Post-tensioned Timber Frames with Supplemental Damping Devices

Tobias Smith

A Thesis presented for the degree of

Doctor of Philosophy

In

Civil Engineering

At the

University of Canterbury

Christchurch, New Zealand

April 2014

Abstract

In recent years the public expectation of what is acceptable in seismic resisting construction has changed significantly. Engineers today live under demands which are far more intensive than their historical counterparts and recent seismic events have shown that preserving life is no longer sufficient, and a preservation of livelihood is now the minimum. This means that after a major seismic event a building should not only be intact but be usable with no or minimal post-quake intervention. In addition to this already high expectation these demands must be met in a green and sustainable fashion with minimal (or even negative) environmental impact. This doctoral project looks to further advance the research into a new and innovative method of timber construction which satisfies (and exceeds) these demands.

In response to these higher expectations recent developments in the field of seismic design have led to the development of damage control design philosophies and innovative seismic resistant systems. Jointed ductile connections for precast concrete structures have been implemented and successfully validated. One of these systems, referred to as the hybrid system, combines the use of unbonded post-tensioned tendons with grouted longitudinal mild steel bars or any other form of dissipation reinforcing device. During the controlled rocking of the system under seismic loading the post-tensioning provides desirable recentering properties, while the devices allow adequate energy dissipation from the system as well as increased moment resistance at column bases and beam-column connections.

The hybrid concept is material independent and in 2004 an extensive campaign was begun to investigate the performance of the hybrid system when applied to large engineered timber members. Numerous small and large scale tests on both subassemblies and full buildings were performed showing that post-tensioned timber meets the seismic resilience demands now imposed by society. Recently this technology has also been applied in practice with over ten structures now using post-tensioned timber walls or frames, or a combination of the two, in New Zealand.

In-spite of the extensive research effort and the acceptance and adoption in practice of post-tensioned timber as a structural system, significant work was still required in the review and refinement of both the system itself and the analytical and numerical methods used to predict and analyse structural performance. The objectives of this research were to review and refine comprehension of the static and dynamic response, analytical and numerical modelling, and design of post-tensioned timber frames under lateral loading. In order to do this a three phase experimental testing campaign was devised and performed including quasi-static testing of an angle dissipative reinforcing device, quasi-static testing of a full-scale beam-column joint and the mono-directional dynamic testing of a 2/3rd scale three storey frame. All testing used glue laminated timber, which had not been previously used in post-tensioned timber structures.

Insight gained from the experimental testing was used to analyse and refine existing analytical modelling techniques. These techniques were split into two categories: 1) modelling of the local behaviour of a post-tensioned timber beam-column joint, with particular focus on stiffness and energy dissipation capacity, and 2) evaluation of the seismic demand (in the form of design base shear) on post-tensioned timber frames looking at current Force Based (FBD) and Displacement Based (DBD) design methods.

This analysis led to the development of recommended alterations in the existing beam-column joint analytical procedure enabling the procedure to provide better prediction of initial and post-yield stiffness. Analysis of the FBD and DBD procedures showed that both methods are capable of providing accurate prediction of seismic demand provided correct assumptions are made regarding system ductility and damping characteristics. Recommendations have been made on how designers can ensure that assumptions are either sufficiently accurate in the beginning of a design or require minimal iteration to be performed. Current numerical modelling techniques have also been compared against the quasi-static and dynamic testing results providing confidence in their accuracy when applied to post-tensioned timber frames. Modelling techniques were also extended to the widely used SAP2000 modelling programme which had not been previously used in post-tensioned timber research.

Although many observations and conclusions were made, a common theme continued throughout this research. This was the importance of the deep understanding of displacements within a post-tensioned timber frame and the impact of these displacements on frame performance. Displacements occur throughout a frame in dissipative reinforcing devices, in the connection of these devices, in beams, columns and joint panels as well as at the interfaces between members. When these displacements are allowed for through proper design excellent seismic performance, possible using this innovative system, is obtained.

Acknowledgements

Over the period of my thesis the input of colleagues, friends and family has been immense. Over the next paragraphs I will attempt to thank some of these contributors however the words written here could never do justice to importance of the advice, help and support they have provided.

Firstly I would like to thank my supervisors Professor Stefano Pampanin, Professor Felice Ponzo and Dr David, Carradine. Without your support (technical, financial and grammatical) this rather ambitious experimental campaign, spanning across the world, would never have been possible.

The financial support of the Structural Timber Innovation Company and Federlegno Arredo have made the testing presented possible.

To my dear friends in Potenza, Antonio di Cesare, Rocco Ditommaso, Domenico Nigro, Gianluca Auletta, Michele Simonetti and Marica Colaianni thank you not only for sharing your wealth of knowledge but also showing me what hospitality means.

To my friends in New Zealand, Andrew Baird, Francesco Sarti, Daniel Moroder, Dennis Pau, Harry Johnston, Sam McHattie, Zeinab Chegini, Varun Joshi, Maxim Millen, James O'Neill, Chris Watson and all other members of the Grizzly Bairds, our technical chat's and the many laughs have been invaluable in maintaining my sanity.

To my family thank you all for your support and for staying up a little late on the odd occasion for a skype call.

Finally I thank my wife Marta. Urban legend tells that I would not have started a PhD if it was not for you but the honest truth is that without your love and support I would have never got through it to the finish.

Table of Contents

Nomenclature

A	Area
A_b	Area of the beam
A_{ex}	External area of the dissipative reinforcement
A_{fuse}	Fuse area of the dissipative reinforcement
A_{pt}	Post-tensioning area
A_{scr}	Area of column face screw reinforcing
A_s	Mild steel reinforcement area
$A_{s,b}$	Beam shear area
$A_{s,col}$	Column shear area
b_A	Width of angle dissipative reinforcing
b_b	Beam section width
b_c	Column section width
c	Neutral axis depth
C_β	Behaviour factor correction for flag shaped system
C_s	Compression force in the mild steel dissipative reinforcement
C_t	Timber compressive force
d_{ex}	Original diameter of the dissipative reinforcement
d_{fuse}	Diameter of fused length of the dissipative reinforcement
E	Young's modulus of mild steel
E_{con}	Interface modified connection modulus
E_{pt}	Post-tensioning modulus of elasticity
$E_{t,para}$	Timber parallel-to-grain Modulus of Elasticity
$E_{t,perp}$	Timber perpendicular-to-grain Modulus of Elasticity
f'_{para}	Timber stress capacity parallel to the grain
f'_{perp}	Timber stress capacity perpendicular to the grain
f_s	Mild steel stress
f_{tb}	Timber bending strength
f_{ts}	Timber shear strength
f_y	Yield stress of mild steel
F_y	Yield strength of dissipative reinforcing
f_u	Ultimate stress of mild steel
G	Dead load
Gt	Shear modulus of timber
g	Acceleration due to gravity ($9.81 m/s^2$)
h	Depth of the section
h_b	Beam section depth
h_c	Column section depth
H_e	Effective height of the equivalent Single-Degree of Freedom (SDOF) structure
h_i	The height of level *i* above the base structure
H_n	Height from the base of the structure to the uppermost seismic weight or mass
I	Modulus of inertia
I_b	Beam modulus of inertia
I_c	Column modulus of inertia
j_d	Lever arm
k_a	Yield displacement modification factor for fuse type reinforcing
K_e	Secant stiffness of the equivalent SDOF structure
k_{gap}	Modulus of elasticity modification factor
K	Initial stiffness
k_{int}	Interface compression rotation factor
k_b	Beam stiffness
k_c	Column stiffness
k_{pt}	Post-tensioning stiffness
$k_{pt,sho}$	Frame stiffness modified for frame shortening

k_{sho}	Frame shortening factor
k_{scr}	Modification factor for screw reinforcement
k_{ss}	Modification factor for stress spreading
k_{μ}	Ductility reduction factor
L	Bay length
L_A	Length of milled section of angle dissipative reinforcing
L_b	Beam length
L_{cant}	Distance from the interface to the point of contra-flexure
L_{ex}	External length of the dissipative reinforcement
L_{fuse}	Fuse length of the dissipative reinforcement
L_t	Total length of the dissipative reinforcement
L_{tube}	Length of anti-buckling tube for fuse type reinforcing
l_{ub}	Un-bonded length of the post-tensioning
m	Seismic mass
$M_{b,col}$	Column base moment
M_{col}	Column moment
M_{cl}	Moment at the column center of a beam-column joint connection
M_{con}	Connection moment
M_{dec}	Decompression moment
m_e	Effective seismic mass
m_i	seismic mass at level *i*
M_{pt}	Post-tensioning moment capacity
M_s	Dissipative reinforcing moment capacity
M_t	Total moment capacity
n	Total number of floors
n_b	Number of beams/bays
n_{col}	Number of columns
n_{gap}	Number of gap openings
n_H	Number of holes in angle dissipative reinforcing
Q	Live load
q_{EPP}	Behaviour factor for an elasto perfectly-plastic system
q_{FS}	Behaviour factor for a flag shaped system
r	Bilinear post-yield stiffness factor (as a ratio of initial stiffness)
R	Non-linear reduction factor for DBD
S_a	Spectral acceleration
S_d	Spectral displacement
S_p	Structural performance factor
T	Structural period
t_A	Thickness of milled section of angle dissipative reinforcing
T_1	Fundamental period structure
T_{pt}	Post-tensioning force
$T_{pt,initial}$	Initial post-tensioning force
T_s	Tension force of the mild steel dissipative reinforcement
V	Shear force
V^*_{col}	Column shear force demand
V_b	Base shear
V_E	Column seismic shear demand
V_{jp}	Shear in the joint panel
W	Seismic weight
w_{ex}	Original width of the dissipative reinforcement
w_{fuse}	Fuse width of the dissipative reinforcement
y_{pt}	Edge distance to the post-tensioning reinforcement level
$y_{s,c}$	Edge distance to the compression reinforcement level
$y_{s,t}$	Edge distance to the tension reinforcement level
Z_b	Beam section modulus
Z_{col}	Column section modulus
ΔT_{pt}	Post-tensioning force increase
α	Post-yield stiffness of dissipative reinforcing
$\alpha_{s,ave}$	Shear coefficient to find the section shear rigidity
$\alpha_{s,cl}$	Shear coefficient to convert average shear to centroidal shear

β	Re-centering ratio
δ	Displacement of dissipative reinforcement attachment
$\delta_{bending}$	Displacement due to bending
δ_{shear}	Displacement due to shear
Δ	Displacement
Δ_d	Design displacement
Δ_{ex}	External displacement of the reinforcement
Δ_{fuse}	Fuse displacement
Δ_i	Horizontal displacement at the i-th level
Δ_{int}	Interface initial compression due to initial PT load
Δ_{pt}	Elongation of the post-tensioning
Δ_s	Elongation of dissipative reinforcing
Δ_y	Yield displacement of dissipative reinforcing
$\Delta\varepsilon_{pt,i}$	Strain increase in post-tensioning
ε_s	Mild steel strain
ε_t	Timber strain
ε_t	Mild steel yield strain
θ	Rotation
θ_b	Elastic beam rotation
θ_c	Elastic column rotation
$\theta_{c,base}$	Elastic column base rotation
θ_{cl}	Rotation at the centerline of the beam-column joint
θ_{con}	Connection rotation
θ_d	Design drift
θ_{gap}	Gap rotation
θ_{imp}	Imposed rotation
θ_{int}	Interface compression rotation
θ_j	Elastic joint panel rotation contribution
θ_t	Total inter-storey drift rotation
θ_y	Yield rotation
μ	Structural displacement ductility factor
μ_A	Displacement ductility demand of dissipative reinforcing angle
ξ	Total equivalent viscous damping
ξ_{EQV}	Equivalent viscous damping defined from area based method
ξ_{el}	Elastic damping
ξ_{hyst}	Hysteretic damping
ρ_k	Characteristic density
ρ_m	Mean density
ϕ	Strength reduction factor
ϕ_{dec}	Decompression curvature
ϕ_H	Diameter of holes in angle dissipative reinforcing
ϕ_0	Material over-strength factor
Ψ	Earthquake imposed action combination factor
ω_f	Dynamic amplification factor

1 Introduction, Motivation and Scope of Research

1.1 INTRODUCTION

Although timber is one of the most ancient materials available in construction, during the last 100 years it has fallen behind both concrete and steel in medium and high rise construction. Increasingly, the importance of timber as a sustainable and efficient option for the future of world construction is being recognized. However, significant steps in the development of the use of this material must still be made to ensure its wide scale adoption.

Parallel to the push in the rise of timber as a desirable construction material it is becoming increasingly obvious that current target performance levels in seismic design are no longer acceptable to developed society. Modern seismic codes indicate that obtaining ductility is critical to seismic performance, however there is a failure to acknowledge that in providing ductility an engineer is accepting that significant damage will occur to a structure in a design level earthquake. The recent Canterbury, New Zealand seismic sequence of 2010 and 2011 has highlighted, especially in the public eye, the failings of this design objective. During these events modern structures performed admirably achieving the life safety objective that they were designed to meet, however, the structural damage in addition to economic pressures has meant that a significant part of the central city has now been demolished.

Recent developments in the field of seismic design have led to the development of damage control design philosophies and innovative seismic resilient systems which provide significantly improved seismic performance. In particular, jointed ductile connections for precast concrete structures have been implemented and validated. One type of jointed ductile connection, originally developed for precast concrete during the U.S.-PRESSS program (PREcast Seismic Structural System), coordinated by the University of California, San Diego, U.S.A., for frame and wall systems has been particularly successful (Priestley et al. 1999). This system, referred to as the ‘hybrid’ system, combines the use of unbonded post-tensioned tendons with grouted longitudinal mild steel bars or any other form of dissipation device. While the post-tensioning provides desirable recentering properties, the dissipation devices allow

adequate energy dissipation as well as increasing moment resistance. During lateral movement, controlled rocking occurs at the beam-column, wall-foundation or column-foundation interface, which gives the "flag-shaped" hysteretic behaviour. When dissipation devices are placed externally they become replaceable so that hysteretic energy dissipation is effectively decoupled from permanent structural damage. This decoupling leads to structures that will not only remain operational after a major earthquake event, but will also limit direct costs associated with repair and indirect financial losses associated with business operation and downtime.

In 2004 the jointed ductile concept developed for concrete structures was applied to large engineered timber members and has been extensively tested at the University of Canterbury using laminated veneer lumber (LVL), in a system known as Pres-Lam (Prestressed-Laminated timber). Over the last seven years extensive medium scale sub-assembly testing has been performed (Palermo et al. 2005; Palermo et al. 2006) as well as larger scale testing (Iqbal et al. 2010; Newcombe et al. 2010). Design procedures which were developed during the U.S.-PRESSS program (Pampanin et al. 2001) and extended by subsequent researchers (Palermo 2004) were applied to this form of timber construction considering the material characteristics of timber (Newcombe et al. 2008).

In 2008 work began on the first ever post-tensioned timber multi-storey building for the Nelson Marlborough Institute of Technology (NMIT) in Nelson, New Zealand combining timber gravity frames with coupled post-tensioned timber walls (Devereux et al. 2011). Following the success of this first structure, eight more post-tensioned timber buildings have been completed or are nearing completion in New Zealand. Three of these structures have used post-tensioned timber frames with two of the three placing dissipative devices at the beam-column connection. These structures are further described in Chapter 2.

In-spite of the extensive research effort and the acceptance and adoption in practice of post-tensioned timber as a structural system, significant work was still required in the review and refinement of both the system itself and the analytical and numerical methods used to predict and analyse structural performance in order to facilitate the efficient design and construction of more post-tensioned timber buildings.

1.2 RESEARCH MOTIVATION

It is inevitable that as new technologies are invented their superior performance will motivate building owners and occupants to consider adopting these technologies in their buildings. This is especially true following a major seismic event, such as the current situation in Christchurch, New Zealand, where the general public is very aware of earthquakes and their effects. New building technologies will require practicing engineers to work beyond their standard skill set and levels of confidence.

It is crucial therefore that researchers, as the developers of these new technologies, are confident in their performance and have a deep understanding of every aspect of their performance and adoption in the marketplace. Guidelines for the design of these new technologies must be clear and concise and will often require simplifications to be made. Only through deep understanding of system performance can these simplifications be made in a conservative and correct manner.

1.3 RESEARCH OBJECTIVES

The objective of this research is to review and refine understanding of the static and dynamic response, analytical and numerical modelling and design of post-tensioned timber frames under lateral loads. In order to achieve this objective a series of research questions have been asked, divided into four groups:

<u>Performance of dissipative reinforcing</u>

1. What forms of dissipative device can be applied at the beam-column joint?
2. How will the design parameters of initial stiffness, yield strength and post-yield stiffness relate to the physical characteristics of the device?
3. How will these dissipative devices be connected to the beam-column joint?

<u>Local performance of post-tensioned beam-column joints</u>

4. How does the ratio of moment capacity provided by the post-tensioning and the moment capacity provided by the dissipative reinforcing relate to the damping capacity?
5. Can the prediction of the initial stiffness of post-tensioned beam-column joints as identified by Newcombe (2012) be improved?
6. Can improved understanding of the contributions of elastic deformations of the beam, column, joint panel and external dissipative reinforcing attachment be obtained and simple analytical methods be developed?

Global performance of post-tensioned frames

7. Is Laminated Veneer Lumber (LVL) interchangeable with other engineered timber materials, such as Glue laminated timber (Glulam)?
8. Do the trends and analytical procedures observed and developed almost entirely during low speed, quasi-static and pseudo-dynamic testing continue to apply during large scale dynamic testing?
9. Are the current methods used for the prediction of the dynamic demand and response of post-tensioned timber frames accurate?
10. How does the dynamic response of a post-tensioned timber frame change when dissipative reinforcing is added to the frame?

Numerical modelling and design of post-tensioned timber frames

11. Do the current methods of numerical computer modelling accurately predict the dynamic performance of post-tensioned timber frames?
12. Can simplifications to these numerical computer modelling procedures be made in order to render their use more acceptable to practising engineers?
13. How do the frame characteristics (bay length, number of bays and number of stories) as well the quantity of dissipative reinforcing, alter section size and required strength and performance?
14. Can the design procedure be refined and simplified in order to make it more linear (with less iteration as is currently required) and easier to use for practicing engineers?

1.4 SCOPE OF RESEARCH

The scope of this research is the assessment and prediction of the seismic performance of post-tensioned timber frames. This research will focus only on the application of alternative dissipative reinforcing types at the beam-column and column-foundation connections and will not include the application of reinforcing at other locations throughout a structure (such as dissipative bracing). The frames considered are one-way and will be designed considering lateral forces only in one direction. The wider body of research into the performance of post-tensioned timber structures will be discussed in Chapter 2 and includes post-tensioned walls and gravity systems, the use of other engineered timber materials such and Laminated Veneer Lumber (LVL) and Cross Laminated Timber (CLT) as well as the seismic

performance of diaphragms. These aspects of post-tensioned timber design will not be included here.

1.5 RESEARCH METHOD AND THESIS CONTENT

The responses to the questions presented in Section 1.3 have been prepared through the use of three phases of experimental testing:

- Quasi-static cyclic testing of dissipative angle reinforcing elements
- Quasi-static cyclic testing of a full-scale glue laminated beam-column joint varying the combination of post-tensioning moment capacity and dissipative reinforcing capacity
- Mono-directional dynamic testing of a two-third scale three storey post-tensioned timber frame with and without the addition of dissipative reinforcing

In addition to the experimental testing three phases of numerical modelling have been performed:

- Development of a non-linear finite element model in order to replicate and predict the cyclic performance dissipative reinforcing elements
- Development of numerical lumped plasticity models in order to replicate and predict the local (beam-column) and global (full frame) static and dynamic performance
- A parametric analysis varying four frame characteristics: bay length, number of bays, number of stories and quantity of dissipative reinforcing

Following a review of the current state of post-tensioned timber design, presented in Chapter 2, the first phase of experimental testing is presented in Chapter 3. This first phase studied the performance of two forms of external dissipative reinforcing devices through the use of two cyclic testing campaigns. The first of the testing campaigns was performed as part of this thesis and the second was sourced from literature. The design of these devices is then discussed and analysed using testing results and finite element modelling. Finally this chapter looks at the flexibility of the external dissipative reinforcement connection. This is critical in design in order to obtain correct dissipative reinforcing performance.

The local behaviour of a post-tensioned timber frame, the behaviour of the beam-column joint, is examined in Chapters 4 and 5. Chapter 4 presents a series of quasi-static tests performed on a full-scale beam-column joint varying the quantity of dissipative reinforcing and the amount of initial force in the post-tensioned tendon or bar. Chapter 5 presents the verification and refinement of the procedure to predict the moment-rotation relationship at the beam-column interface using the results of the beam-column testing. Methods were also developed and are presented to predict the elastic rotations of the beam, column and joint panel as well as the hysteretic damping capacity of the beam-column joint. All procedures were found to be adequately accurate following the application of a few minor adjustments and refinements.

The global dynamic behaviour of a post-tensioned timber frame is examined in Chapters 6 and 7. Chapter 6 presents the dynamic testing of a three-storey two-third scale post-tensioned timber frame. Testing was performed both with and without the addition of dissipative reinforcing up to a maximum peak ground acceleration of 0.9 g. The beam and column members remained undamaged during testing up to the maximum 3.6% drift registered during testing. Chapter 7 first compares the beam-column performance with the design procedures which were developed during the beam-column testing and finds them accurate also under dynamic loading. Chapter 7 then goes on to compare current Force Based Design (FBD) and Displacement Based Design (DBD) methods for predicting seismic demand with testing results. This comparison underlined the importance of understanding ductility during the frame design.

Increasingly, and especially for innovative technologies, practicing engineers rely on the use of numerical modelling programmes to assess the performance of the structural system that has been designed. Chapter 8 examines and refines current numerical modelling techniques which were compared against the quasi-static beam-column and dynamic frame test results.

Chapter 9 presents a parametric study of post-tensioned timber frames which was performed varying the bay length, number of bays, number of stories and the ratio between the moment capacity provided by the post-tensioning and the dissipative reinforcing, All frames were designed using the refined DBD and post-tensioned analytical procedures and had the same performance objective in the form of a design

drift. A comprehensive numerical analysis was then performed using the modelling techniques presented in Chapter 8.

Chapter 10 presents the step by step design procedure for post-tensioned timber frames with dissipative reinforcing devices. Guidance has been provided regarding the selection of section sizes, initial post-tensioning and dissipative reinforcing quantities. Long term effects and target strength hierarchies are also analysed and discussed. Chapter 11 presents the conclusions drawn from research and provides future research recommendations.

All testing performed during the completion of this thesis has been in the structural laboratory of the Department of Structures, Geotechnics and Applied Geology of the University of Basilicata (UNIBAS) in Potenza, Italy.

REFERENCES CHAPTER 1

Devereux, C. P., Holden, T. J., Buchanan, A. H., and Pampanin, S. (2011). "NMIT Arts & Media Building - Damage Mitigation Using Poat-Tensioned Timber Walls." 9th Pacific Conference on Earthquake Engineering, Auckland, New Zealand.

Iqbal, A., Pampanin, S., Palermo, A., and Buchanan, A. H. (2010). "Seismic Performance of Full-scale Post-tensioned Timber Beam-column Joints." 11th World Conference on Timber Engineering, Riva del Garda, Trentino, Italy, 10.

Newcombe, M. (2012). "Lateral Force Design of Post Tensiond Timber Frame and Wall Buildings ", University of Canterbury, Christchurch.

Newcombe, M. P., Pampanin, S., A.Buchanan, and Palermo, A. (2008). "Section Analysis and Cyclic Behavior of Post-Tensioned Jointed Ductile Connections for Multi-Story Timber Buildings." *Journal of Earthquake Engineering*, 12(1), 83–110.

Newcombe, M. P., Pampanin, S., and Buchanan, A. H. (2010). "Global Response of a Two Storey Pres-Lam Timber Building." 2010 New Zealand Society for Earthquake Engineering Conference, Wellington, New Zealand, 8.

Palermo, A. (2004). "The Use of Controlled Rocking in the Seismic Design of Bridges," Politecnico di Milano, Doctoral thesis, Milan.

Palermo, A., Pampanin, S., Buchanan, A., and Newcombe, M. (2005). "Seismic Design of Multi-Storey Buildings using Laminated Veneer Lumber (LVL)." 2005 New Zealand Society for Earthquake Engineering Conference, Wairakei Resort, Taupo, New Zealand.

Palermo, A., Pampanin, S., Fragiacomo, M., Buchanan, A. H., and Deam, B. L. "Innovative Seismic Solutions for Multi-Storey LVL Timber Buildings." *9th World Conference on Timber Engineering*, Portland, U.S.A.

Pampanin, S., Priestley, N., and Sritharan, S. (2001). "Analytical Modelling of the Seismic Behaviour of Precast Concrete Frames Designed with Ductile Connections." *Journal of Earthquake Engineering*, 5(3), 329-367.

Priestley, N., Sritharan, S., Conley, J., and Pampanin, S. (1999). "Preliminary Results and Conclusions From the PRESSS Five-Story Precast Concrete Test Building." *PCI Journal*(November-December 1999), 42-67.

2 The Current State of Post-tensioned Timber Frame Practice

This chapter presents a review of the relevant research and material relating post-tensioned timber frame research. For clarity this is done in four sections. In the first section the development of the post-tensioned timber concept is presented and discussed. Following this, the current methods and techniques for modelling and analysing these types of connections and systems are presented. The addition of supplemental damping through the application of dissipative devices and dissipative reinforcing are then discussed. Finally, previous research programmes which have studied the dynamic performance of timber buildings are discussed.

2.1 THE JOINTED DUCTILE CONNECTION SYSTEM

In the early 1990's a research project was initiated in U.S. with the aim of increasing the use of precast concrete with the aim of developing new materials, concepts and technologies for precast concrete (Priestley 1991). This project (named U.S. PRESSS, PREcast Seismic Structural Systems) recognised the significant advantages of the use of prefabricated elements due to their 'high technology/low labour' attributes. The three phases of this extensive project eventually focused on the experimental and analytical development of 'Jointed Ductile' connections (Priestley 1996) culminating in the pseudo-dynamic testing of a full scale five storey test building at the University of California at San Diego. (Priestley et al. 1999). Very early in this project the advantages of the combination of a Non-Linear Elastic (NLE) and Tension Compression Yielding (TCY) or Coulomb Friction (CF) system were recognised. In particular the combination of post-tensioning tendons/bars and longitudinal non-prestressed mild steel (or in fact some other form of external dissipation device) to make a 'hybrid' (Stanton et al. 1997) joint provided particularly good results.

This combination provides controlled rocking under horizontal loading (such as seismic loading). During this rocking a gap is opened between the beam and column, or wall and foundation yielding the mild steel and elongating the tendon. During rocking the moment capacity provided by the post-tensioning combines with the

moment capacity provided by the yielding of the mild steel which results in the characteristic 'flag-shaped' hysteretic loop shown in Figure 2.1. Provided these systems are properly designed testing has shown that hybrid joints can provide a seismic response that is at least as adequate as that of the equivalent monolithic solution (Pampanin et al. 2000).

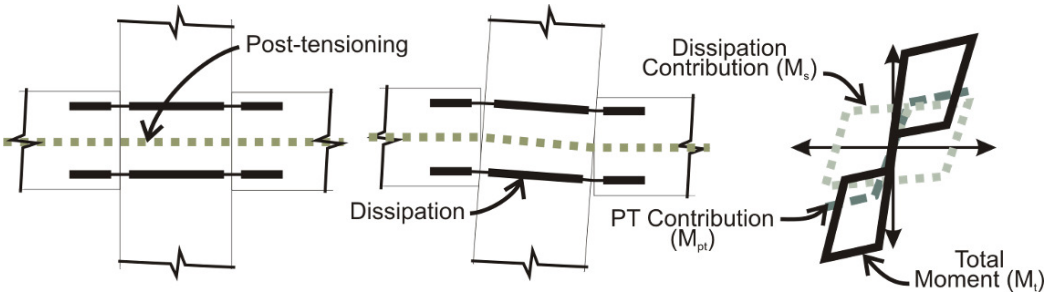

Figure 2.1. Characteristics of a hybrid beam-column joint

The ratio between the moment capacity provided by the post-tensioning (M_{pt}) and the total moment capacity (M_t) is known as the recentering ratio. This ratio is one of the key parameters of the hybrid system as it provides information about the level of hysteretic damping the connection possesses.

Residual displacements are also reduced with a hybrid system. Residual displacements have been identified as being significantly critical to proper limited damage performance (Christopoulos and Pampanin 2004). Residual deformations can results in a building being declared unsafe following a seismic event which provides effectively the same structural result as if the building had collapsed. Residual displacements can also significantly increase the cost of repair. Hybrid joints can either limit or in some cases eliminate residual deformations.

These systems have been shown to be material independent with structural steel options being designed, analysed and tested (Christopoulos et al. 2002).

2.2 POST-TENSIONED TIMBER TESTING

Beginning in 2004 the use of the hybrid jointed ductile connection concept was extended to use with timber elements (Palermo et al. 2005a). This ongoing project combines the use of the concepts developed for use in precast concrete with engineered timber products.

Due to its availability in New Zealand and improved characteristic strength and stiffness Laminated Veneer Lumber (LVL) has been initially used. A veneer based product consisting of wood and adhesive, LVL was first developed during The Second World War for use in airplane propellers and other high strength airplane components. Similar to plywood, LVL is made up of parallel laminations of veneer, glued and processed together to form a new material. The distinguishing difference between LVL and plywood is that in LVL the orientations of the veneer layers all run parallel. The use of thin veneers has the effect of spreading out any defects (Figure 2.2a) in the member thus decreasing variation in the timber properties and increasing the characteristic strength and Modulus of Elasticity (MOE) (Figure 2.2b).

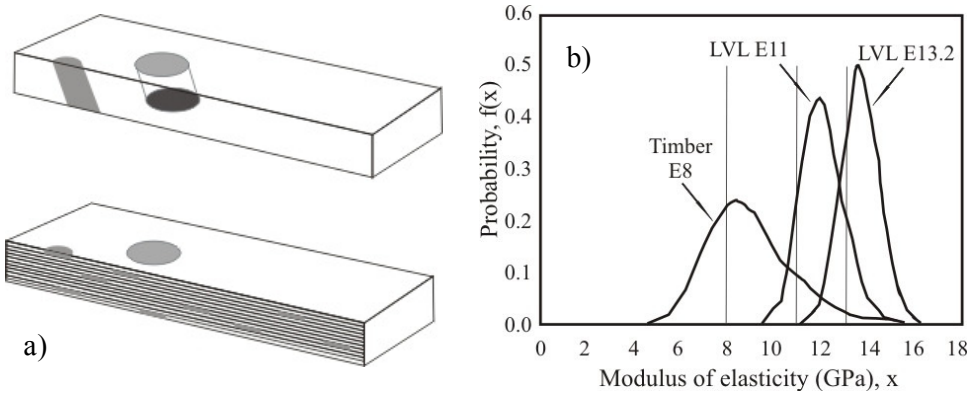

Figure 2.2. a) Spreading of defects in LVL b) increased MOE

2.2.1 Laboratory testing

Extensive medium scale sub-assembly testing has been performed on Beam-Column (Palermo et al. 2006a), Wall-Foundation both single and coupled (Iqbal et al. 2007; Smith et al. 2007) and Column-Foundation (Iqbal et al. 2007; Palermo et al. 2006b) connections. Selected results from these tests are presented in Figure 2.3.

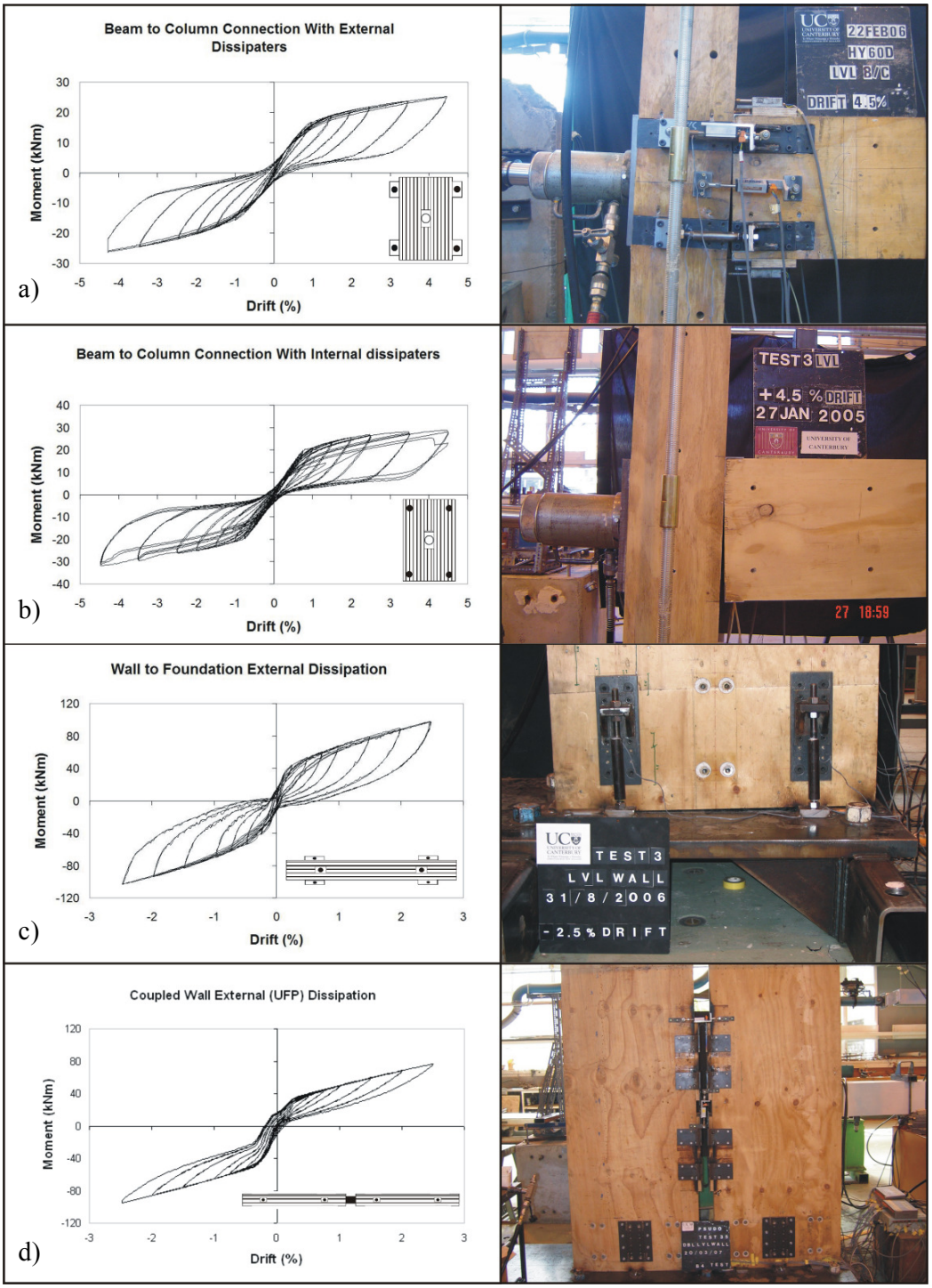

Figure 2.3. a) Beam-column test with external dissipation b) Beam-column test with internal dissipation c) Wall-foundation test with external dissipation d) coupled wall with external UFP dissipation

In all of these tests the distinctive 'flag shape' hysteretic behaviour is apparent. All of the tests displayed significant amounts of hysteretic damping which was achieved through the use of 'fused type' dissipation devices, initially developed for precast

concrete jointed ductile connections (Marriott 2009; Pampanin 2005). Values of up to 15% Equivalent Viscous Damping (EVD) were recorded during testing. This method of dissipation will be further described in Chapter 3. All of these tests however had very small joint to member capacity ratios (i.e. the beam-column interface moment capacity was significantly less than the moment capacity of the beam and the column). This was done in order to ensure the beam and column members remained purely elastic thus enabling a large number of tests to be performed on a single specimen.

Once the principles of the Post-Tensioned timber concept were validated larger scale tests were proposed and performed. The first of these was a full scale internal and external beam-column connection shown in Figure 2.4a (Iqbal et al. 2010). This was followed by a 2/3rd scale frame and wall super-assembly two-storey building tested both with and without flooring shown in Figure 2.4b (Newcombe et al. 2010c). Both of these tests continued to validate the system however it was noted that in both tests there was little gap opening at the 2% design level drift meaning that the mild steel dissipative elements which had proven successful in small scale testing did not activate (or activated nominally). This led to almost elastic behaviour at design drift. This lack of post-decompression rotation has been mainly attributed to the inherent flexibility in timber (Cusiel et al. 2010) in addition to the dissipative devices being too slender. As the large scale test was pushed to higher drift levels (3.5%) yielding of the external dissipaters did occur and equivalent viscous damping values increased (Iqbal et al. 2010).

Figure 2.4. a) Full-scale Beam-Column (Iqbal et al. 2010) and b) 2/3rd scale frame and wall tests (Newcombe et al. 2010c)

2.2.2 Applications in construction

At the beginning of 2010 work was begun on the first ever post-tensioned timber building in Nelson, New Zealand (Devereux et al. 2011). Constructed as part of the campus of the Nelson Marlborough Institute of Technology (NMIT) the building consists of a timber gravity resisting frame and lateral load resisting shear walls. Post-tensioning was used only in the wall elements (Figure 2.5) coupled with U-shaped Flexural Plates (UFP) shown in Figure 2.3d and described further in Section 2.6.

Figure 2.5. Construction of Nelson Marlborough Institute of Technology (NMIT) building 2009

Following this initial post-tensioned timber building eight more applications of post-tensioned timber have been currently applied around New Zealand. Two of these structures have used post-tensioned timber frames complemented by dissipative elements at the beam-column joint: the 3 storey Merritt office building (Figure 2.6a) and the 2 storey Trimble office building (Figure 2.6b). A third structure, constructed for Massey University in Wellington, used post-tensioned timber frames with draped tendons and UFP dissipative devices between the first floor beam and the foundation wall. The advantage of placing the dissipative devices at this location is that under seismic loading they will undergo the maximum amount of displacement possible (i.e. the full interstorey drift). This leads to the maximum possible plastic strains and thus the maximum amount of hysteretic dissipation being obtained. This is not the case when dissipative devices are placed at the beam-column joint as will be discussed further in Section 2.4.2.

Figure 2.6. Applications of post-tensioned timber frames in construction a) the Trimble office building, b) the Merritt office building

2.2.3 Feasibility of the wide scale adoption of post-tensioned timber construction

Several recent projects have also studied the likely cost and construction times of buildings using post-tensioned timber. Smith et al. (2009) compared a 6-storey Laminated Veneer Lumber (LVL) post tensioned timber building with prototype buildings in both precast concrete and steel. The conclusion of this study was that the building would take a similar time to construct and cost roughly 5% more than the $NZD 9.5 million required to construct either the steel or concrete alternatives. This research did however have some limitations due to assumptions made regarding structural system layouts (which were maintained from the concrete structure) and a high cubic meter cost of LVL. The construction of the test building shown in Figure 2.4b, provided valuable cost data for the second study performed by Menendez Amigo (2010) This study compared an open plan 5 storey concrete building with a theoretical post tensioned timber alternative. One conclusion of this study was that the post tensioned timber building would have taken 40% less time to construct due to its fully prefabricated nature. The cost comparison of the two buildings showed an

increase of $NZD 100,000 for the timber building, 8% of the total cost of the building. Recent study (John et al. 2011) has compared instead a real post-tensioned timber building with theoretical steel and concrete contaparts concluding similar cost and time results. Liong (2009) connected the cost difference to manufacturing techniques on post-tensioned timber building which are poorly developed and do not have the required large-scale capacity in New Zealand. An example of this from Liong is displayed in Figure 2.7 which compares the complexity of the supply of a post-tensioned timber structure to the relative simplicity of the supply of an equivalent steel structure.

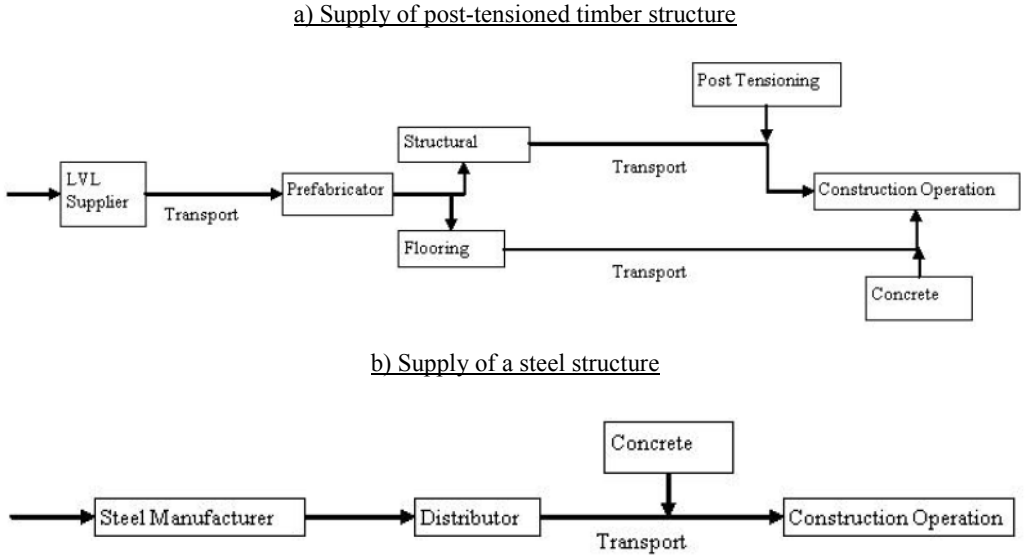

Figure 2.7. Comparison between the supply chain for a) post-tension timber structure and b) steel structure in New Zealand (Liong 2009)

2.3 LONG TERM EFFECTS IN POST-TENSIONED TIMBER BUILDINGS

The post-tensioned timber system relies on a moment connection which comes, in part, from the tensioning of a high strength steel cable or bar. Losses in tension in the steel element reduce the resistance of the connection and may lead to insufficient strength under seismic or gravity loading. Timber when subjected to sustained compression displays viscous properties which can lead to unrecoverable negative displacements. Although significantly more testing is required to understand the relationship between compression deformation and the post-tensioned timber system limited research has been performed and is described.

Davies (2007) performed a year-long experimental campaign subjecting LVL to sustained compression under both uncontrolled and controlled conditions. The results of testing were analysed in order to distinguish between pure creep and machno-sorptive effects and relate these to the changing environmental conditions. The conclusions of this study were that current codes (NZS3603 1993) may be adequate where timber is subjected to compression parallel to the grain however values of long term deformation can be up to 4.5 time larger where compression is perpendicular to the grain (as is the case in a beam-column joint). A limiting value of 40% of the total timber compression strength was suggested in order to mitigate these affects.

Neale (2009) conducted testing for creep effects on the test building shown in Figure 2.4b during its testing phase in the University of Canterbury Structures Laboratory. Neale's study confirmed Davies' evidence that the columns loaded perpendicular to the grain represent the governing factor in terms of structural performance, however due to the short time-frame of recordings, taken over a period of 2 months, values were used as an indication only and no firm conclusions could be made. One important result from the study was the investigation into the use of screws in order to reduce compression perpendicular to grain creep with a modest reduction being observed.

As mentioned above work is ongoing in this field with several projects monitoring creep deformations and tendon losses in real post-tension timber applications (Carradine et al. 2012).

2.4 ANALYTICAL ANALYSIS OF JOINTED DUCTILE SYSTEMS

Rocking connections present an unusual problem in design in that some of the corner stone principles of moment-curvature analysis are violated. Firstly, Bernoulli-Navier theorem of "plane sections remain plane" is violated by the infinite curvature at the rocking interface. Furthermore, the fact that post-tensioning elements are left unbonded means that strain compatibility is violated. In this section the methods of analysing post-tensioned timber system response are presented.

2.4.1 Analysis of the behaviour of the interface of a jointed ductile system

Analysis of a jointed ductile concrete systems

A step-by-step general design procedure which describes the response of a post-tensioned dry jointed connection was initially proposed by Pampanin et al. (2001). This design procedure was based upon the concept of a Monolitic Beam Analogy (MBA) which was used in order to calculate the compression strain in the concrete as part of a complete moment-rotation analysis procedure of the connection. This procedure has been included in the fib guidelines (fib 2004) as well as in the New Zealand concrete design standard (NZS 3101 2006). The MBA considers a global compatibility condition by assuming that the displacement of a post-tensioned system is equal to that of an equivalently reinforced monolithic connection when subjected to the same lateral load. This procedure proposed that if reinforcement is identical, then the elastic deformation will also be identical and therefore was originally developed focusing on the calculation of the plastic system rotation.

Further development of the design procedure lead to the revised Monolitic Beam Analogy (rMBA) when it was recognised that, following decompression, the post-tensioned system is inherently more flexible than the equivalent monolithic element (Palermo 2004). This is due to the fact that following decompression, but before the yielding of the inelastic response of the concrete in compression the post-tensioned element will have and addition displacement/rotation due to the initiation of the gap opening. The analogy has therefore been divided into three regions: before decompression, between decompression and yield of the concrete in compression, and after yield of the concrete in compression. The rMBA procedure was renamed as the Modified Monolithic Beam Analogy (MMBA) and will be named as such in this thesis. The MBA/MMBA has been shown to be material independent through its successful application to the prediction of the performance of steel rocking frames (Christopoulos et al. 2002). The use of unbonded post-tensioned concrete frames has also been extended to gravity dominated frames with the development of the Brooklyn system (Pampanin et al. 2004).

Analysis of a jointed ductile timber systems

In the calculation of the moment-rotation response of a post-tensioned timber jointed ductile connection (wall-foundation, column-foundation or beam–column connection)

the same basic principles are followed as those applied to reinforced concrete, however, some minor alterations had to be made.

As mentioned above, the post-yield behaviour defined in the MMBA procedure refers to the yielding of a typical reinforced concrete section and not specifically the inelastic behaviour of an additional damping device. During the design of a post-tensioned connection it is required that strains in the timber remain below the materials yield strain and therefore the pre-yield form of the MMBA is used in order to calculate the compression strain in the timber.

$$\varepsilon_t = c\left(3\frac{\theta_{imp}}{L_{cant}} + \phi_{dec}\right) \quad \textbf{(2.1)}$$

Where:

ε_t = compression strain at the extreme fibre of the timber beam

L_{cant} = Distance from the interface to the point of contra-flexure

ϕ_{dec} = Decompression curvature

As the timber strain is designed to remain below the yield strain of the material a triangular stress block is used.

The value of L_{cant} depends upon what type of structural form contains the jointed ductile timber connection. For frames L_{cant} is taken as the point of contraflexure of the beam and for the base column the same principle applies. For wall systems the length L_{cant} is taken as the effective height of the wall multi-degree of freedom system (STIC Inc. 2013).

In addition to the considerations relating to the use of the MBA/MMBA as described above, alterations to the jointed ductile reinforced concrete design procedure were required in order to account for the use of timber as a construction material. During the calculation of the material characteristics of timber testing values are read over a code defined gauge length in order to avoid the ‘end effect’ which is present in timber materials (EN408:2003 2003). This end effect is related to the local crushing of the timber fibres and results in a 70% reduction in timber stiffness.

Timber is highly anisotropic and presents a significantly lower stiffness in the perpendicular to the grain direction. Where timber parallel to the grain is bearing on

perpendicular to the grain members (i.e. in a beam-column joint), interaction between the two occurs further reducing the stiffness of the connection.

In order to account for the end-effects and the localized deformation due to bearing perpendicular to the grain, a reduction factor, k_{gap}, has been introduced and a modified 'connection modulus', E_{con}, has been defined (Newcombe 2007). The definition of k_{gap} and the connection modulus is further discussed in Chapter 5.

An alternative analysis method for jointed ductile timber systems

A modified section analysis design procedure for post-tensioned seismic-resisting timber frames has been presented (Pampanin et al. 2006b). This is essentially the same as the MMBA using only the pre-yield region. Recently it has been noted that the use of the MMBA fails to capture the initial performance of post-tensioned members (be it beam-column or wall/column-foundation). This has led to the proposal of empirical formulas based on the results of comprehensive variable analyses (Newcombe et al. 2010a).

2.4.2 Inclusion of elastic deformations in the analysis of jointed ductile timber systems

Section 2.2.1 discussed that when the post-tensioned timber jointed ductile concept was applied to large scale testing of a frame and beam-column subassembly the desired performance was not obtained to the same satisfactory level as observed in the medium scale testing. This occurred because of the delayed activation of the dissipation devices. The principle reason behind this, in addition to errors in the dissipater design, was related to the need to adequately account for the full elastic deformations of the frames during design.

The rotation contributions (Figure 2.8) comprise of the elastic rotations of the beam (θ_b), column (θ_c) and joint panel (θ_j) (Buchanan and Fairweather 1993; Newcombe et al. 2010a). The beam and column rotations can be simply calculated in relation to the moment at the connections using common beam deflections equations. Due to the low shear modulus of timber the large axial forces in the beams induced by the post-tensioning create large elastic shear deformations in the joint panel occur which must also be accounted for (Cusiel et al. 2010). Equations have been proposed to estimate the rotation of the joint panel (Newcombe et al. 2010a).

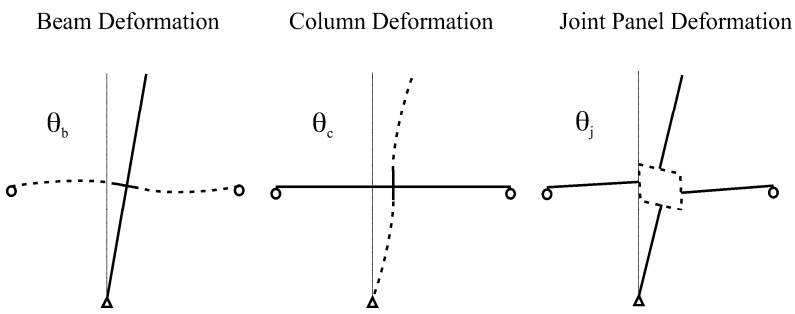

Figure 2.8. Rotation contributions to a post-tensioned timber frame

The acknowledgement of these moment contributions is crucial in the design of any proposed dissipation element as these elements require complete understanding of likely displacements in the area in which they will be placed. Hysteretic dissipations devices (described in Section 2.6) for example are required to yield at a given level of displacement and sustain a certain ductility demand. Failure to understand the displacements which will be sustained by dissipation devices may lead to either late or no activation rendering the system essentially elastic (i.e. zero damping).

2.5 POST-TENSIONED SYSTEM MODELLING

2.5.1 Lumped plasticity models with rotational springs

From the conception of the post-tensioned jointed ductile concept it has been clear that the nature of the controlled rocking mechanism leant itself well to the use of a lumped plasticity approach in modelling (Palermo et al. 2005b; Pampanin et al. 2001). This approach combines the use of effectively zero length (1 mm or less) rotational springs which are located at the rocking interface with elastic frame elements having the appropriate material and section properties. In order to perform this modelling method a section analysis (moment-rotation) procedure must be first performed in order to individuate the contributions of the post-tensioning, steel and gravity loading if present.

2.5.2 Multi-spring models

The use of a multi- (axial) spring model can be seen as a more direct way of predicting/analysing the behaviour of a post-tensioned system. In this model the interface is represented by a series of axial compression only springs whose characteristics are calibrated based on the analysis of the post-tensioned only system. All other components, such as the dissipative devices, are modelled based on their realistic mechanical response. As this the lump plasticity model frame or wall sections

are represented as elastic Giberson members, however, instead of calculating a proposed dissipation and post-tensioned contribution the real force/displacement or force/velocity performance of the dissipation can be set and placed in the system linked by rigid elements. This form of modelling has the advantage that phenomena such as beam elongation, neutral axis depth and tendon elongation can be represented unlike in the rotational spring model.

2.5.3 Finite Element Models (FEM)

A Finite Element Model (FEM) divides the system into a number of sub-domains each represented by a set of equations related to the properties of the original system and based on an appropriate mesh form. This mesh can be increased in order to increase accuracy however it is likely that finer meshing will require increase computational time. Each of these fibres is assigned a stress/strain relationship which is monitored throughout the analysis.

Finite element models have been used to model the response of post-tensioned precast concrete walls by Kurama (2006) using the ABAQUS package. Gap/contact elements were located at the rocking interface between the foundation and wall elements to allow uplift. The finite element model compared well to an equivalent fibre element (lumped plasticity) model, with the lateral response and the uplift and contact during rocking comparing favourable.

2.5.4 Further considerations in modelling

As mentioned recent studies (Cusiel et al. 2010) have also recognised the importance of modelling and accounting for the elastic joint rotation in the calculation of the connection rotation. In order to model this an elastic rotational spring is added in the joint panel region of a post-tensioned timber frame. This procedure was not verified against a wide range of testing results and is reviewed during this thesis.

2.6 DESIGN AND APPLICATION OF DISSIPATION DEVICES

The dissipative devices make up an important part of the hybrid system. Depending on the type of dissipaters used these can add strength and/or stiffness thus increasing capacity as well as adding dissipation reducing demand. This consideration means that the dissipative elements should be thought of more as dissipative reinforcing and not solely as dissipative devices.

The options for the dissipative reinforcing of a building are almost endless in both energy release method (i.e. tension compression yielding, yield in bending, friction sliding, viscous, Figure 2.9), method of control (passive, semi-active, active) and placement (i.e. beam-column, base of wall/frame, in between walls, braced bay, Figure 2.12). Reinforcing can also be displacement proportional or velocity proportional. All of these methods of dissipative reinforcing have been shown to perform well under various loading conditions.

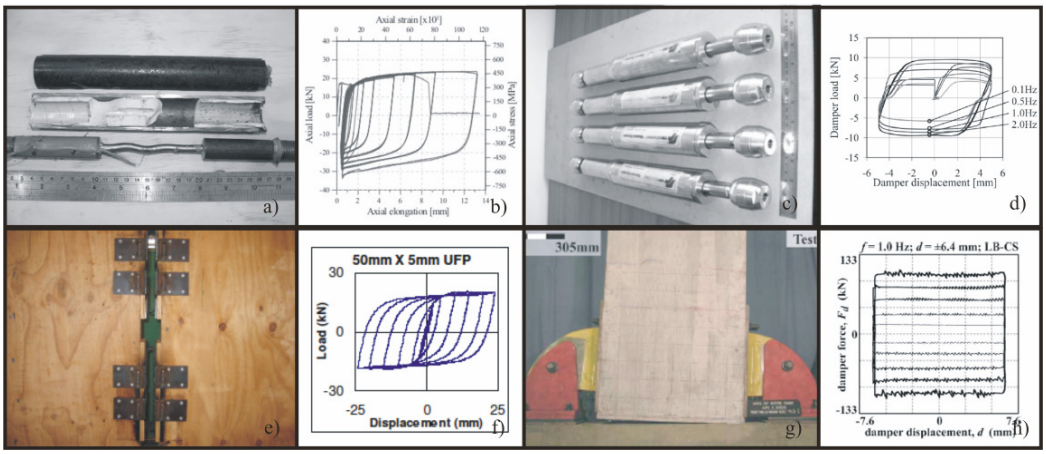

Figure 2.9. Tension compression yield (fuse type) a) dissipation device and b) performance, viscous c) dissipation device and d) performance (Marriott 2009), bending type (U-Shaped Flexural plate, UFP (Kelly et al. 1972)) e) dissipation device and f) performance (Iqbal et al. 2007) and friction type g) dissipation device and f) performance (Morgen and Kurama 2008)

Further consideration is required when considering placement of the dissipation device. As well as the placement in the frame or wall system devices can be either externally accessible or internal to principal structural members. Clear advantages of external systems are their replaceable nature after a seismic event or simply for maintenance purposes. However limitations such as the adequate attachment of the device, fire and restriction of space available may lead to the selection of an internally placed dissipation system.

Due to the almost endless variety of dissipation devices on offer a limited group was selected for study during the duration of this project. This study focussed only on the use of passive devices. With this main subgroup devices in which dissipation is provided hysterically through the tension and compression or flexural yielding of steel were used.

Marriot (2009) and Pampanin et al. (2006a) successfully designed and adopted a 'fused-type' dissipation device in the testing of post-tensioned jointed ductile concrete connections. These devices, which have also been incorporated into design guidelines (NZCS 2010), involve the milling down of a mild steel bar to provide it with a desired length in which plastic deformation is concentrated. This method of deliberate concentration of plastic deformation can be incorporated into either internal or external dissipation devices (Priestley et al. 1999). When attached externally it is suggested that a steel tube be placed around the device and be filled with a sufficiently rigid substance in order to prevent buckling. Amaris (2010) however does note the disadvantage of this protection method when the device is placed in compression with a rapid increase in strength and stiffness being observed as the substance filling the tube is also placed in compression. Fused type dissipative reinforcement has also been referred to as the 'plug & play' devices during application.

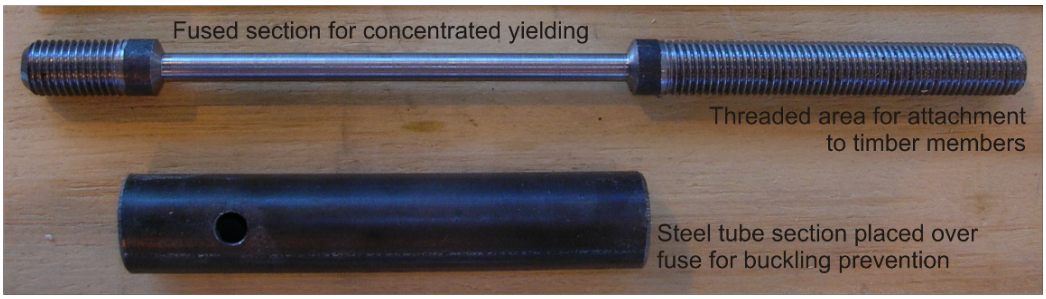

Figure 2.10. Characteristics of the fused type dissipative reinforcing

The fused type dissipative reinforcing uses steel yielded in both tension and compression in order to provide hysteretic damping. Several forms of passive steel device have been proposed which use flexural yielding in order to facilitate energy release. Kelly (1972) proposed the use of a U-shaped Flexural Plate (UFP) which has also been successfully implemented in conjunction with post-tensioned jointed ductile systems, in particular coupled walls, (Priestley et al. 1999) as well as other, more innovative, uses such as base isolation (Cardone et al. 2005). This system (shown in Figure 2.11a) allows for progressive yield as one side of the plate is displaced providing stable loops and large dissipative capacity. Another device using the flexural yield of steel to dissipate energy is the weakened steel angle presented by Ponzo (2011) (shown in Figure 2.11b). As with the fused devices this form of dissipative reinforcing looks to concentrate yielding in a certain controlled area of the

element. This work built upon testing by Kumara and Shen (2004) where steel angles were applied to wall coupling beams providing vertical load resistance and hysteretic capacity. A concentrated yielding area was not provided for during this testing.

Simple design procedure exist for both the fused type dissipation device (NZCS 2010) and also for the UFP (Kelly et al. 1972) which has been elaborated upon by Baird et al. (Baird et al. 2014). Prior to the commencement of the research no design procedure was available in literature for the design of the yielding steel angle. This is therefore one of the objective of this thesis.

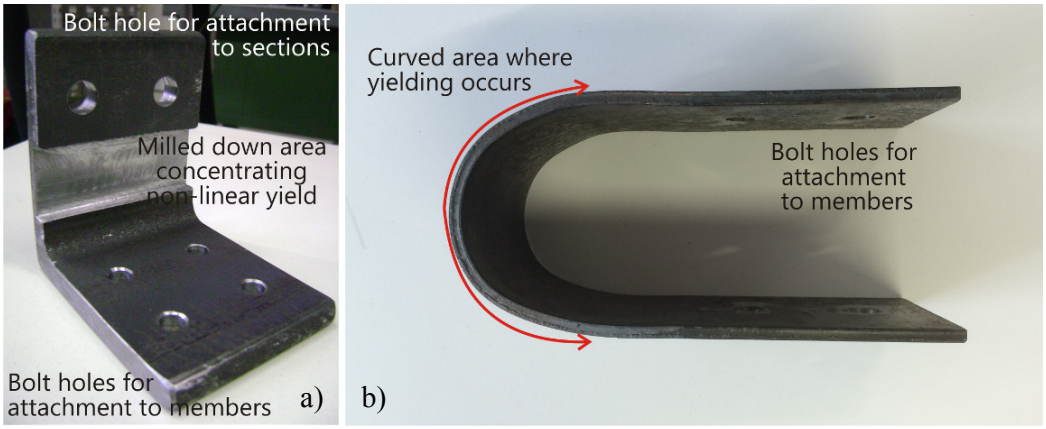

Figure 2.11. Characteristics of a) the yielding steel angle and b) UFP dissipative reinforcing

Above a detailed description of hysteretic steel dissipative reinforcing has been provided. Clearly these devices are not the only method of dissipation available. Friction devices (such as that described by Morgen and Kurama (2004) and shown in Figure 2.9) have the advantage that dissipation is provided as soon as displacement occurs however these devices can have durability issues and require more controlled maintenance. Another innovative solution is the use of super elastic Shape Memory Alloys (SMA). This alloy is essentially a flag-shape in itself which dissipates energy when extended beyond its elastic limit but will return to its original position upon unloading.

The use of displacement proportional dissipation systems are particularly effective under typical far-field excitation however these systems may exhibit lower dissipation characteristics under low-cycle, near field ground motions, this is particularly true for flexible, moderate to long period structures (such as timber). Velocity proportional dampers can be added to mitigate these near fault effects. These dampers can be

added either alone or in parallel with displacement proportional dissipative reinforcing to make up an 'advanced flag shape' system proposed by (Kam et al. 2010) based on analytical-numerical investigations and tested by Marriott et al, (2008) in the form of post-tensioned rocking dissipative concrete and timber walls

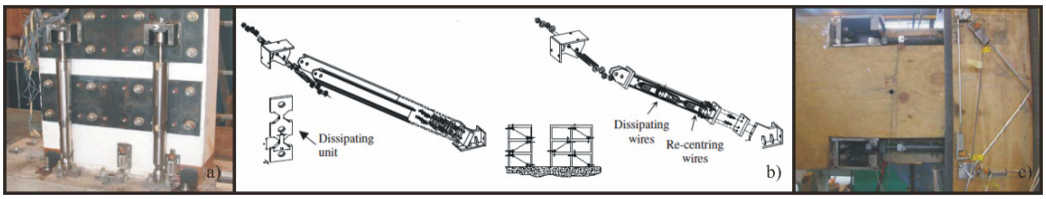

Figure 2.12. Dissipation a) at wall base (Marriott 2009) b) as bracing elements (Cardone et al. 2003) and c) at beam column joint (Iqbal et al. 2010)

2.7 APPLICATION OF DISSIPATIVE REINFORCING TO POST-TENSIONED TIMBER BUILDINGS

In recent years various forms of dissipative reinforcing have been applied to post-tensioned timber structures. All of these devices have aimed to dissipate energy through the hysteretic behaviour of steel. Forms of energy dissipation investigated in conjunction with post-tensioned timber can be split into two main categories: internal and external application. These are discussed separately in this section followed by a discussion of the various forms of dissipation anchorage which have been implemented.

2.7.1 Internal applications of dissipative reinforcing

The first applications of energy dissipation performed during the experimentation into the response of post-tensioned timber under lateral loading were performed by Newcombe et al., (2005). Testing was performed on both a 2/3rd scale beam-column and wall-foundation connection each having two different methods of internal dissipation attachment.

The major difference between the two systems was in the way that the bars were connected to the foundation and in the amount of, and type of, dissipation used (thus altering the recentering ratio discussed previously). In the first test bars were cast into the foundation using a standard hook shaped anchor, these bars did not have a fused length. The second test used TCM couplers and contained a fused length which allowed the bars to be screwed into the foundation after its construction. The results

of testing were positive with both cases achieving high levels of damping. Recentering in the first test was not considered adequate due to a combination of excessive steel contribution and out-of-plane movement. The second test showed much more adequate performance due to correct steel contribution and the addition of shear keys to control out-of-plane movement.

Beam-column testing performed again looked at the effect of including a fused length in design. Both arrangements epoxied bars into both the beam and column. Both systems showed adequate performance with a good balance of PT and steel contribution. Strain gauges placed on the bars displayed that even when a design fuse length is not included little strain penetration is observed. To date, these tests are the only examples of internal dissipation being used in post-tensioned timber testing (Palermo et al., 2006), with the focus of research, development as well as implementation been directed more towards externally placed and replaceable dissipaters. One of the construction applications mentioned in Section 2.2.2 did use internally epoxied bars inside post-tensioned timber walls (Palermo et al. 2012) due to the lack of area available around the walls.

2.7.2 External applications of dissipative reinforcing

External applications of dissipative reinforcing have been the subject of more intensive investigation in relation to their application to post-tensioned timber. Different forms of energy dissipation, although always based on steel yielding, have been applied.

The first investigation into the application of external dissipative reinforcing was that of Loock (2005) and Palermo et al. (2005a) during testing a 2/3rd scale wall-foundation connection was fitted with two forms of fused type dissipative reinforcing. The first external reinforcing used consisted of a fused steel rod epoxied into a timber block. This block was bolted to either the centre or edge of the rocking wall. The second system substituted the timber block with a piece of steel tube which was used for anti-buckling. All tests provided adequate results with the only issues arising from the connection of the device to body of the wall which will be discussed further in Section 2.7.3.

Fuse-type external reinforcing was then applied to a 2/3rd scale beam-column joint by Smith (2006b) providing excellent results in terms of both recentering and energy dissipation. During that year the application of external fused type reinforcing to wall-foundation connections was also revisited (Smith 2006a). This simple form of dissipative reinforcing has also been attached externally to a 2/3rd scale column-foundation connection which was tested in both uniaxially (Pasticier 2006) and biaxially (Iqbal 2011) again with good results.

Finally, two larger scale tests using fused type reinforcing have been performed by Iqbal (2011) on a full scale beam-column joint and Newcombe (2010c) on a 2/3rd scale two storey frame and wall specimen. Both tests did not manage to achieve the dissipative performance seen in previous smaller scale test results. This meant that at design drift levels (2.5%) the system response was nominally elastic and little to no yielding of the dissipative reinforcing was observed.

At the beginning of 2007 a simple form of dissipative reinforcing was attempted in the form of a plywood sheet used to couple a pair of 2/3rd scale post tensioned timber walls (Smith et al. 2007). This form of reinforcing, although simple, exhibited some undesirable characteristics due to the selected method of dissipation. During movement inelastic behaviour was concentrated in the bending and yielding of nails which, following the first cycle, display significant slack and thus loss of initial stiffness.

An alternate form of dissipative reinforcing, applied as part of a couple wall post-tensioned timber system, is that of the U-shaped Flexural Plate (UFP as described above) which was selected as the preferred coupling method during the U.S. PRESSS program (Priestley et al. 1999). UFPs of various sizes were applied and tested by Iqbal (2011) as part of a 2/3rd scale post-tensioned couple timber wall system. Newcombe (2010c) applied UFPs to the frame specimen which described in Section 2.2.1 however although these increase by base moment nominal dissipation was observed.

UFPs have also been applied in construction as part of the Nelson Marlborough Institute of Technology (NMIT) and Trimble building coupled wall lateral resisting system (Devereux et al. 2011)

2.7.3 Attachment of internal and external dissipative reinforcing

As all forms of dissipation currently being applied to post-tensioned timber are dependent on displacement, the attachment the reinforcing used is crucial. Currently internal reinforcement attachment presents one clear option which is the epoxying in of bars allowing a sufficient development length.

The issue with connection details become more prevalent when discussing the attachment of external dissipative reinforcing. As mentioned, one of the main advantages of this class of device is the ability to simply replace it after a seismic event. On the other hand this adds further complication to the connection design. Timber as a material can present issues when a strong, slip free connection is required. The first investigations into external dissipative reinforcing attachment used bolted connections, capable of significant load transfer (Loock 2005; Smith 2006b). The issue with this type of connection was that although large load transfer capabilities were eventually achieved the significant initial slip of the connection lead to delayed yielding and movement during rocking leading to connection damage lead to losses in stiffness. Smith (2006b) looked to solve this issue through the addition of epoxy to the bolted connection. This solution worked well and was adopted in further testing (Iqbal 2011; Pasticier 2006; Smith et al. 2007) however; issues with onsite application and quality control can lead to issues in real world application. Screws have also been utilized for the attachment of both fused type (Smith 2006a) and UFP (Iqbal 2011; Newcombe et al. 2010c) reinforcing however due to the large forces which are required to be transmitted in real world application these solutions may become costly and time consuming for application onsite. An innovative pin solution was also designed and applied for the connection of the fused type devices (Newcombe et al. 2010b) however proved to be overly flexible in application. Further discussion regarding the connection of dissipative reinforcing is presented in Chapter 3.

2.8 CONNECTION DETAILS FOR POST-TENSIONED TIMBER BUILDINGS

As this research project will deal also with the design and testing of a beam-column joint and a three-storey frame specimen required to carry not only lateral loading but

to transfer loading throughout the structure, a study of previously design and tested connections is presented.

2.8.1 Floor to frame/wall load transfer

During seismic loading the forces placed on the lateral resisting system come from masses inside the building, which in most cases are situated on building flooring systems. Therefore, the way in which these floors are able to transmit lateral loading to a frame or wall is crucial in the overall building response.

The connection of the timber diaphragm was first considered in the design of a post-tensioned timber case study building discussed in Section 2.2.3 (Smith 2008). Two methods of transfer were designed: the first (shown in Figure 2.13a) consisted of a type of timber drag bar with the second (Figure 2.13b) being similar to proposed timber concrete composite floor connections, but applied to the beam member. Several simple push out tests were also performed which displayed the load carrying and ductility capacity of the second connection type, however insufficient testing was performed to conclude characteristic strength values.

The diaphragm connection of the floor to frame elements was investigated further (van Beerschoten and Newcombe 2010) in a series of five tests shown in Figure 2.14. These tests involved different combinations of dowel and inclined screws/nails and transferred forces either directly from the topping slab to the beam (termed timber-concrete) or through an additional LVL packing joist (termed timber-timber).

The results of these tests continued to display the feasibility of this method of shear transfer and some useful observations were made: 1) the displacement of the floor is dominated by the connection displacement in almost all cases, thus the floor can be modelled as a single degree of freedom system, 2) the inclination of fasteners increased the initial stiffness of the connection by approximately 4 times and also provided the strongest connection, 3) the inclined timber–concrete screw system (Test 2) showed the highest ductility although failure was in the concrete slab which would lead to costly post-event repair costs, and 4) timber–timber connection failures displayed the lowest post–event repair cost.

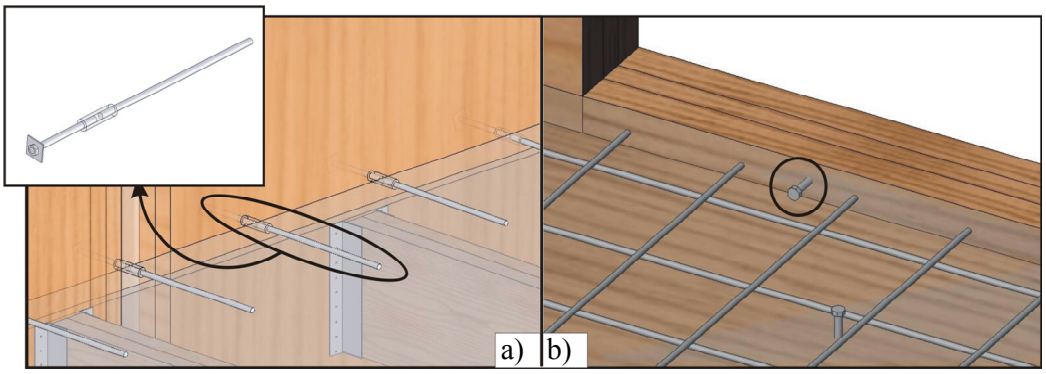

Figure 2.13. a) Wall to floor and b) frame to floor shear connection (Smith 2008)

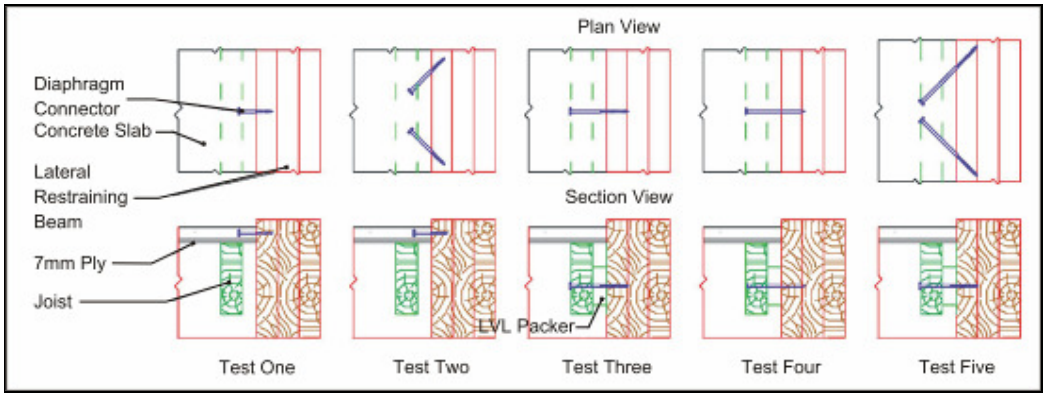

Figure 2.14. Tests performed investigating methods of shear transfer (van Beerschoten and Newcombe 2010)

2.8.2 Wall/column to foundation shear connections

Early in the testing of the post-tensioned timber solution it was realised that although the friction generated by the axial load on the vertical elements (by either gravity or post-tensioning) was sufficient to resist lateral forces, once rocking occurred these elements have a tendency to 'walk' out of plane. In order to address this issue various shear keys have been proposed, being either simple steel angles or half circular steel elements in order to not hinder rocking.

2.8.3 Design for gravity forces

In the design of a structural system the gravity resisting structure can be placed either in parallel with the lateral load resisting system or separated from it. Some vertical load resisting options for post-tensioned timber systems are presented below.

Joist-beam connection

In traditional timber flooring systems joist hangers are often used to transmit gravity loading from floor joists to connecting primary beams. Smith (2008) tested the

performance of large face mounted joist hangers (Figure 2.15a) on a 2/3rd scale beam to column joint in combination with the post-tensioned system. During these single direction quasi-static tests a gap was left of 10cm between the floor joist and the beam in order to ensure the movement of the beam to column connection was unhindered (Figure 2.15b). No significant damage was noted in the floor after testing.

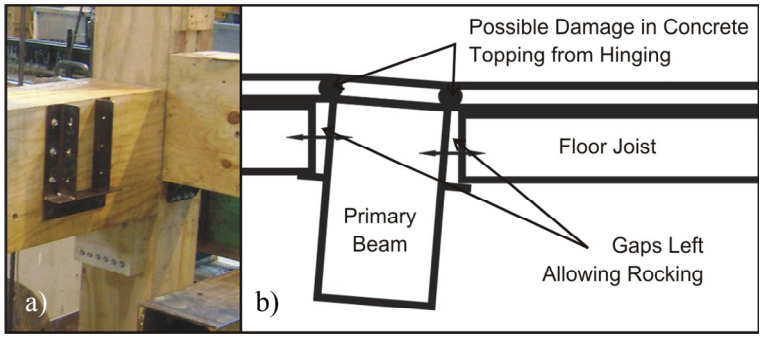

Figure 2.15. a) Joist hanger and b) movement during beam-column rocking (Smith 2008)

The testing of Newcombe et al. (2010b) used a different approach where the joists were top hung from the beam as shown in Figure 2.16a. A small gap was again left in order to ensure rocking was unhindered. During the recent reconstruction of this building (Carradine et al. 2012) the practising engineers involved in the project chose to revert to the use of joist hangers (Shown in Figure 2.16a and b), always maintaining a small gap to ensure unhindered rocking was possible.

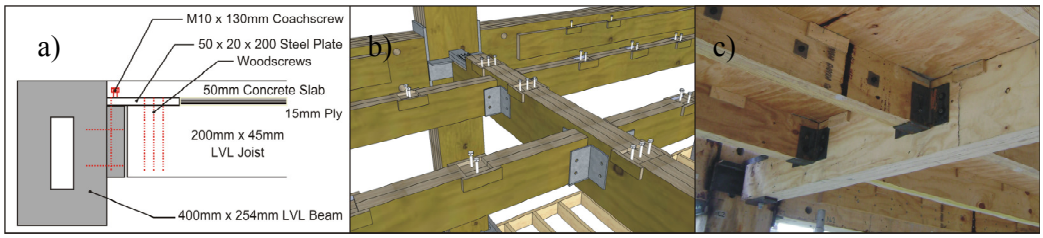

Figure 2.16. a) Top hung joist hanger (Newcombe et al. 2010b) b) and c) face mounted joist hanger

Corbels for Shear Transfer from Primary Beams

Similar principles as those used in the vertical force transfer of floor joists have been applied to vertical force transfer in primary beams (be they gravity only or also seismic resisting) by placing beam members on either timber or steel corbels. Although a post-tensioned connection between a beam and a column often generates adequate friction force to resist gravity loading, current concrete codes for the application of hybrid concrete solutions state that:

"The total vertical shear forces cannot be reliably transferred at the interfaces between precast concrete members by friction induced by post-tensioning. Therefore the design vertical shear force due to factored gravity loads should be transferred by other devices such as corbels or alternative solutions, leaving to the friction contribution induced by the post-tensioning action only the shear components due to seismic loads" (NZS 3101:2006)

Therefore it is recommended that corbels able to resist gravity loading also be applied to post-tensioned timber beam members.

The first study into the use of corbels as part of a beam-column joint was performed by Smith (2008). In this study a small scale post-tensioned timber beam-column joint was subjected to cyclic quasi-static loading using selected corbel options (Figure 2.17a) investigating their effect on the overall system response. A 9 kN concrete weight was applied to the beam to simulate gravity loading (Figure 2.17b). During testing no change was observed on the overall system response with or without the addition of the shear corbel.

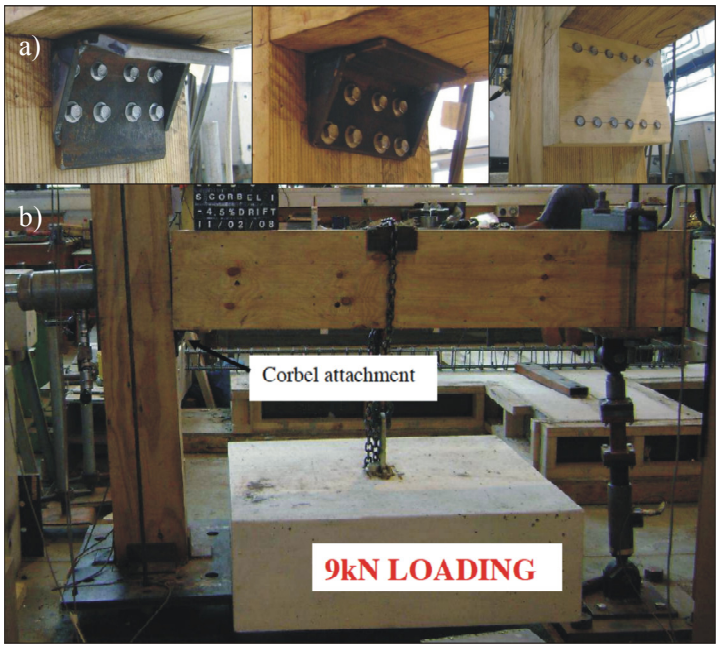

Figure 2.17. a) Corbel types used during tests and b) overall test set-up

During the testing by (Newcombe et al. 2010b), extensive testing (Figure 2.18a) was performed investigating further the use of timber corbels under gravity load (Carradine et al. 2010). During these tests failure was usually through the double

hinging of the screws and the cracking and splitting of the LVL (Figure 2.18b), however ultimate failure of the connection was governed by the attachment of the steel hanger to the beam or joist. During the reconstruction of the building a new steel corbel was designed for the central gravity beam (Figure 2.18c).

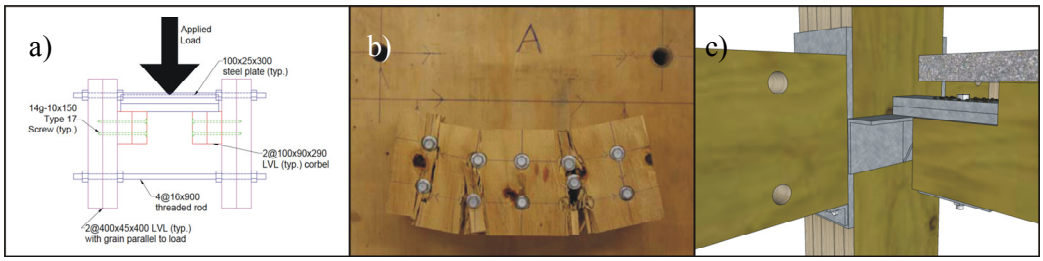

Figure 2.18. a) Timber corbel test set-up and b) response (Carradine et al. 2010) c) application of steel corbel in reconstructed building

2.9 SHAKING TABLE TESTING OF TIMBER BUILDINGS

Unlike other common building materials shaking table testing on timber buildings is very limited.

The largest timber experimental shaking table program to date was that of the NEESWood project which sought to use a series of shaking table tests amongst other investigations in order to safely increase the height of wood framed structures in active seismic zones of the U.S. in addition to mitigating damage to low-rise wood framed structures (van de Lindt et al. 2010). The testing phase of the NEESWood Project began with seismic shaking table testing of a full-scale, two-story, woodframed townhouse building (the "benchmark" test structure) (Filiatrault et al. 2010). Testing of the structure was performed at variously increasing levels of ground motion with observed damage being recorded after each level of excitation. It was seen that under the Maximum Credible Event (MCE) that damage to the sill plate occur with a maximum drift level of 3.5%. A side sway mechanism also began to develop at this drift level which would likely have been the collapse mechanism of the building (Christovasilis et al. 2007).

The results of this testing were then used to design a six storey wood-framed building at the E-Defense shaking table facility in Miki City, Japan. The building displayed maximum drifts of between 2 and 3% and no serious structural damage was observed up to MCE level.

During this project the role of advanced seismic control systems such as additional damping devices and base isolation (Shinde and Symans 2010) was also investigated and discussed. These discussions were based around the aim of reducing damage and downtime and did not focus on collapse prevention which was identified as not being a major issue in properly designed timber frame structures during the early phases of testing.

The above testing focused on what is considered timber panel system of construction. This form of construction relies on structural walls in order to provide both vertical and horizontal load resistance.

Another form of timber panel construction which is beginning to gain widespread adoption in Europe and around the world is the use of cross laminated (cross-lam or x-lam) panels. These solid timber panels, as with the sheathed timber construction described above this system uses timber walls to carry both horizontal and vertical loading.

Progetto Sofie (Ceccotti 2010) began to study the seismic performance of this type of system in 2006 with the testing of a full scale 3 storey structure. Testing then culminated in the full scale shaking of a 7 storey structure at the E-Defense facility (Figure 2.19). In this test, the cross-laminated technology proved adequate in resisting the seismic actions imposed and the ability to offer the flexibility to engineers to re-position hold-down anchors following a major seismic event and even under the maximum possible loading no damage to the timber boards was observed. Test observations have been reported upon by Quenneville and Morris (2007)

Figure 2.19. Seven storey cross laminated timber structure tested by Ceccotti et al. (2010)

Displacements during testing were substantial but still within acceptable limits. One major issue, however, was the 4g acceleration at the top storey of the structure. This acceleration level may endanger lives even if the structure remains undamaged and is due to the rigidity of the system and a lack of damping. Suggestions have been made that due to the nature of the system a prudent method of seismic protection could be the addition of base isolation to the structure.

The two testing series mentioned above focus on the dynamic performance of timber wall systems. The particular application of the post-tensioned timber concept at the centre of this study is in the application to frame systems. Limited dynamic testing has been performed on this type of structure due to the difficulty in providing a timber moment-resisting connection.

One such test however was the testing of Heiduschke at al. (2009) in which a timber moment joint was tested in which the moment connection was provided by a series of pins (Figure 2.20). Two tests were performed one 1/4th scale and one full scale test. Critical damping ratios between 5 and 25% were observed during testing which depended upon the amount of damaged sustained by both the steel pins and the timber members. The 25% damping ratios were however accompanied by severe structural damage, in line with traditional forms of construction.

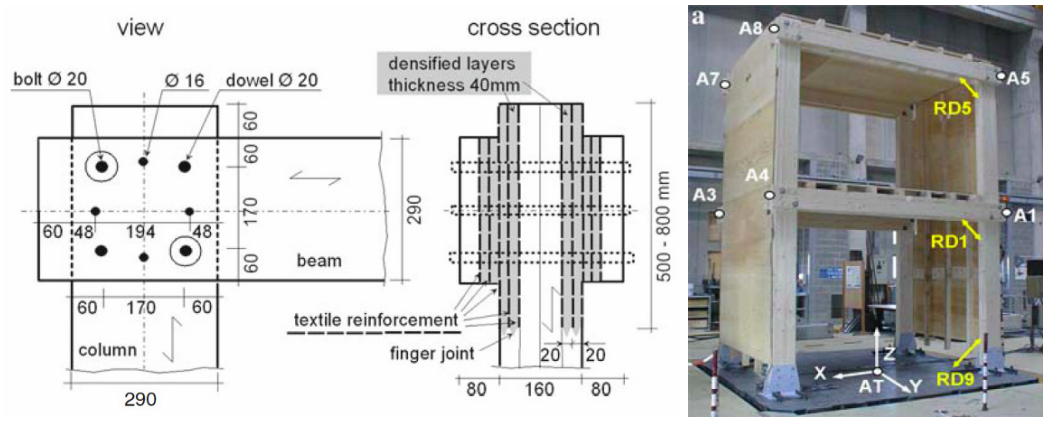

Figure 2.20. Pinned timber frame connection for two storey test frame of Heiduschke (2008)

Pino et al. (2011) has performed the only dynamic testing of the post-tensioned timber system to date. Testing was performed on a 1/4th scale model (Figure 2.21) having either 3 or 5 storeys. As with previous quasi-static testing the system proved the damage free nature of post-tensioned timber frames under seismic loading up to, and beyond, design level earthquakes.

Figure 2.21. Shaking table testing of post-tensioned only test frame (Pino Merino 2011)

As no additional methods of damping were provided the studies focused on the level of elastic damping which can be used with the system. Previous design levels had been conservatively set at 2% however testing showed that up to 5% may be realistic. It was also found that damping values may depend on joint armouring, initial tension value and maximum displacements.

In addition to the seismic testing computer modelling was performed which appeared to underestimate the real seismic response.

REFERENCES CHAPTER 2

Amaris Mesa, A. (2010). "Developments of Advanced Solutions for Seismic Resisting Precast Concrete Frames," University of Canterbury, Christchurch, New Zealand.Doctor of Philosophy in Civil Engineering.

Baird, A., Smith, T., Palermo, A., and Pampanin, S. (2014). "Experimental an Numerical Study of U-Shaped Flexural Plate (UFP) Dissipators for use in Seismic Application." 2014 New Zealand Society for Earthquake Engineering Conference, Auckland, New Zealand.

Buchanan, A. H., and Fairweather, R. H. (1993). "Seismic Design of Glulam Structures." *Bulletin of the New Zealand Society for Eathquake Engineering*, 26(4), 415-436.

Cardone, D., Canio, G. D., Dolce, M., Marnetto, R., Moroni, C., Nicoletti, M., Nigro, D., Pizzari, A., Ponzo, F. C., Renzi, E., Santarsiero, G., and Spina, D. (2003). "Comparison of Different Passive Control Techniques Through Shaking Table Tests." 8th World Seminar on Seismic Isolation, Energy Dissipation and Active Vibration Control of Structures, Yerevan, Armenia, 10.

Cardone, D., Di Cesare, A., Dolce, M., Moroni, C., Nigro, D., Ponzo, F. C., and Nicoletti, M. (2005). "Dynamic Tests on a 1 4 Scaled R/C Existing Building Comparison of Several Isolation Systems." 9th World Seminar on Seismic Isolation, Energy Dissipation and Active Vibration Control of Structures, Kobe, Japan, 8.

Carradine, D., Newcombe, M., and Buchanan, A. H. (2010). "Screwed Corbel Connections in Laminated Veneer Lumber." 11th World Conference on Timber Engineering, Riva del Garda, Trentino, Italy, 8.

Carradine, D., Smith, T., Carter, B., Pampanin, S., Palermo, A., Ponzo, F. C., and Buchanan, A. (2012). "Study of a High Performance Timber Building: Design, Construction and Performance." 12th World Conference on Timber Engineering, Auckland, New Zealand.

Ceccotti, A. (2010). "Il progetto SOFIE sugli edifici di lengo con tecnologia X-LAM: riflessioni a margine delle prove sismiche su tavola vibrante." *Modulo*(360), 278.

Christopoulos, C., Filiatrault, A., Uang, C.-M., and Folz, B. (2002). "Posttensioned Energy Dissipating Connections for Moment-Resisting Steel Frames." *ASCE Journal of Structural Engineering*, 129(9), 1111-1120.

Christopoulos, C., and Pampanin, S. (2004). "Towards performance-based seismic design of MDOF structures with explicit consideration of residual deformation." *ISET Journal of Earthquake Technology*, 41(1), 53-73.

Christovasilis, I. P., Filiatrault, A., and Wanitkorkul, A. (2007). "Seismic Testing of a Full-Scale Two-Story Light-Frame Wood Building : NEESWood Benchmark Test." University of Buffalo, Buffalo.

Cusiel, M. R., Newcombe, M. P., Pampanin, S., Buchanan, A. H., and Palermo, A. (2010). "The Effect of Joint Flexibility on the Seismic Response of Post-tensioned LVL Frames." 14th European Conference on Earthquake Engineering, Ohrid, Republic of Macedonia.

Devereux, C. P., Holden, T. J., Buchanan, A. H., and Pampanin, S. (2011). "NMIT Arts & Media Building - Damage Mitigation Using Poat-Tensioned Timber Walls." 9th Pacific Conference on Earthquake Engineering, Auckland, New Zealand.

Bulletin 27. (2004). "Seismic Design of Precast Concrete Building Structures." fib. International Federation for Structural Concrete

Filiatrault, A., Christovasilis, I. P., Wanitkorkul, A., and van de Lindt, J. W. (2010). "Experimental Seismic Responce of a Full-Scale Light-Frame Wood Building." *Journal of Structural Engineering*, 136(3), 246-254.

Heiduschke, A., Kasel, B., and Haller, P. (2009). "Shake Table Tests of Small- and Full-scale Laminated Timber Frames with Moment Connections." *Bulletin of Earthquake Engineering*, 7, 323-339.

Iqbal, A. (2011). "Seismic Response and Design of Subassemblies for Multi-Storey Prestressed Timber Buildings," University of Canterbury, Christchurch, New Zealand.Doctor of Philosophy in Civil Engineering.

Iqbal, A., Pampanin, S., Buchanan, A., and Palermo, A. (2007). "Improved Seismic Performance of LVL Post-tensioned Walls Coupled with UFP devices." 8th Pacific Conference on Earthquake Engineering, Singapore.

Iqbal, A., Pampanin, S., and Buchanan, A. H. (2010). "Seismic Performance of Prestressed Timber Beam-Column Sub-Assemblies." 2010 New Zealand Society for Earthquake Engineering Conference, Wellington, New Zealand.

John, S., Mulligan, K., Perez, N., Love, S., and Page, I. (2011). "Cost Time and Environmental Impacts of the Construction of the New NMIT Arts and Media Building " *01*, University of Canterbry, Cristchurch.

Kam, W. Y., Pampanin, S., Palermo, A., and Carr, A. J. (2010). "Self-centering Structural Systems with Combination of Hysteretic and Viscous Energy Dissipations." *Earthquake Engineering and Structural Dynamics*, 26.

Kelly, J. M., Skinner, R. I., and Heine, A. J. (1972). "Mechanisms of Energy Absorbtion in Special Devices for use in Earthquake Resistant Structures." *Bulletin of the New Zealand Society for Eathquake Engineering*, 5(3), 63-88.

Kurama, Y. C., and Shen, Q. (2004). "Post-tensioned Hybrid Coupled Wall under Lateral Loads." *Journal of Structural Engineering*, 130(2), 297-309.

Kurama, Y. C., Weldon, B. D., and Shen, Q. (2006). "Experimental Evaluation of Posttensioned Hybrid Coupled Wall Subassemblages." *Journal of Structural Engineering*, 132(7), 13.

Liong, S. (2009). "Supply Chain Analysis for Post Tensioned LVL Buildings in New Zealand," University of Canterbury, Cristchurch, New Zealand.Masters of Engineering Management.

Loock, P. (2005). "LVL Wall with Varied External Dissipation Options." University of Canterbury, Christchurch, New Zealand.

Marriott, D. (2009). "The Development of High-Performance Post-Tensioned Rocking Systems for the Seismic Design of Structures," University of Canterbury, Christchurch, New Zealand.Doctor of Philosophy in Civil Engineering.

Marriott, D., Pampanin, S., Bull, D., and Palermo, A. (2008). "Dynamic Testing of Precast, Post-tensioned Rocking Wall Systems with Alternative Dissipating Solutions." *Bulletin of the New Zealand Society for Eathquake Engineering*, 41(2), 14.

Menendez Amigo, J. (2010). "Feasibility of Multi-Storey Pres-Lam Timber Buildings: Design, Construction and Cost," Edinburgh Napier University, Edinburgh, Scotland.Master of Science in Timber Engineering.

Morgen, B. G., and Kurama, Y. C. (2004). "A Friction Damper for Post-Tensioned Precast Concrete Beam-to-Column Joints." 13th World Conference on Earthquake Enigineering, Vancouver, Canada

Morgen, B. G., and Kurama, Y. C. (2008). "Seismic Response Evaluation of Posttensioned Precast Concrete Frames with Friction Dampers." *Journal of Structural Engineering*, 134(1), 14.

Neale, A. (2009). "Long Term Performance of Post-Tensioned Timber Buildings," University of Canterbury, Christchurch, New Zealand.3rd Professional Year Project.

Newcombe, M. (2007). "Seismic Design of Multistorey Post-Tensioned Timber Buildings," Università degli Studi di Pavia, Pavia, Italy.Master Degree in Earthquake Engineering.

Newcombe, M., Cusiel, M., Pampanin, S., Palermo, A., and Buchanan, A. H. (2010a). "Simplified Design of Post-tensioned Timber Frames." CIB W18 Workshop on Timber Structures, Nelson, New Zealand.

Newcombe, M. P., Pampanin, S., and Buchanan, A. H. (2010b). "Design, Fabrication and Assembly of a Two-Storey Post-Tensioned Timber Building." 11th World Conference on Timber Engineering, Riva del Garda, Trentino, Italy, 9.

Newcombe, M. P., Pampanin, S., and Buchanan, A. H. (2010c). "Global Response of a Two Storey Pres-Lam Timber Building." 2010 New Zealand Society for Earthquake Engineering Conference, Wellington, New Zealand, 8.

NZCS. (2010). *PRESSS Design Handbook*, New Zealand Concrete Society, Wellington New Zealand.

Palermo, A. (2004). "Use of Controlled Rocking in the Seismic Design of Bridges," Doctate Thesis, Technical Institute of Milan, Milan

Palermo, A., Pampanin, S., and Buchanan, A. (2006a). "Experimental Investigations on LVL Seismic Resistant Wall and Frame Subassemblies." First European Conference on Earthquake Engineering and Seismology, Geneva, Switzerland, 10.

Palermo, A., Pampanin, S., Buchanan, A., and Newcombe, M. (2005a). "Seismic Design of Multi-Storey Buildings using Laminated Veneer Lumber (LVL)." 2005 New Zealand Society for Earthquake Engineering Conference, Wairakei Resort, Taupo, New Zealand.

Palermo, A., Pampanin, S., and Carr, A. (2005b). "Efficiency of Simplified Alternative Modelling Approaches to Predict the Seismic Responce of Precast Concrete Hybrid Systems." fib symposium "Keep Concrete Attractive, Budapest, Hungary.

Palermo, A., Pampanin, S., Fragiacomo, M., Buchanan, A. H., and Deam, B. L. (2006b). "Innovative Seismic Solutions for Multi-Storey LVL Timber Buildings." 9th World Conference on Timber Engineering, Portland, U.S.A.

Palermo, A., Sarti, F., Baird, A., Bonardi, D., Dekker, D., and Chung, S. (2012). "From Theory to Practice: Design, Analysis and Construction of Dissipative Timber Rocking Post-Tensioning Wall System for Carterton Events Centre, New Zealand." 15th World Conference on Earthquake Engineering, Lisbon, Portugal.

Pampanin, S. (2005). "Emerging Solutions for High Seismic Performance of Precase/Prestressed Concrete Buildings." *Journal of Advanced Concrete Technology*, 3(2), 207-223.

Pampanin, S., Pagani, C., and Zambelli, S. (2004). "Cable-stayed and suspended post-tensioned solutions for precast concrete frames: the Brooklyn system." New Zealand Concrete Society Conference, Queenstown, New Zealand.

Pampanin, S., Palermo, A., and Amaris, A. (2006a). "Implementation and Testing of Advanced Solutions for Jointed Ductile Seismic Resisting Frames." 2nd International fib Congress, Naples, Italy.

Pampanin, S., Palermo, A., Buchanan, A., Fragiacomo, M., and Deam, B. "Code Provisions for Seismic Design of Multi-Storey Post-Tensioned Timber Buildings." *CIB W18/39*, Florence, Italy.

Pampanin, S., Priestley, M. J. N., and Sritharan, S. (2000). "Passive energy dissipation and self-centering capabilities in precast ductile connections." Second European Conference on Structural Control, Champs-sur-Marne, France.

Pampanin, S., Priestley, N., and Sritharan, S. (2001). "Analytical Modelling of the Seismic Behaviour of Precast Concrete Frames Designed with Ductile Connections." *Journal of Earthquake Engineering*, 5(3), 329-367.

Pasticier, L. (2006). "Experimental and numerical validation of innovative connections for LVL (laminated veneer lumber) frame systems." University of Canterbury, Chrsitchurch, New Zealand.

Pino Merino, D. (2011). "Dynamic Response of Post-Tensioned Timber Framed Buildings," University of Canterbury, Christchurch, New Zealand.Master of Engineering.

Ponzo, F., Di Cesare, A., Nigro, D., and Smith, T. (2011). "Dissipative Steel Angles Devices for the Increased Seismic Performance of Low Level Damping Systems." XXIII Congresso CTA, Lacco Ameno, Ischia, Italy.

Priestley, M. J. N. (1991). "Overview of PRESSS Research Program." *PCI Journal*, 36(4), 50 - 57.

Priestley, M. J. N. (1996). "The PRESSS program – Current status and proposed plans for phase III." *PCI Journal*, 42(2), 22-40.

Priestley, N., Sritharan, S., Conley, J., and Pampanin, S. (1999). "Preliminary Results and Conclusions From the PRESSS Five-Story Precast Concrete Test Building." *PCI Journal*(November-December 1999), 42-67.

Quenneville, P., and Morris, H. (2007). "Japan Kobe Earthquake Shake Table Simulation." *New Zealand Timber Design Journal*, 15(4), 3-8.

Shinde, J. K., and Symans, M. D. (2010). "Integration of Seismic Protection Systems in Performance-Based Seismis Design of Woodframed Structures." Rensselaer Polytecnic Institute.

Smith, T. (2006a). "LVL Rocking Shear Walls: with External Dissipater Attachment," University of Canterbury, Christchurch, New Zealand.3rd Professional Year Project.

Smith, T. (2006b). "Work performed during summer research scholarship on LVL beam column joint." University of Canterbury, Chrsitchurch, New Zealand.

Smith, T. (2008). "Feasibility of Multi Storey Post-tensioned Timber Buildings," University of Canterbury, Christchurch, New Zealand.Master of Engineering.

Smith, T., Fragiacomo, M., Pampanin, S., and Buchanan, A. H. (2009). "Construction Time and Cost for Post-Tensioned Timber Buildings." *Proceedings of the Institution of Civil Engineers*, Construction Materials(CM4), 9.

Smith, T., Ludwig, F., Pampanin, S., Fragiacomo, M., Buchanan, A., Deam, B., and Palermo, A. (2007). "Seismic Response of Hybrid-LVL Coupled Walls Under Quasi-Static and Pseudo-Dynamic Testing." 2007 New Zealand Society for Earthquake Engineering Conference, Palmerston North, New Zealand, 8.

EN408:2003. (2003). "Timber Structures - Structural Timber and Glued Laminated Timber - Determination of some Physical and Mechnical Properties." European Committee for Standardization.

Stanton, J., Stone, W. C., and Cheok, G. S. (1997). "A Hybrid Reinforced Precast Frame for Seismic Regions." *PCI Journal*, 42(2), 20-32.

Structural Timber Innovation Company Inc. (2013). "Post-Tensioned Timber Buildings - Design Guide." Structural Timber Innovation Company, Christchurch, New Zealand.

van Beerschoten, W., and Newcombe, M. (2010). "The Effects of Diaphragm Flexibility on the Response of Post-Tensioned Timber Buildings," University of Canterbury, Christchurch, New Zealand

van de Lindt, J. W., Rosowsky, D. V., Filiatrault, A., Symans, M. D., and Davidson, R. A. (2010). *The NEESWood Project in Review*.

NZS 3602:1993. (1993). "Timber Structures." Standards New Zealand.

NZS 3101:1995. (2006). "Concrete Structures Part 1. The Design of Concrete Structures." Standards New Zealand.

3 Passive Dissipative Reinforcing Devices for Use in Post-tensioned Timber Frames

3.1 PRINCIPAL CONCLUSIONS OF CHAPTER 3

Chapter 3 discusses two forms of passive dissipative reinforcing which are used in post-tensioned timber frame structures. The forms of dissipative reinforcing studied are: the tension-compression yielding fuse type device and an angle device (divided into two categories) which yields in bending. The following principal conclusions are drawn:

Fused type dissipative reinforcing

1. Testing present in literature (Sarti et al. 2013) was used to study the performance of the device which was shown to be stable even at very high strain levels.
2. The tension-compression yielding fuse-type dissipative reinforcing device requires a corrective factor, k_a, in order to accurately predict the yield displacement. This is due to strains (and hence displacements) outside of the fused area impacting significantly on yield displacement.

Angle type dissipative reinforcing

1. The angle device has been proved through an experimental test campaign which built upon concepts described by Kurama and Shen. (2004) and Dolce et al. (2006) (Section 2.6) providing dependable strength and large stable hysteretic loops.
2. Care must be taken to ensure that the ratio between the original angle and the reduced down yielding area is sufficient in order to avoid yielding outside the fused zone. Yielding outside this zone creates significantly pinched hysteretic behaviour which is undesirable.
3. Design charts have been provided for the angle devices based on finite element modelling.

The connection of both (angle and fused reinforcing) devices is a crucial point in post-tensioned timber design and formulas to calculate the stiffness of common connections have been provided.

3.2 INTRODUCTION

As described in Chapter 2 a wide variety of devices are available for the additional damping of structures. In this chapter a selection of these are tested, numerically modelled and discussed. All of these systems are based on the yielding of steel either in tension and compression or in bending.

All of the devices discussed are attached externally to the structure meaning that following a major seismic event if significant damage occurs to the device they can be simply replaced. The attachment of the devices is also crucial in design and will be discussed.

A principal focus of this chapter will be on the prediction of the devices force-displacement characteristics and the design of the devices for the application to post-tensioned timber frames.

This chapter incorporates the results of two experimental studies on the performance of dissipative reinforcing devices. The experimental campaigns are not presented here in their entirety and more details can be found in Sarti et al. (2013), for the fuse type dissipative reinforcing and Di Cesare (2013) for the milled and holed dissipative angles.

3.3 THE FUSE TYPE DISSIPATIVE REINFORCING DEVICE

The first method of dissipative reinforcing which will be analysed and discussed is the fused tension-compression yield (TCY) dissipation method, often referred to as the 'plug and play' dissipation device. This device behaves in a similar manner to traditional concrete reinforcing bars during cyclic motion in that it yields cyclically in tension and compression. The major difference however is that the displacement and area within the bars in which yielding occurs is controlled by the milling down of a certain fuse length (L_{fuse}) to a desired design diameter (d_{fuse}). The bar is covered by an anti-buckling tube (shown in Figure 3.2) which is filled with either grout or epoxy to provide stable hysteretic loops even at very high (up to 5%) strain levels. These

dissipative devices have already been applied to both concrete and timber post-tensioned structures both experimentally and in practice (Figure 3.1a and b) (Cattanach and Pampanin 2008; Sarti et al. 2013). Although testing has been performed on single devices in order to characterise their performance as part of a global post-tensioned concrete or timber system (Amaris Amaris Mesa 2010; Iqbal 2011; Marriott 2009), a comprehensive experimental-numerical campaign was needed to finalize the characterization of the behaviour of the devices themselves. This was performed by Sarti et al. (2013) and led to the refinement of current design procedures which is presented in this Chapter. This design procedure has also been publish in the Post-tensioned Timber Buildings Design Guide (Pampanin et al. 2013)

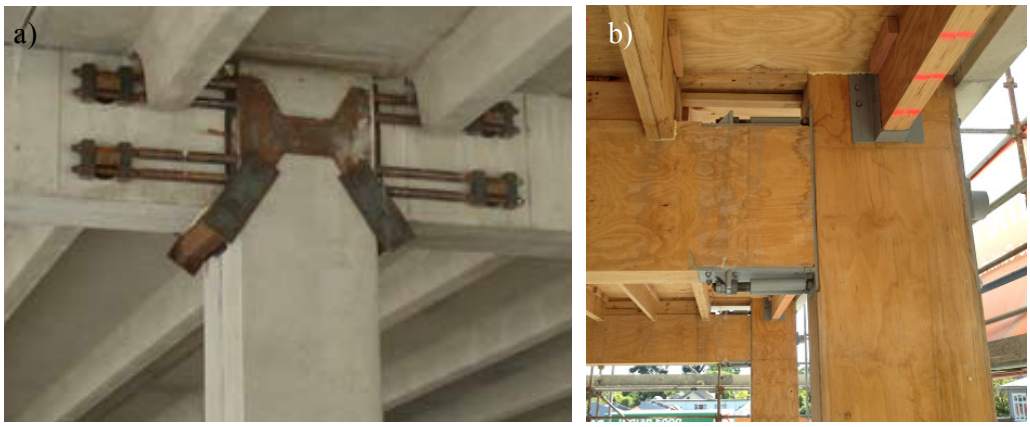

Figure 3.1. Applications of fuse-type dissipative reinforcing devices: a) Learning and Research building, Victoria University, Wellington, New Zealand (Cattanach and Pampanin 2008) and b) Merritt Building (right), Christchurch, New Zealand (Sarti et al. 2013)

The design of the devices centres on the definition of a defined fuse length shown in Figure 3.2. During positive and negative displacements inelastic behaviour will concentrate in this area, and this enables a designer to have control over the force displacement characteristics of the device. The section of tube shown in Figure 3.2 is placed over the yielding fused length of the device and filled (either with epoxy or grout). This prevents excessive bucking of the fused section during displacement.

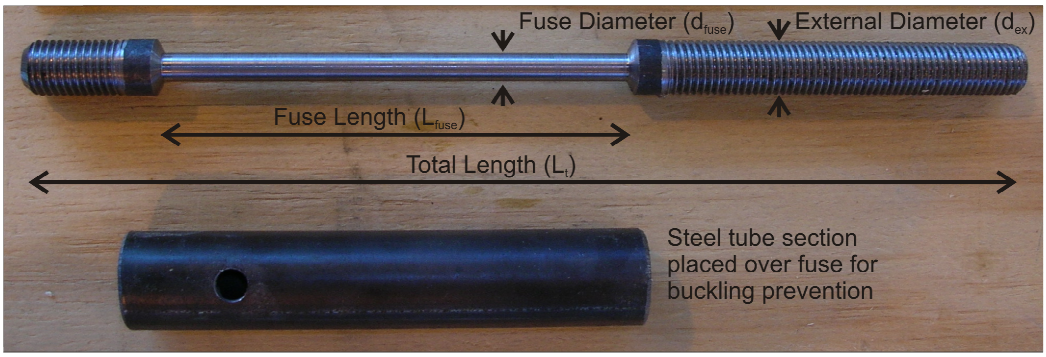

Figure 3.2. Fuse type dissipative reinforcing characteristics

Although extensively tested and already adopted in practice some questions still surrounded the correct design of this form of dissipative reinforcing, in particular relating to the yield displacement, which can be crucial in post-tensioned timber design.

3.3.1 Fuse type dissipative reinforcing testing

A series of tests have been performed by Sarti et al. (2013) investigating the performance of the fuse type dissipative reinforcing under cyclic loading. During this test campaign a total of 17 different specimens were tested on 6 different dissipative reinforcing geometries (Table 3.1). The specimens were loaded in a single direction (initially tension) corresponding with their expected performance when placed at the interface between beam-column, column-foundation or wall-foundation connections.

Table 3.1. Physical characteristics of fuse type dissipative reinforcing tested

Fuse type ID	d_{fuse} mm	d_{ex} mm	L_{fuse} mm	L_t mm
D12L180	12	13.0	180	290
D20L300	20	19.5	300	420
D24L360	24	24.7	360	525
D26L390	26	24.7	390	545
D26L488	26	24.7	488	635
D26L585	26	24.7	585	740

Two force displacement responses for the smallest (D12L180) and largest (D20L300) devices tested are presented in Figure 3.3.

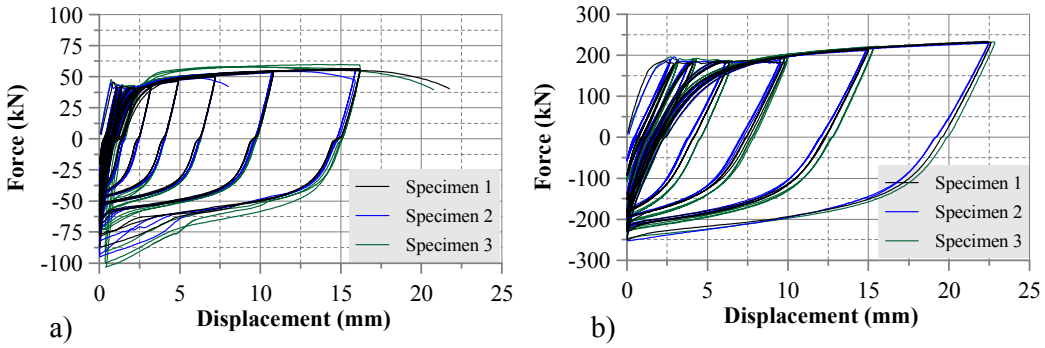

Figure 3.3. Force-displacement response of 3 forms of dissipative reinforcing with a) fuse diameter d_{fuse} = 12 mm and a fuse length L_{fuse} = 180 mm and b) fuse diameter d_{fuse} = 26 mm and fuse length L_{fuse} = 585 mm

The parameters of interest for the design of a post-tensioned timber connection are the yield force (F_y) yield displacement (Δ_y) and the post-yield stiffness (α). Knowing the yield force and displacement the initial stiffness (K) can also be calculated. These factors are important in post-tensioned timber design as they will control the strength of the connection and its dissipative capacity. These values are shown in Table 3.2 averaged across the three repetitions of each dissipative reinforcing configuration.

Table 3.2. Performance characteristics of fuse type dissipative reinforcing tested

Fuse type ID	F_y kN	Δ_y mm	K kN/mm	α kN/mm
D12L180	42	0.6	70	0.9
D20L300	96	0.9	107	1.5
D24L360	155	1.2	129	3.1
D26L390	180	1.3	138	3.8
D26L488	180	1.4	129	3.4
D26L585	180	1.5	120	2.8

3.3.2 Force-displacement back-bone prediction

Current design procedures for the non-prestressed dissipative reinforcement of post-tensioned frames were developed considering a device with a minimal non-fused section and calculate strain (ε_s) by dividing the total dissipative reinforcing elongation (Δ_s) by the fuse length (L_{fuse}, considering the effects of the non-fused length to be negligible):

$$\varepsilon_s = \frac{\Delta_s}{L_{fuse}} \tag{3.1}$$

Once the strain is calculated a stress-strain assumption is made in order to calculate stress and therefore the force in the dissipative reinforcing devices. The choice of this

stress-strain relationship depends on the accuracy required in design and can range from a simple elasto-perfectly plastic assumption to stress-strain relationships derived from characterisation testing or numerical modelling of the devices to be used. The yield force (F_y) is calculated using the characteristic yield stress of the steel (f_y) and the area of the fuse (A_{fuse}):

$$F_y = f_y A_{fuse} \tag{3.2}$$

As post-tensioned frame structures have been adopted in practice, architectural choice, as well as the necessary development of feasible methods of reinforcement attachment has led to the development of fused type devices which have a non-fused length which is no longer negligible.

Figure 3.4a compares the yield force F_y from Equation (3.2) with the yield force measured during testing (Sarti et al. 2013) presented in Table 3.2. The graph shown in Figure 3.4b compares the yield displacements calculated from Equation (3.1), imposing a strain at yield ε_y = 0.0015 and the values measured during testing presented in Table 3.2. In order to help illustrate the adequacy of the equation a 1:1 ratio line has also been drawn on the graph.

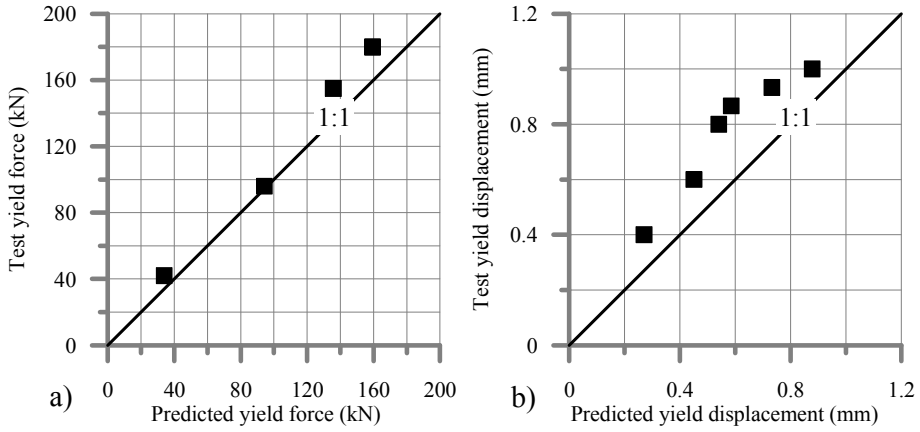

Figure 3.4. Comparison of a) predicted and yield force (F_y) from the cyclic testing of Sarti et al. (2013) b) predicted and test yield displacement (Δ_y) from cyclic testing

The procedure gave adequate prediction of the yielding force of this form of dissipative reinforcing with a slight underestimation due to the use of a characteristic value and not a mean value of yield strength. Figure 3.4b shows however that Equation (3.1) under-estimated significantly the yield displacement. The reason for this error is the assumption that before yield all displacement to which the full device

length is subjected is concentrated in the turned down fused area. This is not the case however with the length of bar outside the fused area also being subjected to stress and therefore strain and displacement.

In order to address this error the way in which the yield displacement is calculated must be rethought and the strain developed outside the fuse area accounted for. The yield displacement (Δ_y), considering yield to be isolated in the fused area ($F_y = f_y A_{fuse}$) can be represented as a series of elongations resulting from the same force F_y:

$$\Delta_y = \frac{f_y A_{fuse} L_{ex1}}{E A_{ex1}} + \frac{f_y A_{fuse} L_{fuse}}{E A_{fuse}} + \frac{f_y A_{fuse} L_{ex2}}{E A_{ex2}} \quad \textbf{(3.3)}$$

Where:

$A_{ex1,2}$ = Area of the device outside of the turned down fused section

A_{fuse} = Area of the turned down fused section

$L_{ex1,2}$ = Length of the device outside the of the turned down fused section

L_{fuse} = Length of the turned down fused section

f_y = Yield stress of steel

E = Young‘s modulus of steel

In most cases $A_{ex1} = A_{ex2}$ therefore a single A_{ex} value can be used:

$$\Delta_y = \frac{f_y A_{fuse} (L_{ex1} + L_{ex2})}{E A_{ex}} + \frac{f_y L_{fuse}}{E} \quad \textbf{(3.4)}$$

The external length can be defined in terms of the total length of the device.

$$L_{ex1} + L_{ex2} = L_t - L_{fuse} \quad \textbf{(3.5)}$$

The total length of the dissipative reinforcing device is defined as the distance between the two points where the device is connected to the structure, not the length of the device itself. Inserting Equation (3.5) and putting the equation in terms of the fuse diameter (d_{fuse}) and external diameter (d_{ex}):

$$\Delta_y = \frac{f_y L_{fuse}}{E} \left(\left(\frac{d_{fuse}}{d_{ex}} \right)^2 \frac{L_t - L_{fuse}}{L_{fuse}} + 1 \right) \quad \textbf{(3.6)}$$

This means that at yield a factor k_a can be defined in order to account for the additional displacement due to strain in the areas between the anchorage of the device and the fused area:

$$\Delta_y = \frac{k_a f_y L_{fuse}}{E} \tag{3.7}$$

$$k_a = \left(\frac{d_{fuse}}{d_{ex}}\right)^2 \frac{L_t - L_{fuse}}{L_{fuse}} + 1 \tag{3.8}$$

Table 3.1 showed the physical characteristics of the fuse type devices used to recalculate the yield displacement which is shown in Figure 3.5. Note that the external diameter of the dissipative reinforcing device (d_{ex}) was smaller in some cases than the fuse diameter (d_{fuse}). This is due to the fact that when calculating the external diameter the net diameter (i.e. the total diameter minus the thread depth) must be used if the non-fused bar length is predominantly threaded.

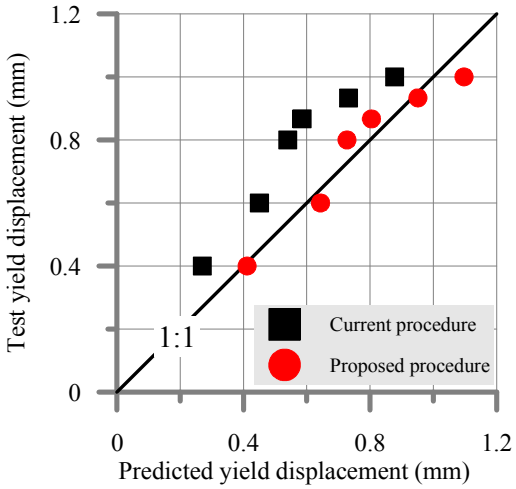

Figure 3.5. Predicted and test yield displacement (Sarti et al. 2013), Δ_y, using current and proposed procedure

As seen the proposed procedure provided an improved prediction of the yield displacement.

During the design of a post-tensioned beam-column connection, which will be further described in Chapter 5, the designer requires the fuse to have a certain strain (ε_s) when subjected to a given displacement (Δ_s). During the design the amount of force required (T_s) is also known. Therefore assuming yield has occurred in the fuse and

strain is constant across the fuse the total displacement is made up of a plastic component within the fuse and an elastic component in the external area:

$$\Delta_s = \varepsilon_s L_{fuse} + \frac{T_s\left(L_t - L_{fuse}\right)}{EA_{ex}} \quad \textbf{(3.9)}$$

Rearranging (3.9) and solving for the fuse length gives:

$$L_{fuse} = \frac{\Delta_s - \varepsilon_{ex} L_t}{\varepsilon_s - \varepsilon_{ex}} \quad \textbf{(3.10)}$$

$$\varepsilon_{ex} = \frac{T_s}{EA_{ex}} \quad \textbf{(3.11)}$$

3.3.3 Fuse type dissipative reinforcing design recommendations

Based on experimental testing (Sarti et al. 2013) and observed behaviour the following recommendations are made for the design of fuse type dissipative reinforcing:

- The fuse diameter should be no less than 75% of the external diameter. This is in order to avoid yielding outside of the fused area due to strain hardening:

$$d_{fuse} \leq 0.75 d_{ex} \quad \textbf{(3.12)}$$

- The total length of the anti-buckling tube shall be sufficient to ensure that the fuse length remains covered during maximum elongation. A simple approach is to assume a maximum strain inside of the fused area of 6% which leads to a minimum tube length of $1.12L_{fuse}$ (both positive and negative displacements are allowed for):

$$L_{tube} \geq 1.12 L_{fuse} \quad \textbf{(3.13)}$$

- The threaded portion of the device shall be considered as part of the total device length, L_t, and its net area shall be greater than or equal to the area of the unthreaded section. If this is not the case (i.e. where the device is fabricated from a threaded rod) the external area is to be taken as the net area of the thread.

- For manufacturing purposes enough clearance between the external diameter of the dissipative reinforcing bar and the restraining tube shall be provided. This will assist the fabrication of the dissipative reinforcing. Values of between 4 and 10 mm larger than the external diameter (d_{ex}) are suggested.

- The external part of the dissipative reinforcing device is not buckling restrained; therefore, buckling of this external length should be given due consideration.

3.4 THE DOG BONE DISSIPATIVE REINFORCING DEVICE

The dog bone dissipative reinforcing devices stemmed from the testing of the fuse type device; however it is derived from a flat plate and not a round bar. This renders the device simpler to attach by providing a workable flat surface as shown in Figure 3.6.

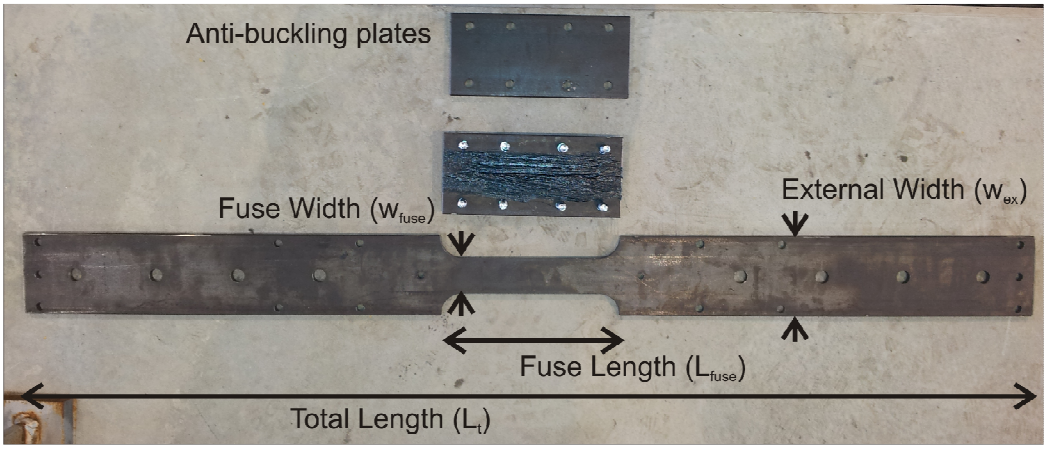

Figure 3.6. Dog-bone dissipative reinforcing device design characteristics

As with the fuse type dissipative reinforcing device elastic deformations outside of the fuse area must be considered. Equation (3.10) should be used in the calculation of the fuse length (L_{fuse}). Further study is required in order to fully understand the behaviour of this form of device specifically regarding anti-buckling measures (shown in Figure 3.6), this however falls outside the scope of this research and has been presented by Armstrong et al. (2014).

3.5 THE ANGLE DISSIPATIVE REINFORCING DEVICE

The yielding angle dissipative reinforcing system is based on the DIS-CAM system developed at the University of Basilicata in Potenza, Italy which has already been

successfully used in the retrofit of reinforced concrete and masonry structures. The dissipation device (Dolce et al. 2006) consisted of a steel angle, weakened as shown in Figure 3.7 by drilling holes and milling down thus removing a significant amount of the angles cross section.

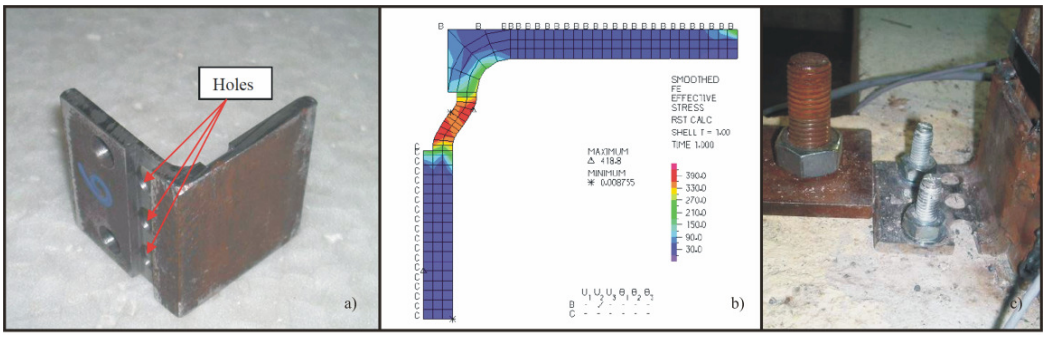

Figure 3.7. a) DIS-CAM weakened angle, b) finite element yield prediction and c) installation at the column base

Although it has been successfully applied as part of wider sub-assembly testing no previous comprehensive experimental campaign has been undertaken in order to fully understand the behaviour of the yielding angle or provide design recommendations. Due to the desire to use the yielding angle as a form of dissipative reinforcing for the current research a comprehensive experimental test campaign was performed which is summarised here. Finite element models and analytical calculations have been made coupled with experimental testing in order to characterize the performance of the angle system.

In total 22 different angle types were tested with two different methods of providing an area of concentrated yielding. The presentation of the testing results will be split into these two groups. In the first of these groups the concentrated yield area was created by milling down a certain section of the angle. In the second case the yielding area was created using holes drilled into the angle face. In addition to this angles were taken from two different sources: equal angle sections and steel hollow section tubes. In order to provide an angle section the steel hollow tubes were halved.

Two different steel strengths were used during testing: S275 and S355 in accordance with the Italian code NTC (2008). The properties of these materials are shown in Table 3.3.

Table 3.3. Material properties

Young's modulus		E	210 GPa
S275	Yield strength	f_y	275 MPa
	Ultimate strength	f_u	430 MPa
S355	Yield strength	f_y	355 MPa
	Ultimate strength	f_u	510 MPa

The milled angle

The basic form of the milled angle is shown in Figure 3.8. A segment of angle was used and milled down to provide a region of concentrated yielding dissipating energy through the inelastic behaviour of steel. The variables used to control the characteristics of angle performance were the thickness of the milled area (t_A), the height of the milled area (L_A) and the width of the angle (b_A). One further parameter was the way in which the transition was made to the yielding area of the milled down angles. Four different options were chosen as shown in Figure 3.8.

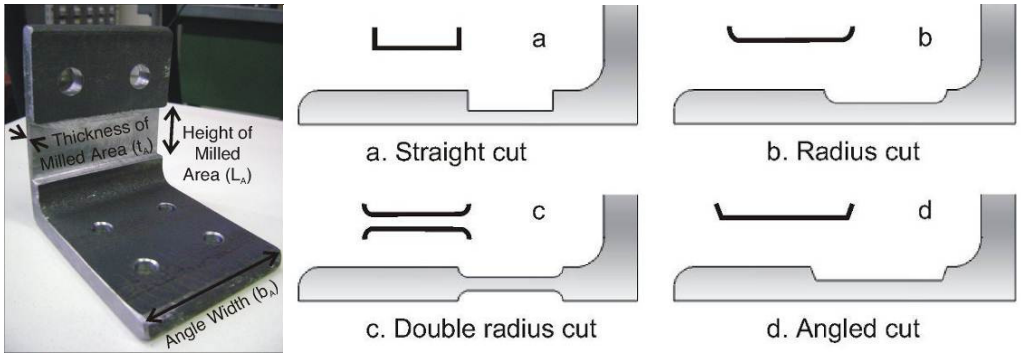

Figure 3.8. Definition of milled angle dissipative reinforcement parameters

The holed angle

The basic form of the holed angle is shown in Figure 3.9. Simpler in principle than the milled angle and therefore easier to manufacture, the angles were characterised by the drilling a certain number (n_H) of holes of a certain diameter (ϕ_H). The drilling of these holes causes the same concentration of yielding as occurs in the milled angles.

As mentioned a total of 22 different angle configurations have been tested. Some of the testing was repeated leading to a total of 29 individual angle tests.

Figure 3.9. Definition of holed angle dissipative reinforcing parameters

Testing included variations of the following general parameters:

1. Source material, steel square hollow tube (T) or a length of equal angle (A)
2. Method of yield concentration, milled (R) or holes (H)
3. Angle thickness (t)
4. Angle width (b_A)
5. Type of steel, S275 or S355

Parameters varied relating only to milled angles:

1. Thickness of milled area (t_A)
2. Height of milled area (L_A)
3. Transition method; a, b, c or d (Figure 3.8)

Parameters varied relating only to holed angles:

1. Number of holes (n_H)
2. Diameter of holes (ϕ_H)

Results are presented in the way in which they related to the changes made in these parameters. An overview of the angles tested in the structural laboratory of the University of Basilicata, Potenza is presented in Table 3.4.

Table 3.4. Identification and characteristics of angles tested (all values are in mm)

Angle ID	A/T	R/H	t	b_A	Tran	t_A	L_A	ϕ_H	Steel
ID0	A	R	10	80	a	4	30	-	S355
ID1.1	A	R	10	80	b	4	36	-	S355
ID1.2	A	R	10	80	c	4	33	-	S355
ID2	A	R	10	80	b	6	36	-	S355
ID3	A	R	10	80	b	6	46	-	S355
ID3 2A/2B	A	R	10	80	b	6	46	-	S275
ID4 A/B	A	R	10	80	b	7	39	-	S275
ID5 A/B	A	R	10	80	d	6	40	-	S275
ID6 A	T	H	8.5	80	-	-	-	2 x 28	S355
ID6 B	T	H	8.5	80	-	-	-	2 x 30	S355
ID7 A	A	H	8.5	80	-	-	-	2 x 30	S275
ID7 B	A	H	8.5	80	-	-	-	2 x 28	S275
ID8 A	A	R	8.5	160	d	6	40		S275
ID8 B	A	R	10	160	d	6	40		S275
ID9	A	R	8.5	80	d	6	40		S275
ID10 1A/1B	T	H	6	80	-	-	-	2 x 24	S355
ID10 2A/2B	T	H	6	80	-	-	-	2 x 30	S355
ID11 A	A	H	10	80	-	-	-	2 x 30	S275
ID11 B	A	H	10	80	-	-	-	2 x 28	S275
ID12	A	H	10	160	-	-	-	4 x 30	S275
ID13	A	H	8.5	160	-	-	-	4 x 30	S275
ID14 A/B	T	H	6	160	-	-	-	4 x 30	S355

3.5.1 Definition of performance characteristics

Several factors have been used in order to define the performance of the steel angles. These are: the initial stiffness (K), the yield strength F_y, the yield displacement (Δ_y), the ductility (μ_A) and the hardening ratio (α).

Figure 3.10 shows the way in which the angle performance characteristics were defined. Similar to the fused type dissipative reinforcing, angle dissipative reinforcing is characterised by: the yield force (F_y), yield displacement (Δ_y), ultimate force (F_u), ultimate displacement (Δ_u), initial stiffness (K), post-yield stiffness (α) and ductility (μ).

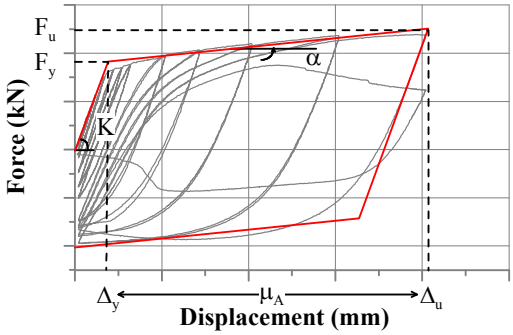

Figure 3.10. Definition of dissipative angle reinforcing performance characteristics

3.5.2 Test setup

Testing was performed using a hydraulic jack fixed to a steel testing rig as shown in Figure 3.11. Several different test configurations were used during the experimental campaign, however the principles of each test set up were the same: the bottom edge of the angle was bolted to the test rig and the plate (in the centre of the testing rig) was moved up or down in accordance with the loading protocol. This plate was used for the initial part (ID0 – ID3) of the test regime but was replaced by the steel block shown in Figure 3.11c (for ID4 onwards). Force and displacement were measured from the movement of the plate and the reaction on the plate.

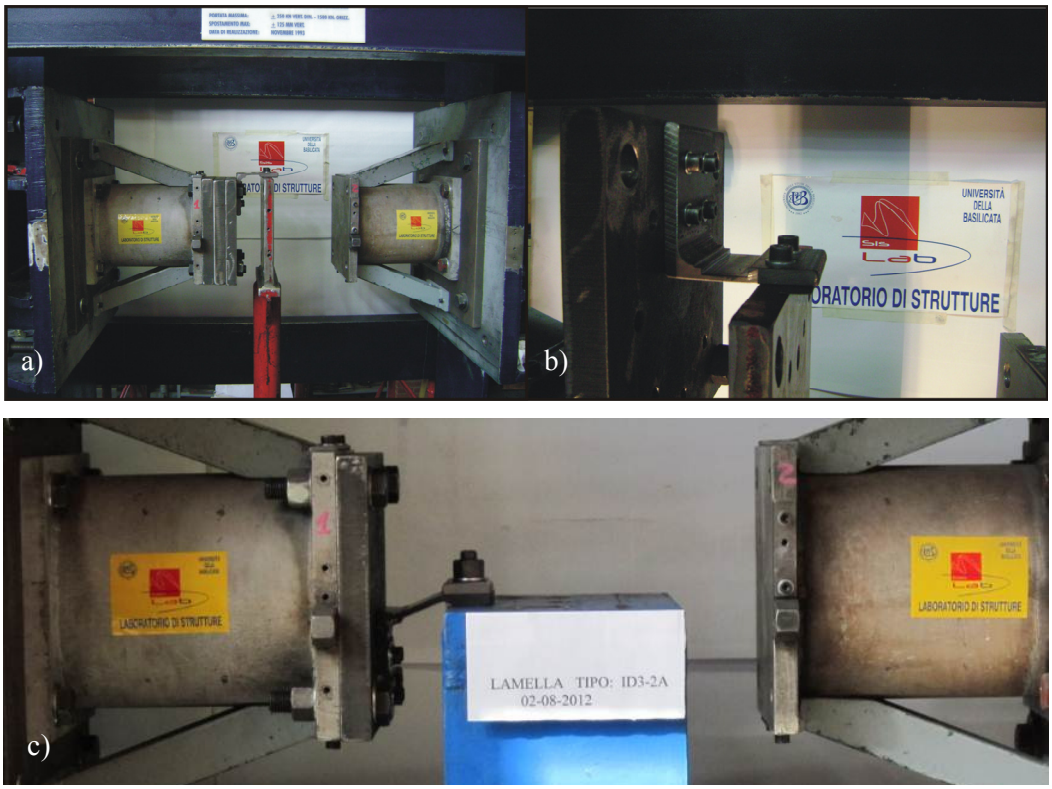

Figure 3.11. Angle dissipative reinforcing test set up a) original set up with moving plate, b) angle attached to moving plate and c) modified test set up using moving block

The angle was loaded at a velocity of 0.5 mm/s and only in a single direction corresponding with its expected performance when placed at the interface between a beam-column, column-foundation or wall-foundation connection (as with the fuse type device testing). Two cycles at each displacement level were applied with displacement and reaction load being recorded. The complete loading protocol is displayed in Figure 3.12.

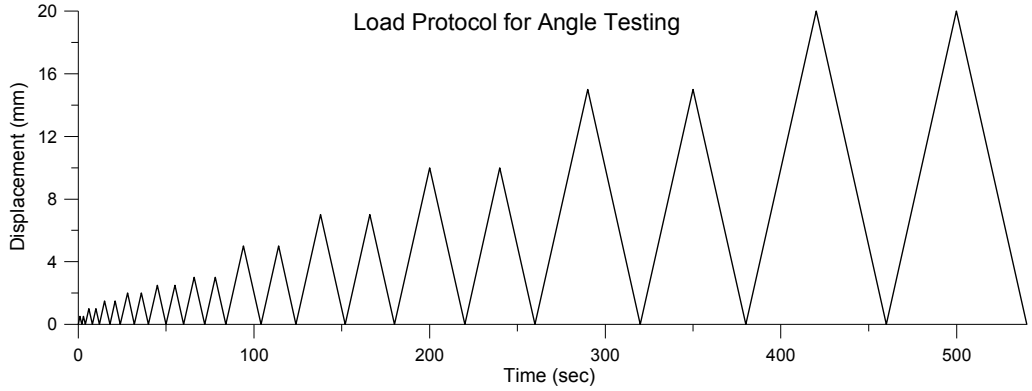

Figure 3.12. Loading protocol for the testing of angle dissipative reinforcing

3.5.3 Testing results

This section provides a summary of the key testing results for both the milled and holed angles. For a comprehensive report on the performance of both angle configurations refer to Smith et al. (2014).

Milled angles

Eleven of the 22 angle configurations tested created concentrated yielding through the milling down of a certain section of steel area. A selection of results from these tests is presented in Figure 3.13 with a selection of testing photos shown in Figure 3.14.

The first test performed was that of ID0 which had a straight cut transition zone. This led to the sudden low cycle fatigue failure shown in Figure 3.14a and the reduced hysteretic capacity shown in Figure 3.13a. In order to mitigate this effect a series of different transition zones were used all of which were successful in eliminating low cycle fatigue. ID1.1 and ID1.2 utilized two methods of radius cut with force-displacement testing results displayed in Figure 3.13c. As seen there is no significant difference in testing results and therefore the less time consuming single radius cut was utilised for future testing.

Angle ID3 was selected for the beam-column joint test campaign which will be described in Chapter 4. This angle possessed the required strength capacity of approximately F_y = 15 kN and did not display the pinching of hysteretic loops or the sudden fracture observed in other angle tests.

The testing results of angles ID4 A and B are shown in Figure 3.13d and compared to the performance of the benchmark ID3. This figure illustrates the way in which the

characteristics of the angle can be altered in order to change the system performance. The ID4 angles were made out of a lower steel strength compared to ID3 and therefore the milled thickness (t_A) was increased (from 6 mm to 7 mm) and the height of the milled area (L_R) was decreased (from 46 mm to 40 mm). As shown this had the effect of increasing the angles strength beyond that of angle ID3.

The change in parameters from ID3 to ID4 also led to undesirable second order effects degrading the angle performance. This led to the significant pinching observed in the hysteresis loops due to the yielding of the base of the angle shown in Figure 3.14b. A minimum ratio between the original angle thickness (t_A) and the milled angles thickness (t_A) of 2:3 should be maintained in order to ensure that this undesirable behaviour does not occur.

Finally Figure 3.13e shows angle ID5 where the results of the benchmark specimen were replicated with the low strength S275 steel by decreasing the height of the milled area (from 46 mm to 40 mm). Angle ID5 also adopted another form of transition, the angled cut. This transition proved to be successful and simple and is now recommended for all milled angle dissipative reinforcing. The angle ID5 was adopted during the shaking table test series as described in Chapter 6.

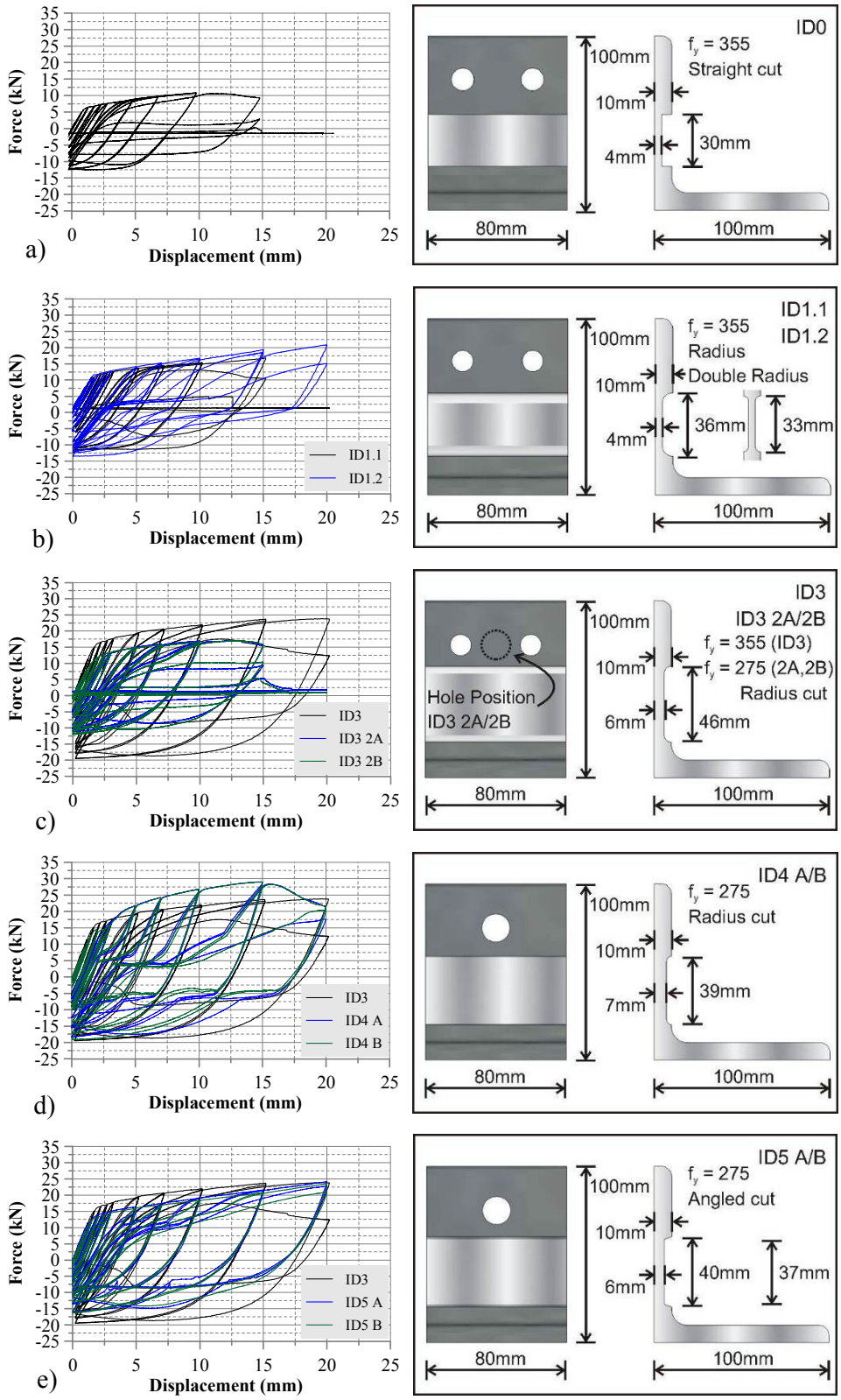

Figure 3.13. Angle dissipative reinforcing characteristics and testing results for milled dissipative reinforcing angles: a) ID0, b) ID1.1, ID1.2 c) ID3, ID3 2A, ID3 2B, d) ID3, ID4 A, ID4 B and e) ID3, ID5 A, ID5 B

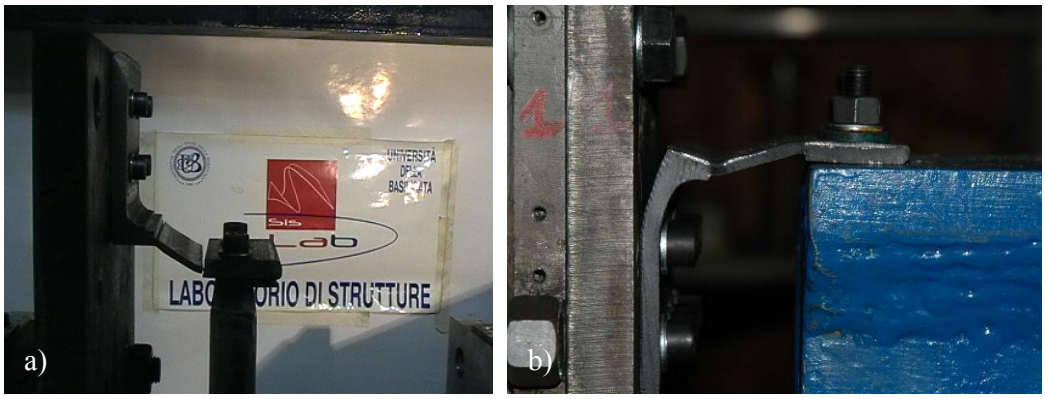

Figure 3.14. End of test milled dissipative reinforcing angles: a) ID0 showing low cycle fatigue failure and b) ID4 B showing yielding outside of the intended, milled down, area

Holed angles

The remaining 11 of the 22 angle forms tested created concentrated yielding through the drilling of holes removing part of the steel area. A selection of results from these tests is presented in Figure 3.15 with a selection of testing photos shown in Figure 3.16.

The first series of testing, ID6 and ID7 was designed to replicate the performance of the benchmark test ID3 with holed angles fabricated from tube and angles respectively. Figure 3.15a shows the comparison between the results of ID3 and ID6 where it can be seen that the force-displacement characteristics were successfully replicated.

Slight pinching can be seen in the loops of ID6 A with the onset of the failure mode of yielding in the angle base attachment (i.e. outside of the intended yielding area) as also seen in the milled angle tests. The full degradation of behaviour seen in the performance of angle ID4 was not observed however due to the reinforcement placed on the bottom of the angle seen in Figure 3.16a. An alternative to this would be to use a thicker angle. Testing of both angles ID6 A/B (Figure 3.15a) and angles ID7 A/B (Figure 3.15b) was successful in that they both displayed adequate dissipation represented by stable hysteretic loops. This means that the holed angles can be made from either a steel tube or an angle section with no change in the dissipative reinforcing performance.

Angle ID10 2 was created and designed in order to provide a significantly lower strength demand of F_y = 8 kN using the FE modelling described in Section 3.5.6. The results of ID6 2 are shown in Figure 3.15c with the photo in Figure 3.16b showing the angle during testing. As shown both angles provided adequate amounts of dissipation with a significant reduction of yield strength due to the reduction of angle thickness (t_A).

The final test series displayed in Figure 3.15d is that of angle ID14. This angle was developed for a column-foundation connection instead of a beam-column connection for which all previously displayed angles were defined. Angle ID14 was twice the width of ID10 2 however 4 holes and not 2 were used. As expected angle ID14 provided twice the strength of ID10 2.

No angle during the holed angle testing fractured under cyclic loading however stiffness degradation was observed in the later, large displacement cycles. This was related to the angle yielding outside of the holed area. The significance of the high ductility capacity of the holed angles will be discussed further in Section 3.5.4.

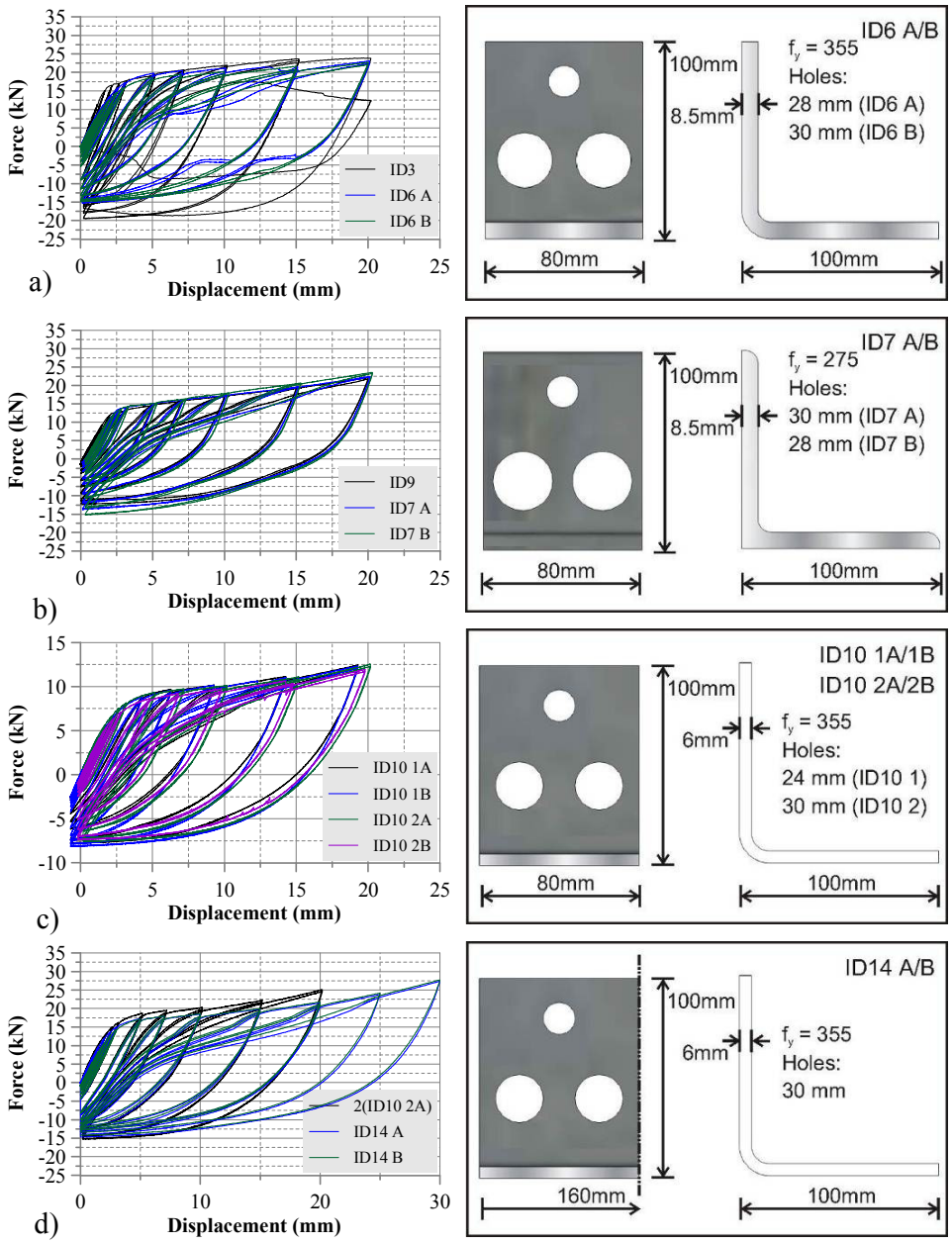

Figure 3.15. Angle characteristics and testing results for holed dissipative reinforcing angles: a) ID3, ID6 A, ID6 B, b) ID7 A, ID7 B, c) ID10 1A, ID10 1B, ID10 2A, ID10 2B and d) 2 times ID102A, ID14 A, ID 14 B

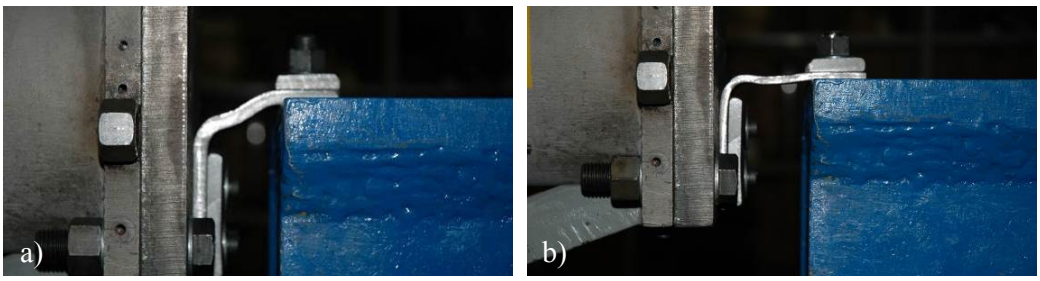

Figure 3.16. Photos during holed dissipative reinforcing angle testing of a) ID6 B and b) ID10 B

3.5.4 Summary of all tests

A summary of the angle performance characteristics is presented in Table 3.5. This section will compare the angles in relation to these parameters. The maximum tested displacement ductilities of the angles are shown in Figure 3.17.

During testing it was noted that significant displacements were occurring adding to the recorded displacement of the angle that led to increased displacement values being recorded. These were created by movements in the testing frame which meant the angle was not attached to a fixed point. As displacements were not measured directly across the angle but instead relied on readings from the ram this resulted in registered displacement values being 2.5 times larger than what the angle was actually subjected to. This has been confirmed during full scale beam-column testing described in Chapter 4 and through finite element modelling which is discussed in Section 3.5.6. Values shown in Table 3.5 have been calibrated to remove this error in displacement.

Table 3.5. Summary of angle performance characteristics from testing

Angle ID	F_y kN	Δ_y mm	F_u kN	Δ_u mm	μ	K kN/mm	α kN/mm
Milled							
ID0	6.8	0.50	11.0	4.0	8.0	13.6	1.20
ID1.1	12.0	0.70	17.0	6.0	8.6	17.1	0.94
ID1.2	12.0	0.70	21.0	8.0	11.4	17.1	1.23
ID2	25.0	1.00	33.0	7.5	7.5	25.0	1.23
ID3	19.0	0.75	24.0	6.0	8.0	25.3	0.95
ID3 2A/2B	12.0	0.70	17.0	6.0	8.6	17.1	0.94
ID4 A/B	20.0	0.80	29.0	6.0	7.5	25.0	1.73
ID5 A/B	14.2	0.60	24.0	8.0	13.3	23.7	1.32
ID8 A	23.5	0.80	49.0	12.0	15.0	29.4	2.28
ID8 B	25.5	0.75	41.5	8.0	10.7	34.0	2.21
ID9	13.0	0.80	22.0	8.0	10.0	16.3	1.25
Holed							
ID6 A	18.5	1.00	23.0	8.0	8.0	18.5	0.64
ID6 B	18.5	1.00	22.5	8.0	8.0	18.5	0.57
ID7 A	14.5	1.10	22.5	8.0	7.3	13.2	1.16
ID7 B	14.5	1.10	23.5	8.0	7.3	13.2	1.30
ID10 1A/1B	8.2	1.10	12.5	7.6	6.9	7.5	0.66
ID10 2A/2B	8.2	0.90	12.5	8.0	8.9	9.1	0.61
ID11 A	23.5	1.00	35.0	8.0	8.0	23.5	1.64
ID11 B	23.5	1.00	37.0	8.0	8.0	23.5	1.93
ID12	34.0	1.00	68.0	12.0	12.0	34.0	3.09
ID13	30.0	1.10	58.0	12.0	10.9	27.3	2.57
ID14 A/B	16.0	0.90	25.0	12.0	13.3	17.8	0.81

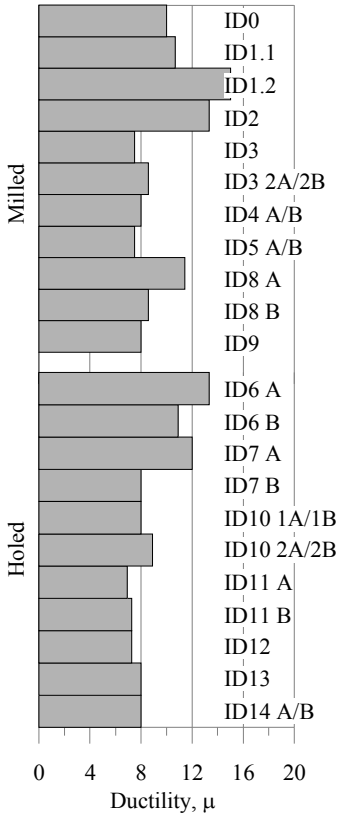

Figure 3.17. Displacement ductility of angles

Comparison of angle thickness, L

Direct comparisons regarding the change in angle width were made for both the milled and holed angles. The milled angles ID5 and ID9, identical except for a change in L from 10 mm to 8.5 mm displayed a reduction in the key parameters with reductions of 25% and 30% in ductility and stiffness respectively. The same comparison was made between the holed angles ID11 A and ID 7 A. Although in this case a similar trend was observed for stiffness with a 40%, while reduction the ductility remained constant. Although the reason behind the reduction in stiffness for the holed angle was clear, and accompanied by a reduction in yield strength (F_y) from 23.5 kN to 14.5 kN, the reason behind the stiffness reductions in the milled angles was slightly less clear, however perhaps it was related to yield of the angle outside of the desired area. While for a holed angle a reduction in width is accompanied by a subsequent reduction in strength for a milled angle this is not the case as the strength is controlled by the milled width (t_A) and not the angle width (t). As mentioned, minimum ratios between t and t_A of 2:3 are suggested.

Comparison of angle width, b_A

As mentioned in Section 3.5.3 the doubling of the angle width from 80 mm to 160 mm led to a two-fold increase in yield strength. As shown in Table 3.5 this was accompanied by a complementary increase in stiffness. On average a 40 % increase in stiffness was seen for both the milled and holed angles with a doubling of width.

Comparison of milled and holed angles

It has been seen that very similar force-displacement responses were obtained by using either method (milled or holed) of creating a concentrated yielding area. Comparisons of initial stiffness shows that in general milled angles are slightly stiffer than holed angles with a 27% increase in stiffness between angle ID6 A and ID3.

Testing did find, however, that the holed angles had a significantly larger ductile capacity when compared to their milled angle counterparts. All testing of milled angles was performed until a significant loss in strength was observed due to low cycle fatigue failure. This was not observed during the holed angle testing with no angles being tested until failure (fracture). This can be seen through the higher ultimate displacements of the holed angles which have an average Δ_u = 9.2 mm

compared to an average of Δ_u = 7.2 mm for the milled specimens. Ductility demand values of the holed angle dissipative reinforcing are not larger than the milled specimens however due to the increased yielded displacements of the holed angle specimens.

3.5.5 Simplified design method

A simplified design method has been developed based on the static bending of the angle under displacement. Making the assumption that the angle acts as a fixed-fixed beam under a unit displacement the shear force at yield (F_y) can be calculated from the yield moment of the angle (M_y):

$$F_y = \frac{2M_y}{L_A} \tag{3.14}$$

$$M_y = f_y Z = f_y \frac{b_A t_A^2}{6} \tag{3.15}$$

Therefore combining (3.14) and (3.15) F_y is obtained:

$$F_y = \frac{f_y b_A t_A^2}{3L_A} \tag{3.16}$$

Figure 3.18 shows the way in which the parameters of b_A, t_A and L_A are defined for both the milled and holed angles. The parameter f_y is the yield strength of the steel.

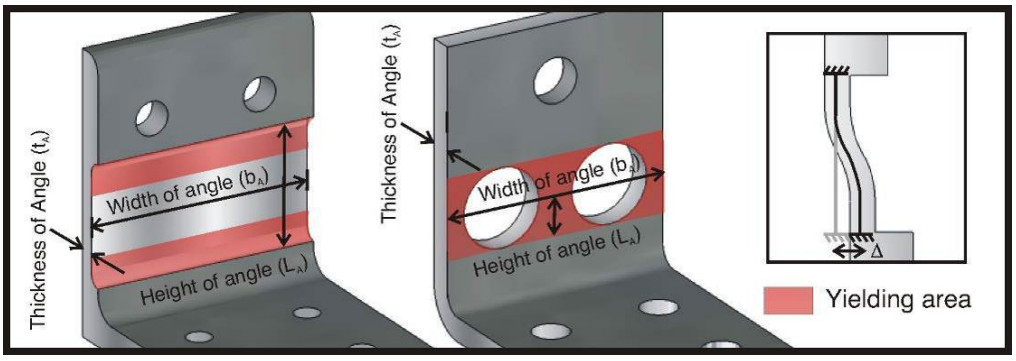

Figure 3.18. Definition of design parameters for the simplified design of milled and holed angle dissipative reinforcement

Figure 3.19 below shows a comparison between the estimates provided by the simplified procedure presented above and the test results. As shown the procedure

provided a conservative estimate of the angle strength by under-estimating the yield strength of the angle in all but one case.

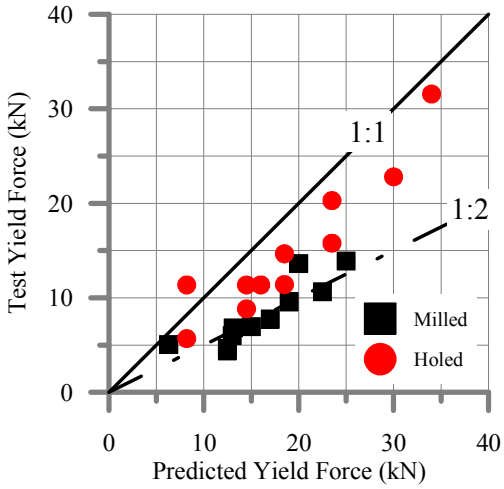

Figure 3.19. Comparison of estimated yield force values (F_y) provided by Equation (3.16) with milled and holed dissipative reinforcement testing results

The estimation for the milled angles was more conservative than that of the holed angles. This was likely due to the under-estimation of the thickness of the milled area. Due to the radius or angle transition zone used yielding does not occur only in the area with the fully reduced section but also in the transition zone giving an effective thickness and thus section modulus which is larger than the milled thickness alone. Figure 3.19 shows that a factor of two between the procedure and testing results seems to be appropriate as a rough estimate. This conclusion, however, is limited to the observations made during this testing and as such relates to the limited material and geometric characteristics used.

3.5.6 Numerical analysis

A finite element model has been developed in order to both replicate the testing results shown above and in order to provide design tables.

The ABAQUS finite element programme (ABAQUS Inc. 2011) was used to model the behaviour of each of the dissipative angles presented above. A 3D deformable solid made up of 2 mm tetrahedral mesh elements was used. The steel material was modelled using a plastic yield model with (combined) cyclic hardening. The boundary conditions of the angle were set in order to mimic as closely as possible the loading of the steel angle. The displacements of the numerical model have been calibrated in

order to remove the frame displacements described above. The mesh arrangement and boundary conditions for the angle ID3 are shown in Figure 3.20.

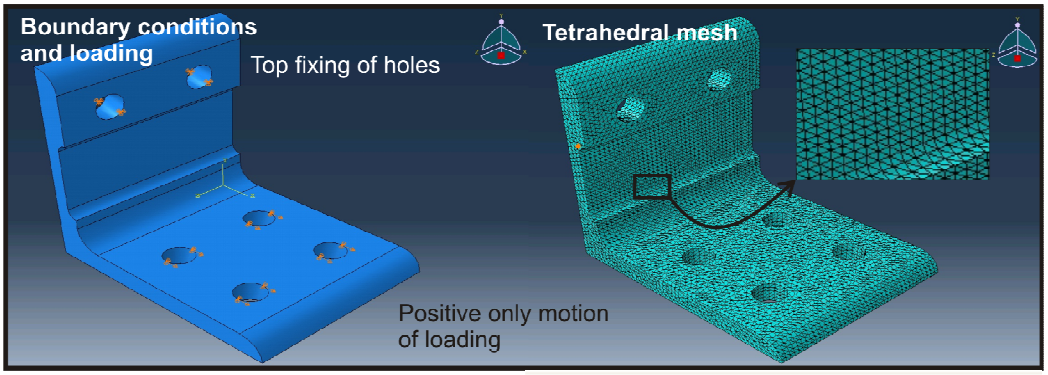

Figure 3.20. Meshing and boundary conditions of ABAQUS model

The finite element model was run using the same displacement cycles as testing however only one single cycle was applied at each displacement level. Fatigue was not accounted for in the model. This is not anticipated to be an issue for the holed dissipative reinforcing angles however further investigation is required in order to understand the impact that fatigue will have on the milled dissipative angle reinforcement.

Comparison between a selected angle case and the ABAQUS model of the milled and holed angles and the testing results of each are shown in Figure 3.21 (a full comparison can be found in Smith et al. (2014). As shown the models provided a sufficiently accurate representation of the angles performance with close prediction of the key parameters of stiffness, both pre and post yield, yield strength/displacement and ultimate strength/displacement. More detailed discussion of the milled and holed angle response is presented below.

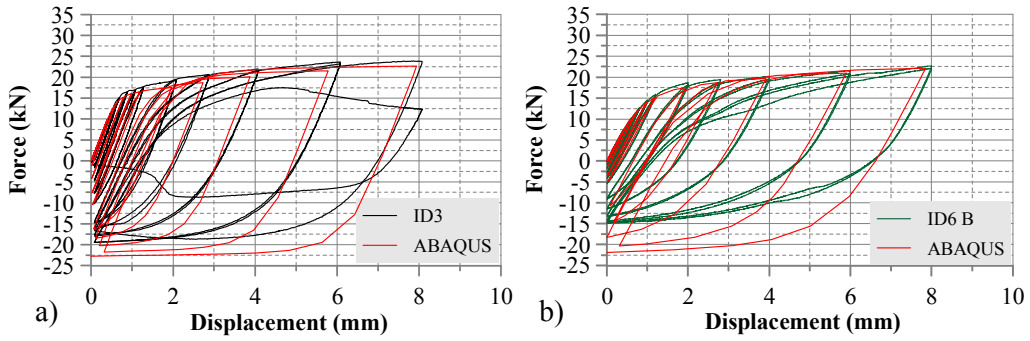

Figure 3.21. Comparisons between the force-displacement results of the FEM ABAQUS model and the milled dissipative reinforcing angle ID3 and the holed dissipative reinforcing angle ID6 B

Milled angles

The numerical prediction of the cyclic behaviour of the angles was accurate for all angles except those in which significant pinching of the hysteretic response was observed (such as angle ID4 A/B shown in Figure 3.13d). As mentioned previously this pinching was caused by yielding occurring outside of the milled area.

A comparison was made between the stress distribution at maximum displacement of the benchmark angle ID3 (Figure 3.22a) and those of ID4 (Figure 3.22b) and ID9 (Figure 3.22c) which displayed a significantly pinched hysteretic response. In this figure the areas in grey represent areas of the angle in which the elastic limit of the steel has been exceeded. The stress distribution in ID3 shows that as the ratio between t and t_A (which is on the limit of the 2:3 ratio suggested) is sufficient and yielding is effectively restricted to within the milled area. Angle ID4 however displayed significant yielding outside of the milled area created due to the amount of angle which was milled down not being sufficient (i.e. the angle strength created by the milled area is too large). This was also the case for angle ID9 where the angle original width (t) was reduced. This meant that although the strength of the angle was similar to that of angle ID3 A/B which worked well, the reduction of the angle original width reduced the angle capacity outside of the milled area to an unacceptable level. Although modelling indicates that this is likely to be an issue, the reinforcing used similar to that shown in Figure 3.16 was sufficient in order to stop this occurring and therefore no pinching of the hysteretic loops was observed. Figure 3.23 shows the strain which occurred in a selection of the angles at maximum displacement. The strain levels show clearly that although yielding was occurring outside of the milled

area the majority of plastic strains were still concentrated in the desired area of the angle.

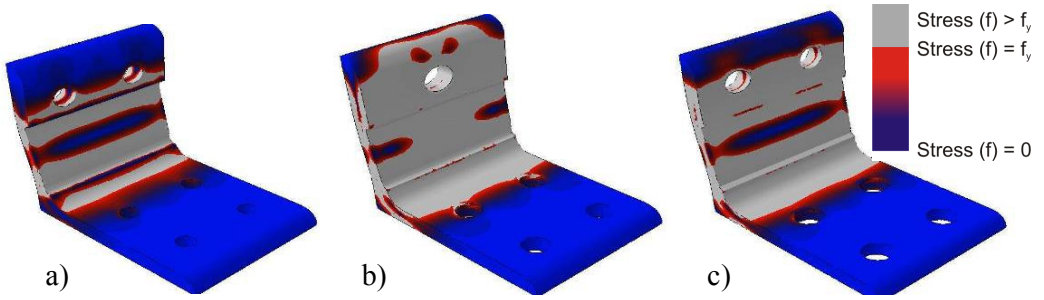

Figure 3.22. Stress distribution at maximum displacement for milled angles a) ID3, b) ID4 and c) ID9

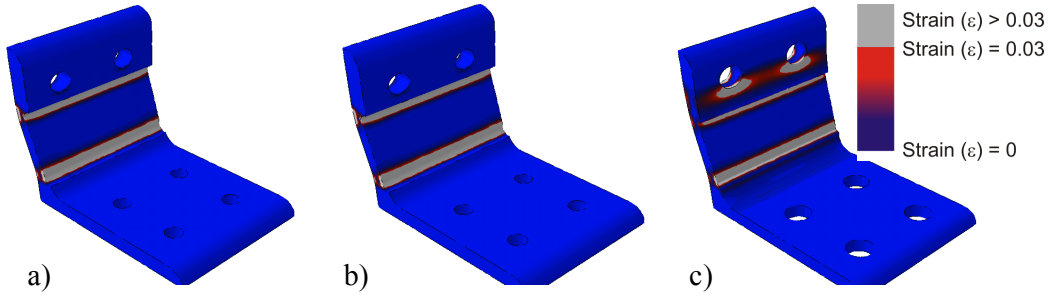

Figure 3.23. Strain distribution at maximum displacement for milled angles a) ID3, b) ID4 and c) ID9

Holed angles

As with the milled angles the cyclic behaviour of the holed angles was predicted with sufficient accuracy except where pinching of the hysteretic loops is evident.

The distribution of stress in the angle at the maximum displacement point is shown for angle ID6 (Figure 3.24a), ID7 A (Figure 3.24b), and ID10 2 (Figure 3.24c). These figures display the way in which the yielding of the angle occurred over a significantly larger area compared to the milled angles. This had the effect of increasing ductility due to a larger spreading of plastic strains. One thing that can be noticed however is how yielding had a tendency to also occur where the top of the angle is attached. This supports the necessity of the use of the reinforcing placed on the top of the angles seen during the holed angle testing.

Figure 3.25 shows the strain which occurred in a selection of the holed angles at maximum displacement. Strain levels show that although yielding was occurring outside of the holed areas the majority of plastic strain was concentrated below each hole.

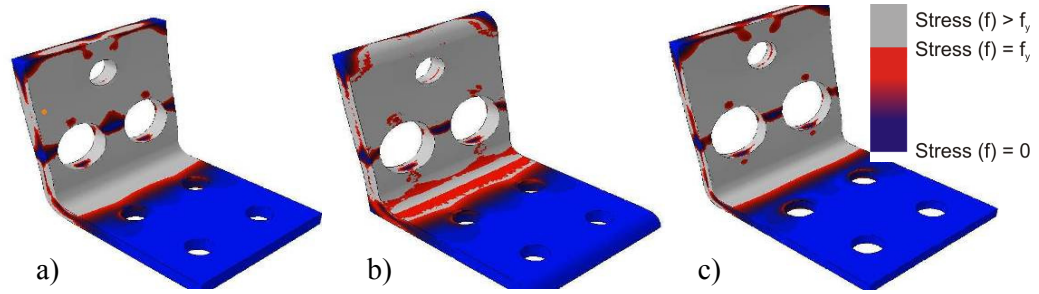

Figure 3.24. Stress distribution at maximum displacement for milled angles a) ID6 B, b) ID7 A and c) ID10 2

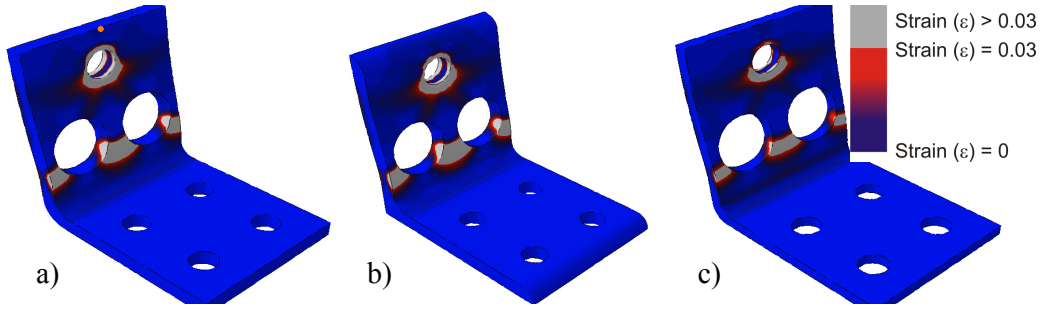

Figure 3.25. Strain distribution at maximum displacement for milled angles a) ID6 B, b) ID7 A and c) ID10 2

3.5.7 Design charts for the design of yielding steel angles

The numerical model developed has been used in order to produce design tables listing characteristic yield forces and displacements for both the milled and holed dissipative angles. These enable a designer to specify a dissipative reinforcing angle by stating a desired yielding force (F_y) and displacement (Δ_y). The following considerations have been made in defining the tables for the milled angles:

1. Four standard angle sizes have been used which are (all measurements in mm):
   i. 100 x 100 x 10 (which has been used for most of the testing presented)
   ii. 150 x 150 x 18
   iii. 200 x 200 x 20
   iv. 250 x 250 x 25

2. The two steel grades used during testing (S275 and S355) have been used in addition to the Australasian steel Grade 300 (F_y = 300MPa, F_u = 440MPa, E = 200GPa) (NTC08 2008; NZS 3404:Part 1:2009)

3. Angles have been dimensioned to ensure that yielding is unlikely outside of the milled area under Ultimate Limit State loading

The following considerations have been made in defining the tables for the holed angles:

1. Four standard angle sizes have been used with varying thicknesses (all measurements in mm):
   i. 100 x 100 x 12, 10 and 8
   ii. 150 x 150 x 18, 14, 12 and 10
   iii. 200 x 200 x 24, 22, 10, 18 and 16
   iv. 250 x 250 x 28, 26, 24, 22 and 20

2. Three steel grades have been used; S275, S355 and Australasian Grade 300

3. For the 250 and 200 equal angles a single hole of variable size has been used. For the 150 and 100 equal angles two holes have been used.

Loading of the numerical model was performed monotonically as shown in Figure 3.26a. As shown this slightly underestimated forces (10 – 15% at yield, 15 – 20% at ultimate). A slight alteration in the way in which the displacement was imposed was also made with displacement being imposed to the section through the angle as shown in Figure 3.26b. The design charts (Figure 3.27 and Figure 3.28) are presented for a 100 mm angle width.

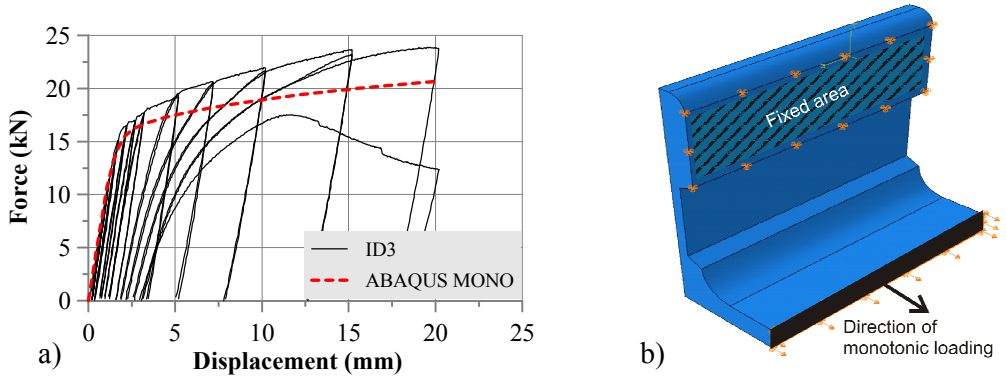

Figure 3.26. a) Monotonic loading versus ID3 test results b) displacement loading point (milled angle shown)

3.6 DESIGN TABLES FOR HOLED AND MILLED ANGLES

Figure 3.27 and Figure 3.28 present an example of the design tables for the milled and holed angles respectively. Entering with either a milled height and thickness (milled angles) or an angle thickness and hole size (holed angles) an engineer can find the design yield strength and displacement of the given angle arrangement. Values are shown per 100 mm of angle. The full design charts are presented in APPENDIX A. These charts have not been corrected to allow for cyclic loading

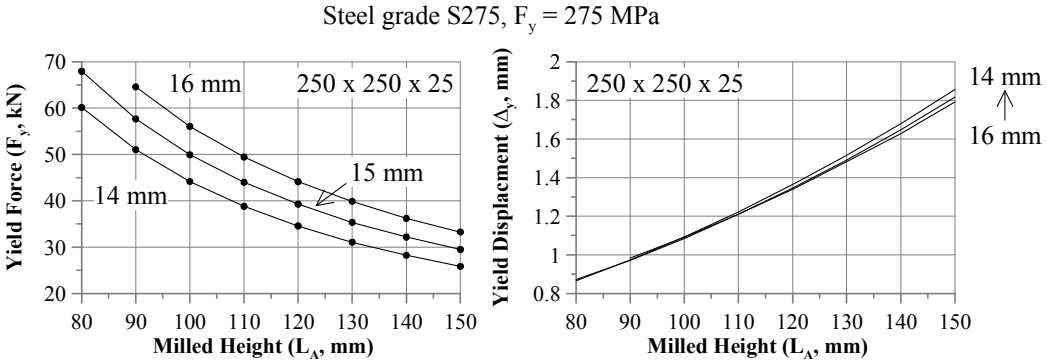

Figure 3.27. Milled angle design chart for angle 250 x 250 x 25 steel grade S275 thickness of milled area t_R = 14 mm, 15 mm and 16 mm, yield force (F_y) and displacement (Δ_y) per 100 mm

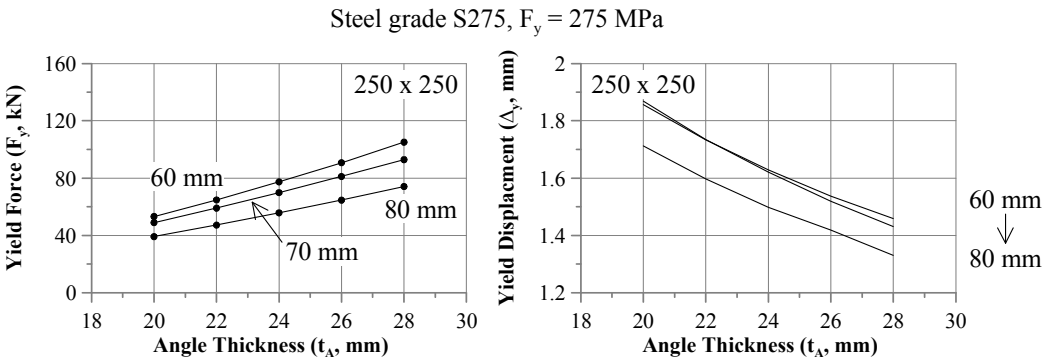

Figure 3.28. Holed angle design chart angle 250 x 250 Grade 300 steel hole diameter ϕ_H = 60 mm, 70 mm and 80 mm, yield force (F_y) and displacement (Δ_y) per 100 mm

3.7 COMPARISON OF DESIGN TABLES AGAINST TESTING RESULTS

In order to gauge the adequacy of the design tables presented above a comparison was made between the yield force (F_y) and displacement (Δ_y) values obtained from testing (presented in Table 3.5) and the design table curves. This comparison is shown in Figure 3.29 for the milled dissipative reinforcing angles. Comparison between the holed angle results and the design charts was not possible due to the different angle widths used.

Comparison between the design curves and the results of the milled angle testing shows that the design charts were able to adequately predict the yield for of the reinforcing. The yield displacement however was not as well predicted with the design charts underestimating the test values. The design charts do however provide a reasonable estimate (within 0.4 mm) with the exception of one outlier.

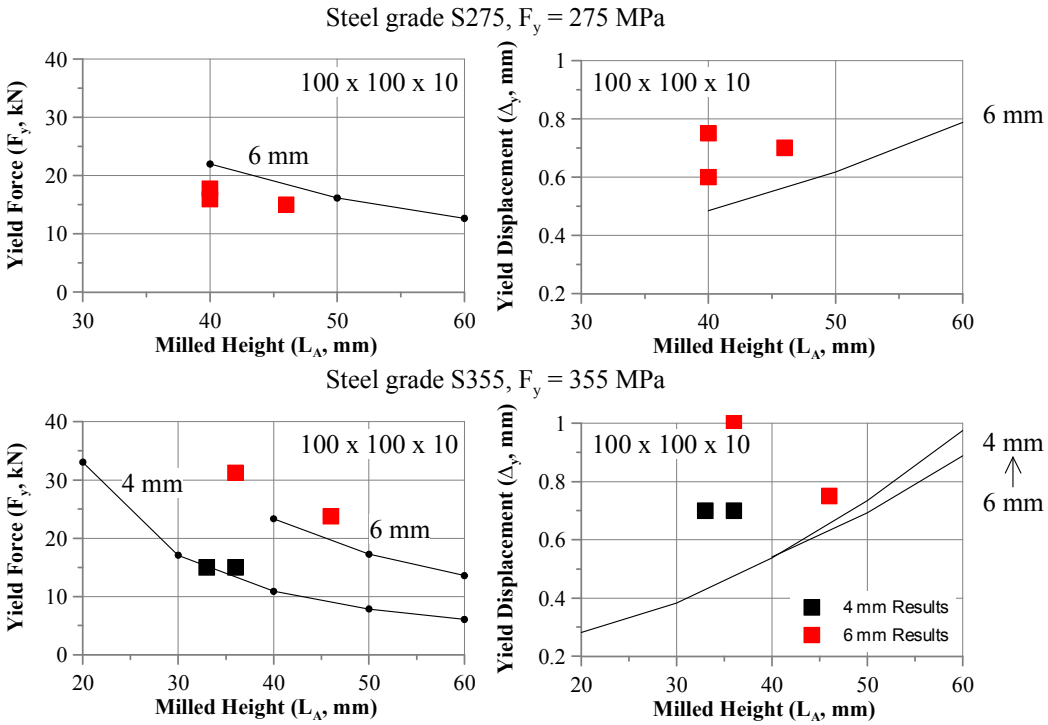

Figure 3.29. Comparison between design curves found through ABAQUS modelling and testing results for the milled reinforcing angles thickness of milled area t_R = 4 mm and 6 mm

3.8 POST YIELD STIFFNESS

If a simple elasto-perfectly-plastic assumption is not made in design a designer will require a post-yield stiffness (α from Figure 3.10) as input. The post-yield stiffness of the dissipative reinforcing is crucial as the re-centering ratio, defined at the ratio between the moment capacity provided by the post-tensioning and the total moment capacity (i.e. post-tensioning plus dissipative reinforcing), is not calculated at yield but at a certain design drift. The actual force in the dissipative reinforcing at the performance point can only be calculated if the post-yield stiffness is known. Figure 3.30 displays the post yield ratios as calculated from the monotonic loading of the ABAQUS model for a selected milled angle configuration. The full tables are presented in APPENDIX A.

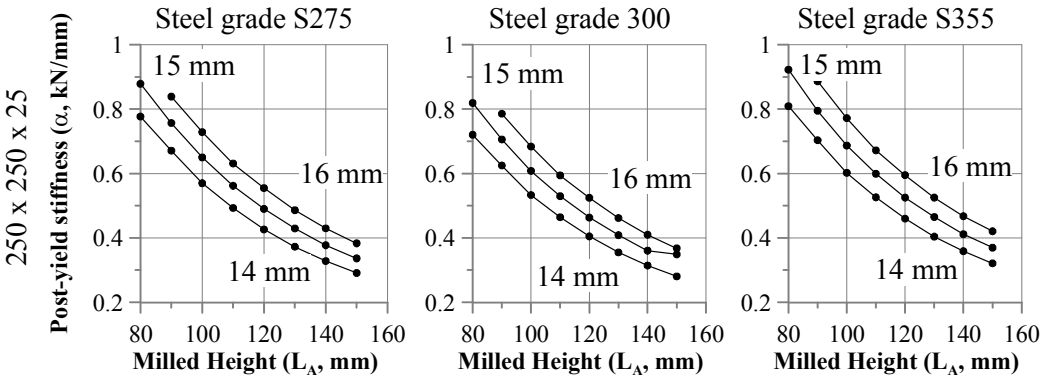

Figure 3.30. Post-yield stiffness (α) design charts for 250 x 250 x 25 per 100 mm of angle thickness of milled area t_R = 14 mm, 15 mm and 16 mm

3.9 FURTHER CONSIDERATIONS IN THE DESIGN OF PASSIVE DISSIPATIVE REINFORCING DEVICES

Two different methods of providing additional reinforcement and energy dissipation capacity to post-tensioned timber systems have been presented and the design of each standalone device has been discussed either based on the use of design charts or formulas based on the characteristics of the device. All of the above devices depend on displacements in order to activate and therefore the movement of whatever method of connection is used must be considered.

3.9.1 Effect of displacements on dissipative reinforcing device connections

Yielding steel devices rely on displacement in order to provide hysteretic energy dissipation. It is therefore crucial that a good understanding of what displacement demand will be imposed on a dissipative reinforcing device is obtained, minus any slipping or elastic connection displacement. Numerous methods of shear transfer between steel and timber exist however little information is available regarding the stiffness of these connections. The method of steel to timber shear attachment used during this body of work was vertical screws (the beam-column connection and frame testing presented in Chapters 4 and 6). The methods used in order to calculate their stiffness are presented in addition to another common form of steel to timber connection.

Timber rivets

The stiffness of a group of rivets in shear has been defined by (Zarnani and Quenneville 2012). When loaded parallel to the grain the displacement of the rivet group is defined as:

$$\delta_l = 4\left[1-\sqrt{1-\frac{N_l^*}{\phi_r Q_{r,l}}}\right] \quad \textbf{(3.17)}$$

Where:

δ_l = The displacement of the rivet group

N_l^* = Rivet group demand

$\phi_r Q_{r,l}$ = Rivet group capacity as calculated by Zarnani and Quenneville (2012)

When loaded perpendicular to the grain the displacement of the rivet group is defined as:

$$\delta_p = 5.5\left[1-\sqrt{1-0.99\frac{N_p^*}{\phi_r Q_{r,p}}}\right] \quad \textbf{(3.18)}$$

Where:

δ_p = The displacement of the rivet group

N_p^* = Revit group demand

$\phi_r Q_{r,p}$ = Revit group capacity as calculated by (Zarnani and Quenneville 2012)

Vertical screws

Screws are more commonly used when compared to rivets and therefore more information is available regarding their stiffness. Although the current New Zealand timber code (NZS 3602:1993) does not provide any information regarding screw displacement Appendix C3 of the Australian timber code (AS 1720.1-2010) does. This code states however that for the case of metal to timber connections the equations overestimate connection slip which may lead to under-estimation of device strain and failure.

For this reason the equation provided in Table 7.1 of the European timber code (EN 1995-1-1:2004) should be used:

$$K_{ser} = \rho_m^{1.5}\, d/23 \tag{3.19}$$

Where:

K_{ser} = Stiffness of a single screw

ρ_m = Mean density of the timber

d = External diameter of the screw

Equation (3.19) provides the stiffness of a single screw in a timber to timber connection. For a timber to steel connection the stiffness K_{ser} is multiplied by a factor of two. The total displacement a screw group thus becomes:

$$\delta = \frac{N^*}{2n_s \rho_m^{1.5}\, d/23} \tag{3.20}$$

Where:

N^* = Screw group demand

n_s = Number of screws in screw group

A significant issue with this equation is that it uses the mean density of timber ρ_m. This value is not easily found in literature and no accurate method of converting the more common characteristic value, ρ_k to this mean value exists.

In this body of research reference is made to two different engineered timber products: the European glue laminated timber GL32h and the New Zealand Laminated Veneer Lumber LVL11. The characteristic density for these two materials are ρ_m = 480 kg/m^3 (DIN EN 1995-1-1:NA:2010) and ρ_m = 599 kg/m^3 (Quenneville and Franke 2011) respectively.

3.10 CONCLUSIONS FROM CHAPTER 3

This chapter has presented a selection of dissipative reinforcing methods based on the cyclic yielding of steel under displacement.

The first method presented was based on the yielding in tension and compression of a steel bar or plate which was reduced over a certain area in order to control strains.

This form of dissipative reinforcing has already been adopted throughout New Zealand however, a slight modification is necessary in order to accurately calculate the yield displacement. A corrective factor, k_a, has been derived in order to do this.

The second method of dissipative reinforcing was based on a yielding steel angle developed for use in the retrofit of poorly detailed reinforced concrete structures. During movement the angle yields in bending over an area which has been weakened either through the reduction of the angles width (milled angle) of the drilling of holes (holed angle). An extensive experimental campaign has been performed of quasi-static cyclic testing. This testing showed the effectiveness of the angles as a dissipative reinforcing system however it did highlight some issues which need to be addressed regarding the strength of the area outside the weakened zone. The ratio between the strength of the weakened zone and the remaining angle section must be controlled either through the use of a sufficiently large initial section or the local reinforcing of the angle in problem areas.

A simplified design method which can be used in order to gain a rough estimate of angle size has been provided however this was not sufficiently accurate for detailed design. A finite element model, which has been confirmed against testing results, was therefore used in order to provide design tables for both the milled and holed angle types. These tables provide the design yield strength of the angle for a range of angle sizes providing yield strength from $F_y = 6 – 85$ kN (milled angles) and $F_y = 13 – 133$ kN (holed angles). The use of these design charts is presented in Chapter 10 where the full design procedure for post-tensioned timber frames is presented.

Finally brief consideration has been made to the stiffness of the dissipative reinforcement connection. This connection is typically a steel-timber shear connection and although codes provide methods of strength calculation the stiffness, crucial in understanding the response of a displacement dependant device, is often neglected. Following a brief discussion equations were presented for the calculation of the stiffness of two common steel to timber shear connections. The adequacy of the stiffness formulas for a group of timber rivets in shear has been confirmed through the testing of Zarnani and Quenneville (2012). The adequacy of the stiffness formulas for groups of vertical screws is less certain however were assumed to be adequate.

REFERENCES CHAPTER 3

ABAQUS Inc. (2011). "Abaqus FEA." ABAQUS Inc., Providence, Rhode Island, United States, Finite element analysis software.

Amaris Mesa, A. D. (2010). "Developments of Advanced Solutions for Seismic Resisting Precast Concrete Frames," University of Canterbury, Christchurch, New Zealand.Doctor of Philosophy in Civil Engineering.

Armstrong, T., Smith, T., Pampanin, S., and Buchanan, A. H. (2014). "Experimental testing of Pres-Lam beam column joint details." 2014 New Zealand Society for Earthquake Engineering Conference, Auckland, New Zealand.

AS 1170.1-2010. (2010). "Timber Structures - Design methods." Standards Australia.

Cattanach, A., and Pampanin, S. (2008). "1st Century Precast: the Detailing and Manufacture of NZ's First Multi-Storey PRESSS-Building." NZ Concrete Industry Conference, Rotorua.

Di Cesare, A., Ponzo, F. C., Nigro, D., Simonetti, M., Smith, T., and Pampanin, S. (2013). "Experimental testing and numerical analysis of steel angles as hysteretic energy dissipating devices." Il XV Convegno di Ingegneria Sismica, Associazione Nazionale di Ingegneria Sismica, Padova, Italia.

Dolce, M., Moroni, C., Nigro, D., Ponzo, F. C., Santarsiero, G., Croce, M. D., Canio, G. D., Ranieri, N., Caponero, M., Berardis, S., Goretti, A., Spina, D., Lamonaca, B., and Marnetto, R. (2006). "TREMA Project Experimental Evaluation of the Seismic Performance of a R/C 1/4 Scaled Model Upgraded with the DIS-CAM System " 2nd International fib Congress, Naples, Italy.

NTC. (2008). "Norme Tecniche per le Costruzioni." Il Ministro delle Infrastrutture.

Iqbal, A. (2011). "Seismic Response and Design of Subassemblies for Multi-Storey Prestressed Timber Buildings," University of Canterbury, Christchurch, New Zealand.Doctor of Philosophy in Civil Engineering.

Kurama, Y. C., and Shen, Q. (2004). "Post-tensioned Hybrid Coupled Wall under Lateral Loads." *Journal of Structural Engineering*, 130(2), 297-309.

Marriott, D. (2009). "The Development of High-Performance Post-Tensioned Rocking Systems for the Seismic Design of Structures," University of Canterbury, Christchurch, New Zealand.Doctor of Philosophy in Civil Engineering.

Normung, D. I. f. (2010). "National Annex - Nationally determined parameters - Eurocode 5: Design of timber structures. Part 1-1: General - Common rules for buildings." Deutches Institut fur Normung, Berlin.

Pampanin, S., Palermo, A., and Buchanan, A. (2013). "Post-Tensioned Timber Buildings - Design Guide." Structural Timber Innovation Company, Christchurch, New Zealand.

Quenneville, P., and Franke, S. (2011). "Bolted and dowelled connections in Radiata pine and laminated veneer lumber using the European Yield Model." *Australian Journal of Structural Engineering*, 12(1), 13-28.

Sarti, F., Smith, T., Palermo, A., Pampanin, S., Bonardi, D., and Carradine, D. M. (2013). "Experimental and analytical study of replaceable Buckling Restrained Fuse type (BRF) mild steel dissipaters." 2013 New Zealand Society for Earthquake Engineering Conference, Wellington, New Zealand.

Smith, T., Simonetti, M., Di Cesare, A., Ponzo, F. C., Carradine, D., Pampanin, S., and Nigro, D. (2014). "Angle dissipaters: Experimental campaign and analytical study." University of Canterbury, Christchurch, New Zealand.

EN 1995-1-1:2004. (2004). "Design of Timber Structures Part 1-1: General - Common Rules and Rules for Buildings." European Committee for Standardization.

Zarnani, P., and Quenneville, P. (2012). "Timber Rivet Connection Design Guide." University of Auckland, Auckland.

NZS 3602:1993. (1993). "Timber Structures." Standards New Zealand.

NZS 3404:Part 1:2009. (2009). "Steel Structures Standard Part 1: Materials, Fabrication, and Construction." Standards New Zealand.

4 Study of the Local Response of Post-Tensioned Timber Frames through Beam-column Testing

4.1 PRINCIPAL CONCLUSIONS OF CHAPTER 4

Chapter 4 presents the quasi-static testing of an exterior full-scale post-tensioned beam-column connection. The following principal conclusions are drawn:

1. Testing of post-tensioned glue laminated timber displayed essentially the same characteristics as when laminated veneer lumber was used.
2. Increases in initial post-tensioning values led to an increase in moment capacity.
3. Addition of the dissipative angle reinforcing presented in Chapter 3 led to an increase in moment capacity and hysteretic energy dissipation as well as an average 1.6 times increase in post-yield stiffness
4. Testing was performed with and without additional vertical shear loading on the beam with no change in response.
5. Hysteretic damping, measured as Equivalent Viscous Damping, ranged between 7% and 16% depending on the ratio between the moment capacity provided by the reinforcing and the total moment capacity (taken as the factor β). Increased hysteretic damping was coupled with increased residual displacement.
6. Elastic rotation contributions of the beam, column and joint panel combined to make up 20 - 25% of the total rotation of the beam-column joint.

4.2 INTRODUCTION

This chapter presents the design and quasi-static testing of a full scale beam-column joint. Testing was split into three separate phases: post-tension only testing, post-tension testing including the application of the angle dissipative reinforcing devices previously described in Chapter 3 (a 'hybrid' system) and testing including the application of a factored gravity load (with and without dissipative reinforcing).

Firstly the test model is presented and the test set-up described followed by detailed description of testing results. Testing is analysed both in terms of the local response of

the beam-column connection (i.e. at the interface between the beam and column) and the overall response of the beam-column joint.

4.3 PROTOTYPE BUILDING DESIGN

The post-tensioned beam-column joint used for the quasi-static testing campaign was extracted from the prototype building shown in Figure 4.1a and b. The building was a five storey regular office type structure with a bay length of 4.6 m and a tributary width of 5 m. Seismic loading was simulated proposing that the building was situated in Potenza, Italy which can be considered as a moderate-high seismic zone (PGA = 0.31 g, soil type B – dense sand, gravel or very stiff clay). In design a structural factor of q = 4 (Table 8.1 EN 1998-1:2003) was used.

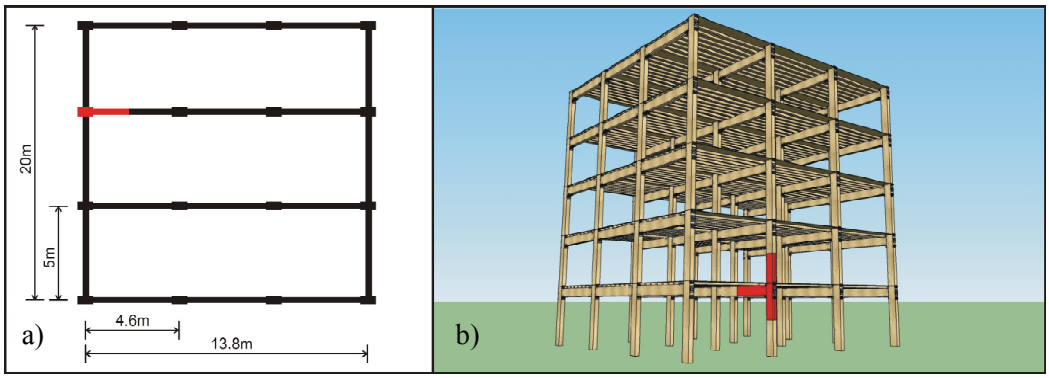

Figure 4.1. Prototype structure a) in plan and b) rendering showing beam-column joint used for testing

The force based design procedure used gave a design moment M_n = 49.4 kNm. The design of the prototype structure is shown in Appendix B.

4.4 THE POST-TENSIONED TIMBER BEAM-COLUMN JOINT

The full scale beam-column joint, shown in Figure 4.2, was made from glulam grade GL32h (EN 1995-1-1 2004) and both the column and the beam were 483 x 240 mm. A 0.6" 7-wire strands high strength steel tendon (f_y = 1530 MPa; f_u = 1760 MPa) was placed at the centre of the beam having a diameter of 15.2 mm. Following the first test program this was replaced with a larger high strength steel bar (f_y = 1050 MPa) with a net diameter of 26.5 mm. A summary of material characteristics is shown in Table 4.1.

Table 4.1. Timber and post-tensioning element material properties

Glulam GL32h			Post-tension Tendons		
Strength			Yield Strength	1530	MPa
Bending	32	MPa	Ultimate Strength	1760	MPa
Compression Parallel to Grain	29	MPa	Elastic Modulus	201	GPa
Compression Perp to Grain	3.3	MPa	Area	165	mm^2
Shear	3.8	MPa			
Elastic Modulus			Post-tension Bar		
Characteristic. Parallel to Grain	11.1	GPa	Yield Strength	1050	MPa
Characteristic Perp to Grain	0.46	GPa	Elastic Modulus	170	MPa
Shear	0.85	GPa	Area	552	mm^2

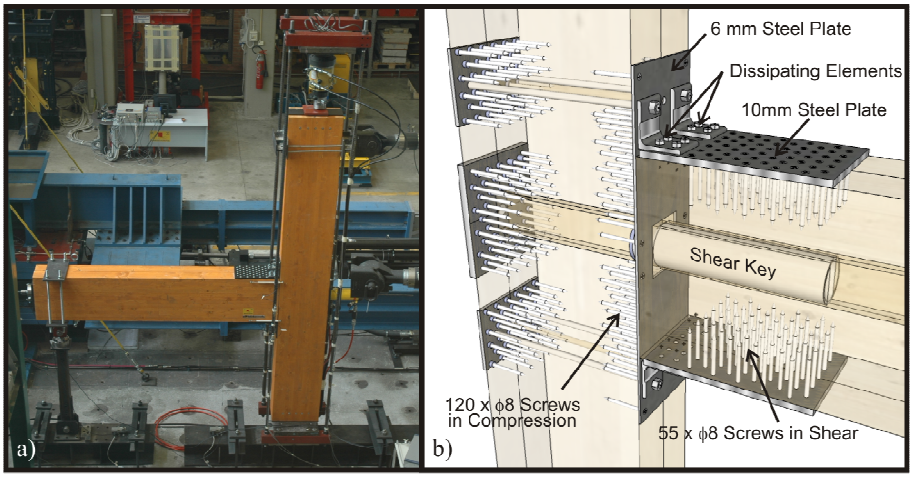

Figure 4.2. a) Beam-column joint assembled and b) details of beam-column joint showing dissipating elements and shear key

Due to the nature of timber as an orthotropic material it is undesirable to have excessive loading in the weaker perpendicular-to-grain direction. As displayed in Figure 4.2b the column member (where compression occurs perpendicular to the grain) was reinforced through the use of ϕ 8 mm, 120 mm long screws.

During Phase 2 of testing steel dissipative angles (ID3) as described in Chapter 3 were added to the beam-column joint (Figure 4.2b) as additional non-post-tensioned reinforcing. The attachment of the dissipating elements was designed using screws placed perpendicular to the direction of loading. Section 3.9 discussed the way in which movement of this type of connection reduces the ductility demand on the reinforcement, therefore reducing its effectiveness. In order to allow for the maximum exploitation of the movement created by the gap opening the connection was significantly over-designed having a resistance of three times the expected loading during testing this also increased the stiffness of the connection (as discussed in Section 3.9.1). This limited elastic displacement and maximised dissipative reinforcing displacements.

Although a significant amount of friction was created at the beam-column interface, current practice dictates that this form of moment connection (in both timber and concrete construction) must be able to support some quantity of gravity load without relying on friction at the interface. This creates an alternate load path if, for some reason, the friction at the interface is lost. As displayed in Figure 4.2b, in the design of the beam-column joint a 101.6 mm diameter 5 mm thick steel tube (f_y = 275 MPa) was glued into the beam with a protruding length of 40 mm. The fact that the steel tube is hidden inside the beam-column joint (in addition to being aesthetically more pleasing) assists the fire resistance of the system by avoiding the use of exposed steel. The tube was designed for a total factored gravity shear load of approximately 80 kN which was based on the tributary width of 5 m x 2.3 m taken from the prototype building.

During the design phase concerns were raised that if the steel shear key sat inside a cavity which was approximately the size of the tube itself during rocking the tube may block the beam rotation and have an adverse effect on system response by becoming wedged inside the column pocket. In order to mitigate this possibility a 10 mm gap was left above the tube where it was seated inside the column. This meant that during rocking the tube was free to move up inside this pocket and the beam was free to rotate. The aim of this was to allow the tube to rock freely on its support while the beam rocked on the column face.

4.5 FABRICATION OF BEAM-COLUMN JOINT

The fabrication of the beam-column joint was performed over a period of two weeks by Holzbau Sud in Calitri, Italy. Although the beam and column were of the same dimension slightly different methods of fabrication were used. Due to the presence of the space inside the beam member to accommodate the post-tensioning tendon two separate segments (as shown in Figure 4.3) were glued together after a hollow was made in each part using a computer numerical controlled (CNC) woodworking machine. The column was made of a single segment of glulam in which a hole was made for the tendon to be placed.

Figure 4.3. a) Half of beam member with tendon gap removed, b) beam member with shear key and c) column member with screw reinforcement (photos courtesy of HOLZBAU SUD)

4.6 EXPERIMENTAL SET-UP

In order to reproduce the moment conditions in the specimen under seismic loading a series of three hinges, placed at the points of contra-flexure, were used. The column member was loaded horizontally and fixed to the reaction floor using steels pins representing perfect hinges (Figure 4.4c). The end of the beam was fixed on a double pinned lever considered to be a pin joint on a roller. The test apparatus consisted of:

- An MTS ram with a capacity of +490 kN and -290 kN applying controlled horizontal displacements (+/- 250 mm) applied to the top of the column and attached to a reaction wall (Figure 4.4a).
- An ENERPACK jack having a capacity of 1500 kN for the application of a constant vertical load (simulating vertical load from the floors above) (Figure 4.4a).
- An ENERPACK jack having a capacity of 300 kN used to apply the tendon load which was connected directly to the test specimen (Figure 4.4b).

A summary sketch of the test set-up used is shown in Figure 4.5.

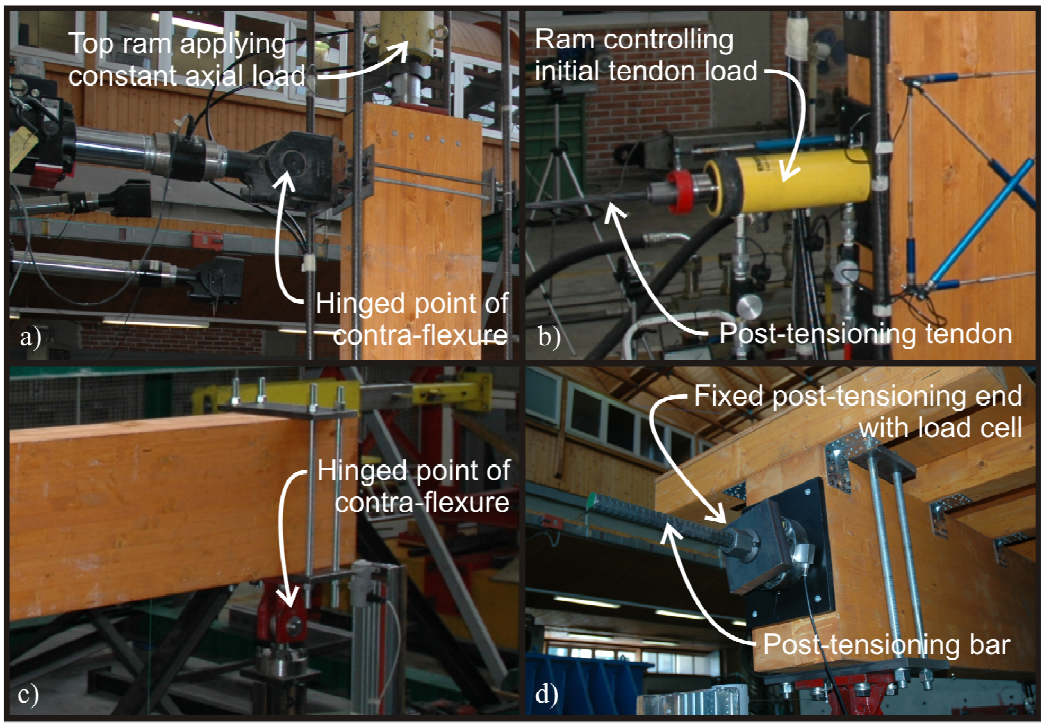

Figure 4.4. a) Top ram for displacement application, b) ram for tendon load (showing tensioned tendon) c) beam hold-down hinge and d) beam post-tension end connection (showing tensioned bar)

The instrumentation placed to record the local and global effects during testing included 25 acquisition channels as displayed in Figure 4.6. Three load cells were used to record the load in the tendon, the axial load force, and the hold down force in the beam. All other instrumentation was used to measure relative displacements in various positions.

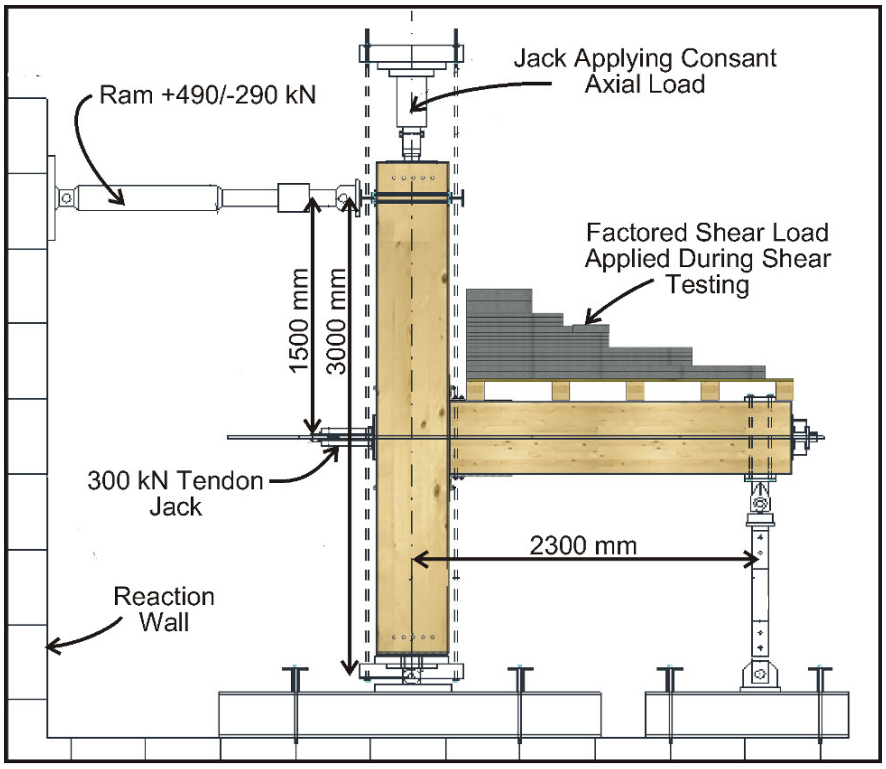

Figure 4.5. Full scale post-tensioned timber beam-column joint test set-up

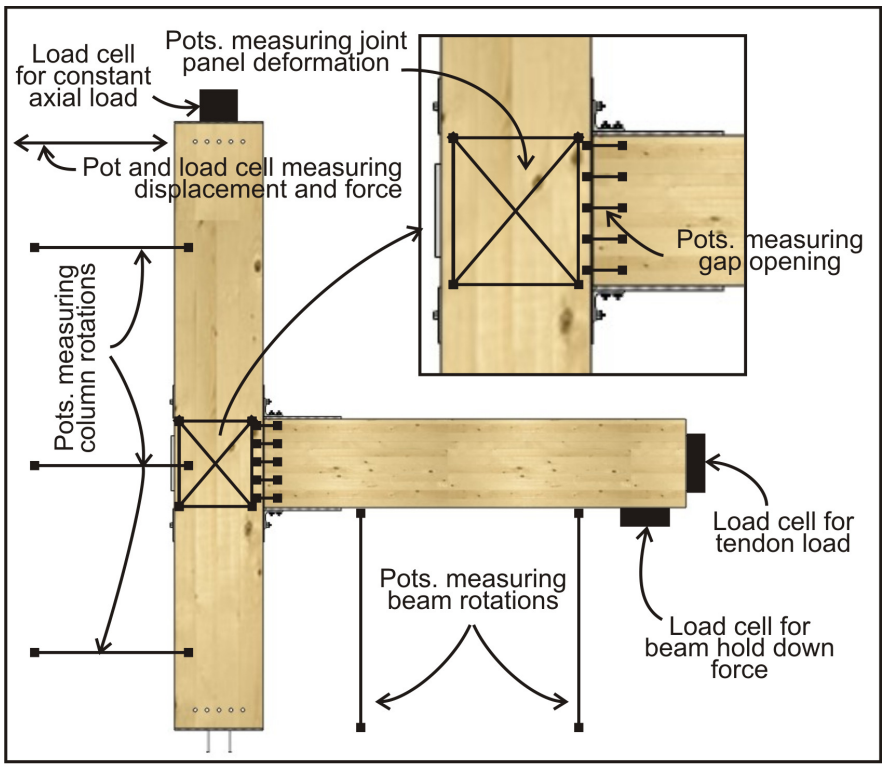

Figure 4.6. Test instrumentation for full scale post-tensioned timber beam-column joint

4.7 TESTING PROGRAM

A total of 21 tests were performed varying; 1) the amount of initial force in the post-tensioning and type of post-tensioning used, 2) the application and amount of dissipative reinforcing and, 3) the presence of shear loading. From the total of 21 tests, 13 key tests (covering all considered permutations of the above parameters) have been identified as shown in Table 4.2.

Table 4.2. Key tests in beam-column testing

Test Name	Tendon Load	Angles	PT Type	β	M_{con}
1) PT ONLY					
PT ONLY 50KN	50 kN	N/A	7 Wire Strand 0.6”	1.00	20 kNm
PT ONLY 100KN	100 kN	N/A	7 Wire Strand 0.6”	1.00	30 kNm
PT ONLY 150KN	150 kN	N/A	7 Wire Strand 0.6”	1.00	40 kNm
PT ONLY 200KN	200 kN	N/A	26mm Bar	1.00	58 kNm
PT ONLY 250KN	250 kN	N/A	26mm Bar	1.00	68 kNm
2) WITH DISSIPATIVE REO					
PT 150KN 1 ANGLE	150 kN	1+1	7 Wire Strand 0.6”	0.72	55 kNm
PT 100KN 2 ANGLES	100 kN	2+2	7 Wire Strand 0.6”	0.49	61 kNm
PT 150KN 2 ANGLES	150 kN	2+2	7 Wire Strand 0.6”	0.56	69 kNm
PT 200KN 2 ANGLES	200 kN	2+2	26mm Bar	0.66	84 kNm
PT 250KN 2 ANGLES	250 kN	2+2	26mm Bar	0.69	91 kNm
3) WITH SHEAR					
PT 150KN WITH SHEAR	150 kN	N/A	7 Wire Strand 0.6”	1.00	40 kNm
PT 100KN 2 ANGLES WITH SHEAR	100 kN	2+2	7 Wire Strand 0.6”	0.49	61 kNm
PT 150KN 2 ANGLES WITH SHEAR	150 kN	2+2	7 Wire Strand 0.6”	0.56	69 kNm

The ratio between the moment capacity provided by the post-tensioning (M_{pt}) and the total moment capacity (M_t) is given by the ratio β (Figure 4.7). The total moment consists of the moment capacity provided by the post-tensioning and the moment capacity provide by the dissipative reinforcement (M_s) meaning the factor is calculated as:

$$\beta = \frac{M_{pt}}{M_t} = \frac{M_{pt}}{M_s + M_{pt}} \tag{4.1}$$

Although a simple concept, this ratio provides the cornerstone in the understanding of the system performance. Clearly, during design this choice affects both damping and moment capacity of the system and therefore changing this value has a direct effect on both capacity and demand.

During the experimental campaign the size of the structural members, building layout and mass were not altered, however different values of post-tensioning and steel moment capacity contributions (thus variations in the value β) were investigated.

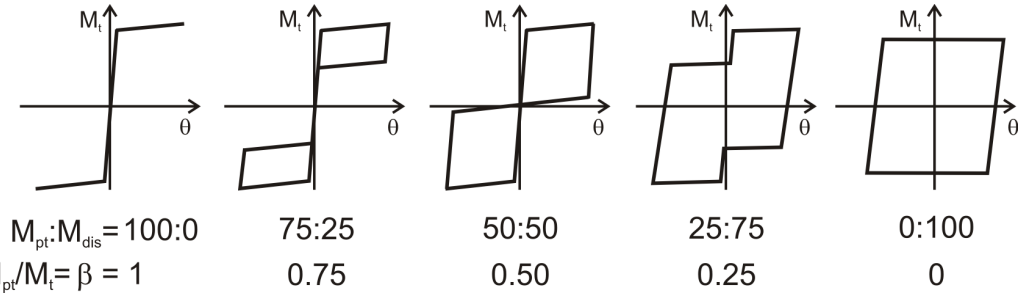

Figure 4.7. Connection moment response of an idealised flag-shaped system with varying levels of the parameter β

Alternative methods of calculating this ratio exist such as the ratio, λ, presented in the fib (fib 2004) and New Zealand (NZS3101 2006) post-tensioned concrete design information. This factor is defined as:

$$\lambda = \frac{M_{pt}}{M_s} \tag{4.2}$$

The factor β has been used in this work as when low moment resistance capacity is provided by the dissipative reinforcing (i.e. low values of Ms), which is more common in post-tensioned timber frame structures compared to their concrete counterparts, the factor λ tends towards infinity.

In the design of the test specimen the predicted moment capacity M_t and recentring ratio β were calculated using the post-tensioned timber design method which is described in Chapter 5. The results of these predictions are shown in Table 4.2.

The test cases shown in Table 4.2 were based around the design case of PT 150KN 2 ANGLES which satisfied the required building demand (ϕM_t = 0.9 x 69 kN = 62 kN > 49 kN) and had an adequate recentering ratio (β ≈ 0.55). The order of tests shown in Table 4.2 is not the chronological order in which testing was performed.

All tests used a modified version of the ACI loading protocol (ACI T1.1-01 & ACI T1.1R-01 2001; ACI T1.2-03 2003) as shown in Figure 4.8. This protocol applies increasing levels of inter-storey drift (as column top displacement) with two cycles

being applied at each drift level. A maximum drift level of 2.5 % was reached in each test.

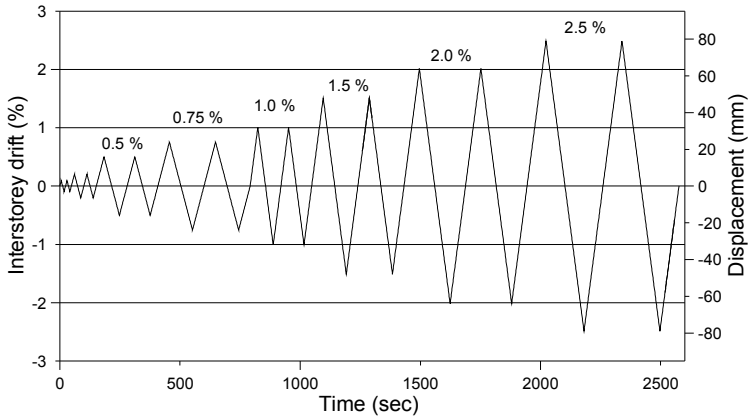

Drift (%)	Disp. (mm)
0.10	3
0.20	6
0.50	16
0.75	24
1.00	32
1.50	48
2.00	64
2.50	79

Figure 4.8. Load protocol used in all testing

4.8 RESULTS OF FULL SCALE BEAM-COLUMN TESTING

4.8.1 Post-tensioned only testing

The first tests to be performed were without the addition of the steel dissipative reinforcing devices or the application of shear loading. A post-tensioned only joint has only one contributor to the moment capacity of the connection with differing moment capacities being obtained by altering the initial post-tensioned values. As shown in Table 4.2 five different levels of initial post-tensioning were applied during testing. Results of the first three tests (PT ONLY 50KN, 100KN and 150KN) are shown in Figure 4.9. Shown in the figure are: force/moment versus displacement/drift response, force in the post-tensioning tendon versus displacement/drift and the neutral axis depth versus displacement/drift response.

It can be seen clearly in Figure 4.9 how an increase in initial post-tensioning affected the response of the beam-column joint for all three parameters presented. In terms of force/moment versus displacement/drift the most evident difference was the increase in moment capacity, M_{con}, which at 2.5 % drift seemed to increase almost linearly with M_{con} = 23 kNm, 32 kNm and 42 kNm for PT ONLY 50KN, 100KN and 150KN, respectively.

Looking at the interaction between the force in the post-tensioning cable and drift the way in which opening of the gap increased the post-tension force can be seen. This

increase in post-tension force is what led to the post gap opening stiffness which can be seen in Figure 4.9a. From Figure 4.9b it can be seen that the increase in post-tensioning with drift decreased with increasing values of initial post-tensioning. This was due to a combination of factors, one of which can be seen in Figure 4.9c which shows the neutral axis depth versus drift. As mentioned in Section 4.4 during the test program the post-tensioning cable was replaced with a high strength steel bar and two more post-tensioned only tests were performed. The results of these two tests are shown in Figure 4.10.

Figure 4.9 and Figure 4.10 show the way in which moment capacity, post-tensioning force and neutral axis depth are linked. In addition to the obvious impact that an increased post-tensioning force had on moment capacity, with increases in initial post-tensioning force the compression area also increased creating and increased neutral axis depth.

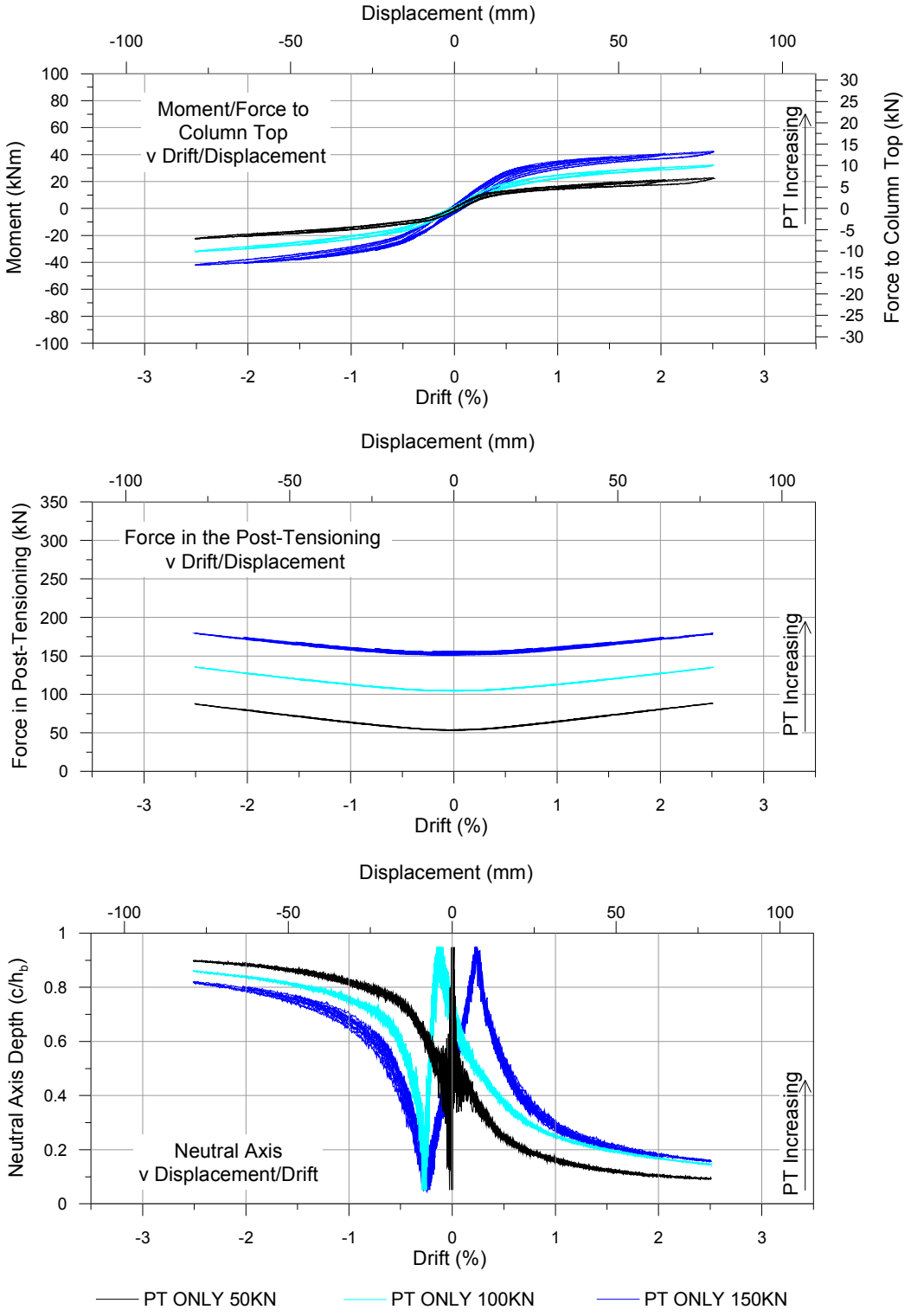

Figure 4.9. Test results for PT ONLY 50KN, PT ONLY 100KN and PT ONLY 150KN

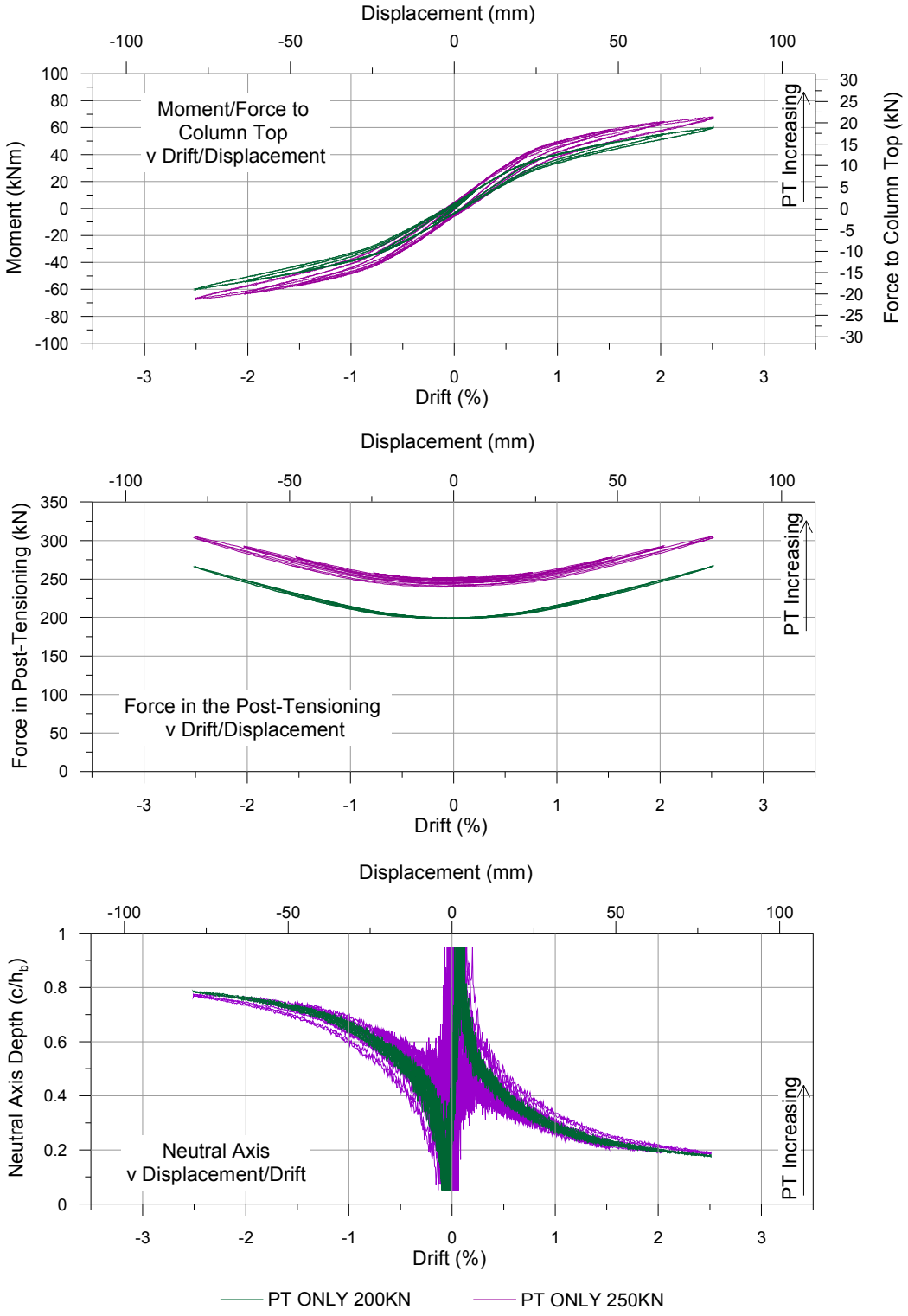

Figure 4.10. Test results for PT ONLY 200KN and PT ONLY 250KN

The trends previously described continue in Figure 4.10 with one major exception. In Figure 4.10b a larger increase in post-tensioning force with drift is seen. This was simply due to the significantly larger area of the post-tensioned bar (552 mm^2

compared with 165 mm^2). This means that although the rate of displacement and strain increases did decrease the larger area meant that higher force increases were present. A summary of all five post-tension only tests performed is shown in Figure 4.11 which illustrates the increased post gap opening post-tensioning force and the subsequent increase in post gap opening stiffness in terms of moment/force versus displacement/drift response.

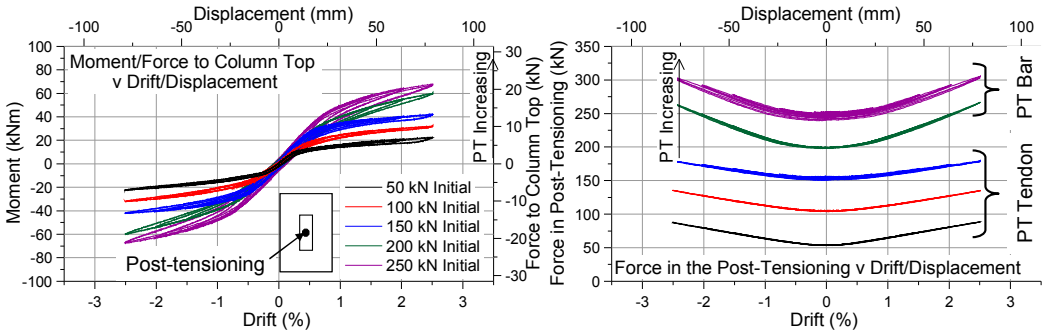

Figure 4.11. Summary of PT ONLY full scale beam-column joint testing results

Photos of the PT ONLY test series at maximum drift levels are shown in Figure 4.12. This test presented the largest amount of gap opening out (10 mm from beam edge to column face at 2.5% drift) of all testing as clearly seen in the figure.

Figure 4.12. Photo summary of PT ONLY 50 kN testing at the maximum 2.5 % drift

Post-tensioned only rotation contributions

As mentioned during the literature review in Chapter 2 one of the key factors in the design of a post-tensioned timber frame is proper understanding of the various rotation contributions which go into making up the total rotation of the frame. This key concept will be revisited in subsequent sections regarding connection design procedures. As shown in Figure 4.6 a series of five displacement potentiometers were

placed across the beam-column connection meaning that the rotation across the connection could be calculated. Figure 4.13 shows the results for the five PT ONLY tests in terms of moment versus connection rotation.

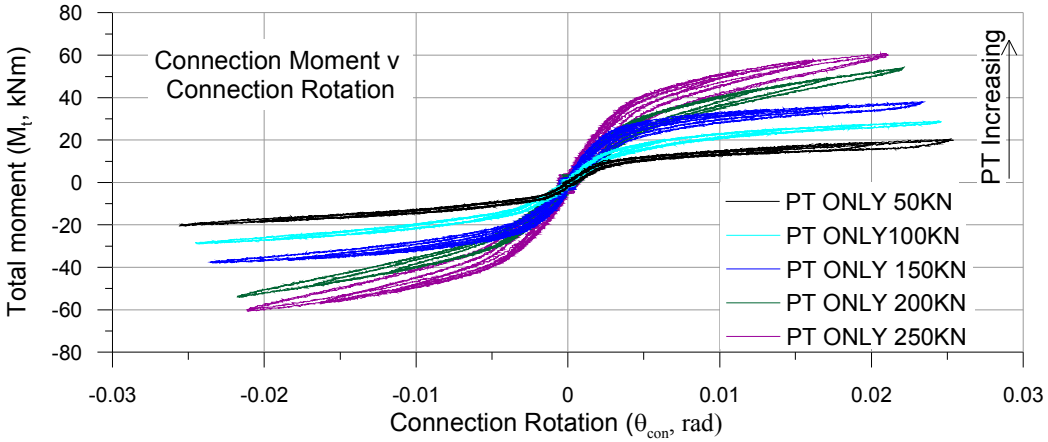

Figure 4.13. Total moment versus rotation graphs for PT ONLY test series

The first point of interest shown in Figure 4.13 is that the beam-column connection clearly had an initial stiffness value, suggesting rotations were occurring in the connection region before decompression. This has previously not been considered as part of a jointed ductile system and will be discussed further in Section 5.3.4. The initial stiffness of the connection seemed to increase with initial post-tensioning value and it can also be seen that the geometric yield point (which presents as a change in slope in the moment-rotation response) seemed to remain similar regardless of initial post-tension value.

Another clear difference between each test is the way in which the total rotations were distributed throughout the beam-column joint. As shown in Figure 4.11 all tests were carried out up to a maximum drift of 2.5% (thus giving a maximum total rotation θ_t = 0.025 rad) however as the initial post-tensioning increased the maximum rotation in the connection decreased. This means that as the initial post-tensioning increased the rotations outside the beam-column connection (i.e. in the column and beam) must have increased. This will be further discussed in Section 4.11.

4.8.2 Post-tensioning with dissipative reinforcing testing results

As mentioned in Section 4.7 on completion of the PT ONLY testing the reinforcing steel angles introduced in Chapter 3 were added to the beam-column joint for Phase 2 of the test programme. As with the PT ONLY testing five different tests were

performed with three tests being performed with the post-tensioning tendon and two tests with the use of the post-tensioning bar. The results of the first three tests performed, those with the use of the post-tensioned tendon, are shown in Figure 4.14. This figure clearly shows the way in which the addition of the steel angle elements increased the hysteretic damping of the beam-column joint. The figure also shows the way in which the selection of the recentering ratio (β) affected the amount of damping present.

From the results it can also be seen that the differing amounts of dissipative reinforcing applied had little to no effect on the increase in post-tensioning value or the neutral axis depth, providing the initial post-tensioning value remained constant. This is as expected as at high levels of drift the elements were yielding both in tension and compression and thus cancelled each other out in the force equilibrium equation leaving the force in the post-tensioning to determine the size of the compression area and subsequent strain/force increases in the post-tensioned element.

The final cycle of all three tests did however show a loss in moment capacity. This was due to the failure of the dissipative angles in bending as discussed in Section 3.5. This failure mechanism is displayed during the maximum drift cycle of test PT 150KN 2 ANGLES in Figure 4.16. This testing was performed prior to the development of the holed dissipative reinforcing angles discussed in Chapter 3 and therefore these elements, which are not susceptible to this type of failure, were not considered.

Upon study of the results of the PT 150KN 2 ANGLES test it was clear that the hysteretic damping present was less than what was expected. It was also noted that during testing frequent clicking noises were coming from the dissipative reinforcing connection. Instrumentation was subsequently placed in order to measure the displacement between the steel angle and the reinforcement attachment steel plate as well as the steel plate and the beam. During the subsequent tests displacements of up to 2 mm were recorded between the plate and the beam with less significant displacement (0.2 mm) between the dissipative device and the plate. Although a displacement of 2 mm may seem insignificant it is important to note that the total displacement to which the steel angle was subjected due to the gap opening was 9 mm and therefore over 22 % of displacement was lost through the plate sliding. This loss

had a significant impact on ductility demand as well as delaying the yielding of the device thus impacting negatively on dissipation capacity. For following testing the screws attaching the plate to the beam face were tightened (before test PT 100KN 2 ANGLES) which significantly reduced this sliding and increased the effectiveness of the dissipative devices. This result is in support of the discussion regarding the rigidity of dissipative reinforcing connections presented in Section 3.9.

The final two hybrid tests involved the use of the high strength bar described in Section 4.4. The results of these two tests (PT 200KN 2 ANGLES and PT 250KN 2 ANGLES) are shown in Figure 4.15. As seen all testing displayed stable hysteretic damping loops of varying levels depending on the amount of reinforcing used and the amount of initial post tensioning. It can also be seen that due to the low yield displacement of the ID3 angle device (0.7 mm as shown in Table 3.5) dissipation begins almost congruently with gap opening allowing each hybrid solution to dissipate as much as physically possible.

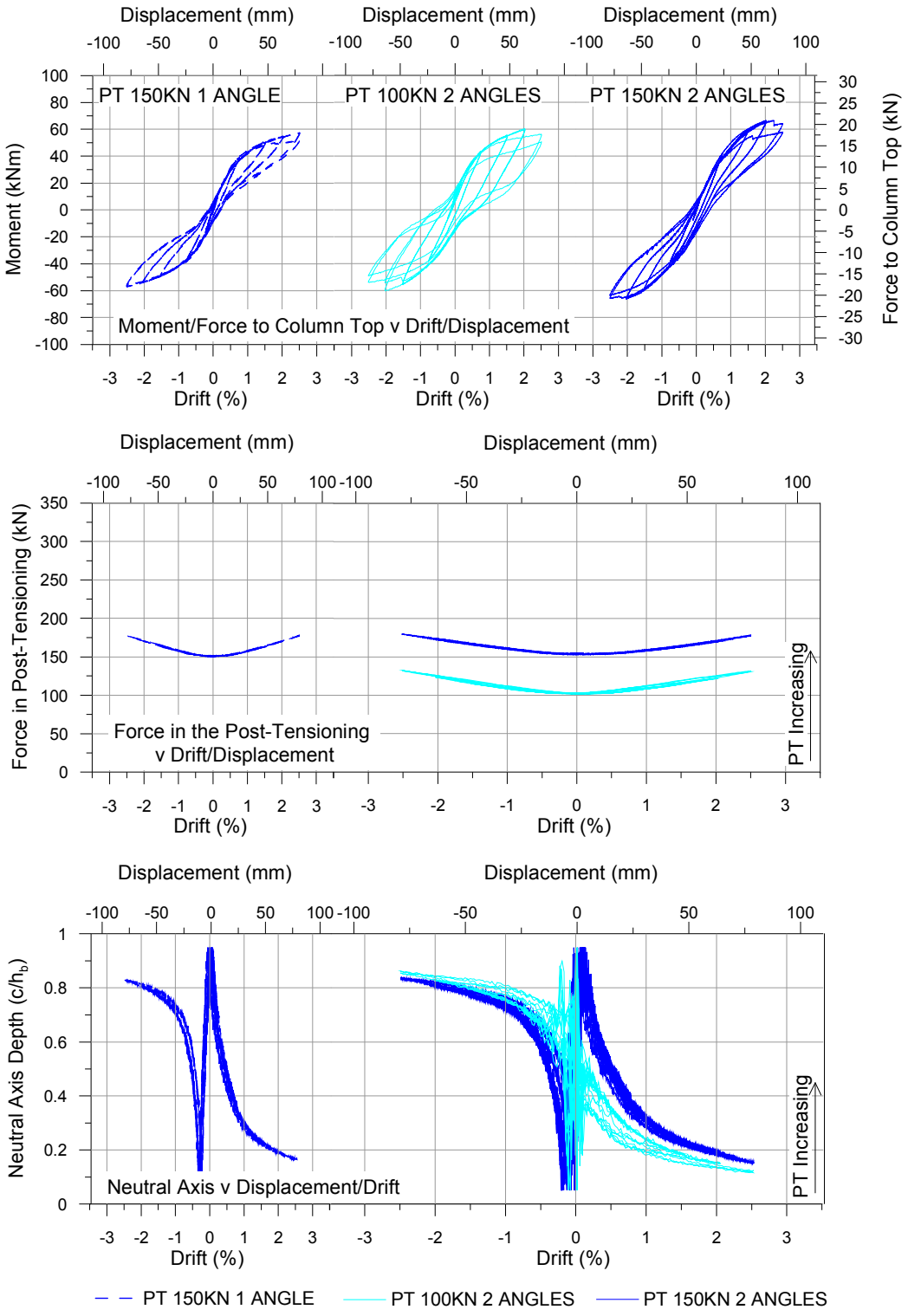

Figure 4.14. Test results for PT 150KN 1 ANGLE, PT 100KN 2 ANGLES and PT 150KN 2 ANGLES

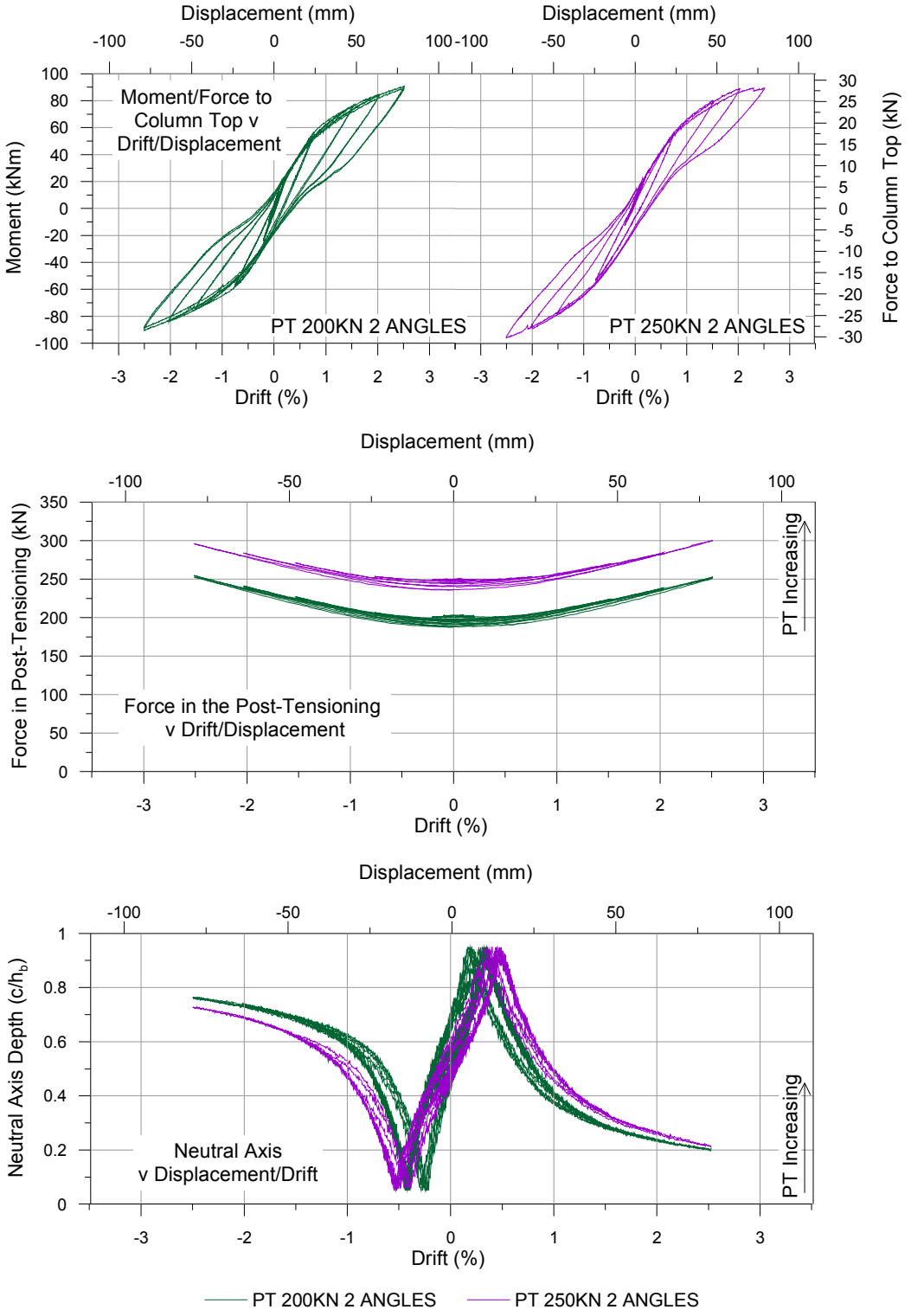

Figure 4.15. Test results for PT 200KN 2 ANGLES and PT 250KN 2 ANGLES

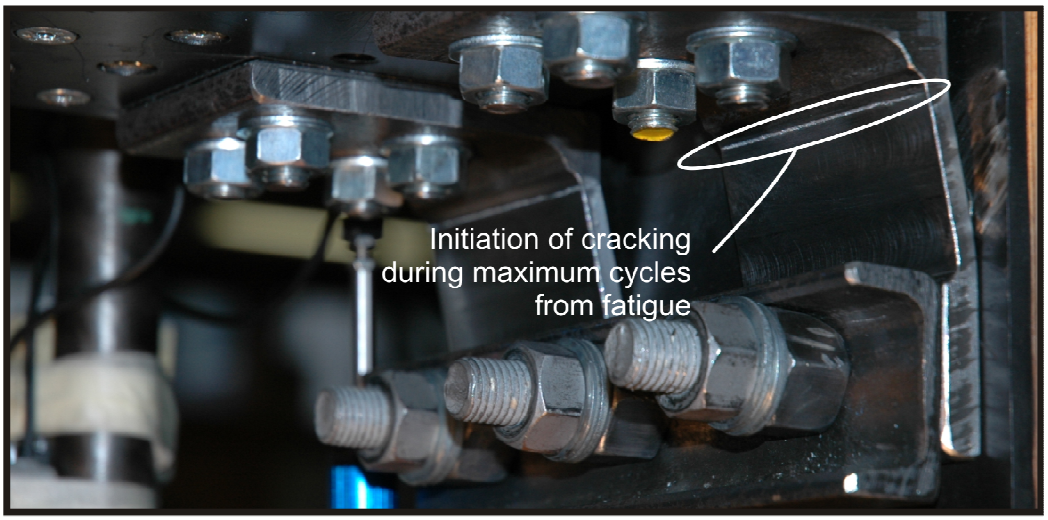

Figure 4.16. Failure of milled dissipative reinforcing angles during maximum cycle of test PT 150KN 2 ANGLES

4.8.3 Testing with Shear Loading

In the design of the beam-column joint a steel tube was inserted into the beam which rested inside a pocket cut into the column (Figure 4.2b)

The key to any shear transfer system in a rocking connection is that it must be able to transfer shear forces without hindering the rocking motion crucial to system performance. For this reason previous solutions used in the design of post-tensioned timber buildings have opted to support the beam from below through the use of either a steel angle or a timber corbel. As shown in Figure 4.17 a triangular arrangement of steel mass was applied to the beam-column joint in order to simulate gravity shear loading on the beam. This mass was applied to a small section of timber floor which was added to the system. This mass simulated the full gravity dead loading and 30% of the 3 kPa live loading of an office structure (G + 0.3Q, approx. 50 kN and resulting in 34 kN shear force at the column face). The triangular force distribution which was used in order to simulate gravity loading is also shown.

It is noted that this load distribution does not respect the way in which the beam would be loaded as part of a complete frame system, however, as these conditions are already not respected due the presence of the beam end hinge shown in Figure 4.4c the goal of the load configuration was to concentrate as much of the loading as a shear force at the column face as possible.

Several comparisons between test configurations with (in colour) and without (in black) shear loading are displayed in Figure 4.18 which shows direct comparisons of the key parameters (force/moment, tendon force and neutral axis depth) for identical tests with and without loading. From these graphs the success of the shear transfer system is displayed clearly as rocking was allowed to occur unhindered under seismic displacement as displayed by the almost identical performance of the beam-column joint with and without the shear loading.

Figure 4.17. Application of joint gravity load to full scale beam-column joint

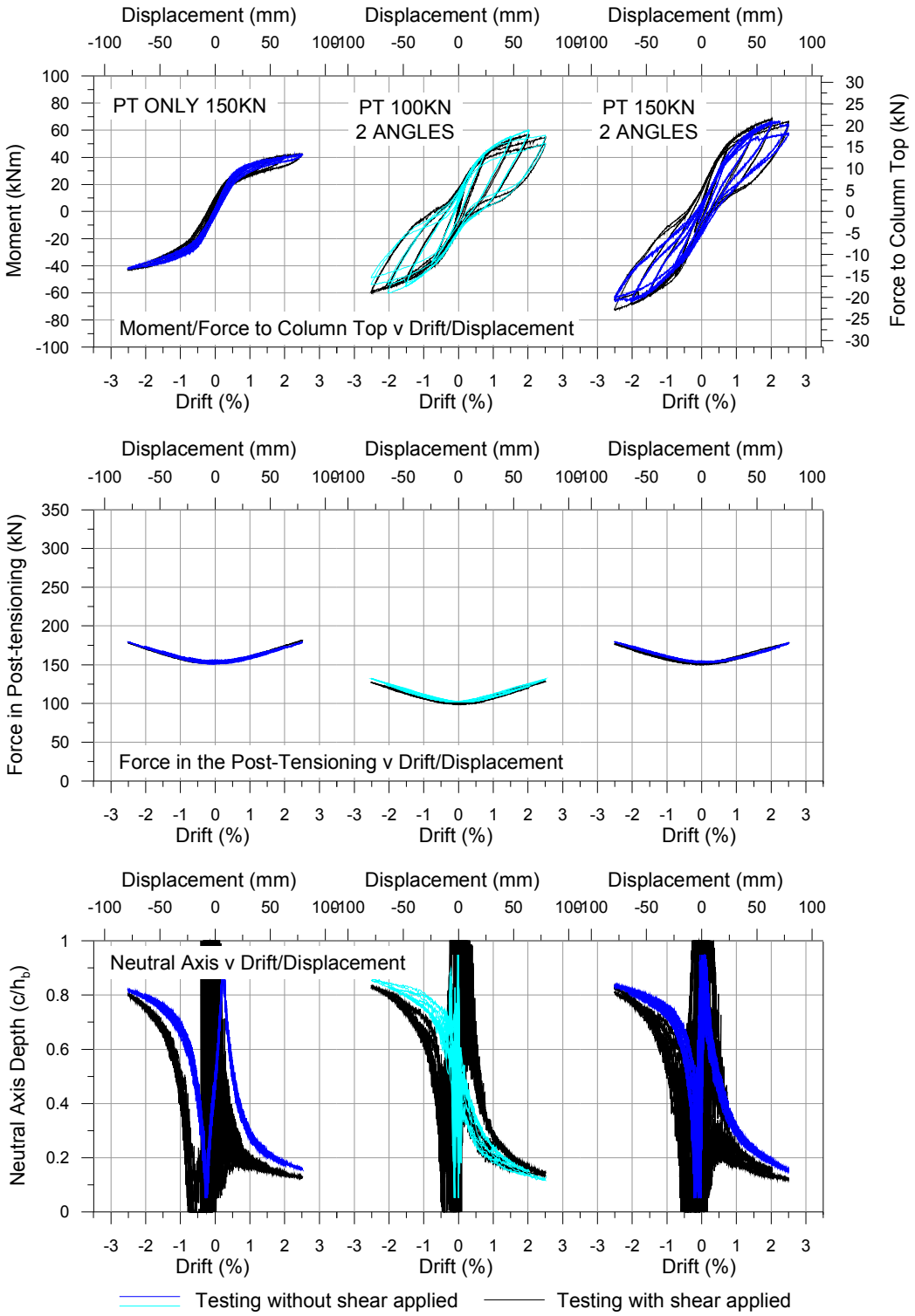

Figure 4.18. Comparison of testing with and without shear loading

4.9 EQUIVALENT VISCOUS DAMPING (EQV)

In order to further analyse the contribution to system performance of the dissipating steel angles, a study was performed to calculate the equivalent viscous damping (ζ_{EQV}) of each of the ANGLE test series system responses described previously. To do this the equation proposed by Jacobsen (1960) was used. This formula equates the energy absorbed by hysteretic steady-state cyclic response at a given displacement level to the equivalent viscous damping of the substitute structure. The formula is represented as a fraction of the critical damping:

$$\zeta_{EQV} = \frac{A_h}{2\pi F_m \Delta_m} \tag{4.3}$$

Where:

A_h = The area within one complete cycle of stabilized force-displacement response

F_m = Maximum force achieved in the loop

Δ_m = Maximum displacement achieved in the loop

This procedure has been shown to be acceptable for the estimation of EQV for systems with relatively low levels of energy absorption in hysteretic response which the flag shaped systems can be considered to be (Chopra 2001). Figure 4.19 shows the Equivalent Viscous Damping for each of the ANGLES test series. The dashed line in the figure indicates the behaviour of the second cycle.

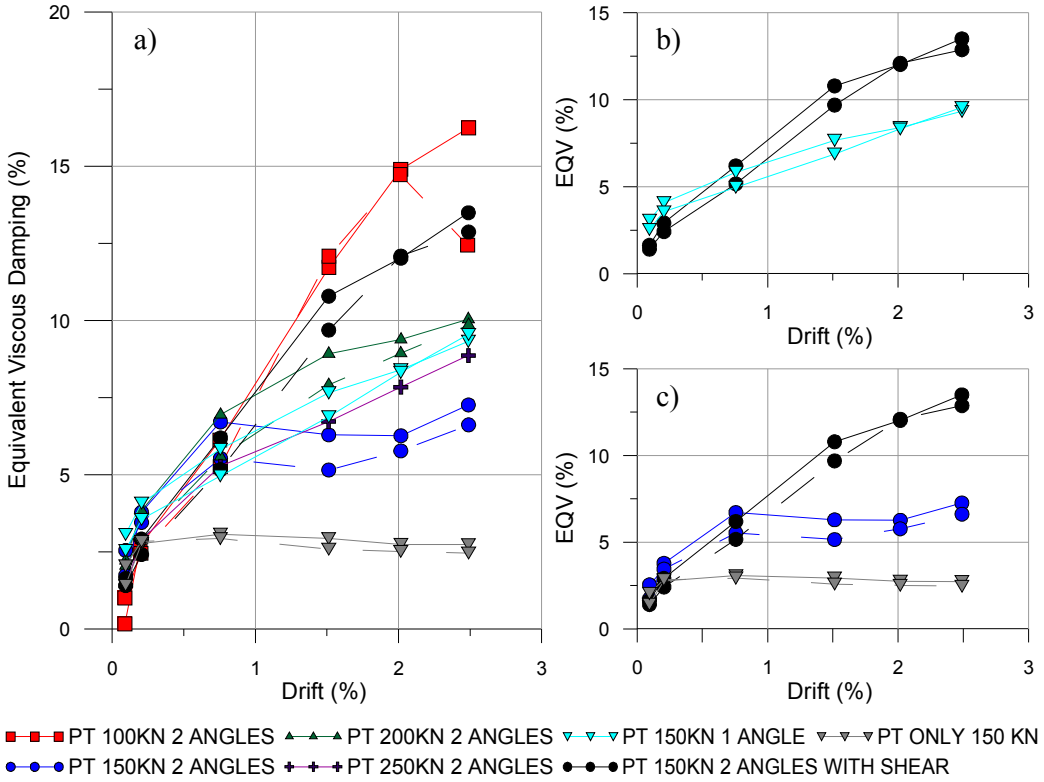

Figure 4.19. Comparison of equivalent viscous damping a) all configurations, b) 150 kN initial single and double angle and c) 150 kN double angle with and without shear (dashed lines in the figures indicate the behaviour of the second cycle)

As expected, Figure 4.19a shows that when the quantity and placement of the dissipating reinforcing angles was constant, increasing the amount of initial post-tensioning force decreased the amount of damping in the system (through a reduction in β). One exception to this was the PT 150KN 2 ANGLES test which presented a lower dissipation value when compared to PT 250KN 2 ANGLES which was due to the slipping of the attachment plate as previously described.

A comparison between the PT 150KN 2 ANGLES test with and without shear loading is shown in Figure 4.19c which displays the significant improvement of the system dissipation due to the tightening of the connection screws. This highlights the crucial role which the connection of the dissipative reinforcing device plays in the overall performance of the system as discussed in Section 3.9. It can be seen however that even with a poor dissipative reinforcing connection the value of equivalent viscous damping was approximately double that of the post-tensioning only system from 2% to 6 – 7%.

The dashed lines show that low or no degradation of the dissipative capacity of the system was observed between the 1st and 2nd cycle. However, it can be seen from the final point of the second cycle of test PT 100kN 2 ANGLES a reduction in damping occurred. This corresponded to the fracture of a single dissipative reinforcing device (accompanied by a reduction in moment capacity shown in Figure 4.14). The fracture was related to fatigue failure of the element due to the high number of cycles to which they were subjected. It is worth noting however that cyclic testing in this manner is particularly demanding with regards to cyclic fatigue and during a real seismic event often only 2 or 3 large cycles will be required of the structure.

The equivalent viscous damping value of one of the post-tensioning only tests was also calculated and shown in Figure 4.19a as a grey line. It can be seen that the value was stable at around 2.5%. The same effect in increasing or decreasing system dissipation can be seen Figure 4.19b where the initial post-tensioning force was constant (150kN) with a single (1+1) or double (2+2) angles (increasing β). It can be seen how the amount of dissipation went from 2 – 5% to 5 – 12% with the addition and activation of the angles.

4.10 RESIDUAL DISPLACEMENTS

In the section above the effects of the ratio between the moment contribution of the post-tensioned element and the total moment capacity of the beam-column joint (β) on equivalent viscous damping has been discussed. It is important to note however that with this increased amount of dissipative capacity the residual displacements of the structure also increase.

The effects of residual displacement on post-earthquake recovery have already been discussed in Section 2.1 relating to the way in which post-event displacements can have a significant impact on the recoverability of a structure. In fact, in some cases although a structure has performed relatively well during a seismic event, large residual displacements lead to costly repair or even a complete loss of the structure.

Figure 4.20 shows the way in which the dissipative capacity of a beam to column joint (measured as EQV) relates to residual drift after each test cycle.

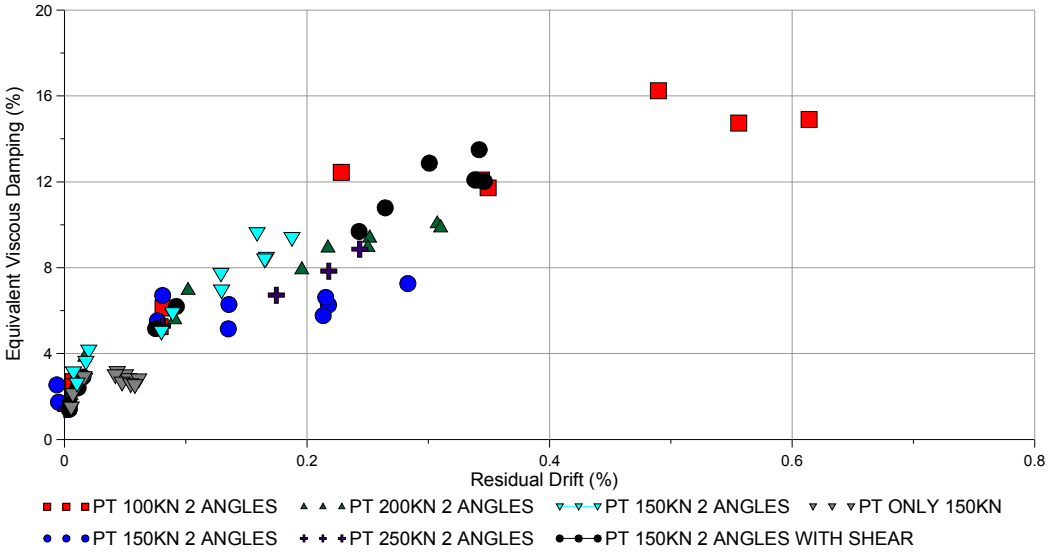

Figure 4.20. Equivalent viscous damping versus residual drift for beam-column testing

Figure 4.20 shows an almost linear relationship between EQV and residual drift with residual drifts increasing as maximum drift and thus damping increases. It is important to note however that seismic action is not well represented by the quasi-static loading protocol selected for this testing. In a real event, small cycle accelerations/displacements occur following the main shock which contribute significantly to the reduction of residual displacements. Residual displacements under dynamic loading are further discussed in Sections 6.5.1 and 6.6.1.

4.11 ROTATION CONTRIBUTIONS IN THE BEAM-COLUMN JOINT

For the design of a post-tensioned timber connection it is crucial to understand the rotation and amount of gap opening which will occur at a given level of drift. The contributions to the total frame rotation (θ_t) are shown in Figure 4.21. The first three of these are elastic rotations and thus fully recoupable at the end of a displacement cycle. These relate directly to the moment capacity of the beam-column connection and are named: the elastic beam deformation (θ_b) composed of both shear and flexural deformations, the elastic column deformation (θ_b) composed of both shear and flexural deformations, and the joint deformation (θ_j) made up of only shear deformations. The final contribution is the deformation occurring at the connection between the beam and column, the connection rotation (θ_{con}). It is this latter deformation that directly affects the performance of a post-tensioned timber frame and therefore is of the greatest interest. Formulas for the calculation of these rotation contributions are presented in Section 5.4.

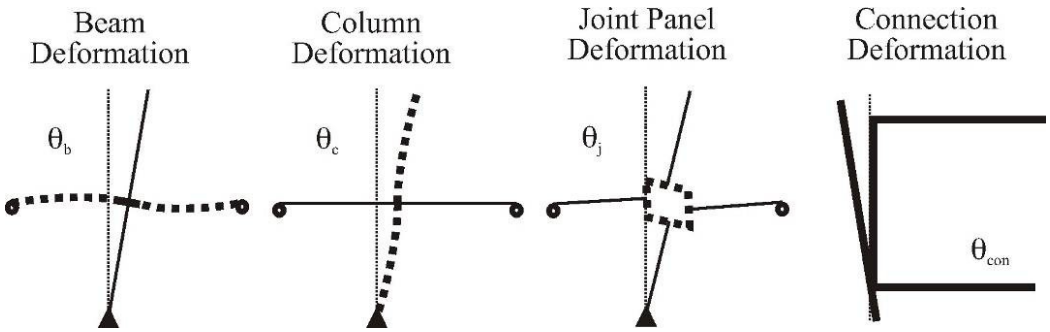

Figure 4.21. Contributions to the total rotation of a post-tensioned beam-column joint.

Figure 4.22 shows the beam, column, joint and connection rotation contributions to the testing performed without the application of the dissipating angle. Rotation contributions are shown both as a percentage of the total rotation (top) and as absolute values (bottom, in radians).

Figure 4.22 shows the way in which the elastic rotation contributions (θ_b, θ_c, θ_j) represented a significant proportion of the total system rotation (θ_t). It can also be seen that the contributions of the elastic rotation contributions increased with higher moment capacity of the joint. It is seen that in the most extreme case, PT ONLY 250KN, 20 – 25% of total rotation was provided by elastic rotations.

The importance of understanding this fact in design is described further in Section 5.4.5. It should be noted that the accuracy of data at low drift levels may not be high due to rotations being deduced from very low level displacements.

Figure 4.23 shows the beam, column, joint and connection rotation contributions to the testing performed with the application of the dissipative angle reinforcing. Rotation values for the testing are shown in red with the PT ONLY testing having the same initial post-tensioning value being shown alongside in black.

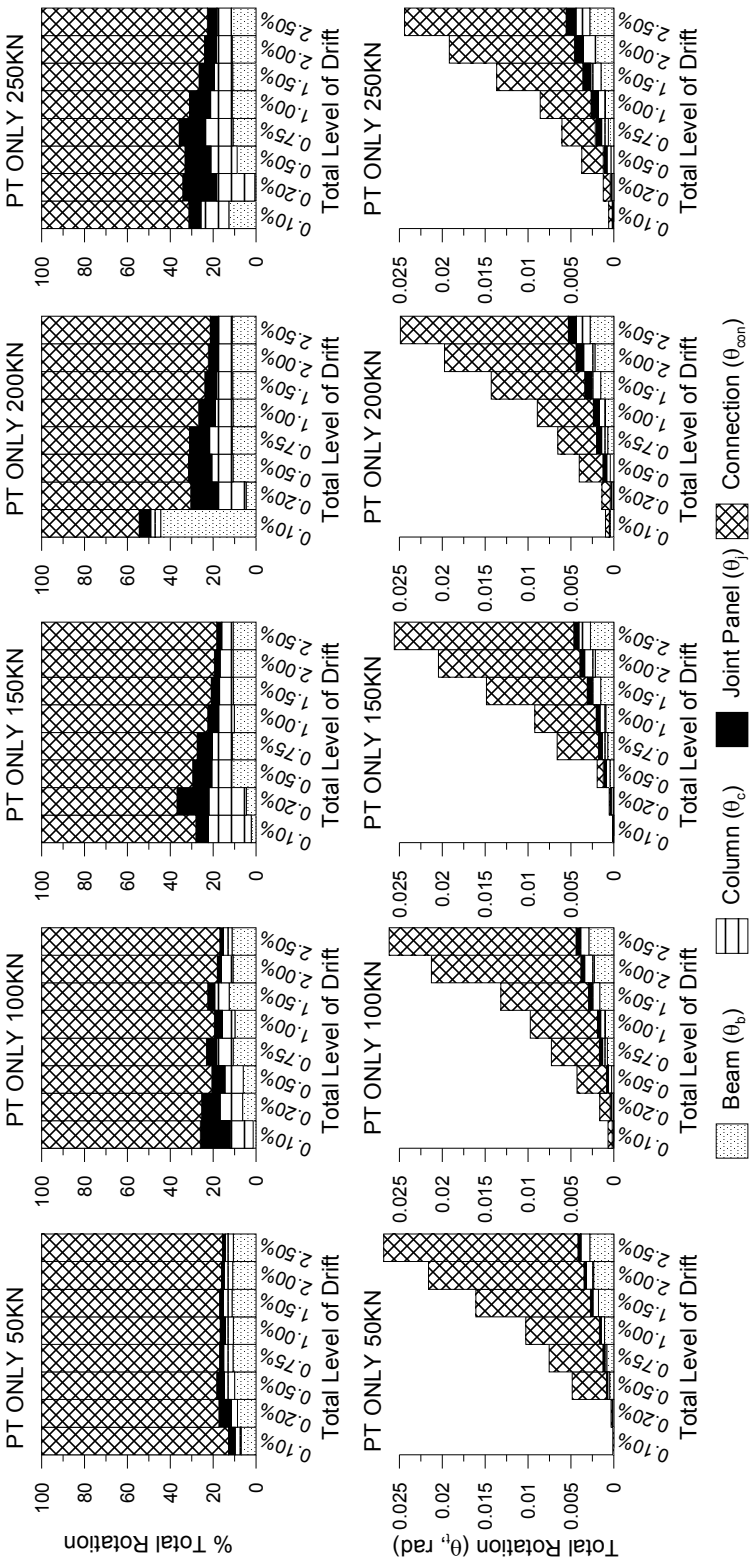

Figure 4.22. Rotation contributions for PT ONLY 50KN, PT ONLY 100KN, PT ONLY 150KN, PT ONLY 200KN and PT ONLY 250KN

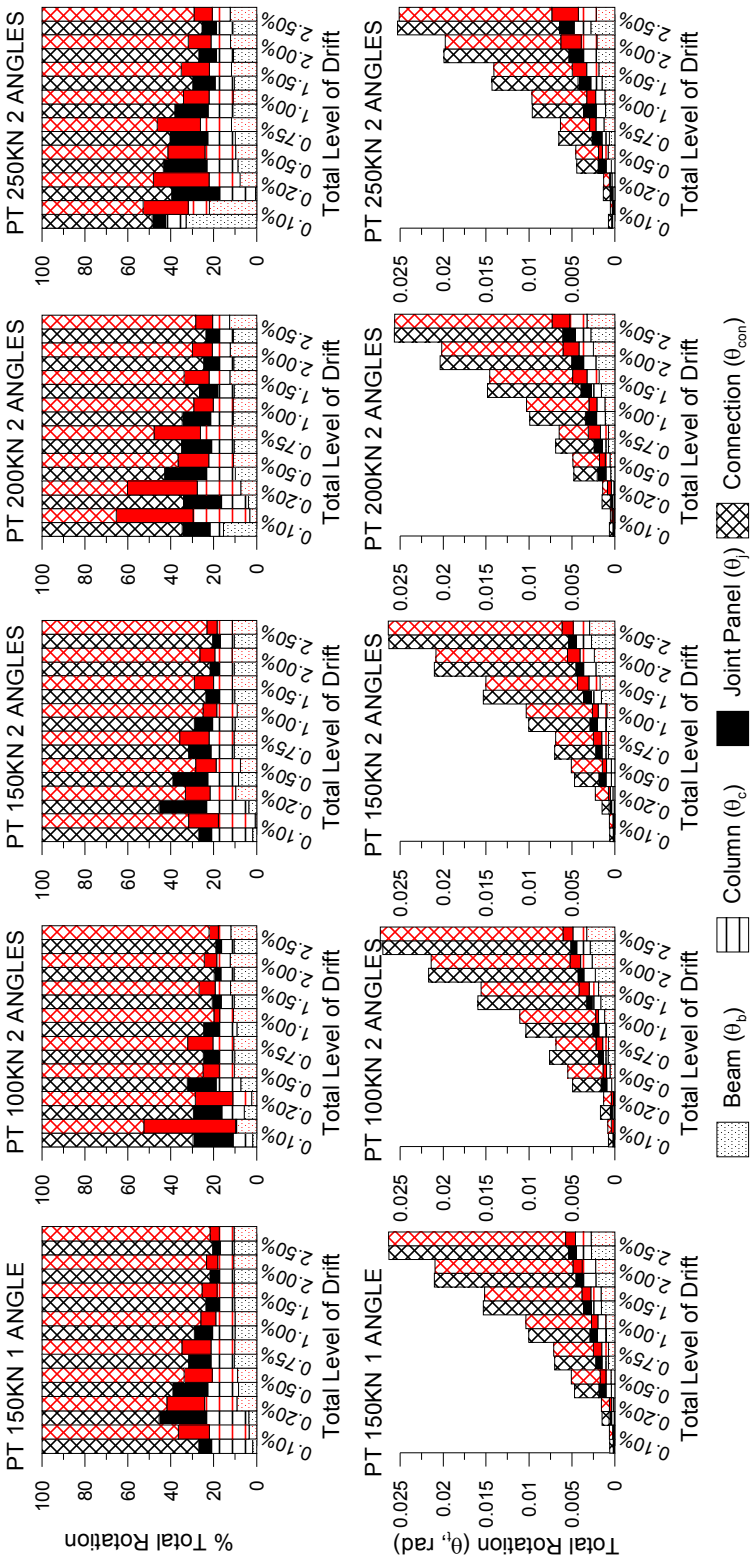

Figure 4.23. Rotation contributions for PT 150 KN 1 ANGLE, PT 100KN 2 ANGLES, PT 150KN 2 ANGLES, PT 200KN 2 ANGLES and PT 200KN 2 ANGLES (in red) compared to corresponding PT ONLT test cases Solutions (in black)

Figure 4.23 again shows the way in which the increase in moment capacity increased the contributions of the elastic deformations. This can be seen two-fold in Figure 4.23;

firstly as with the PT ONLY testing, an increase in initial post-tensioning value led to an increase in elastic contributions. Secondly it can be seen that an increase in elastic contributions occurred between testing having the same initial post-tensioning value with and without the angle devices. With the addition of the angle devices the moment capacity of the beam-column connection was increased and therefore elastic rotations were increased.

4.12 CONCLUSION FROM CHAPTER 4

In this chapter the quasi-static testing of a full-scale post-tensioned beam-column connection has been presented extending post-tensioned timber technology to the use of glue laminated timber and applying a new form of mild steel hysteretic reinforcing.

Testing has been performed quasi-statically on an external beam-column joint taken from a 5-storey prototype office structure. 21 tests have been performed on varying test configurations from which 13 key tests have been selected and presented.

The PT ONLY series of 5 tests (moment capacity provided solely from the post-tensioning tendon/bar) displayed that the re-centering, damage-free characteristics of post-tensioned timber, which have been displayed through the testing of the system in combination with laminated veneer lumber are retained when glue laminated timber is used.

The PT ONLY test series also displayed the way in which the post-tensioning bar or tendon related to the post-gap-opening stiffness of the beam-column joint. Testing showed that when the same post-tensioning is retained, be it a single tendon or a bar, increases in initial post-tensioning force led to an increased neutral axis depth.

The ANGLES test series consisted of 5 tests with moment capacity contributions being provided by the post-tensioning and the dissipative angle reinforcing presented in Chapter 3. The ratio between the moment capacity provided by the post-tensioning and the total capacity of the connection has been introduced as the factor β. The addition of the angle reinforcing both increases moment capacity, hysteretic damping, and post-gap-opening stiffness.

Testing results have been compared between the beam-column joint with and without the presence of a vertical shear load. No significant change in test response was

observed showing the shear transfer system to be effective. This shear transfer system was a steel tube glued into the beam and resting in a pocket inside the column.

The increase in hysteretic damping provided by the reinforcing has been measured as Equivalent Viscous Damping (EQV). Values of EQV range between 7% and 16% depending on the ratio between the moment capacity provided by the reinforcing and the total moment capacity. Increased hysteretic damping created increased (static) residual displacement.

Finally the contributions to the total beam-column rotation were presented. This showed that the elastic rotation contributions of the beam, column and joint panel made up a significant proportion of the total rotation (between 18 - 25 %). Indications were clear that these elastic rotations depended on moment capacity, be it from initial post-tensioning values or steel reinforcing.

REFERENCES CHAPTER 4

Chopra, A. K. (2001). *Dynamics of Structures: Theory and Applications to Earthquake Engineering*, Prentice-Hall, Upper Saddle River, NJ, USA.

ACI T1.1-01 & ACI T1.1R-01. (2001). "Acceptance Criteria for Moment Frames Based on Structural Testing." American Concrete Institute. A. C. Institute

ACI T1.2-03. (2003). "Special Hybrid Moment Frames Composed of Discretely Jointed Precast and Post-tensioned Concrete Members." American Concrete Institute. A. C. Institute

fib Bulletin 27. (2004). "Seismic Design of Precast Concrete Building Structures." fib

Jacobsen, L. S. (1960). "Damping in Composite Structures." 2nd World Conference on Earthquake Engineering, Tokyo and Kyoto, Japan.

EN 1995-1-1:2004. (2004). "Design of Timber Structures Part 1-1: General - Common Rules and Rules for Buildings." European Committee for Standardization.

NZS 3101:1995. (2006). "Concrete Structures Part 1. The Design of Concrete Structures." Standards New Zealand.

5 Analytical Modelling of the Local Response of Post-Tensioned Timber Frames

5.1 PRINCIPAL CONCLUSIONS OF CHAPTER 5

Chapter 5 presents procedures for assessment of the capacity of a post-tensioned frame and compares this against the beam-column joint test results presented in Chapter 4. The following principal conclusions are drawn.

1. Following decompression, the elastic form of the Modified Monolithic Beam Analogy accurately predicted the moment-rotation response of the post-tension beam-column joint

2. Prior to decompression an interface compression rotation occurred dependent on the conditions (e.g. reinforcing, size) of the column face.

3. Although the standard practice in concrete structures is to assume that strain increases in the post-tensioned elements following decompression are directly related to the gap opening, elastic shortening of the timber frame elements (beam and column) led to reduced strain increases in the post-tensioned beam-column joint. This reduction must be accounted for.

4. Formulas are presented in order to calculate the elastic contributions of the beam (θ_b) column (θ_c) and joint panel (θ_j). These elastic rotations made up a significant part of the total beam-column rotations.

5. Current methods for calculating the Area Based Damping/Equivalent Viscous Damping slightly overestimated damping for low values of recentering ratio (low β), however values were acceptable.

5.2 INTRODUCTION

This chapter presents the theoretical and analytical approach to modelling a post-tensioned timber beam-column connection which have been developed based on first principles and then confirmed using the results obtained for the beam-column joint presented in Chapter 4.

This chapter will look at the prediction of beam-column joint behaviour through the application and refinement of current design procedures. The chapter will then use these equations to predict local (moment-rotation at the connection) and global (force displacement of the full beam-column joint) behaviour of the beam-column joint discussed in Chapter 4.

Current procedures are first described and compared against testing results. This comparison leads to the recommendation that minor refinements of the procedure must be applied. The chapter looks at design procedures for analysing an existing frame. This means that section sizes, initial post-tensioning and dissipative reinforcing values are known and a capacity is calculated for a given drift. Chapter 10 will address frame design.

5.3 THE MOMENT-ROTATION RESPONSE OF A POST-TENSIONED BEAM-COLUMN JOINT

5.3.1 Moment-rotation response before decompression ($0 < \theta_{imp} < \theta_{dec}$)

Before the onset of gap opening it has been proposed (Newcombe et al. 2008) that zero rotation occurs at the interface between the beam and column until the decompression moment (M_{dec}) is surpassed which is calculated as:

$$M_{dec} = \frac{T_{pt,initial} Z_b}{A_b} \quad \textbf{(5.1)}$$

Where:

$T_{pt,initial}$ = Initial post-tensioning force (kN)

Z_b = Beam elastic section modulus (m^3)

A_b = Beam Area (m^2)

For a rectangular section which does not have a large cavity for the post-tensioned element (i.e. $Z_b \approx b_b h_b^2/6$ and $A_b \approx b_b h_b$) this can be simplified to:

$$M_{dec} = T_{pt,initial} \frac{h_b}{6} \quad \textbf{(5.2)}$$

Where:

h_b = Height of the beam (m)

5.3.2 Moment-rotation response after decompression before timber yield ($\theta_{dec} < \theta_{imp} < \theta_y$)

The development of the Modified Monolithic Beam Analogy (MMBA) has been discussed in Chapter 2 in the way in which it is currently applied to timber. Figure 5.1 shows the nomenclature used in the design of a beam-column as part of a post-tensioned timber frame:

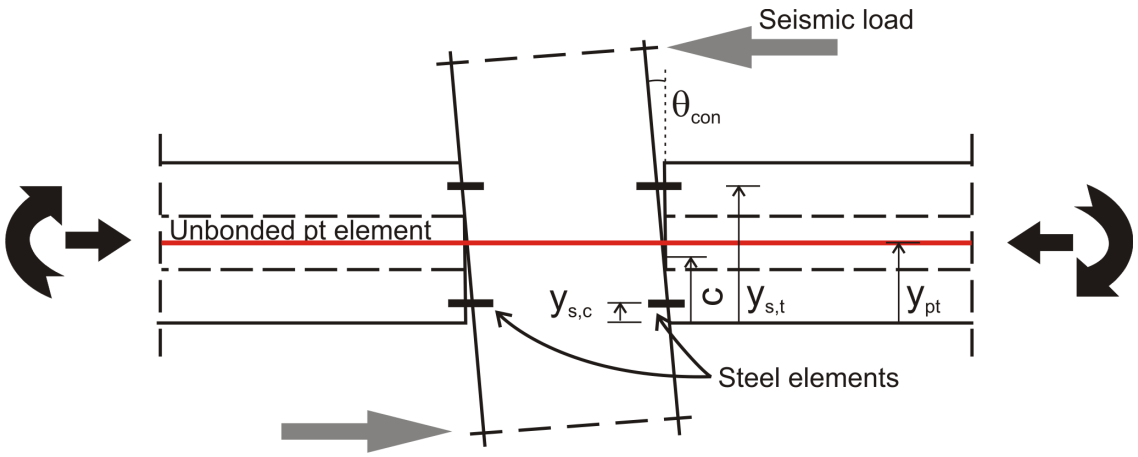

Figure 5.1. MMBA nomenclature for a beam-column joint

Where:

θ_{con} = Connection rotation (rad)

$y_{s,c}$ = Distance between the extreme bottom fibre and the dissipative compression reinforcing (m)

$y_{s,t}$ = Distance between the extreme bottom fibre and the dissipative tension reinforcing (m)

$y_{s,pt}$ = Distance between the extreme bottom fibre and the post-tension element (m)

c = Neutral axis depth (m)

The application of this procedure for a post-tensioned timber beam-column joint with external non-prestressed reinforcement is as follows.

1. Impose a rotation.

A rotation is imposed on the beam-column joint related to the total design drift of the structural frame. In addition the centreline rotation must be transformed to represent the rotation at the beam-column joint. This is done using a simple geometric shift considering a

rigid body assumption and does not account for the elastic deformations of the frame elements which will be discussed in Section 5.4.

$$\theta_{con} = \frac{\theta_{cl}}{\left(1 - \frac{h_c}{L_b}\right)} \tag{5.3}$$

Where:

θ_{con} = Rotation imposed on the beam-column joint (i.e. rotation at the beam-column interface) (rad)

θ_{cl} = Rotation at the centreline of the beam-column joint (rad)

h_c = Column height (m)

L_b = Bay length (m)

2. Assume a neutral axis depth (c).

The neutral axis depth is the point at which the compression zone between the beam and the column ends (Figure 5.1). Initially this value is estimated, iterations are then performed in order to satisfy equilibrium requirements.

3. Evaluate the force in the unbonded post-tensioned elements (T_{pt}).

In order to do this the additional force (ΔT_{pt}) in the post-tensioning due to the opening of the gap at the interface is calculated and added to the initial strain in the post-tensioned element ($T_{pt,initial}$).

$$T_{pt} = T_{pt,initial} + \Delta T_{pt} \tag{5.4}$$

$$\Delta T_{pt} = \Delta\varepsilon_{pt} E_{pt} A_{pt} \tag{5.5}$$

Where:

E_{pt} = Young's modulus of the post-tensioned element (kN/m^2)

A_{pt} = Area of the post-tensioned element (m^2)

$\varepsilon_{pt,\delta}$ = Change in strain in the post-tensioned element

$$\Delta\varepsilon_{pt} = \frac{n_{gap}\Delta_{pt}}{l_{ub}} \tag{5.6}$$

Where:

n = Number of gaps opening along length of the post-tensioned element

l_{ub} = Unbonded length of the tendon from anchorage to anchorage (m)

Δ_{pt} = Displacement between the beam end at the column face due to gap opening (m)

$$\Delta_{pt} = \theta_{imp}\left(y_{pt} - c\right) \tag{5.7}$$

Where:

y_{pt} = Distance between the extreme fibre of the beam and the post-tensioned element centreline (m)

4. Evaluate the force in non-post-tensioned reinforcing elements (T_s and C_s)

The displacements of the tension and compression dissipative reinforcing elements are calculated in the same way as for the post-tensioning:

$$\Delta_{s,t} = \theta_{con}\left(c - y_{s,t}\right) \tag{5.8}$$

$$\Delta_{s,c} = \theta_{con}\left(c - y_{s,c}\right) \tag{5.9}$$

In Chapter 3 the way in which the force-displacement response of the dissipative reinforcing elements is to be calculated was discussed. Using this relationship in combination with the displacements found in Equations (5.8) and (5.9) the force in the tension and compression reinforcing (T_s and C_s respectively) is calculated as a function of their displacement.

$$T_s = f\left(\Delta_{s,t}\right) \tag{5.10}$$

$$C_s = f\left(\Delta_{s,c}\right) \tag{5.11}$$

5. Evaluate the force in the timber at the beam-column interface (C_t)

As it is desirable that the timber remain elastic, the elastic form of the MMBA equations is used in order to calculate the strain in the timber.

$$\varepsilon_t = c\left(3\frac{\theta_{imp}}{L_{cant}} + \phi_{dec}\right) \tag{5.12}$$

Where:

ε_t = Strain at the extreme fibre of the timber beam

L_{cant} = Distance from the face of the column to the point of contra-flexure, for seismic only loading this is taken as half the beam length (m)

ϕ_{dec} = Decompression curvature (m^{-1})

$$\phi_{dec} = \frac{2T_{pt,i}}{k_{gap}E_{t,par}b_b h_b^2} \quad \textbf{(5.13)}$$

Where:

k_{gap} = Factor accounting for the stiffness of the beam to column interface and timber end effect (discussed in Section 5.3.6)

$E_{t,para}$ = The average parallel to grain stiffness of the timber (to be found from the manufacturers technical guidance) (kN/m^2)

Knowing the strain in the timber and assuming a triangular stress block the stress in the timber is calculated:

$$C_t = 0.5k_{gap}\varepsilon_t E_{t,par}b_b c \quad \textbf{(5.14)}$$

6. Check equilibrium

In Step 1 a neutral axis depth (c) was assumed, therefore equilibrium across the interface is now checked to ensure this value is accurate:

$$C_t + C_s - T_s - T_{pt} = 0 \quad \textbf{(5.15)}$$

7. If equilibrium is not satisfied the value of neutral axis depth is updated

Once the tension and compression contributions satisfy equilibrium requirements the moment capacity of the joint can be calculated.

5.3.3 Moment rotation comparison for PT ONLY 50KN, 150KN and 250KN

Figure 5.2 shows the connection moment vs. connection rotation response for tests PT ONLY 50KN, 150KN and 250KN. As can be seen, the MMBA provided reasonable prediction of the moment capacity of the beam-column joint it however did not capture well the initial stiffness of the connection, tending to overpredict testing values. The understanding of the initial stiffness of a beam-column joint and the subsequent impact that it has on the rotation at which gap opening occurs is critical to the correct design of the non-reinforced dissipative

reinforcing elements. As the reinforcing elements also provide hysteretic damping to the frame through the use of some form of concentrated yielding area (see Section 4.11) incorrect rotation values will lead to incorrect yield area design and thus delay of yielding and reduced hysteretic capacity.

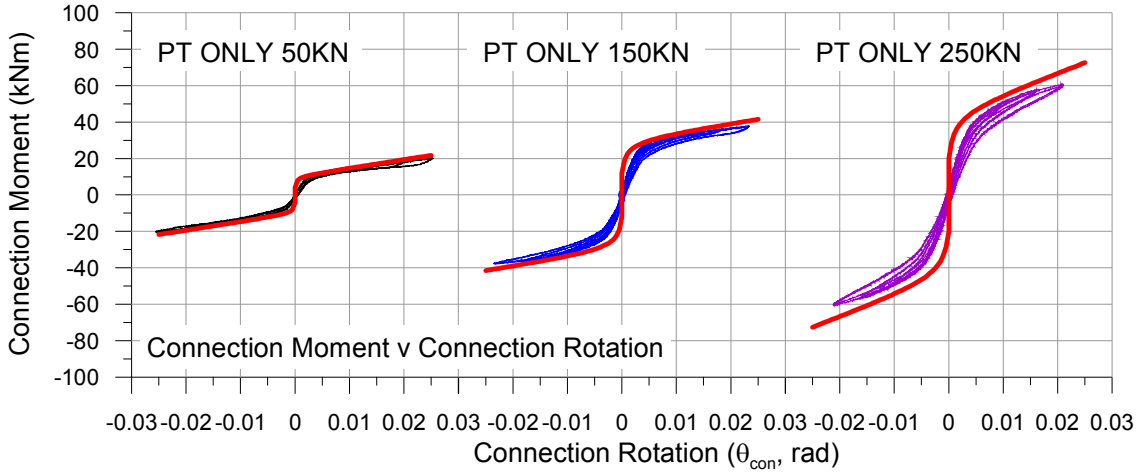

Figure 5.2. Connection moment v rotation for PT ONLY 50KN, 150KN, 250KN compared with MMBA results (in red)

5.3.4 Interface compression deformation θ_{int}

The current form of the MMBA fails to correctly predict the initial stiffness of a post-tensioned beam-column joint. This fact can have a major impact on the accuracy of the full design procedure and can lead to reduced damping capacity and thus higher than anticipated seismic load.

The interface compression deformation (θ_{int}) was first proposed in a paper by van Beerschoten et al. (2011) which described the presence of an additional rotational component due to compression perpendicular to grain deformation at the column face. In this paper the connection rotation was split into two separate rotation components: the aforementioned interface compression rotation and the gap rotation (θ_{gap}). A spring model was applied in order to predict the initial stiffness which will be simplified in the following paragraphs.

In order to better understand the effect of the interface compression deformation on initial stiffness a simple model has been made in ABAQUS (ABAQUS Inc. 2011) where a rigid block ($E \approx \infty$) (the beam) was initially compressed into a low modulus ($E_{t,perp}$ = 460 MPa representing GL32h European glulam) element (the column) which was fully supported along its bottom surface. This initial compression was representative of the application of the initial

tension force to the post-tensioning. Following this the rigid block representing the beam was translated sideways at its end simulating movement due to seismic motion. Figure 5.3 shows the results of this simulation (with colour indicating vertical movement).

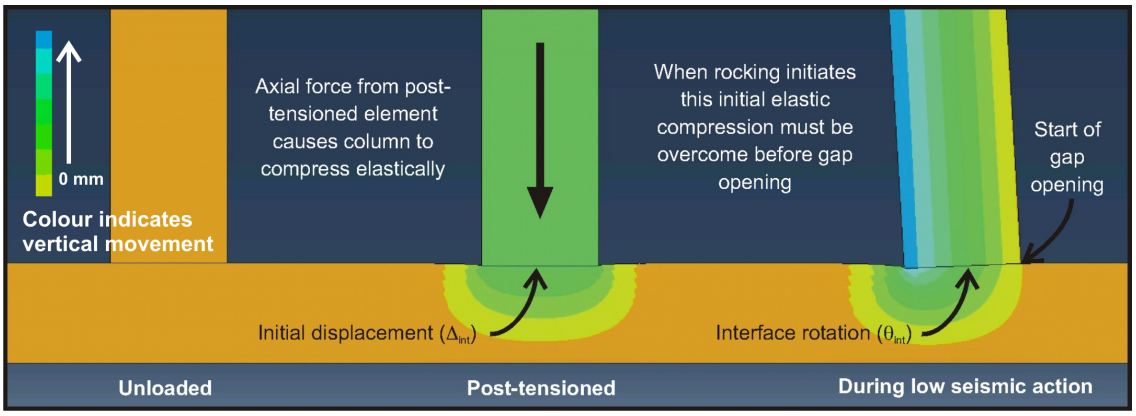

Figure 5.3. Interface compression deformation simulation

The interface deformation shown in Figure 5.3 occurs for any jointed ductile post-tensioned system however, due to the low elastic modulus of timber when compressed perpendicular to the grain (55 times less than that of concrete and 430 times less than steel), it has a much more significant effect for a post-tensioned timber joint.

The interface rotation is elastic and therefore its calculation is relatively straight forward and can be obtained through the following equation:

$$\theta_{\text{int}} = \frac{2\Delta_{\text{int}}}{h_b} \tag{5.16}$$

$$\Delta_{\text{int}} = k_{\text{int}} \frac{T_{pt,i} h_c}{2E_{t,perp} h_b b_b} \tag{5.17}$$

Where:

Δ_{int} = Initial displacement of beam face into column under stress (m)

k_{int} = Interface compression factor which accounts for load shearing and interface reinforcement (described in the following paragraph)

Upon merging equation (5.16) and (5.17) the equation for the interface compression rotation is obtained:

$$\theta_{\text{int}} = k_{\text{int}} \frac{T_{pt,i} h_c}{E_{perp} h_b^2 b_b} \tag{5.18}$$

The interface compression factor, k_{int}

Testing investigating the displacement of a timber block loaded perpendicular to the grain has been performed in order to understand the effects of stress-spreading (Blaβ and Gorlacher 2004) and screw reinforcement (Watson et al. 2013). Following these two testing campaigns a simplified model was developed in order to create a comparison between the test case (having a length allowing stress spreading to occur and with the presence of reinforcement as shown in Figure 5.4a) and a block of timber having a uniform compressive stress and no reinforcing as shown in Figure 5.4b.

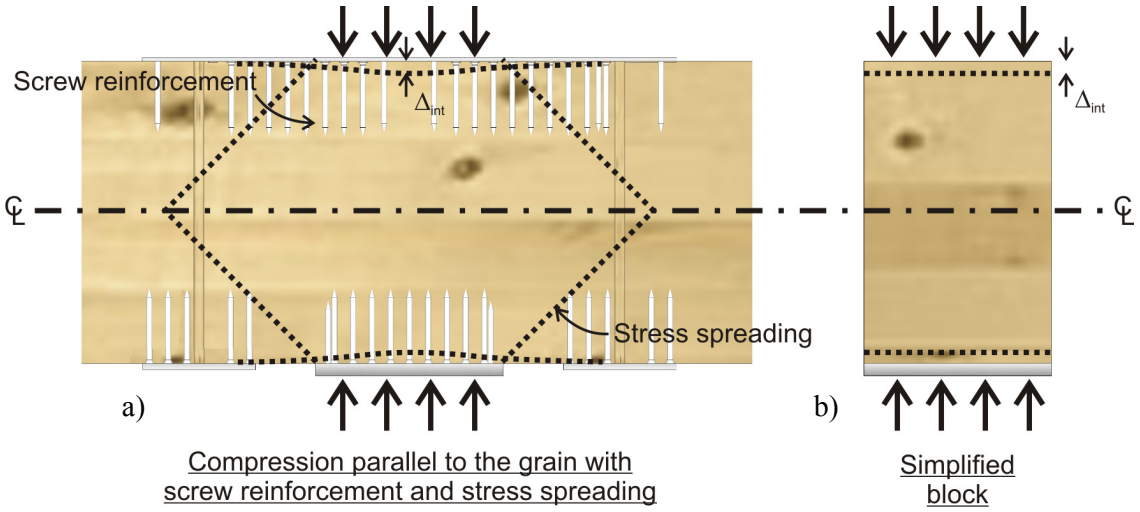

Figure 5.4. Deformation of a timber block under perpendicular to the grain compression loading a) with and b) without stress spreading and screw reinforcement

Two formulas have been defined by Watson et al. (2013) in order to account for the stress spreading (k_{ss}) and screw reinforcement (k_{scr}). The first of these was based on the work performed by Blaβ and Görlacher (2004) and is defined as:

$$k_{ss} = \frac{h_c}{b_L \ln\left(\frac{h_c}{b_L} + 1\right)} \tag{5.19}$$

Where:

b_L = The length of the loaded area (taken as the beam height h_b) (m)

The second equation accounting for the screw reinforcement derived by Watson et al. (2013) is defined as:

$$k_{scr} = 1 + 54\frac{A_{scr}}{A_t}\left(\frac{l_s}{h_c}\right)^{1.26} \quad \textbf{(5.20)}$$

Where:

At = Total area in compression (m^2)

A_{scr} = Total area of screw reinforcing (m^2)

l_s = Total length of screw (m)

The interface compression factor, k_{int}, is calculated by multiplying the stress spreading factor, k_{ss}, and the screw reinforcement factor, k_{scr}:

$$k_{\text{int}} = \frac{1}{k_{scr}k_{ss}} \quad \textbf{(5.21)}$$

Design chart values for the stress spreading factor and screw reinforcing factor over standard post-tensioned frame characteristics are shown in Figure 5.5. The screw reinforcing design chart provides factors up to screw reinforcing ratios of 3% as it is considered difficult and impractical to obtain ratios of above this value (Watson et al. 2013). Using these design charts a range of interface compression factor between k_{int} = 0.85 (no reinforcing, deep beam/shallow column which is not recommended in design) and k_{int} = 0.2 (maximum 3% reinforcing and shallow beam/deep column). The standard range for the factor k_{int} is expected to be between 0.4 and 0.6.

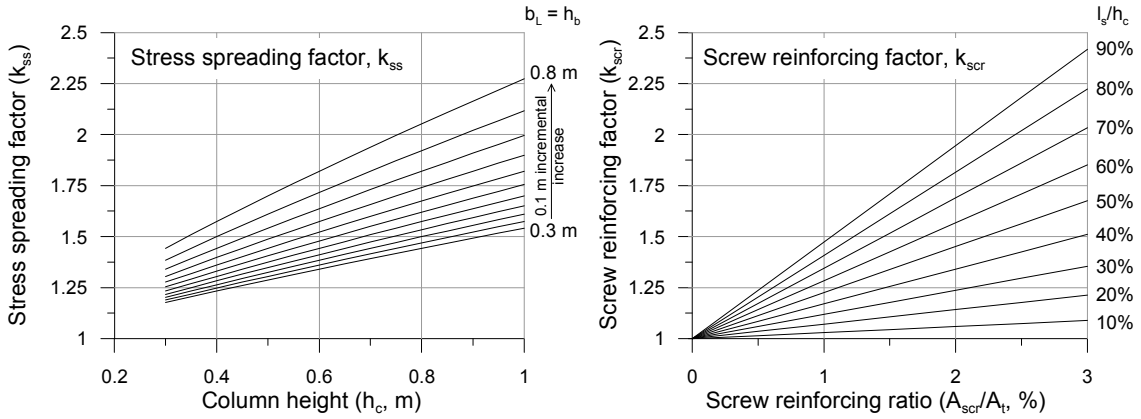

Figure 5.5. Design chart values for the stress spreading factor and screw reinforcing factor over standard post-tensioned frame characteristics

5.3.5 The effect of frame shortening on post-tension strain and the frame shortening factor, k_{sho}

In Section 5.3.2 the increase in post-tensioning during rocking motion is calculated using Equations (5.5) and (5.6). Combining these two formulas the following equation is obtained:

$$\Delta T_{pt} = \frac{n_{gap} \Delta_{pt} E_{pt} A_{pt}}{l_{ub}} \tag{5.22}$$

During the testing described in Chapter 4 the displacement of the tendon due to gap opening (Δ_{pt}) was measured along with the level of tension in the tendon (T_{pt}). Figure 5.6 displays a comparison between two values of tension in either the bar or tendon during testing. This is compared with the values obtained using Equation (5.22) which are shown in red.

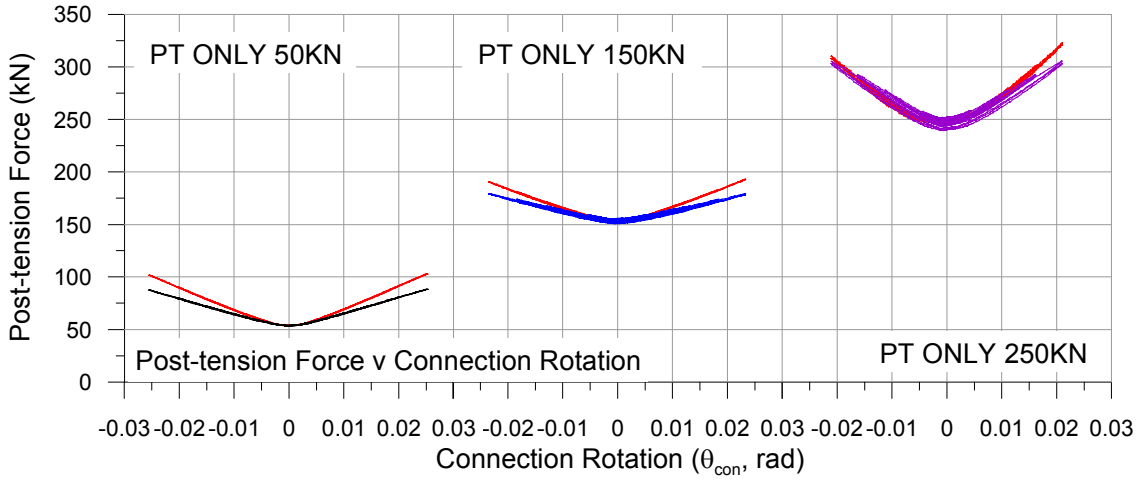

Figure 5.6. Comparisons between actual post-tension values and theoretical values (shown in red) for Equation (5.22)

Figure 5.6 shows the way in which Equation (5.22) significantly over-predicted the increase in post-tensioning due to gap opening. This over-prediction is due to the effect that beam shortening had on the overall elongation of the post-tensioned element. Chapter 4 discussed the way in which timber deflects under loading both parallel and especially perpendicular to the grain direction. The elongation of the tendon created by gap opening, which creates the additional strains created calculated using Equation (5.6), are in part cancelled out by the elastic deformations in the beams and columns created by the increase in post-tension force. This influence was first discussed by Newcombe (2012) however no guidance was provided on how to incorporate this factor into design.

The frame system can be thought of as a series of springs in series where the stiffness of the modified system ($k_{pt,sho}$) becomes:

$$\frac{1}{k_{pt,sho}} = \frac{1}{k_{pt}} + n_b \frac{1}{k_b} + n_{col} \frac{1}{k_c} \quad \textbf{(5.23)}$$

Where:

n_b = Number of beams

n_{col} = Number of columns

The stiffness of the individual elements can be calculated by modifying the first principal formula:

$$K = \frac{EA}{L} \quad \textbf{(5.24)}$$

Where:

K = The stiffness of the element (kN/m)

E = The Young's modulus of the element (kN/m^2)

A = The area of the element (m^2)

L = The length of the element (m)

The stiffness of the beam (k_b) is defined as:

$$k_b = \frac{0.7 E_{t,para} A_b}{L_b} \quad \textbf{(5.25)}$$

Where:

$E_{t,para}$ = Average modulus of elasticity of timber parallel to the grain (kN/m^2)

A_b = Area of the beam (m^2)

L_b = Beam length (face to face) across the bay which the post-tensioning acts (m)

The factor of 0.7 is applied in order to account for the end effects discussed in Section 5.3.6. The stiffness of the columns is defined using the equations presented in Section 5.3.4:

$$k_c = \frac{E_{t,perp} A_b}{k_{\text{int}} h_c} \tag{5.26}$$

Where:

$E_{t,perp}$ = Modulus of elasticity of timber perpendicular to the grain (kN/m^2)

The stiffness of the post-tensioning is defined as:

$$k_{pt} = \frac{E_{pt} A_{pt}}{l_{ub}} \tag{5.27}$$

Adding these factors together the modified stiffness of the post-tensioning can be found ($k_{pt,sho}$) and the modification factor, k_{sho}, can be found:

$$k_{sho} = \frac{k_{pt,sho}}{k_{pt}} \tag{5.28}$$

The factor k_{sho} depends on numerous physical frame characteristics and as such the development of design charts is not possible. Values of k_{sho} are however expected to range between 0.7 and 0.9 for typical post-tensioned timber frame design.

5.3.6 Connection E-modulus modification factor, k_{gap}

Equation (5.13) refers to the factor, k_{gap}, which represents a further alteration of the reinforced concrete design procedure in order to account for the use of timber as a construction material. During the material properties characterisation of timber, testing values are obtained over a code defined gauge length (EN408:2003) in order to avoid the 'end effect' which is present in timber materials. This end effect is related to the local crushing of the timber fibres and leads to reduced stiffness at the end of timber members and results in an average 70% reduction in timber stiffness.

In addition to this end effect, timber as a material is highly anisotropic and presents a significantly lower stiffness in the perpendicular to the grain direction. Where timber parallel to the grain is bearing on perpendicular to the grain members, interaction between the two occurs further reducing the stiffness of the connection.

In order to account for the end-effects and the localized deformation due to bearing perpendicular to the grain, a reduction factor, k_{gap}, has been introduced. Values of k_{gap} to be used in the design of post-tensioned timber structures are presented in Table 5.1.

Table 5.1. k_{gap} values for post-tensioned timber structures

	Occurrence	k_{gap}
Situations where no perpendicular to the grain action is present	Wall-foundation, column-foundation connection, beam-column connections with concrete columns	0.7
Situations where perpendicular to grain action is present but adequate measures have been made to protect the perp to grain crushing timber	Beam-column joints reinforced with screws, epoxied in rods etc.	0.55
Situations where perpendicular to grain action is present and no effort has been made to protect perp to grain crushing of timber	Unreinforced beam-column joints (not recommended)	0.1

The connection modulus (E_{con}) has been referred to in Chapter 2. E_{con} is defined as:

$$E_{con} = k_{gap} E_{t,para} \tag{5.29}$$

5.3.7 Comparison between testing moment-rotation results and post-tensioned timber beam-column design method

The procedure presented above has been applied in order to predict the performance of the beam-column joint presented in Chapter 4. This has been done for the joint both with and without the addition of the steel angle reinforcement presented in Chapter 3. The characteristic strength values used during testing were presented in Table 4.1 and are repeated in Table 5.2 combined with the values of the various factors described above.

Table 5.2. Timber and post-tensioning element material properties and design factors for beam-column testing presented in Chapter 4

Glulam GL32h				Post-tension tendons			
Strength				Yield strength	f_y	1530	MPa
Compression parallel to grain	f'_{para}	29	MPa	Ultimate strength	f_u	1760	MPa
Compression perp to grain	f'_{perp}	3.3	MPa	Elastic modulus	E_{pt}	201	GPa
Shear	f_{ts}	3.8	MPa	Area	A_{pt}	165	mm^2
Elastic modulus				Post-tension bar			
Characteristic perp. To grain	$E_{t,perp}$	0.46	GPa	Yield strength	f_y	1050	MPa
Average parallel to grain	$E_{t,para}$	13.7	GPa	Elastic modulus	E_{pt}	170	MPa
Shear	G_t	0.85	GPa	Area	A_{pt}	552	mm^2
Area of screw reo. (Section 4.4)	A_{scr}	3920	mm^2				
Unbonded Length	L_{ub}	3.28	m				
Design parameters							
Stress spreading factor	k_{ss}	1.44		Screw reinforcement factor	k_{scr}	1.32	
Timber end effect factor	k_{con}	0.55		Timber interface factor	k_{int}	0.53	
Beam shortening factor (tendon)	k_{sho}	0.89		Beam shortening factor (Bar)	k_{sho}	0.74	

The beam shortening factor was calculated as described in Section 5.3.5 however a slight modification was necessary to account for the additional compression of the jack used to

apply tension which was left as part of the system during testing (jack stiffness = 162,000 kNm^{-1}). As the beam did not have a significantly large hole for the tensioning element Equation (5.2) was used to calculate the decompression moment.

Post-tensioned only testing

Figure 5.7 and Figure 5.8 show the connection moment (θ_{con}), post-tension force (T_{pt}), normalized neutral axis depth (c/h_b) and the tendon elongation due to gap opening (Δ_{pt}) from the five post-tensioned only tests performed. These results are compared with results obtained from the design procedure presented above.

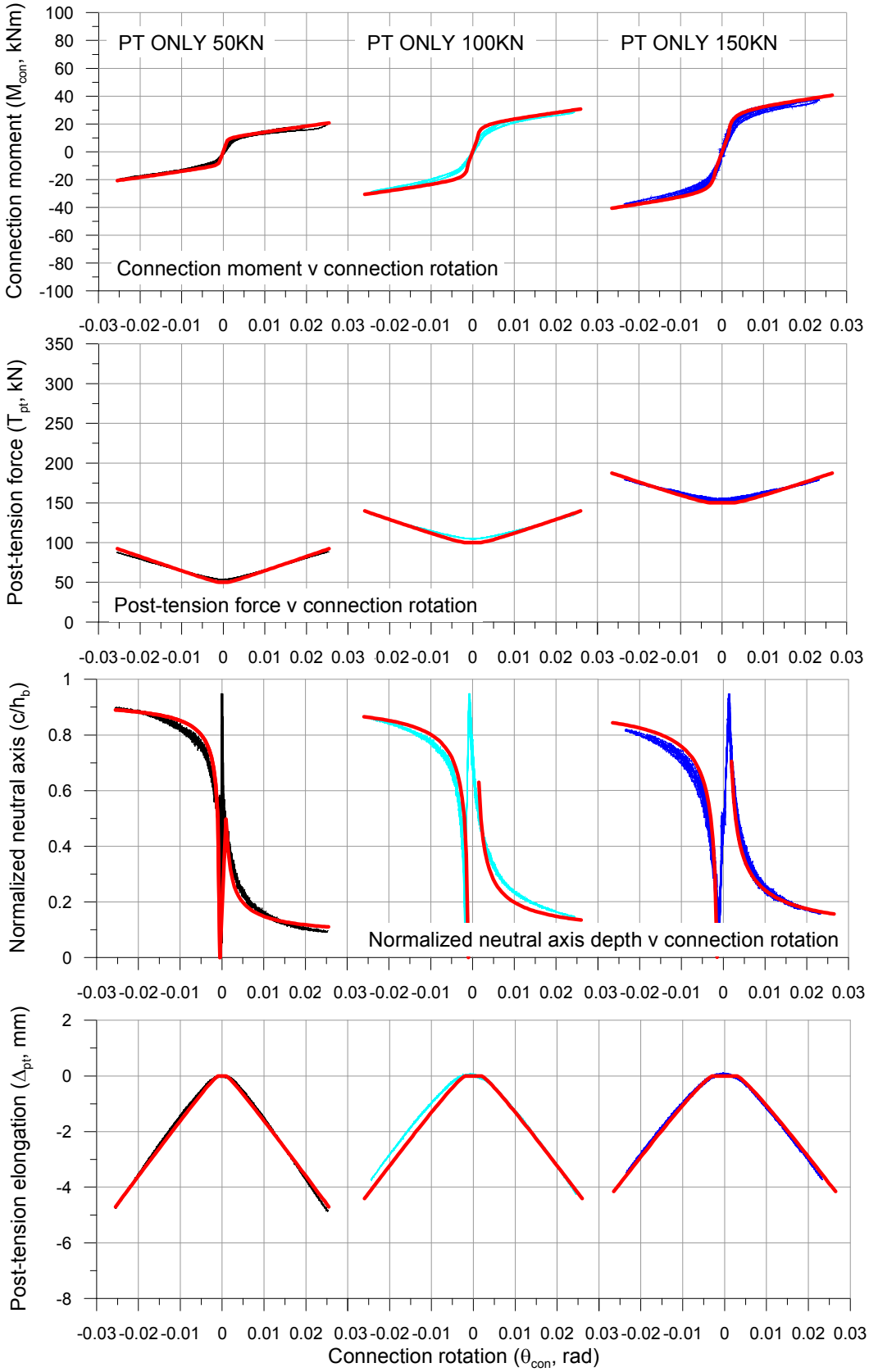

Figure 5.7. Comparisons of test results with design procedure (in red) for PT ONLY 50KN, 100KN and 150KN

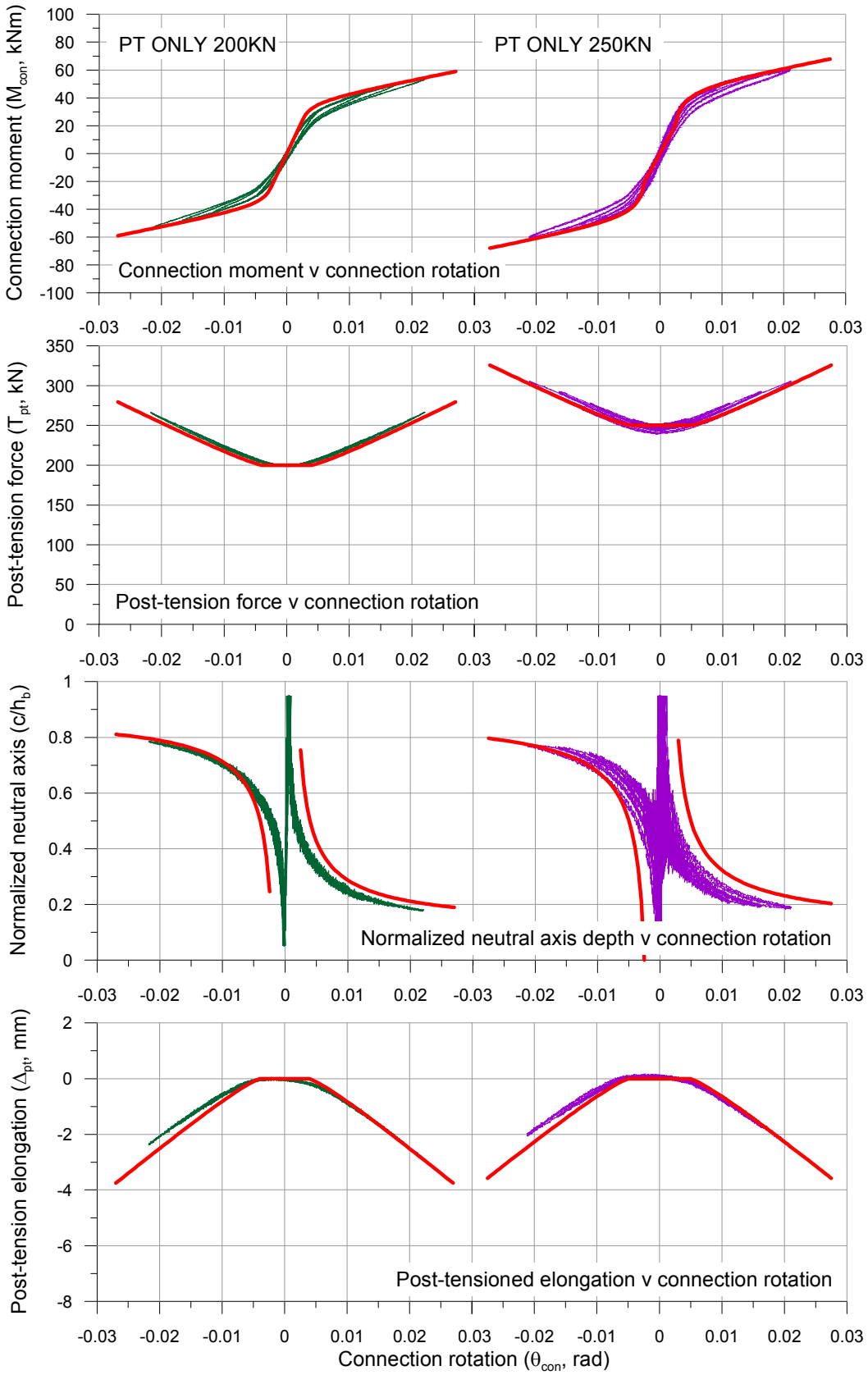

Figure 5.8. Comparisons of test results with design procedure (in red) for PT ONLY 200KN and 250KN

Figure 5.7 and Figure 5.8 show the accurate prediction of the behaviour of a post-tensioned beam-column joint obtained using the current design procedure. The inclusion of the interface compression deformation and the elastic beam shortening improved performance predictions compared to the original procedures which did not include these effects.

Figure 5.7 does show however that although the shortening factor has been included, the procedure still slightly over-estimated the increase in post-tensioning force while accurately predicting the tendon elongation due to gap opening. This would tend to indicate that further losses were present in the tendon system. Figure 5.8 shows that a more accurate representation of the increase in post-tensioning force was obtained for the PT ONLY 200KN and 250KN tests. As mentioned in Section 4.4 these two tests used a different method of post-tensioning (bars and not tendons) and therefore a different method of post-tensioning anchorage. While the post-tensioning bars used a simple threaded nut the tendon uses a cone and collet system which can be more susceptible to losses as it tightens. Both systems had the same anchorage plate size and therefore stress distribution onto the column and beam was identical. It is possible to therefore assume that the anchorage of the post-tensioning bars provides fewer losses under short term loading than those of the post-tensioning tendons however further research would be necessary to confirm this.

Although Figure 5.7 shows almost exact agreement between test results and the design procedure, results shown in Figure 5.8 seemed to overestimate the neutral axis depth in the positive direction. This would indicate that the beam-column interface was stronger than estimated. The exact source of this increase has not been determined, however during later testing some torsional effects were noted as the beam rotated around its long axis which may have led to slight errors in displacement readings. This would also explain the asymmetrical nature of the post-tension elongation.

Testing with dissipation

The procedure for the analysis of post-tensioned timber frame connections has also been used in order to provide the back-bone curves for the test series including the dissipative reinforcing angles. Figure 5.9 and Figure 5.10 show the connection moment (M_{con}), post-tension force (T_{pt}), normalized neutral axis depth (c/h_b) and the tendon elongation due to gap opening (Δ_{pt}) from the five tests performed.

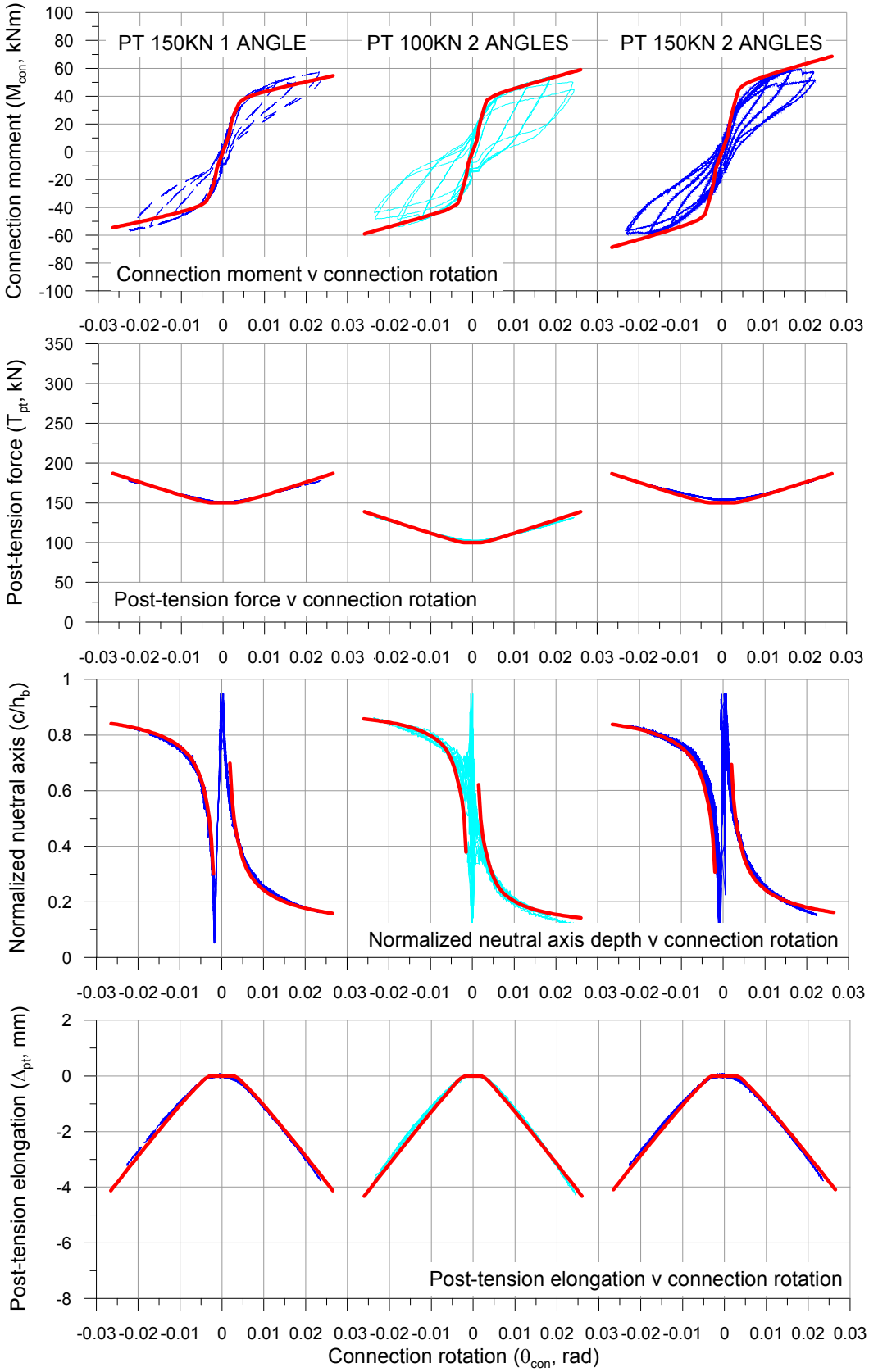

Figure 5.9. Comparison of test results with design procedure (in red) for PT 150KN 1 ANGLE, PT 100KN 2 ANGLES and PT 150KN 2 ANGLES

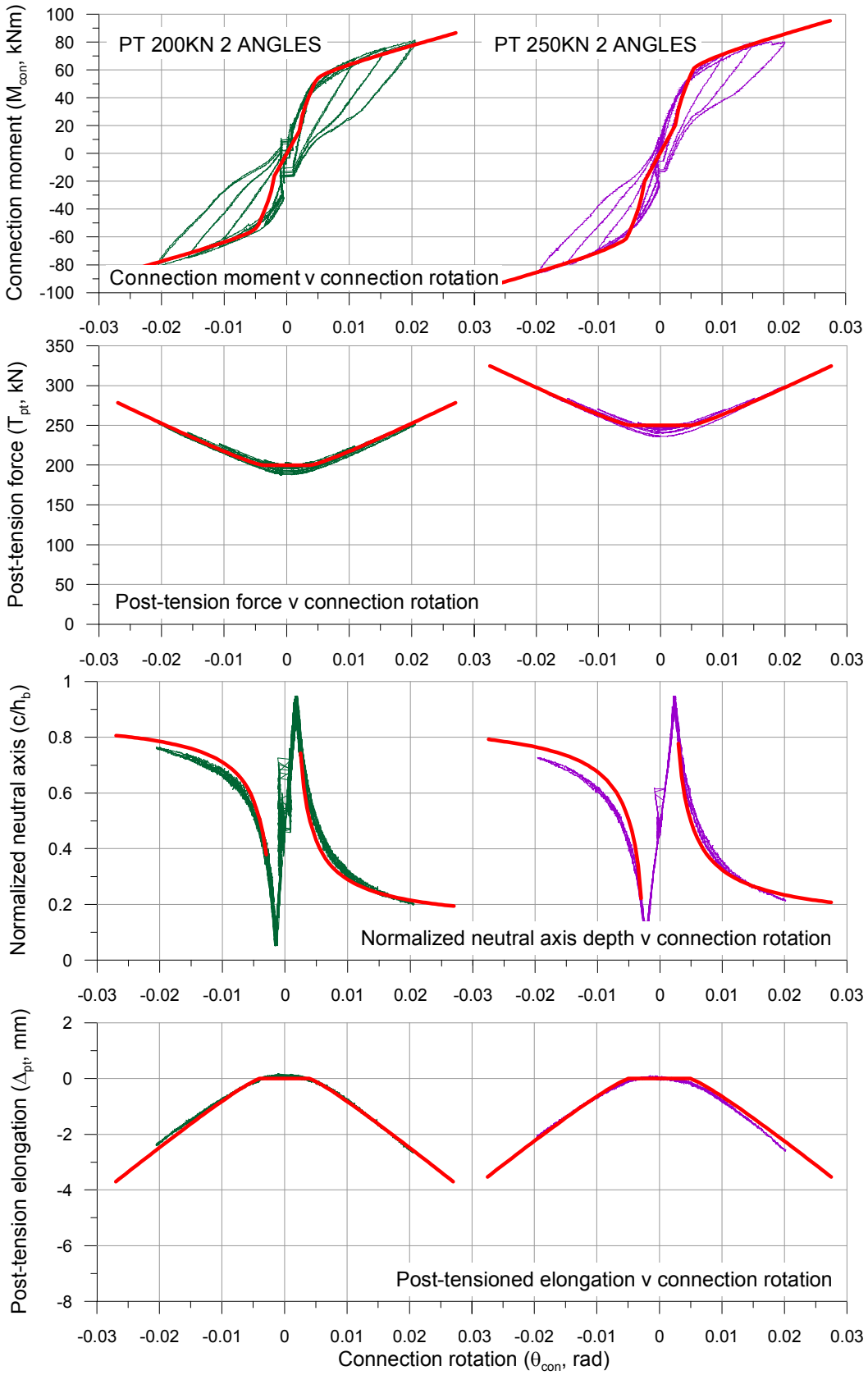

Figure 5.10. Comparison of test results with design procedure (in red) for PT 200KN 2 ANGLES and PT 250KN 2 ANGLES

As shown the design procedure accurately predicted the performance of the beam-column joint with the addition of the reinforcing angles. An exception to this is the test PT 150KN 2 ANGLES for which the procedure over-predicted performance. This is likely due to the reduced contribution of the angles due to the slipping angle connection plate described in Section 4.9.

5.4 FORCE DISPLACEMENT RELATIONSHIP OF A POST-TENSIONED TIMBER FRAME

In the design of a post-tensioned timber frame it is important to understand the amount of rotation which will occur at the beam-column connection (θ_{con}) in order to calculate the connection moment capacity and, as a consequence, the global frame behaviour. During the design of a building drift limits are specified to which the building must adhere during its predicted maximum load case. As described in Section 4.11 the total displacement (Δ_t) of a post-tensioned timber frame is made up of several contributing displacement sources (Figure 5.11): the elastic beam deformation (θ_b), the elastic column deformation (θ_c), and the joint deformation (θ_j), and the connection deformation (θ_{con}). Previously in this section the connection deformation was separated into two contributions: the interface compression deformation (θ_{int}) and the gap deformation (θ_{gap}). The design procedure used to calculate the rotational behaviour has been presented above, while the following section will address the calculation of the elastic deformation contributions of the beam, column and joint panel.

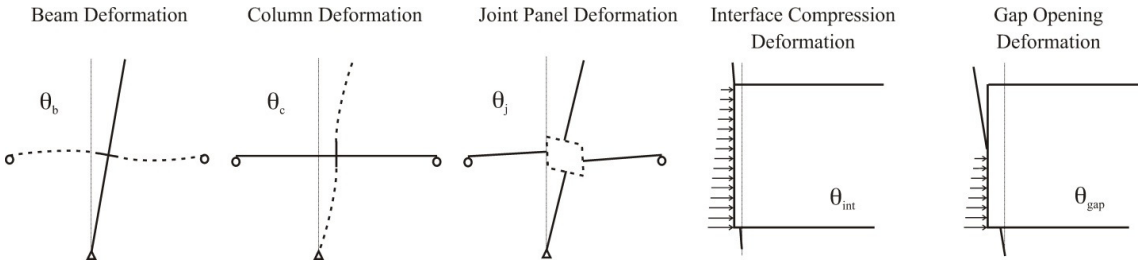

Figure 5.11. Rotation contributions to a post-tensioned timber beam-column joint

5.4.1 Beam and column rotations, θ_b and θ_c

The calculation of the beam and column deformations (Figure 5.12) can be derived using simple beam theory.

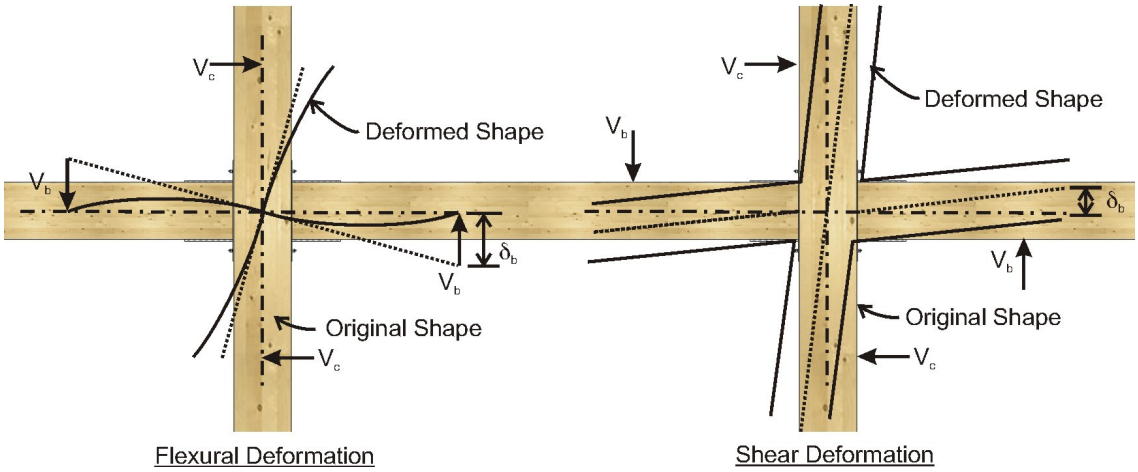

Figure 5.12. Beam-column joint flexural and shear deformations

Beams (θ_b)

The calculations of the flexural and shear deformations of beams are based on the following cantilever arrangement:

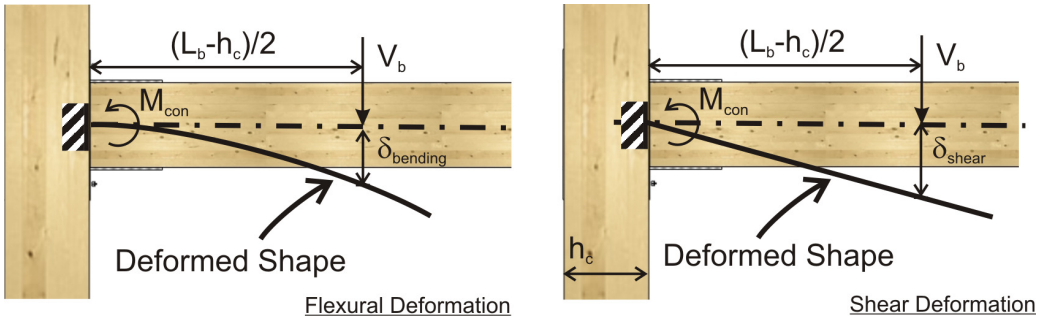

Figure 5.13. Flexural and shear deformations of cantilever

Using moment area theorem the deflection of a cantilever under a point load is:

$$\delta_{bending} = \frac{V_b \ell^3}{3E_{t,para} I_b} \quad \textbf{(5.30)}$$

Where:

$\delta_{bending}$ = Beam end deflection due to bending (m)

V_b = Beam end point load (kN)

ℓ = Cantilever length (in this case $(L_b-h_c)/2$ as shown in Figure 5.13 where L_b is total bay length and h_c is the height of the column) (m)

$E_{t,para}$ = Timber elastic modulus (kN/m^2)

I_b = Second moment of inertia of the beam (m^4)

Rearranging (5.30) and expressing it in terms of total rotation of the beam due to bending ($\theta_{bending} = 2\delta_{bending}/(L_b-h_c)$) and the moment at the connection interface ($M_{con} = V_b(L_b-h_c)/2$, considering actions from horizontal frame loading):

$$\theta_{bending} = \frac{M_{con}(L_b - h_c)}{6E_{t,para}I_b} \tag{5.31}$$

The shear deformation calculations are based on the same cantilever arrangement, the shear deformation of a cantilever under a point load is:

$$\delta_{shear} = \alpha_{s,cl}\frac{V_b \ell}{G_t A_b} \tag{5.32}$$

Where:

δ_{shear} = Beam end deflection due to shear (m)

$\alpha_{s,cl}$ = Shear coefficient to convert average shear to centroidal shear ($\alpha_{s,cl}$ can be taken as 3/2 for rectangles)

G_t = Timber shear modulus (kN/m^2)

A_b = Area of the beam (m^2)

Rearranging (5.32) and expressing it in terms of total rotation of the beam due to shear ($\theta_{shear} = 2\delta_{shear}/(L_b-h_c)$) and the moment at the connection interface ($M_{con} = V_b(L_b-h_c)/2$, considering actions from horizontal frame loading):

$$\theta_{shear} = \alpha_{s,cl}\frac{2M_{con}}{G_t A_b(L_b - h_c)} \tag{5.33}$$

In order to find the total rotation of the section in relation to the column face, the terms for the bending rotation (5.31) and the shear rotation (5.33) are combined:

$$\begin{aligned}\theta_{b,con} &= \theta_{bending} + \theta_{shear} \\ &= \frac{M_{con}(L_b - h_c)}{6E_{t,para}I_b} + \alpha_{s,cl}\frac{2M_{con}}{G_t A_b(L_b - h_c)} \\ &= M_{con}\left(\frac{(L_b - h_c)}{6E_{t,para}I_b} + \frac{2\alpha_{s,cl}}{G_t A_b(L_b - h_c)}\right)\end{aligned} \tag{5.34}$$

During design however all of the elastic rotation contributions must be calculated about a common point. In this case the common point is taken as the centreline of the beam-column joint. Simple geometry states:

$$\theta_b = \theta_{b,con}\left(\frac{L_b - h_c}{L_b}\right) \tag{5.35}$$

Therefore combining (5.34) and (5.35) the beam rotation contributions taken about the centreline of the column are obtained:

$$\theta_b = \frac{M_{con}}{L_b}\left(\frac{(L_b - h_c)^2}{6E_{t,para}I_b} + \frac{2\alpha_{s,cl}}{G_t A_b}\right) \tag{5.36}$$

Columns (θ_c)

The calculations of the flexural and shear deformation of internal columns are based on the following cantilever arrangement:

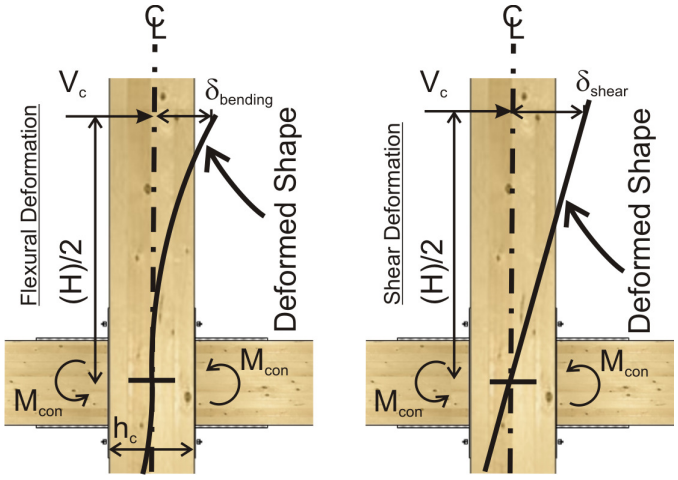

Figure 5.14. Flexural and shear deformation of cantilever

Using moment area theorem the deflection of a cantilever under a point load is:

$$\delta_{bending} = \frac{V_b \ell^3}{3E_{t,para}I_c} \tag{5.37}$$

Where:

$\delta_{bending}$ = Column end deflection due to bending (m)

V_c = Column end point load (kN)

ℓ = Cantilever length (in this case (H)/2 as shown in Figure 5.13 where H is the interstorey height) (m)

$E_{t,para}$ = Timber elastic modulus (kN/m^2)

I_c = Second moment of inertia of the column (m^4)

Rearranging (5.37) and expressing it in terms of total rotation of the column due to bending ($\theta_{bending} = 2\delta_{bending}/H$) and the moment at the connection interface ($M_{con} = V_cH(L_b\text{-}h_c)/2(L_b)$, considering actions from horizontal frame loading):

$$\theta_{bending} = \frac{M_{con}H}{6E_{t,para}I_c}\frac{L_b}{(L_b - h_c)} \tag{5.38}$$

The shear deformation calculations are based on the same cantilever arrangement, the shear deformation of a cantilever under a point load is:

$$\delta_{shear} = \alpha_{s,cl}\frac{V_c\ell}{G_t A_c} \tag{5.39}$$

Where:

δ_{shear} = Column end deflection due to shear (m)

$\alpha_{s,cl}$ = Shear coefficient to convert average shear to centroidal shear (α_s can be taken as 3/2 for rectangles)

G_t = Timber shear modulus (kN/m^2)

A_b = Area of the column (m^2)

Rearranging (5.39) and expressing it in terms of total rotation of the column due to shear ($\theta_{shear} = 2\delta_{shear}/H$) and the moment at the connection interface ($M_{con} = V_bH(L_b\text{-}h_c)/(2L_b)$, considering actions from horizontal frame loading):

$$\theta_{shear} = \alpha_{s,cl}\frac{2M_{con}}{G_t A_c H}\frac{L_b}{(L_b - h_c)} \tag{5.40}$$

In order to find the total rotation of the column section the terms for the bending rotation (5.37) and the shear rotation (5.39) are combined:

$$\begin{aligned}\theta_c &= \theta_{bending} + \theta_{shear} \\ &= \frac{M_{con}H}{6E_{t,para}I_c}\frac{L_b}{(L_b - h_c)} + \alpha_{s,cl}\frac{2M_{con}}{G_t A_c H}\frac{L_b}{(L_b - h_c)} \\ &= \frac{M_{con}L_b}{(L_b - h_c)}\left(\frac{H}{6E_{t,para}I_c} + \frac{2\alpha_{s,cl}}{G_t A_c H}\right)\end{aligned} \tag{5.41}$$

These contributions are already taken about the centreline of the column and therefore need not be converted.

In the case of an external column Equation (5.41) is divided by two due to the moment at the column centreline being $M_{con,cl}/2$.

Comparison between theory and testing results

Figure 5.15 shows the comparison between the formulas derived above with experimental testing results for beam rotation, (5.34, θ_b) and column rotation (5.41, θ_c). Equation (5.41) has been divided by two due to the beam-column joint being external.

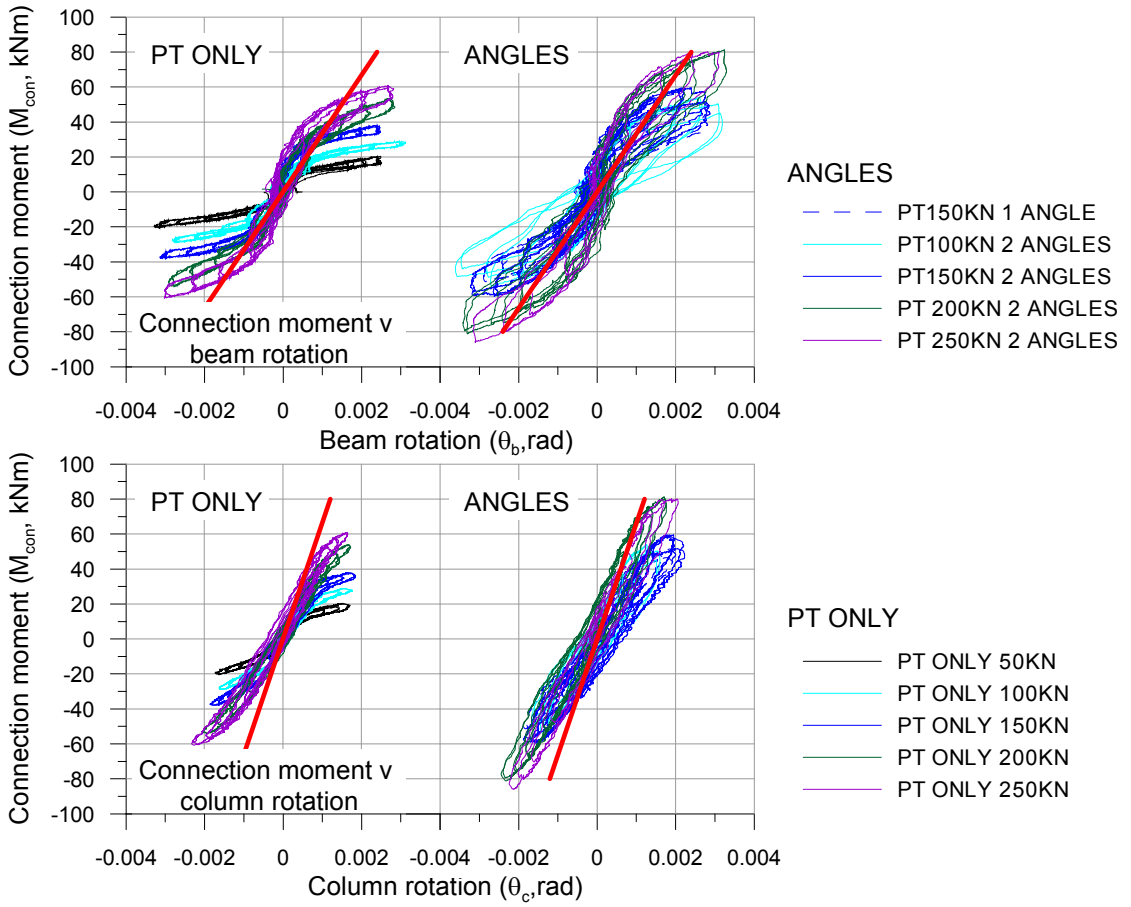

Figure 5.15. Comparisons between testing results and beam and column rotation formulas (in red)

The formulas used to describe the rotation of the column provided an adequate description of the contributions of the column rotations to the total beam-column joint.

Although the predictions of beam rotations were satisfactory, errors are observed where the rotations of the beam became non-linear following gap opening. This was likely due to the placement of the potentiometers, shown in Figure 4.6 of Chapter 4, from which the beam rotations were derived. During testing, data from these potentiometers were compromised as the displacement values included displacements due to both the total drift of the specimen

and additional displacements from gap opening. Further study is therefore required for the confirmation of the beam rotation formula.

5.4.2 Joint rotations, θ_j

Due to the low shear modulus of timber, the column joint panel rotations cannot be ignored in the calculation of the total beam-column joint rotation contributions (Cusiel et al. 2010). This section looks at how these deformations can be estimated simply during design and provides comparisons between the results obtained with those of testing.

Section 5.4.1 provided the way in which the column rotations, θ_c, can be described in relation to the moment at the connections face, M_{con}. This calculation was based on the assumption of a single moment acting at the centre of the beam-column joint. Figure 5.16 shows the difference in the forces, moments and shears arising from the assumptions made in the equation for θ_c and the actual situation present in a beam-column joint under moment.

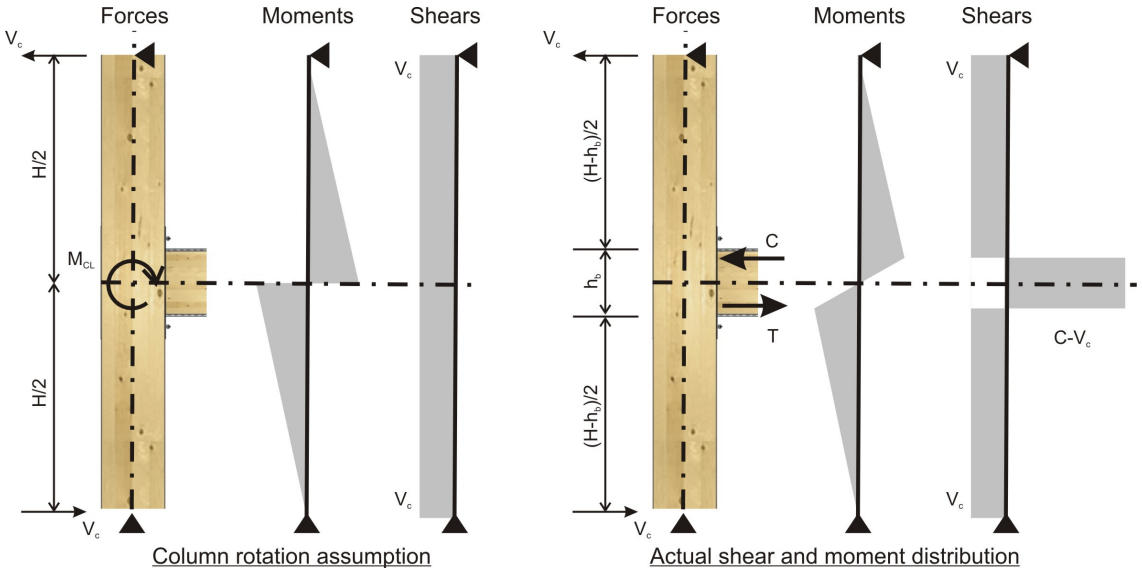

Figure 5.16. Flexural and shear deformation of the column in a post-tensioned timber beam-column joint

As shown, the contributions to rotation from column moment are described with adequate accuracy and therefore do not need to be considered. However, shear contributions are not well represented and therefore a correction, by way of the additional joint rotation term θ_j is introduced.

Shear rotation in the joint panel is due to the change in force created by the addition of shear stresses in the columns due to the force couple created by the moment at the connection, $M_{con,}$ denoted V_{jp} and shown in Figure 5.17. When decompression occurs for an approximately full rectangular section, such as a typical beam in a post-tensioned seismic frame, the moment M_{con} can be decoupled by the lever arm giving:

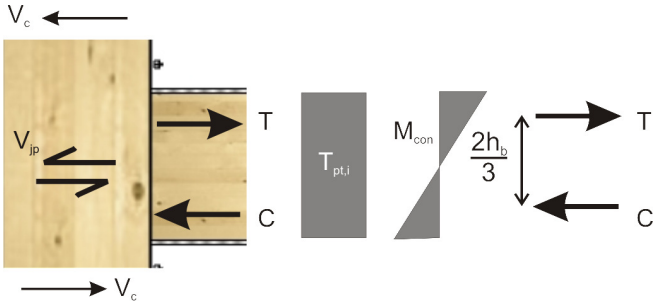

Figure 5.17. Joint panel moment couple for an external joint

$$V_{jp} = \frac{3M_{con}}{2h_b} \tag{5.42}$$

Following decompression this lever arm will increase towards the full section height (h_b) which will also be the case when the reinforcement/dissipation devices are added. This will not however be accounted for in the design meaning that the following procedure provides a conservative estimate of joint rotation.

The shear stress (τ_{jp}) in the column is calculated as:

$$\tau_{jp} = \frac{V_{jp}}{\alpha_{s,ave} A_c} \tag{5.43}$$

Where:

$\alpha_{s,ave}$ = Shear coefficient in order to find the shear rigidity of the section

For a rectangular section the factor $\alpha_{s,ave}$ is calculated as:

$$\alpha_{s,ave} = \frac{10(1+\nu)}{12+11\nu} \tag{5.44}$$

Where:

ν = Poisson's ratio (taken as 0.55 for glue laminated timber)

The rotation in the column joint panel is then simply the shear stress, τ_{jp}, divided by the shear modulus, G. By doing this, and combining equations (5.42) and (5.43) an equation for the

calculation of the joint panel rotation, θ_{jp}, in terms of the connection moment, M_{con}, is obtained:

$$\theta_{jp} = \frac{3M_{con}}{2\alpha_{s,ave}A_c h_b G_t} \quad \textbf{(5.45)}$$

Figure 5.17 shows the case of an external beam-column joint for which Equation (5.45) was developed. For an internal joint this equation remains the same when no dissipative reinforcement is present. When additional reinforcement is also applied to the connection the moment couple is increased by a factor of (2 – β). β is the recentering ratio ($\beta = M_{pt}/M_t$) of the beam-column joint as described in Chapter 4. In order to explain the reason for this reference is made to Figure 5.18. As shown, due to the fact that the post-tensioning tendon is unbonded and passes through the column without transferring any force to the column, the force couple is provided by the two compression contributions of each beam. In order to calculate these force couples the connection moment M_{con} is again conservatively divided by a lever arm of $2h_b/3$.

In the case where dissipation is attached to the beams and columns an additional contribution to the joint rotation occurs which must be added to the single connection contribution provided by M_{con}. This is provided by the steel contribution to the total moment capacity: $M_{con,s} = (1 - \beta)M_{con}$ giving a total contribution to the joint panel deformation of: $M_{con} + (1-\beta)M_{con} = (2 - \beta)M_{con}$.

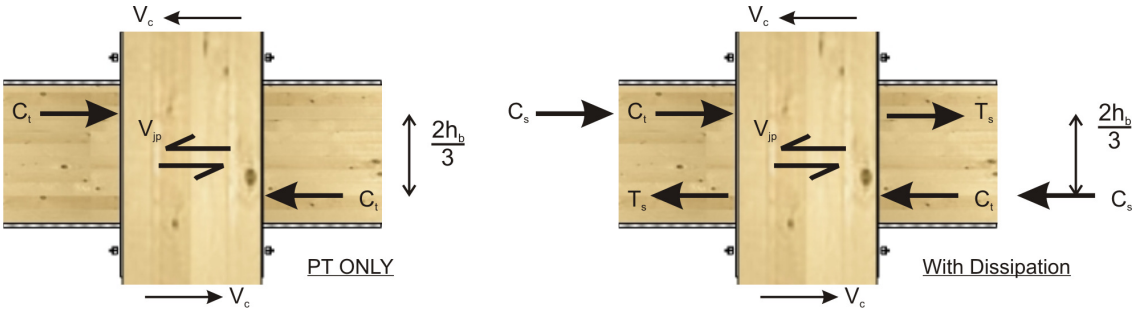

Figure 5.18. Shear deformation contributions for an internal beam-column joint with and without dissipation

Comparison between theory and testing results

Figure 5.19 shows comparisons between the testing results obtained from the beam-column and the theoretical procedure. In measuring the column joint shear it is not possible to separate out the contributions of the column shear and therefore these must be subtracted giving (5.46).

$$\theta_{jp} = \frac{3M_{con}}{2\alpha_{s,ave}A_c h_b G_t} - \frac{M_{con}L_b}{\alpha_{s,ave}H(L_b - h_c)A_c G_t} \quad \textbf{(5.46)}$$

The procedure provided an accurate estimation of the initial stiffness of the beam-column joint under moment. A change in stiffness was observed following gap opening created as the lever arm increases to become more than two-thirds of the beam height. This increase was more evident when the steel elements were attached due to their effect in increasing the lever arm.

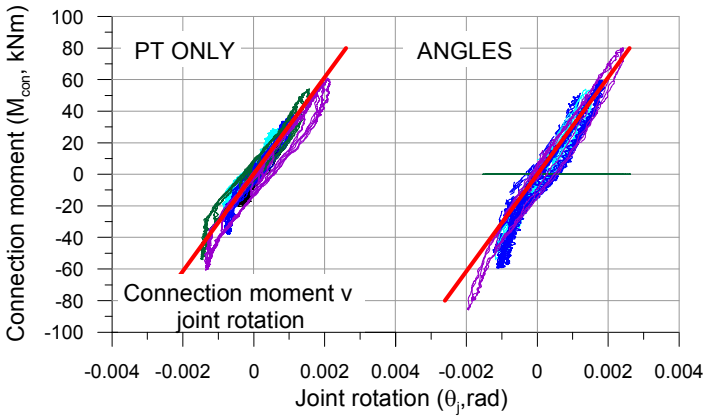

Figure 5.19. Comparisons between testing results and joint panel rotation formulas (shown in red)

Rotation contributions calculated from centreline moment

In some cases it may be necessary to calculate beam, column and joint rotations based on the beam-column centreline moment, M_{cl}, and not the connection moment, M_{con}. In this case the equations presented above become:

$$\theta_b = \frac{M_{cl}(L_b - h_c)}{L_b^2}\left(\frac{(L_b - h_c)^2}{6E_t I_b} + \frac{2\alpha_{s,cl}}{G_t A_b}\right) \quad \textbf{(5.47)}$$

$$\theta_c = M_{cl}\left(\frac{H}{6E_t I_c} + \frac{2\alpha_{s,cl}}{G_t A_c H}\right) \quad \textbf{(5.48)}$$

$$\theta_{jp} = \frac{3M_{cl}}{2\alpha_{s,ave}A_c h_b G_t}\frac{L_b - h_c}{L_b} \quad \textbf{(5.49)}$$

5.4.3 Column base rotations, $\theta_{c,base}$

Although column base connection rotations do not influence the performance of the beam-column joint presented in this section they will have an impact on overall frame design. The column base rotations ($\theta_{c,base}$) are defined as presented in this section.

The calculations of the flexural and shear deformation of columns are based on the following cantilever arrangement:

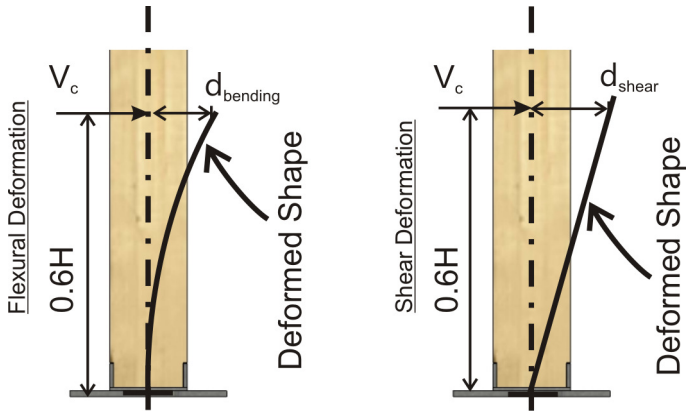

Figure 5.20. Flexural and shear deformation of cantilever

Using moment area theorem the deflection of a cantilever under a point load is:

$$\delta_{bending} = \frac{V_c \ell^3}{3E_{t,para} I_c} \quad \textbf{(5.50)}$$

Where:

$\delta_{bending}$ = Column end deflection due to bending (m)

V_b = Column end point load (kN)

ℓ = Cantilever length (in this case 0.6H as shown in Figure 5.20 this is a design choice and will be discussed further in Chapter 10) (m)

$E_{t,para}$ = Timber elastic modulus (kN/m^2)

I_c = Second moment of inertia of the beam (m^4)

Rearranging (5.50) and putting it in terms of total rotation of the beam due to bending ($\theta_{bending} = \delta_{bending}/0.6H$) and the moment at the connection interface ($M_{con} = V_b 0.6H$, considering actions from horizontal frame loading):

$$\theta_{bending} = \frac{M_{con} H}{5E_{t,para} I_b} \quad \textbf{(5.51)}$$

The shear deformation calculations are based on the same cantilever arrangement, the shear deformation of a cantilever under a point load is:

$$\delta_{shear} = \alpha_{s,cl} \frac{V_c \ell}{G_t A_c} \quad \textbf{(5.52)}$$

Where:

δ_{shear} = Beam end deflection due to shear (m)

$\alpha_{s,cl}$ = Shear coefficient to convert average shear to centroidal shear (α_s can be taken as 3/2 for rectangles)

G_t = Timber shear modulus (kN/m^2)

A_c = Area of the column (m^2)

Rearranging (5.52) and putting it in terms of total rotation of the beam due to shear ($\theta_{shear} = \delta_{shear}/0.6H$) and the moment at the connection interface ($M_{con} = 0.6HV_c$, considering actions from horizontal frame loading):

$$\theta_{shear} = \alpha_{s,cl} \frac{M_{con}}{0.6 G_t A_c H} \quad \textbf{(5.53)}$$

In order to find the total rotation of the section the terms for the bending rotation (5.51) and the shear rotation (5.53) are combined:

$$\begin{aligned} \theta_{c,base} &= \theta_{bending} + \theta_{shear} \\ &= \frac{M_{con} H}{5 E_{t,para} I_b} + \alpha_{s,cl} \frac{M_{con}}{0.6 G_t A_c H} \\ &= M_{con} \left(\frac{H}{5 E_{t,para} I_c} + \alpha_{s,cl} \frac{1}{0.6 G_t A_c H} \right) \end{aligned} \quad \textbf{(5.54)}$$

5.4.4 Force displacement response of beam-column joint

The force-displacement behaviour of the frame is calculated by combining all of the above contributions to the connection rotation response presented in Figure 5.7, Figure 5.8, Figure 5.9 and Figure 5.10. Combining these responses for the beam-column joint testing resulted in the graphs presented in Figure 5.21.

Figure 5.21 shows the way in which the design procedure for the calculation of the force-displacement predicted the backbone behaviour of a beam-column joint system with sufficient accuracy. In some cases (PT 200KN and PT 250KN 2 ANGLES) the design procedure provides conservative results.

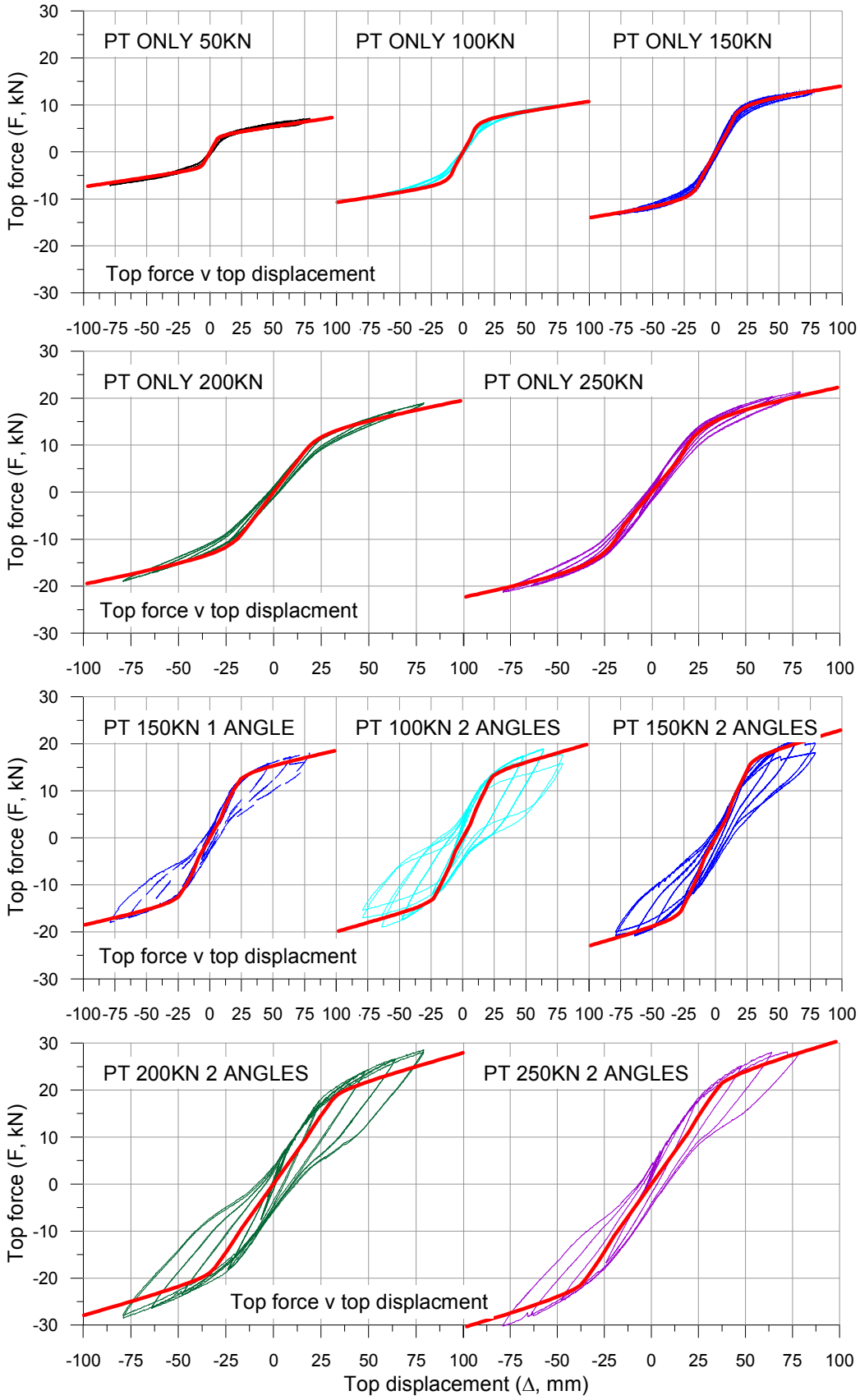

Figure 5.21. Force-displacement comparisons of test results with design procedure results (in red) for all tests

5.4.5 Consequences of elastic deformations on gap opening and energy dissipation

Both of the dissipation devices presented in Chapter 3 require gap opening in order to yield and thus dissipate energy through hysteresis. Figure 5.22 reproduces Figure 4.22 and 4.23 of Section 4.11, showing the percentage and total rotation contributions to the total rotation of the beam-column joint (θ_t).

As mentioned in Section 4.11, a two fold increase in elastic rotation contributions was observed, including an increase due to increased initial post-tensioning force, $T_{pt,initial}$, and an increase due to the additional moment capacity from the dissipation devices (i.e. decreases in β).

From Figure 5.22 it can be seen that the interface rotation (θ_{int}) made up a significant part of the total connection rotation (θ_{con}). It can also be seen that this contribution increased with an increase in post-tensioning which is congruent with Equation (5.17). Comparing the raw interface rotation values between testing with and without the addition of dissipative devices it can be seen that no increase in interface rotation occured, again in congruence with Equation (5.17) which is a function only of the initial post-tensioning value.

All of the elastic rotation contributions mentioned combined to suggest that the gap rotation (θ_{con}) was significantly smaller than the total rotation (θ_t). Table 5.3 shows the recorded gap opening of each angle test (θ_{gap}) along with the recorded gap opening as a percentage of the total recorded rotation and the drift of the beam –column joint at which gap opening occurred (including elastic rotation contributions).

Table 5.3. Recorded gap opening during angle tests at maximum (2.5%) drift

	θ_y (rad)	θ_{gap} (rad)	θ_{gap} (%)
PT 150KN 1 ANGLE	0.008	0.019	74
PT 100KN 2 ANGLES	0.007	0.019	70
PT 150KN 2 ANGLES	0.009	0.018	67
PT 200KN 2 ANGLES	0.010	0.014	53
PT 250KN 2 ANGLES	0.010	0.014	57

Although some inconsistencies existed due to instrumentation error the general trend of decreasing gap opening with increasing moment capacity were seen. This occured to the point where for the test PT 250KN 2 ANGLES at the design drift of 2.5% only 50 – 60% of the total rotation is in the opening of the gap. Recalling that the dissipation devices performance is dependent on gap opening, if these elastic rotations are not allowed for during design, significant reductions in dissipation occur.

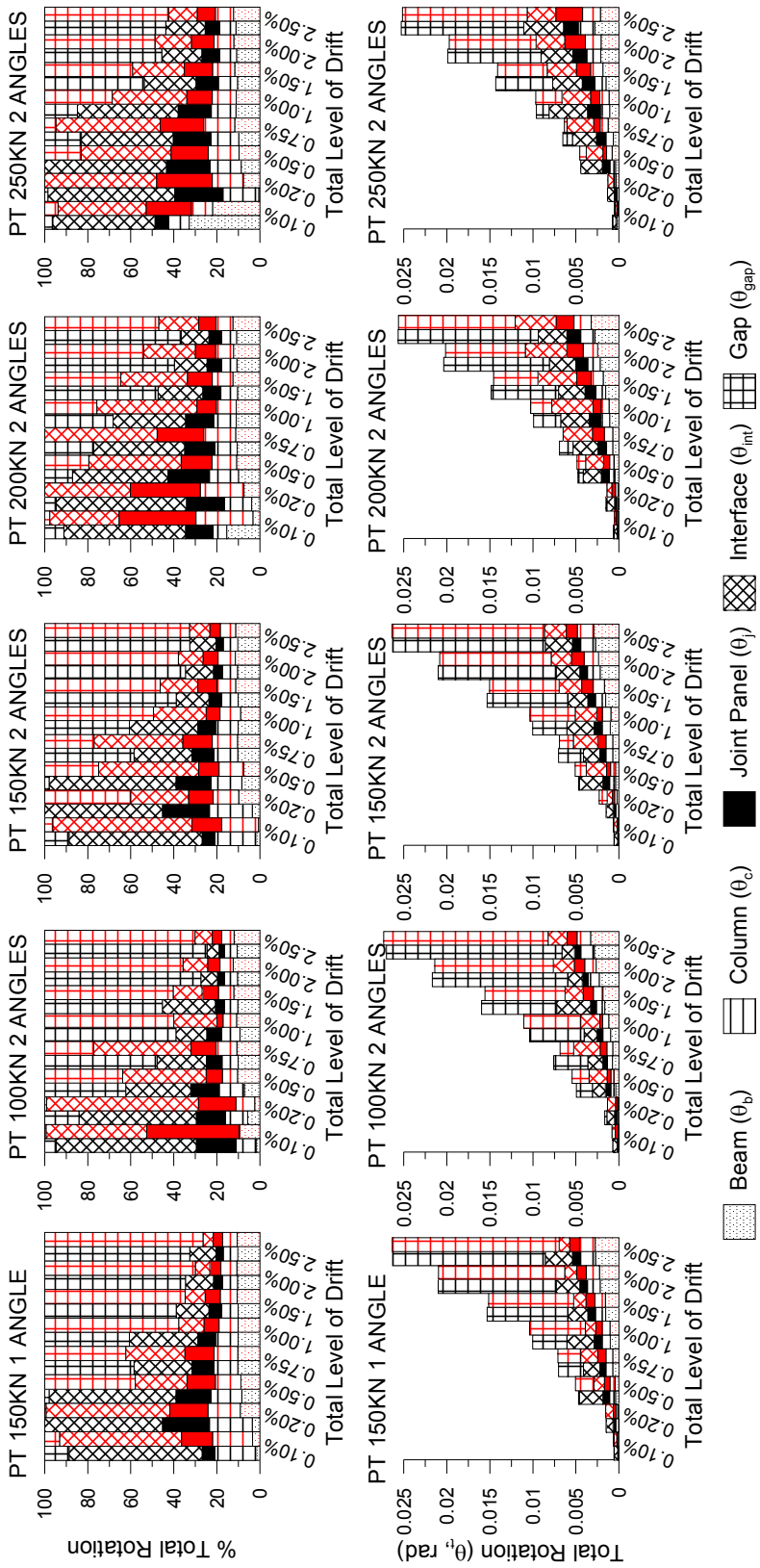

Figure 5.22. Rotation contributions for all angle tests (in black) compared with design procedure results (in red)

5.5 CALCULATION OF EQUIVALENT VISCOUS DAMPING

Section 4.9 provided comparison of the equivalent viscous damping values between the angle tests and evaluations of these damping values with relation to the total drift of the beam-column joint. In design it is necessary to know the amount of equivalent viscous damping which will be obtained from a beam-column joint during a certain drift level in order to calculate design base shear.

Priestley et al. (2007) defined the area based damping/equivalent viscous damping (EQV) for a flag shaped system based on the simplified flag shaped loop shown in black in Figure 5.23. Equation (5.55) applied the formula proposed by Jacobsen (1960) as discussed in Section 4.9 and defined the area within the idealised flag-shaped loop shown in black in Figure 5.23.

As shown in Figure 5.23 the recentering ratio of the system (shown as β_{2007}) was not defined by Priestley et al. (2007) in the same way as it is defined here for a post-tensioned timber system. Therefore Equation (5.56) must be substituted providing the final equation for the prediction of area based damping for post-tensioned timber frame systems as shown in Equation (5.57).

In design, the quantity of area based damping capacity present in a post-tensioned timber frame must be estimated before design as will be discussed further in Chapter 10.

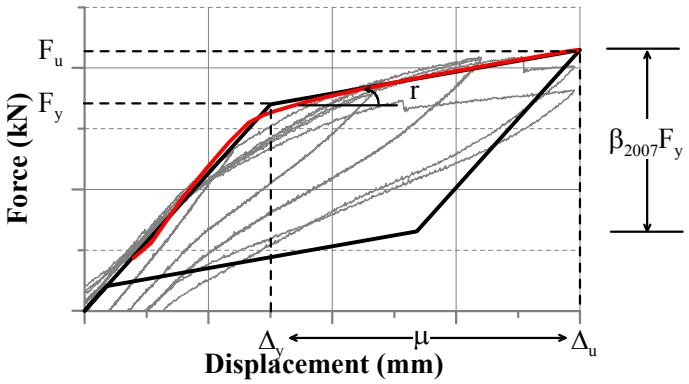

$$\xi_{hyst} = \frac{\beta_{2007}(\mu - 1)}{\mu\pi(1 + r(\mu - 1))} \quad \textbf{(5.55)}$$

$$\beta_{2007} = 2(1 - \beta) \quad \textbf{(5.56)}$$

$$\xi_{hyst} = \frac{2(1 - \beta)(\mu - 1)}{\mu\pi(1 + r(\mu - 1))} \quad \textbf{(5.57)}$$

Figure 5.23. Area based damping parameter definition

The amount of area based damping is predicted using r (as a ratio of the initial stiffness), β and μ values derived from the design procedure presented in this chapter, however as shown in Figure 5.23 when the simplified loop is defined this loop provides only an approximate estimation of the actual area based damping present during testing (shown in grey) and presented in Figure 4.19.

Figure 5.24 shows a comparison between the values of area based damping recorded during testing and the values given by Equation (5.57). The values derived from Equation (5.57) were based on the force displacement results derived from the design procedure as presented in Figure 5.21. The graphs are presented in terms of ductility as for a specific test the parameters r and β remain constant with the amount of damping present being a factor only of the ductility μ.

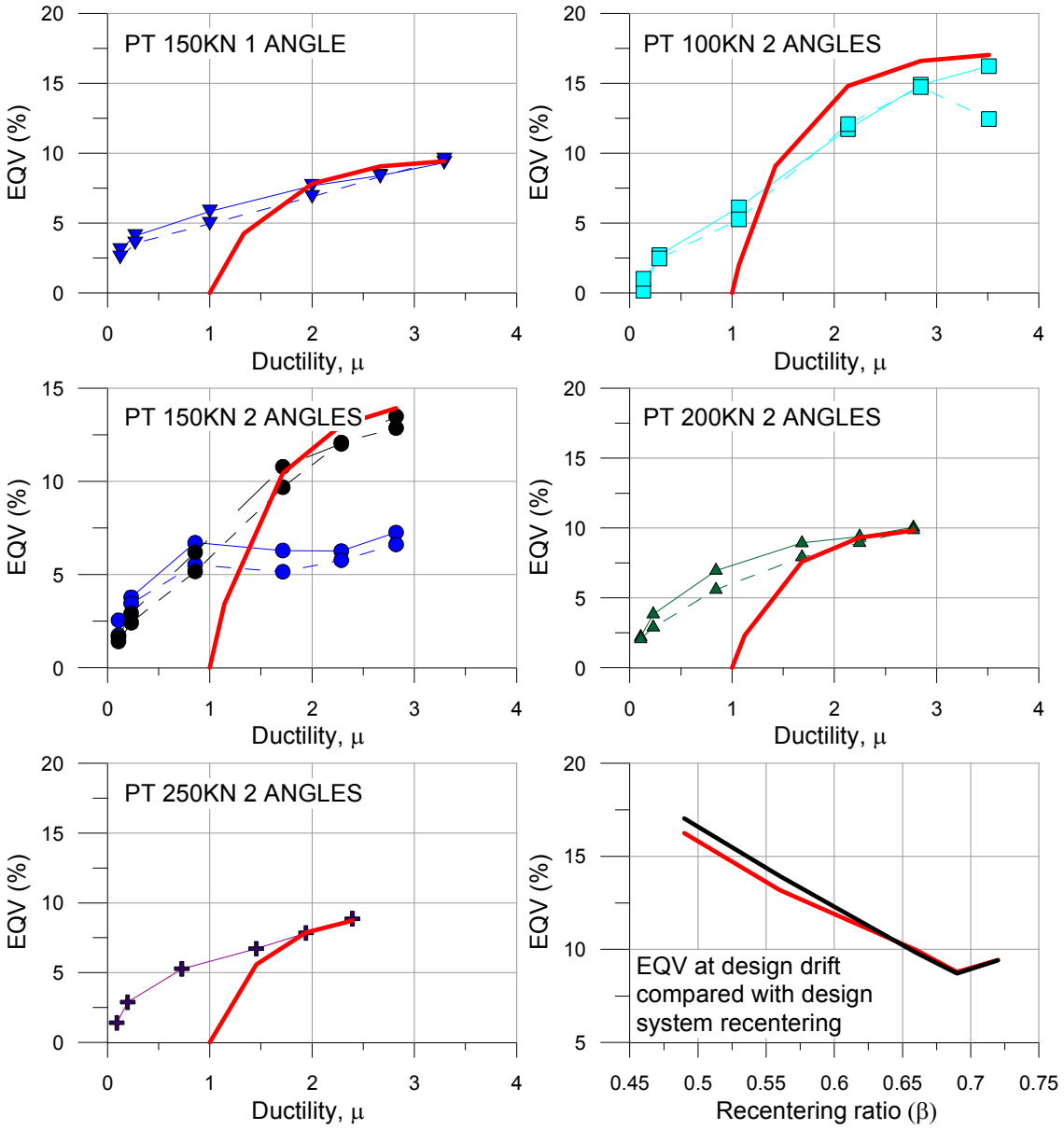

Figure 5.24. Comparison between equivalent viscous damping (EQV) recorded during testing (coloured) and results obtained from Equation (5.57) (in red)

Figure 5.24 shows that the equation provided a reasonably accurate (all within 15% for maximum values of ductility) estimate of area based damping when compared against the

testing results obtained. The final graph however shows that the accuracy decreased with decreasing values of β (i.e. increased levels of damping). Table 5.4 shows the ratio between the recorded value of EQV and the equation value at the design drift level of 2.5% A maximum error of 0.95 occurred with a value of $\beta = 0.49$ and within a normal design range of ($0.55 < \beta < 0.65$) a ratio of approximately 0.95 was observed. These comparisons have been made against the first cycle dissipative values. When this formula is used in the design of post-tensioned timber frames the slight degradation observed during testing should also be accounted for. This point will be discussed further in Chapter 7.

Table 5.4. Error summary between EQV recorded during testing and Equation (5.57)

	β (rad)	ξ_{test} (%)	$\xi_{analyical}$ (%)	$\frac{\xi_{analytical}}{\xi_{test}}$
PT 150KN 1 ANGLE	0.72	10.6	9.3	0.95
PT 100KN 2 ANGLES	0.49	19.1	16.2	0.95
PT 150KN 2 ANGLES	0.56	15.4	13.5	1.01
PT 200KN 2 ANGLES	0.66	10.9	10.0	1.01
PT 250KN 2 ANGLES	0.69	9.5	8.9	1.00

5.6 CONCLUSIONS FROM CHAPTER 5

Chapter 5 has presented the analysis method used to calculate the lateral response of a post-tensioned timber frame. Formulas have been presented in order to predict the full force-displacement, or moment-drift response.

At the local beam-column level focus was made on the moment-rotation response of the joint. This was split into two stages: before and after the beam decompresses from the column face creates a gap between the column face and the beam end.

Before decompression an interface compression rotation (θ_{int}) occurs relating to the initial post-tensioning value ($T_{pt,initial}$). Formulas have been proposed in order to calculate the effect which stress spreading and screw reinforcing have on the stiffness of the interface based on compression block testing from literature.

Following decompression, the elastic form of the Modified Monolithic Beam Analogy is used with minor changes made accounting for the increased flexibility of timber. A corrective value, k_{gap}, has been introduced accounting for two inherent timber properties: the end grain effect and the interaction between the stiffer parallel to the grain direction and the softer perpendicular to grain direction. A second factor, k_{sho}, has been introduced to account for

frame shortening in the calculation of the increase in post-tensioning during gap opening (ΔT_{pt}).

The moment-rotation response analysis procedure has been compared against the moment-rotation response of the beam-column joint presented in Chapter 4.

Equations have been presented and derived in order to calculate the contributions of the beam (θ_b), column (θ_c) and joint panel (θ_j) elastic rotations to global response. These were compared against the beam-column test results presented in Chapter 4. Although joint panel and column rotations were predicted sufficiently, the beam rotation results appeared to be compromised by other system rotations and further investigation is required. Equations have also been presented for the joint-panel rotation of an internal joint with and without reinforcing which required experimental validation.

The global (force/moment versus displacement/drift) response of the beam-column joint presented in Chapter 4 has been calculated and compared against testing results.

These elastic rotations have been presented together in order to study the way in which the individual rotation components make up the total rotation showing that in some cases only 50% of the total rotation consisted of gap rotation. Attention has been drawn to the way in which a reduced gap rotation can negatively impact on system response.

Finally current methods for calculating the Area Based Damping/Equivalent Viscous Damping have been compared against the beam-column joint testing from Chapter 4. Comparisons showed that the current procedure was adequate but slightly overestimated damping for low values of recentering ratio (low β) however values were acceptable.

This chapter has presented the procedure from an analysis view point. Chapter 10 will discuss how this procedure is used in design.

REFERENCES CHAPTER 5

ABAQUS Inc. (2011). "Abaqus FEA." ABAQUS Inc., Providence, Rhode Island, United States, Finite element analysis software.

Blaβ, H. J., and Gorlacher, R. (2004). "Compression perpendicular to the grain." 8th World Conference on Timber Engineering, Lahti, Finland, 435 - 440.

Cusiel, M. R., Newcombe, M. P., Pampanin, S., Buchanan, A. H., and Palermo, A. (2010). "The Effect of Joint Flexibility on the Seismic Response of Post-tensioned LVL Frames." 14th European Conference on Earthquake Engineering, Ohrid, Republic of Macedonia.

Jacobsen, L. S. (1960). "Damping in Composite Structures." 2nd World Conference on Earthquake Engineering, Tokyo and Kyoto, Japan.

Newcombe, M. (2012). "Lateral Force Design of Post Tensiond Timber Frame and Wall Buildings ", University of Canterbury, Christchurch.Doctor of Philosophy.

Newcombe, M. P., Pampanin, S., A.Buchanan, and Palermo, A. (2008). "Section Analysis and Cyclic Behavior of Post-Tensioned Jointed Ductile Connections for Multi-Story Timber Buildings." *Journal of Earthquake Engineering*, 12(1), 83–110.

Priestley, M. J. N., Calvi, G. M., and Kowalsky, M. J. (2007). *Displacement-Based Seismic Design of Structures*, IUSS Press.

EN408:2003. (2003). "Timber Structures - Structural Timber and Glued Laminated Timber - Determination of some Physical and Mechnical Properties." European Committee for Standardization.

van Beerschoten, W. A., Smith, T., Palermo, A., Pampanin, S., and Ponzo, F. C. "The Stiffness of Beam to Column Connection in Post-Tensioned Timber Frames." *CIB W18 Workshop on Timber Structures*, Alghero, Italy.

Watson, C. P., van Beerschoten, W., Smith, T., Pampanin, S., and Buchanan, A. H. "Stiffness of Screw-Reinforced LVL in Compression Perpendicular to the Grain." *CIB W18 Workshop on Timber Structures*, Vancover, Canada.

6 Study of the Global Behaviour of Post-Tensioned Timber Frames Utilising Dynamic Frame Testing

6.1 PRINCIPAL CONCLUSIONS OF CHAPTER 6

Chapter 6 presents investigations into the global performance of post-tensioned timber frames utilizing dynamic testing of a two third scale three-storey building. The following principal conclusions are drawn:

1. Several deficiencies in the connection of the dissipative reinforcing have led to reduced amounts of stiffness and strength leading to displacements beyond the design levels. Despite this, little to no damage occurred to frame members

2. The addition of dissipative reinforcing decreased displacements by 32% when the frame was subjected to a series of records at 75% of target PGA (PGA = 0.44 g relating the seismic hazard in Southern Italy). This was accompanied by an 18 % increase in base shear and no increase in floor acceleration.

3. The maximum floor acceleration recorded during testing was at the third floor of the structure (0.9 g) and was 1.7 times PGA. The ratio between third floor acceleration decreased as seismic intensity was increased due to the initiation of non-linearity (gap opening and dissipative reinforcing yield) in the frame.

4. The fundamental initial period of the post-tensioned timber frame was independent of the presence of dissipative reinforcing. This was due to the fact that the dissipative reinforcing requires a certain level of displacement to occur to begin working and as such their contribution is not captured by initial stiffness.

5. The elastic (equivalent viscous) damping of the frame was calculated as ξ_{el} = 1.49% and 1.84% for tests PT100_0.60 and PT100_1.00 respectively. These values are relatively low for a structural system (typical values used for concrete ξ_{el} = 5%).

6. Hysteretic damping of the frame was calculated as being ξ_{hyst} = 4.2% for tests PT100_0.60 averaged across the total signal and all tests (PGA100%). A maximum hysteretic damping value of ξ_{hyst} = 7.8% was recorded.

6.2 INTRODUCTION

Following the confirmation of local system performance through the full scale testing of a single beam-column joint, the global performance of post-tensioned timber framed structures was investigated. This was done through the dynamic testing of a two-third scale three-storey post-tensioned timber framed structure.

This chapter will first describe the characteristics of the test specimen followed by a description of instrumentation and input loading. Two different testing configurations were used, one with and one without the dissipative reinforcing angles described in Chapter 3. The results of these two tests will be described separately in terms of displacements/drifts, accelerations and forces, and then compared between tests. Finally the total (elastic and hysteretic) damping of the structure is evaluated and discussed.

6.2.1 The prototype structure

The prototype structure was three stories in height and had a single bay in both directions. As with the beam-column joint described in Chapter 4 all design was performed in accordance with the current version of the Italian design codes (NTC 2008). The interstorey height of the prototype building was 3 m and the frame footprint was 6 m by 4.5 m. The building was designed to represent an office structure (live loading Q = 3 kPa) with the final floor being a rooftop garden. A summary of vertical loadings is described in Section 6.4.2. The flooring of the building was made from solid Glulam panels. Seismic loading governed the lateral resistance design of the building.

6.2.2 The test model

The test frame (shown in Figure 6.1) was made from Glulam grade GL32h (EN 1995-1-1 2004). A scale factor of 2/3 was applied to the prototype structure resulting in a specimen interstorey height of 2 m and a footprint of 4 m x 3 m. Seismic loading during testing was mono-directional and applied along the north-south axis of the building (Figure 6.1a). Post-tensioning was applied in both directions in order to

provide structural stability. Many of the design elements developed and verified during the first stage of the project, as described in Chapter 4, were reapplied to the test structure.

Section sizes used in the frame are shown in Figure 6.2. Connection detailing is described in Section 6.3.

Figure 6.1. Test set-up for 2/3rd scale, 3-storey dynamic frame specimen

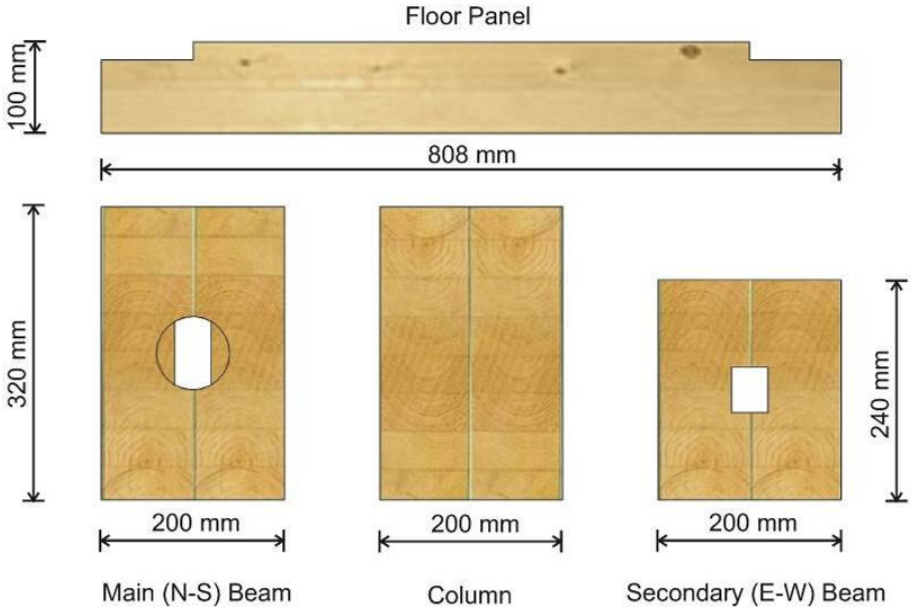

Figure 6.2. Design section sizes used in 2/3rd scale, 3-storey dynamic test frame

6.2.3 Test frame naming convention

Due to the three dimensional nature of the frame it was necessary to develop a naming convention during testing as shown in Figure 6.3. A simple north/south convention was used with the south side of the frame being closest to the reaction wall (i.e. the point of loading). In addition an internal/external convention was used to nominate beam and column faces.

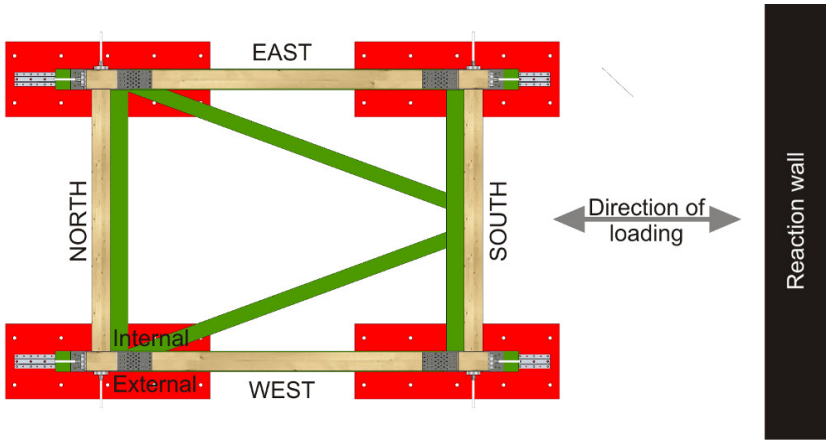

Figure 6.3. Naming convention of shaking table test frame

6.3 TEST FRAME CONNECTION DETAILING AND CONSTRUCTION

Most of the connection detailing of the frame specimen followed the developments of the beam-column testing described in Chapter 4. This section further describes the modifications made in order to transfer these concepts into a complete post-tensioned timber frame.

6.3.1 Beam-column connection in the principal (N-S) direction

The beam-column connection (Figure 6.4) in the principal direction was based on the connection type developed during the beam-column testing presented in Chapter 4. Passing through the centre of the beam was a single 26.5 mm diameter threaded post-tensioned bar. The high strength steel bar was identical to the bar used during the beam-column testing where initial post-tensioning was above $T_{pt,initial}$ = 150 kN, with a yield strength f_y = 1050 N/mm^2 and a Young's modulus of 170 kN/mm^2.

As during beam-column testing screws were used to protect the column face with 22 ϕ 8 mm screws being applied to the column face in contact with the beam and 30 screws being applied beneath the post-tensioning anchorage plate (All screws were

fully threaded and 80 mm in length). 28 ϕ 8 mm 120 mm long screws were used to fix each dissipative reinforcing attachment plate to the timber. The dissipative reinforcing was attached to the column through the use of M16 bolts which passed through the width of the column and back onto a backing plate. Where this plate contacted with the column, 10 ϕ 8 mm, 80 mm long screws were used as reinforcing. Vertical loading was transferred through a ϕ 76.1 mm steel tube that extended 66 mm from the beam and sat inside the column.

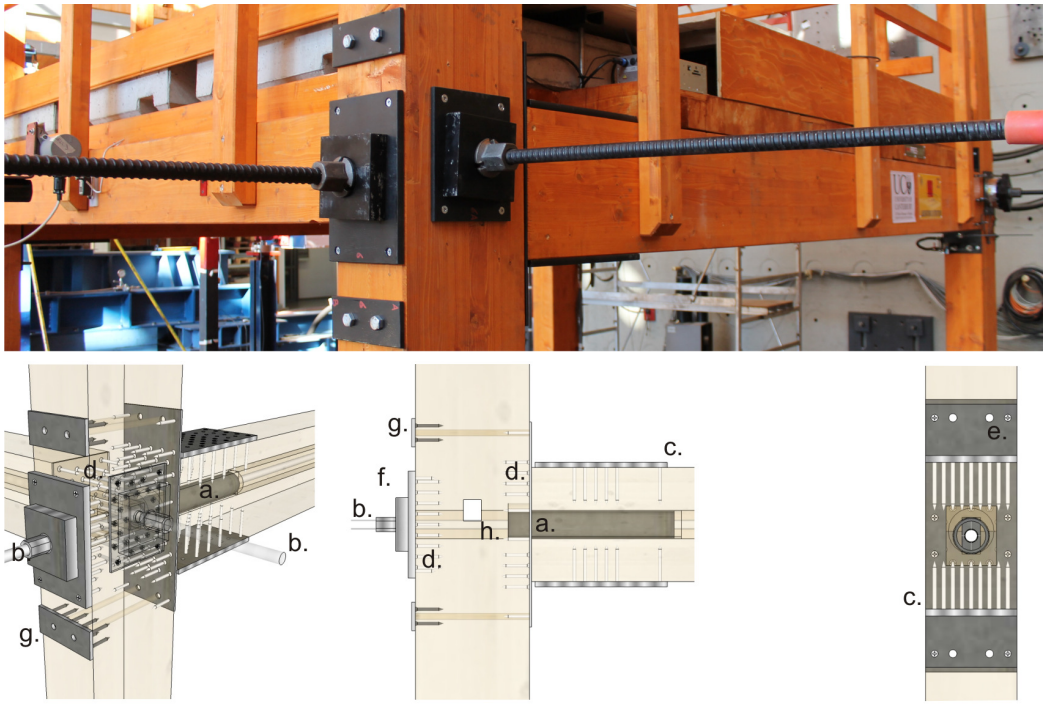

a. Tube shear key
b. Post-tensioned bar
c. Dissipative Reinforcement attachment plate
d. Column reinforcement
e. Drilled Holes for dissipative reinforcing
f. Post-tensioned anchor plate
g. Dissipative reinforcing backing plate
h. Hole for secondary post-tensioned bar

Figure 6.4. Beam-column connection used in 2/3rd scale, 3-storey dynamic test frame

6.3.2 Beam-column connection in the secondary (E-W) direction

As mentioned in Section 6.2.2 post-tensioning was used in both directions in order to provide stability. The beam-column connection in the secondary direction was similar to that in the principal direction. A single ϕ 26.5 mm bar passed through the centre of the beam section. 22 ϕ 8 mm, 80 mm long screws were used to reinforce both where the beam and the post-tensioning backing plate bore on the column.

6.3.3 Column-foundation connection

The detailing of the column-foundation connection is displayed in Figure 6.5. The base of the column was fitted with a steel shoe which was left free to rock on a base plate (which was used to represent the building foundations in the case of the test building). Four ϕ 20 mm bars of 300 mm length which were welded to the base plate were glued (using epoxy) into the base of the column.

Shear transfer was performed in a similar manner to the beam-column shear transfer method tested in Chapter 4. A ϕ 76.1 mm steel tube was welded to the steel shoe which extended 15 mm and slotted into a cavity in the base plate. As shown in Figure 6.5 holes were drilled and tapped in the steel shoe in order to enable the attachment of the dissipative reinforcing devices. In order to keep the base of the column as aesthetically pleasing as possible, the steel shoe was recessed into the column.

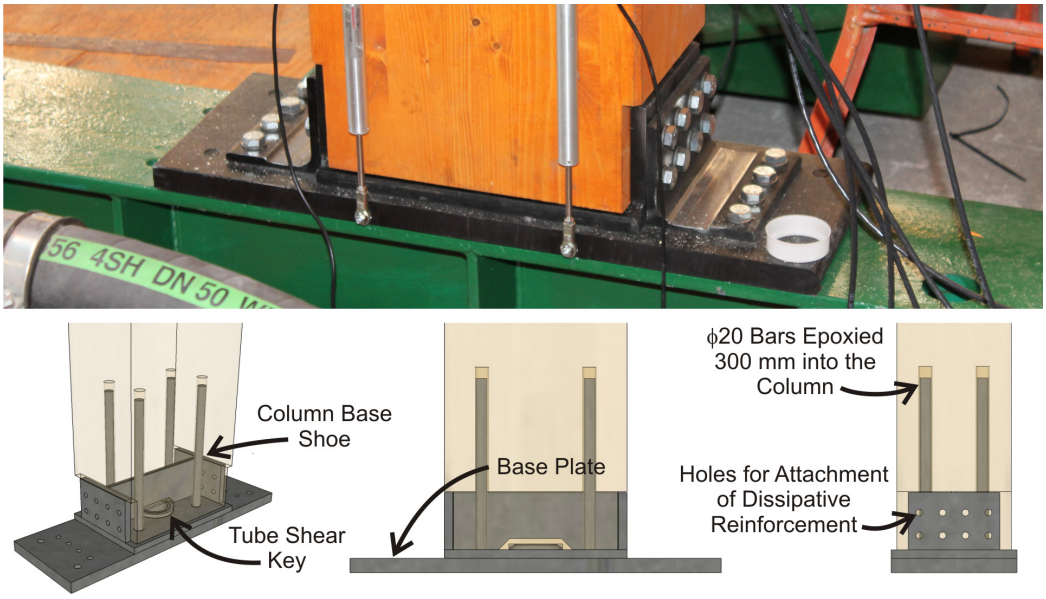

Figure 6.5. Column-foundation connection used in 2/3rd scale, 3-storey dynamic test frame

6.3.4 Flooring

The floor was made from a series of deep glulam beams turned on their sides in order make solid flooring panels (Figure 6.6). Each 808 mm wide panel was connected to the next using a 20 mm thick strip of plywood which was screwed (ϕ 6 mm 80 mm length) at 150 mm centres.

Attachment to the parameter beams was through the use of 16 pairs of skewed VGZ (fully-threaded with a conical head) screws ϕ 7 mm, 220 mm in length in the N-S direction and 15 pairs of skewed HBS (partially, 75 mm-threaded, screws with a conical head) ϕ 6 mm, 240 mm in length in the E-W direction. During design the decision was made to skew these screws due to the significant increase in both stiffness and strength when screws are inclined.

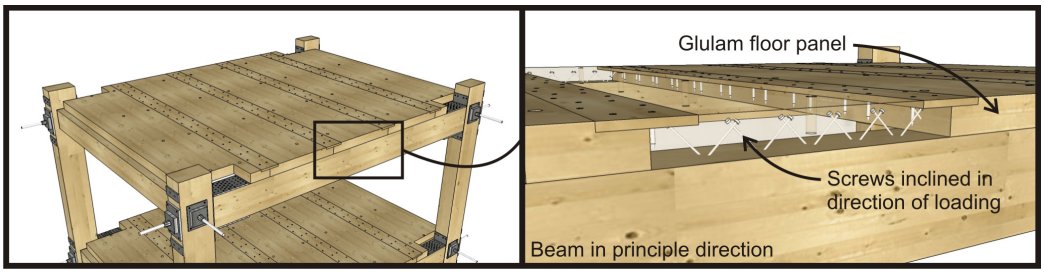

Figure 6.6. Timber flooring used in 2/3rd scale, 3-storey dynamic test frame

Skewing of the screws in their direction of loading was also performed in order to mitigate the tearing of the flooring panel during loading. As gap opening occurs, the flooring panel adjacent would have been placed in tension as it was attached both to the primary and secondary beams. As seen in Figure 6.6 a section of the floor was cut out in order to allow the attachment of dissipating devices and it was possible that stress concentrations would have occurred in the corner of the cut section. By significantly increasing the stiffness of the screw group in the loaded (N-S) direction when compared to those of the secondary (E-W) direction which were skewed in the opposite direction to loading, a fuse was created which allowed the flooring panel to slide over the top of the secondary beam. In order to further reduce tensions in the corner cut the screw groups in both directions began at least 500 mm from the column.

This method of protection proved successful; however a full study of the effectiveness of this protection method is outside of the scope of this body of work. For more information into the performance of the flooring and the floor diaphragm refer to Moroder et al. (2014).

6.3.5 Model fabrication

As with the beam-column joint described in Chapter 4, the fabrication of the frame (Figure 6.7) was performed by Holzbau Sud SpA. Fabrication followed the same

procedure as the beam-column joint members with the extensive use of Computer Numerical Controlled (CNC) machines in order to provide the required cavities in members (for post-tensioning, and shear keys)

Figure 6.7. a) First stage of glulam fabrication, b) beams being pressed together and c) reinforcing screws being placed on column face

During fabrication errors were made in the production of the beams in the principal direction. Following the gluing together of the two sections the beam was planned down. This removed approximately 7 to 10 mm from each side of the section leaving the beam having a total height of 305 mm instead of the original design specifications of 320 mm.

The impact of the change in section size on frame construction meant that the beam needed to be raised 10 mm to meet the flooring panels described in Section 6.3.4. Because of this the internal tube corbel (shown in Figure 6.4) was not in contact with the column pocket and vertical force transfer across the beam-column interface was through friction only.

The movement of the beam up to the meet to flooring panels also created a slight asymmetry in the beam-column connection as the post-tensioned bar was no longer central to the beam. This asymmetry increased for the testing with dissipative reinforcing as 10 mm shims were required to be inserted between the bottom reinforcing attachment plate and the angle reinforcing device. This alteration of lever arm led to a 1 kNm (6%) and 2 kNm (7%) asymmetry between the positive and negative rotation directions for testing without and with dissipative reinforcing, respectively.

6.3.6 Model construction

Construction of the test model in the structural laboratory was performed over a period of 2 days by a work force of 5 people and utilized the 'balloon frame' method (Smith et al. 2009). Figure 6.8 shows the construction sequence of the test frame.

Firstly each longitudinal (i.e. in the principal direction) frame was laid out in a working area beside the shaking table and the post-tensioning was loaded on the ground to an initial value (200 kN) in order to provide stability while each frame was lifted into place. Once both frames were assembled they were lifted into place and the column base reinforcement was attached.

Following the erection of both frames the secondary beams were positioned and tensioned (50 kN), forming the complete skeleton frame. The external flooring panels were then placed on the first two floors, followed by the screwing of the first floor. Once the floor was complete the guardrail was placed followed by the additional masses which will be described in Section 6.4.2. The frame was then completed by the placement of the second floor and its mass and the third floor and mass.

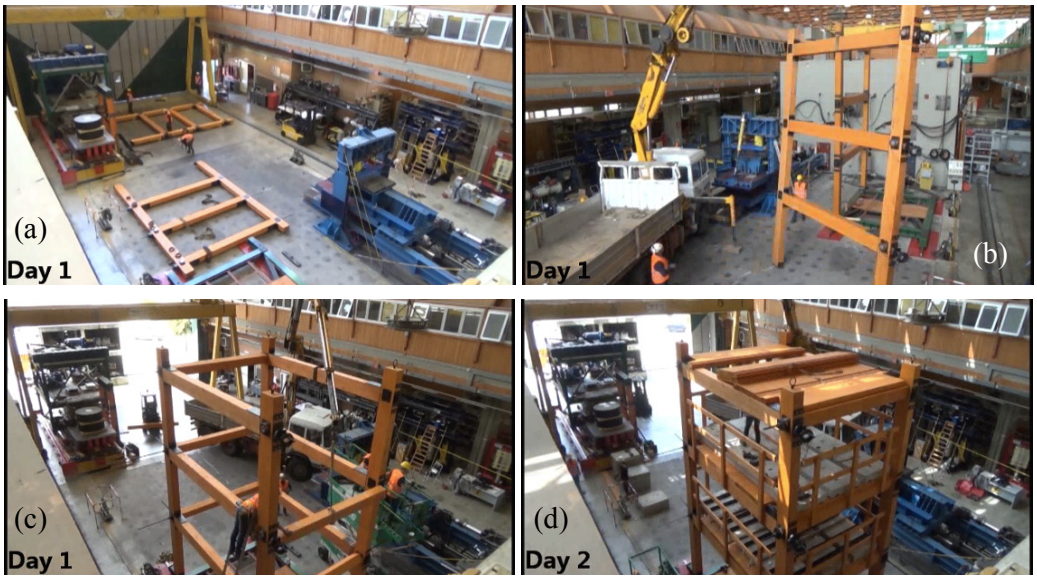

Figure 6.8. Construction sequence of test frame: a) loading of principal frames on ground, b) lifting of principal frames into place, c) completion of skeleton frame and d) placement of top floor

6.4 EXPERIMENTAL SET-UP

Testing was performed under dynamic loading in real time. This was done using a shaking foundation testing rig. Due to the fact that the frame is of 2/3rd scale, mass similitude had to be maintained. This meant that additional mass was added which also represented the presence of a factored live load. Following the definition of the test apparatus, instrumentation of the structure is described along with the two test configurations.

6.4.1 The shaking foundation

The testing apparatus consisted of a shaking foundation (Figure 6.9) present in the laboratory of the University of Basilicata. The foundation had a single degree of freedom in the N-S direction and consisted of a steel frame made up of HEM300 structural steel sections. The foundation was driven by an MTS 244.41 dynamic actuator which has a capacity of ± 500 kN and a stroke of ± 250 mm. The actuator was fixed to a hinge at the base of the foundation and pushed against the 6 m thick strong wall used during the beam-column test programme. Pressure for the actuator was provided by 3 MTS SilentfloTM 505-180 hydraulic pumps.

The foundation was situated upon 4 SKF frictionless sliders (model LLR HC 65 LA T1) with one each situated under the four columns. These sliders sat upon a series of levelling plates set upon grout-pads to ensure that a system with a coefficient of

friction of less than 1% was obtained. The table was displacement controlled and therefore seismic input was supplied as table displacement over a specific time interval.

Figure 6.9. Shaking foundation used in 2/3rd scale, 3-storey dynamic test frame

6.4.2 Similitude scaling for dynamic testing

As mentioned in Section 6.2.2 the model was scaled to two-thirds the size of the prototype building (scale factor $\lambda = 2/3$). In doing this a constant stress, constant acceleration law was selected to avoid the scaling of acceleration and as material densities are not easily scaled. The scale factors used when applying this scaling law are presented in Table 6.1. In the table P has been used to represent the Prototype and S has been used to represent the Scale Structure.

Table 6.1. Similitude scaling factors used for dynamic frame testing

Parameter	Symbol	Unit	Test-prototype relationship	Test-prototype scale factor
Stress	σ	σ	$\sigma_S = \sigma_P$	1
Acceleration	a	a	$a_S = a_P$	1
Length	L	L	$L_S = \lambda L_P$	λ
Force	F	$F = \sigma L^2$	$\sigma_S L_S^2 = \sigma_P \lambda^2 L_P^2$	λ^2
Moment	M	M = FL	$F_S L_S = \lambda^2 F_P \lambda L_P$	λ^3
Mass	m	m = F/a	$F_S/a_S = \lambda^2 F_P/a_P$	λ^2
Mass Density	ρ	$\rho = m/L^3$	$m_S/L_S^3 = \lambda^2 m_P/(\lambda L_P)^3$	λ^{-1}
Time	T	$T = (L/a)^{0.5}$	$(L_S/a_S)^{0.5} = (\lambda L_P/a_P)^{0.5}$	$\lambda^{0.5}$
Velocity	v	v = L/T	$L_S/T_S = \lambda L_S/(\lambda^{0.5} T_S)$	$\lambda^{0.5}$
Weight	W	W = F		λ^2

6.4.3 Additional masses

The necessity to add mass to the frame came from two sources: the mass due to the scaling of the test frame and the mass due to live loading. As mentioned above the prototype building was taken to be an office structure which also had a rooftop garden.

In order to calculate the total required mass, first the mass of the prototype building was calculated. As mentioned above the flooring consisted of solid timber panels (150 mm thick in the prototype structure) and was assumed to be covered by a grout and screed layer followed by flooring. The final floor was planned as a rooftop garden consisting of waterproofing measures, levelling concrete and soil. The live load values for an office structure were Q = 3 kN/m^2 for the two inhabited levels and Q = 2 kN/m^2 for the open roof. A glass façade (and balustrade in the case of the roof level) was considered to surround the building. In combining the various loadings the following formula was used:

$$m_i = G_1 + G_2 + \psi_E Q \tag{6.1}$$

Where:

m_i = The seismic mass of the floor

G_1 = Dead load of structural elements

G_2 = Dead load of non-structural elements

Q = Live loading

Ψ_E = Seismic combination factor

A summary of these loads is shown in Table 6.2.

Table 6.2. Seismic loads of prototype building

Floor	G_1				G_2		Q	Area	Mass*
	Flooring (kN/m^2)	Beams (kN)	Columns (kN)	Façade (kN/m)	Office (kN/m^2)	Rooftop (kN/m^2)	(kN/m^2)	(m^2)	(kN)
1 and 2	0.65	10.8	7.5	0.9	2.2		3	26.9	139.5
3 (Roof)	0.65	10.8	3.7	0.56		3.4	2	26.9	136.1

* This is the total seismic mass of the unscaled prototype structure

In order to calculate the required amount of mass to be added to the test frame the masses of the prototype building were multiplied by the scale factor of $(2/3)^2$ as explained in Section 6.4.2. This was due to the fact that the materials used in the test model remained the same and only the size of members was scaled. Following this the mass of the test building itself was calculated and subtracted from the required scaled mass. The remaining mass (i.e. the difference between the scaled mass and the mass of the test frame) was added to the frame using concrete blocks and steel channels. A summary of the masses of the test frame is shown in Table 6.3.

Table 6.3. Additional mass requirement for test frame

Floor	Scaled mass	Test specimen			Additional elements*	Total specimen	Mass required
	(kN)	Flooring (kN)	Beams (kN)	Columns (kN)		(kN)	(kN)
1 and 2	62.0	5.5	3.0	2.2	5.2	15.9	46.1
3 (Roof)	60.5	5.5	3.0	1.7	5.3	15.5	45.0

* Additional elements included the timber balustrade (for security), timber floor covering and attachment plates

The additional mass required was made up of a combination of concrete blocks and steel hold downs. 12 blocks each weighting 3.3 kN were spread out across the flooring as shown in Figure 6.10.

Figure 6.10. Additional mass arrangement used in 2/3rd scale, 3-storey dynamic test frame

The concrete blocks were held in place by 2.8 m lengths of UPN100 steel section (0.1 kN/m). A summary of the additional mass is shown in Table 6.4 along with the total test structure weight.

Table 6.4. Total mass of test structure

Floor	Total Specimen	Added Mass			Total mass	Target Mass
	(kN)	Concrete (kN)	UPN (kN)	Total (kN)	(kN)	(kN)
1 and 2	15.9	39.6	2.2	41.8	57.7	62.0
3 (Roof)	15.5	39.6	2.2	41.8	57.3	60.5
				Total	172.7	

6.4.4 Instrumentation

Instrumentation of the structure consisted of a combination of potentiometers, load cells and accelerometers. The west view of the instrumentation of the test structure is shown in Figure 6.11.

Fourteen horizontal accelerometers (two at each floor in each direction and one in each direction on the shaking foundation) were placed on the structure in addition to a two vertical accelerometers at the first and third floor. Accelerometers were placed in pairs on each floor in opposite (South-west and North-east) corners of the structure.

The displacements of each floor were measured directly with 2 potentiometers connected to each floor level and an external reference frame. By using a set of 2 potentiometers spaced as far apart from one another as possible any torsional response of the frame was recorded. A potentiometer was also attached to the shaking foundation.

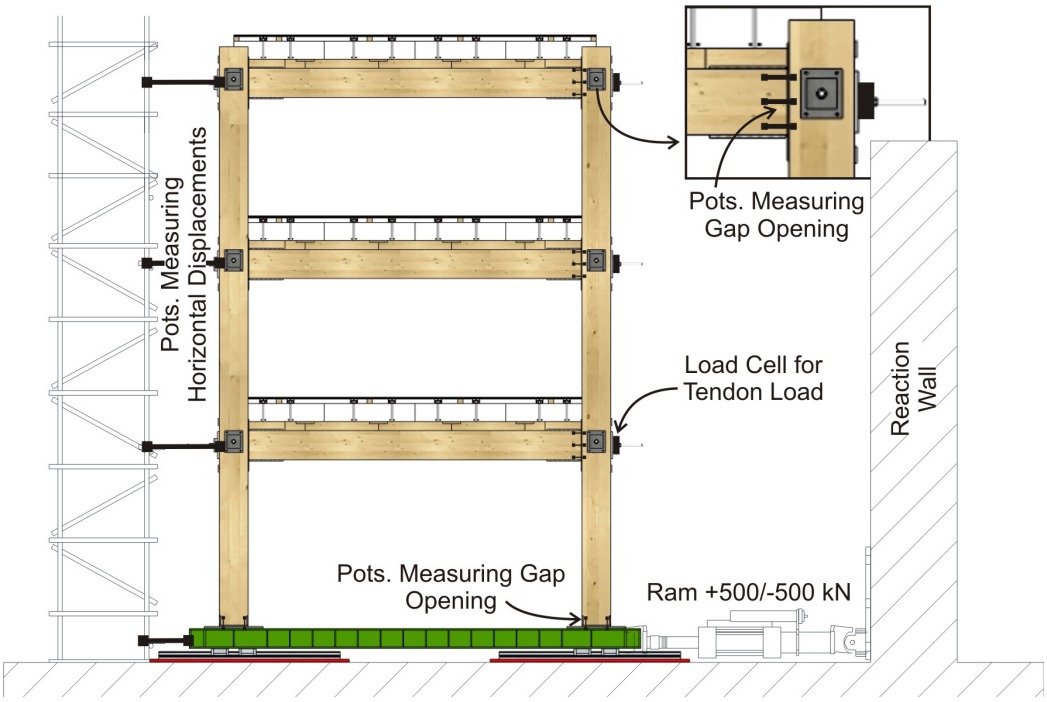

Figure 6.11. West view of frame and instrumentation

Tension in the post-tensioning cables was measured directly for 6 of the 12 post-tensioning bars in the structure with three load cells placed in the direction of loading and three in the transverse direction.

Local deformations were also recorded across the gap opening, similar to the beam-column test program. These were recorded using a series of 3 potentiometers placed across the beam-column interface of one column on each floor. In addition six potentiometers were used at the base of the column (Figure 6.11) in order to record the rocking that occurred between the column and the foundation. Base shear was measured directly using the load cell attached to the dynamic actuator.

In total 48 channels of data were used to record the real-time performance of the structure. This was assisted by various video and image equipment.

The acquisition of data was performed though the use of two separate stations, one recording accelerations and one recording all other data. Both of these acquisitions systems registered at 200 Hz.

6.4.5 Test configurations

Chapters 4 and 5 have described the way in which the alteration of initial post-tensioning values in combination with the recentering ratio β changes the capacity of a post-tensioned timber joint. Section 5.5 then went on to compare the impact that the choice of β has on the dissipative capacity of the beam-column joint. Therefore it can be concluded that altering β not only impacts on the capacity but also on demand. Investigation of this concept is the basis of the dynamic test program.

Two test cases were selected as shown in Table 6.5; one PT ONLY and one with the addition of the milled dissipative steel angles described in Chapter 3 and used during the beam-column testing of Chapter 4. The first option was named PT100_1.00 which had an ultimate connection moment capacity of M_{con} = 17 kN. This load case was designed using Displacement Based Design (Priestley et al. 2007) which will be discussed in Chapters 7 and 10. As mentioned, adding steel without reducing the post-tension moment contribution (PT100_0.60) has the effect of both increasing capacity and decreasing demand. This test case was expected to create a decrease in displacement without increasing acceleration and therefore base shear.

Table 6.5. Experimental cases for dynamic frame testing

Name	$T_{pt,i}$	β	Moment capacity at 2% total rotation		
			M_{pt}	M_s	M_{con}
Hybrid case (with the addition of steel elements)					
PT100_0.60	100 kN	0.60	15.4	11.8	26.2
Post-tension only case					
PT100_1.00	100 kN	1.00	16.7	0.0	16.7

In order to further illustrate and confirm the effect of altering both the initial post-tensioning and the reinforcing contributions, Acceleration Displacement Response Spectra (ADRS) have been constructed for each of the two test cases as shown in Figure 6.12.

The ADRS were constructed by plotting the push-over displacement (base shear versus the displacement at the effective single degree of freedom height) against the non-linear demand spectra. The non-linear acceleration and displacement spectra were

constructed by multiplying the elastic design spectrum by the factor R defined as (Priestley et al. 2007):

$$R = \sqrt{\frac{7}{2+\xi}} \tag{6.2}$$

Where:

ξ = the system damping ratio of the structure taken as a combination of the elastic damping, ξ_{el}, and the hysteretic damping, ξ_{hyst}

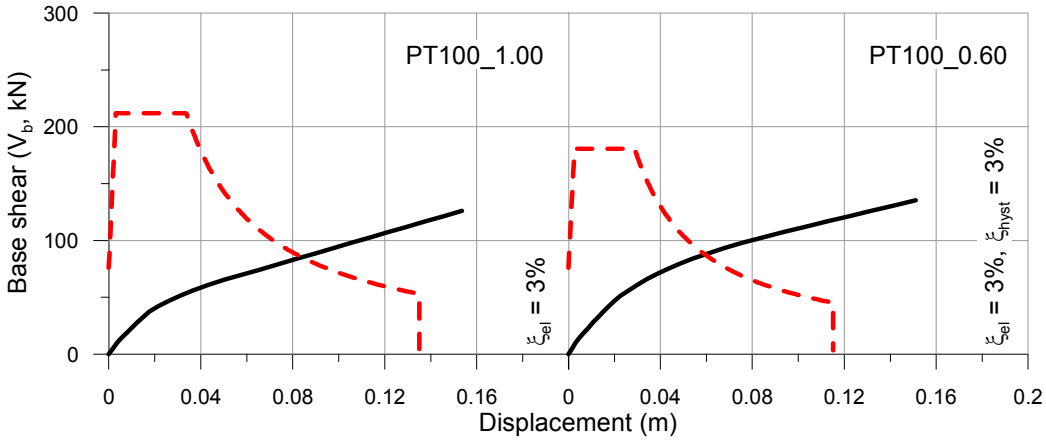

Figure 6.12. ADRS spectra for the shake-table test cases comparing push-over frame response (in solid black) with design demand (in dashed red)

As shown in Figure 6.12 the case without the addition of dissipative reinforcing (PT100_1.00) had an increased seismic demand when compared to the case with the addition of dissipative reinforcing (PT100_0.60). This case has been plotted against a spectrum which has been slightly increased (R = 1.18) compared to the code spectrum in order to account for the fact that post-tensioned timber systems typically display low levels of elastic damping taken as 3% (Pino Merino et al. 2010).

PT100_0.60 had a significantly reduced performance point (i.e reduced displacements) due to the addition of the steel angles. As shown this had the effect of both increasing strength (larger base shear capacity shown by black line, Figure 6.12) and reducing demand with a diminished damped spectrum (red line Figure 6.12). It is important to note however that this decrease in total displacement led to a decrease in ductility, which, as displayed in Equation 5.57 of Section 5.5 leads to reduced damping.

The structure was first tested (subjected to the full test regime) with the addition of the dissipative reinforcing angles (PT100_0.60). Upon completion the angles were removed and PT ONLY testing was performed (PT100_1.00). This was possible due to the damage free nature of post-tensioned timber.

6.4.6 Seismic input

The input for the shaking table testing was based on a site within Italy with high seismic hazard. The code spectrum which was used when selecting the records was defined in accordance with the current Eurocode for seismic design (EN 1998-1:2003 2003) having a PGA of $a_g = 0.35$, a soil factor of S = 1.25 (Soil class B – medium soil) and a return period of 1 in 475 years giving a PGA for the design spectrum of 0.4375.

The testing input was a set of 7 spectrum compatible earthquakes selected from the European strong-motion database (Figure 6.13). The characteristics of these are shown in Table 6.6. In order to maintain similitude (Table 6.1) the time scale of the acceleration inputs was scaled by a factor of $(2/3)^{0.5}$. Four of the earthquakes were also scaled in acceleration in order to ensure the average of their spectral acceleration matched as closely as possible the code acceleration spectrum.

Table 6.6. Earthquake characteristics

ID Code	Location	Date	M_W	PGA (g)	PGV (ms^{-1})	Epicentral Dist. (km)	Scale factor
001228x	Izmit, Turkey	17/08/99	7.6	0.357	0.332	47	1.5
000196x	Montenegro, Serbia	15/04/79	6.9	0.454	0.388	25	1.0
000535y	Erzican, Turkey	13/03/92	6.6	0.769	1.077	13	1.5
000187x	Tabas, Iran	16/09/78	7.3	0.926	0.844	57	1.0
000291y	Campano Lucano, It	23/11/80	6.9	0.264	0.413	16	1.5
004673y	South Iceland	17/06/00	6.5	0.716	0.720	15	1.5
004677y	South Iceland	17/06/00	6.5	0.227	0.208	21	1.0

Three of the earthquakes shown were selected in order to provide a second, smaller group of test inputs (001228x, 000196x and 000535y). These records were selected as their average provided an adequate representation of the design spectra as shown in Figure 6.13. As the average of the earthquake inputs was studied for comparison with the design spectrum the demand of each individual earthquake was either above (e.g. record 000535y) or below (e.g. record 001228y) the design spectrum. As a consequence it was expected that frame response was also above or below design values (depending on input) with the average response providing the target values.

The single earthquake 000196x was identified as being the record most representative of the design spectrum.

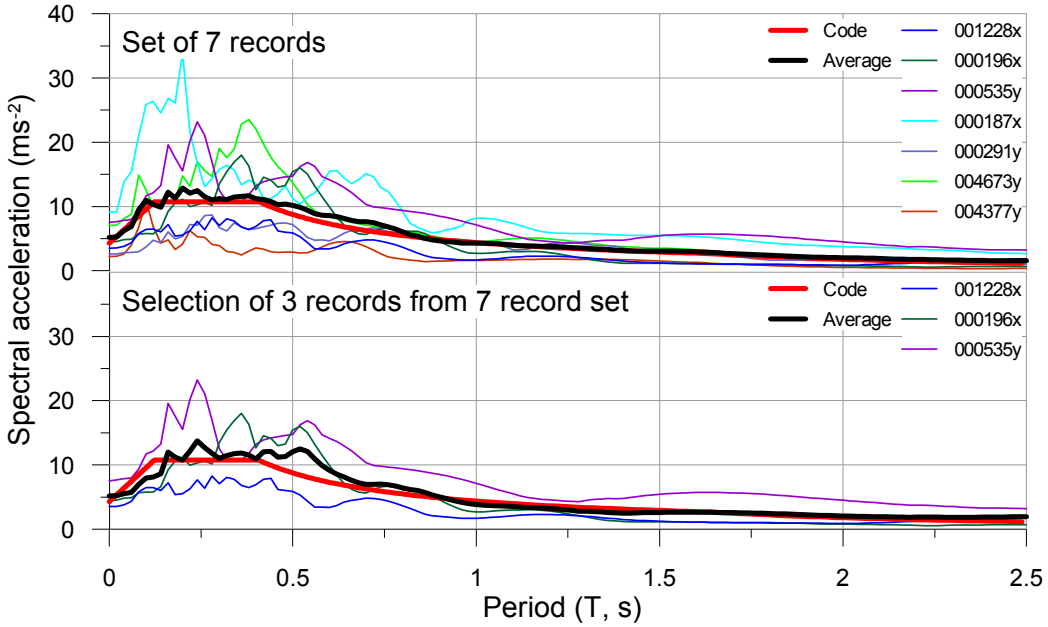

Figure 6.13. Selected earthquake input for shaking table testing

6.4.7 Dynamic identification of test frame

For each test case dynamic identification was performed before seismic testing was begun. Dynamic identification testing of the model was carried out in order to find its first three natural frequencies of vibration and considered a number of different excitation sources including: hammer impact excitations and sine-sweep ground motion.

In Figure 6.14 the Fast Fourier transforms used in order to identify the dynamic characteristics of the frame are shown along with the experimental natural frequencies ($f_{i,exp}$) corresponding to translational modes along the testing direction. These results corresponded to the hammer impact test response on the third floor or the structure which provided the clearest representation of the structural modes. The periods corresponding to these modes are also shown.

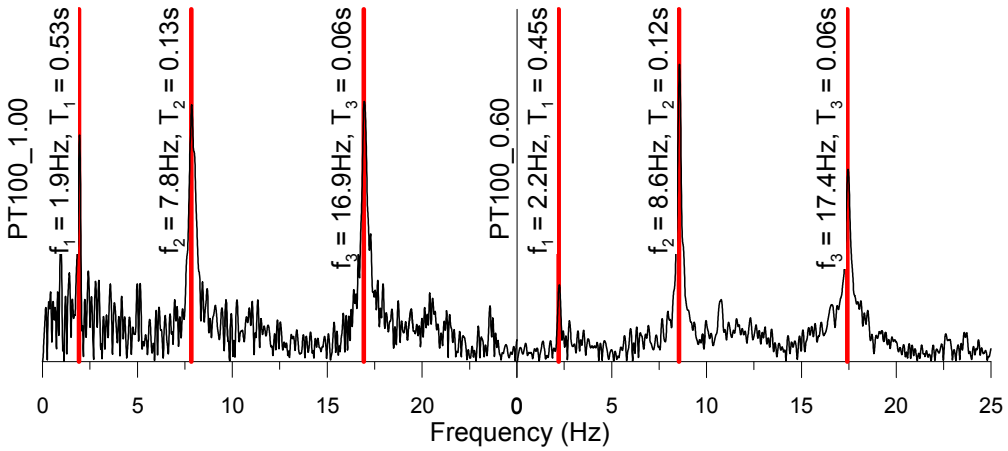

Figure 6.14. Fast Fourier transforms of dynamic test model 3rd floor acceleration response under hammer impact

Figure 6.14 displays a slight change in natural frequency between the test configurations with (PT100_0.60) and without (PT100_1.00) the dissipative reinforcing. As the mass remained effectively identical between the two tests this result implied a reduction in stiffness occurred between tests PT100_0.60 and PT100_1.00.

A possible reason for this reduction in stiffness was the creation of minor damage to the frame. As mentioned above, the PT100_0.60 test case was performed before the PT ONLY case of PT100_1.00. During PT100_0.60 testing large drift levels were reached which may have damaged structural elements. This point is discussed further in Section 6.5.6.

6.5 TEST RESULTS PT100 β = 0.60

In total 20 key dynamic tests were performed on the specimen with an initial post-tensioning value $T_{pt,initial}$ = 100 kN and a dissipative reinforcing level in order to obtain a re-centering ratio β = 0.60 at a total frame drift of θ_t = 2 %. Dissipative reinforcing angles were placed at the beam-column joint interface at each level (2 x ID5 top and bottom as presented in Chapter 3, F_y = 14.2 kN, Δ_y = 0.60 mm) and at the column base (1 x ID8 B both sides as presented in Chapter 3, F_y = 25.5 kN, Δ_y = 0.75 mm).

The test matrix is shown in Table 6.7. As shown the structure was subjected to the set of three earthquakes up to 100% of their PGA. The full set of seven earthquakes was performed at 50% of PGA. A single record (001228x) was applied at 125% of PGA.

Table 6.7. Test matrix for PT100_0.60 shaking table testing (numbers indicate test sequence)

% PGA	001228x	000196x	000535y	000187x	000291y	004673y	004677y
10	1	2	3				
25	4	5	6				
50	7	8	9	11	12	13	14
75	10	15	16				
100	17	18	19				
125	20						

During any dynamic campaign it is important to control the input acceleration. As mentioned in Section 6.4.1 the shaking foundation was displacement controlled. During testing the frequency content of the seismic input measured by the accelerometers placed on the shaking foundation was controlled and compared against the desired input shown in Figure 6.13. An example of this comparison is shown in Figure 6.15 for the PT100_0.60 testing at 100% of PGA.

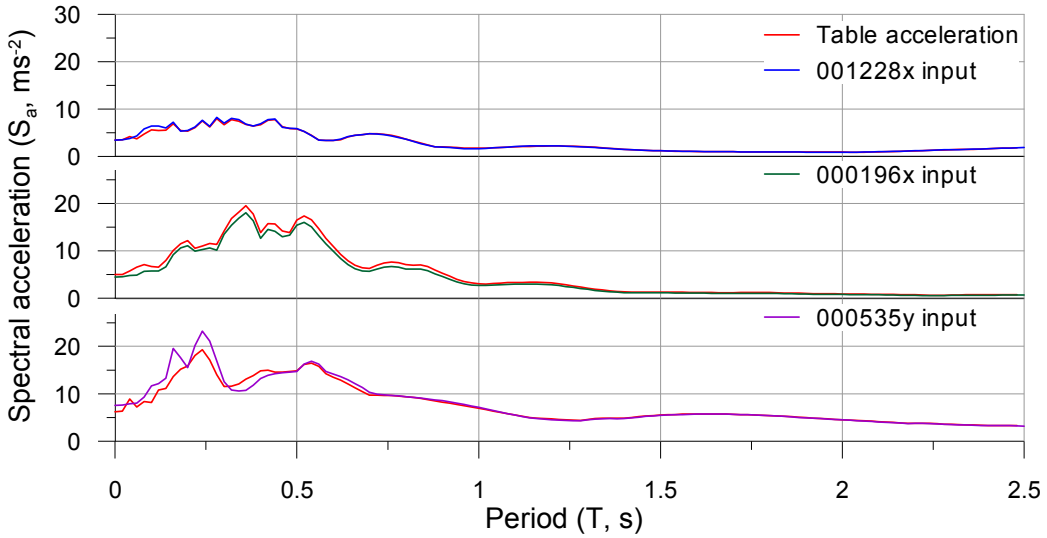

Figure 6.15. Comparison between desired and actual frequency content for testing PT100_0.60 under earthquakes 001228x, 000196x and 000535y at 100% PGA.

As shown the input and the recorded spectral accelerations were sufficiently accurate across all period ranges, in fact within the range of the fundamental frequency of testing values were almost identical. A small issue can be seen in the low period (high frequency) range of earthquake 000535y which may have had a slight impact on the response of the higher modes of the building.

Visually the frame performed as expected with no damage occurring throughout the testing regime. Figure 6.16 shows the total input force as measured by the dynamic actuator versus the drift recorded at the first floor of the structure. The force in the dynamic actuator was used and not a force = mass x acceleration approach was used

due to the two acquisition systems used (as described in Section 6.4.4) being slightly out of phase. Comparison of the actuator data with the F = ma approach was performed however with average results being within ± 5%.

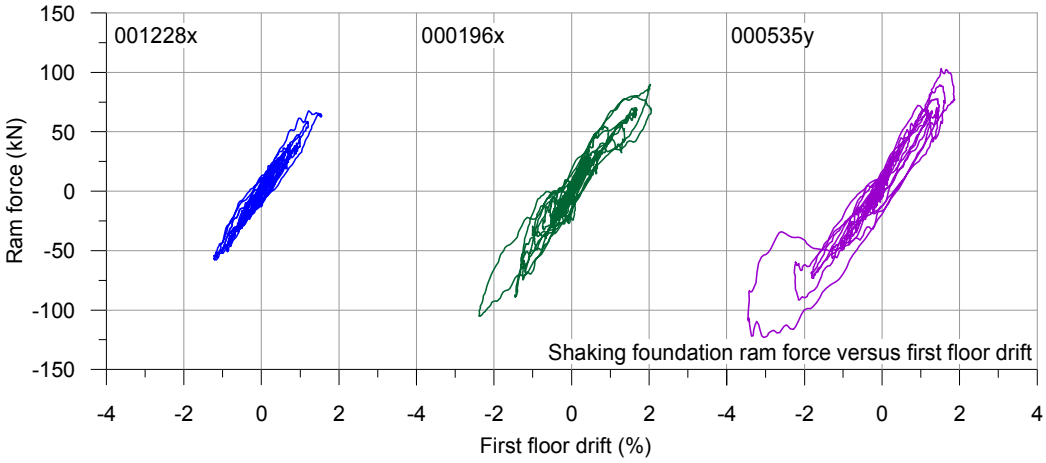

Figure 6.16. Shaking foundation ram force versus first floor drift for PT100_0.60 testing 100%PGA

Figure 6.16 shows, at larger drift levels above approximately 2%, the development of the typical flag-shaped loops found during the beam-column testing of Chapter 4, however the nonlinear response of the structure seemed to develop later than expected. A full analysis of the testing regime PT100_0.60 is presented in the following paragraphs.

6.5.1 Drift and displacement response of test structure

Displacement response of the structure was recorded using a series of seven (six distributed up the building and one at the base) string potentiometers as described in Section 6.4.4. Knowing the floor displacement responses, interstorey drifts were able to be calculated.

Maximum displacement response of structure

The maximum displacement responses of the test structure are shown in Figure 6.17 for each of the three earthquakes used at varying levels of PGA. The average of the results is shown in black. The solid lines denote the movement recorded on the west side of the frame with the dashed line denoting the movement on the East side. Displacements in Figure 6.31 are relative to the movement of the shaking foundation.

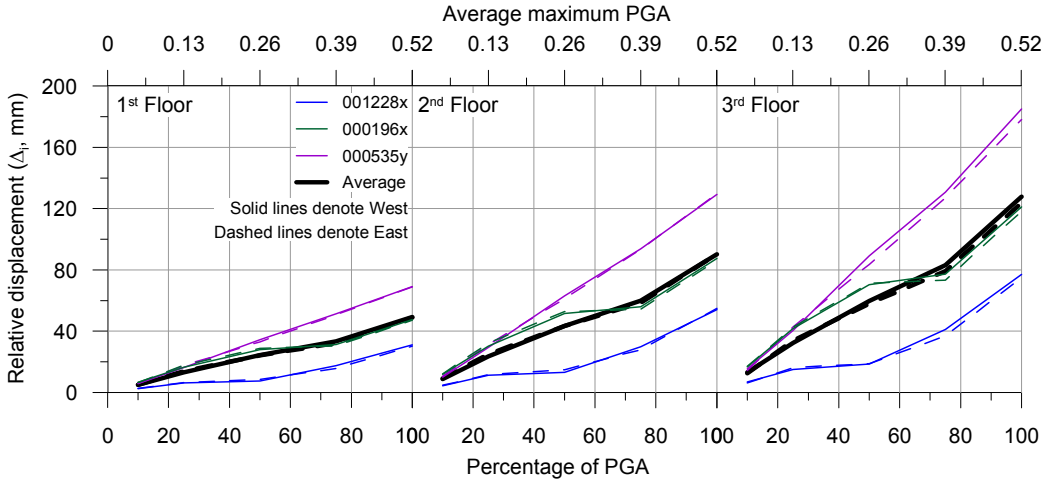

Figure 6.17. Maximum displacements of test frame at increasing levels of PGA for PT100_0.60

Figure 6.17 shows an almost linear increase in the average maximum displacement with increasing PGA up until 75%. Following this point a slight increase in rate was observed. This was consistent with the onset of gap opening. The frame also appeared to be responding symmetrically, with the East and West displacements being equal (i.e. negligible torsional response) with the exception of a slight increase in the West displacements on the final floor.

Maximum drift response of test structure

From the displacement recordings it was possible to calculate frame drifts which are shown in Figure 6.18.

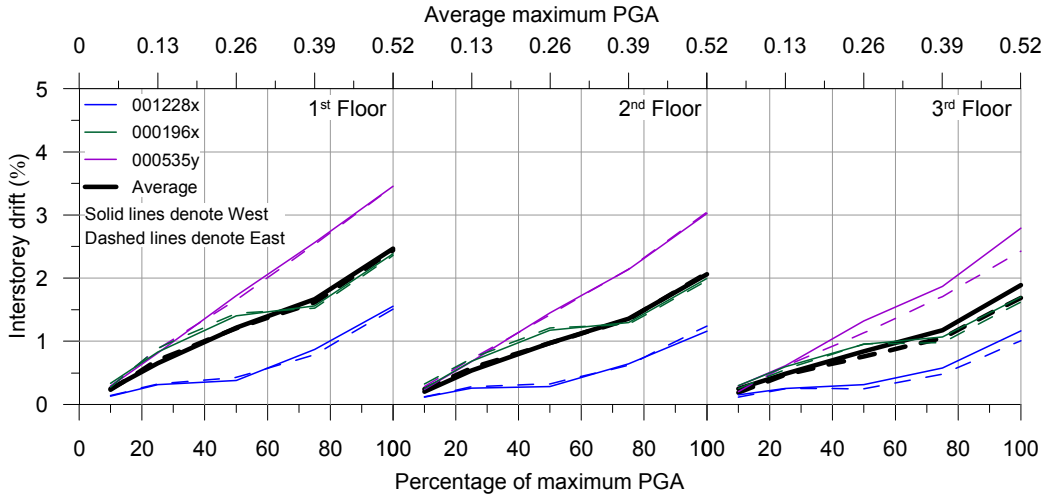

Figure 6.18. Maximum drifts of test frame at increasing levels of PGA for PT100_0.60

As with the maximum displacement measurements, Figure 6.18 shows an almost linear increase in drift up until the PGA level of 75% and the frame seems to be

responding symmetrically with the exception of the final floor which displayed slightly larger drifts on the West side.

The maximum average drift levels occurred at the first level of the frame and were significantly larger (2.46%) than design drift levels which were expected to be around 1.6% for the test case PT100_0.6. Although the reduction of the beam depth from 320 mm to 305 mm will have in part created larger displacements, further performance issues with the test frame were recognised which created this increased drift. These will be discussed in Sections 6.6.4 and 6.5.5. The maximum recorded drift of the first floor of the test frame was 3.46% which occurred during the 000535y record at 100% (PGA = 0.77 g). Maximum drift levels remained roughly equal up the structure with average maximum drifts of 2.45%, 2.07%, and 1.78% for the 1st, 2nd and 3rd stories, respectively.

Residual drift of test structure

Chapter 2 discussed the important role which residual displacements can have in post-earthquake recovery. Figure 6.19 shows the residual drifts following each test for PT100_0.60. As shown, a general increasing trend of residual drift was measured with a maximum value of 0.12% being recorded during testing. Although no set standard for the gauging of the acceptability of residual drift exists this value is likely to be negligible. It can also be seen that this value only occurred on one occasion with average values of less than 0.05% drift being measured. Residual drifts also show that a slight residual torsion was exhibited

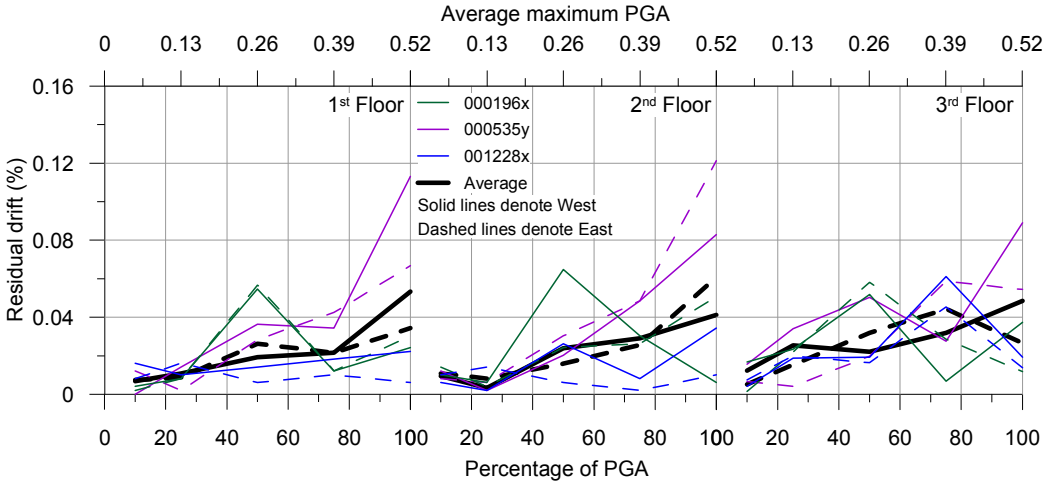

Figure 6.19. Residual drifts of test frame at increasing levels of PGA for PT100_0.60

6.5.2 Acceleration response of test structure

As mentioned in Section 6.4.5 and throughout Chapter 4 one of the principal functions of the dissipative reinforcing angles used is to reduce displacements without the increase of accelerations and therefore base shear and internal actions. Figure 6.20 displays the maximum accelerations of the test frame PT100_0.60 at increasing levels of PGA. The amplification of acceleration up the structure can be measured as a ratio between the maximum floor acceleration and the PGA as shown in Figure 6.21.

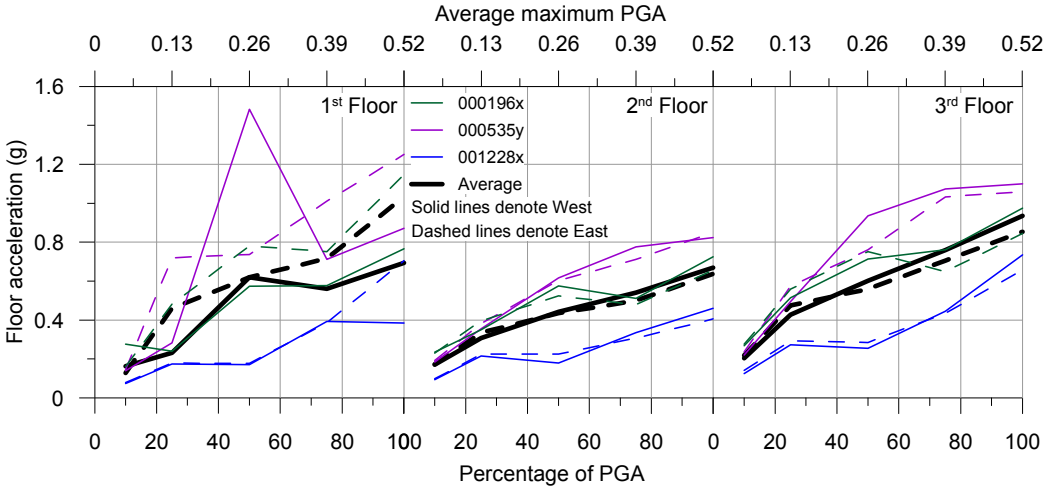

Figure 6.20. Maximum accelerations of test frame at increasing levels of PGA for PT100_0.60

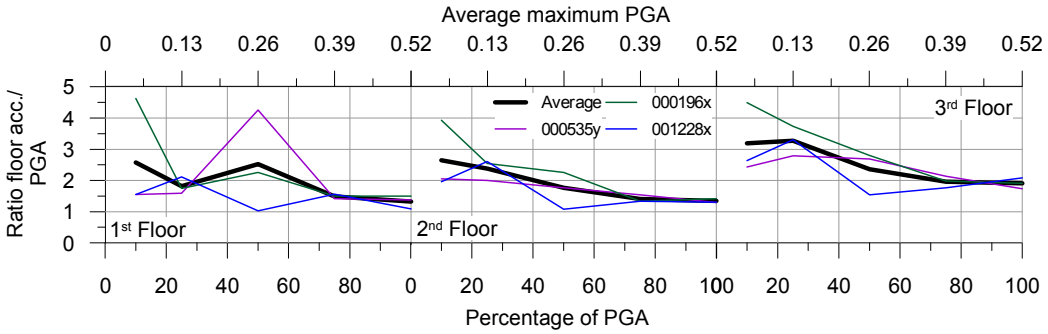

Figure 6.21. Ratio of floor acceleration to PGA at increasing levels of PGA for PT100_0.60

Maximum average floor accelerations of 0.86, 0.66 and 0.90 were measured for the 1st, 2nd and 3rd floors, respectively. Both the second and third floors displayed a steady increase in floor acceleration until testing reached 75% of PGA where acceleration plateaued (especially in the case of earthquake 000535y). This is correspondent with onset of non-linear structural response and congruent with the increase in displacement and drift observed in Figure 6.17 and Figure 6.18.

The first floor however displayed an erratic acceleration response. Although the average of the readings displayed the same increasing trend of the 2nd and 3rd floor, alternating spikes in both the East and West acceleration readings were recorded. Although it is difficult to conclude what the source of these spikes was for certain, one possible source was the initial 'let-go' of the flooring units creating slipping between the flooring and the test frame. As accelerometers were placed on flooring panels and not on the frame itself this would manifest as an acceleration spike. This hypothesis may explain why the spikes in acceleration: a) were alternating between the East and West side (i.e. flooring does not slip simultaneously on both sides), b) only occurred during stronger motion earthquakes (i.e. with larger displacement demands than those previous), c) seemed to occur on the first floor (where rotational demand is greatest). In addition to these facts, during the 50% PGA testing series significant 'timber-timber slipping' noises were heard which were not reproduced during subsequent testing. Minor spikes were also observed at other floors as drift levels increased.

As described in Chapter 2 the amplification of accelerations up the structure can be of particular concern for low damping system such as post-tensioned timber. The amplification up the structure showed a maximum of 4.6, 3.9 and 4.5 for the first, second and third floors respectively. Amplifications decreased with increasing PGA percentage which was expected as the structure became more non-linear (both with gap opening and yielding of the dissipative reinforcing). Overall a maximum amplification under strong motion of 2.1 (001228x PGA100%) was recorded for the final floor of the structure.

6.5.3 Base shear response of test structure

The base shear response of the structure with increasing levels of PGA is presented in Figure 6.22. This was calculated using the accelerations discussed in Section 6.5.2 and the masses presented in Table 6.4. Although a load cell was placed on the dynamic actuator these readings included the weight of the

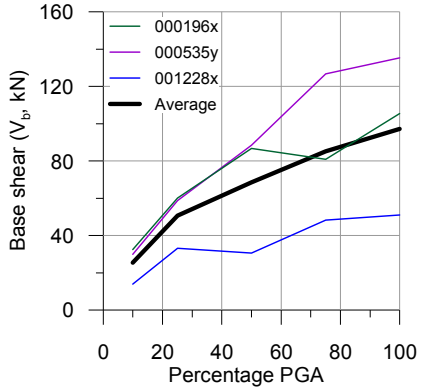

Figure 6.22. Maximum base shear of test frame at increasing levels of PGA for PT100_0.60

shaking foundation and provided higher values than what was actually present during testing.

As expected the base shear display the same general trend as the accelerations presented above. A maximum average base shear of 97 kN was recorded which was similar to the design level base shear presented in Figure 6.22 (represented by the intersection of the frame capacity, in black, and demand, in red).

6.5.4 Local response of beam-column joints

As discussed in Chapter 4 and Chapter 5 the performance of the beam-column joint in a post-tensioned timber frame controls the performance of the entire system. Potentiometers were placed across the 1st, 2nd and 3rd floor south-west beam-column interface. In addition, a load cell measured the amount of tension present in each post-tensioned bar of the West frame during testing. This instrumentation allowed the evaluation of the response of each individual beam-column interface during testing. In addition, visual evidence was collected during testing which further enabled the evaluation of the beam-column connection behaviour. This was done through the placement of a video camera at the beam-column joint interface of the Level One South-West column.

Moment-rotation response

Due to the presence of the angles it was not possible to deduce the total moment-rotation response of the beam-column joint, it was however possible to calculate the moment contribution of the post-tensioning. The moment contribution provided by the post-tensioning (M_{pt}) is shown in Figure 6.23 along with the post-tensioning force (T_{pt}) and the normalised neutral axis depth (c/h_b) against the connection rotation (θ_{con}). Results are shown for earthquakes 001228x, 000196x and 000535y at PGA100%.

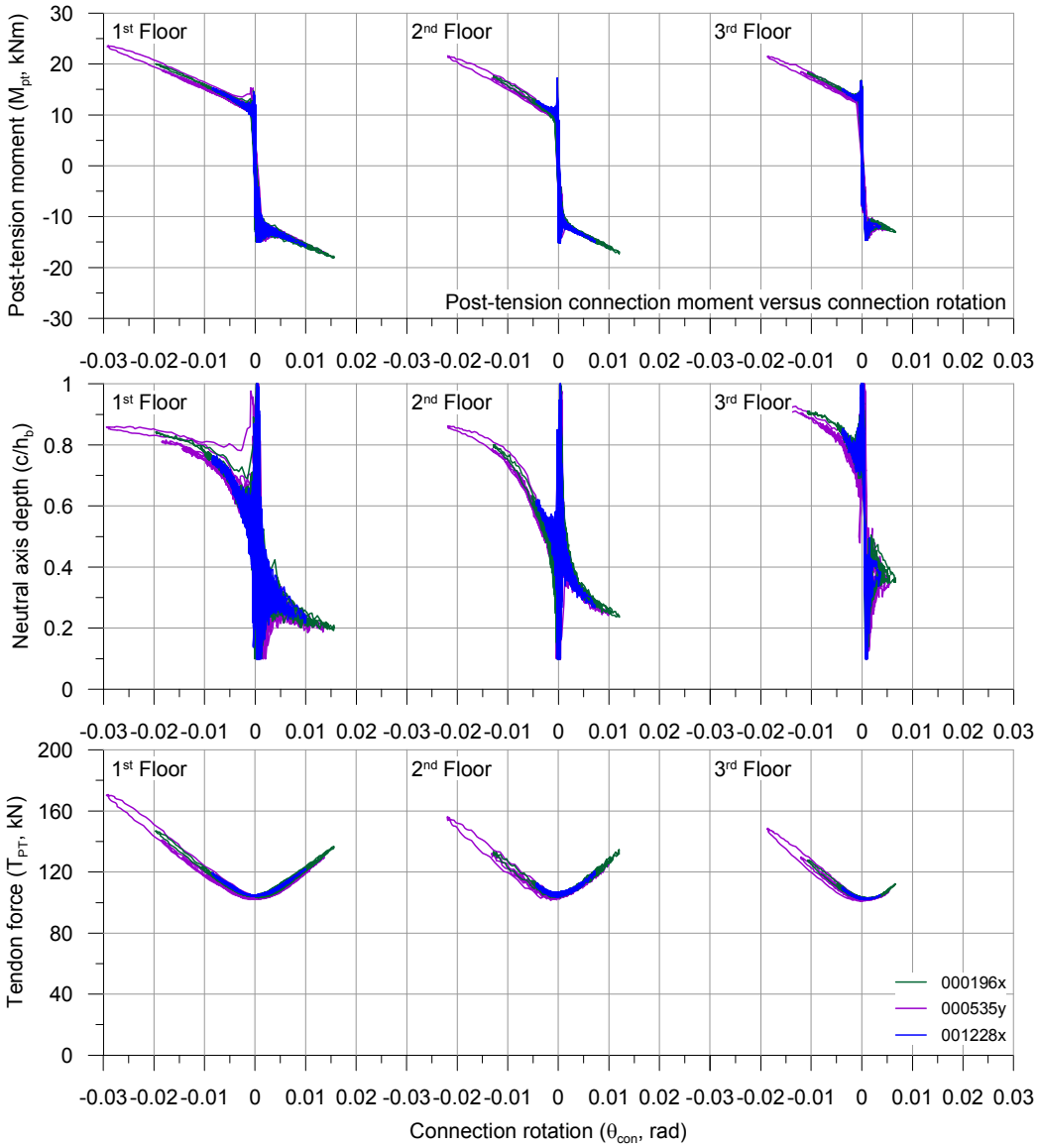

Figure 6.23. Post-tensioning moment, post-tensioning force and normalized neutral axis depth versus connection rotation for PT100_0.60 dynamic testing PGA100%

As expected, Figure 6.23 shows that the behaviour of the beam-column joint as part of a full frame system was the same as the response of the beam-column joint subassembly tested in Chapter 4 and analysed in Chapter 5.

The graphs display the non-linear elastic behaviour of the post-tension moment contribution and also the way in which the beam-column joint remained undamaged throughout testing. This is evident in the way that the neutral axis and moment response performed in the same manner both during testing and among tests. No losses were observed in the post-tensioning tendons.

Rotational response

Chapter 5 provided discussion on the way in which the elastic rotations of the frame create reductions in connection rotation. Figure 6.24 shows the maximum rotations for the test frame at increasing levels of PGA. The solid lines on the graph show the maximum total rotations (as derived from the interstorey drift), and the dashed lines show the maximum recorded connection rotations. The ratios between these two values are also shown in the bottom graph of Figure 6.24.

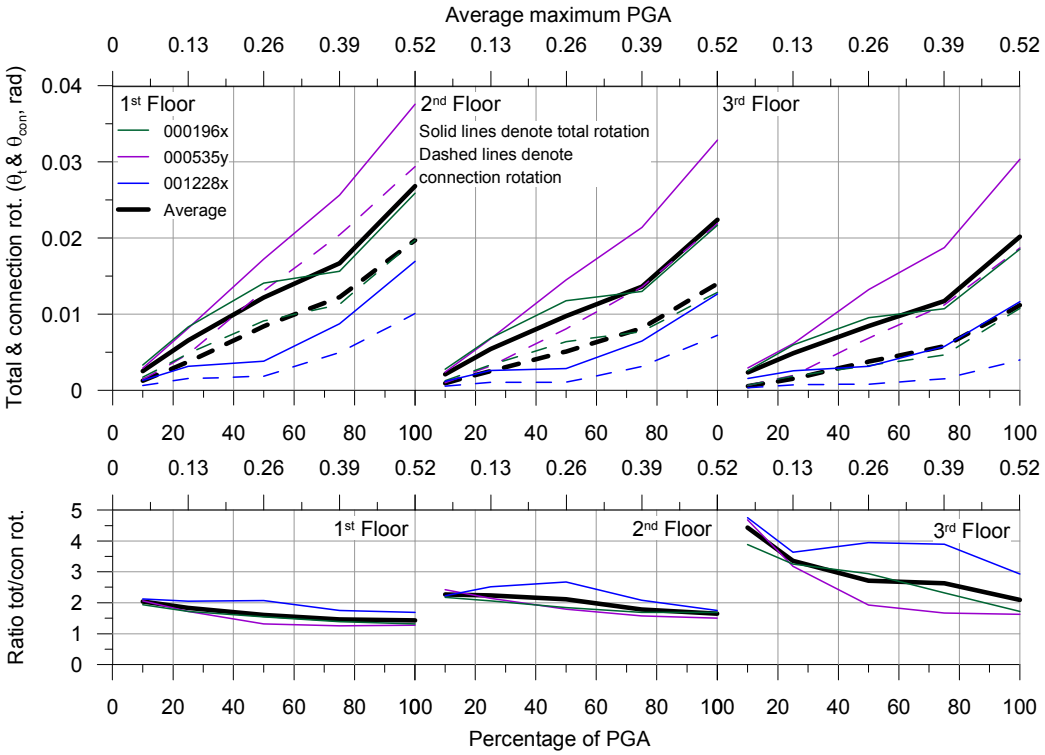

Figure 6.24. Maximum total and connection rotations and ratios (West-side frame) of test frame to connection rotations at increasing levels of PGA for PT100_0.60

As discussed in Section 5.4 the maximum connection rotations (θ_{con}) of post-tensioned timber frames are considerably reduced when compared to the total rotation (θ_t) of the frame. Average ratios between the total frame and connection rotations of the first two floors ranged between 2.3 and 1.4. The third floor presented higher average ratios ranging between 4.4 and 2.1. These higher ratios stemmed from both larger column rotations caused by altered system mechanics (i.e. the lack of column above the joint with which to share moment) and decreased total rotations as explained below.

The ratio between the two rotations showed a decreasing trend, with the ratio between the connection and total frame rotation decreasing with increasing total rotation. This was congruent with the statements made in Chapter 5 which provided moment dependant equations for the calculation of the rotation contributions for the beam (θ_b), column (θ_c) and joint panel (θ_j). The rate of increase in moment capacity decreases with increased connection moment as the gap opens and dissipative reinforcing yields. This means that the ratio between the total frame and connection rotation decreases following this point of non-linearity. This can be seen above in three ways; the ratio decreased with increasing PGA, the ratio was smaller for stronger earthquakes, and the ratio was smaller for the lowest level of the frame which had the highest connection rotations.

This change in ratio between the total frame and connection rotations following the point of non-linearity of the beam-column interface is further shown by a direct comparison between the total and connection rotations during testing as shown in Figure 6.25. The graph shows a clear transition in the ratio between the total and connection rotation (seen as a change in slope) which corresponded with the point of gap-opening as shown in Figure 6.23. As the beam-column joint at each level possessed the same design capacity the rotational response at each floor was also similar. Figure 6.25 shows the total rotation of the frame translated to the column face using Equation 5.3 in order to enable a direct comparison.

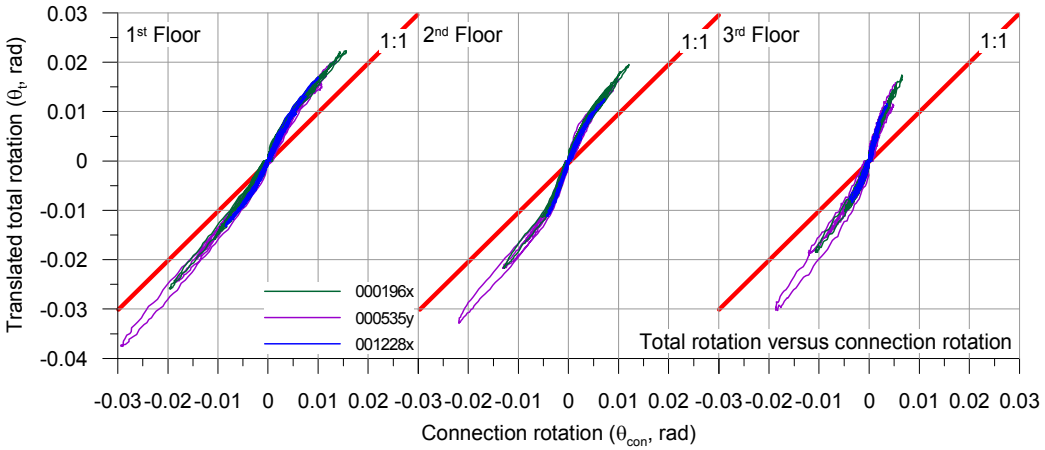

Figure 6.25. Total frame rotation versus connection rotation for PT100_0.60 testing 100%PGA

Visual inspection of beam-column joint behaviour

During testing a video camera was placed at one of the beam-column joint interfaces in order to provide a visual record of its performance. Figure 6.26 shows the beam-column joint, with a focus on the dissipative reinforcement connection, during test 000535y at PGA100%.

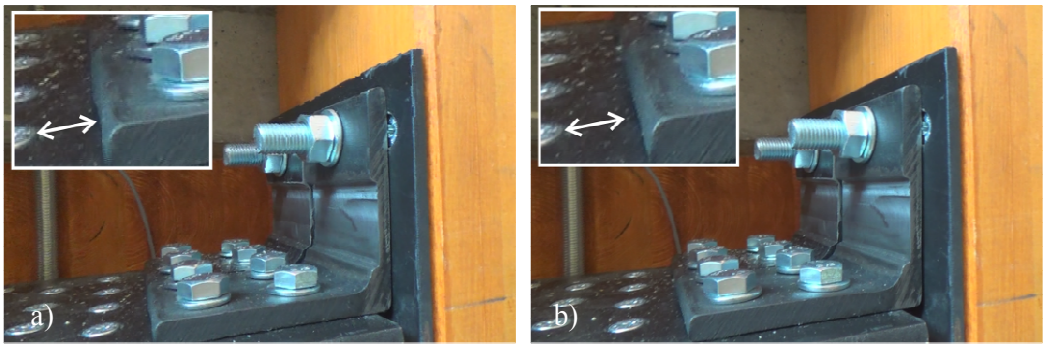

Figure 6.26. Performance of PT100_0.60 beam-column joint interface during test 000535y PGA100% at a) maximum negative drift and b) maximum positive drift

Figure 6.26 shows slipping of the dissipative connection during testing. This reduced the effectiveness of the reinforcing by decreasing both stiffness and dissipative capacity. Although the slipping shown is approximately 3 mm this represented almost half of the expected reinforcing displacement and was 6 times the yielding displacement. It is likely that this fact led or at least was a contributing factor to the increased drifts and displacements mentioned in Section 6.5.1.

Slipping between the base of the dissipative reinforcing and the connection plate also explains why the dissipative loops shown in Figure 6.16 were low in spite of the significant levels of gap opening shown in Figure 6.23. It is unclear the degree to which this slipping occurred during testing with only one of the connections being recorded. It is clear however that yielding did occur during test 000535y due to the flag shape response shown in Figure 6.16.

This slipping was related to the necessity to create holes in the dissipative reinforcing angle which were larger than the fixing blots (+ 2mm on the radius). This was done to enable the angles to be placed without specific sizing of each individual angle.

6.5.5 Local response of column-foundation joints

The local response of the column foundation joint was monitored in two ways; through the use of a series of 6 potentiometers placed across the zone of expected gap opening between the column shoe base and the steel foundation, and the placement of a video camera at the base of the North-East column.

Through study of the experimental data it was difficult to deduce the moment-rotation response of the column base due to the constantly changing axial load in the column. It was however possible to evaluate the rotation and displacement response and visually study the column performance.

Visual inspection of beam-column joint behaviour

As with the beam-column joint interface the movement of the column base against the column foundation was recorded visually. Figure 6.27 clearly demonstrates a deficiency in the frame performance.

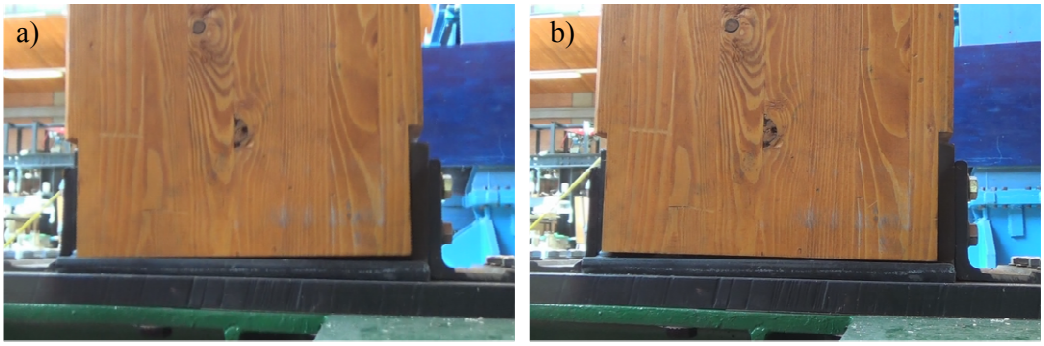

Figure 6.27. Performance of PT100_0.60 North-East column-foundation interface during test 000535y 100%PGA at a) maximum negative drift and b) maximum positive drift

During the frame movement rocking was occurring between the base of the timber column and the steel shoe insert and not between the insert and the foundation as designed. This rendered the dissipative devices at the base of each column inactive thus reducing stiffness, strength and dissipative capacity. Due to there being no visual damage externally in any of the four column bases following testing, the likely cause of this is the failure of the interface between the glued-in bars and the drilled holes into which they were placed. Inspection of this connection following testing indicated that the standard practice placement a bleed hole to ensure full bond was not performed which may have led to the joint failure.

Rotational response

The rotational response of the column base was calculated using the potentiometers shown in Figure 6.11. Table 6.8 displays the maximum measured column base rotations during PGA100% testing for the columns which were instrumented. These values are shown alongside the maximum Level One rotations measured.

Table 6.8. Comparison between the maximum Level One (L1) rotations and measured column rotations

	L1 rot. (rad)	NW col. ext. (rad)	SW col. ext. (rad)	SW col. int. (rad)
001228x	0.017	0.017	0.012	0.014
000196x	0.026	0.024	0.025	0.021
000535y	0.038	0.029	0.040	0.040

Table 6.8 shows that the values of the maximum Level One rotations and the maximum column rotations were very similar. This tends to confirm that the column base had little-to-no moment capacity during testing due to the fact that moment capacity would have acted to restrict rotations.

In addition to the rotations, the absolute values of displacement between the North-West column base and the shaking foundation, from the column base potentiometers described in Section 6.4.4, were analysed. Figure 6.28 displays these displacements during the PGA100% testing sequence of PT100_0.60.

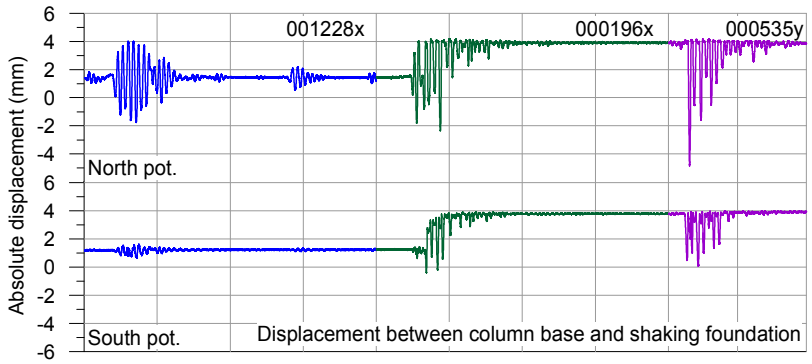

Figure 6.28. Displacements of North-West column during for PT100_0.60 PGA100% testing (internal)

Figure 6.28 displays a significant (3.8 mm) amount of residual displacement, linked to the failure of the glued in rods, between the column base and the rocking foundation. These residual displacements occurred during test 000196x and remained almost constant during test 00535y. These residual displacements following the 000196x test were symmetric for this column with values of 3.6 mm and 3.2 mm being recorded

externally. Residual displacements were however negligible with values of 0.2 mm and -0.1 mm being measured following testing (000535y).

In addition to these residual displacements it can be seen that the column base displayed asymmetric rocking behaviour during testing. This is especially evident during test 001228x. Increased displacements on one side of the column (South pot.) corresponded to the changing levels of axial load during seismic testing with increased axial load (and therefore displacement) in one load direction. However, during test 001228x the difference between the two displacement maximums seemed disproportionate to this effect. During test 000196x the behaviour became more symmetric corresponding with the onset of significant levels of residual drift. It is likely that this was caused by delayed failure of one side of the epoxied bars. These tension bars then subsequently failed during test 000196x, leading to increased displacements and more symmetric displacement behaviour. This failure also created the residual displacements seen in Figure 6.28.

Through a combination of instrumentation and visual inspection it can be confirmed that this failure occurred for three of the four column connection (North-East, North-West and South-West). It is therefore likely that failure also occurred in the fourth (South-East) column which was not observed directly.

6.5.6 Dynamic characteristics following testing

Section 6.4.7 discussed the dynamic identification of the test frame before each phase of testing (PT100_0.60 and PT100_1.00). Figure 6.14 showed that the frame had decreased fundamental frequencies before the PT100_1.00 test series. It was suggested that this change in dynamic characteristics may not have been due to a change in the dynamic behaviour of the frame created by the removal of the dissipative reinforcing, but due to slight damage during the PT100_0.60 testing. Figure 6.29 shows the Fast Fourier transform of the tail of third floor acceleration response of test 000535y 100% PGA on PT100_0.60. This was performed for the tail of each earthquake record at every intensity level. As shown the Fundamental Frequencies were identified to be 1.9 Hz, 7.9 Hz and 16.6 Hz for the first, second and third modes, respectively. These values were very similar to values recorded before PT100_1.00 testing (1.9 Hz, 7.8 Hz and 16.9 Hz) upon removal of the dissipative reinforcing. Figure 6.29 also shows the fundamental period of the structure calculated

using the third floor accelerations recorded following the end of the strong motion of each test (each test is represented as a dot with three tests for each level of PGA%).

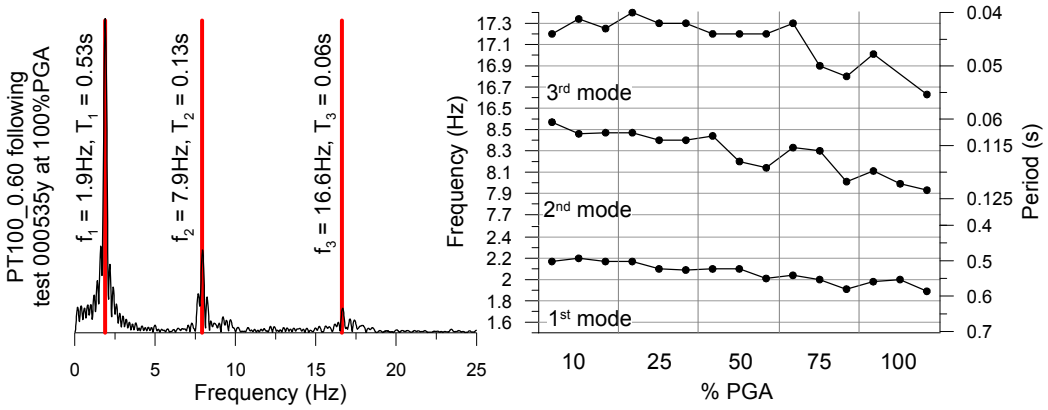

Figure 6.29. Fast Fourier transform of dynamic test model PT100_0.60 3rd floor acceleration response following test 00535y 100% PGA (left) and fundamental frequencies of test model over testing sequence (right)

Figure 6.29 clearly shows a decreasing trend in the dynamic test frames fundamental frequencies during the test sequence. The major changes occurred during larger levels of PGA percentage and specifically during the second (000196x) and third (000535x) tests of each sequence. Previous sections have discussed how during testing cracking noises where heard accompanied by spikes in both floor acceleration and displacement. These have been attributed to the initial slipping and loosening of the flooring panels which may have also lead to decreases in fundamental frequencies.

Section 6.5.5 showed that during high seismic intensity levels the column base connections failed and rendered the dissipative reinforcing placed at these connections ineffective. It has been proposed that this failure did not occur simultaneously at all columns or on all sides of a single column as supported by the displacements shown in Figure 6.28. It is therefore likely that changes in fundamental frequencies were also linked to changes in the column base stiffness caused by these failures.

Of interest however is the fact that the addition and subtraction of dissipative reinforcing at the beam-column joint had a negligible impact of the fundamental frequency of a post-tensioned timber structure. Section 7.4 further discusses this point.

6.6 TEST RESULTS PT100 β = 1.00

In total 17 key dynamic tests were performed on the specimen with an initial post-tensioning value $T_{pt,initial}$ = 100 kN at all floor levels and dissipative reinforcing levels in order to obtain a re-centering ratio β = 1.00 at a total frame drift of θ_t = 2 % at the beam-column joint (i.e. no dissipative reinforcing). Dissipative reinforcing angles were placed at the column base (1 x ID8 B both sides) for stability.

The testing matrix is shown in Table 6.9. As shown the structure was subjected to the set of three earthquakes up to 75% of their PGA. The full set of 7 earthquakes was performed at 50% of PGA. A single record (001228x) was applied at 100% of PGA. Testing was stopped before test 000196x PGA100% due to excessive drift at the first floor level creating concerns about the structure going beyond instrumentation limits.

Table 6.9. Test matrix for PT100_1.00 shaking table testing (numbers indicate test sequence)

% PGA	001228x	000196x	000535y	000187x	000291y	004673y	004677y
10	1	2	3				
25	4	5	6				
50	7	8	9	10	11	12	13
75	14	15	16				
100	17						

As with the PT100_0.60 testing no visible damage (i.e. crushing or splitting of timber members) was observed throughout the testing sequence. Figure 6.30 shows the total input force as measured by the dynamic actuator versus the drift at the first floor of the structure. As shown the overall response of the structure displayed similar characteristics as the PT ONLY testing presented in Chapter 4. A full analysis of the testing regime PT100_0.60 is presented in the following paragraphs. A comparison between testing with (PT100_0.60) and without (PT100_1.00) dissipative reinforcing is presented in Section 6.7.

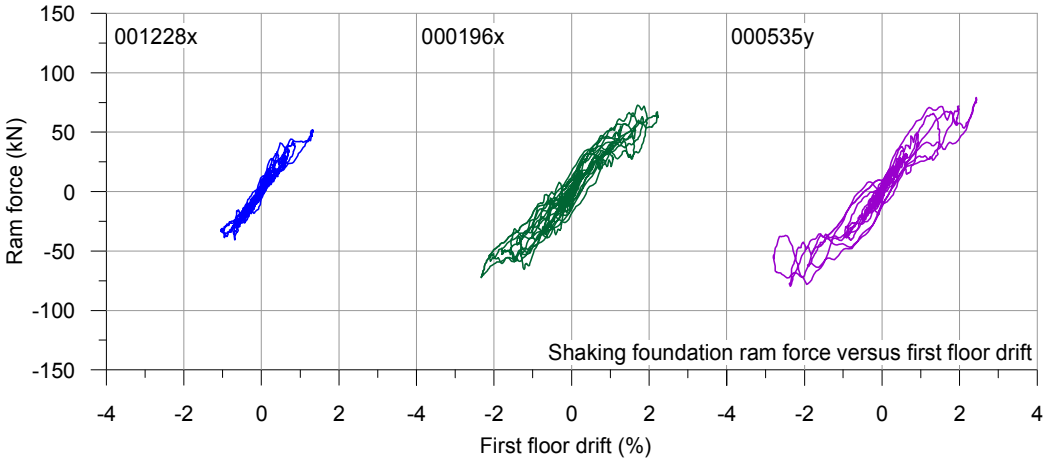

Figure 6.30. Shaking foundation ram force versus first floor drift for PT100_1.00 testing 75%PGA

6.6.1 Drift and displacement response of test structure

As with the PT100_0.60 testing string potentiometers were used to measure the displacement and hence the drift of the PT100_1.00 structure.

Maximum displacement and drift response of structure

The maximum displacement response of the test structure is shown in Figure 6.31a with the maximum drift response shown in Figure 6.31b. Responses are shown for each of the three earthquakes used at varying levels of PGA. The average of the results is shown in grey. The solid lines denote the movement recorded on the West side of the frame with the dashed line denoting the movement on the East side.

Drift and displacement levels increased with increasing PGA percentage with a maximum 1st storey drift of 2.9% being reached during earthquake 000535y at 75% PGA. The average maximum drift at PGA75% was equal to 2.2, 2.0 and 1.9% for the 1st, 2nd and 3rd levels, respectively. The building appeared to be responding symmetrically except for a slight increase in the displacements of the west side of the structure on the third floor. Overall the increases in displacement and drift with increasing PGA percentages appeared to be linear however; a slight change in the rate of increase following the 25% PGA test series was seen. Displacements in Figure 6.31 are relative to the movement of the shaking foundation.

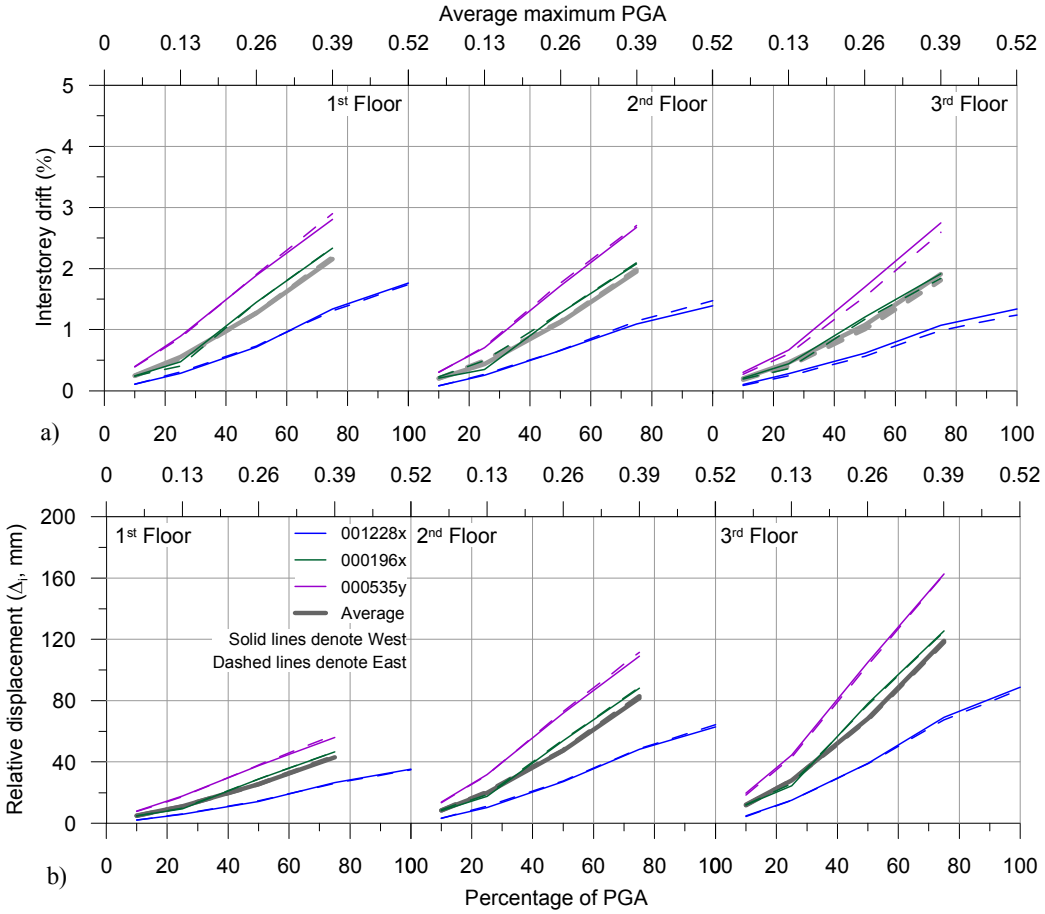

Figure 6.31. Maximum a) drifts and b) displacements of test frame at increasing levels of PGA for PT100_1.00

As with the PT100_0.60 test series drifts are higher than design levels for PT100_1.00. It was anticipated that this test series would have an average design drift of 2.0% at PGA100% however the frame had already reached this value at 75% PGA. During this stage of testing no dissipative reinforcing was used at the beam-column connections however dissipative reinforcing was in place at the base of each column. It is likely that the failure of the column base connection, as described in Section 6.5.5, led to the increased drifts observed during testing by effectively eliminating the moment capacity at the column base.

Residual drift of test structure

Figure 6.32 shows the residual drifts following each test for PT100_1.00. Chapter 5 provided descriptions of the way in which a PT ONLY ($\beta = 0$) beam-column joint presents minimal residual drifts following beam-column rotation. Figure 6.32 supports this observation with negligible average displacements of less than 0.03%

throughout all testing. It is likely that the residual drifts were also reduced by the decreased effectiveness of the dissipative reinforcing at the column base as described in Section 6.5.5. This was due to the relationship between the presence of dissipation and residual drifts (decreased β, increased residual displacements) discussed in Section 4.10. Residual rotations at the column base would have created residual drifts up the height of the test frame.

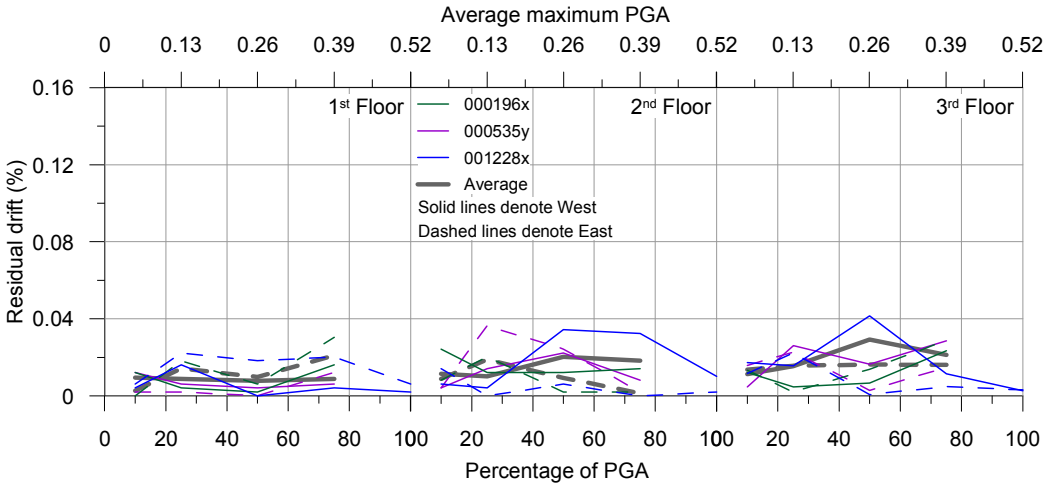

Figure 6.32. Residual drift of test frame at increasing levels of PGA for PT100_1.00

6.6.2 Acceleration response of test structure

The PT100_1.00 test series did not include dissipative reinforcing at the beam-column joint and therefore had nominal dissipative capacity. Figure 6.33 displays the maximum accelerations of the test frame PT100_0.60 at increasing levels of PGA.

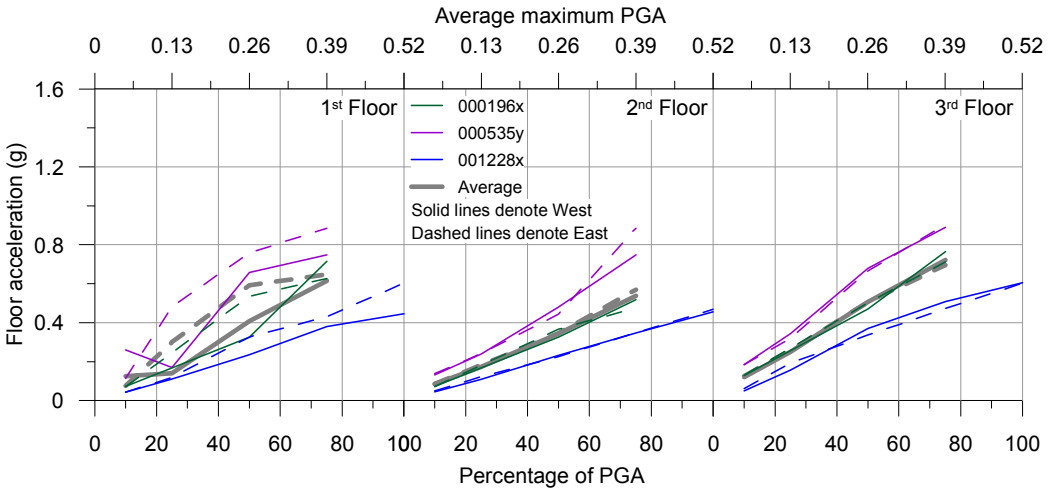

Figure 6.33. Maximum accelerations of test frame at increasing levels of PGA for PT100_1.00

The amplification of acceleration up the structure can be measured as a ratio between the maximum floor acceleration and the PGA as shown in Figure 6.34.

As shown the amplification of acceleration was equal to approximately 1.6, 1.4 and 1.9% for the first, second and third floors for testing with 75% PGA, respectively. These values did not change significantly during testing. Both the linear increase in accelerations and the lack of variation of the ratios presented in Figure 6.34 depart from the observations made during PT100_0.60 test. Further discussion of this point is presented in Section 6.7.2.

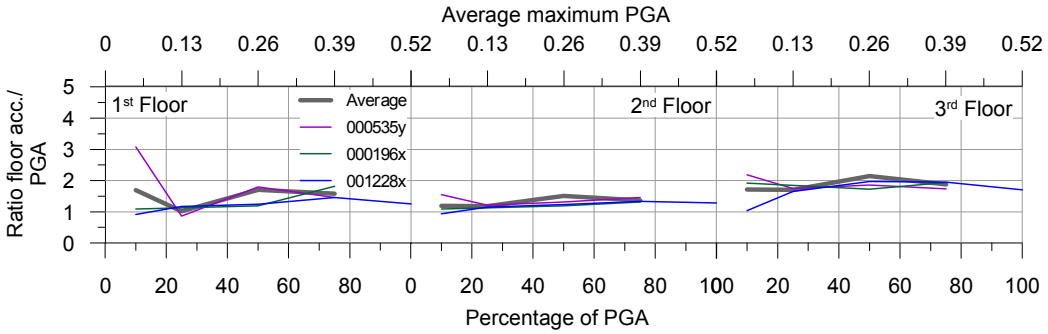

Figure 6.34. Ratio of floor acceleration to PGA at increasing levels of PGA for PT100_1.00 (West-side frame)

6.6.3 Base shear response of test structure

The base shear response of the test structure has been calculated using the accelerations presented in Section 6.6.2 and the masses presented in Table 6.4 in the same manner as Section 6.5.3. The base shear response of the structure with increasing levels of PGA is presented in Figure 6.35.

As expected the base shear displays the same general trend as the accelerations presented above. A maximum average base shear of 72 kN was recorded. Although it was not possible to directly compare this value to the design

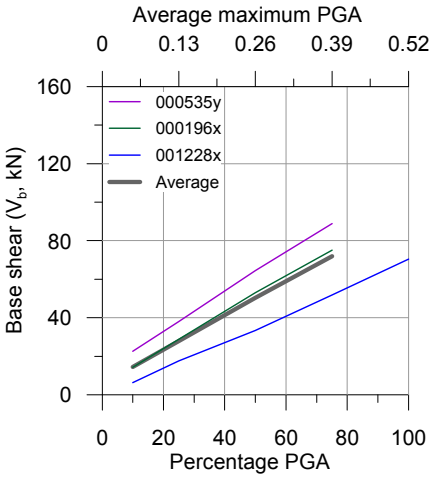

Figure 6.35. Maximum base shear of test frame at increasing levels of PGA for PT100_1.00

values shown in Figure 6.12, if the linear trend is assumed to continue a value of approximately 91 kN would be obtained. This value is similar to the performance point (i.e. the intersection of capacity and demand) presented in Figure 6.12.

6.6.4 Local response of beam-column joints

As already mentioned in Section 6.6.2, PT100_1.00 testing did not contain the use of dissipative reinforcing. Due to this fact a direct evaluation of the moment contribution of each joint was possible. The same instrumentation and visual recording techniques as described in Section 6.5.4 were used to evaluate beam-column joint performance for the PT100_1.00 test series.

Moment-rotation response

As the beam-column joint did not possess dissipative reinforcing angles the total moment behaviour of the beam column joint could be calculated. The moment contribution provided by the post-tensioning (M_{pt}) and therefore the total moment capacity of the beam-column joint (M_{con}) is shown in Figure 6.36 along with the post-tensioning force (T_{pt}) and the normalised neutral axis depth (c/h_b) against the connection rotation (θ_{con}). Results are shown for earthquakes 001228x, 000196x and 000535y at PGA75%.

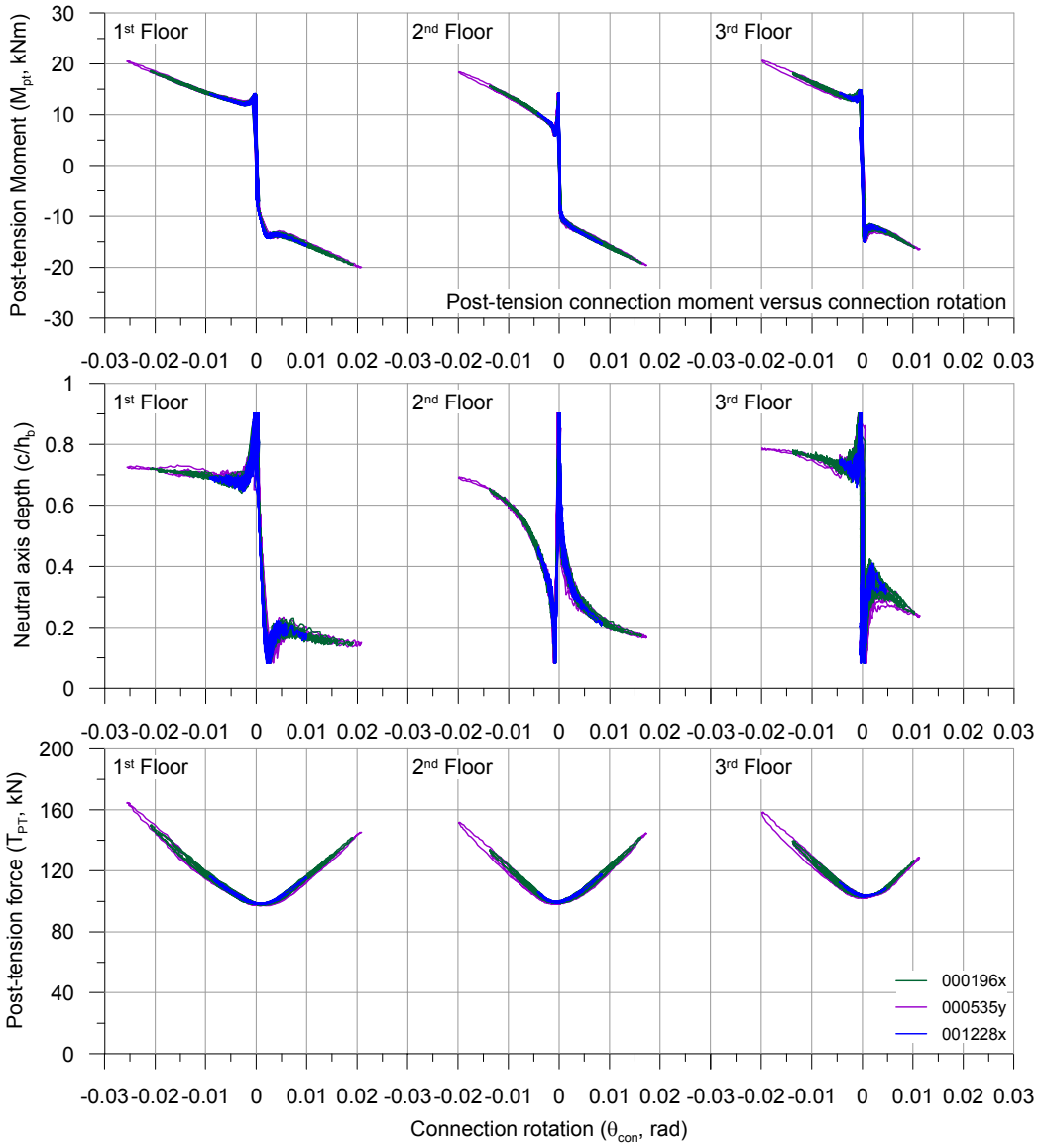

Figure 6.36. Post-tensioning moment, post-tensioning force and normalized neutral axis depth versus connection rotation for PT100_1.00 dynamic testing PGA75%

Figure 6.36 shows the response of the non-linear elastic system responded in the same way as observed during PT100_0.60 testing and in the beam-column tests discussed in Chapter 4 and 5. No losses in either post-tensioning force or moment capacity were noted throughout the testing sequence, indicating that the beam-column joint remained undamaged throughout testing.

Rotational response

Figure 6.37 shows the maximum rotations for the test frame at increasing levels of PGA. The solid lines on the graph show the maximum total rotations (as derived from

the interstorey drift) and the dashed lines show the maximum recorded connection rotations. The ratios between these values are also shown in the bottom graph of Figure 6.37.

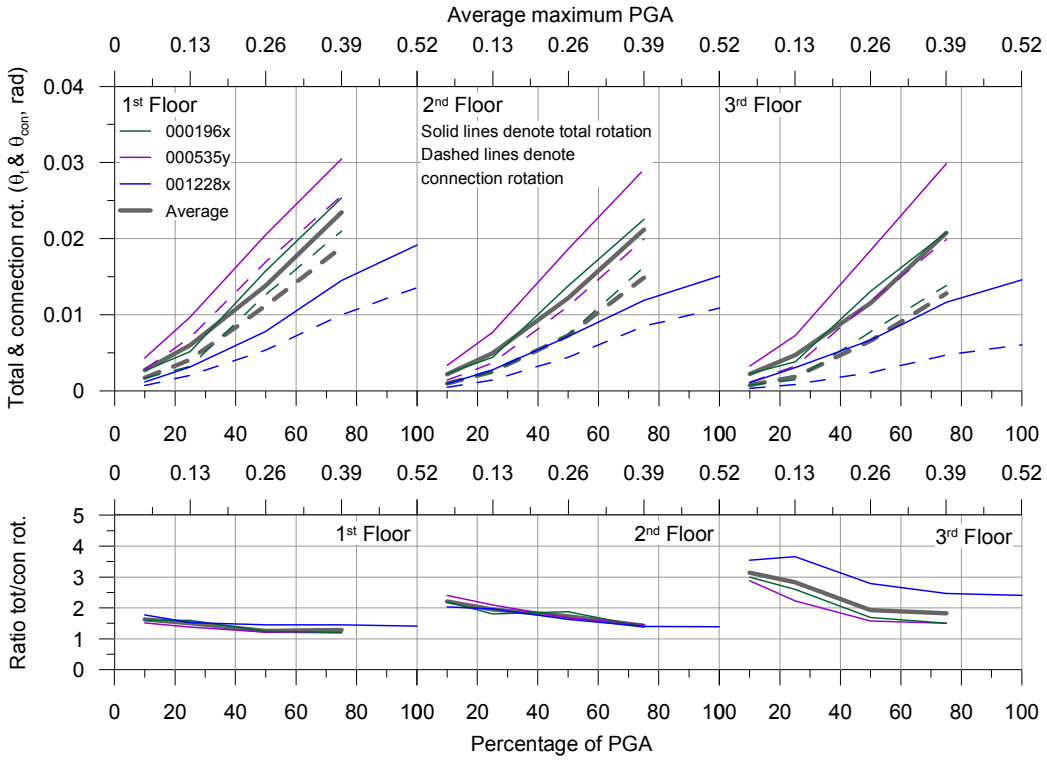

Figure 6.37. Maximum total frame and connection rotations and ratios of test frame at increasing levels of PGA for PT100_1.00

A maximum average connection rotation of 0.019 rad was recorded at the first level of the structure during test. This value was smaller than the total rotation values of the frame which had maximum averaged values of 0.023 rad.

The ratios between the total frame and the connection rotations were approximately the same for the first two levels of the structure, ranging between 1.5 and 2, however the third level displayed an increased ratio and larger scatter. The reasons for this increase have already been discussed in Section 6.5.4. As with the ratios shown in Figure 6.37 the results decreased with increasing levels of PGA, are smaller for stronger earthquakes and are smaller at the first floor.

6.6.5 Local response of column-foundation joints

Section 6.5.5 already discussed the way in which deficiencies in the performance of the column-foundation performance contributed to increased drifts and displacements

of the test structure. The PT100_1.00 test series contained no dissipative reinforcement at the beam-column joint; however dissipative reinforcement was placed at the column base. As no improvements of the column base behaviour were made between the testing of PT100_0.60 and PT100_1.00 it was expected that the column base behaviour displayed the same deficiencies described in Section 6.5.5

Rotational response

The rotational response of the column base was calculated using the potentiometers shown in Figure 6.11. Table 6.10 displays the maximum measured column base rotations during PGA75% testing for the columns which were instrumented. These values are shown alongside the maximum Level One rotations measured.

Table 6.10. Comparison between the maximum level one rotations and measured column rotations

	L1 rot. (rad)	NW col. ext. (rad)	SW col. ext. (rad)	SW col. int. (rad)
001228x	0.015	0.014	0.011	0.010
000196x	0.025	0.025	0.026	0.024
000535y	0.030	0.025	0.031	0.030

Table 6.10 shows that as with PT100_0.60, testing column rotational values were similar to the total rotational response of Level One. This once again indicated that the column base possessed minimal moment capacity indicating that the deficiencies observed in Section 6.5.5 were also occurring during PT100_1.00 testing as expected.

6.7 COMPARISONS BETWEEN TESTING WITH AND WITHOUT DISSIPATIVE REINFORCING

Two testing series were performed and have been presented above. The first series, PT100_0.60, had an initial post-tensioning value at each level of $T_{pt,initial}$ = 100 kN and dissipative reinforcing angles placed at both the beam-column joint interface at each level (2 x ID5 top and bottom as presented in Chapter 3, F_y = 14.2 kN, Δ_y = 0.60 mm) and at the column base (1 x ID8 B both sides as presented in Chapter 3, F_y = 25.5 kN, Δ_y = 0.75 mm). The second series, PT100_1.00, had an initial post-tensioning value at each level of $T_{pt,initial}$ = 100 kN and dissipative reinforcing angles at the column base (1 x ID8 B both sides).

The effects of adding dissipative reinforcing to a post-tensioned timber systems has already been discussed extensively in Chapters 4 and 5 as well as in Section 6.4.5,

with the overall aim being the decrease of displacement without an increase in floor accelerations and base shears.

Figure 6.38 shows the shaking foundation ram force versus first floor drift for both test series subjected to 001228x, 000196x and 000535y at PGA75%. The following paragraphs compare in more detail the performance of the two test series studying the displacement/drift and acceleration/force responses.

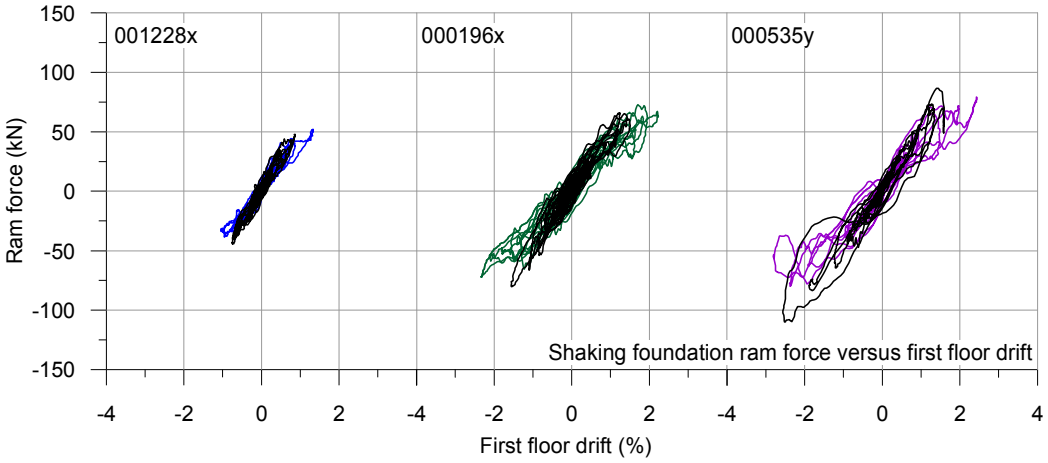

Figure 6.38. Shaking foundation ram force versus first floor drift for PT100_0.60 (shown in black) and PT100_1.00 testing PGA75%

6.7.1 Comparison of drift response of test structure

Figure 6.39 shows the maximum average drift of the three levels of the test structure for the two configurations PT100_0.60 (with dissipative reinforcing) and PT100_1.00 (without reinforcing). The figure clearly shows that under dynamic loading the addition of the dissipative angle reinforcing reduced maximum drifts for similar loads. An average reduction in drift at PGA75% of 32% was recorded.

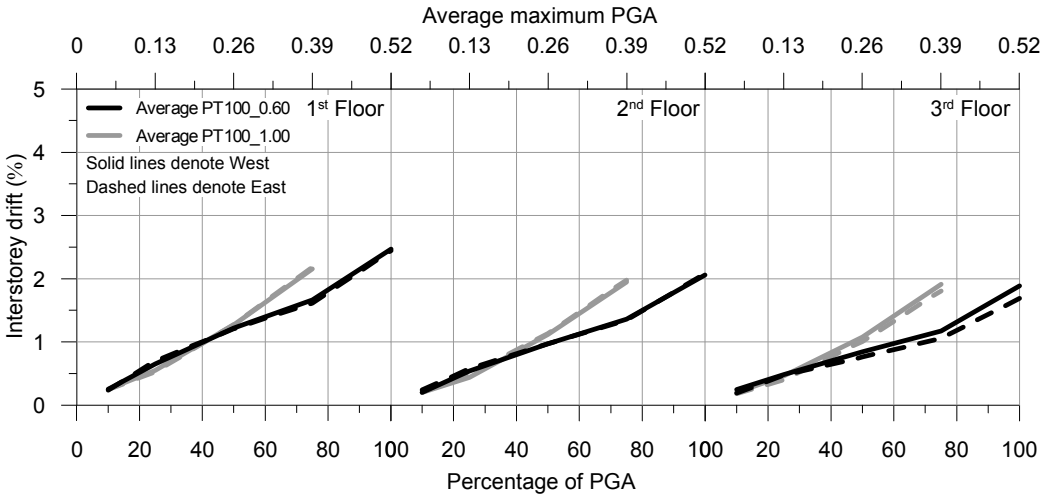

Figure 6.39. Comparison of maximum drifts of test frame at increasing levels of PGA

Figure 6.39 shows that at low levels of seismic action the two systems responded very similarly in terms of drift. Following the PGA50% level the response differed with a rapid increase in the PT100_1.00 drift levels while the increase in PT100_0.60 drift levels remained constant. The PT100_0.60 test series displayed the same rapid increase in drift following the PGA75% test series. As described in Chapter 5 the point of gap-opening is a function only of the amount of initial post-tensioning across the interface, however in a dissipative reinforced system, following gap-opening the joint also has the stiffness and strength provided by the angles in order to resist rotation leading to later onset of non-linear behaviour.

Residual drifts have been shown for test series PT100_0.60 and PT100_1.00 in Figure 6.19 and Figure 6.32, respectively. The first of these figures showed that, as expected and discussed in Section 4.10, a system which contains dissipative reinforcing will present minor amounts of residual drift (averaging less than 0.05%). The second figure shows that without the dissipative reinforcing residual drifts were mostly insignificant (averaging less than 0.03%). These values are not considered significant as they are under limits for which post-event remediation would generally be required (Priestley et al. 2003).

Finally Figure 6.39 shows that despite the deficiencies in the performance of the beam-column and column-foundation connections due to sliding of the dissipaters' attachments, the presence of the dissipative reinforcing did have an impact on system response.

6.7.2 Acceleration response of test structure

Figure 6.39 clearly shows a reduction in maximum average drift between test PT100_0.60 and PT100_1.00. As mentioned in Chapters 4 and 5 the reduction in drift comes from two sources, the increased strength of the joint when the dissipative angles are added and the system damping which they provide. Figure 6.40 shows the average maximum floor accelerations for the two test configurations with increasing percentages of PGA along with the average ratio between floor acceleration and PGA for the west side of the structure.

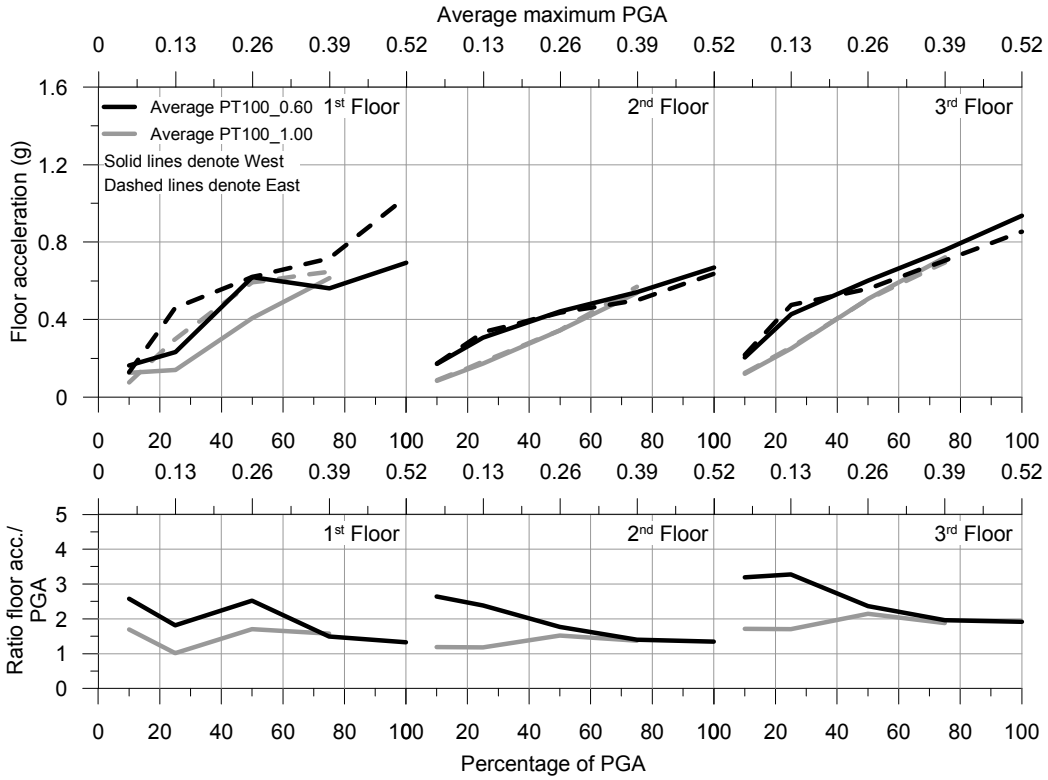

Figure 6.40. Comparisons of maximum average accelerations and ratios (West-side frame) of test frame at increasing levels of PGA

Figure 6.40 shows that as levels of PGA% increased the differences in floor acceleration between the PT100_0.60 and PT100_1.00 testing decreased. For low levels of PGA% a slight increase in floor acceleration is observed. It is likely that this was due to the increased stiffness of the structure before the initial slipping of the floors (as discussed in Section 6.5.2) and the failure of the column base connection (as discussed in Section 6.5.5). These two factors led to a reduced building stiffness as evidenced by a higher building period (as discussed in Section 6.5.6).

The ratios of PGA to floor acceleration are also presented in Figure 6.40 and as shown this ratio was approximately between 1.5 and 2 at higher levels of PGA% for both PT100_0.60 and PT100_1.00 testing. The ratios in testing varied for lower levels of PGA for test PT100_0.60, however this same change in ratio was not seen in the PT100_1.00 testing. It is possible that this was due to the alteration in the boundary conditions of the structure with a reduction in column base stiffness due to the failure of the column base connection. This reduction remains for the PT100_1.00 testing leading to an unaltered ratio between floor acceleration and PGA.

Table 6.11 shows the maximum average east and west floor accelerations at PGA75% along with the percentage difference between PT100_0.60 and PT100_0.60. Overall no significant increase in maximum average floor acceleration due to the addition of the dissipative reinforcing existed despite a 32 % reduction in maximum average drift mentioned in Section 6.7.1.

Table 6.11. Comparison between the maximum Level One rotational and measured column rotation

	Max. Ave. Acc. W	Max. Ave. Acc. E	Max. Ave. Acc. W	Max. Ave. Acc. E	Max. Ave. Acc. W	Max. Ave. Acc. E
	PT100_0.60		PT100_1.00		% Difference	
Level 1	0.561	0.716	0.614	0.647	- 9 %	+ 10 %
Level 2	0.541	0.499	0.537	0.570	+ 7 %	- 14 %
Level 3	0.760	0.705	0.721	0.696	+ 5 %	+ 1 %

In order to further understand the acceleration response of the structure, in Figure 6.41 the time history acceleration and displacement response at each level of the structure during testing has been compared for test 000535y at PGA75%. Several aspects of the systems dynamic response are evident. Firstly it is evident that during the strong motion portion of the response (after the first main cycle) the two signals were out of phase. Secondly it can be seen that the signals returned to being in phase towards the end of the motion. Thirdly, higher frequency acceleration response was reduced but not completely removed by the addition of dissipative reinforcement.

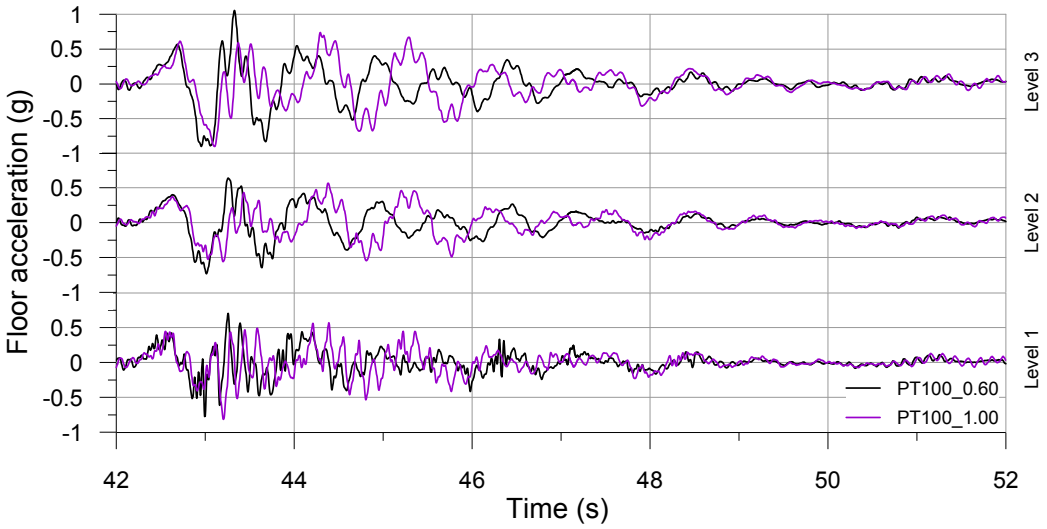

Figure 6.41. First, second and third floor acceleration response of PT100_0.60 and PT100_1.00 during test 000535y PGA75%

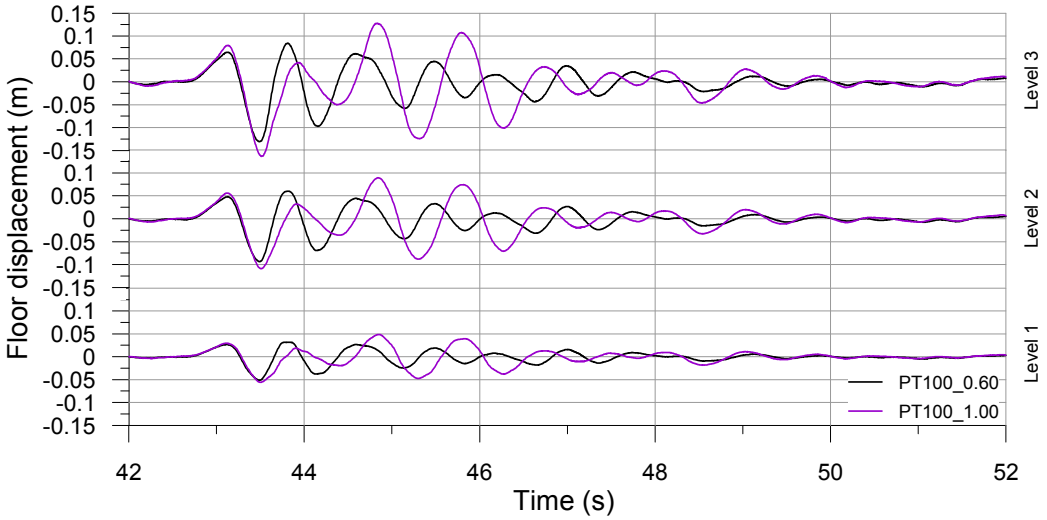

Figure 6.42. First, second and third floor displacement response of PT100_0.60 and PT100_1.00 during test 000535y PGA75%

The elongation of the 1st period of PT100_1.00 during strong motion was due to the gap opening of the structure reducing stiffness. Although a small amount of gap opening did occur during the PT100_0.60 testing, as evidenced by the flag shaped loop shown in Figure 6.30, it did not occur for as long. This created a change in period between the two test configurations. Upon completion of the ground motion the two systems return to being in phase as their elastic dynamic characteristics were the same (as discussed in Section 6.5.6).

Further comparisons of the acceleration responses of PT100_0.60 and PT100_1.00 are presented on the left of Figure 6.43 where the response is shown together for each

test. As mentioned above the effects of the higher modes on the frame were evident in both tests however, they were moderately reduced with the addition of the dissipative reinforcing which presented as reduced variations in acceleration between floors.

The maximum base shears with increasing levels of PGA are shown on the right of Figure 6.43. As expected, the increase in floor accelerations at lower PGA% levels led to high base shears for the PT100_0.60 structure. What is unusual however is that the base shear of the PT100_0.60 test series remained higher even if the maximum average accelerations became approximately equal (as shown in Figure 6.40). It is likely that in this particular case it was the higher modes that were reducing the base shear of test PT100_1.00 with floors acting against each other reducing the total amount. This will not however be the case for all structures. The presence of higher modes increases demand on the columns which will not be considered if a first mode assumption is made in design.

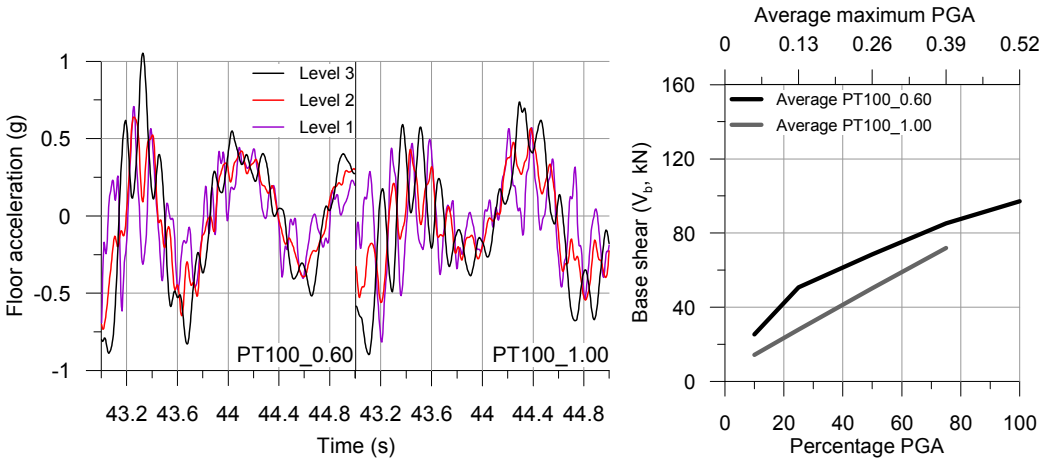

Figure 6.43. First, second and third floor response of PT100_0.60 and PT100_1.00 to test 000535y PGA75% (left) and maximum average base shear of test frame at increasing levels of PGA (right)

6.7.3 Summary table of PT100_0.60 and PT100_1.00 testing results

Sections 6.5, 6.6 and 6.7 have presented, discussed and compared the results of the dynamic testing of test frame configurations PT100_0.60 and PT100_1.00. Table 6.12 summarises the numerical values of the testing parameters discussed.

Table 6.12. a) Summary table of PT100_0.60 and PT100_1.00 testing results

		Displacement (Δ, m)												Drift (θ_d, %)											
		1st floor				2nd floor				3rd floor				1st floor				2nd floor				3rd floor			
	%PGA	001228x	000196x	000535y	AVE	001228x	000196x	000535y	AVE	001228x	000196x	000535y	AVE	001228x	000196x	000535y	AVE	001228x	000196x	000535y	AVE	001228x	000196x	000535y	AVE
PT100_0.60	10	2.7	6.6	5.8	5.0	4.6	12.0	10.3	9.0	6.6	17.0	14.9	12.8	0.13	0.30	0.29	0.24	0.12	0.29	0.26	0.22	0.13	0.28	0.25	0.22
	25	6.4	17.2	16.9	13.5	11.5	31.2	30.4	24.4	15.7	42.3	41.7	33.2	0.32	0.86	0.85	0.68	0.27	0.71	0.70	0.56	0.25	0.58	0.61	0.48
	50	8.1	28.5	33.8	23.4	14.0	52.2	62.1	42.8	18.8	70.8	86.4	58.7	0.40	1.42	1.69	1.17	0.30	1.19	1.43	0.98	0.28	0.96	1.23	0.82
	75	16.6	30.9	51.0	32.8	28.9	55.2	93.6	59.2	39.1	75.3	128.9	81.1	0.83	1.54	2.55	1.64	0.63	1.28	2.14	1.35	0.53	1.02	1.79	1.11
	100	30.7	47.4	69.0	49.1	54.5	86.9	129.5	90.3	76.0	119.6	181.6	125.7	1.54	2.37	3.45	2.45	1.20	1.98	3.03	2.07	1.09	1.66	2.61	1.79
PT100_1.00	10	2.2	4.8	7.8	4.9	3.3	8.6	13.6	8.5	4.6	12.0	19.0	11.9	0.11	0.24	0.39	0.25	0.08	0.22	0.30	0.20	0.09	0.20	0.29	0.19
	25	5.9	9.7	17.6	11.1	10.8	18.2	31.7	20.2	15.0	25.2	43.9	28.0	0.30	0.44	0.88	0.54	0.26	0.42	0.71	0.47	0.26	0.40	0.64	0.43
	50	14.5	29.0	37.9	27.1	27.5	54.2	72.4	51.4	39.0	77.7	104.2	73.6	0.72	1.45	1.89	1.36	0.66	1.27	1.74	1.22	0.59	1.19	1.62	1.13
	75	26.4	46.7	57.0	43.4	48.4	88.3	110.3	82.4	68.3	125.4	162.5	118.7	1.32	2.34	2.85	2.17	1.12	2.09	2.69	1.96	1.03	1.88	2.67	1.86
	100	35.0			35.0	63.6			63.6	88.0			88.0	1.75			1.75	1.43			1.43	1.29			1.29

		Acceleration (g)												Ratio floor acceleration to peak ground acceleration											
		1st floor				2nd floor				3rd floor				1st floor				2nd floor				3rd floor			
	%PGA	001228x	000196x	000535y	AVE	001228x	000196x	000535y	AVE	001228x	000196x	000535y	AVE	001228x	000196x	000535y	AVE	001228x	000196x	000535y	AVE	001228x	000196x	000535y	AVE
PT100_0.60	10	0.08	0.22	0.14	0.15	0.10	0.23	0.19	0.17	0.13	0.27	0.23	0.21	1.6	4.6	1.5	2.6	2.0	3.9	2.1	2.6	2.6	4.5	2.4	3.2
	25	0.18	0.36	0.50	0.35	0.22	0.37	0.37	0.32	0.28	0.54	0.53	0.45	2.1	1.7	1.6	1.8	2.6	2.5	2.0	2.4	3.3	3.7	2.8	3.3
	50	0.17	0.68	1.11	0.65	0.20	0.55	0.61	0.45	0.27	0.73	0.85	0.62	1.0	2.3	4.3	2.5	1.1	2.3	1.8	1.7	1.5	2.8	2.7	2.3
	75	0.39	0.66	0.86	0.64	0.32	0.50	0.74	0.52	0.44	0.70	1.05	0.73	1.6	1.5	1.4	1.5	1.3	1.3	1.5	1.4	1.8	2.0	2.1	2.0
	100	0.54	0.96	1.06	0.85	0.43	0.69	0.84	0.65	0.70	0.91	1.08	0.90	1.1	1.5	1.4	1.3	1.3	1.4	1.3	1.3	2.1	1.9	1.7	1.9
PT100_1.00	10	0.04	0.07	0.19	0.10	0.05	0.07	0.13	0.08	0.05	0.13	0.18	0.12	0.9	1.1	3.1	1.7	0.9	1.1	1.6	1.2	1.0	1.9	2.2	1.7
	25	0.11		0.33	0.22	0.12		0.24	0.18	0.17		0.33	0.25	1.2		0.9	1.0	1.2		1.2	1.2	1.7	0.0	1.7	1.1
	50	0.28	0.43	0.71	0.47	0.23	0.35	0.46	0.35	0.35	0.49	0.67	0.50	1.2	1.2	1.8	1.4	1.2	1.2	1.3	1.2	2.0	1.7	1.9	1.8
	75	0.40	0.67	0.82	0.63	0.35	0.50	0.82	0.55	0.49	0.74	0.90	0.71	1.5	1.8	1.5	1.6	1.3	1.3	1.5	1.4	2.0	1.9	1.7	1.9
	100	0.52			0.52	0.46			0.46	0.60			0.60	1.3			1.3	1.3			1.3	1.7	0.0	0.0	0.6

		Total rotation (θ_t, rad)												Connection rotation (θ_{con}, %)											
		1st floor				2nd floor				3rd floor				1st floor				2nd floor				3rd floor			
	%PGA	001228x	000196x	000535y	AVE	001228x	000196x	000535y	AVE	001228x	000196x	000535y	AVE	001228x	000196x	000535y	AVE	001228x	000196x	000535y	AVE	001228x	000196x	000535y	AVE
PT100_0.60	10	0.001	0.003	0.003	0.002	0.001	0.003	0.003	0.002	0.001	0.003	0.002	0.002	0.001	0.002	0.001	0.001	0.001	0.001	0.001	0.001	0.000	0.001	0.001	0.001
	25	0.003	0.009	0.008	0.007	0.003	0.007	0.007	0.006	0.003	0.006	0.006	0.005	0.002	0.005	0.005	0.004	0.001	0.003	0.003	0.002	0.001	0.002	0.002	0.001
	50	0.004	0.014	0.017	0.012	0.003	0.012	0.014	0.010	0.003	0.010	0.012	0.008	0.002	0.009	0.013	0.008	0.001	0.006	0.008	0.005	0.001	0.003	0.007	0.004
	75	0.008	0.015	0.025	0.016	0.006	0.013	0.021	0.014	0.005	0.010	0.018	0.011	0.005	0.011	0.020	0.012	0.003	0.008	0.014	0.008	0.001	0.005	0.011	0.006
	100	0.015	0.024	0.035	0.025	0.012	0.020	0.030	0.021	0.011	0.017	0.026	0.018	0.010	0.020	0.029	0.020	0.007	0.013	0.022	0.014	0.004	0.011	0.019	0.011
PT100_1.00	10	0.001	0.002	0.004	0.002	0.001	0.002	0.003	0.002	0.001	0.002	0.003	0.002	0.001	0.002	0.003	0.002	0.000	0.001	0.001	0.001	0.000	0.001	0.001	0.001
	25	0.003	0.004	0.009	0.005	0.003	0.004	0.007	0.005	0.003	0.004	0.006	0.004	0.002	0.003	0.007	0.004	0.001	0.002	0.004	0.003	0.001	0.001	0.003	0.002
	50	0.007	0.014	0.019	0.014	0.007	0.013	0.017	0.012	0.006	0.012	0.016	0.011	0.005	0.013	0.017	0.012	0.004	0.007	0.011	0.008	0.002	0.008	0.012	0.007
	75	0.013	0.023	0.029	0.022	0.011	0.021	0.027	0.020	0.010	0.019	0.027	0.019	0.010	0.021	0.026	0.019	0.008	0.016	0.020	0.015	0.005	0.014	0.020	0.013
	100	0.018			0.018	0.014			0.014	0.013			0.013	0.014			0.014	0.011			0.011	0.006			0.006

b) Summary table of PT100_0.60 and PT100_1.00 testing results continued

Residual displacement (%)

	%PGA	1st floor 001228x	000196x	000535y	AVE	2nd floor 001228x	000196x	000535y	AVE	3rd floor 001228x	000196x	000535y	AVE
PT100_0.60	10	0.01	0.00	0.01	0.01	0.01	0.01	0.01	0.01	0.01	0.01	0.04	0.02
	25	0.01	0.01	0.01	0.01	0.01	0.01	0.00	0.01	0.01	0.01	0.02	0.01
	50	0.01	0.06	0.03	0.03	0.02	0.04	0.03	0.03	0.01	0.03	0.03	0.02
	75	0.01	0.01	0.04	0.02	0.01	0.03	0.05	0.03	0.03	0.00	0.01	0.02
	100	0.01	0.03	0.09	0.04	0.02	0.03	0.10	0.05	0.01	0.02	0.04	0.02
PT100_1.00	10	0.01	0.01	0.01	0.01	0.01	0.02	0.00	0.01	0.01	0.01	0.00	0.01
	25	0.02	0.01	0.00	0.01	0.00	0.02	0.03	0.01	0.01	0.00	0.01	0.01
	50	0.01	0.00	0.00	0.01	0.02	0.01	0.02	0.02	0.02	0.00	0.01	0.01
	75	0.01	0.02	0.01	0.01	0.02	0.01	0.01	0.01	0.01	0.01	0.01	0.01
	100	0.00			0.00	0.01			0.01	0.00			0.00

Base shear (V_b, kN)

	%PGA	001228x	000196x	000535y	AVE
PT100_0.60	10	13.8	32.5	29.9	25.4
	25	33.2	60.1	58.8	50.7
	50	30.5	86.7	88.4	68.5
	75	48.2	80.9	126.8	85.3
	100	51.0	105.3	135.3	97.2
PT100_1.00	10	6.3	14.2	22.6	14.4
	25	17.7		38.1	27.9
	50	33.3	53.0	64.4	50.2
	75	51.7	75.0	88.9	71.9
	100	70.5			70.5

Ratio total rotation to connection rotation

	%PGA	1st floor 001228x	000196x	000535y	AVE	2nd floor 001228x	000196x	000535y	AVE	3rd floor 001228x	000196x	000535y	AVE
PT100_0.60	10	2.2	1.8	2.1	1.9	2.3	2.3	2.7	2.4	4.2	4.2	4.0	4.1
	25	2.1	1.8	1.8	1.8	2.6	2.1	2.2	2.2	3.6	3.1	3.2	3.2
	50	2.2	1.6	1.3	1.5	2.9	1.9	1.8	1.9	3.5	3.0	1.8	2.3
	75	1.7	1.4	1.2	1.3	2.0	1.7	1.6	1.7	3.6	2.2	1.6	1.9
	100	1.5	1.2	1.2	1.2	1.7	1.5	1.4	1.5	2.7	1.5	1.4	1.6
PT100_1.00	10	1.6	1.5	1.4	1.4	1.8	2.1	2.2	2.1	3.1	2.7	2.5	2.6
	25	1.4	1.4	1.3	1.3	1.9	1.7	1.9	1.9	3.1	2.7	2.0	2.3
	50	1.4	1.1	1.1	1.2	1.5	1.7	1.6	1.6	2.5	1.5	1.4	1.6
	75	1.3	1.1	1.1	1.2	1.3	1.3	1.4	1.3	2.2	1.4	1.3	1.5
	100	1.3			1.3	1.3			1.3	2.1			2.1

6.8 ELASTIC AND INELASTIC DAMPING

The final study of the post-tensioned timber dynamic test results involved the evaluation of the elastic and inelastic damping of the frame. During a seismic event the presence of damping reduces demand on a structure. The total equivalent viscous damping of a structure (ξ) is made up of two sources the; elastic damping (ξ_{el}) and the hysteretic damping (ξ_{hyst}). Damping values from both of these sources are evaluated and compared in this section.

6.8.1 Elastic damping, ξ_{el}

Elastic damping is used to introduce damping not captured by the hysteretic model represented by the codified reduction methods and will be further discusses in Section 7.5. This damping has a number of sources of which the most important is the typical simplification that the hysteretic model has a perfectly linear response in the elastic range. Damping can also result from impact damping, foundations and the interaction between structural and non-structural elements.

Many methods can be used in order to evaluate the elastic damping of a building. During the analysis of the test structure the half-power bandwidth (HPB) method (Ewins 1994) was used. This method estimates the damping using the frequency range, in combination with a Welch Fourier analysis (Welch 1967). The HPB method returns significant results in the analysis of a stationary system (i.e. no significant non-linear response) therefore it has been applied using the forced vibration hammer identification testing described in Section 6.4.7. In the application of the HPB method, firstly, the amplitude of each (in this case the first) natural frequency is obtained. Two more frequencies are then taken that have amplitudes equal to the amplitude of the natural frequency divided by the square-root of two. The distance between these two points will increase as damping increases thus damping is taken as the ratio between these points. Results are shown for each accelerometer placed on the test structure (e.g. L1 SW is the accelerometer placed at the South-West corner of Level One).

Table 6.13. Elastic damping coefficients (%) for test PT100_0.60 and PT100_1.00

	L1 SW	L1 NE	L2 SW	L2 NE	L3 SW	L3 NE	Ave.
PT100_0.60	1.63	1.53	1.46	1.52	1.40	1.40	1.49
PT100_1.00	1.91	1.72	1.85	1.77	1.90	1.90	1.84

Table 6.13 shows the nominal amount of elastic damping that was present in the post-tensioned timber frame structure. As shown average values of ξ_{el} = 1.49% and 1.84% were calculated for tests PT100_0.60 and PT100_1.00, respectively. Test configuration PT100_1.00 showed slightly elevated elastic damping likely due to the reduction in stiffness created by the PT100_0.60 series testing (as discussed in Section 6.5.6). It is important to note however that an experimental model is without many of the sources of elastic damping present in a normal structure (partitions, cladding etc.).Values were therefore expected to be lower than in a real post-tensioned timber structure which contains these elements.

6.8.2 Hysteretic (non-linear material) damping, ξ_{hyst}

The hysteretic damping of post-tensioned timber structures has already been discussed in both Section 4.9 and 5.5. As with elastic damping several methods are available which can be used to evaluate inelastic damping, such as the method proposed by Jacobsen (1960) used in Section 4.9. The evaluation of hysteretic damping during dynamic testing is complicated by the forced nature of the system response.

The total damping of the forced dynamic system was evaluated using a method proposed by Mucciarelli and Gallipoli (2006) for the simple non-parametric analysis (NonPaDAn) of the damping factor of buildings. This simple method allows the calculation of damping values from a single short input, also under forced conditions, using statistical analysis of decreasing peaks in the displacement, velocity, or acceleration time history response.

The damping factor is estimated using the logarithmic decrement method on a minimum of three consecutive decreasing peaks separated by the same period T (within a bracket of ± the tolerance level as a function of T).

As shown in Section 5.5, in order to have hysteretic damping gap opening and dissipative reinforcing, yield must occur. With increased displacement beyond yield (i.e. increased ductility) the equivalent viscous damping of a post-tensioned timber structure also increases. During seismic response therefore, damping increases with stronger ground motion.

Table 6.14 shows the total damping coefficients (ξ) for each of the three main test inputs at increasing levels of PGA%. The NonPaDAn method averages damping across the length of the sample therefore two values are shown for each test; the full response (over the entire acceleration response of the structure, weak and strong motion) and the strong response (over the strong motion acceleration response of the structure). The average of the results obtained using the response of the West and East side accelerometers of Level Three are shown.

Table 6.14. Total equivalent viscous damping (ξ) coefficients for test PT100_0.60

	001228x		000196x		000535y	
PGA%	Full	Strong	Full	Strong	Full	Strong
10	4.4	4.9	3.0	2.2	3.3	2.6
25	3.5	4.3	5.6	7.3	4.3	5.7
50	3.6	6.7	4.2	7.9	4.2	6.1
75	4.2	6.3	4.9	5.8	3.9	5.6
100	4.5	6.8	4.5	5.5	5.4	5.9

The average total damping across the three earthquakes at PGA100% was ξ = 4.3 % across the full response and ξ = 5.9 % across the strong motion response section. The elastic damping coefficient of the frame calculated in Section 6.8.2 was ξ_{el} = 1.5 % indicating that the average hysteretic damping across the three earthquakes at PGA100% was ξ_{hyst} = 2.8 % across the full response and ξ_{hyst} = 4.2 % across the

strong motion response section. This was less than the planned level of design damping due to the deficiencies in system response discussed in Sections 6.5.4 and 6.5.5.

A NonPaDAn analysis has also been performed on the acceleration response of test configuration PT100_1.00 at PGA75%. The average total damping across the three earthquakes at PGA100% was ξ = 4.9 % across the full response indicating that the average hysteretic damping across the three earthquakes at PGA75% was ξ_{hyst} = 3.0 % across the full response. Test PT100_1.00 did not contain the use of dissipative reinforcing at the beam-column joint indicating that the timber system itself is capable of providing nominal amounts of hysteretic dissipation during strong motions. This is consistent with the findings of Pino (2011).

The total response of the PT100_1.00 system was very similar to the PT100_0.60 response (ξ_{hyst} = 2.8 % for PGA75%) tending to indicate that when averaged across the entire response the damping characteristics of the two configurations are very similar. This is not unexpected as the dissipative reinforcing will only provide damping during the maximum frame response cycle of which few occur during the total frames responses. In fact from Figure 6.16 it can be seen that only one clear flag shaped hysteretic loop occurred during all tests (being the maximum frame response under 000535y at 100%PGA). Performing the area EQV analysis method suggested by Jacobsen (1960) as discussed in Section 4.9, the equivalent viscous damping value of this loop is ξ_{hyst} = 7.8 %.

6.9 CONCLUSIONS FROM CHAPTER 6

The dynamic testing of a two-third scale post-tensioned timber frame has been used to investigate the global performance of the post-tensioned timber system under real-time seismic loading. This testing has confirmed that the observations made regarding the low damage lateral performance of post-tensioned frames during quasi-static testing of parts (as described Chapter 4) and a full frame (As described in Chapter 2 by Newcombe (2012)) are correct also for real-time dynamic loading as indicated during the small scale testing of Pino et al. (2010)

Two testing configurations have been used, one with (PT100_0.60) and one without (PT100_1.00) the use of dissipative reinforcing discussed in Chapter 3. Dissipative

reinforcing was placed at the column-foundation connection for all testing. The system did not respond as designed with deficiencies in the connection of the dissipative reinforcing leading to lower strength capacity and hysteretic damping. Despite these deficiencies in the performance of the post-tensioned timber frame, several significant observations have been made during the analysis of testing results.

The first of these deficiencies related to the slipping of the dissipative angle reinforcing at the beam-column joint against the reinforcement attachment plate. This had a direct impact on system stiffness and damping with a reduction in stiffness due to increased total (angle plus slip) yield displacement and damping due to reduced maximum displacement. It was unclear the degree to which this slipping occurred during testing with only one of the connections being monitored visually. It was clear however that yielding of the beam-column joint dissipative reinforcement did occur during test 000535y (100%PGA level) due to the flag shape response shown in Figure 6.16.

The second deficiency in system response was due to the failure of the epoxied bar connection at the column base leading to rocking occurring between the timber column and its steel base and rather than steel base and the foundation as had been designed. This led to the dissipative reinforcing placed at the column-foundation connection not contributing to the moment capacity of the base connection or to the hysteretic damping of the system as a whole.

In addition to these two deficiencies errors in the production of the beams in the principal direction led to beam depths being 5% less than design values (305 mm instead of 320 mm). This lead to further increases in drift compared with design values.

These deficiencies would be avoided through careful control of the production of the post-tensioned frame and a simplification of connection design. This highlights the critical importance of quality control measures being in place during fabrication and construction crucial in ensuring that the details perform as designed provide desired performance. Further discussion regarding future research around connection simplification is discussed in Section 10.2.

Although the above deficiencies had a significant impact on system response several significant observations have been made regarding system performance. Comparisons between the two systems with (PT100_0.60) and without (PT100_1.00) dissipative reinforcing showed a 32% decrease in drift during PGA75% testing. The reason for this decrease was two-fold: firstly the PT100_0.60 system had a larger capacity when compared to the PT100_1.00 and secondly the PT100_0.60 had a higher hysteretic energy dissipation capacity due to the yielding of the dissipative reinforcing (which did occur but was however less than designed).

Comparisons of accelerations between the two test configurations showed that the 32% decrease in drift was not accompanied by an increase in acceleration, but and by an 18% increase in base shear. It would be expected that both of these values (acceleration and base shear) would be higher if only strength was increased between PT100_1.00 and PT100_0.60 indicating that the dissipative reinforcing was impacting positively on system strength. The presence of the dissipative reinforcing also reduced the effects of the higher modes on the frame response. Ratios between PGA and floor acceleration did not exceed 2 for high PGA testing.

The comparison of maximum drifts and accelerations between the two test configurations confirmed that the addition of dissipative reinforcing reduces drift without significant increases in base shear. Dissipative reinforcing also limits the increases in accelerations up the building.

Study of the frequency and period response of the structure before each of the test configurations displayed a slight change in the fundamental frequencies of the frame. As masses remained essentially constant between test configurations this change must have been related to a loss in stiffness. Further analysis showed that this was not a change due to the removal of the dissipative reinforcing but due to the accumulation of minor damage throughout testing. It is believed that the major reason for this change was likely to have been the failure of the epoxied rods at the column base mentioned above. It is possible that the onset of slipping between the frame members and flooring panels also contributed to this loss in stiffness. It is therefore possible to conclude that the inclusion of dissipative reinforcing has little to no impact on the dynamic characteristics of a post-tensioned timber frame.

A comparison between the damping properties of the frame has shown that on average elastic damping values were ξ_{el} = 1.5% for both frames. Hysteretic damping values were ξ_{hyst} = 4.2% across the strong motion response section at PGA100%. The values of damping over the full test response did not vary greatly between the PT100_0.60 and PT100_1.00 tests which was not unusual due to the fact that the non-linear behaviour of the reinforcing is usually isolated to one or two cycles of the response. Isolating one of these cycles provided an equivalent viscous damping value of ξ_{hyst} = 7.8%.

One key observation from testing is that although clear deficiencies were present in the frame these did not lead to any significant damage of the frame members.

REFERENCES CHAPTER 6

Ewins, J. D. (1994). *Modal testing: theorey and practise*, Reasearch Studies Press.

NTC. (2008). "Norme Tecniche per le Costruzioni." Il Ministro delle Infrastrutture.

Jacobsen, L. S. (1960). "Damping in Composite Structures." 2nd World Conference on Earthquake Engineering, Tokyo and Kyoto, Japan.

Moroder, D., Smith, T., Simonetti, M., Ponzo , F. C., Di Cesare , A., Nigro, D., Pampanin, S., and Buchanan, A. H. (2014). "Experimental Behaviour of Diaphragms in Post-tensioned Timber Frame Buildings." Second European Conference on Earthquake Engineering and Seismology, Istanbul, Turkey, August 25 - 29.

Mucciarelli, M., and Gallipoli, M. R. (2006). "Estimate of Frequency and Damping for Large Sets of Buildings in Dense Urban Areas." First European Conference on Earthquake Engineering and Seismology, Geneva, Switzerlanf.

Newcombe, M. (2012). "Lateral Force Design of Post Tensiond Timber Frame and Wall Buildings ", University of Canterbury, Christchurch.Doctor of Philosophy.

Pino Merino, D. (2011). "Dynamic Response of Post-Tensioned Timber Framed Buildings," University of Canterbury, Christchurch, New Zealand.Master of Engineering.

Pino Merino, D., Pampanin, S., Carradine, D., Deam, B., and Buchanan, A. H. (2010). "Dynamic Responce of a Multi-Storey Post-Tensioned Timber Building." 11th World Conference on Timber Engineering, Riva del Garda, Trentino, Italy, 8.

Priestley, M. J. N., Calvi, G. M., and Kowalsky, M. J. (2007). *Displacement-Based Seismic Design of Structures*, IUSS Press.

Priestley, N., Pampanin, S., and Christopoulos, C. (2003). "Performance-based seismic response of frame structures including residual deformations pat II: Multi-degree of freedom systems." *Journal of Earthquake Engineering*, 07(01), 119-147.

Smith, T., Fragiacomo, M., Pampanin, S., and Buchanan, A. H. (2009). "Construction Time and Cost for Post-Tensioned Timber Buildings." *Proceedings of the Institution of Civil Engineers*, Construction Materials(CM4), 9.

EN 1998-1:2003. (2003). "Design of structures for earthquake resistance - Part 1: General rules, seismic actions and rules for buildings." European Committee for Standardization.

EN 1995-1-1:2004. (2004). "Design of Timber Structures Part 1-1: General - Common Rules and Rules for Buildings." European Committee for Standardization.

Welch, P. D. (1967). "The Use of Fast Fourier Transform for the Estimation of Power Spectra: A Method Based on Time Averaging Over Short." *IEEE Transactions on Audio Electroacoustics*, AU-15, 70-73.

7 Analytical Modelling of the Global Seismic Response of Post-tensioned Timber Frames

7.1 PRINCIPAL CONCLUSIONS OF CHAPTER 7

Chapter 7 presents the procedure for the assessment of the global seismic response of a post-tensioned frame and compares this against the dynamic frame test results presented in Chapter 6. The following principal conclusions are drawn.

1. A study of the local response of the post-tensioned timber frame under dynamic loading showed the equations presented in Chapter 5 to be accurate and slightly conservative.

2. Methods used for the estimation of the initial period of the frame were analysed:

    - For a quick estimation the empirical method suggested by NZS1170.5 (2004) for steel frame structures provided, for this specific case, a sufficiently accurate prediction.

    - For more detailed information a structural modelling programme should be used. This model does not need to contain information regarding the local response of the beam-column joint interface and can contain only information regarding section sizes.

3. Two methods of calculation of base shear under a given seismic loading have been investigated; Force Based Design (FBD) and Displacement Based Design (DBD). Both of these methods provided adequate prediction of seismic base shear provided correct assumptions were made regarding the ductility and damping of the post-tensioned timber frame. These two parameters were shown to provide significant error in base shear if not correctly predicted.

7.2 INTRODUCTION

Chapter 6 presented the dynamic testing of a 3-storey post-tensioned timber frame. During the design of this frame various assumptions were made regarding dynamic

characteristics in order to evaluate seismic demand and thus provide the required capacity. These assumptions are evaluated in this chapter.

Two prominent methods were used in order to evaluate the design seismic demand on a post-tensioned timber frame: Force Based Design (FBD) and Displacement Based Design (DBD). Discussion regarding the analytical response will revolve around these two methods covering the initial period of the structure, damping, ductility and the effects of these on base shear.

Figure 6.13 of Chapter 6 presented the code based acceleration spectrum considered when the input earthquakes were selected during testing. This spectrum provides the foundation from which the seismic demand is determined (for both FBD and DBD). Figure 7.1 shows the acceleration and the (pseudo-) displacement spectra for the average of the inputs used during dynamic testing along with the code base acceleration spectra used when considering input suitability.

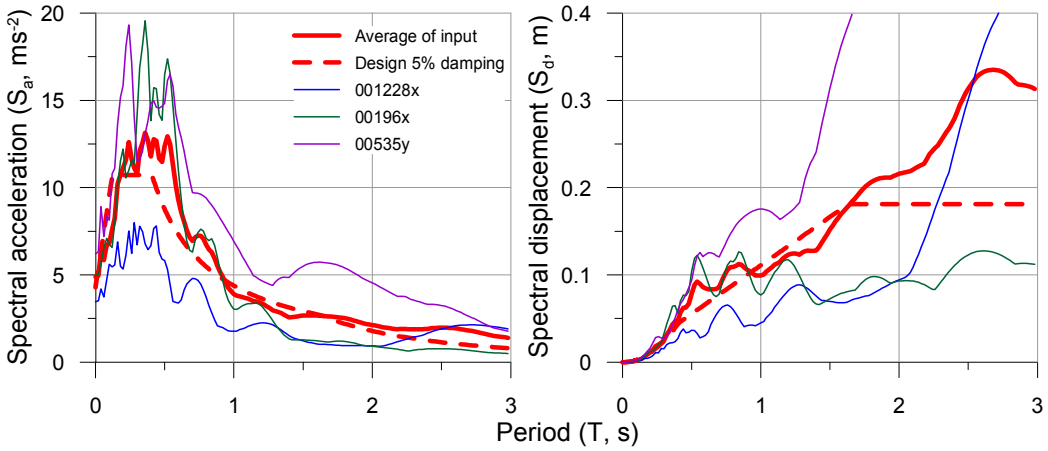

Figure 7.1. Code and input elastic acceleration and displacement spectra used during the design of the post-tensioned timber test frame

The spectra shown in Figure 7.1 have already been reduced in order to represent the inherent 'elastic' damping of the system. Values used in elastic damping will be discussed in Section 7.5.

During FBD an initial period of the structure must be assumed which will be discussed in Section 7.4. For both FBD and DBD the impact of non-linear behaviour must be estimated. Chapter 6 discussed the way in which post-tensioned timber frames provide non-linear behaviour (damping and ductility) in order to reduce seismic demand. During FBD and DBD design the elastic spectra presented above are

reduced to represent the effect that this non-linear behaviour has on demand. The conclusion of this is the obtaining of a design base shear, V_b, which will be described in Section 0. During both DBD and FBD assumptions are made regarding the systems dynamic performance and issues relating these assumptions are discussed.

Before the analysis of the global behaviour is carried out the ability of the local analytical procedure presented in Chapter 5 to predict the dynamic local response of the frame is briefly analysed.

7.3 ANALYTICAL MODELLING OF THE LOCAL RESPONSE OF THE POST-TENSIONED TIMBER FRAME

Chapter 5 presented analytical modelling techniques for the design of post-tensioned timber frames. The chapter focused on the two principal aspects of the frame design: understanding the local moment-rotation response and the rotational contributions of the joint panel, beam and column.

As discussed in Chapter 6 the moment rotation response of the test specimen with the dissipative reinforcing (PT100_0.60) could not be evaluated due to the uncertainty surrounding the exact force-displacement performance of the dissipative reinforcing. This section therefore only looks at the performance of the PT ONLY PT100_1.00 testing.

7.3.1 Analytical moment, neutral axis and post-tensioning-connection rotation response of PT100_1.00

The moment rotation response has been calculated using the procedure presented in Chapter 5 and compared against the testing results presented in Figure 6.23 of Chapter 6. These comparisons are displayed in Figure 7.2. The design procedure presented in Chapter 5 provides a sufficiently accurate prediction of the connection moment capacity versus connection rotation response of the connection.

Overall it can be seen that the prediction was slightly conservative in some cases where prediction of the neutral axis was larger than recorded values. The amount of post-tensioning force throughout testing was also well represented by the design procedure. Due to the way in which the moment response was calculated it was not possible to draw conclusions regarding the initial stiffness of the connection.

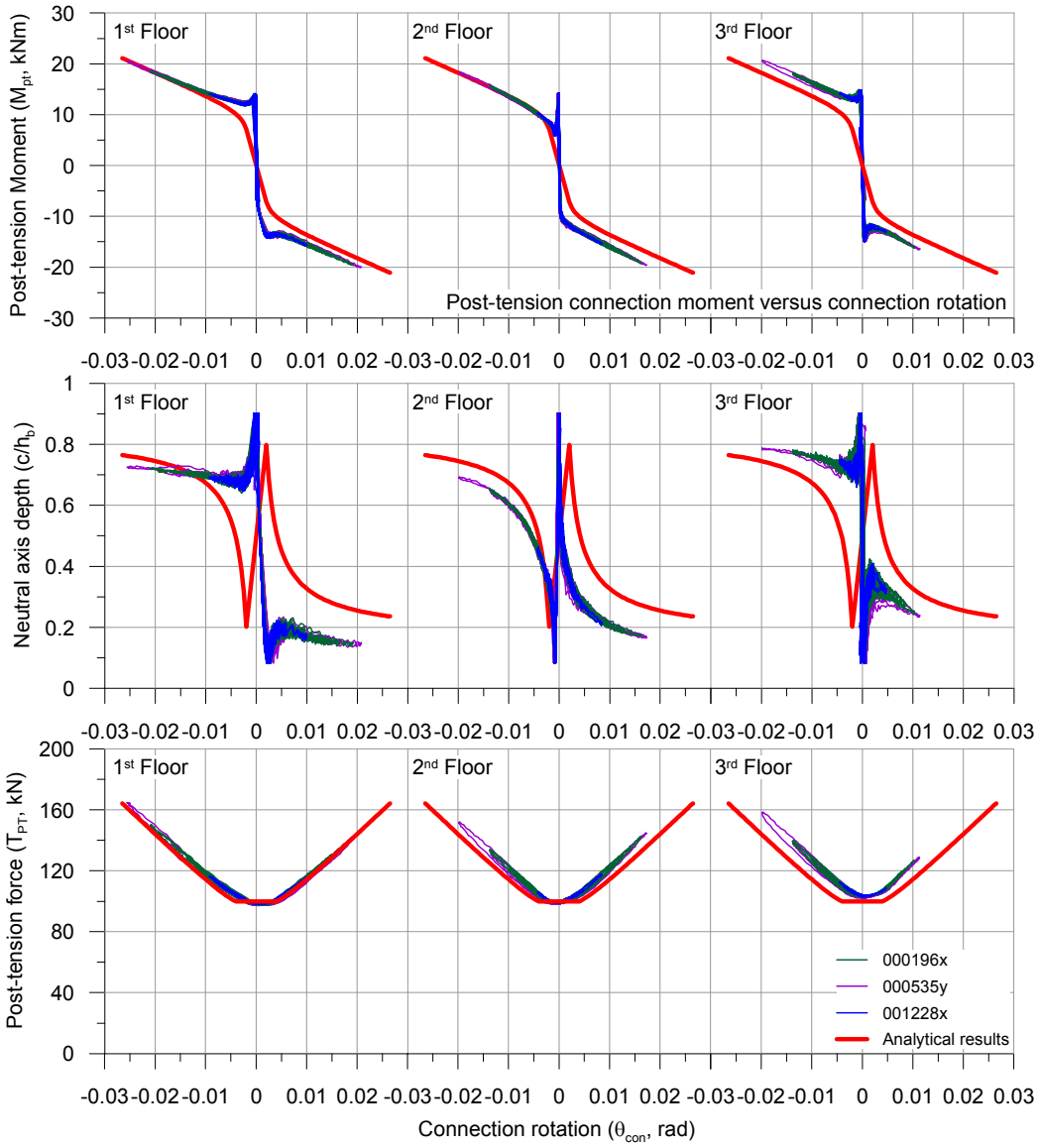

Figure 7.2. Comparison of test results versus design procedure moment, neutral axis and post-tensioning-connection rotation response of PT100_1.00 PGA75%

7.3.2 Analytical beam, column and joint panel rotation response of PT100_1.00

The beam, column and joint panel rotations have been calculated as outlined in Chapter 5 and added to the connection moment-connection rotation procedure above in order to provide the moment-drift response of the frame. These have been compared to the connection moment-drift response of the frame in Figure 7.3. The combined moment-drift procedure provided a sufficiently accurate representation of the total moment-drift response of the frame. The procedure on the whole can be seen to be conservative with predicted analytical frame response showing lower capacity

when compared to testing results. As with the comparisons made in Section 7.3.1 it was not possible to draw conclusion regarding initial stiffness.

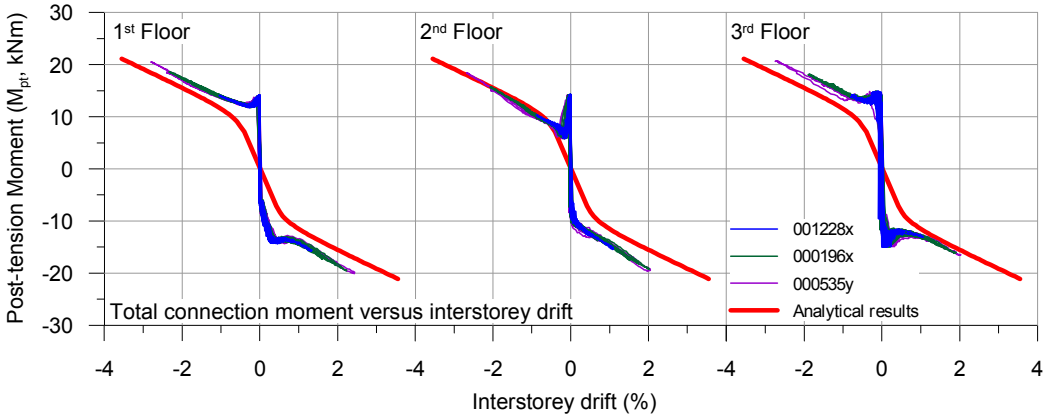

Figure 7.3. Comparisons of test results with design procedure moment-drift response of PT100_1.00

Figure 6.25 of Chapter 6 compared total rotations of the frame with the connection rotations at each beam column joint. In order to further analyse the adequacy of the beam, column and joint panel rotations presented in Chapter 5, Figure 7.4 has been made for the PT100_1.00 test configuration. The red line on the graph shows the analytical relationship as defined in Chapter 5.

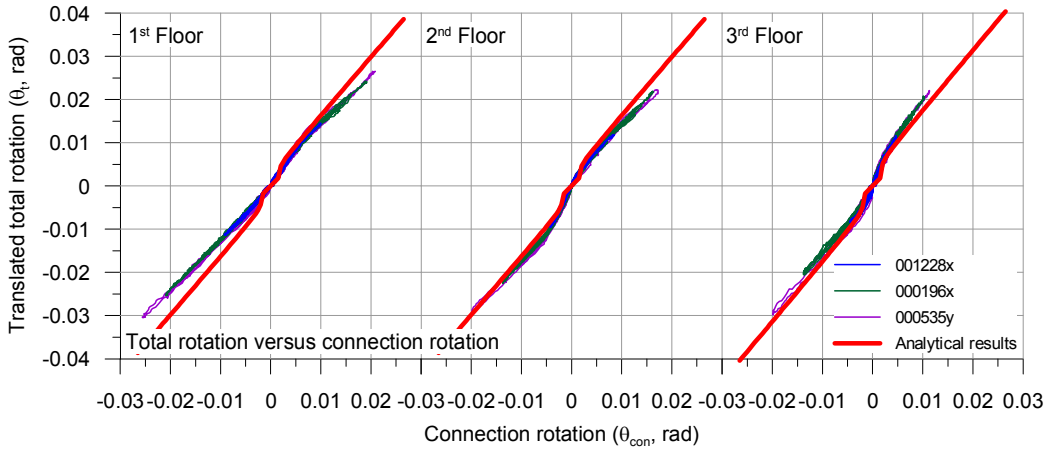

Figure 7.4. Total rotation versus connection rotation for PT100_1.00 testing PGA75% compared with analytical results

The figure shows that, as with the MMBA, the analytical procedure provided a sufficiently accurate representation of the relationship between the total rotation of the frame and the connection rotation at the joint panel interface for Level 2 and 3 of the structure. The analytical procedure seemed to overestimate the elastic contributions at the first floor predicting lower connection rotations at a given level of total rotation.

Overall this over estimation of the elastic contributions was probably connected with conservative assumptions made regarding shear values and points of contraflexure during the definition of the beam, column and joint panel rotations presented in Chapter 5. This fact has already been supported during the beam-column testing as discussed in Section 5.4.4. The possible over estimation of these elastic contributions meant that connection rotations were larger than design values. This led to increased moment capacity and damping creating an overall positive effect on building response. This must be considered however when determining the ultimate capacity of dissipative reinforcing and post-tensioning elements. Factors of safety must therefore be carefully considered.

7.4 EVALUATION OF INITIAL PERIOD AND STRUCTURAL FREQUENCY

During testing the initial period of each of the two structural configurations was measured. Several methods were used in order to evaluate the dynamic characteristics of the frame test specimen with the hammer impact test providing the best results. Section 6.4.6 discussed the fundamental period of the structure before the commencement of testing of each test configuration. Table 7.1 shows these values.

Table 7.1. Dynamic characteristics of test frame configurations before testing

	First mode	Second mode	Third mode
PT100_0.60	2.2Hz (0.45s)	8.6Hz (0.12s)	17.4 Hz (0.06s)
PT100_1.00	1.9Hz (0.53s)	7.8Hz (0.13s)	16.9 Hz (0.06s)

Table 7.1 shows that a change in the dynamic characteristics of the frame was observed with all three first modes decreasing in frequency between testing with and without dissipative reinforcing. The mass between the two test configurations remained equal, therefore this change in characteristics must have been related to a reduction in stiffness. Section 6.5.6 found by comparing the dynamic characteristics of the frame during the PT100_0.60 test sequence that the reduction in stiffness was related to the accumulation of minor damage in the frame and not to the removal of the dissipative elements. It is likely that the change in dynamic characteristics was related to an alteration of the boundary conditions of the frame due to damage created at the column base during the PT100_0.60 test series discussed in Chapter 6.

The evaluation of the initial period of the equivalent first (assumed dominant) mode of the frame is a fundamental requirement in a FBD approach in order to determine

the spectral acceleration and thus the design base shear. During the use of FBD it is the fundamental period of an equivalent single degree of freedom elasto-plastic system that is required in order to derive spectral acceleration from the code defined spectrum. In order to define the fundamental period of the elasto-plastic system it is the secant to yield stiffness that is required. Figure 7.5 shows how in concrete structures this requirement can mean that ambient vibrations do not provide adequate values of the fundamental period of the equivalent elasto-plastic system. This is due to the way in which the non-linear behaviour of concrete develops with initial stiffness of the system being related to the onset of cracking and not the onset of yield. This means that the fundamental period values derived are in general lower (due to higher stiffness) than the fundamental period of the elasto-plastic system.

Significant attention has been given to the calculation and estimation of the elastic displacements of post-tensioned timber frames throughout the experimental testing campaigns presented in Chapters 4 and 6. The combination of these elastic deformations creates a frame which is notably more flexible than the concrete equivalent. This increased flexibility means that issues with the use of ambient vibrations to evaluate initial period do not occur in post-tensioned timber frames. As shown in Figure 7.5 the low initial stiffness of the post-tensioned timber frame means that there is negligible difference between the initial and the secant to yield stiffness in a post-tensioned timber frame.

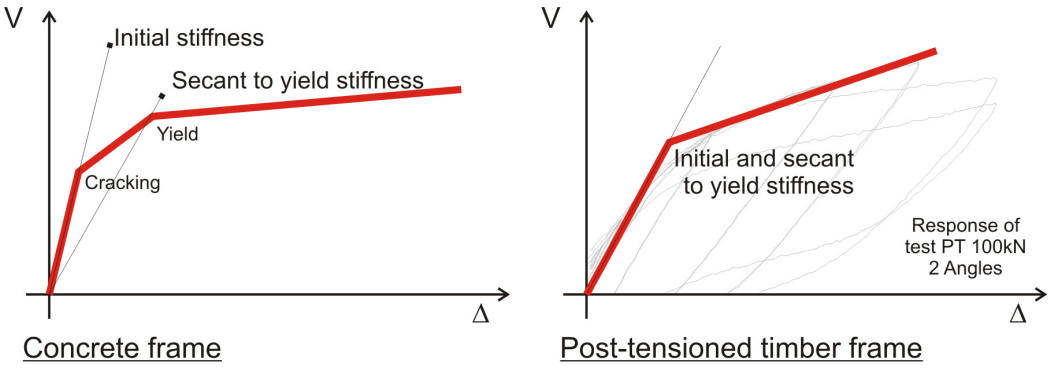

Figure 7.5. Comparison of traditional concrete and post-tensioned timber elasto-plastic system assumptions

A number of code-based equations or approaches are available to estimate the initial period. Four of these code-based methods have been used and are compared against the actual frame values presented in Table 7.1.

For three of the four methods an elastic numerical model was required. This was done using the SAP2000 (Computers and Structures CSI Computers and Structures Inc. 2004) numerical modelling programme. Chapter 8 will discuss the way in which the characteristics of post-tensioned timber frames are modelled numerically, presenting methods for representing the gap-opening described in Chapter 5. The numerical model used in this section does not account for these non-linear rotations and is intended to remain purely elastic. Actual member sizes (h_b = 305 mm) have been used in modelling.

7.4.1 Method one – The Rayleigh method

The first of the four methods used was the Rayleigh method (NZS1170.5 2004) which requires assumptions to be made regarding dynamic characteristics of the system. The first mode period (T_1) is calculated using the following formula:

$$T_1 = 2\pi \sqrt{\frac{\sum_{i=1}^{n} W_i \Delta_i^2}{g \sum_{i=1}^{n} F_i d_i}} \qquad \textbf{(7.1)}$$

Where:

Δ_i = Horizontal displacement of the centre of mass at level i (ignoring the effects of torsion) (m)

g = Gravitational constant (ms^{-2})

F_i = Displacing force at level i, coming from the equivalent static distribution of the base shear (kN)

W_i = Seismic weight at level i (tonnes)

When using the Rayleigh method several assumptions must be made regarding column boundary conditions and system dynamic characteristics. The boundary conditions at the base of the columns impact significantly on the displacements under load and therefore the estimation of initial period. As described in Section 6.5.5 during testing the test frame responded in an almost pin based manner presenting only nominal amounts of base moment capacity. The column bases have therefore been modelled as pinned.

Figure 7.1 showed the elastic acceleration and displacement spectra which were used when selecting the seismic input during the frame specimen testing. These are reduced in order to account for the non-linear response of the structure when calculating the base shear. Chapter 5 described the numerous factors which impact the non-linear response and the damping capacity of a post-tensioned timber frame. During the use of the Rayleigh method the base shear distributed up the structure is reduced in order to represent non-linear behaviour. This has been done in accordance with the current New Zealand Seismic code NZS1170.5 (NZS 1170.5 2004) which will be discussed further in Section 7.6.1.

Equation (7.1) provides a first value of the initial period which is then used to calculate an updated base shear. If this new base shear is significantly different from the base shear used the procedure is repeated until convergence is obtained. The initial period of the test frame calculated using the Rayleigh method was $T_1 = 0.41$s.

7.4.2 Method two – Empirical methods

Most modern codes provide empirical methods for the calculation of initial period. Two of these methods have been considered, being those presented by the Italian (NTC08 2008) and New Zealand (NZS1170.5 2004) seismic codes as follows:

Section 7.3.3.2 NTC08 (2008)

$$T_1 = C_1 H^{3/4} \tag{7.2}$$

Section C4.1.2.2 NZS1170.5 (2004)

$$T_1 = 1.0 k_t h_n^{0.75} \tag{7.3}$$

Where:

H, h_n = Height to the uppermost seismic mass, normally the building height (m)

C_1, k_t = Modification factor for structural type

Equation (7.3) is provided for structural calculations pertaining to the Serviceability Limit State (SLS). Normally the intention under this level of loading is that the structure remains elastic. The period values used have been taken from elastic readings and therefore this formula will be used.

No modification factor exists for post-tensioned timber, however as it can be considered to be a flexible system the values proposed for steel frames have been suggested as adequate. These values are C_1 = 0.085 and k_t = 0.11 for NTC08 and NZS1170.5, respectively. Table 7.2 displays period values calculated using these empirical methods.

Table 7.2. Initial periods of test frame as provided by the empirical methods

NTC08	T_1 = 0.33
NZS1170.5	T_1 = 0.42

Table 7.2 clearly shows a difference in the two period values provided by the empirical methods. As these are calibrated factors this is likely representative of the differences in buildings used and assumptions made during the calibration of the factors.

7.4.3 Method three – Empirical and numerical method

A second empirical method is suggested by the New Zealand codes based on the displacement of the building when the gravity loading on the building is applied horizontally as follows:

$$T_1 = 2\sqrt{d} \tag{7.4}$$

Where:

d = Elastic displacement at the top of the building due to the gravity loads being applied in a horizontal direction (in this case the seismic weight, dead load plus 30% of live load) (m)

The SAP2000 numerical model used for Method 1 in Section 7.4.1 has again been used with pinned column bases. The initial period provided for the test specimen by the empirical and numerical method was T_1 = 0.52

7.4.4 Method four – Numerical method

Using the SAP2000 model that was developed for estimation of the period for Methods One and Three, a modal analysis was performed to determine the fundamental period of the structure. In order to gauge the importance of column base conditions a pinned based and a fixed base model were used for comparison.

These models not only provided the fundamental period of the structure but also provide higher mode periods. Table 7.2 displays period values calculated using these empirical methods for the first three modes.

Table 7.3. First three mode periods provided by the numerical method

	1st mode	2nd mode	3rd mode
Pinned base	$T_1 = 0.51$	$T_2 = 0.12$	$T_3 = 0.06$
Fixed base	$T_1 = 0.34$	$T_2 = 0.10$	$T_3 = 0.05$

7.4.5 Method summary compared with testing results

A summary of the different estimations of the fundamental period, depending on the methods used for the estimation is given in Table 7.4

Table 7.4. Summary of test specimen periods provided by analytical and numerical methods

Test results			
PT100_0.60	$T_1 = 0.45$	$T_2 = 0.12$	$T_3 = 0.06$
PT100_1.00	$T_1 = 0.53$	$T_2 = 0.13$	$T_1 = 0.06$
Method one			
	$T_1 = 0.41$		
Method two			
NTC08	$T_1 = 0.33$		
NZS1170.5	$T_1 = 0.42$		
Method three			
	$T_1 = 0.52$		
Method four			
	1st mode	2nd mode	3rd mode
Pinned base	$T_1 = 0.51$	$T_2 = 0.12$	$T_3 = 0.06$
Fixed base	$T_1 = 0.34$	$T_2 = 0.10$	$T_3 = 0.05$

Comparisons with testing results showed that all methods, with the exception of Method Two as proposed by NTC08, provided, in this specific case, sufficiently accurate values of the initial period. Method Three using the empirical model proposed by NZS1170.5 and Method Four which used the numerical modelling program SAP2000 provided an almost exact prediction of the modes of the structure when a pinned base was assumed.

The model used for the SAP2000 analysis did not contain any information regarding the strength or stiffness of the beam-column joint. This indicates that as observed in Section 6.5.6 the initial period of a post-tensioned timber structure is dependent on the size and stiffness of structural members.

In summary, Methods One and Two (NZS1170.5) provided sufficiently accurate predictions of initial period, providing slightly lower values than those recorded from the actual test frame. Due to the form of the acceleration spectrum, as shown in Figure

7.1, this underestimation will generally lead to conservative values of base shear. While Method Three provides an almost exact estimation of the initial period, as a numerical approximate method, care must be taken in its use.

If possible during design a simple elastic modal analysis should be performed which will provide the most accurate estimation of initial period. This model does not need to contain information regarding the beam-column interface connection behaviour. It is crucial however that correct assumptions be made regarding the flexibility of the column base. Providing moment capacity at the base of the column of the built post-tensioned timber frame will not create a fixed base and is likely only to slightly reduce the period of the real structure.

7.5 ELASTIC DAMPING

As discussed in Section 6.8.1 elastic damping is used to introduce damping not captured by the hysteretic model represented by the codified reduction methods (i.e. the factor q discussed in Section 7.4.1). Typically elastic damping values of $\xi_{el} = 0.05$ are used for concrete structures (represented in most codes by the presentation of a 0.05 damped design spectrum). Steel structures typically are given lower elastics damping values ($\xi_{el} = 0.02 – 0.03$).

The work by Pino Merino (2011) on the dynamic testing of post-tensioned timber frames has already been described in Chapter 2 and suggested that total damping values (considered to be elastic due to the lack of dissipative devices) varied from around $\xi_{el} = 0.02$ to 0.05 as maximum drifts ranged from $\theta_d = 0$ to 2.5%. It was also stated however during this work that slight damage was observed during larger drift cycles and therefore damping values were not strictly elastic.

Further dynamic testing performed by Marriot (2009) of a post-tensioned timber wall showed elastic damping values to be at the lower end of the range suggested above with $\xi_{el} = 0.02$.

Additional work has been performed by Smith et al. (2012) regarding the study of a full scale post-tensioned timber frame and wall building that was subjected to the 2010 – 2011 Canterbury seismic sequence. Three accelerometers were placed throughout the building and over 2000 separate seismic events were recorded.

The damping of the structure was analysed using the statistical NonPaDAn method (Mucciarelli and Gallipoli 2006) which provided an average value of ξ_{el} = 0.03 in both building directions. Upon further analysis the relationship between building displacement and damping values were also demonstrated to vary with amplitude as was shown during the testing of Pino Merino et al. (2010).

The elastic damping values of the three storey test structure have been evaluated during the dynamic identification of the structure giving a range of elastic damping values between ξ_{el} = 0.014 to 0.019. As mentioned in Section 6.8.1 however, the frame model was without many of the sources of elastic damping present in a normal structure. Therefore it appears that an average damping value of ξ_{el} = 0.03 is acceptable for post-tensioned timber frames.

7.6 HYSTERETIC DAMPING

Hysteretic damping and the way in which it can be estimated for a post-tensioned timber system has been discussed in Section 5.5 which presented a relationship between the equivalent viscous damping, ξ_{EQV}, the post-yield stiffness ratio, r, and the ductility, μ.

As mentioned in Section 7.2 two principal methods can be considered when calculating the design base shear of a post-tensioned timber structure: Force Based Design (FBD) and Displacement Based Design (DBD). These two methods treat the contributions of non-linearity (and hence hysteretic damping) in different ways.

7.6.1 Force based design (FBD)

The evaluation of the reduction of the elastic acceleration spectrum due to the non-linear response of the structure has been considered according to two different code based methods. The first of these is found in the New Zealand seismic code NZS1170.5 (2004). The second in the Italian design code NTC08 (2008). It must be noted that, as described above, both of these methods of reduction have been based on a supposed elasto-perfectly plastic hysteretic behaviour which is significantly different from the flag shaped hysteresis displayed by a post-tensioned timber system. It is important to also note that both of these methods apply a general factor accounting for non-linear behaviour and do not separate the effects of ductility and damping. A third alternative method, based on the work by Cardone et al. (2008), is

also presented. This method specifically addresses the impact of the recentering ratio (β) on system damping and separates out the impact of ductility and damping on the non-linear dynamic response of post-tensioned timber frames.

Evaluation of spectral reduction in accordance with NZS1170.5

The New Zealand seismic code allows the reduction of the design spectrum by:

$$\frac{S_p}{k_\mu} \tag{7.5}$$

Where:

S_p = The structural performance factor which for buildings having a ductility larger that 2 is taken as 0.7 and for buildings having $1 \leq \mu \leq 2$ is taken as:

$$S_p = 1.3 - 0.3\mu \tag{7.6}$$

It has been suggested that for post-tensioned timber structures the structural performance factor be set to 1 (STIC 2013).

For most soil classes (apart from the softest soils) the factor k_μ is taken as:

$$k_\mu = \mu \text{ for } T \geq 0.7$$
$$k_\mu = \frac{(\mu - 1)T}{0.7} + 1 \text{ for } T < 0.7 \tag{7.7}$$

Evaluation of spectral reduction in accordance with the NTC08

The Italian seismic code allows the reduction of the design spectrum through the use of a structural performance factor ($q = q_0 K_R$) based on structural type (q_0) and regularity (K_R). Timber structures are separated into two groups: structures of high ductility (Type A) and structures of low ductility (Type B) with values of q_0 ranging between 2 and 5. None of these structural classes refer to the use of timber in structural frames, therefore it is difficult to propose what a likely structural factor would be for a post-tensioned timber frame in design. These factors can be based on the parametric analysis of any structural system and Chapter 9 will provide a brief discussion regarding the reduction factors found during the limited parametric analysis performed during this body of research. However, a much more significant

number of cases should be considered before confident estimations of the factor q_0 can be made.

Alternative measure for the calculation of the behaviour factor, q

Cardone et al. (2008) presented methods for the calculation of the behaviour factor, q, for flag-shaped hysteretic models. A series of non-linear time-history analyses were carried out using 14 earthquake records relevant to 2 different site-conditions. The maximum seismic response of a single degree of freedom flag-shaped system was derived and compared to that of an Elasto-Perfectly Plastic (EPP) single degree of freedom system. Although this study referred to the use of shape memory alloys, which also present a flag-shaped hysteretic loop, it can be easily adapted for use with post-tensioned timber structures. It can also be tentatively applied to the multi degree of freedom frame.

The procedure proposed by Cardone et al. (Cardone et al. 2008) is based around the behaviour factor formula for an EPP system, q_{EPP}, as proposed by Newmark and Hall (1973):

$$q_{EPP} = \begin{cases} 1 & T = 0 \\ \sqrt{2\mu - 1} & T = T_g \\ \mu & T > T_C \end{cases} \quad \textbf{(7.8)}$$

Where:

T_g = Characteristic period of the ground motion (i.e. the period associated with the peak spectral acceleration taken as the beginning of the constant acceleration part of the code defined spectrum) (s)

T_C = Corner period associated with the transition between the constant acceleration and constant velocity part of the spectrum (s)

The values of T_g and T_C for the code spectrum used in the design of the test frame were 0.121 and 0.407, respectively. Between T = 0, T_g and T_C a linear relationship for q_{EPP} is used. Once the behaviour factor for the EPP system is known, two correction factors are used in order to account for the flag shaped hysteretic behaviour presented by the post-tensioned timber system as follows.

$$q_{FS} = C_\beta q_{EPP} \quad \textbf{(7.9)}$$

$$C_\beta = -2\beta^2 + 1.8\beta + 1 \quad \textbf{(7.10)}$$

Where:

q_{FS} = The structural behaviour factor for the flag shape system

C_β = The q correction factor based on the recentering ratio of the frame (β)

A second correction factor was also proposed based on the post-yield stiffness, however, it was concluded that this effect was negligible and could be ignored. The equation above was also only developed for a single value of elastic period (T = 0.3s) and it was expected that values would vary for different initial periods. Tentatively a relationship between period and the correction factor was proposed where a linear relationship can be used between values as follows.

$$C_\beta = \begin{cases} 1 & T = 0 \\ C_\beta & T = T_g \\ 1 & T = 0.8 \end{cases} \quad \textbf{(7.11)}$$

7.6.2 Displacement based design (DBD)

Displacement based design uses a reduction factor, R, which is a function of the total structural damping (Priestley et al. 2007):

$$R = \left(\frac{7}{2 + \xi} \right)^\alpha \quad \textbf{(7.12)}$$

Where:

ξ = the system damping ratio of the structure taken as a combination of the elastic damping ξ_{el} and the hysteretic damping ξ_{hyst} as described in Equation (7.13) (%)

α = is equal to 0.5 and 0.25 for far-field and near field seismic spectra, respectively.

This reduction factor is then used to adjust the displacement spectrum in order to account for inelastic behaviour.

Elastic damping in DBD, ξ_{el}

Elastic damping values have been discussed above concluding that values of $\xi_{el} = 0.03$ (3%) are appropriate for post-tensioned timber structures. Priestley et al. (2007)

suggested that a correction factor (κ) should be used to account for the fact that the secant stiffness for the equivalent single degree of freedom system is used in DBD. Elastic damping values are normally provided relative to the initial stiffness of the system and therefore should be reduced for consideration with non-linear response. This conclusion, however, has been drawn when considering high stiffness, high ductility systems such as reinforced concrete, where differences between the initial, tangential and secant stiffness can vary greatly. Newcombe et al. (2011) have proposed that because the secant and tangent stiffness of the post-tensioned system will not vary greatly the elastic damping will not significantly reduce with ductility. This observation is supported by the moment-drift response shown in Figure 7.3 and total building response shown displayed in Chapter 6. A post-tensioned timber frame system has low-initial stiffness, high post-yield stiffness and generally low ductility demand, meaning that the initial, tangential and secant stiffnesses do not vary greatly when compared for example with traditional reinforced concrete or even post-tensioned concrete structures. It is therefore suggested that no correction factor is required for post-tensioned timber frames (i.e. $\kappa = 0$).

Hysteretic damping in DDBD, ξ_{hyst}

The hysteretic damping of post-tensioned timber frames has been discussed in several sections during both the full-scale beam-column testing presented in Chapter 4 and the dynamic three-storey frame testing presented in Chapter 6.

As with elastic damping, Priestley et al. (2007) suggested that values of hysteretic damping should be corrected. In the case of hysteretic damping this is in order to account for the random nature of seismic input. Correction values have been proposed based on non-linear time history analyses for low-damping flag shaped hysteretic loops ranging between 0.8 and 1.2 depending on ductility (0.8 and 1.2 for $\mu = 2$ and 6, respectively).

Due to the large amount of elastic deformation in a post-tensioned timber frame, ductility values of higher than 3 are unlikely, indicating that a reduction factor between 0.8 and 1 would be appropriate. Observations in Section 5.5 showed that the formula for calculating the area within a flag-shaped loop had a ratio of approximately 0.9 when compared to measured values within a normal recentering range ($0.55 < \beta < 0.65$). Considering these two points it is suggested that a factor of 0.7 be

conservatively applied to the hysteretic damping values calculated for post-tensioned timber frames. This means that for a post-tensioned timber frame the total damping, ξ, is equal to:

$$\xi = \xi_{el} + 0.7\xi_{hyst} = 0.03 + 0.7\xi_{hyst} \quad \textbf{(7.13)}$$

As mentioned above the value of 0.7 is conservative as this value is dependent on system ductility and target recentering ratio. Further research may improve this value or define it as a function of these two parameters.

7.7 EVALUATION OF MAXIMUM BASE SHEAR

The evaluation of the maximum base shear of the frame is key to understanding the seismic demand on a structure. Two approaches (FBD and DBD) have been used to calculate the base shear of the frame using the assumptions made above in order to calculate period and non-linear reductions.

7.7.1 Base shear calculation according to Force Based Design (FBD)

In order to calculate the design Ultimate Limit State base shear according to Force Based Design (FBD) two parameters must be either calculated or estimated (with the latter of the two options being the most likely). These are: 1) the initial period of the building (as described in Section 7.4) and 2) the spectrum reduction factor (as described in Section 7.6.1).

The spectrum reduction factors described in Section 7.6.1 are all reliant on accurate knowledge of the ductility demand on the frame during seismic excitation. During design it is not expected that the ductility of the frame will be known before the base shear of the frame is calculated. Guidance on reducing ductility errors in design is provided in Chapter 10. For the remainder of this chapter the correct ductility, as measured during testing and presented in Chapter 6, will be used. Design values of the recentering ratio have been used. An initial first mode period of T = 0.53s has been used for both frames as by the end of the PT100_0.60 test series (i.e. during maximum response) this was the first mode of the frame as described in Section 6.5.6.

The spectrum reduction factors have been calculated using the two methods presented in Section 7.6.1 and are presented in Table 7.5. The method used in the Italian code

NTC08 (NTC 2008) has not been compared as an appropriate q_0 factor is not provided as discussed in Section 7.6.1.

As mentioned above, recent post-tensioned timber design guidelines (STIC 2013) suggest that if the New Zealand code is to be used in design that the S_p factor be set to 1 for all cases. Reduction values calculated with $S_p = 1$ are also displayed in Table 7.5.

Table 7.5. Elastic acceleration spectrum reduction factors

	PGA	Ductility	AS/NZS1170	AS/NZS1170 ($S_p = 1$)	Alternative procedure
PT100_0.60	100%	2.5 / 1.6 = 1.6	$\frac{S_p}{k_\mu} = \frac{0.82}{1.45} = 0.56$	$\frac{1}{k_\mu} = 0.69$	$q_{FS} = 1.82$
PT100_1.00	75%	2.2 / 1.1 = 2.0	$\frac{S_p}{k_\mu} = \frac{0.7}{1.75} = 0.40$	$\frac{1}{k_\mu} = 0.57$	$q_{FS} = 1.84$

Table 7.5 shows that for test PT100_0.60 the two procedures provided very similar reduction factors (1/1.82 = 0.55). For PT100_1.00 however the results of the procedures differed with the alternative procedure, which accounts for both ductility and the recentering ratio, providing a more conservative reduction value of 1/1.84 = 0.54.

The maximum base shear during each test was measured and presented in Chapter 6. It was possible to convert these into design accelerations by dividing the maximum base shear by the building mass. This maximum building response was then averaged amongst the three seismic inputs and compared with the average input spectrum in order to find the average reduction factor measured during testing. The results of these analyses are shown in Figure 7.6.

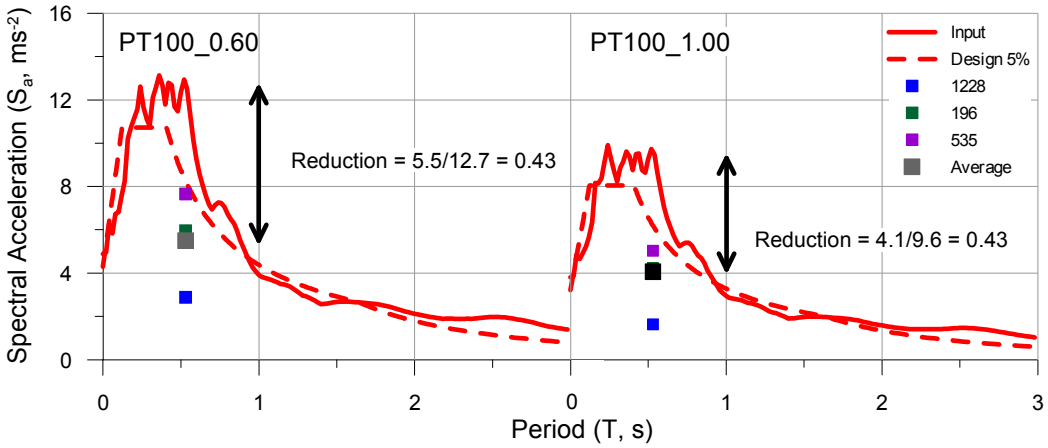

Figure 7.6. Comparisons of input motion and spectral response for dynamic frame testing

Figure 7.6 shows that spectral reduction factors (i.e. the ratio between the elastic spectrum at T_1 and the response of the test frame) of 0.43 have been found for both PT100_1.00 and PT100_0.60 testing. These values were within the range of the reduction factors calculated using the two methods presented. The AS/NZS1170 method provided the closest estimation for any test predicting a reduction of 0.40 for the PT100_1.00 testing set. This was possibly a simple coincidence however as no information is considered regarding the dissipative capacity of the system. From these results it does appear, however, that building ductility had a larger impact on system response than system damping. The alternative procedure correctly predicted that system base shear response would be similar with and without the additional dissipation for these low ductility systems. On the whole the procedure provided a conservative estimate of the reduction factor. NZS1170.5 estimations became more conservative when S_p was set equal to 1.

It is important to note that, although both procedures provided reasonably accurate estimations of the spectral acceleration and therefore base shear, they were based on actual values of both initial period and ductility. Section 7.4 showed the wide range of initial periods possible depending on the assumptions made with a 0.2 second range between the maximum and minimum value.

The most important contributors are the assumptions surrounding the ductility of the structure. Previous chapters have discussed the increased elastic deformations of timber when compared to more traditional multi-storey construction materials. Behaviour factors of 5 (equating more or less to a ductility of 5) do not seem feasible when considering that if yield occurs at 0.8% drift, a maximum drift of 4% will be

experienced. These values should be considered more as what is feasible under maximum response and not as the design value. Ductility values used in design must either be correct from the beginning (requiring excellent engineering judgement or luck) or checked and iterated upon once design is completed. An alternative to this is the use of a closed-form Force Based Design procedure in order to simplify the required iterations on the initial stiffness and ductility (Sporn and Pampanin 2013).

The observations made above are significant, however they are only based on two data points.

7.7.2 Base shear calculation according to Displacement Based Design (DBD)

Section 7.6.2 discussed the reduction factor R used to account for system damping in displacement based design. As mentioned this is a combination of the elastic damping (which has been set at 3%) and 70% of the hysteretic damping (calculated as in Section 5.5). In calculation of the reduction factor (Table 7.6) a value of $\alpha = 0.5$ has been used.

Table 7.6. Elastic displacement spectrum reduction factors for DBD assuming $\alpha = 0.5$

	Ductility	Post-yield stiffness	Hysteretic damping	Total Damping	Reduction factor
PT100_0.60	2.5 / 1.6 = 1.6	r = 0.27	$\xi_{hyst} = 0.08$	$\xi = 0.09$	R = 0.81
PT100_1.00	2.2 / 1.1 = 2.0	r = 0.08	$\xi_{hyst} = 0.00$	$\xi = 0.03$	R = 1.18

In order to use a displacement based design approach two operations must be performed; the Multi-Degree Of Freedom (MDOF) system must be converted into an equivalent Single Degree Of Freedom (SDOF) system and the 5% damped elastic acceleration spectrum provided by the design code must be converted into a 5% damped elastic displacement spectrum. This section provides a brief description of how to perform these two operations. For more information and the equations used refer to Chapter 10 where the full post-tensioned timber displacement based design procedure is discussed.

Conversion of the MDOF system to a SDOF system (Table 7.7 and Table 7.8) followed the procedure set out in Priestley et al. (2007) which follows the method proposed by Shibata and Sozen (1976). This procedure is independent of strength depending only on geometry and mass, however as with the FBD design levels of ductility and maximum displacement were used, meaning that the procedure was performed individually for each frame. The average critical displacement for both

frames occurred at Level One with values of 0.049 m (2.45%) and 0.043 m (2.15%) occurring for tests PT100_0.60 and PT100_1.00, respectively.

Table 7.7 and Table 7.8 calculated the displaced shape of the structure in relation to the critical displacement which occurred at the first floor. In doing this a linear distribution of displacement was assumed as proposed by Priestley et al. (2007) for low rise structures. Comparisons of the assumed deformed shapes against the maximum average testing results are shown in Figure 7.7. It shows that the linear assumption provided a good estimation of the displaced shape of the frame.

Table 7.7. Equivalent SDOF system for PT100_0.60 MDOF test frame

Level	m_i (t)	h_i (m)	δ_i	Δ_i (m)	$m_i\Delta_i$	$m_i\Delta_i h_i$	$m_i\Delta_i^2$
3	5.8	6.0	1.00	0.148	0.85	5.15	0.127
2	5.8	4.0	0.67	0.099	0.57	2.30	0.057
1	5.8	2.0	0.33	0.049	0.28	0.57	0.014
∑	17.4				1.70	8.02	0.198

Table 7.8. Equivalent SDOF system for PT100_1.00 MDOF test frame

Level	m_i (t)	h_i (m)	δ_i	Δ_i (m)	$m_i\Delta_i$	$m_i\Delta_i h_i$	$m_i\Delta_i^2$
3	5.8	6.0	1.00	0.130	0.75	4.52	0.098
2	5.8	4.0	0.67	0.087	0.50	2.02	0.044
1	5.8	2.0	0.33	0.043	0.25	0.50	0.011
∑	17.4				1.50	7.04	0.153

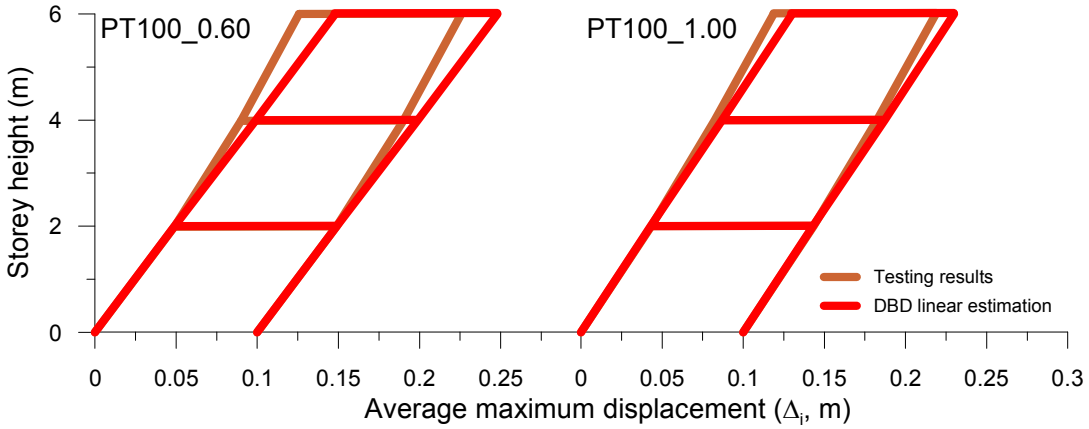

Figure 7.7. Assumed DBD displaced shape comparisons with testing results

Priestley et al. (2007) state that for structures with more than 4 storeys an idealized first mode shape should be used to estimate displaced shape. This appeared also to hold for post-tensioned timber buildings with the shape of the test structure (especially the higher capacity PT100_0.60 test case) clearly beginning to approach the form of an idealized first mode.

The next step in the displacement based design procedure was to calculate the effective displacement, mass and height of the structure. This has been performed and is presented in Table 7.9.

Table 7.9. DBD design parameters for test series PT100_0.60 and PT100_1.00

	Effective displacement	Effective mass	Effective height
PT100_0.60	Δ_d = 0.116 m	m_e = 14.7 t	H_e = 4.71 m
PT100_1.00	Δ_d = 0.102 m	m_e = 14.7 t	H_e = 4.71 m

In order to complete the DBD procedure the elastic acceleration spectra shown in Figure 7.1 was converted into an elastic pseudo-displacement spectrum and multiplied by the reductions factors presented in Table 7.6. Once the inelastic displacement spectrum was defined the design displacement, Δ_d, was used to find the effective period, T_e, of the equivalent SDOF system (Figure 7.8).

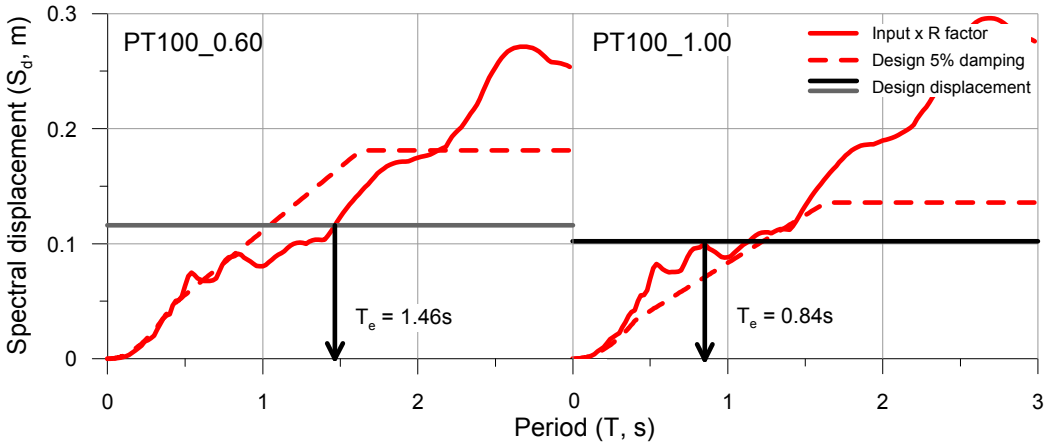

Figure 7.8. Reduced design displacement spectrum used to find effective period (T_e) of structure as part of DBD procedure

Once the effective period of the SDOF system was found the base shear of the structure was calculated using Equation (7.14).

$$V_b = K_e \Delta_d = \frac{4\pi^2 m_e}{T_e^2} \Delta_d \qquad \textbf{(7.14)}$$

Where:

K_e = the secant stiffness of the equivalent SDOF system

Doing this provided base shears of V_b = 31.6 kN and V_b = 83.9 kN for PT100_0.60 and PT100_1.00, respectively. Comparing the DBD base shear values with the average testing value of PT100_1.00 (V_b = 71.9 kN) shows the DBD base shear to be

reasonably accurate and slightly conservative. Comparisons between the DBD base shear values and the average testing values of PT100_0.60 (V_b = 97.2) however, displays that for this specific case the DBD procedure severely underestimates base shear values.

The reason for this underestimation is twofold; errors made in the calculation of the reduction factor due to the assumptions made in design not being true during system response, and due to the nature of DBD these errors are amplified during the design procedure.

Section 6.8.2 of Chapter 6 described the hysteretic damping calculated during testing and using the area based method calculated a maximum hysteretic damping of ξ_{hyst} = 7.8%. Although this value is similar to the calculated damping value (ξ_{hyst} = 8%) presented in Table 7.6, it corresponded with the maximum drift recorded during testing (θ_t = 3.5%) and not the average value used during the DBD (θ_d = 2.5%).

Chapter 6 discussed the various deficiencies in performance encountered during testing and how these led to reduced performance of the post-tensioned timber frame. It is highly likely that these have also led to high values of frame recentering ratio due a reduced contribution of the dissipative reinforcing. In the calculation of the hysteretic damping of the frame at a certain level of total drift, the total recentering ratio must be used which, in this case, was likely to be higher than β = 0.6.

In addition to this fact it is noted that the formula used for calculating the hysteretic damping of the flag-shaped post-tensioned timber system is particularly sensitive to ductility values in the likely ductility range of a post-tensioned timber frame (μ = 1 – 2.5). Although in Chapter 6 an estimation of ductility was made using the actual test results, this estimation has been based on a backbone curve and a selected value of yield drift based on a ‘best fit’ method. This method is objective and as such contains a certain level of error.

The actual levels of damping where measured in Section 6.8.2 using the NonPaDAn method, providing an average total damping of ξ = 4.5%. Using this value provided a significantly different reduction factor of R = 1.04. In fact, and as for the PT ONLY case, an increase in spectrum was seen due to the fact that damping is below the 5% value used by the code spectrum.

This error in reduction factor was then increased by the second source of error in DBD. When the new R value was applied to the spectrum the effective period was reduced to $T_e = 0.84$ (approximately a 43% decrease) and a new base shear value (V_b = 95 kN) was found. This new base shear value was three times the original value. This value was almost exactly the value found during testing (V_b = 97.2 kN). The reason for this rapid increase lies in the use of Equation (7.14) where any small change in effective period is squared, creating large changes in base shear.

It is therefore evident that, as with FBD, extreme care must be taken in the estimation of ductility levels and recentering ratios which are crucial in understanding system damping. Errors in these assumptions or, as was the case with the test frame, if the system does not provide the desired design response can lead to significant underestimation of seismic demand.

As with FBD, these observations are significant, however they are only based on two data points.

7.7.3 Summary of base shear calculations following the FBD and DBD approach

Table 7.10 provides a summary of the base shear values calculated using the FBD and DBD design procedures for the PT100_0.60 and PT100_0.60 testing series. The average maximum base shears registered during testing are also provided.

Table 7.10. PT100_0.60 and PT100_1.00 base shear values using the FBD and DBD analytical procedures

	PGA	FBD		DBD	Testing
		NZS1170.5	Alt. Procedure		
PT100_0.60	100%	V_b = 126.6	V_b = 123.3	V_b = 95.0*	V_b = 97.2
PT100_1.00	75%	V_b = 67.8	V_b = 92.2	V_b = 83.9	V_b = 71.9

*This base shear was modified in order to represent measured levels of damping

The table above shows that all of the analytical procedures used provided sufficiently accurate (within 30%) estimations of the average maximum base shear for the frame when subjected to the seismic loading used.

7.8 CONCLUSIONS FROM CHAPTER 7

Chapter 7 has presented analytical methods for understanding the global seismic response of post-tensioned timber frames. The principal outcome of these methods

was the design level of base shear, V_b, which was compared with the testing results presented in Chapter 6.

Prior to the study of the global response of the frame the local response of the beam-column joints at each level was analysed. Comparisons were made with the analytical procedures presented in Chapter 5. The first of these comparisons looked at the behaviour of the beam-column interface under dynamic loading and showed that the analytical procedure provides accurate predictions of the moment, post-tensioning force and neutral axis depth response. Comparisons of the neutral axis depths versus connection rotation behaviour indicated that the systems became slightly stiffer under dynamic loading leading to conservative estimations of moment capacity.

The second comparison made using the local frame response looked at the beam, column and joint panel elastic rotations and compared them with the analytical formula presented in Chapter 5. Comparisons showed that for the second and third floor the equations used provided accurate representations of the elastic frame contributions accurately predicting the ratio between total and connection rotations. At the first floor level the formulas overestimated the quantity of elastic rotations. This was likely due to the assumptions made regarding the distribution of moment in the column being inaccurate for the first level (the point of contra-flexure in the column was not at mid height as assumed). Overestimation of elastic rotations will lead to conservative designs (increased connection rotations and therefore increased dissipation and moment capacity), however, this possibility must be considered when designing post-tensioning and dissipative reinforcing in order to avoid failure from increased strain demand.

The first aspect of the global seismic response of the frame studied was an investigation into the methods available for the estimation of initial period of frames. All of the methods used except one (the NTC08 empirical method) provided, in this specific case, sufficiently accurate estimations of initial period which was shown to also be representative of the secant to yield period for post-tensioned timber structures. If a quick estimate of the buildings initial period is required the empirical method proposed by NZS1170.5 is adequate (this should be checked however following detailed design). The most accurate representation of the global frequency characteristics of the frame was the construction of a simple frame model in the

structural analysis program SAP2000. It was shown that in this case this model did not need to possess information regarding the beam-column interface response in order to provide accurate results.

Finally two methods of calculating the likely impact of seismic loading on a post-tensioned timber frame were analysed; Force Based Design (FBD) and Displacement Based Design (DBD). These two methods were used to calculate base shear values using the input spectrum discussed in Section 6.4.5. Two factors have been shown to impact on the base shear of the frame; the ductility and the hysteretic damping. Chapter 6 discussed the damping and ductility response of the post-tensioned timber test frame and described how in the design of any jointed ductility system (such as post-tensioned timber) the two factors are not necessarily linked. This is due to the introduction of the re-centering ratio, β, which represents the amount of dissipative steel moment capacity the frame possess. A post-tensioned only system ($\beta = 1$) will have ductility but will possess only minimal amounts of hysteretic damping.

Current FBD procedures do not necessarily recognise the amount of damping a seismic resistant system possesses with reduction factors being based on only ductility. The base shears calculated using the NZS1170.5 procedure was one example of this. Using this procedure provided base shear values which were conservative when damping was present (even if in minimal quantities), however results became unconservative for PT ONLY testing. Removal of the structural performance factor, ($S_p = 1$) increased the conservative nature of the dissipative PT100_0.60 and made the PT ONLY PT100_1.00 system slightly conservative. The PT100_1.00 base shear value calculated using the NZS1170.5 procedure was close to the measured value however this was likely a result of the low frame ductility (leading to only a minor reduction). Larger frame ductilities are likely to provide significantly unconservative results. The alternative FBD reduction procedure, which does separate out ductility and damping, remained conservative in both cases.

The DBD procedure is capable of separating out ductility and damping during the reduction of the displacement spectrum to account for non-linear behaviour. DBD provided very accurate prediction of base shear for test PT100_0.60 (within 2%) and an accurate prediction of the PT100_1.00 (within 14%) base shear value. Although these the two base shear values were eventually calculated with accuracy, the original

assumptions made regarding the PT100_0.60 ductility and recentering performance led to a base shear value which was a third of the measure value. It was observed that DBD is particularly sensitive to errors made in the calculation of damping, particularly for low damping ranges. This is particularly critical for post-tensioned timber frames which possess low levels of ductility where the hysteretic damping formula is the most sensitive.

Provided assumptions made regarding ductility and damping are sufficiently accurate, both procedures produce accurate estimations of likely base shear. Further discussion of the use of damping and ductility in FBD and DBD design is presented in Section 10.2.1.

REFERENCES CHAPTER 7

Cardone, D., Di Cesare, A., Ponzo, F. C., and Blonna, B. (2008). "Evaluation of Behaviour Factor for Flag-Shaped Hysteritic Models." International Conference on Engineering Optimization, Rio de Janeiro, Brazil.

CSI Computers and Structures Inc. (2004). "SAP2000: Static and Dynamic Finite Analysis of Structures." Berkeley, CA, USA.

NTC. (2008). "Norme Tecniche per le Costruzioni." Il Ministro delle Infrastrutture.

Marriott, D. (2009). "The Development of High-Performance Post-Tensioned Rocking Systems for the Seismic Design of Structures," University of Canterbury, Christchurch, New Zealand.Doctor of Philosophy in Civil Engineering.

Mucciarelli, M., and Gallipoli, M. R. (2006). "Estimate of Frequency and Damping for Large Sets of Buildings in Dense Urban Areas." First European Conference on Earthquake Engineering and Seismology, Geneva, Switzerlanf.

Newcombe, M. P., Marriott, D., Kam, W. Y., Pampanin, S., and Buchanan, A. H. (2011). "Design of UFP-coupled Post-tensioned Timber Shear Walls." 9th Pacific Conference on Earthquake Engineering, Auckland, New Zealand, 10.

Newmark, N. M., and W. J. Hall. (1973). "Procedures and criteria for earthquake resistant design." National Bureau of Standards, U.S. Dept. of Commerce.

Pino Merino, D. (2011). "Dynamic Response of Post-Tensioned Timber Framed Buildings," University of Canterbury, Christchurch, New Zealand.Master of Engineering.

Pino Merino, D., Pampanin, S., Carradine, D., Deam, B., and Buchanan, A. H. (2010). "Dynamic Responce of a Multi-Storey Post-Tensioned Timber Building." 11th World Conference on Timber Engineering, Riva del Garda, Trentino, Italy, 8.

Priestley, M. J. N., Calvi, G. M., and Kowalsky, M. J. (2007). *Displacement-Based Seismic Design of Structures*, IUSS Press.

Shibata, A., and Sozen, M. (1976). "Substitue Structure Method for Seismic Design in R/C." *ASCE Journal of Structural Engineering*, 102(1), 1 - 18.

Smith, T., Carradine, D., Pampanin, S., Ditomasso, R., and Ponzo, F. C. (2012). "The Seismic Performance of a Post tensioned LVL Building During the 2011 Canterbury Earthquake Sequence." 15th World Conference on Earthquake Engineering, Lisbon, Portugal.

Sporn, B., and Pampanin, S. (2013). "A “retrofit” solution for Force-Based Design: eliminating the need for iteration and initial period estimation." 2013 New Zealand Society for Earthquake Engineering Conference, Wellington, New Zealand.

Structural Timber Innovation Company Inc. (2013). "Post-Tensioned Timber Buildings - Design Guide." Structural Timber Innovation Company, Christchurch, New Zealand.

NZS 1170.5:2004. (2004). "Structural Design Actions Part 5 : Earthquake Actions - New Zealand." Standards New Zealand.

8 Non-linear Numerical Modelling of the Local and Global Behaviour of Post-tensioned Timber Frames

8.1 PRINCIPAL CONCLUSIONS OF CHAPTER 8

Chapter 8 presents numerical modelling developed to predict the local and global response of the beam-column testing presented in Chapter 4 and the frame testing presented in Chapter 6. The following principal conclusions are drawn:

1. The local (force/moment versus displacement/drift and hysteretic) response of a post-tensioned timber beam-column joint can be accurately modelled using non-linear models calibrated against the analytical design procedure presented in Chapter 5.

2. The two modelling techniques used (rotational springs or the more complex multi-(axial) springs) and the two modelling programs used (RUAUMOKO and SAP2000) provide very similar local (beam-column interface) behaviour.

3. The global (acceleration, base shear and drift) response of a post-tensioned timber frame can be adequately (with limited error) modelled applying the local modelling techniques.

4. The accuracy of the global numerical model relies strongly on the accurate prediction of the column base performance. If the column base is left to rock, it is recommended that the base of the column not be simply made ‘fixed’ or ‘pinned’ but be represented using the same modelling techniques used for the modelling of the beam-column interface (i.e. the use of a rotational or multi-spring element).

8.2 INTRODUCTION

Increasingly in the design of structures, engineers rely on the use of Non-Linear Time History (NLTH) analysis in order to verify building performance under design seismic loading. This is even more common when novel construction techniques are used such as post-tensioned timber. In the use of these models several trade-offs are made between complexity, accuracy, programming time, and processing time. In

design it is crucial that simple models exist which provide sufficiently accurate building response without requiring a large amount of time in either processing or programming.

During the course of the post-tensioned timber project several authors have used computer numerical modelling in order to successfully replicate testing results (Iqbal et al. 2010; Newcombe et al. 2010), however little work has been done to truly predict joint behaviour (i.e. blindly predict results without relying on calibrations against experimental test results). This analysis will thus include errors related to the analytical procedure presented and discussed in Chapter 5 but it will also provide information regarding the level of confidence a design engineer can have in current numerical modelling techniques.

In order to address this knowledge gap this chapter will be split into two separate parts; the first of these will look at the local static cyclic response of a post-tensioned timber frames with the second addressing the dynamic behaviour of post-tensioned timber frames. Comparisons will be made with the beam-column and frame testing results presented in Chapters 4 and 6, respectively. Several modelling techniques will be used and two finite element computer programmes will be compared.

8.3 NUMERICAL MODELS AND MODELLING TOOLS USED: BEAM-COLUMN JOINT STATIC RESPONSE

From the conception of the post-tensioned jointed ductile concept it has been clear that the nature of the controlled rocking mechanism lent itself well to the use of a lumped plasticity approach in modelling (Palermo et al. 2005). This approach combines the use of elastic elements with springs which represent the non-linear (gap opening) rotations in the system. This method of modelling has been used in the design predictions of the beam-column joint described in Chapter 4 both with and without the dissipating steel angles.

8.3.1 Modelling methods

Recently two methods have been studied and applied to post-tensioned timber; a series of parallel rotational springs or the more complex multi-spring model made up of linear compression only springs (Figure 8.1). Both of these methods rely on calibration using the analytical MMBA design procedure described in Chapter 5.

When not considering secondary effects such as beam elongation or timber crushing, the simpler rotational spring model has been shown to be sufficiently accurate (Newcombe et al. 2010). The rotational spring model does not however predict directly the value of post-tensioning force (T_{pt}) or the neutral axis depth (c), nor does it directly calculate the force (T_s or C_s) or displacement (Δ_s) and strains of steel elements. The use of the rotational spring also does not subject the elastic beam elements to the axial force created by the post-tensioning which is captured by a multi-spring approach.

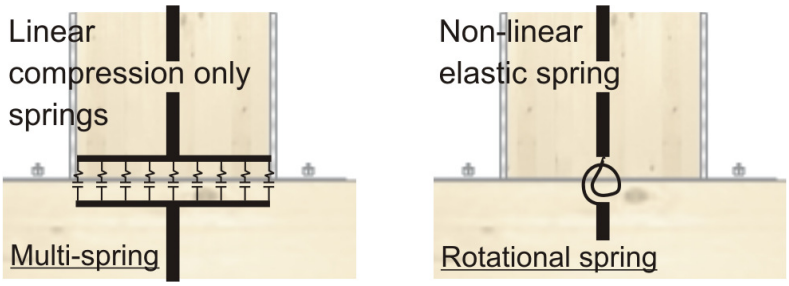

Figure 8.1. a) Rotational spring model and b) multi-spring model used to model interface behaviour in post-tensioned timber buildings

Chapter 5 provided discussion on the way in which the rotation of the beam-column joint panel has a significant impact on the response of a post-tensioned timber system. In order to model this a rotational spring is added in the joint panel region. The stiffness of the rotational spring, k_{jp}, was calculated using Equation (8.1) which has been derived from Equation (5.45) from Chapter 5.

$$k_{jp} = \frac{2\alpha_{s,ave} A_c h_b G_t}{3} \frac{L_b}{L_b - h_c} \quad \textbf{(8.1)}$$

Where:

$\alpha_{s,ave}$ = Shear coefficient in order to find the shear rigidity of the section, defined in Equation 5.44

A_c = Area of the column (m)

h_b = Height of the beam (m)

G_t = Shear modulus of timber (kN/m^2)

L_b = Bay length (m)

h_c = Column height (m)

The final term in Equation (8.1), $(L_b/(L_b-h_c)$, is necessary due to the fact that standard practice is to place the spring representing the joint rotation at the beam column centerline (shown in Figure 8.2). The joint rotation is related to the connection moment M_{con} and therefore an increases in stiffness must occur in order to account for the fact that in its position in the model the spring will be subjected to M_{cl} and not M_{con} ($M_{cl} = M_{con}(L_b/(L_b-h_c))$).

8.3.2 Modelling tools

Previously all modelling of post-tensioned timber beam-column joints has been performed using the finite element program RUAUMOKO (Carr 2006) using both multi-spring and rotational spring approaches (Newcombe et al. 2010).

Although a very powerful modelling tool the RUAUMOKO programme is not wide spread or widely used in engineering practise around the world. For this reason the SAP2000 structural calculation program (CSI Computers and Structures Inc. 2004) was also used and compared both with testing results and output from the RUAUMOKO analysis. SAP2000 does not contain a built in multi-spring model therefore only a rotational spring model was used.

8.3.3 Model characteristics

The beam-column joint models have been set up combining elastic elements with the springs elements described in Section 8.3.1. A summary of the two models used in shown in Figure 8.2.

The two rotational spring models were essentially identical however, the length of the rotational spring differs between the two models. In the RUAUMOKO analysis the standard practice of setting the spring length to 1 mm (to approximate a zero-length) was employed however this proved unstable when applied to the SAP model and a 10 mm spring length was used. A rigid link was used to connect the joint panel rotational spring to the interface rotational springs or multi-spring.

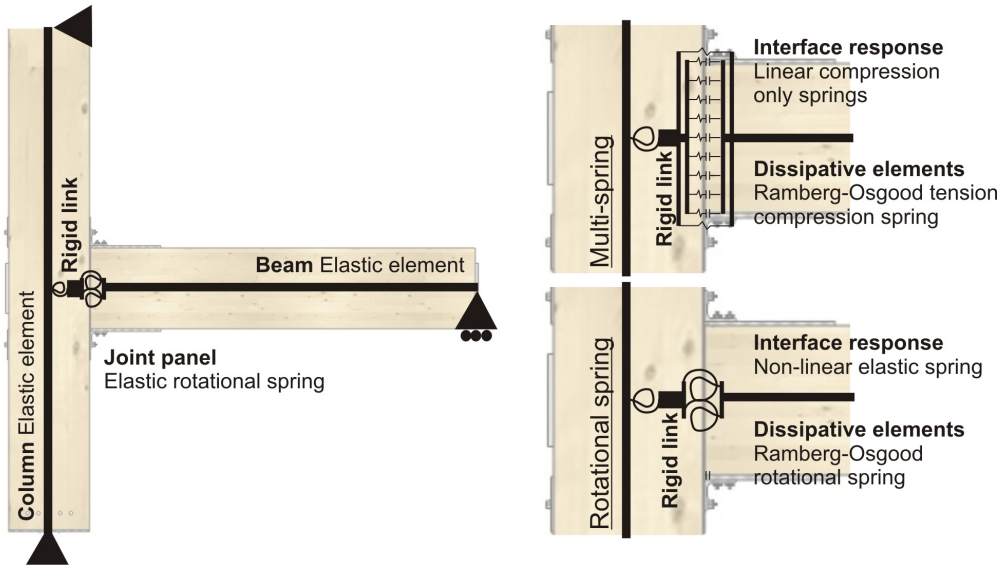

Figure 8.2. Summary of multi-spring and rotational spring models for use in local beam-column numerical modelling predictions for post-tensioned timber frame connections

The multi-spring model

As the multi-spring model can accurately predict the gap opening and resulting displacements axial springs were used to represent the performance of the yielding steel angles. These were calibrated against testing results obtained for a single angle element subjected to cyclic axial loading taken from the dissipative reinforcing testing described in Chapter 3. A Bounded Ramberg-Osgood hysteretic rule was used (Kaldjian 1967).

Although the multi-spring model can accurately predict the displacement of the joint following decompression it cannot capture accurately the interface compression rotation , θ_{int}, introduced in Section 5.3.4. In order to represent these rotations a final rotational spring is introduced between the column rigid link and the multi-spring element. The stiffness of this spring element is defined from Equation (5.18) of Section 5.3.4 by merging the Equation (5.18) with the equation for the calculation of the decompression moment of a rectangle ($M_{dec} = T_{pt,initial}h_b/6$):

$$k_{\text{int},\theta} = \frac{E_{perp} I_b}{k_{\text{int}} h_c} \tag{8.2}$$

Where:

k_{int} = Interface compression factor which accounts for load shearing and interface reinforcement

E_{perp} = Perpendicular to the grain timber stiffness (kN/m^2)

I_b = Section modulus of the beam (m^4)

The interface compression spring is input as a non-linear elastic rotational spring that works up until decompression at which point the stiffness is set to be almost infinite as the interface compression does not impact on interface behaviour following this point. Table 8.1 shows a summary of the hysteretic loops used for the multi-spring model.

Table 8.1. Summary of spring hysteretic properties of multi-spring numerical model

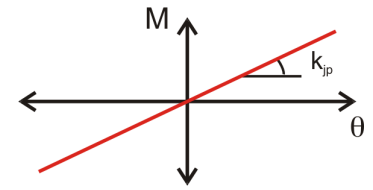

Joint Panel		
Initial stiffness	k_{jp}	kNm/rad

Multi-spring model – RUAUMOKO Only

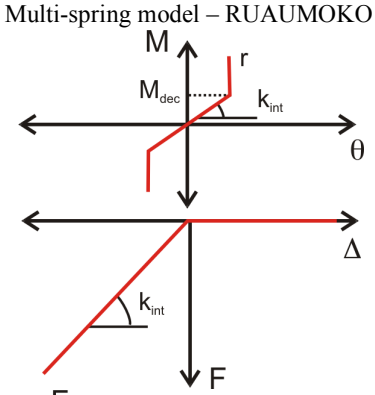

Non-linear elastic spring (Interface compression)		
Decomp. moment	M_{dec}	kNm
Initial stiffness	k_{int}	kNm/rad
Bi-linear factor	r	*

Multi-spring		
Number of springs	n	
Axial stiffness	k	kN/m

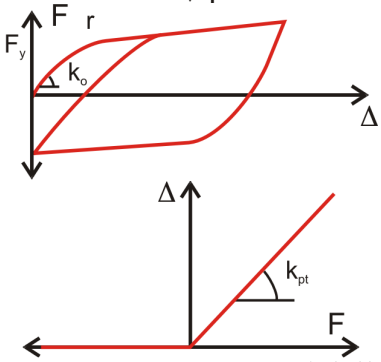

Bounded Ramberg-Osgood spring (dissipative elements)		
Yield force	F_y	kN
Initial stiffness	k_o	kN/m
R-O factor	r	*

Linear elastic spring (post-tensioning)		
Initial stiffness	k_{pt}	kN/m

* The bi-linear factor and R-O factor are input in terms of a fraction of the initial stiffness, k

The rotational spring model

The parameters of the rotational springs were set to match the predicted rotational response. Post-tensioning was represented using tri-linear elastic elements for both models with Bounded Ramberg-Osgood and Buoc-Wen rotational spring models

(Wen 1980) used to represent the steel elements in the RUAUMOKO and SAP2000 models, respectively.

Table 8.2. Summary of spring hysteretic properties of rotational spring numerical model

Rotational spring model

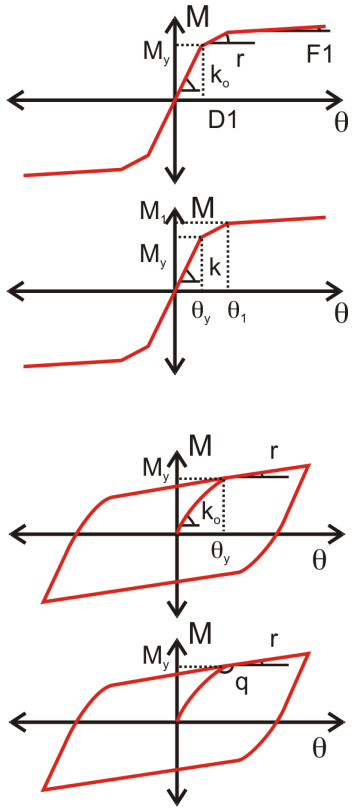

Non-linear elastic rotational spring (post-tensioning)		
RUAUMOKO		
Yield Moment	M_y	kNm
Initial stiffness	k_o	kN/m
Post-yield stiffness	r	*
Post-onset stiffness	F1	*
Disp. multiplier	D1	**
SAP 2000		
Yield Moment	M_y	kNm
Yield rotation	θ_y	Rad
Initial stiffness	ko	kN/m
Onset moment	M_1	kNm
Onset rotation	θ_1	Rad
Max moment	M_2	kNm
Max rotation	θ_2	Rad
Bounded Ramberg-Osgood spring (dissipative elements)		
RUAUMOKO		
Yield moment	M_y	kN
Initial stiffness	k_o	kN/m
Post-yield stiffness	r	*
SAP 2000		
Initial stiffness	k_o	kN/m
Yield moment	M_y	kN
Post-yield stiffness	r	*
Yield exponent	q	

* The post-yield and on-set stiffness' are input in terms of a fraction of the initial stiffness, k

** The displacement multiplier is input as a fraction of the yield displacement, Δ_y

8.3.4 Model calibration

All analysis results presented in this chapter have been calibrated against the moment rotation response provided by the design procedure described in Chapter 5 and have not been calibrated against experimental test results.

Calibration of the multi-spring element was performed by altering the stiffness of the element until the three parameters of connection moment (M_{con}), post-tension force (T_{pt}) and neutral axis depth (c) were accurately predicted for the PT ONLY 150 kN design procedure predictions (Figure 8.3). Following calibration it was simply necessary to change the initial compression value across the gap (due to post-tensioning elements) in order to predict the performance of the different initial testing states.

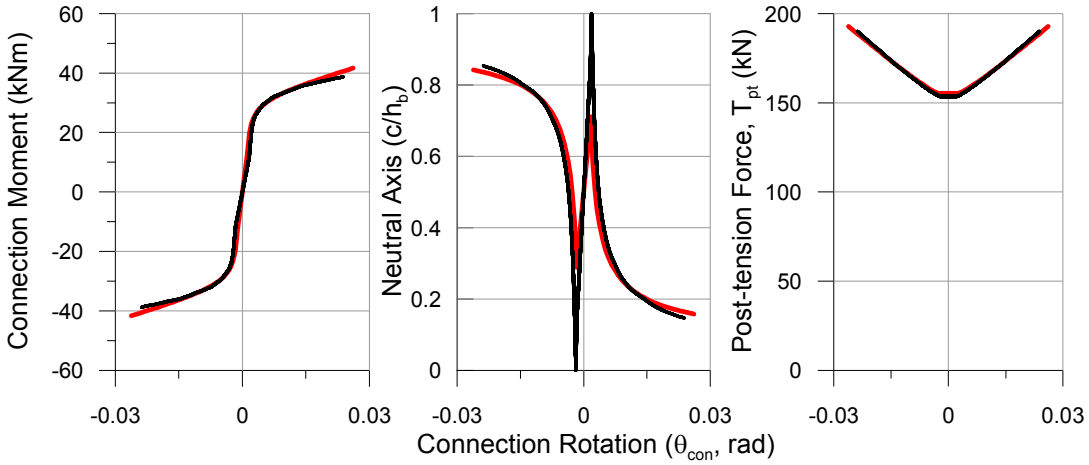

Figure 8.3. Calibration of multi-spring model (in black) against design procedure (in red)

RUAUMOKO offers the opportunity to select the method of stiffness distribution used during modelling, a linear distribution of stiffness was selected.

Calibration of the Ramberg-Osgood axial springs was done against the angle axial testing results described in Chapter 3. Table 8.3 shows the input values used for the multi-spring analysis.

Table 8.3. RUAUMOKO multi-spring inputs for PT ONLY and ANGLE testing, all springs 1 mm in length

Joint Panel	k_{jp}		
Initial stiffness	30094		
Multi-spring model – RUAUMOKO Only			
Interface compression	M_{dec} (kNm)	k_{int} (kNm/rad)	r
$T_{pt,i}$ = 50 kN	4.3	10731	10000
$T_{pt,i}$ = 100 kN	8.5	10731	10000
$T_{pt,i}$ = 150 kN	12.5	10731	10000
$T_{pt,i}$ = 200 kN	16.0	10731	10000
$T_{pt,i}$ = 250 kN	20.1	10731	10000
Multi-spring	n	k (kN/m)	
All models	10	500,000	
Dissipative elements	F_y (kN)	k_o (kN/m)	r
Single angle	19	25500	8
Post-tensioning	k_{pt} (kN/m)		
$T_{pt,i}$ = 50, 100, 150 kN	9078		
$T_{pt,i}$ = 200, 250 kN	22117		

Calibration of the rotational springs was done by simplifying the backbone curves provided by the design procedure into either tri-linear (post-tensioning) or Ramberg-Osgood and Bouc-Wen (dissipative angles) approximations. An example of this is shown in Figure 8.4 for the PT 150KN 2 ANGLES test case.

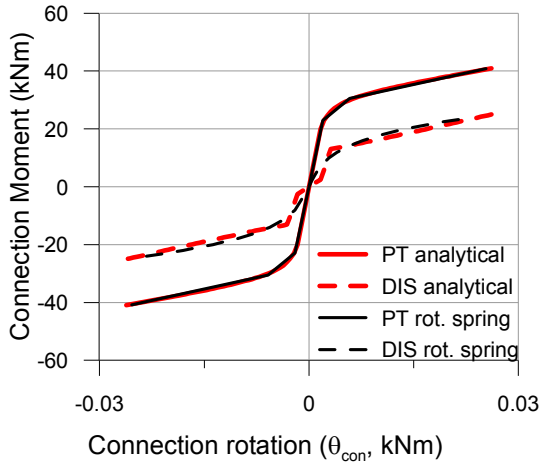

Figure 8.4. Example of rotational spring model calibration for test PT 150KN 2 ANGLES

Table 8.4, Table 8.5 and Table 8.6 show the input characteristics for each test case across all three of the models/analysis programmes used.

Table 8.4. RUAUMOKO and SAP 2000 rotational spring model input values for PT ONLY testing

RUAUMOKO							
Test	k_o (kNm/rad)	M_y (kNm)	r	F1	D1		
PT ONLY 50kN	10000	8.0	0.159	0.044	3.125		
PT ONLY 100kN	10333	15.5	0.167	0.045	3.080		
PT ONLY 150kN	11905	20	0.240	0.044	2.976		
PT ONLY 200kN	11600	23.2	0.355	0.086	2.870		
PT ONLY 250kN	12000	30	0.331	0.095	2.612		
SAP2000							
Test	k_o (kNm/rad)	M_y (kNm)	θ_y (rad)	M_1 (kNm)	θ_1 (rad)	M_2 (kNm)	θ_2 (rad)
PT ONLY 50kN	10000	8	0.0008	10.7	0.0025	20.8	0.0254
PT ONLY 100kN	10333	15.5	0.0015	20.9	0.0046	30.5	0.0254
PT ONLY 150kN	11905	20.0	0.0017	29.5	0.0050	40.1	0.0254
PT ONLY 200kN	11600	23.2	0.0020	38.6	0.0057	59.3	0.0265
PT ONLY 250kN	12000	30	0.0025	46	0.0065	67.4	0.0254

Table 8.5. RUAUMOKO rotational spring model input values for ANGLE testing

RUAUMOKO - PT					
Test	k_o (kNm/rad)	M_y (kNm)	r	F1	D1
PT 150KN 1 ANGLE	11450	22.9	0.143	0.045	3.265
PT 100KN 2 ANGLES	10067	15.1	0.178	0.049	2.893
PT 150KN 2 ANGLES	11450	22.9	0.173	0.042	2.920
PT 200KN 2 ANGLES	12727	28.0	0.239	0.077	2.627
PT 250KN 2 ANGLES	11897	34.5	0.287	0.085	2.314
RUAUMOKO - ANGLES					
Test	k_o (kNm/rad)	M_y (kNm)	r		
PT 150KN 1 ANGLE	3000	10	5.5		
PT 100KN 2 ANGLES	7000	20	6		
PT 150KN 2 ANGLES	7000	18	5		
PT 200KN 2 ANGLES	6000	18.5	5.5		
PT 250KN 2 ANGLES	6000	18.5	5.5		

Table 8.6. SAP2000 rotational spring model input values for ANGLE testing

SAP2000 - PT							
Test	k_o (kNm/rad)	M_y (kNm)	θ_y (rad)	M_1 (kNm)	θ_1 (rad)	M_2 (kNm)	θ_2 (rad)
PT 150KN 1 ANGLE	11450	22.9	0.0020	30.3	0.0065	40.4	0.0261
PT 100KN 2 ANGLES	10067	15.1	0.0015	20.2	0.0043	30.7	0.0258
PT 150KN 2 ANGLES	11450	22.9	0.0020	30.5	0.0058	39.9	0.0254
PT 200KN 2 ANGLES	12727	28.0	0.0022	38.9	0.0058	59.4	0.0265
PT 250KN 2 ANGLES	11897	34.5	0.0029	47.5	0.0067	67.9	0.0269

SAP2000 - ANGLES			
Test	k_o (kNm/rad)	M_y (kNm)	r
PT 150KN 1 ANGLE	2432	9	0.0949
PT 100KN 2 ANGLES	5758	19	0.0734
PT 150KN 2 ANGLES	5000	19	0.0823
PT 200KN 2 ANGLES	3900	19.5	0.0953
PT 250KN 2 ANGLES	4167	20	0.0815

8.4 RESULTS OF NUMERICAL MODELLING: BEAM-COLUMN JOINT

The models presented above have been run and their results have been compared against the testing results presented in Chapter 4. This section discusses these comparisons; firstly the multi-spring model is compared, followed by the rotational spring models.

8.4.1 Multi-spring analysis results

The multi-spring model is capable of predicting the parameters of moment-drift, post-tensioning-drift and neutral axis-drift response. These parameters have been compared against the beam-column experimental testing results presented in Chapter 5 and are used to judge the adequacy of the numerical modelling methods described above.

PT ONLY testing

Comparisons between the multi-spring model and testing results for the PT ONLY test series are shown in Figure 8.5 and Figure 8.6. The figures show that the multi-spring model provided accurate predictions of the moment-drift response of the beam-column joint.

Accurate prediction of the increase in post-tensioning was also provided, however, as shown in Figure 8.6 errors in initial post-tensioning values (shown at low drift levels) increase with increasing values of initial post-tensioning. This is due to the fact that the axial spring providing the axial properties of the post-tensioning is compressed at

the beginning of the analysis. This can be allowed for by increasing the initial post-tensioning by an initial offset value.

The multi-spring model also provided adequate prediction of the neutral axis depth, however errors were present. These errors appeared to increase with increasing levels of post-tensioning. This trend was also observed in the comparisons with the analytical procedure presented in Chapter 5. A number of factors may be causing this to occur however it is likely that the issue was related to the assumptions surrounding the interface compression deformation.

The interface compression deformation causes an offset of the neutral axis values. Further research is required in order to fully understand the impact of the interface compression deformation on modelling, however, if a multi-spring model is to be used in analysis it should be calibrated against initial post-tensioning values near to those which are to be used in design.

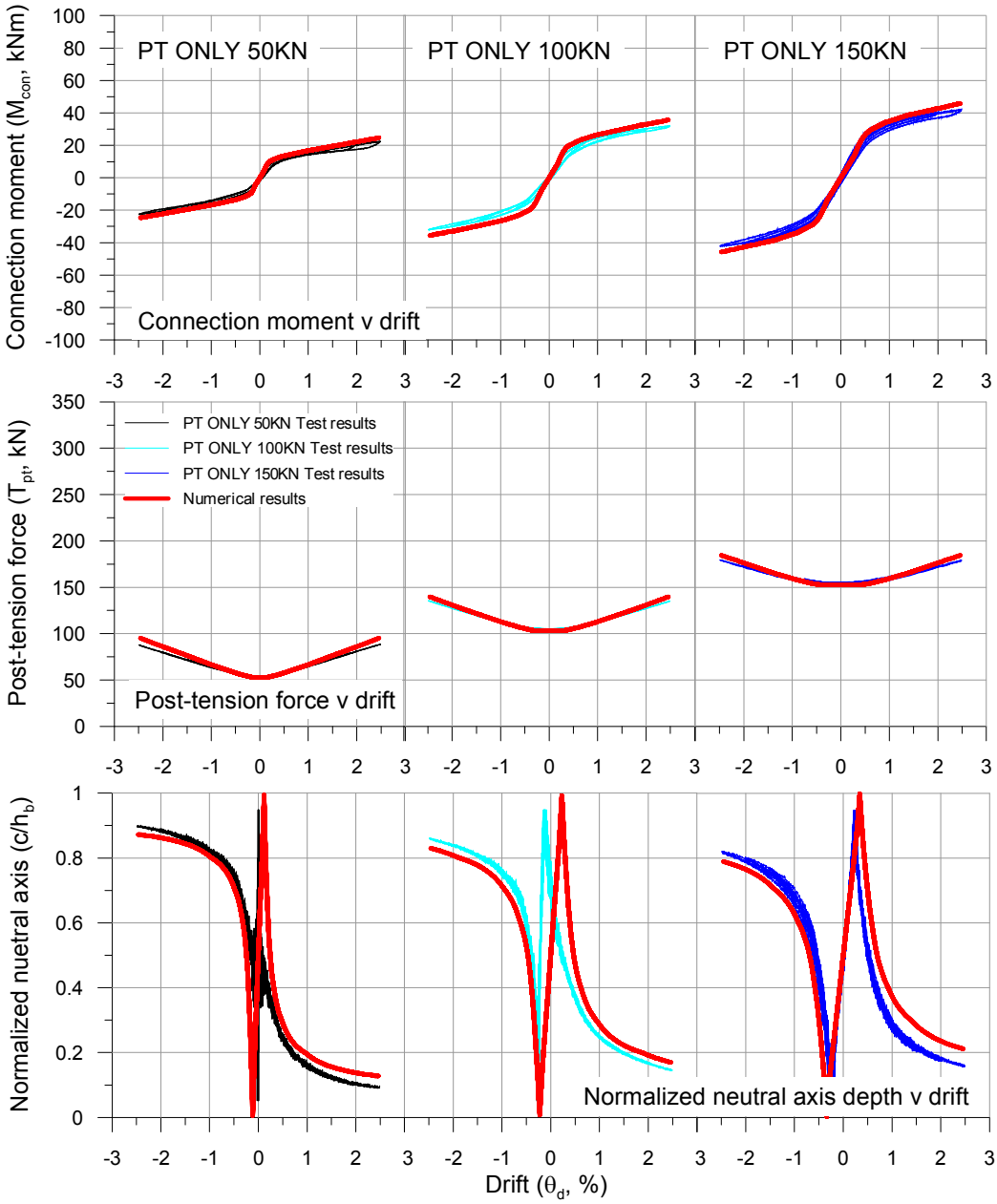

Figure 8.5. Comparisons of Multi-spring numerical modelling results with testing results for PT ONLY 50kN, 100kN and 150kN

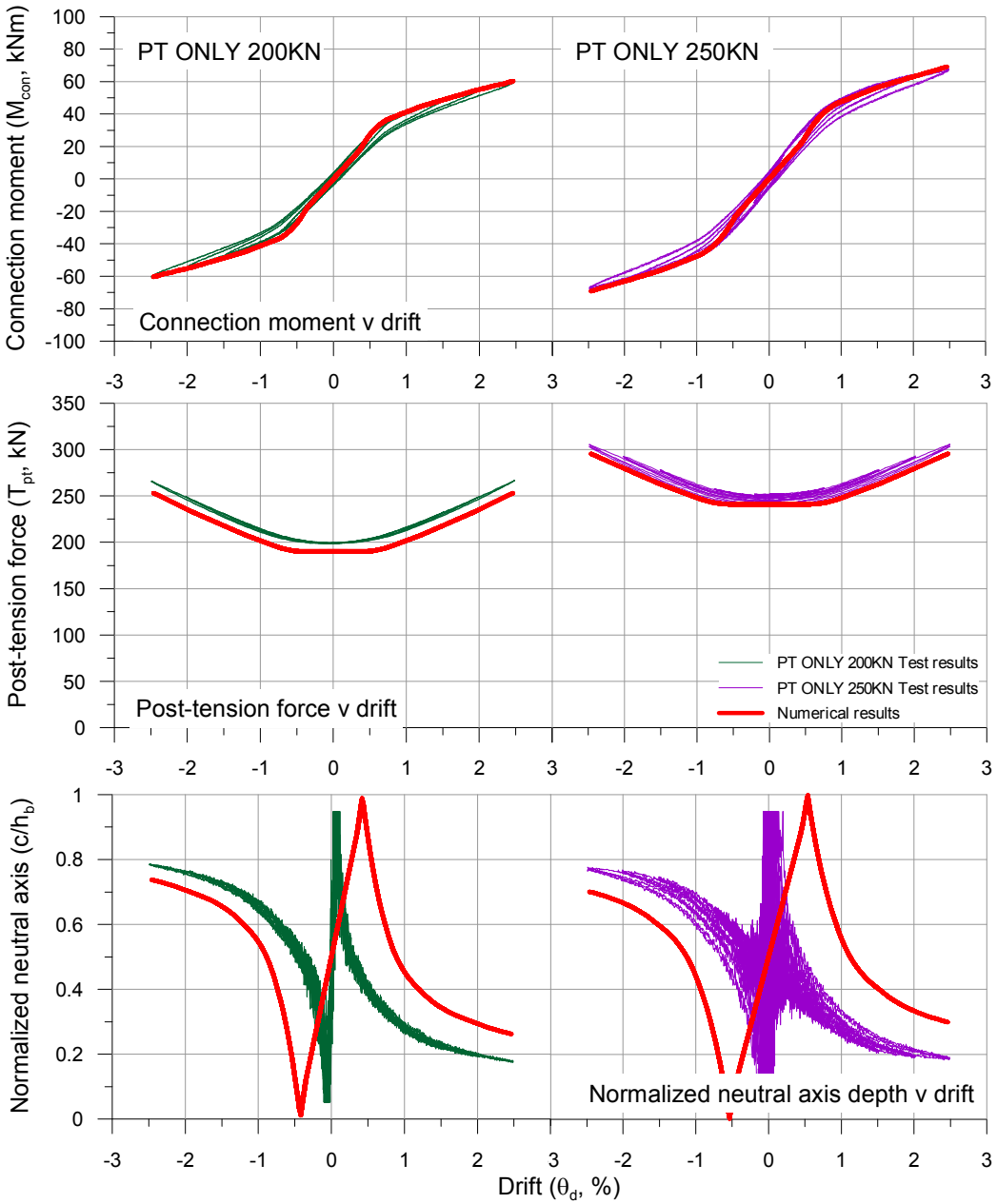

Figure 8.6. Comparisons of Multi-spring numerical modelling results with testing results for PT ONLY 200kN and 250kN

ANGLE testing

Figure 8.7 and Figure 8.8 show comparisons between the multi-spring model and testing results for the ANGLES test series.

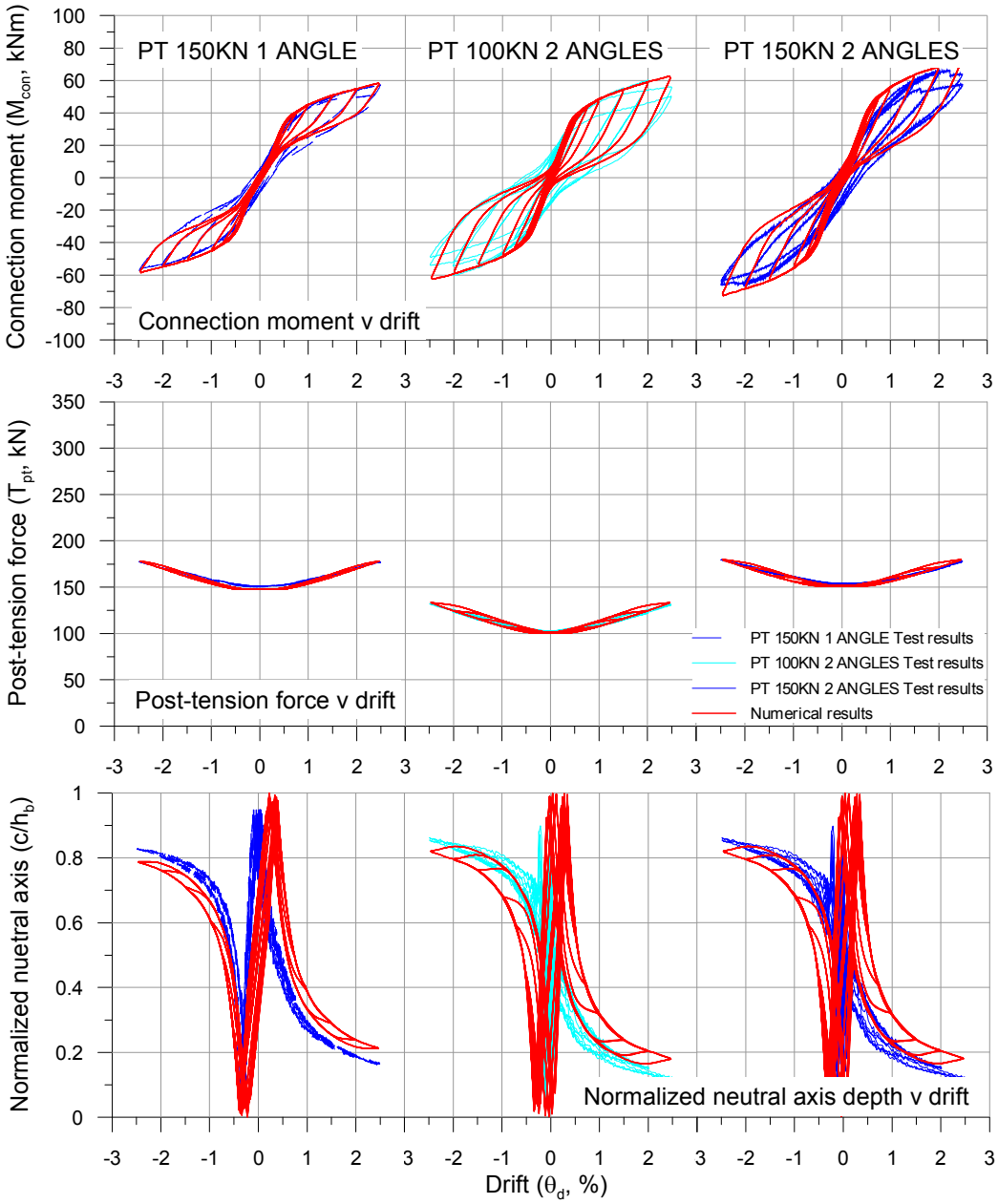

Figure 8.7. Comparisons of Multi-spring numerical modelling results with testing results for PT 150kN 1 ANGLE, PT 100kN 2 ANGLES and PT 150kN 2 ANGLES

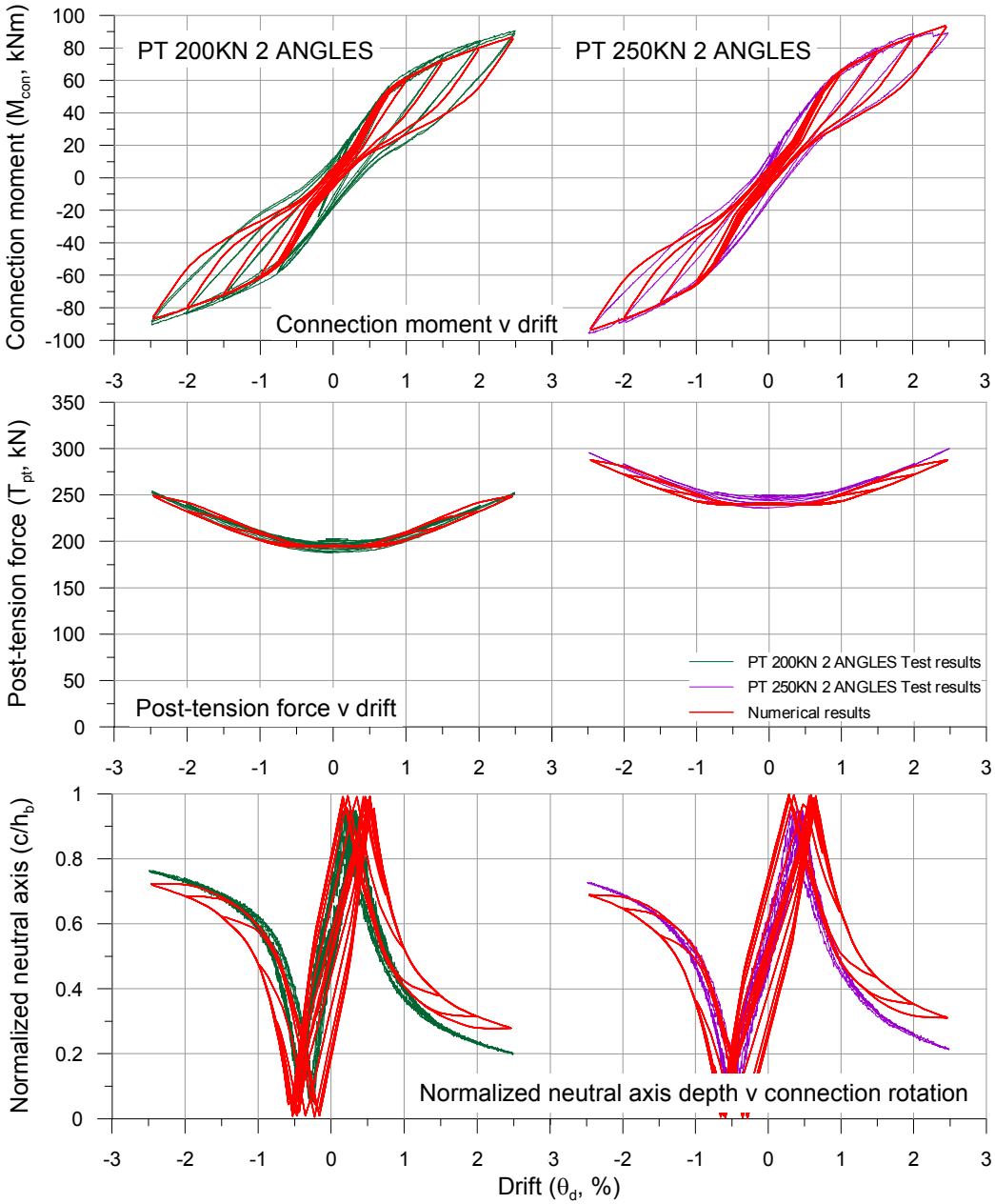

Figure 8.8. Comparisons of Multi-spring numerical modelling results with testing results for PT 200kN 2 ANGLES and PT 250kN 2 ANGLES

The multi-spring model provides accurate predictions of the moment-drift performance and the post-tensioning response of the beam-column joint with dissipative reinforcing. In addition, an improved prediction of the neutral axis depth is obtained (although still slightly over predicted).

The hysteretic contribution of the dissipative angles is also well captured by the model with sufficient prediction of the hysteretic contribution and the unloading

stiffness. Further discussion of representations of hysteretic damping in the models is presented in Section 8.4.3.

All results show a slightly pinched behaviour due to the way in which the interface compression deformation was modelled as described in Section 8.3.1.

8.4.2 Rotational spring analysis results

The rotational spring model will only provide moment-drift output. As previously discussed both RUAUMOKO and SAP2000 have the ability to model lumped plasticity using rotational springs.

PT ONLY testing

The results for the RUAUMOKO and SAP2000 rotational spring models are shown in Figure 8.9 and Figure 8.10 for the PT ONLY test series. As shown both models provide similar and adequate prediction of the moment-drift response of the beam-column joint. The results obtained for both the RUAUMOKO and SAP200 numerical analysis cases are very similar, suggesting both programmes are adequate for use with regards to this type of modelling.

Results for both models of the PT ONLY 200kN and PT ONLY 250kN test cases show slight over prediction of response. It is therefore suggested that conservative assumptions be made when calibrating post-tensioned only timber systems (i.e. curves should be fitted conservatively compared to analytic procedures).

ANGLES testing

The results for the RUAUMOKO and SAP2000 rotational spring models are shown in Figure 8.11 and Figure 8.12 for the ANGLES test series. As shown both models provide similar prediction of the moment-drift response of the beam-column joint. As with the PT ONLY modelling both RUAUMOKO and SAP2000 provide adequate (within 5% error of maximum values) predictions of the moment-drift response of the post-tensioned beam-column joint with the addition of the reinforcing angles.

Figure 8.11 and Figure 8.12 show that the Ramberg-Osgood (RUAUMOKO) and Buoc-Wen (SAP2000) models slightly underestimate the hysteretic damping contribution of the reinforcing angles. This is further discussed in Section 8.4.3.

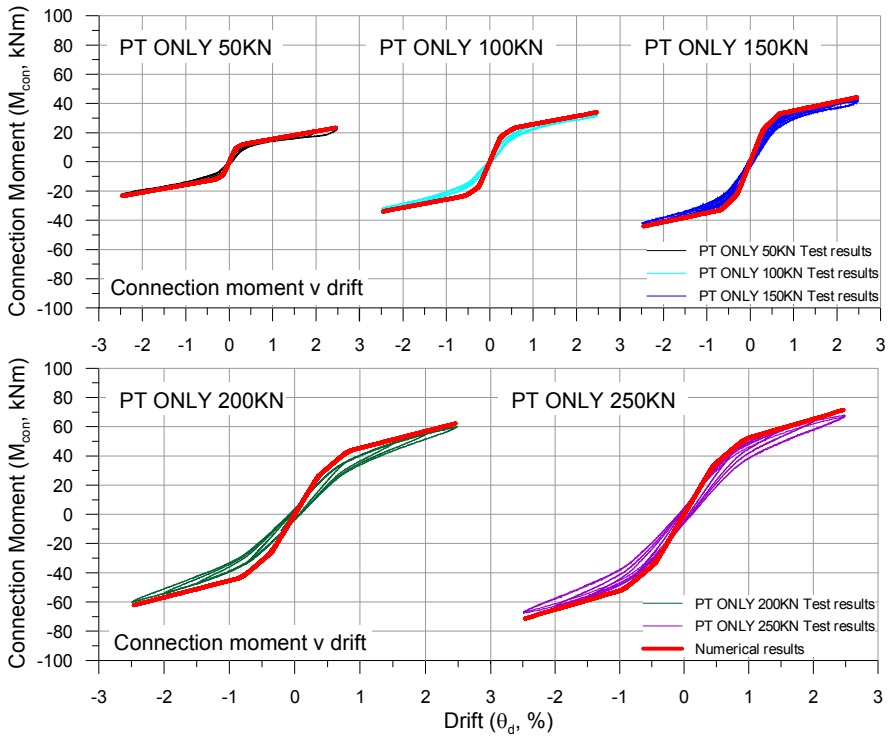

Figure 8.9. RUAUMOKO comparisons of rotational spring numerical modelling results with testing results PT ONLY 50kN, 100kN, 150kN, 200kN and 250kN.

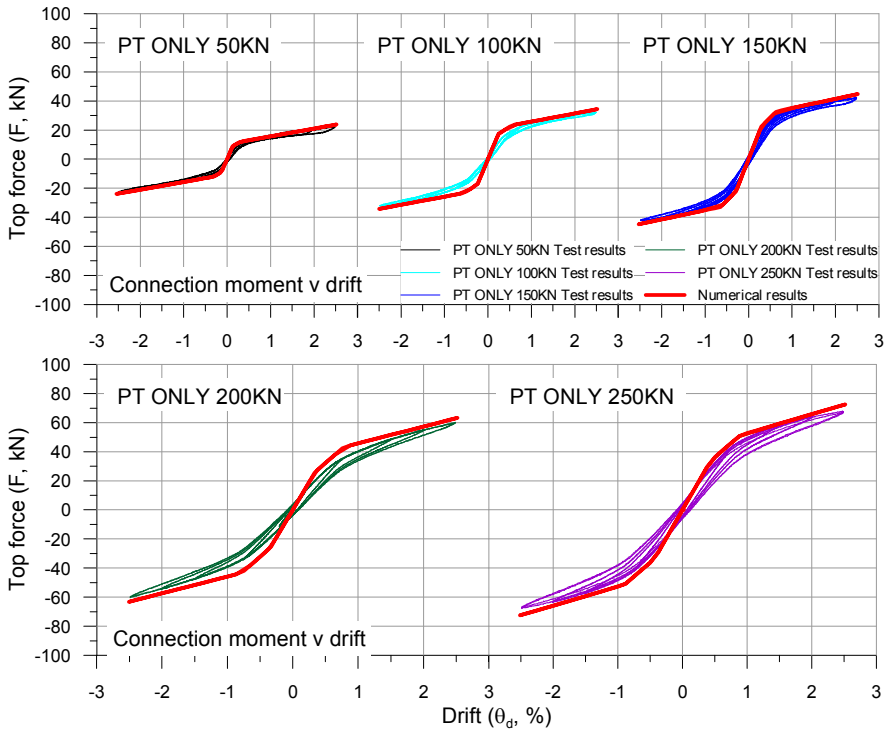

Figure 8.10. SAP2000 comparisons of rotational spring numerical modelling results with testing results PT ONLY 50kN, 100kN, 150kN, 200kN and 250kN.

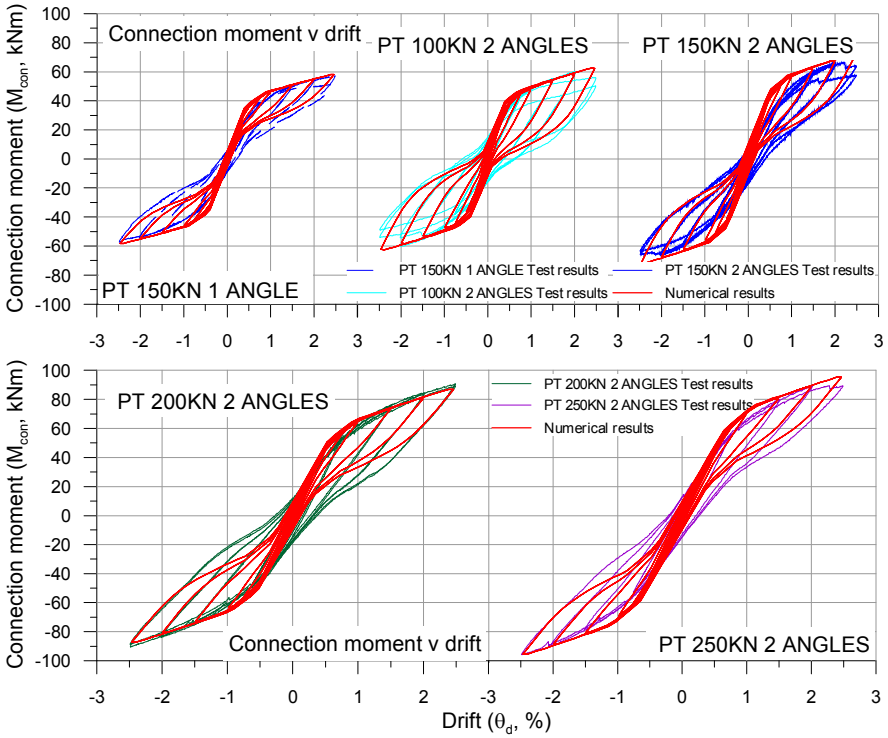

Figure 8.11. RUAUMOKO comparisons of rotational spring numerical modelling results with testing results PT 150kN 1 ANGLE, PT 100kN 2 ANGLES, PT 150kN 2 ANGLES, PT 200kN 2 ANGLES and PT 250kN 2 ANGLES.

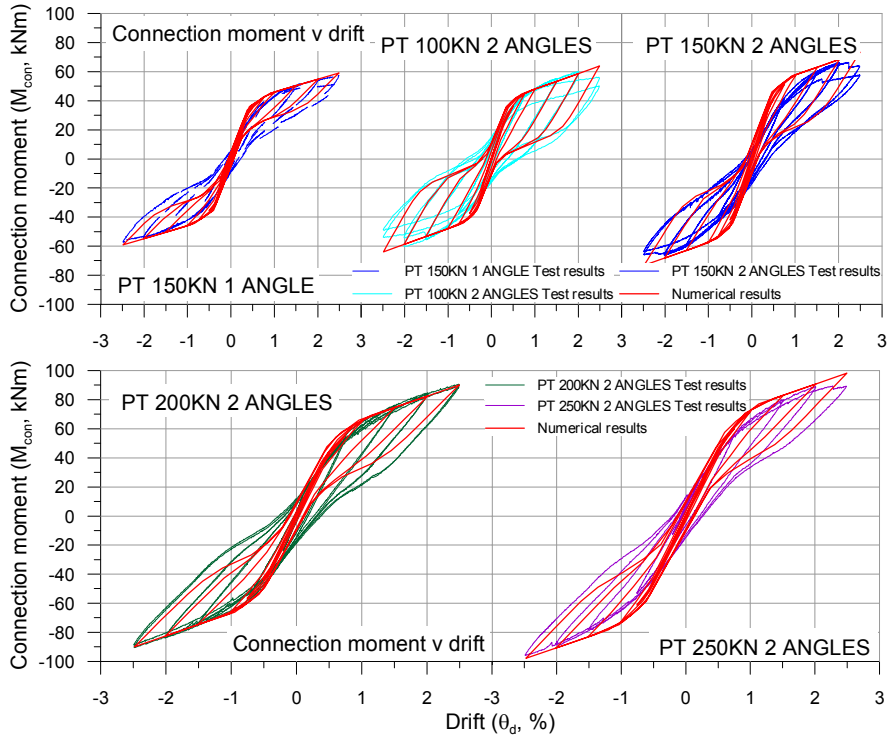

Figure 8.12. SAP2000 comparisons of rotational spring numerical modelling results with testing results PT 150kN 1 ANGLE, PT 100kN 2 ANGLES, PT 150kN 2 ANGLES, PT 200kN 2 ANGLES and PT 250kN 2 ANGLES.

8.4.3 Modelling of Equivalent Viscous Damping (EQV)

Section 8.4.2 discussed the way in which the use of the rotational spring model calibrated against the analytical procedure presented in Chapter 5 slightly underestimated hysteretic response. Section 4.9 introduced Equivalent Viscous Damping (EQV) which is used to measure hysteretic damping from cyclic behaviour. Figure 8.13 shows the EQV calculated for the ANGLE test series for each of the modelling techniques used.

As shown all of the models provide adequate (within 10% error) representation of the EQV values following spring yield (modelling does not account for the small amount of hysteretic damping present before reinforcing yield). Contrary to the observations made in Section 8.4.2, the RUAUMOKO multi-spring and rotational spring models provide almost identical representation of the EQV, with the rotational spring providing slightly lower values. This is due to the pinching of the multi-spring model loop mentioned previously that counteracts the apparent increased area of the hysteretic loop of the multi-spring model furnishing similar EQV values in both models.

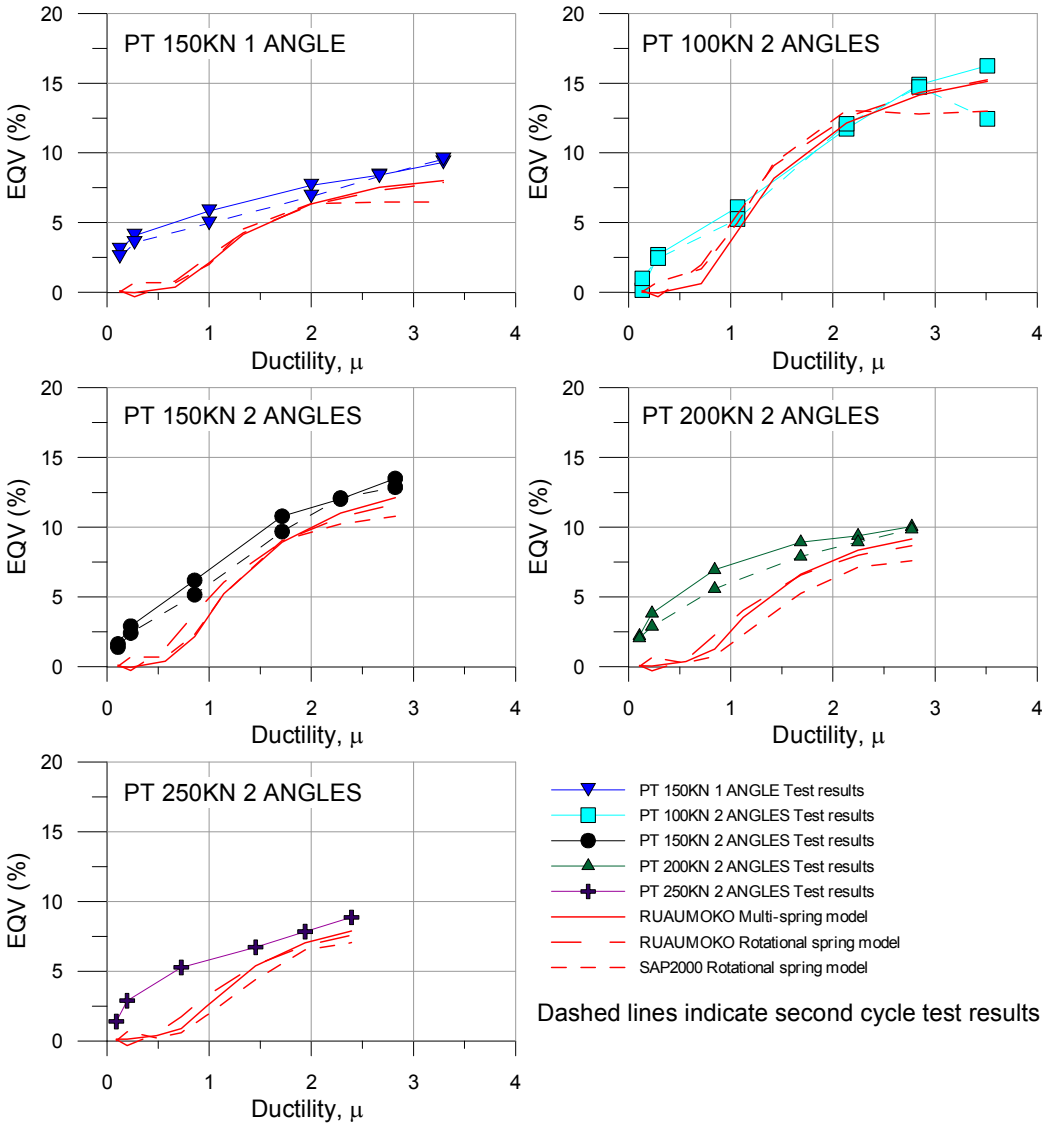

Figure 8.13. Comparison of equivalent viscous damping modelling and testing results for ANGLE test series for all models

Comparisons between the RUAUMOKO and SAP2000 rotational models shows that the SAP2000 model presents lower hysteretic damping. In addition, the values of EQV in the SAP2000 rotational model plateau for higher ductility levels. In order to understand the reason for this, the two models have been compared for the PT 150KN 2 ANGLES test case in Figure 8.14.

As shown although the two models have been calibrated against the same analytical procedure result the form of the hysteretic loops differs. The initial stiffness of the RUAUMOKO rotational spring is higher and in addition the model provides a better

representation of the unloading characteristics of steel (Bauschinger effect), this leads to larger area being enclosed by the loop and creates larger values of EQV.

The reason for the plateau observed in the SAP2000 model is also evident in Figure 8.14. As shown, the unloading of the rotational spring is transposed linearly for larger levels of displacement. As shown in Section 4.9 the formula for EQV is divided through by an equivalent triangle. This means that beyond a certain displacement level the increase in the area of the Bouc-wen model does not lead to an increase in EQV.

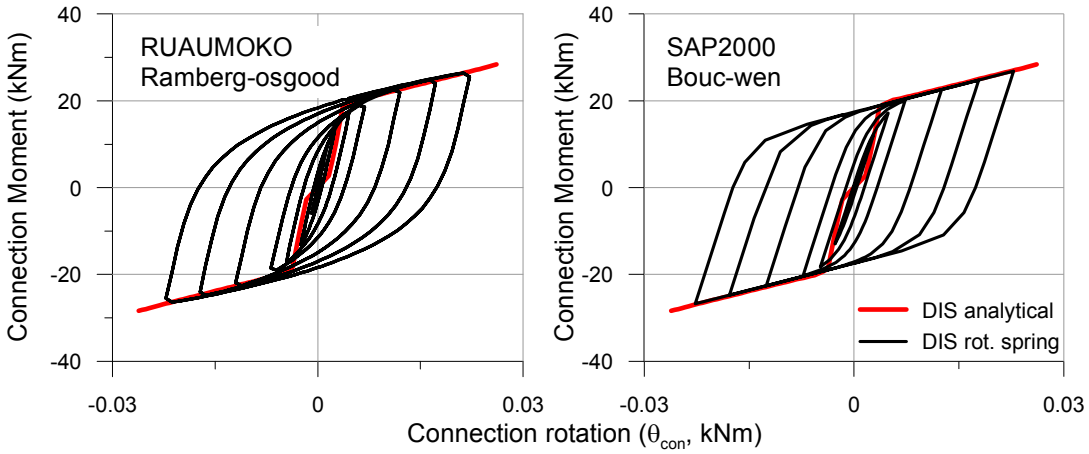

Figure 8.14. Dissipation rotational spring models for PT 150KN 2 ANGLES RUAUMOKO and SAP2000 models

8.5 NUMERICAL MODELS AND MODELLING TOOLS USED: FRAME TEST DYNAMIC RESPONSE

Chapter 6 presented the results of shaking table testing of a three-storey frame. As mentioned in Section 6.4.4 numerical models were developed during specimen design in order to predict behaviour and to assist in the placement of instrumentation.

The following sections describe the models developed and compare the results provided with the results obtained for the experimental testing presented in Chapter 6.

8.5.1 Modelling methods and tools

As with the beam-column testing models described in Section 8.3 and 8.4 the numerical modelling programmes RUAUMOKO and SAP2000 were used.

Section 8.4 described the adequacy of the rotational spring model in predicting beam-column performance. Rotational springs have therefore been used to model performance due to their simplicity when compared to the multi-spring model and issues surrounding column shears when the multi-spring model is applied to a frame. As mentioned in Section 8.3.1, the use of rotational springs at the beam-column interface means that beam members were not subjected to the axial forces created by the post-tensioning.

8.5.2 Model characteristics and calibration

Figure 8.15 shows the model used to predict system behaviour in both RUAUMOKO and SAP2000. The beam-column joint was represented in the same way as described in Section 8.3.3 with a combination of rotational springs being assembled to represent the post-tensioning, reinforcement and joint panel contributions.

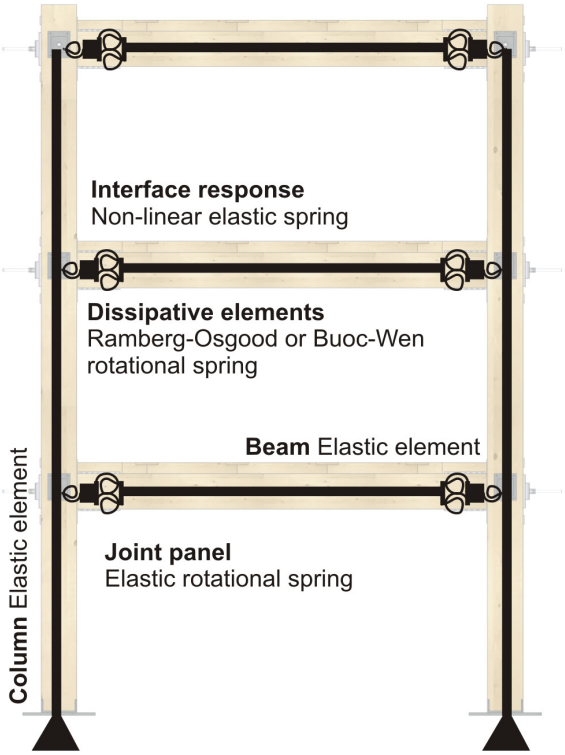

Figure 8.15. SAP2000 and RUAUMOKO frame numerical models

Figure 8.15 shows a perfectly pinned based column-foundation connection for the frame. As shown in Section 6.3.3 reinforcement was applied to the column base providing moment capacity. This moment capacity acts in addition to the moment capacity provided by gravity (through the column axial load). As the column-

foundation connection has moment capacity a truly pinned assumption is likely to over-predict displacement and under-predict base shears. Figure 8.16 shows the options considered in order to better represent the response of the column-foundation connection.

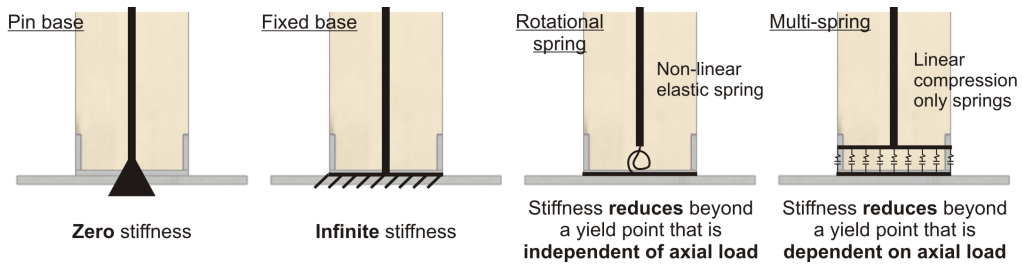

Figure 8.16. Base connection modelling options considered for frame numerical model

As shown in Figure 8.16 four options were considered of increasing complexity. A fixed based assumption was made; replacing the first, pinned based assumption. This option is considered adequate in predicting response until column-base gap opening, however, following gap opening it is likely to under-predict displacement and over-predict base shear. This is due to the fixed based model being infinitely stiff and not being able to account for the sudden drop in stiffness when gapping occurs.

The third option shown in Figure 8.16 allows for the drop in stiffness due to gap opening through the use of a rotational spring. This is calibrated in the same manner as the beam-column joint as described in Section 8.3.4. During this calibration the static value (i.e. without lateral earthquake loading) of column axial load is used, however, during seismic loading this value will not remain constant. During some of the stronger motions used axial load in the column was observed to become positive (i.e. the column went into tension). This means that the moment contribution will have dropped to zero, a factor which is not considered in the rotational spring column-foundation model.

The final solution was the use of a calibrated multi-spring as shown in the far right diagram in Figure 8.16. This option provided the most accurate representation of the column-foundation connection accounting for the sudden loss of stiffness due to gap opening but also allowing for the change in capacity due to changing axial load.

As mentioned in Section 8.3.2 SAP2000 does not have a proprietary multi-spring model and therefore a multi-spring was created using two axial gapping springs (gap elements as defined in SAP2000).

As described in Chapter 6 two different frame configurations were tested. The rotational spring parameters for each of these configurations are displayed in Table 8.7 and Table 8.8 for the RUAUMOKO and SAP2000 models, respectively.

Table 8.7. RUAUMOKO rotational spring model input values for ANGLE testing

RUAUMOKO - PT					
Test	k_o (kNm/rad)	M_y (kNm)	r	F1	D1
PT100_0.60	3400	8.5	0.353	0.133	1.8
PT100_1.00	3696	8.5	0.236	0.123	2.7
RUAUMOKO - ANGLES					
Test	k_o (kNm/rad)	M_y (kNm)	r		
PT100_0.60	2600	11.5	7.5		

Table 8.8. SAP2000 rotational spring model input values for ANGLE testing

SAP2000 - PT							
Test	k_o (kNm/rad)	M_y (kNm)	θ_y (rad)	M_1 (kNm)	θ_1 (rad)	M_2 (kNm)	θ_2 (rad)
PT100_0.60	3400	8.5	0.0025	10.9	0.0045	20.8	0.0265
PT100_1.00	3969	8.5	0.0023	11.9	0.0062	21.1	0.0265
SAP2000 - ANGLES							
Test	k_o (kNm/rad)	M_y (kNm)	r				
PT100_0.60	1961	10	0.1096				

Chapter 6 discussed how the dissipative reinforcing angles placed at the column base were rendered ineffective by deficiencies in the production of the angle connection shoe. For this reason both the rotational spring and multi-spring base numerical models do not include elements representing the dissipative reinforcing at the base of the columns.

Elastic damping values of 3% have been used across all modes for the frame modelling done using the RUAUMOKO program. In SAP2000 a Rayleigh damping model has been used with elastic damping values being set to 3% for the first and second mode (T = 0.53 and 0.13 s) this was due to the fact that it is not possible in the SAP2000 programme to set damping across all modes (which is preferable as the use of Rayleigh damping may over-damp higher modes). The use of this value was based on a combination of the frame testing results presented in Chapter 6 and previous research suggestions as discussed in Section 7.5.

8.6 RESULTS OF NUMERICAL MODELLING: FRAME TEST DYNAMIC RESPONSE

This section compares the results of the numerical analysis using the models and tools described in Section 8.5 with the results of tests PT100_0.60 and PT100_1.00 as described in Chapter 6. In Chapter 6 a large amount of response parameters were analysed in order to evaluate the adequacy of frame performance. These included: displacement, drift, acceleration at each level as well as the total base shear, system dynamic characteristics (frequency and period) and damping. In this section three parameters have been selected as 'key indicators' which are the following: acceleration at the third floor, base shear of the building and drift of the first level. The acceleration of the third floor and the drift at the first level have been selected because the maximum acceleration and drift occurred at these points during testing. The base shear has been selected as it provides a definitive indication of the seismic demand on the frame.

As with the numerical analysis of the full-scale beam-column joint both RUAUMOKO and SAP2000 have been used in analysis. However the full suite of input (i.e. PGA = 10 – 50%) was not used in the case of SAP2000 due to the program requiring a significant amount of processing time with only the maximum PGA cases being applied (100% for PT100_0.60 and 75% for PT100_1.00).

8.6.1 Comparison of time history acceleration, base shear and drift response between NLTH analysis and testing results

The first comparisons made between the NLTH analysis and testing results compared the time history 3rd floor accelerations, base shears and 1st level drifts over time. Figure 8.17 and Figure 8.18 show the testing and NLTH response to earthquake 000196x obtained from RUAUMOKO and SAP2000, respectively. The results shown are for the multi-spring base model which has been developed for both tests PT100_0.60 and PT100_1.00 for RUAMOKO and test PT100_0.60 SAP2000. A model for testing PT100_1.00 using SAP2000 was not successfully developed as the low damping system (containing only the 3% elastic damping) was unable to converge using the integration methods provided by the program. This was only an issue with the SAP2000 PT100_1.00 multi-spring based model.

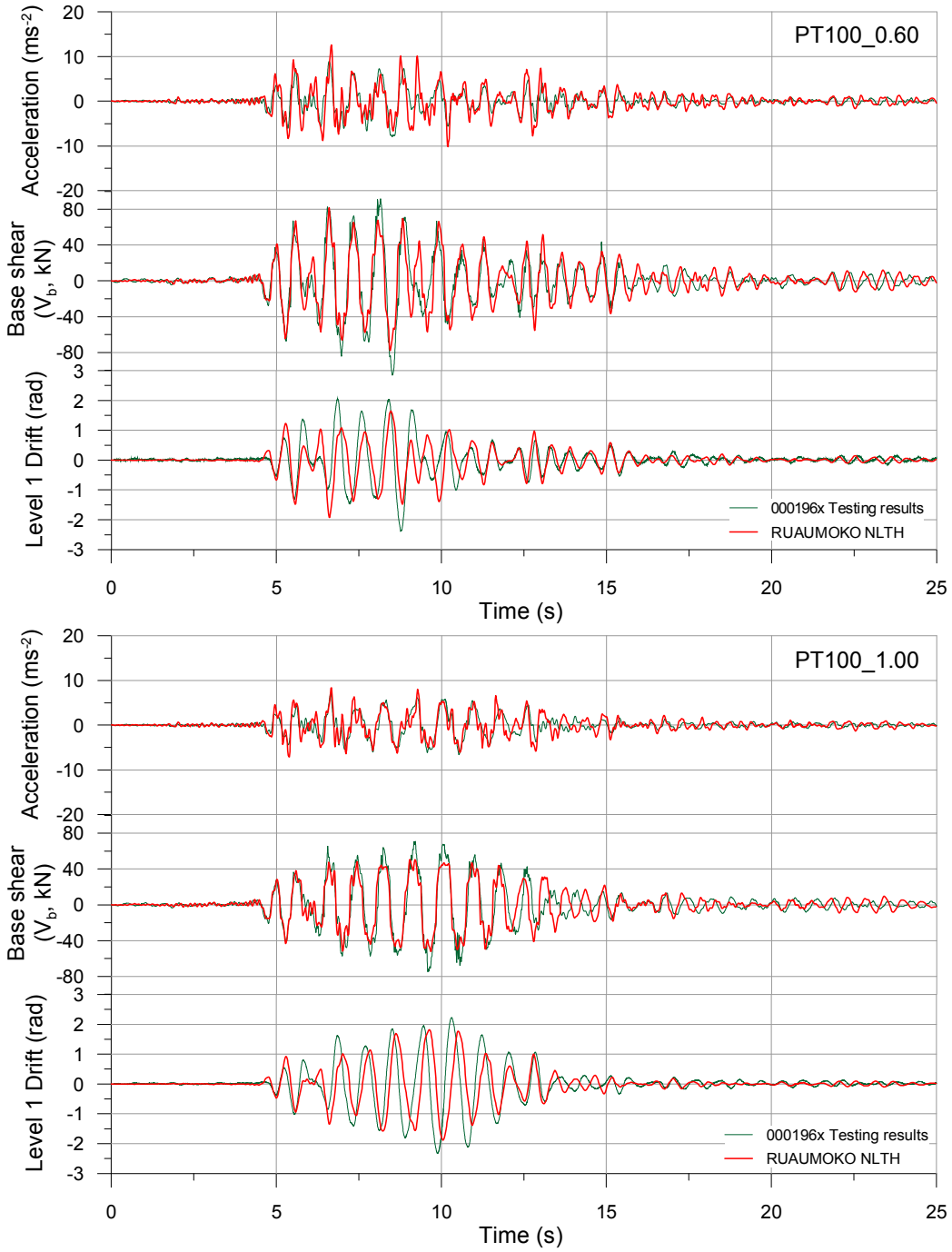

Figure 8.17. Comparisons between RUAUMOKO multi-spring base numerical model and testing results for 000196x earthquake loading: PT100_0.60 (PGA100%)(top) and PT100_1.00 (PGA75%) (bottom)

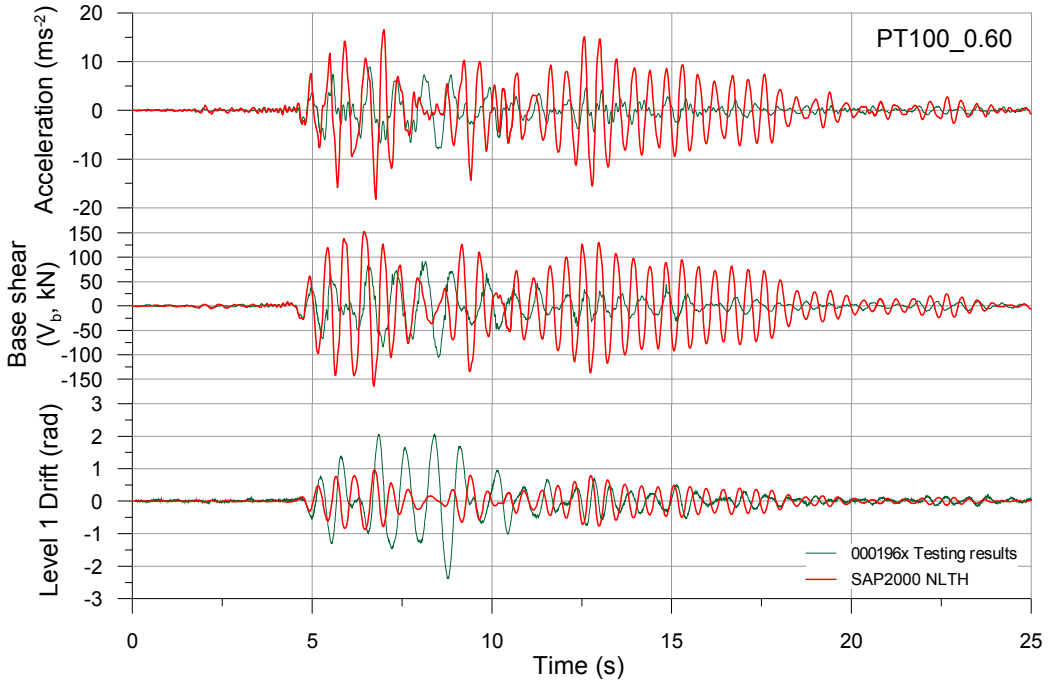

Figure 8.18. Comparisons between SAP2000 multi-spring base numerical model and testing results for 000196x earthquake loading PT100_0.60 (PGA100%)

Comparisons between the results of the RUAUMOKO numerical models show that the models predicted all of the three key indicators with sufficient accuracy in both form and amplitude. Direct comparison of the maximum values from NLTH against testing results is presented in Section 8.6.2 however from Figure 8.17 it can be seen that NLTH tended to slightly under-predict the base shear and drift for both PT100_1.00 and PT100_0.60. Acceleration of the 3rd floor provides the most accurate match between testing results and NLTH in this (000196x) case. Figure 8.17 also shows that the models appeared to become marginally out of phase during the tail of the frame response. This is most noticeable in the drift response of the frame for test PT100_1.00. This is likely to have been created by minor differences in the non-linear (rocking) dynamic response of the model when compared to the test frame. This may be due to overestimation of elastic damping in the RUAUMOKO model. In addition it is possible that the model had difficulty in accurately predicting the higher modes of the structure which were more prevalent in the PT ONLY testing (as described in Section 6.7.2).

Comparisons between the results of the SAP2000 numerical model shows that the multi-spring based model developed does not adequately predict the response of the frame. The model over-predicts the third floor acceleration and base shear and under-

predicts the first floor drift. This type of error indicates that the base connection in the model is stiffer than in the test frame.

8.6.2 Comparisons of maximum acceleration, base shear and drift response between NLTH analysis and testing results with different base boundary conditions

Section 8.5.2 discussed the way in which the choice of boundary conditions, in this case the column base connection, are modelled can have a significant impact on the response and therefore accuracy of the model. Four separate column base boundary conditions have been used during the NLTH analysis of the frame (Figure 8.16). In order to evaluate the effectiveness of these base connection models the maximum values of the selected key indicators provided by models incorporating the four column base connection boundary conditions have been compared with the testing results. Figure 8.19 and Figure 8.20 show this comparison for the RUAUMOKO and SAP2000 NLTH analyses respectively.

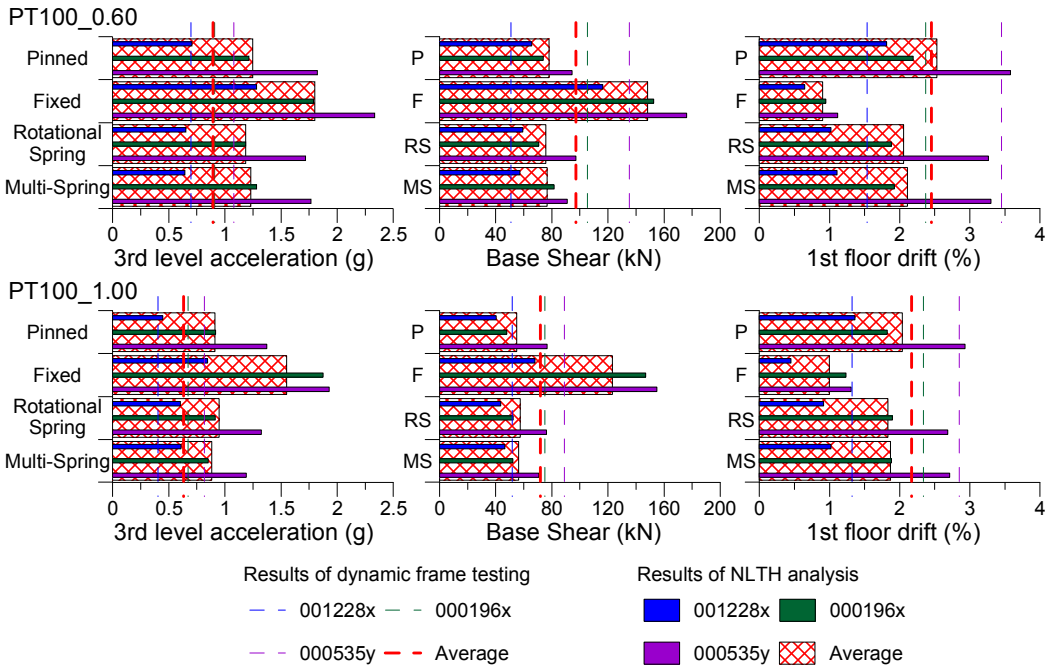

Figure 8.19. Comparisons between RUAUMOKO NLTH and testing results for the pinned, fixed, rotational and multi-spring column base boundary condition models

Figure 8.19 shows that the RUAUMOKO pinned, multi-spring and rotational spring base connection models all provide very similar results in terms of maximum response. For this particular case these models also provide the most accurate

prediction of the model response. This is not unexpected as the base connection response described in Section 6.5.5 displayed very little moment resistance (i.e. a pinned connection).

For both the PT100_1.00 and PT100_0.60 testing series the pinned, multi-spring and rotational-spring models overestimate the acceleration at the third level (average error 27% for PT100_0.60 and 31% for PT100_1.00), underestimate the base shear (average error 20% for PT100_0.60 and PT100_1.00) and slightly underestimate 1st level drift (average error 9% for PT100_0.60 and 12% for PT100_1.00). The fact that the model under-estimates base shear but overestimates third-floor acceleration may indicate that the model is not accurately representing the higher modes which were clearly present during testing (as described in Section 6.7.2). This theory is supported by the slightly increased accuracy of the PT100_0.60 which reduced these higher mode effects.

Figure 8.19 shows that for both the PT100_1.00 and PT1000.60 configurations a fixed base model does not adequately predict frame response.

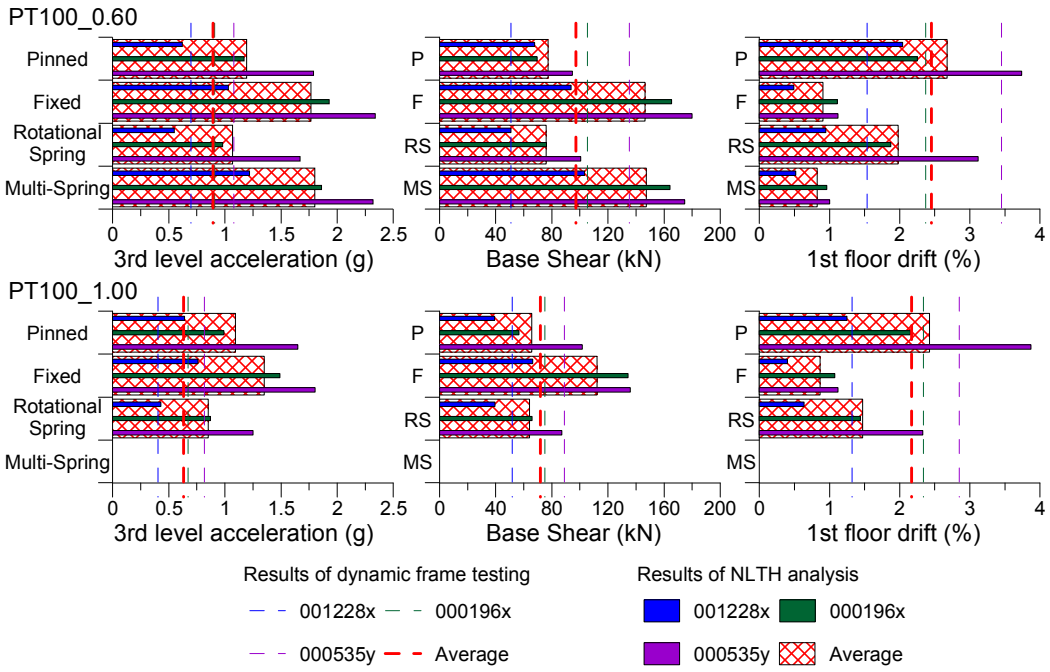

Figure 8.20. Comparisons between SAP2000 NLTH and testing results for the pinned, fixed, rotational and multi-spring column base boundary condition models

Figure 8.20 shows that as with the RUAUMOKO model, the pinned and rotational spring results provided using SAP2000 were reasonably similar and provided accurate

predictions of the maximum frame responses. Again as with the RUAUMOKO model the pinned and rotational spring based SAP2000 models overestimate the acceleration at the third level (average error 21% for PT100_0.60 and 35% for PT100_1.00) and underestimate the base shear (average error for 21% PT100_0.60 and 10% for PT100_1.00). One difference between the RUAUMOKO and SAP2000 modelling however is that while the rotational spring model underestimates 1st level drift (19% error PT100_0.60 and 32% for PT100_1.00) the pinned model overestimates the maximum values (8% error PT100_0.60 and 11% for PT100_1.00).

Figure 8.18 showed the significant error which occurred in the comparisons of the multi-spring SAP2000 model and testing results. Figure 8.20 shows that the response of the multi-spring model was very similar to that of the fixed base model indicating that the multi-spring element used did not adequately represent the performance of the column base.

8.6.3 Comparisons of maximum acceleration, base shear and drift response between NLTH analysis and testing results with increasing levels of PGA%

Figure 8.21 shows comparisons of maximum testing results and RUAUMOKO numerical analysis for the 3rd floor acceleration, base shear and 1st floor drift with increasing levels of PGA%. This analysis was performed for the multi-spring based model and therefore only the RUAUMOKO program was used.

Figure 8.21 shows that the trends observed in Section 8.6.3 in the comparison between the non-linear time history analysis and the testing results (over-prediction of acceleration and under-prediction of base shear and drift) hold true also when considering low levels of input excitation. In general with increasing levels of PGA% the error between the numerical model and the testing results increases. The low seismic (PGA = 10 – 25%) performance of the frame does however appear to be captured very well for most of the key indicators used.

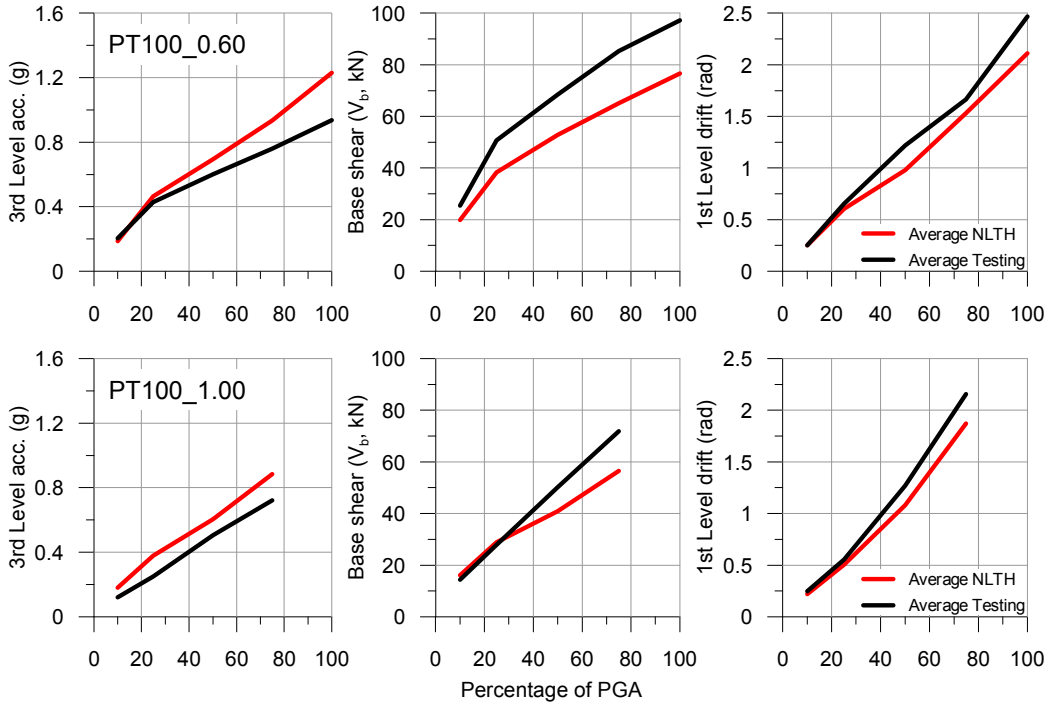

Figure 8.21. Comparison of maximum testing results and RUAUMOKO analysis for the 3rd floor acceleration, base shear and 1st floor drift with increasing levels of PGA%

8.7 CONCLUSIONS FROM CHAPTER 8

Chapter 8 has presented discussions on the numerical modelling of post-tensioned timber frames. This has been done by comparing numerical models developed to represent both the local quasi-static beam-column response presented in Chapter 4 and the global dynamic frame response presented in Chapter 6. All of the springs used during the input of the numerical models presented have been calibrated against the analytical design methods presented in Chapter 5 and not against testing results. Two numerical modelling programs were used: RUAMOKO and SAP2000. Two forms of non-linear elements were used: the rotational spring which contains information regarding the moment-rotation behaviour of the beam-column interface (calibrated against analytical procedures presented in Chapter 5) and the multi-spring model which represented the actual behaviour interaction between beam and column (through the use of axial springs in series) combined with axial springs to represent the post-tensioned and dissipative reinforcing behaviour.

The numerical modelling of the quasi-static beam-column performance provided confirmation that the local, force/moment versus displacement/drift, behaviour of a post-tensioned timber frame can be accurately represented through the use of either a

rotational or multi-spring model in either RUAUMOKO or SAP2000. Although the models all differ in the way in which they model the hysteretic behaviour of the dissipative reinforcing, all three models provided vary similar values of equivalent viscous damping. It is therefore suggested that the simpler rotational spring model is used for the non-linear modelling of post-tensioned timber frames instead of the more complex and less computationally stable multi-spring model. It must be noted however that the rotational spring model does not provide correct information regarding the amount of displacement across the gap (which is provided by the multi-spring model). Therefore if information is required regarding gap opening the multi-spring model must be used or back-calculated using the analytical MMBA procedure presented in analytical MMBA procedure presented in Chapter 5.

The numerical modelling of the global performance of the post-tensioned timber frame confirmed global seismic response of a post-tensioned timber frame can be adequately (errors in the range of maximum 20 – 25%) represented through non-linear time history analysis. Three key indicators selected for comparison between the testing results and the numerical models were the 3rd level acceleration, the base shear and the 1st level drift.

Comparison of these key indicators showed the importance of making correct assumptions regarding the base connection conditions of a post-tensioned timber frame. Both the RUAUMOKO and SAP2000 numerical models provided adequate representation across all three key indicators for the pinned based and rotation spring models and provided significant error for a fixed base model. These results were congruent with the observations made in Section 6.5.5 which described the nominal moment capacity of the column base (i.e. pinned).

A multi-spring model was also used in order to represent the performance of the base connection in both RUAUMOKO and SAP2000. Although the RUAUMOKO model provided accurate prediction of the three key indicators the SAP2000 model performed more as a fixed base element and requires further development if it is to be used in the numerical modelling of post-tensioned timber frames.

The above observations regarding the critical role that the modelling of the column base plays in the accuracy of the numerical model led to the conclusion that, although

it may not be necessary to use a multi-spring model at the beam-column interfaces, in a frame it is crucial that the column boundary condition is correctly modelled. For the test cases presented a pinned model was adequate however it is likely that this would not be the case if dissipative reinforcing elements contributed significantly to moment capacity as would have been the case if the failure of the epoxied base connection had not occurred as described in Section 6.5.5. It is therefore suggested that the response of column base be at least modelled using a properly calibrated rotational spring in order to provide confidence in numerical modelling outcomes.

REFERENCES CHAPTER 8

Carr, A. (2006). "RUAUMOKO." A. Carr, Christchurch, New Zealand, Inelastic Dynamic Analysis Software.

CSI Computers and Structures Inc. (2004). "SAP2000: Static and Dynamic Finite Analysis of Structures." Berkeley, CA, USA.

Iqbal, A., Pampanin, S., Palermo, A., and Buchanan, A. H. (2010). "Seismic Performance of Full-scale Post-tensioned Timber Beam-column Joints." 11th World Conference on Timber Engineering, Riva del Garda, Trentino, Italy, 10.

Kaldjian, M. J. (1967). "Moment-curvature of Beams as Ramberg-Osgood functions." *Journal of the Structural Division, American Society of Civil Engineers*, 93(ST5), 53-65.

Newcombe, M. P., Pampanin, S., and Buchanan, A. H. (2010). "Numerical Modelling and Analysis of a Two-Storey Post-Tensioned Timber Frame with Floor Diaphragms." 14th European Conference on Earthquake Engineering, Ohrid, Republic of Macedonia.

Palermo, A., Pampanin, S., and Carr, A. (2005). "Efficiency of Simplified Alternative Modelling Approaches to Predict the Seismic Responce of Precast Concrete Hybrid Systems." fib symposium "Keep Concrete Attractive, Budapest, Hungary.

Wen, Y. (1980). "Equivalent Linearization for Hysteretic Systems under Random Excitation." *ASME Journal for Applied Mechanics*, 47(1), 150-154.

9 Parametric Analysis of the Seismic Design and Performance of Post-tensioned Timber Frames

9.1 PRINCIPAL CONCLUSIONS OF CHAPTER 9

Chapter 9 presents the design and assessment with Non-Linear Time History analysis of 81 post-tensioned timber frame configurations varying the number of stories and bays, the bay length and the recentering ratio. These principal conclusions were drawn:

1. As with any structural frame system, increasing bay length and number of stories increased moment demand and thus section sizes and required moment capacity (i.e. initial post-tensioning values and dissipative reinforcing).

2. When compared with a post-tension only frame, the allocation of 20% of moment capacity to dissipative reinforcing ($\beta = 0.8$) led to a 45% decrease in design spectral acceleration demand, approximately 25% reduction in section area and approximately 45% reduction in the required initial post-tensioning force. The allocation of 40% of moment capacity to dissipative reinforcing ($\beta = 0.6$) led to a 62% decrease in design spectral acceleration demand, approximately 42% reduction in section area and approximately 71% reduction in the required initial post-tensioning force.

3. Drift response from the NLTH analysis was compared against the 1.8% design value showing that due to the use of safety factors in design all frames responded with design drifts that were lower than the 1.8% value.

4. The presence of higher modes impacted moderately on frame response. Amplification factors were recommended to address the impact of higher modes in design.

9.2 INTRODUCTION

The penultimate chapter of this thesis presents a study of the way in which several frame design parameters impact the seismic response of post-tensioned timber frames

through the use of a parametric design and Non-Linear Time History (NLTH) analysis.

The parametric analysis was performed incorporating the information gathered throughout this research regarding the global (through the use of Displacement Based Design (DBD) presented in Chapter 7) and local (through beam-column and column-foundation analytical analysis techniques presented in Chapter 5) performance of post-tensioned timber frames. Using this information 81 separate frame configurations have been designed varying recentering ratios (β), number of stories (n), number of bays (n_b) and bay length (L). Frames were designed to a Design-Basis Earthquake (DBE) intensity level. These 81 frames have then been modelled using the NLTH analysis techniques described in Chapter 8 and subjected to the set of 7 earthquake records used in the dynamic frame testing described in Chapter 6.

Following the presentation of the setup of the parametric analysis the results of the study will be separated into two sections: the presentation of the results of the design performed according to a DBD approach (which provided the design characteristics of each frame), and the results of the NLTH analysis (which provided the seismic performance of each frame).

How to use DBD and the design of post-tensioned timber frames will not be covered in this chapter and can be found in Chapter 10.

9.3 SETUP AND VARIABLES STUDIED DURING PARAMETRIC ANALYSIS

The parametric analysis presented in this chapter varied a selection of four parameters: the recentering ratio (β), the number of stories (n) and bays (n_b), and the bay length (L). Three different values of each parameter were used as shown in Table 9.1 and Figure 9.1. All permutations of these variables were considered totalling 81 frame types.

Table 9.1. Parameter definition for variable analysis

Recentering ratio	β	0.6, 0.8, 1.0
Number of Stories	n	3, 5, 7
Number of Bays	n_b	1, 3, 5
Bay Length	L	4m, 6m, 8m

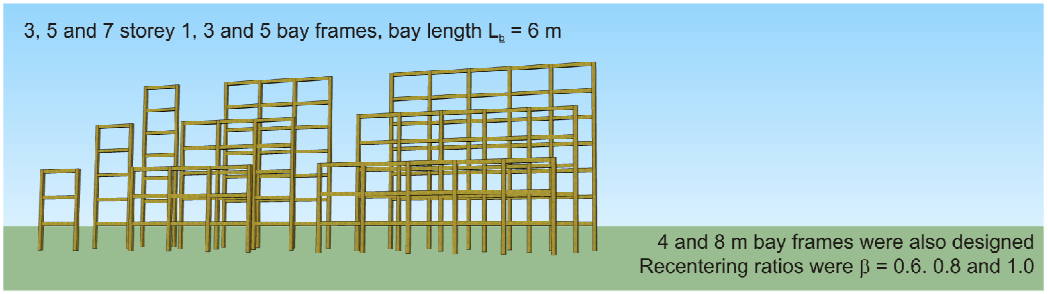

Figure 9.1. Sketch of a selection of frames used during parametric analysis

In order to make the study practical a series of assumptions were required in order to facilitate the analyses:

- The building was an office structure (live load Q = 3 kPa), with exception of the final floor which has a roof top penthouse. This resulted in a total seismic flooring weight (dead plus 30% of live loading) of 5.1 kPa.
- Each frame had a tributary width of 2.5 m and was considered as the external frame of a building with frames spaced at 5 m centre to centre.
- The building was situated in Southern Italy and was therefore designed for the seismic hazard of that region (i.e. PGA=0.44 g). This was the same seismic hazard used in the design of the test frame presented in Chapter 6.
- Displacement Based Design (DBD) was used in order to calculate design base shear. In order to do this a design drift of θ_d = 1.8% under Ultimate Limit State (ULS) loading was selected. A ductility of μ = 2 and a post yield ratio of r = 0.1 was assumed in order to calculate the spectrum reduction due to hysteretic damping.
- A linear extrapolation of the design displacement spectrum was assumed following the constant (plateau) displacement region of the code defined spectrum (shown as a dashed line in Figure 9.10).
- Section sizes aimed to have a ratio between height (h_c, h_b) and width (b_c, b_b) as close as possible to 3:2. Section sizes were increase in 0.05 m increments. An example beam and column are displayed in Figure 9.2.
- Beam sizes and column sizes were selected to be the same.
- Post-tensioned elements were selected as 26.5 mm high strength steel bars (A_{pt} = 552 mm). Where one bar was not sufficient several (up to 4) bars were used. All post-tensioning was placed at the centre of the beam.

- Fused type dissipative reinforcing was used in frames with recentering ratios ($\beta=M_{pt}/M_t$) less than 1. Dissipative reinforcing was placed at 100 mm from the external edge of each beam and at 50 mm from the external edge of each column. Grade300 steel (f_y = 300 MPa) was used.
- Frames were considered to be 'seismic only' meaning that they carried no gravity loading.
- A generic Laminated Veneer Lumber, LVL11, engineered timber was considered as the beam and column material. Material properties are presented in Table 9.2.

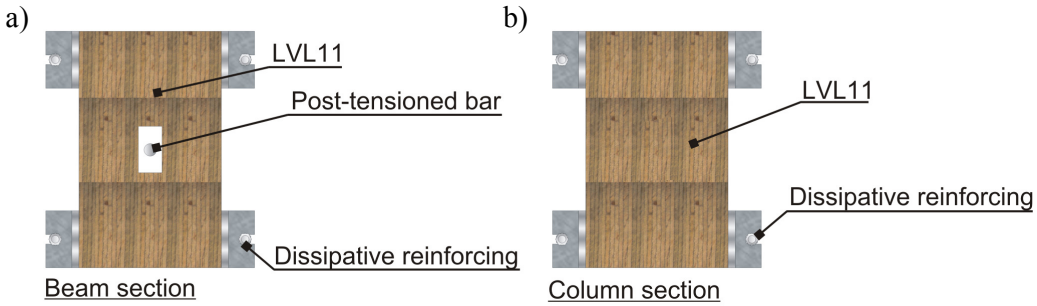

Figure 9.2. Example of typical a) beam and b) column used for parametric analysis of post-tensioned timber frames.

Table 9.2. Material properties used for parametric analysis of post-tensioned timber frames.

LVL11				Post-tension Bar			
Strength				Yield strength	f_y	1050	MPa
Bending	f_{tb}	48.0	MPa	Elastic modulus	E_{pt}	170	MPa
Compression parallel to grain	f'_{par}	45.0	MPa	Area	A_{pt}	552	mm^2
Compression perp. to grain	f'_{perp}	42.0	MPa				
Shear	f_{ts}	6.0	MPa	Dissipative reinforcing			
Elastic modulus				Yield Strength	f_y	300	MPa
Characteristic para. to grain	$E_{t,para}$	11.0	GPa	Ultimate strength	f_u	440	MPa
Shear	G_t	0.55	GPa	Elastic Modulus	E	200	MPa

9.4 DISPLACEMENT BASED DESIGN RESULTS FROM PARAMETRIC ANALYSIS FRAME DESIGN

In order to analyse the seismic performance of the 81 case frames selected each frame required physical properties. In order to provide the frames with this information, Displacement Based Design (DBD) was used which provided the design seismic demand for each structure, the base shear was then distributed through the building using the equilibrium method first described in Priestley (2007) and elaborated upon by the New Zealand Concrete Society (NZCS 2010). This section describes the results of the DBD and the frame characteristics it provided.

Design characteristics for the three storey frame were uniform up the building height. The section sizes, initial post-tensioning and dissipative reinforcing values were revised for the five and seven storey buildings above the third and fourth stories, respectively.

9.4.1 Design base shear

The seismic hazard used in the parametric analysis was the same hazard used for the frame design described in Chapter 6. This was then reduced using the reduction factor (R, from Section 7.6.2) in order to allow for the hysteretic damping properties of the frame using the Equation (5.57) of Chapter 5. System damping is independent of height and the number or length of bays therefore only three different reduction factors were used relating to the three recentering ratios selected. Ductility and post-yield ratios are not available during this stage of design and therefore had to be estimated. As suggested in Chapter 7 an elastic damping value of ξ_{el} = 3% was used for all cases.

Table 9.3. Elastic, hysteretic and total damping and reduction factors used for parametric analysis

Recentering ratio	ξ_{el}	ξ_{hyst}	ξ	R
$\beta = 1$	0.03	0.00	0.03	1.18*
$\beta = 0.8$	0.03	0.06	0.07	0.88
$\beta = 0.6$	0.03	0.12	0.11	0.73

*As the design spectrum is damped to 5% a damping ratio of 3% results in an increase of the design spectrum

The use of DBD requires the definition of an equivalent single degree of freedom system which provides an effective system design displacement (Δ_d), height (H_e), mass (m_e) and period (T_e). As described in Chapter 7 these values are then used to calculate the system base shear.

This was done for each of the parametric frames providing the SDOF systems values which are presented in Table 9.4. As can be seen in the table not all of the design DBD parameters were affected by the variables used. Both the design displacement and effective height were only changed by a change in the total height of the building. This was expected as all frames were designed to target the same drift. The effective mass altered with changes in number of stories, bay length and the number of bays. All of these parameters directly impact on the building floor area and thus mass. The effective period changed with building height and recentering ratio. Changes due to recentering ratio occurred due to the alteration of the demand spectrum by the factor R shown in Table 9.3.

Table 9.4. Effective SDOF system characteristics defined by DBD

		Design displacement (Δ_d, m)									Effective mass (m_e, t)								
		$n_b = 1$			$n_b = 3$			$n_b = 5$			$n_b = 1$			$n_b = 3$			$n_b = 5$		
		$L_b = 4$ m	$L_b = 6$ m	$L_b = 8$ m	$L_b = 4$ m	$L_b = 6$ m	$L_b = 8$ m	$L_b = 4$ m	$L_b = 6$ m	$L_b = 8$ m	$L_b = 4$ m	$L_b = 6$ m	$L_b = 8$ m	$L_b = 4$ m	$L_b = 6$ m	$L_b = 8$ m	$L_b = 4$ m	$L_b = 6$ m	$L_b = 8$ m
n = 3	β = 1	0.151	0.151	0.151	0.151	0.151	0.151	0.151	0.151	0.151	13	20	27	40	60	80	67	100	134
	β = 0.8	0.151	0.151	0.151	0.151	0.151	0.151	0.151	0.151	0.151	13	20	27	40	60	80	67	100	134
	β = 0.6	0.151	0.151	0.151	0.151	0.151	0.151	0.151	0.151	0.151	13	20	27	40	60	80	67	100	134
n = 5	β = 1	0.195	0.195	0.195	0.195	0.195	0.195	0.195	0.195	0.195	22	33	45	67	101	134	112	168	223
	β = 0.8	0.195	0.195	0.195	0.195	0.195	0.195	0.195	0.195	0.195	22	33	45	67	101	134	112	168	223
	β = 0.6	0.195	0.195	0.195	0.195	0.195	0.195	0.195	0.195	0.195	22	33	45	67	101	134	112	168	223
n = 7	β = 1	0.263	0.263	0.263	0.263	0.263	0.263	0.263	0.263	0.263	31	46	61	92	138	183	153	229	306
	β = 0.8	0.263	0.263	0.263	0.263	0.263	0.263	0.263	0.263	0.263	31	46	61	92	138	183	153	229	306
	β = 0.6	0.263	0.263	0.263	0.263	0.263	0.263	0.263	0.263	0.263	31	46	61	92	138	183	153	229	306

		Effective height (H_e, m)									Effective Period (T_e, s)								
		$n_b = 1$			$n_b = 3$			$n_b = 5$			$n_b = 1$			$n_b = 3$			$n_b = 5$		
		$L_b = 4$ m	$L_b = 6$ m	$L_b = 8$ m	$L_b = 4$ m	$L_b = 6$ m	$L_b = 8$ m	$L_b = 4$ m	$L_b = 6$ m	$L_b = 8$ m	$L_b = 4$ m	$L_b = 6$ m	$L_b = 8$ m	$L_b = 4$ m	$L_b = 6$ m	$L_b = 8$ m	$L_b = 4$ m	$L_b = 6$ m	$L_b = 8$ m
n = 3	β = 1	8.4	8.4	8.4	8.4	8.4	8.4	8.4	8.4	8.4	0.94	0.94	0.94	0.94	0.94	0.94	0.94	0.94	0.94
	β = 0.8	8.4	8.4	8.4	8.4	8.4	8.4	8.4	8.4	8.4	1.27	1.27	1.27	1.27	1.27	1.27	1.27	1.27	1.27
	β = 0.6	8.4	8.4	8.4	8.4	8.4	8.4	8.4	8.4	8.4	1.52	1.52	1.52	1.52	1.52	1.52	1.52	1.52	1.52
n = 5	β = 1	12.9	12.9	12.9	12.9	12.9	12.9	12.9	12.9	12.9	1.21	1.21	1.21	1.21	1.21	1.21	1.21	1.21	1.21
	β = 0.8	12.9	12.9	12.9	12.9	12.9	12.9	12.9	12.9	12.9	1.63	1.63	1.63	1.63	1.63	1.63	1.63	1.63	1.63
	β = 0.6	12.9	12.9	12.9	12.9	12.9	12.9	12.9	12.9	12.9	1.95	1.95	1.95	1.95	1.95	1.95	1.95	1.95	1.95
n = 7	β = 1	17.5	17.5	17.5	17.5	17.5	17.5	17.5	17.5	17.5	1.63	1.63	1.63	1.63	1.63	1.63	1.63	1.63	1.63
	β = 0.8	17.5	17.5	17.5	17.5	17.5	17.5	17.5	17.5	17.5	2.21	2.21	2.21	2.21	2.21	2.21	2.21	2.21	2.21
	β = 0.6	17.5	17.5	17.5	17.5	17.5	17.5	17.5	17.5	17.5	2.63	2.63	2.63	2.63	2.63	2.63	2.63	2.63	2.63

Base shear result calculated using the above DBD design parameters are shown in Figure 9.3. It is noted that the relationships shown in Figure 9.3 are not specific to post-tensioned timber buildings and are material independent.

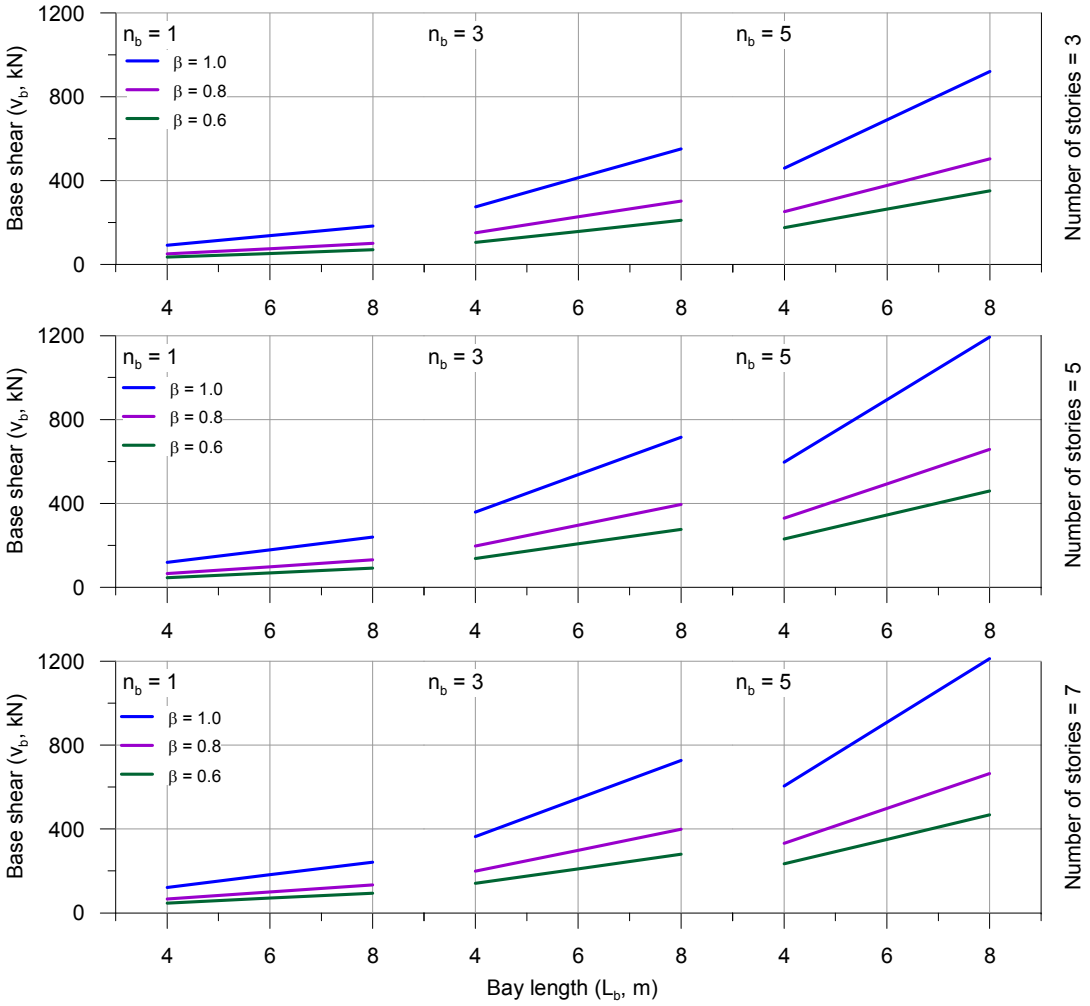

Figure 9.3. Frame base shear calculated using DBD for parametric analysis

Figure 9.3 displays the way in which the base shear of the structure related to increases in the number of stories, number and length of bays and decreases in recentering ratio. As shown all of these factors impacted on the base shear of the structure, however as discussed above, it is unclear if these changes were related to an alteration of the buildings dynamic characteristics (i.e. an alteration of building effective period as concluded from DBD) or simply a change in the buildings mass. In order to individuate these two effects, the spectral acceleration (S_a defined as the base shear divided by the seismic mass) has been calculated for each frame and is shown in Figure 9.4.

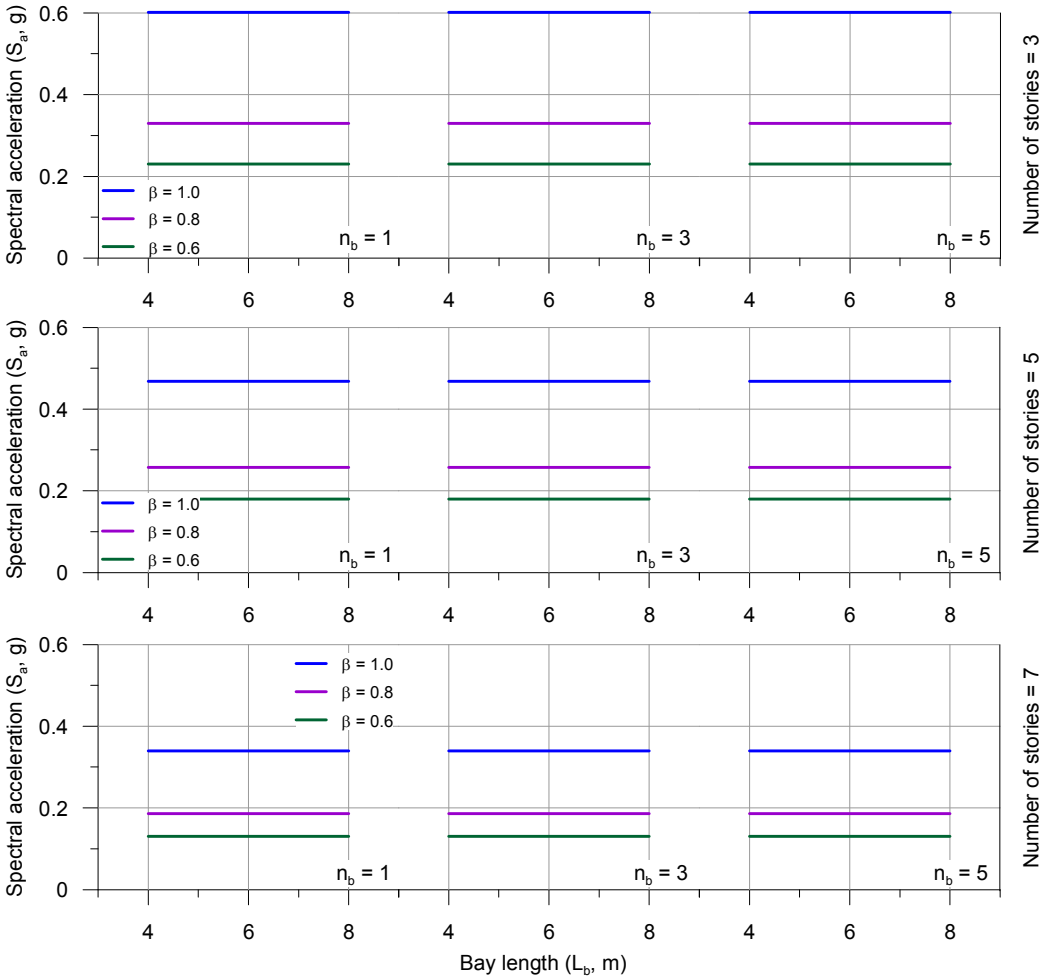

Figure 9.4. Frame spectral acceleration calculated using DBD for parametric analysis

Figure 9.4 shows that although the base shear changed with the number of bays and the bay length this, when following the DBD procedure, did not impact on the dynamic characteristics of the building. This means that, for a given number of storeys and re-centering ratio the effective period of the structure (as defined by DBD) will remain equal regardless of the number of bays or the bay length. The spectral acceleration reduced when the number of stories increased which is expected as the period of the building elongates.

It is evident from Figure 9.4 the significant impact that adding dissipative reinforcing had on the design base shear provided by DBD. It is also evident that this impact was not linear. When 20% of the moment capacity was allocated to the dissipative reinforcing ($\beta = 0.8$) a 45% reduction occurred in the spectral acceleration. When 40% of the moment capacity was allocated to the dissipative reinforcing ($\beta = 0.6$) a 62% reduction in the spectral acceleration was observed. This reduction was not

linked to any parameter other than the allocation of the moment capacity in the frame (i.e. the value of β).

9.4.2 Design frame characteristics

Section 9.4.1 has presented the base shear and spectral accelerations calculated using Displacement Based Design (DBD). The results of this were the calculation of moment demands for each beam-column connection of each frame. As mentioned this was done using the equilibrium method which uses static equilibrium in order to distribute the base shear within the frame. Using these moment demands the section sizes (h_b, h_c, b_b and b_c), initial post-tensioning force ($T_{pt,initial}$) and area of dissipative reinforcing (A_s) were calculated.

Beam and column section sizes

The equilibrium method provided beam shears at each floor for each frame. Section 9.4.1 discussed the way in which the spectral acceleration did not change with increases in either bay length or bay width; this meant that the beam shear at each floor also did not change. Although this is true the design of a post-tensioned timber beam-column joint is a function of the moment demand on the joint. Increases in the number of bays in the frame will not impact on the moment demand however, increases in bay length have a linear relationship with demand with a longer bay length creating a larger demand.

Chapter 5 showed that the elastic frame deformations of the beam (θ_b), column (θ_c) and joint panel (θ_j) are a function of the moment at the beam-column joint and the beam and column section sizes. This chapter also discussed the negative impact that these elastic rotations can have on frame performance. In order to ensure that the design ductility of two was obtained, section sizes were selected to ensure that the sum of the elastic rotations did not exceed one third of the design drift when subjected to the design moment. (i.e. $\theta_b + \theta_c + \theta_j < 0.6\%$ under design moment). This objective meant that section sizes were able to be selected regardless of initial post-tensioning values and dissipative reinforcing quantities thus reducing iteration in the design procedure. Figure 9.5 shows the beam heights used for the post-tensioned timber frame parametric analysis. Further discussion regarding the sizing of beam and column members is described in Section 10.2.2.

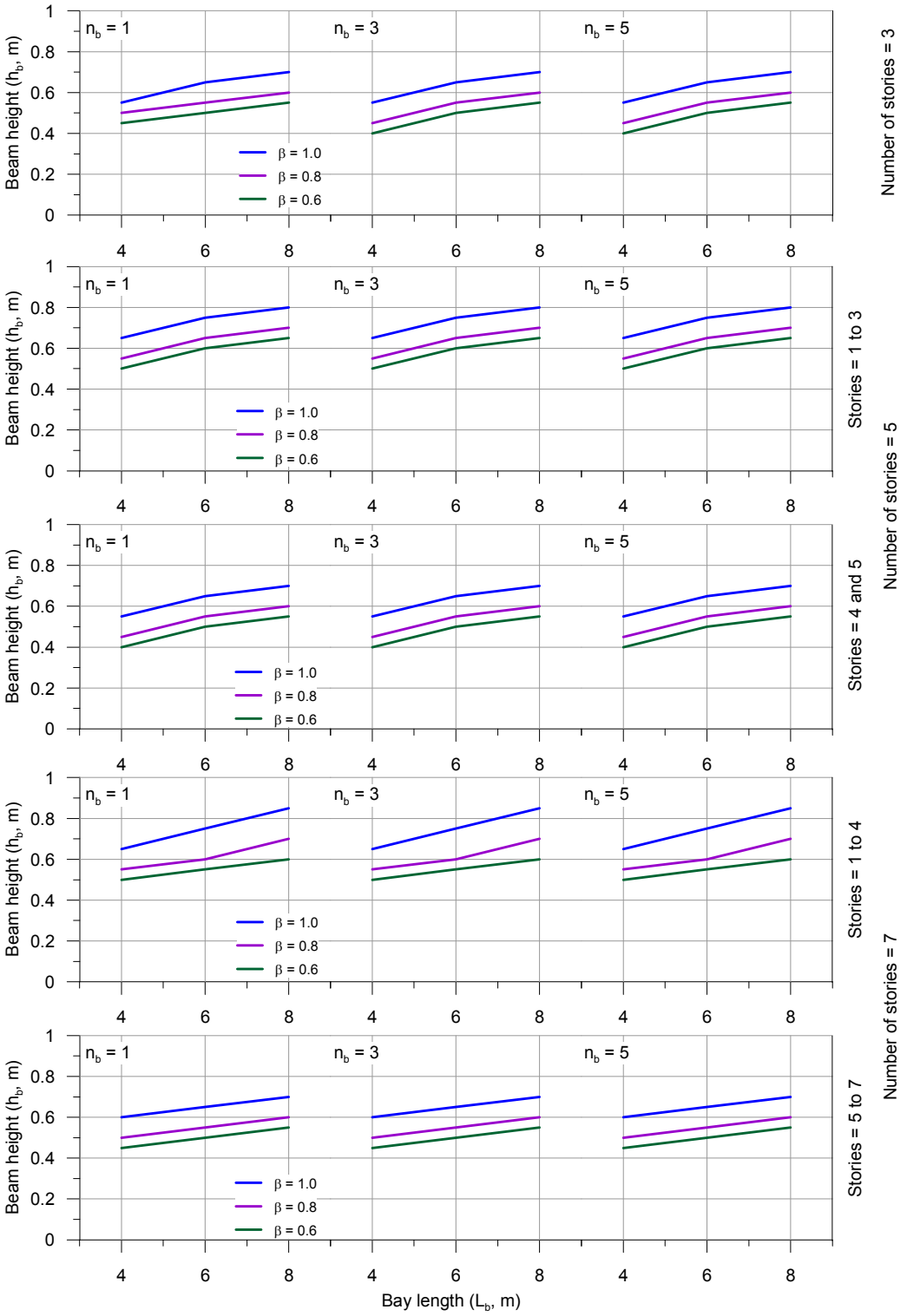

Figure 9.5. Design beam heights (h_b) calculated using post-tensioned timber design procedure for parametric analysis

Figure 9.5 shows beam heights between h_b = 0.4 m (n = 3, β = 0.6) and h_b = 0.85 m (levels 1 to 4, n = 7, β = 1.0). Beam widths increased with beam heights from b_b = 0.3

m to b_b = 0.5 m. This means that the beam area varied between A_b = 0.12 m^2 to A_b = 0.425 m^2 which was an increase of 250%.

The same trends observed in Section 9.4.1 with relation to the base shears provided by the DBD procedure followed on to the beam and column characteristics. Due to identical moment demand beam characteristics when the number of bays was increased did not change. When the bay length was increased the moment demand increased and the beam depths were increased in order to keep the elastic rotations below the target 0.6% value.

With an increased number of stories moment demand also increases (due to an increased total overturning moment). This increased moment demand also led to an increase in beam height. As an example, the beam height increased from h_b = 0.6 m (n = 3, L_b = 8 m, β = 0.8) to h_b = 0.7 m (n = 7, L_b = 8 m, β = 0.8) with an increase in the number of stories from 3 to 7.

Allocating a proportion of the moment resistance to dissipative reinforcing ($\beta < 1$) also impacted on the beam depth. As an example the beam height increased from h_b = 0.5 m (n = 3, L_b = 6 m, β = 0.6) to h_b = 0.55 m (n = 3, L_b = 6 m, β = 0.8) and h_b = 0.65 m (n = 3, L_b = 6 m, β = 1.0) with increasing values of β. The beam area in these cases displayed a 27% decrease when 20% of moment capacity was allocated to the dissipative reinforcing and a 42% decrease when 40% of moment capacity was allocated to the dissipative reinforcing. When extrapolated to a whole building scale this creates a notable difference in the required volume of timber.

These beam sizes have been concluded based on the design-basis earthquake and not serviceable levels of drift. Traditional systems tend to restrict serviceable drift limits in order to avoid damage to structural elements when subjected to low intensity earthquakes. A post-tensioned timber frame however is capable of sustaining moderate levels of drift without damage (i.e. no dissipative reinforcing yielding) and as such drift limits will be imposed by non-structural elements and comfort levels inside the structure during low intensity events. Further research is required in order to define serviceable drift limits for post-tensioned timber buildings.

Initial post-tensioning values and dissipative reinforcing area

Selection of the required initial post-tensioning and dissipative reinforcing area was performed using the post-tensioned timber frame design procedure presented in Chapter 5. Several design choices were made during this design: 1) the initial stress in the post-tensioned bar would remain below 60% of yield (< 300 kN, i.e. if $T_{pt,initial}$ > 300, more than 1 bar was used) and 2) the diameter of the fused type reinforcing would be increased at 1 mm intervals. The results of the design are shown in Figure 9.6 and Figure 9.7.

Figure 9.6 displays the initial post-tensioning force required for each of the parametric frame cases. Trends similar to those observed for the base shear and the beam depth were found. Only minor change was observed with increases in the number of bays due to changes in the elastic joint panel rotations (as described in Section 5.4.2) and alterations of impacts of frame shortening (Section 5.3.5) on the increase in post-tensioning force following gap opening.

Increasing the bay length increased the moment demand in the frame. As a consequence the initial post-tensioning was also increased. When 100% of the seismic resistance was provided only by the post-tensioning ($\beta = 1$) this increase was more rapid as all of the additional moment capacity was provided by the post-tensioning. As portions of the moment capacity were allocated to the dissipative reinforcing ($\beta < 1$) there was a decrease in the rate of post-tensioning increase. This was also due to the decrease in the rate of base shear increase shown in Figure 9.3.

With an increased number of stories the moment demand increased. This increased moment demand led to an increased initial post-tensioning force. As an example, the initial post-tensioning force increased from $T_{pt,initial}$ = 400 kN ($n_b = 3$, $n = 3$, $L_b = 8$ m, $\beta = 0.8$) to $T_{pt,initial}$ = 650 kN ($n_b = 3$, $n = 7$, $L_b = 8$ m, $\beta = 0.8$) with an increase in the number of stories.

Figure 9.6 shows that allocating a proportion of the moment resistance to dissipative reinforcing ($\beta < 1$) impacted significantly on the initial post-tensioning required. Allocating 20% of the moment capacity to the dissipative reinforcing resulted in an average 45% reduction in initial post-tensioning force. Allocating 40% of the moment capacity to the dissipative reinforcing resulted in an average 71% reduction in initial

post-tensioning force. Reductions in post-tensioning force are important for post-tensioned timber structures as minimizing initial post-tensioning force minimizes the compression perpendicular to the grain in the column. This will reduce the required amounts of column face reinforcing and post-tension anchorage requirements.

Figure 9.7 displays the amount of dissipative reinforcing required to match moment capacity to moment demand for the parametric frame cases. Similar trends were seen for the dissipative reinforcing as for the beam height and the initial post-tensioning force; no significant change was observed with increased bay number and dissipative reinforcing areas were increased with bay length and number of bays.

It can be noted in Figure 9.7 that increases in dissipative reinforcing area were not as smooth as the increases in initial post-tensioning shown in Figure 9.6 and in some cases general trends observed for other cases were not followed (e.g. comparison between $n_b = 3$, $n = 7$, $L_b = 6$ m, $\beta = 0.8$ and $n_b = 3$, $n = 7$, $L_b = 8$ m, $\beta = 0.8$). This was due to two factors related to the design choice of increasing the reinforcing area by 1 mm diameter increments. This choice meant that increases in the strength of the dissipative reinforcing were limited by finite increments in the strength of dissipative reinforcing. In addition to this fact during design it is unlikely that a combination of beam depth, post-tensioning force and dissipative reinforcing area satisfies exactly the desired recentering ratio. An example of this is shown in Table 9.5 for the frame cases $n_b = 3$, $n = 7$, $L_b = 6$ m, $\beta = 0.8$ and $n_b = 3$, $n = 7$, $L_b = 8$ m, $\beta = 0.8$ where a decreased amount of dissipative reinforcing was required against the general increasing trend. A design reduction factor $\phi = 0.9$ (Pampanin et al. 2013) was used.

Table 9.5. Design parameters and capacity at $\theta_d = 1.8\%$ of parametric study cases $n_b = 3$, $n = 7$, $L_b = 6$ m, $\beta = 0.8$ and $n_b = 3$, $n = 7$, $L_b = 8$ m, $\beta = 0.8$ levels 1 to 4

Recentering ratio	h_b (m)	b_b (m)	$T_{pt,initial}$ (kN)	A_s (mm)	M_s (kNm)	M_{pt} (kNm)	ϕM_t (kNm)	M^*_{con} (kNm)	β
$n_b = 3$, $n = 7$, $L_b = 6$ m, $\beta = 0.8$	0.6	0.4	550	2 ϕ13	36	131	150	> 142	0.78
$n_b = 3$, $n = 7$, $L_b = 8$ m, $\beta = 0.8$	0.7	0.45	650	2 ϕ12	40	183	201	> 192	0.82

Average dissipative reinforcing yield force values were $F_y = 54$ kN and $F_y = 86$ kN for $\beta = 0.8$ and $\beta = 0.6$ respectively. The maximum dissipative reinforcing yield force was provided by the first four levels of the $n = 7$, $L_b = 8$ m, $\beta = 0.6$ case with $F_y = 136$ kN. Ratios of dissipative steel area to beam area ranged between 0.07% ($n = 1$, L_b

= 8 m, β = 0.8) and 0.2% (n = 7, L_b = 8 m, β = 0.8). In general reinforcing ratios decreased with increasing bay length.

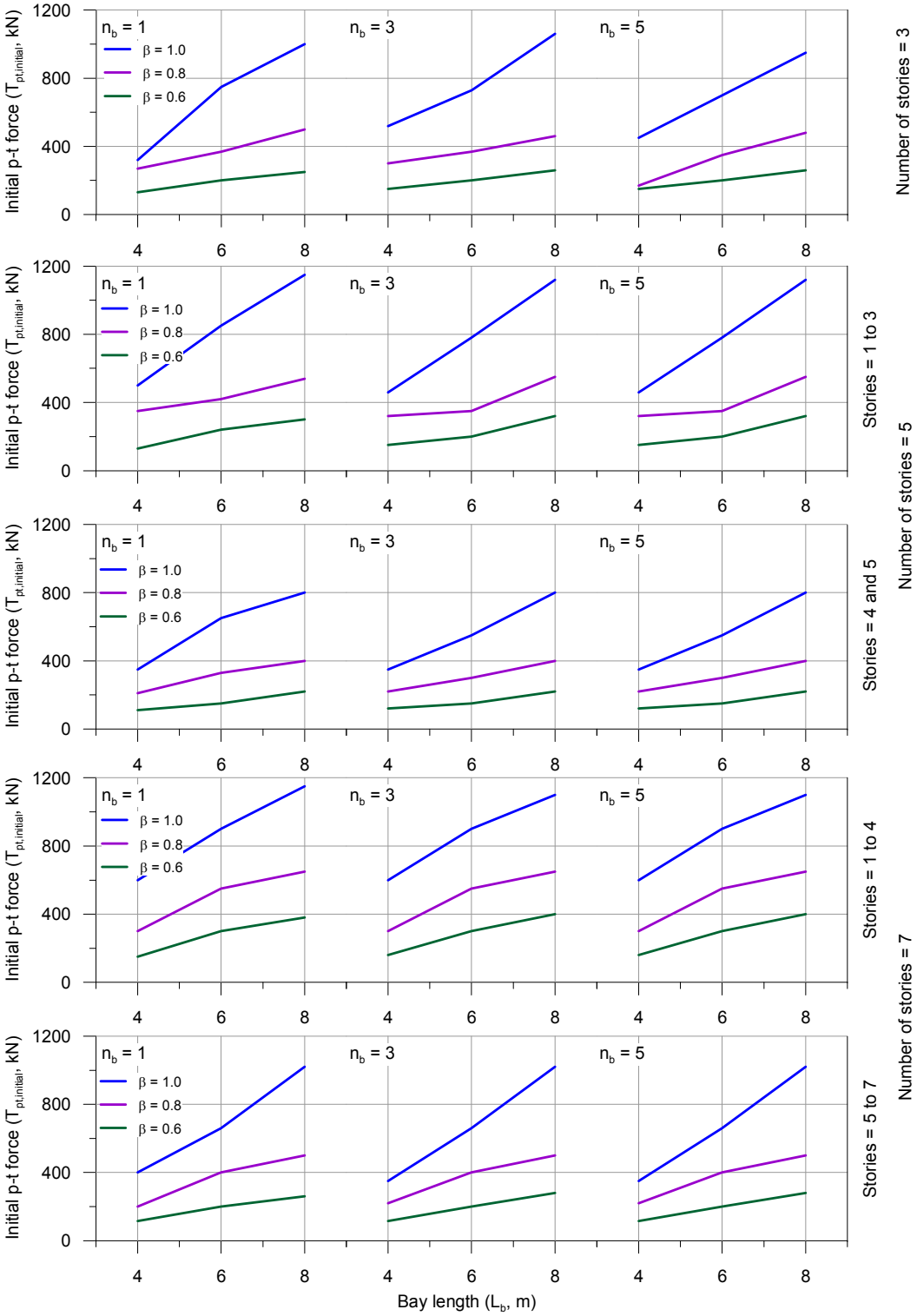

Figure 9.6. Design initial post-tension force ($T_{pt,initial}$) calculated using post-tensioned timber design procedure for parametric analysis

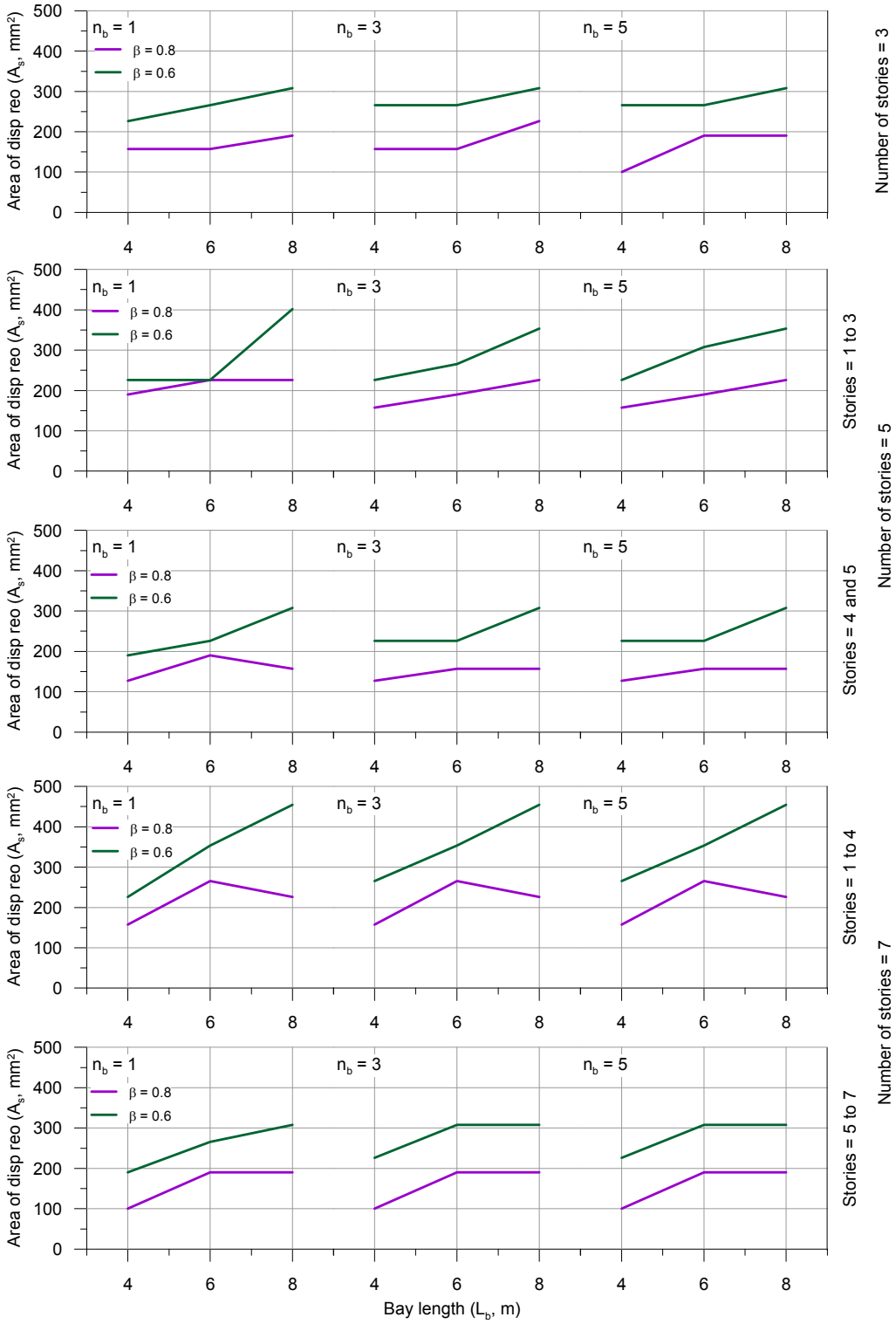

Figure 9.7. Design dissipative reinforcing area (A_s) calculated using post-tensioned timber design procedure for parametric analysis

Column base moment capacity

Column base moment capacity comes from two sources: the column axial load and any additional reinforcing present at the column base. During the distribution of forces within the frame a point of contraflexure at 60% up the height of the first floor column was considered. This assumption meant that the column base needed to be provided with moment capacity. During design the moment capacity of the column was calculated using the same design procedure as used for the beam-column joint. No vertical post-tensioning was considered inside the columns and where the moment capacity provided by the axial load was not sufficient additional dissipative reinforcing was added.

9.5 RESULTS OF NON-LINEAR TIME HISTORY ANALYSIS OF PARAMETRIC POST-TENSIONED TIMBER FRAMES

Section 9.4 has presented a series of 81 frames which have been designed following the Displacement Based Design (DBD) procedure. During the use of this design procedure an input in the form of a target drift (θ_d = 1.8%) was used. As a consequence, according to the assumptions made by the design procedure, frame response should provide this drift at the first floor when subjected to the design level input. No P-Delta effects were considered during the analysis.

This section analyses frame response using Non-Linear Time History (NLTH) analysis. Several key indicators were selected in order to analysis frames response: drift, base shear, acceleration and ductility demand.

9.5.1 Parametric frame modelling and input

The parametric frames were modelled using the numerical techniques described in Chapter 8. Each frame was represented using a combination of elastic beam elements (representing the beams and columns) and rotational springs (representing beam-column interface, joint panel performance and column base performance). Calibration of the moment rotation springs was performed following the guidance presented in Section 8.3.4.

Due to the large amount of analyses (7 per frame case totalling 567 earthquakes) which were performed the more time efficient RUAUMOKO numerical modelling

program was used. The seismic input used was the set of seven earthquakes described in Section 6.4.6 used during the dynamic frame testing.

9.5.2 Acceleration Displacement Response Spectrum (ADRS) of parametric frames

Pushover analyses of the parametric frames were performed and Acceleration Displacement Response Spectrum (ADRS) were constructed for each frame in the same manner as described in Section 6.4.5. A selection of these analyses (for the β = 0.8, L_b = 6 m) are presented in Figure 9.8.

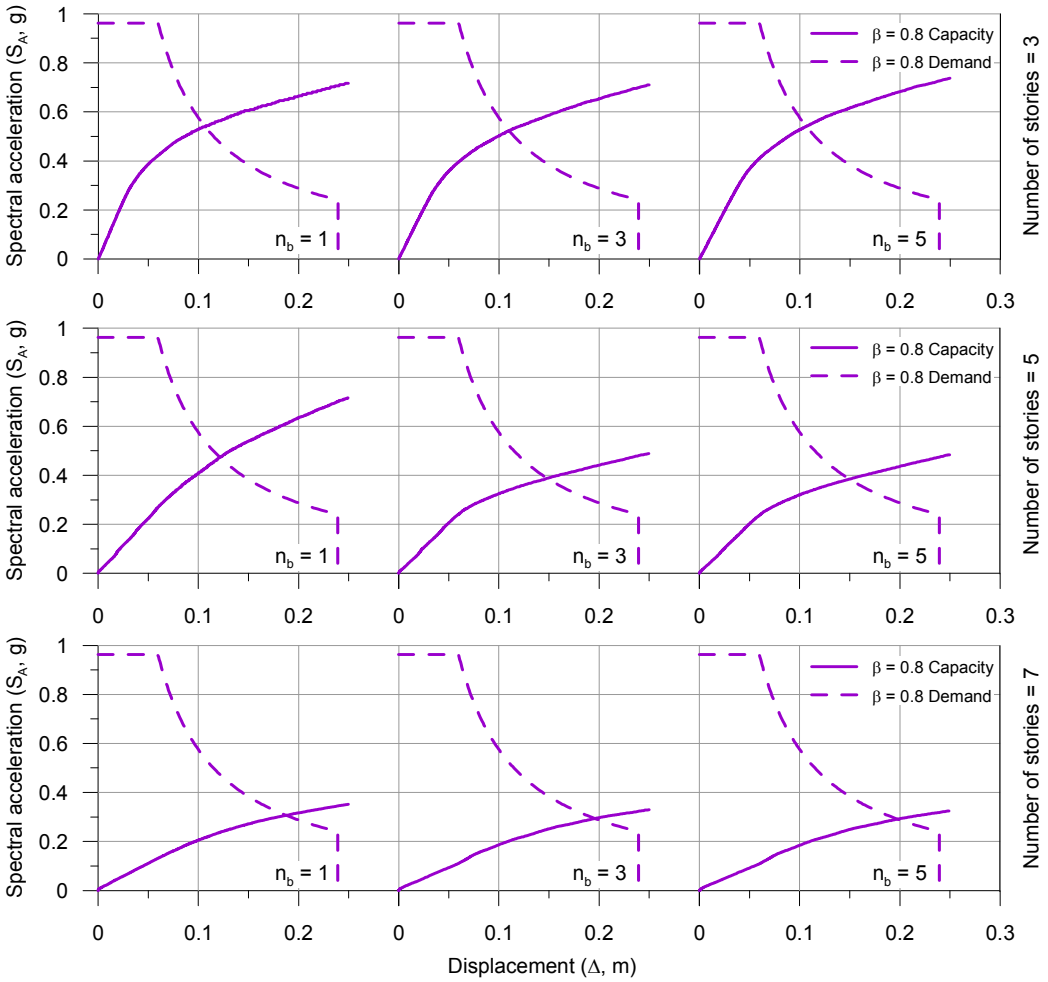

Figure 9.8. ADRS spectra of β = 0.8, L_b = 6 m parametric frames

From Figure 9.8 the significant flexibility of the parametric post-tensioned timber frames can be seen. Each of the frames displayed notable amount of elastic deformation before yield leading to the low system displacement ductility values

(target $\mu = 2$) characteristic of these frames. The analyses also displayed the nominal difference between initial and post-yield stiffness noted in Chapter 7.

9.5.3 Drift results of NLTH analysis of parametric post-tensioned timber frames

The design of the parametric post-tensioned timber frames analysed using NLTH analysis used a design drift of $\theta_d = 1.8\%$. This related to the drift of the first floor of the frame structure which is nominated as the 'critical' level in DBD based on the assumption that the first mode shape will dominate seismic performance. Figure 9.9 shows that the average first floor drift frame response from Non-Linear Time History (NLTH) analysis across all considered frames.

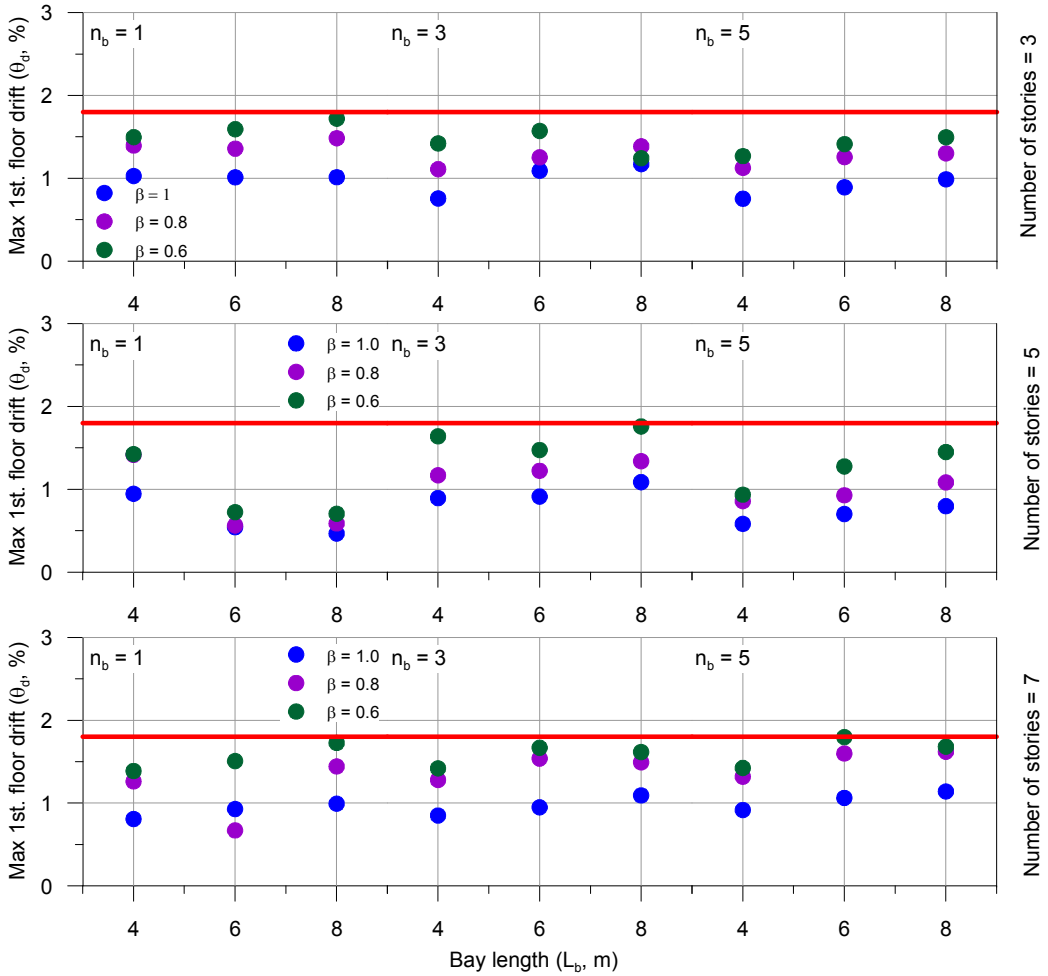

Figure 9.9. Average maximum first floor drift response results from NLTH frame parametric analysis

The average first floor drift frame response from was 1.3% (coefficient of variation = 0.26) which was close (within 0.5% drift) to the 1.8% design value for all frame cases

considered. In all cases the first floor drift response of the parametric frames was less than the target value of 1.8%. The reason for this was two-fold:

1) During design a factor of safety was used which will be further discussed in Chapter 10. This means that the frame was inherently stronger than the required capacity thus reducing displacements,
2) During the selection of dissipative reinforcing and initial post-tensioning values the standard practice of ensuring capacity was greater than demand was used. This meant that in all cases connections were stronger than demand adding further strength.

Figure 9.9 also displays significant variation in average drift which is due to earthquake selection. During the selection of the seismic input used for the post-tensioned timber frame testing presented in Chapter 6 the average spectral acceleration of the set of seven earthquakes was compared against the code acceleration spectrum. Figure 9.10 shows the spectral displacements of the set of seven earthquakes used for shaking table testing and the parametric analysis. In addition, Figure 9.10 shows the range of initial period of the three, five and seven storey parametric frame structures taken from the non-linear time history models.

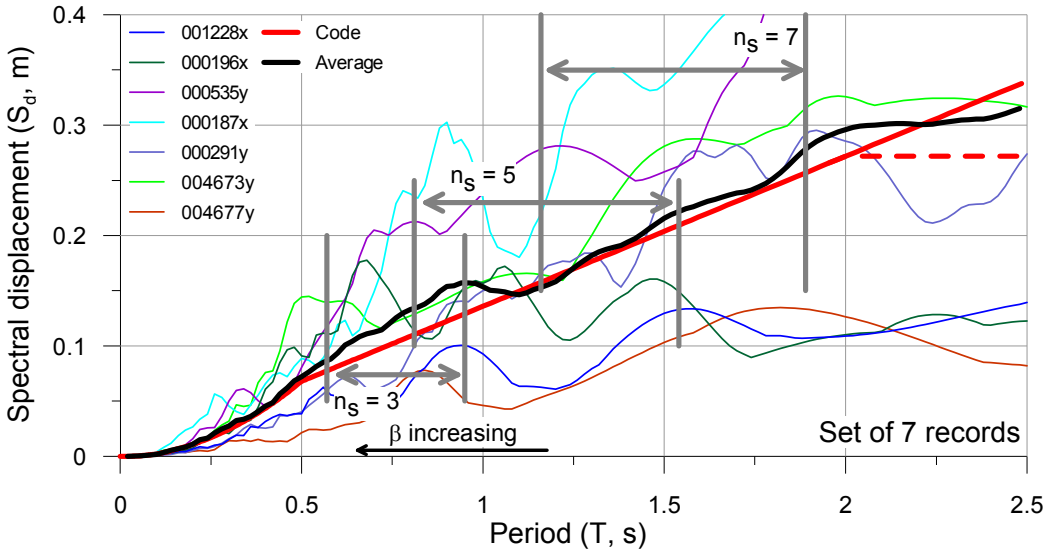

Figure 9.10. Spectral displacement of selected earthquake inputs for shaking table testing and parametric analysis

Figure 9.10 shows that over two period ranges (≈ 0.6 s to 1 s and 1.6 s to 2.3 s) the average displacement spectrum of the set of seven earthquakes, specifically the

000187x and 000535y records, used for the parametric analysis does not match well the displacement spectrum. The first zone of elevated spectral displacement impacted strongly on the response of the three storey structures leading to the elevated first floor drift response of these structures. This has impacted less on the $\beta = 1.0$ cases due to their larger section sizes (and thus lower initial periods) which meant they were further away from the high displacement demand area.

The second area of increased spectral displacement occurred over a section of the seven storey structure period range and thus an increase in drift for the higher period (low β) was also observed.

From these observations it can be concluded that if during design NLTH analysis is to be used in order to assess likely frame drift response consideration of the displacement demand must also be made when selecting suitable input accelerograms. Due to the increased flexibility of post-tensioned timber frames displacement is likely to be a critical factor. As shown in this section scaling a set of earthquakes to the acceleration design spectrum as specified by most design codes (NTC08 2008; NZS1170.5 2004) may not lead to an adequate fit in terms of displacement demand. However, it is considered to be appropriate that this practice remain thus keeping the scatter typical in earthquake ground motion and representative of the uncertainties in ground motion response. This will likely provide the same scatter in response observed during this study which is then check against maximum limits. If displacement response is found to be excessive, the displacement spectrum should be checked to ensure that demands are not excessive

9.5.4 Base shear results of NLTH analysis of parametric post-tensioned timber frames

Displacement Based Design (DBD) was used in order to calculate the values of design base shear which were then distributed through each of the parametric frames in order to calculate beam shears and moment demands. Section 9.4.1 discussed the results of the DBD and presented the design base shears for each of the parametric frames. Figure 9.11 displays the design base shears calculated using DBD as solid lines and the average maximum base shear from the Non-Linear Time History (NLTH) analysis as points.

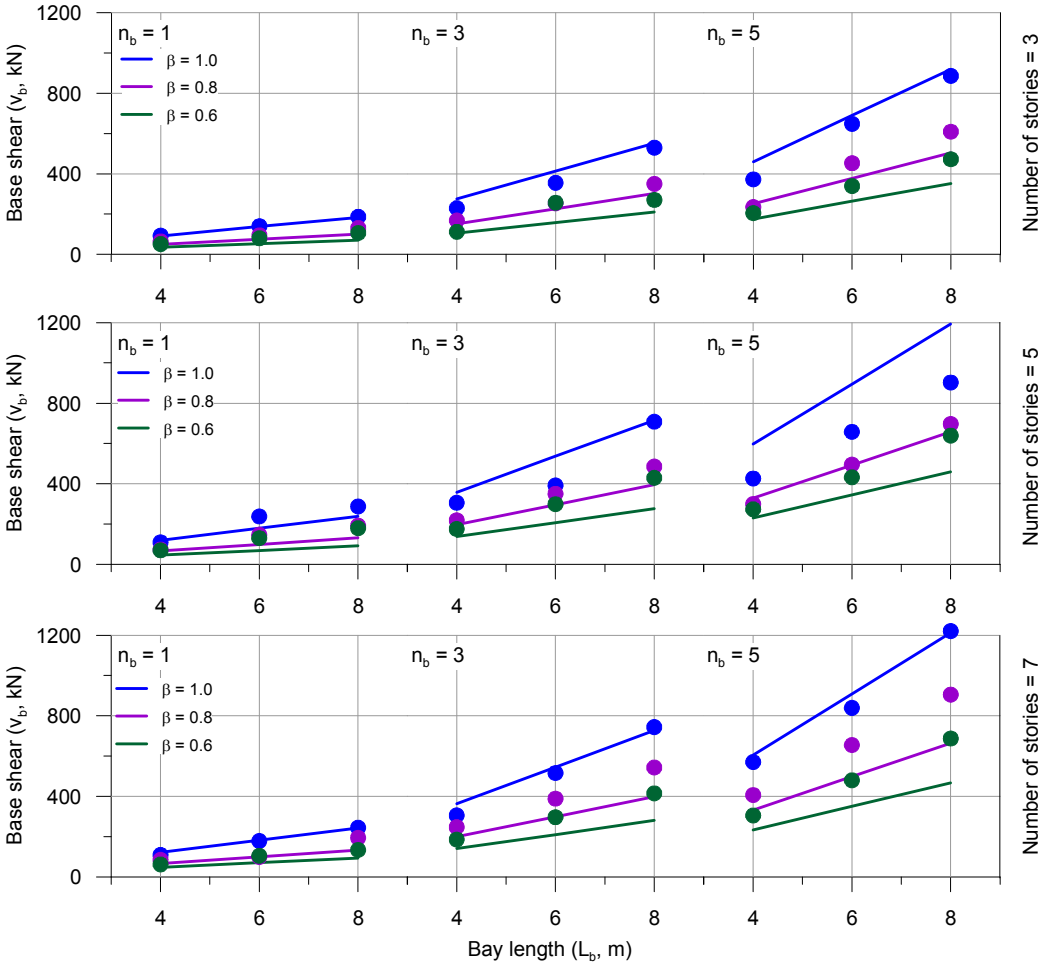

Figure 9.11. Comparisons between frame DBD parametric base shear and NLTH analysis results

Figure 9.11 shows reasonable agreement between the base shear calculated through the use of DBD and the NLTH results. Figure 9.12 shows the ratio between the DBD and NLTH values which averaged 1.1. Figure 9.12 also shows that the frames having high values of β provided comparisons against the NLTH results which tended to be more conservative than those with lower values of β. Although this may indicate that some of the assumptions surrounding the calculation of the impact of hysteretic damping on frame demand are not conservative, it is more likely that this is related to the set of earthquakes used in the analysis. This point does however require further study.

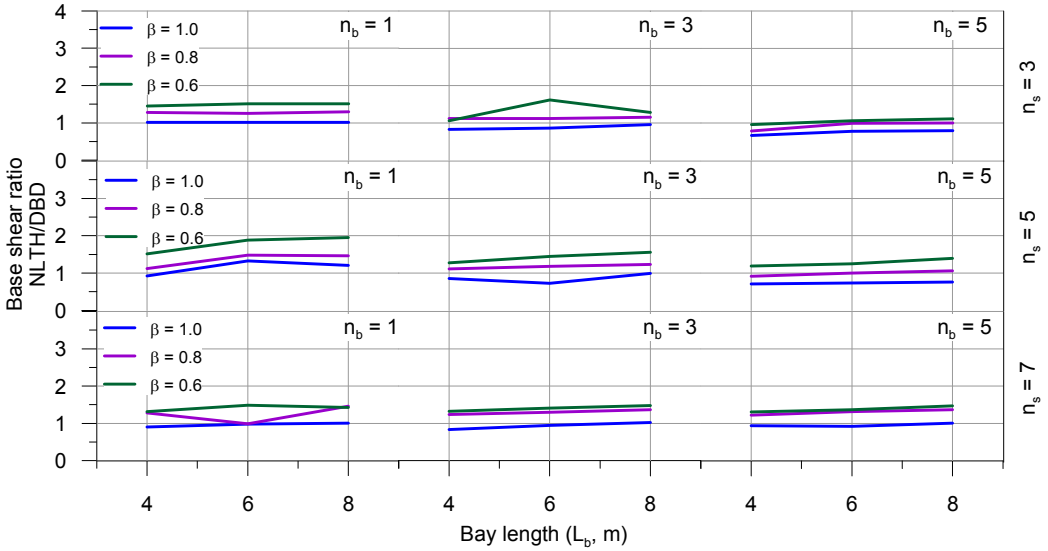

Figure 9.12. Ratio between frame DBD parametric base shear and NLTH analysis results

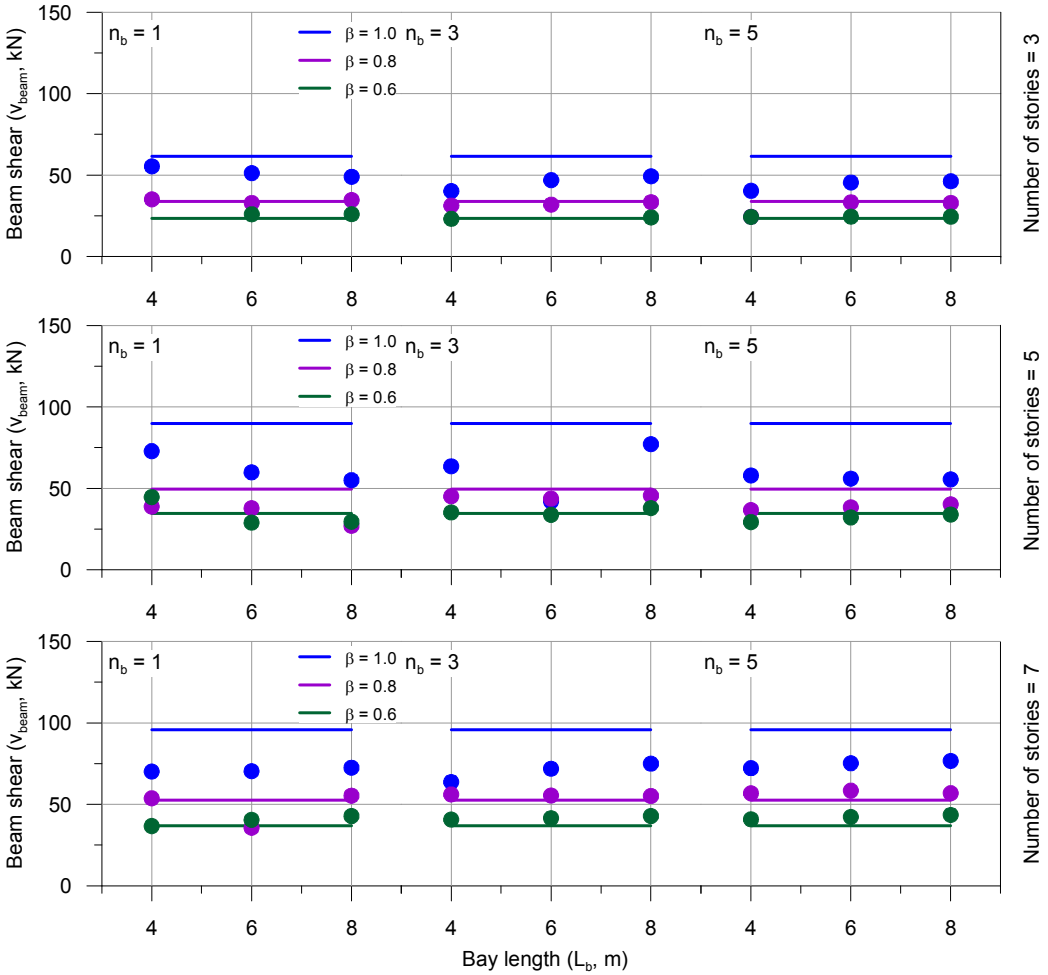

Figure 9.13. Comparisons between frame DBD parametric level one beam shear and NLTH analysis results

Figure 9.13 shows that the beam shear values provided by the NLTH analysis were significantly more conservative (average ratio 0.87) than the base shear values.

The beam and column section sizes, initial post-tensioning values and dissipative reinforcing design were selected using the moment demand at the beam-column joint interface which is related to the beam shear. Thus the base shear value calculated using DBD, which provided a sufficiently accurate prediction of beam shear, were conservative for use during post-tensioned timber frame design. The increased column shears observed in Figure 9.11 and Figure 9.12 were related to the impact of the higher modes on the frame response that are discussed further in Section 9.6.

9.5.5 Acceleration results of NLTH analysis of parametric post-tensioned timber frames

Post-tensioned timber is a low damping system and can be at risk to excessive amounts of acceleration. Figure 9.14 displays the average top floor acceleration results provided by the NLTH analysis of the post-tensioned timber frames.

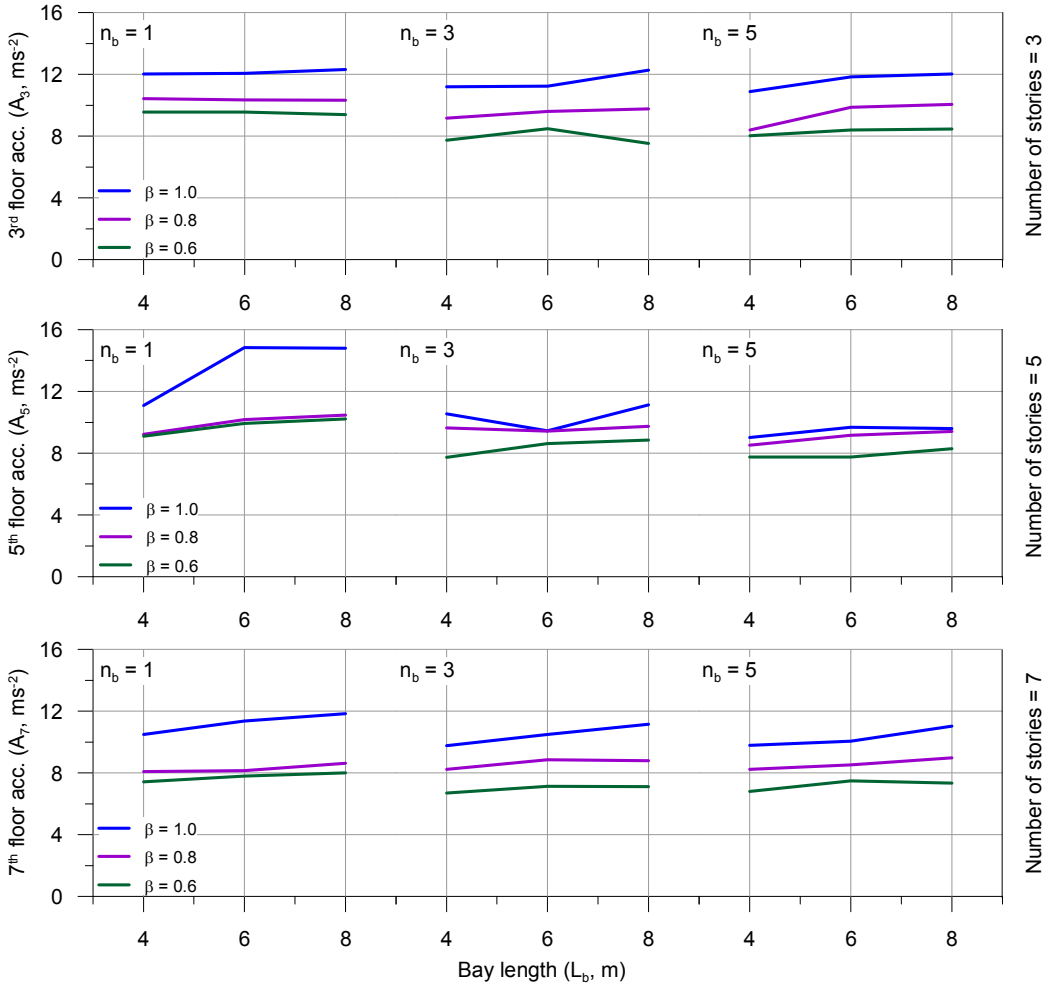

Figure 9.14. Average top floor accelerations from NLTH analysis of parametric frames

Chapters 6 and 7 have discussed the way in which a post-tensioned timber frame reduces accelerations through non-linearity (created by gap opening and non-linearity in dissipative reinforcing) and damping (through the hysteretic energy absorption of dissipative reinforcing). Figure 9.14 shows a maximum top floor acceleration of 14.84 ms^{-2} (1.5 g) was registered across all permutations. This was also the maximum average acceleration registered at any floor during the NLTH analysis.

The acceleration values from the NLTH analysis of the frames showed similar trends to the base shear calculated using DBD (Figure 9.3). Allocating 20% of the moment capacity to the dissipative reinforcing resulted in an average 17% reduction in acceleration. Allocating 40% of the moment capacity to the dissipative reinforcing resulted in an average 27% reduction in acceleration. Maximum average accelerations did not vary greatly with increases in either bay length or number of bays.

9.5.6 Ductility demand results of NLTH analysis of parametric post-tensioned timber frames

Section 9.3 described the assumptions made in the design of the parametric post-tensioned timber frames. One of the crucial assumptions made was the frame ductility which was set as $\mu = 2$. This ductility was then used in order to calculate the impact of damping on the frame response.

Several chapters have highlighted the impact that the elastic rotations of post-tensioned timber frames have on damping stating that excessive elastic deformations reduce damping. Elastic rotations reduce damping by reducing the ductility demand impacting on non-linearity and hysteretic energy release.

In order to ensure a displacement ductility $\mu = 2$ was obtained, the elastic deformations under design loading were limited to 0.6% ($1/3^{rd}$ of the total design drift) through the sizing of the beam and column members. The average ductility demand of the external beam-column joint from the NLTH analysis is shown in Figure 9.15. This was calculated by dividing the average maximum beam-column interface rotation from the NLTH analyses by the yield rotation of the first floor spring.

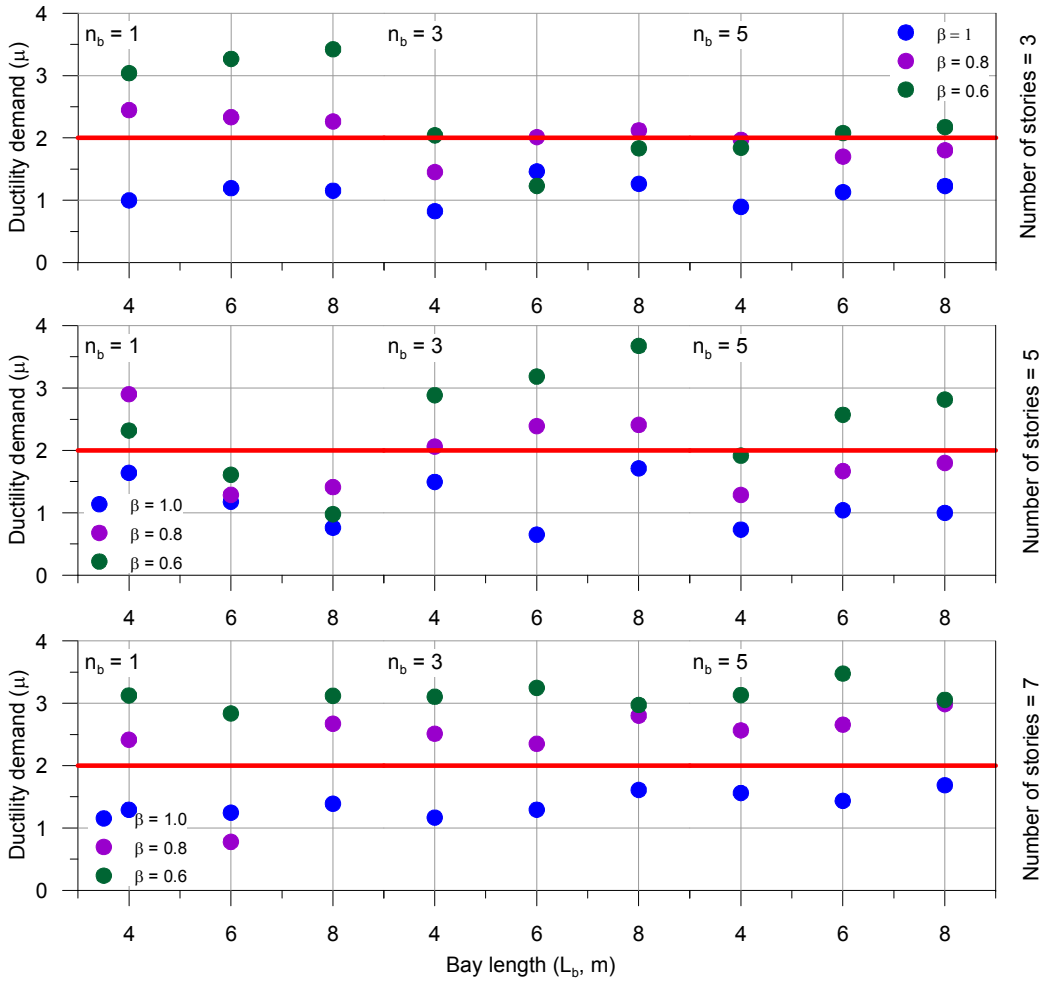

Figure 9.15. Average displacement ductility demand from NLTH analysis of parametric frames

Figure 9.15 shows that imposing the limit of 1/3rd of the total design drift was not successful in ensuring that a ductility of at least $\mu = 2$ was obtained at the first level. This in part has been created by the reduced levels of maximum drift created by the points discussed in Section 9.5.3. Average ductility values of 1.99 were, however, recorded across all permutations indicating that overall the strategy of reducing elastic drift levels to control ductility works well.

It is important to note that Figure 9.15 shows the first floor ductility demand and not the ductility demand of the entire frame which is the factor considered during design.

9.6 THE EFFECTS OF HIGHER MODES ON POST-TENSIONED TIMBER FRAMES

Higher modes refer to frame vibration frequencies beyond the first mode. These modes have high frequencies (and thus lower periods) than the principal mode.

During seismic motion it is principally the first mode of vibration that is excited and thus dominates frame response. However, as systems become taller and more flexible the frequencies of the higher modes decrease and begin to influence frame response. This creates accelerations and displacements which do not adhere to the shape of the first mode (Figure 9.16).

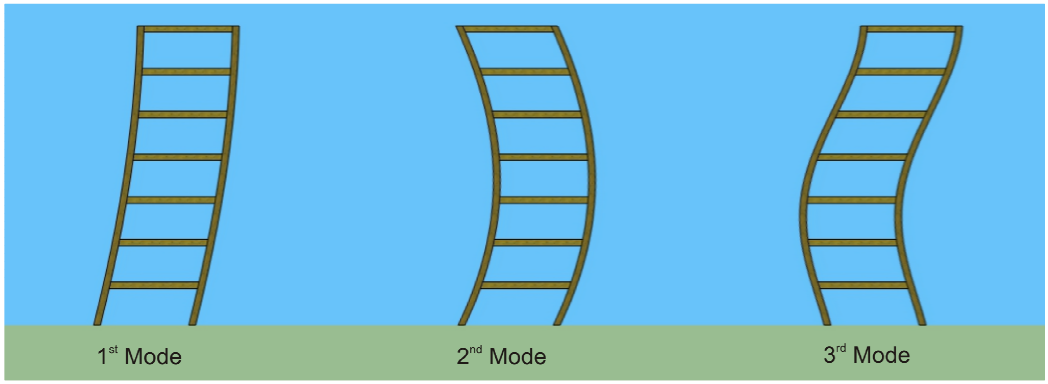

Figure 9.16. First, second and third mode shapes in post tension timber frames

Force Base Design (FBD) and Displacement Based Design (DBD) both assume that the first mode is dominating frame response (assuming a SDOF system). This not only influences the base shear calculation but also the way in which the base shear is distributed throughout the building and thus internal design forces.

Section 6.7.2 discussed the clear evidence of high modes influencing the column shear of the post-tensioned timber test frame. Higher modes have also been discussed in Section 9.5.4. Figure 9.13 showed however that these column shears did not impact on the beam shear and thus beam-column moment demand, initial post-tensioning or dissipative reinforcing quantities. Higher modes will impact on floor accelerations thus impacting on diaphragm forces, column shears and foundation design through increased base shear.

Although the design of the foundations and diaphragms to resist these forces will not be covered, this section will look at the parametric frame cases where higher modes had a significant impact on frame response and discuss how these higher modes should be addressed during design frame member design.

9.6.1 Higher modes observed in parametric post-tensioned timber frames

Higher modes influenced the parametric frame response through the deviation of frame accelerations and displacements (and thus drifts) from the assumed first mode

shapes. When frame response is first mode dominant, accelerations and displacements increase up the building height. The influence of higher modes alters this trend.

Influence of higher modes on floor acceleration

Figure 9.17 shows the strong motion floor acceleration results of the parametric frame case n_b = 3, n = 7, L_b = 6 m, β = 1.0 when subjected to the 000196x ground motion. The figure clearly displays the influence of the higher modes on the frame acceleration response. In Figure 9.17 the response of the first, second and third modes are indicated on the graph.

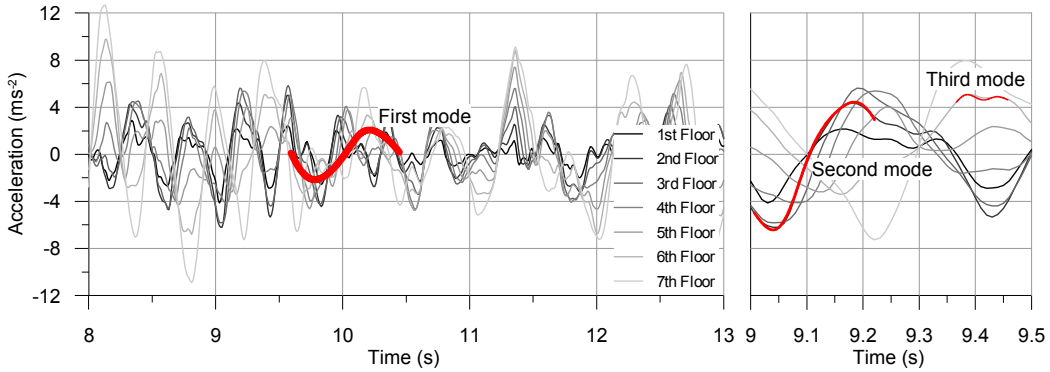

Figure 9.17. Floor acceleration response of frame n_b = 3, n = 7, L_b = 6 m, β = 1.0 to earthquake 000196x

Higher modes impact on the floor level which provides the maximum acceleration response. When the first mode is dominant, maximum acceleration occurs at the top storey of the frame. The presence of higher modes alters this with maximum accelerations occurring in other floors up the height of the frame. This has been used in order to gauge the effects of the studies parameters (n_b, n, L_b, β) on the presence of higher mode accelerations in post-tensioned timber frames. Figure 9.18 shows the ratio between the top floor average acceleration (which would be the maximum in a first mode dominated frame) and the maximum average acceleration across all levels. The floor at which the maximum average accelerations occurred is shown beside each point on the graph.

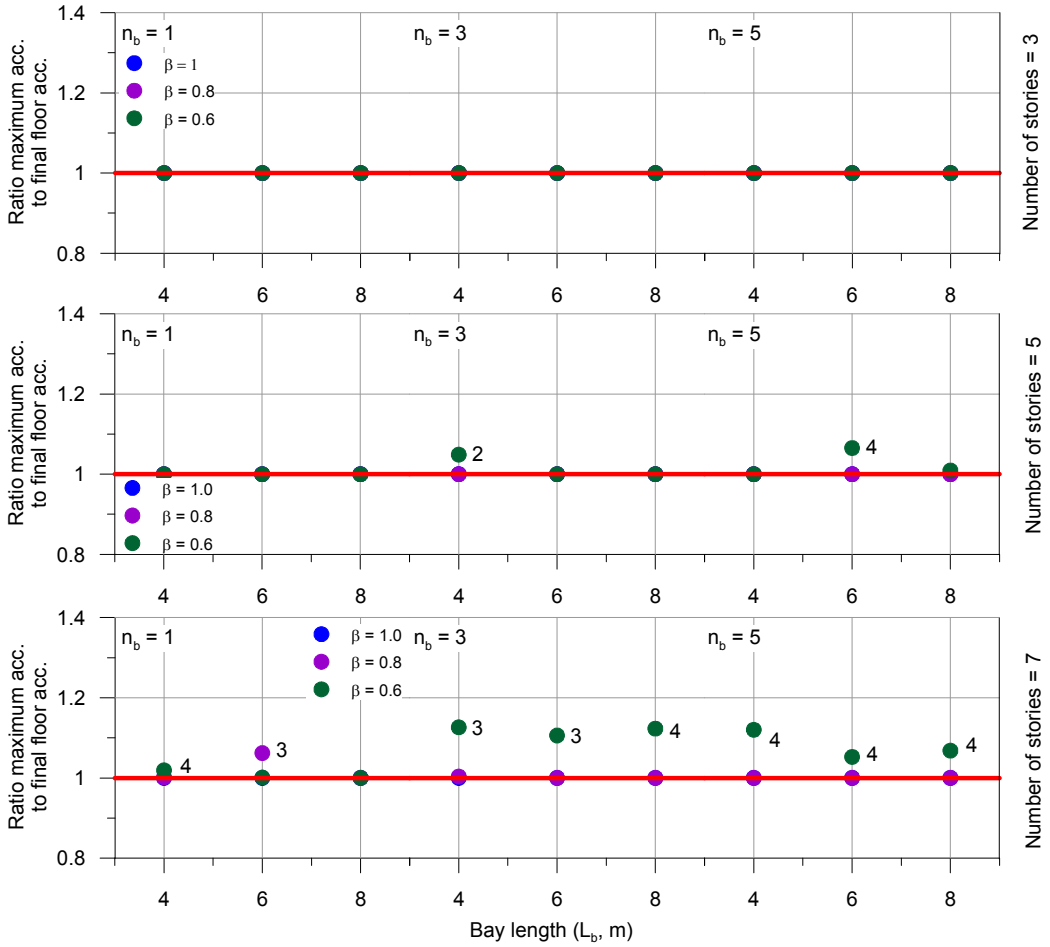

Figure 9.18. Presence of higher mode accelerations in parametric post-tensioned timber frames (numbers indicate floor at which maximum average acceleration occurred)

Figure 9.18 shows that higher modes impacted on the accelerations for several of the parametric frames. Higher modes had the smallest impact on the three storey frames with higher modes becoming more relevant with increasing building height. The results shown in Figure 9.18 suggested that variations in the recentering ratio and bay length do not impact on the presence of high mode accelerations in post-tensioned timber frames. The observation that recentering ratio does not impact on higher modes is contrary to the observations made during frame testing and requires further investigation. The results shown in Figure 9.18 also suggested that the number of bays did not impact on the presence of higher modes which also contradicts expectations and requires further investigation.

Figure 9.19 further highlights the impact that higher modes had on the acceleration response of the frames showing maximum accelerations at each floor for the 3, 5 and 7 storey, 3 by 4 m bay structures with $\beta = 0.8$. It can clearly be seen in this figure that

as the number of stories increased the second mode shape impacted on accelerations. This led to acceleration forms up the structure similar to the displaced shapes shown in Figure 9.16.

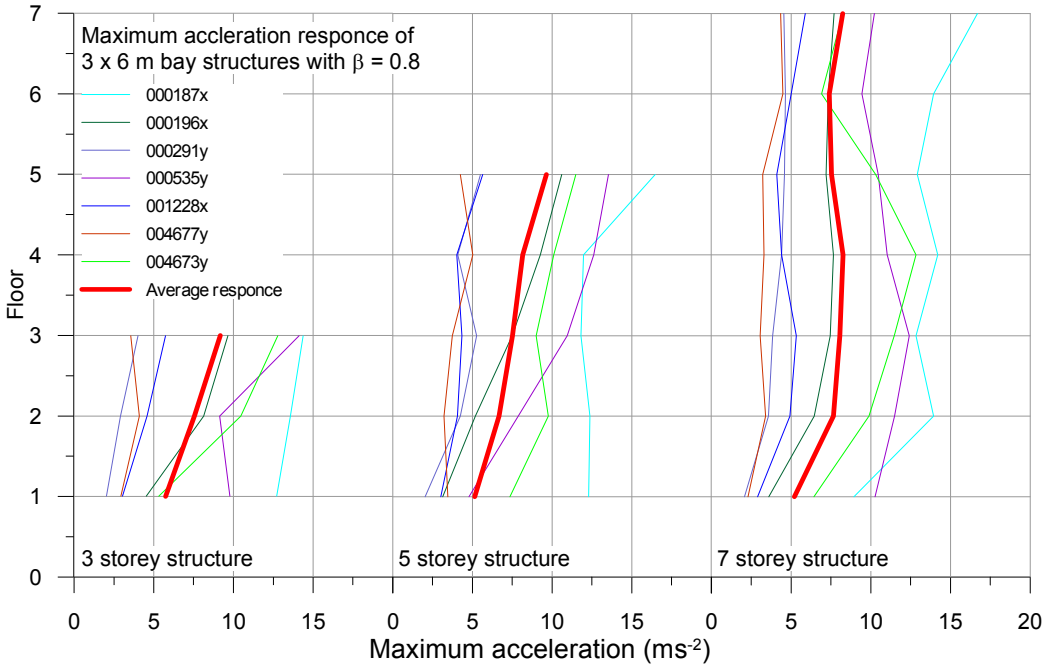

Figure 9.19. Maximum acceleration NLTH results for the 3, 5 and 7 storey 3 by 4 m bay structures with $\beta = 0.8$

Accelerations influence the amount of loading which must be transmitted through the floor diaphragm to the post-tension timber frame and higher modes must be considered. This is the subject of an on-going study at the University of Canterbury.

Influence of high modes on column shears

The increased accelerations which have occurred in the frames due to higher modes created forces in the columns that, in some cases, were above those provided by Displacement Based Design (DBD). Figure 9.20 shows the ratio between the column shears provided at each level by DBD and the maximum average column shear at each level provided by Non-Linear Time History analysis.

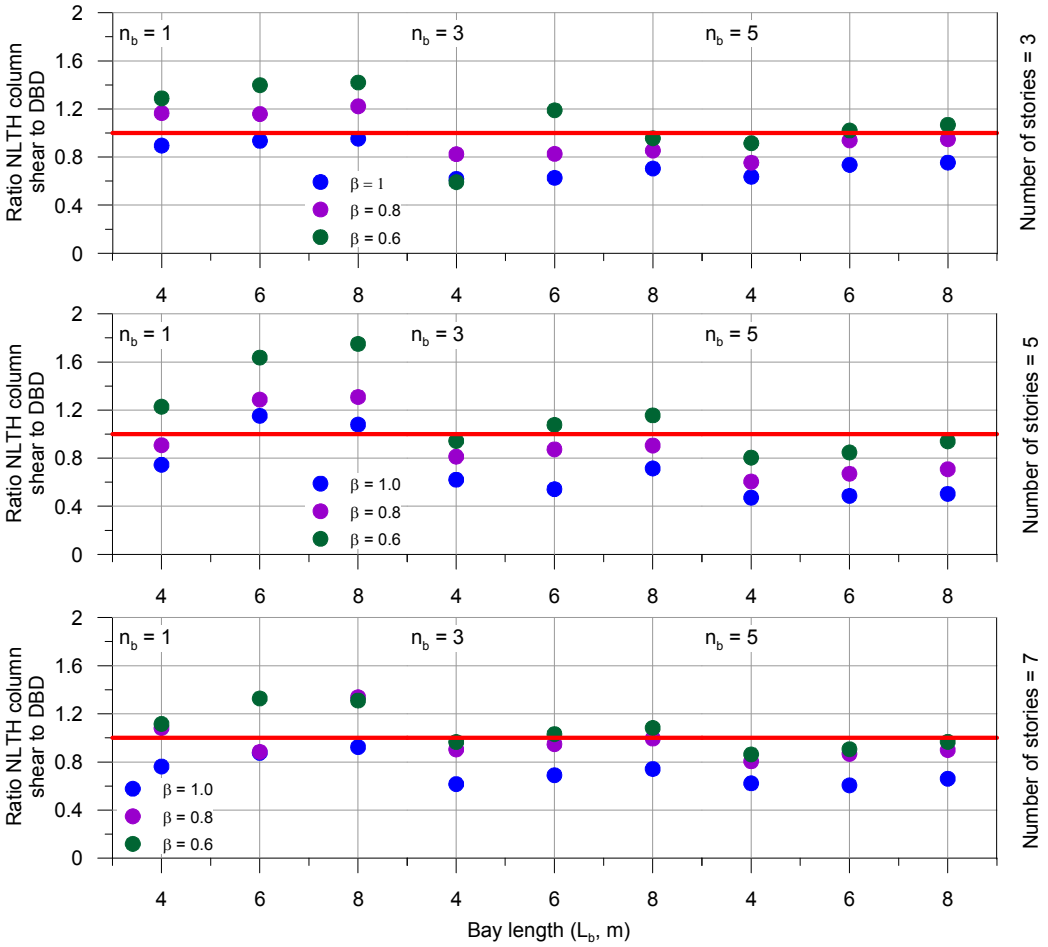

Figure 9.20. Ratio between column shears provided by DBD and NTLH analysis

Figure 9.20 shows that a maximum ratio between the maximum column shear provided by DBD and the NLTH results of 1.8 was obtained, however, mostly column shears were within DBD predicted values.

The ratio between the DBD and NLTH column shears increased as more moment capacity was allocated to the dissipative reinforcing (i.e. decreasing levels of β). Average ratios of 0.7, 0.9 and 1.1 were recorded for β = 0.6, 0.8 and 1, respectively. This is likely due to the fact that decreasing the recentering ratio impacted on the overall shear in the column (as shown in Figure 9.11) however did not, in this study, reduce the impact of the higher modes. Thus the additional shears provided by the higher modes made up a larger proportion of the total shear for the low β cases leading to larger ratios. Allowing for these higher column shears in design is discussed in Section 9.6.2.

Influence of higher modes on interstorey drift

As with floor accelerations higher modes impact, though to a lesser extent, on floor displacements and thus interstorey drifts. Figure 9.21 shows the strong motion floor drift results of the parametric frame cases n_b = 3, n = 7, L_b = 6 m, β = 1.0 when subjected to the 000196x ground motion over the same time period as shown in Figure 9.17.

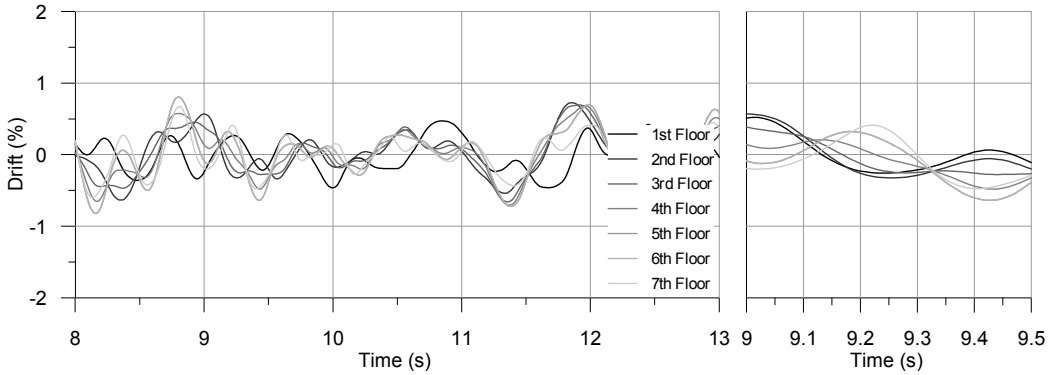

Figure 9.21. Interstorey drift response of frame n_b = 3, n = 7, L_b = 6 m, β = 1.0 to earthquake 000196x

As expected, the interstorey NLTH results shown in Figure 9.21 were smoother than the acceleration response however the effects of the higher modes were still evident.

As with the accelerations this impacts on where the maximum drift occurs in the frame. Figure 9.22 shows the ratio between the first floor drift (which would be the maximum in a first mode dominated frame) and the maximum drift across all levels. The results shown support the observation made from Figure 9.21 that the accelerations in the frame were more susceptible to higher modes than the frame drifts. Higher modes did not impact on frame drift for any of the three storey cases. Higher modes did impact slightly on the drift response for the five and seven storey cases and the anomalies noted for the 5 storey single bay case were again highlighted. The bay length did not impact on the higher mode drifts however there was a general indication that increasing the factor β increased the ratio between the first floor drift and the maximum drift.

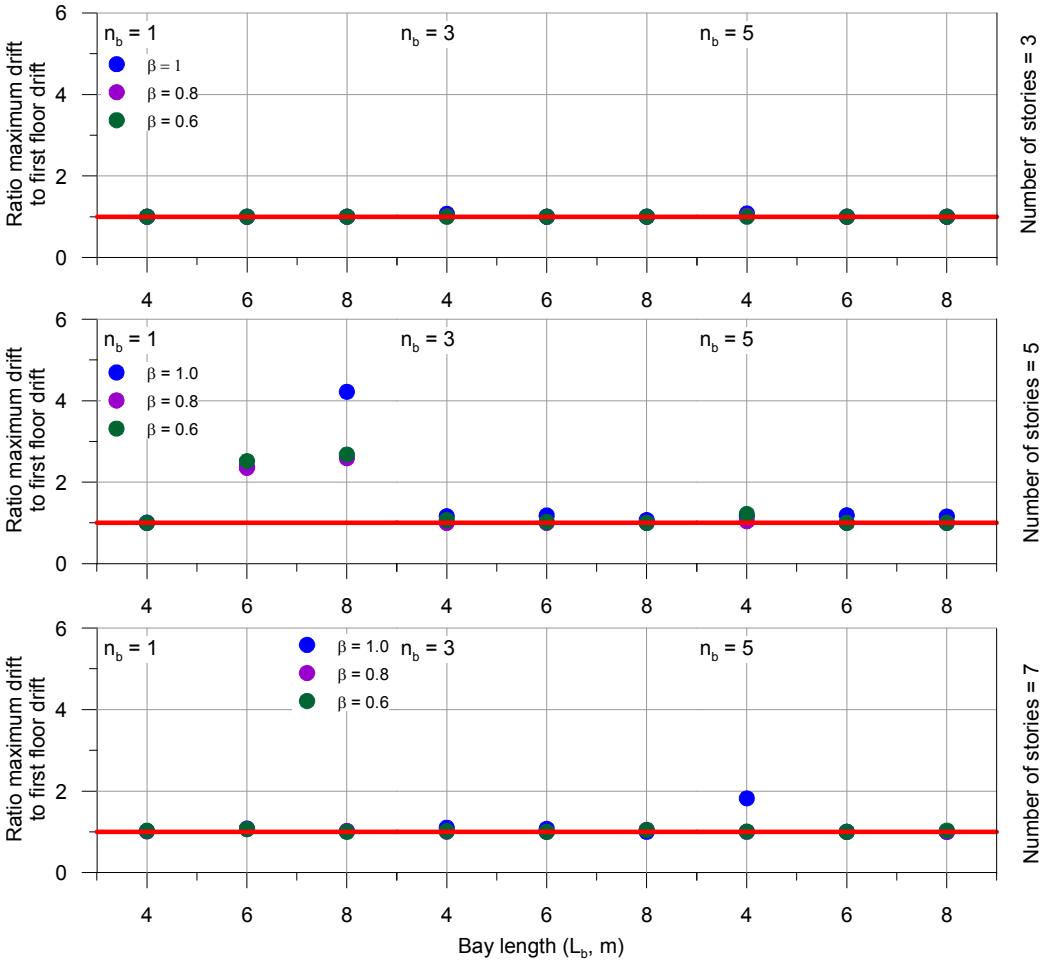

Figure 9.22. Presence of higher mode drifts in parametric post-tensioned timber frames

9.6.2 Allowing for higher modes in post-tensioned frame design

Section 9.6.1 described the impact that modes beyond the first mode had on the response of the parametric frames. It is important to note that due to the inherent flexibility of timber as a material, higher modes will impact on the response of most post-tensioned timber frames and must be assessed in order to judge their significance.

Section 9.5.4 showed that higher modes did not impact on beam shear and therefore do not need to be considered when designing beam and column sizes or initial post-tensioning and dissipative reinforcing values.

Section 9.6.1 showed that the higher modes did have an impact on column shear and therefore require consideration when verifying column shear and moment capacity. Newcombe (2012) suggested a series of factors in order to account for the impact of

high modes on column shear and moment demand which have been reviewed using the results of the Non-Linear Time History analysis of the parametric frames.

Firstly the dynamic amplification factor for higher mode effects (ω_f) must be calculated. This formula also includes an overstrength factor, ϕ_o. In the post-tensioned timber design guidelines (STIC 2013) a value of $\phi_o = 1.25$ has been suggested for post-tensioned timber frames. The dynamic amplification factor is then calculated as:

$$\omega_f = 1.66 + 0.13\left(\frac{\mu}{\phi_o} - 1\right) \quad \textbf{(9.1)}$$

Using the design ductility of $\mu = 2$ Equation (9.1) provided results of $\omega_f = 1.74$. The use of this amplification factor in the calculation of the moment demand is discussed in Section 10.3.2.

Newcombe (2012) also suggested a formula in order to calculate the column shear demand (V^*_{col}):

$$V^*_{col} = \phi_o V_E + 0.1\mu V_E \quad \textbf{(9.2)}$$

Where:

V_E = The column shear demand provided by the considered seismic load (kN)

Equation (9.2) essentially provides an amplification of V_E of $\phi_o + 0.1\mu$. Using the design level ductility of $\mu = 2$ provides an amplification of 1.45 which is conservative for the frames designed. These recommendations have been based on the parametric cases provided which contained only one value of target ductility $\mu = 2$. Further analysis is required in order to confirm the observations made.

9.7 ELASTIC SPECTRUM REDUCTION FOR THE FORCE BASED DESIGN (FBD) OF POST-TENSIONED TIMBER FRAMES

The parametric frames described in this chapter were designed using displacement based design and incorporated that procedures method of allowing for non-linear behaviour and ductility. The performance of the parametric frames has confirmed the adequacy of these procedures.

Chapter 7 discussed the Force Based Design (FBD) method of estimating seismic demand and Section 7.6.1 presented two methods which can be used to account non-linear behaviour and ductility in FBD: the method presented in the New Zealand code NZS1170.5 (2004) and the alternative method presented by Cardone et al. (2008). Both of these methods provide reduction factors, based on system displacement ductility, which are applied to the elastic design spectrum in order to define an inelastic spectrum. These factors are therefore a ratio between the elastic spectrum at the fundamental period (T_1) and the proposed non-linear response of the structure.

Figure 9.23 shows the ratio between the acceleration base response and the elastic response (at T_1) of each parametric frame. The base acceleration response was calculated by dividing the maximum base shear response of the structure by the structural mass. The spectral acceleration of each frame (i.e. acceleration from the acceleration spectrum at T_1) was then divided through by the base response giving:

$$Ratio = \frac{S_a(T_1)}{V_{b,\max} \Big/ \sum_{n=1}^{i} m_i} \qquad \textbf{(9.3)}$$

Where:

$S_a(T_1)$ = Elastic spectral acceleration at T_1 (g)

$V_{b,max}$ = Maximum base shear from NLTH analysis (kN)

m_i = Mass of floor i (t)

The maximum allowed values suggested by the NZS1170.5 and alternative procedures are also displayed in Figure 9.23. The design ductility of $\mu = 2$ has been used during these calculations.

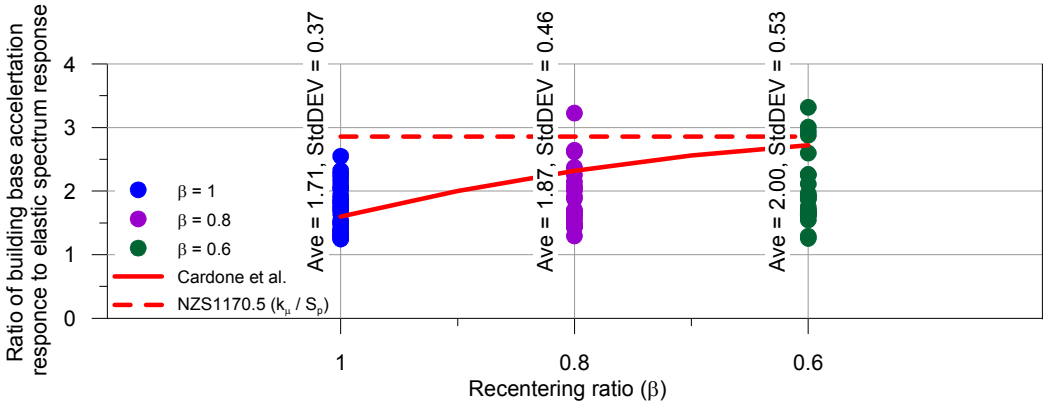

Figure 9.23. Spectral reduction factor for force based design, comparison with NZS1170.5 and alternative procedures

Figure 9.23 shows that the alternative procedure provided an indication of the general trend of values however was not conservative in its estimations.

As previously discussed in Chapter 7 the procedure suggested by NZS1170.5 became less conservative with increasing β values up to when β = 0.6 where the procedure approached the non-conservative predictions of the alternative procedure.

From these results it is suggested that with increased concentrated research effort the alternative procedure could be refined in order to provide conservative results and more accurate design. The procedure provided by NZS1170.5 should be used cautiously for high β values, especially if higher ductility levels are targeted. It is also noted that the base shear values used in this approximate evaluation included the higher mode response described in Section 9.6. The FBD design procedure is based on a SDOF assumption and as such future research should aim to isolate only the first mode for comparison.

9.8 CONCLUSIONS FROM CHAPTER 9

Chapter 9 has presented the design and analysis of 81 parametric post-tensioned timber frames. These frames have varied number of stories, number of bays, the length of these bays and the amount of dissipative reinforcing capacity. The chapter was divided into two parts, the design of the parametric frames using Displacement Based Design (DBD) and the analysis of these frames using Non-Linear Time History (NLTH) analysis. Finally the presence and impact of higher mode on the frame response was discussed.

Each of parametric frame was designed to a target level drift of $\theta_d = 1.8\%$. The DBD design procedure, in combination with the design decision to limit elastic rotations to approximately 0.6% provided beam and column section sizes, initial post-tensioning values and required quantities of dissipative reinforcing. Beam heights ranged between $h_b = 0.4$ m ($n = 3$, $\beta = 0.6$) and $h_b = 0.85$ m (levels 1 to 4, $n = 7$, $\beta = 1.0$). Beam areas ranged between $A_b = 0.12$ m^2 to $A_b = 0.425$ m^2 which was an increase of 250%. Beam height did not change with an increase in the number of bays however as expected an increase of bay length did lead to an increase in beam height (and therefore area). Decreasing the value of recentering ratio, β, from 1 to 0.8 led to a 27% reduction in beam area. Decreasing β from 1 to 0.6 led to a 42% reduction in beam area.

Similar trends were observed regarding the initial post-tensioning required to resist moment demand. Minimal change was noted with an increase in the number of bays and moderate increase (approximately 30%) with an increase in number of stories from 3 to 7. A significant increase in initial post-tensioning was observed with an increase in bay length. This was particularly important for the $\beta = 1$ post-tensioned only cases which are required to resist any additional moment demand only through increase in post-tensioning force. The effect of allocating a percentage of moment resistance to the dissipative reinforcing was twofold by decreasing demand and providing moment capacity. Decreasing post-tensioning forces is particularly important as the stresses they create can lead to significant long-term creep issues. Any reduction in post-tensioning force will mitigate these effects. Increases in the quantity of dissipative reinforcing required for the $\beta = 0.8$ and 0.6 parametric frames generally followed the same trends as observed for the initial post-tensioning force.

Following the DBD design of the post-tensioned timber frames NLTH analysis using the modelling techniques discussed in Chapter 8 was performed. The set of seven spectrum compatible earthquakes used during the dynamic frame testing described in Chapter 6 was applied to the frame and several key indicators were analysed.

DBD uses a target First Floor drift in order to provide seismic demand, therefore the first comparison made was that of the first floor drift. The first floor drifts of the frames were shown to be less than design values due to a series of design choices and safety factors.

Chapter 2 discussed how low damping systems, such as post-tensioned timber, can be susceptible to dangerous increases in acceleration. From the results of the NLTH analysis it was seen that the non-linearity of the post-tensioned timber frame is sufficient to keep floor accelerations within reasonable limits (maximum 1.5g corresponding to a record with PGA of 0.77 g). Allocating 20% of the moment capacity to the dissipative reinforcing resulted in an average 17% reduction in acceleration. Allocating 40% of the moment capacity to the dissipative reinforcing resulted in an average 27% reduction in acceleration.

One of the major focuses of Chapter 9 has been the assessment of the impact of higher modes on the response of post-tensioned timber frames. Methods of allowing for these higher modes in design have been discussed and presented in the form of amplification factors to be applied to column shears. These values proved conservative for the cases studied however further analysis is recommended.

Higher modes have also been shown to impact on the floor displacements of the n = 7 frames. These increased displacements led to increased drifts which would require careful consideration during the design of the non-structural elements (cladding etc.) for the already flexible post-tensioned timber frame system.

Finally the ratio between the elastic design spectra and the non-linear response of each of the parametric frames was calculated and compared with the two procedures presented in Section 7.6.1. The failure of the NZS1170.5 to account for the recentering ratio indicted that care should be taken in its use for low β (i.e. low damping) systems. The alternative procedure suggested by Cardone et al. (2008) provided non-conservative results but may be refined in order to provide a more robust estimation of this ratio in Force Based Design.

In conclusion from the design and NLTH analysis of 81 separate post-tensioned timber frames, the bay length and number of stories increases the section sizes and required moment capacity as expected for any structural system. The addition of dissipative reinforcing decreases section size and, more importantly, initial post-tensioning force. Higher modes have proven to be an issue in post-tensioned frame response and require careful consideration during design.

It is important to note that this parametric analysis has only considered one of the sources of building load: Ultimate Limit State earthquake loading. Serviceability earthquake loading and wind loading are likely to govern some of the tall cases studied and as such require further analysis.

REFERENCES CHAPTER 9

Cardone, D., Di Cesare, A., Ponzo, F. C., and Blonna, B. (2008). "Evaluation of Behaviour Factor for Flag-Shaped Hysteritic Models." International Conference on Engineering Optimization, Rio de Janeiro, Brazil.

Il Ministro delle Infrastrutture. (2008). "Norme Tecniche per le Costruzioni." Secondary Norme Tecniche per le Costruzioni, Secondary Infrastrutture, I. M. d., ed., Il Ministro delle Infrastrutture, Italia.

Newcombe, M. (2012). "Lateral Force Design of Post Tensiond Timber Frame and Wall Buildings ", University of Canterbury, Christchurch.

NZCS. (2010). *PRESSS Design Handbook*, New Zealand Concrete Society, Wellington New Zealand.

Pampanin, S., Palermo, A., and Buchanan, A. (2013). "Post-Tensioned Timber Buildings - Design Guide." Structural Timber Innovation Company, Christchurch, New Zealand.

Priestley, M. J. N., Calvi, G. M., and Kowalsky, M. J. (2007). *Displacement-Based Seismic Design of Structures*, IUSS Press.

Structural Timber Innovation Company Inc. (2013). "Post-Tensioned Timber Buildings - Design Guide." Structural Timber Innovation Company, Christchurch, New Zealand.

Standards New Zealand. (2004). "Structural Design Actions Part 5 : Earthquake Actions - New Zealand." Secondary Structural Design Actions Part 5 : Earthquake Actions - New Zealand, Secondary Zealand, S. N., ed., Standards New Zealand, New Zealand.

10 Procedure for the Seismic Design of Post-tensioned Timber Frames

10.1 INTRODUCTION

Each chapter of this thesis has looked into the assessment and prediction of the performance of post-tensioned timber frame structures with additional dissipative reinforcing. This final chapter will bring together the aspects discussed and present the procedure for the design of a post-tensioned timber framed building with dissipative reinforcing. A summary of the design of a post-tensioned timber frame is shown in Figure 10.1.

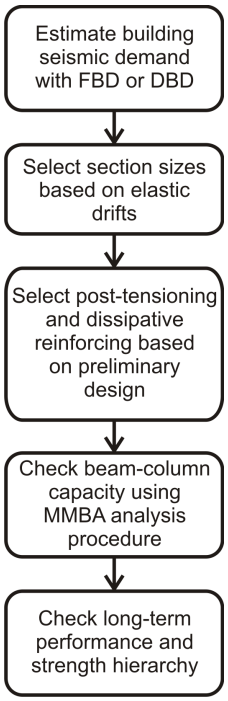

Figure 10.1. Summary of the design of a post-tensioned timber framed building

10.2 OVERVIEW OF POST-TENSIONED FRAME DESIGN

The design of a post-tensioned frame can be divided into two parts; determination of vertical and horizontal actions, and the sizing of beams, columns, post-tensioning and reinforcing in order to resist these actions.

10.2.1 Determination of vertical and horizontal actions

Determination of vertical actions is performed by using the tributary area of each column. Several methods exist for the determination of horizontal actions on post-tensioned timber frames; traditional Force Based Design (FBD, as already discussed in Section 7.7.1), Displacement Based Design (DBD, as already discussed in Section 7.7.2), and Corrected Force Based Design (CFBD presented by Sporn and Pampanin (2013)). The application of FBD and DDBD will be discussed in this chapter. A flow chart summary of the two methods used is presented in Figure 10.2 and discussed further in the following paragraphs.

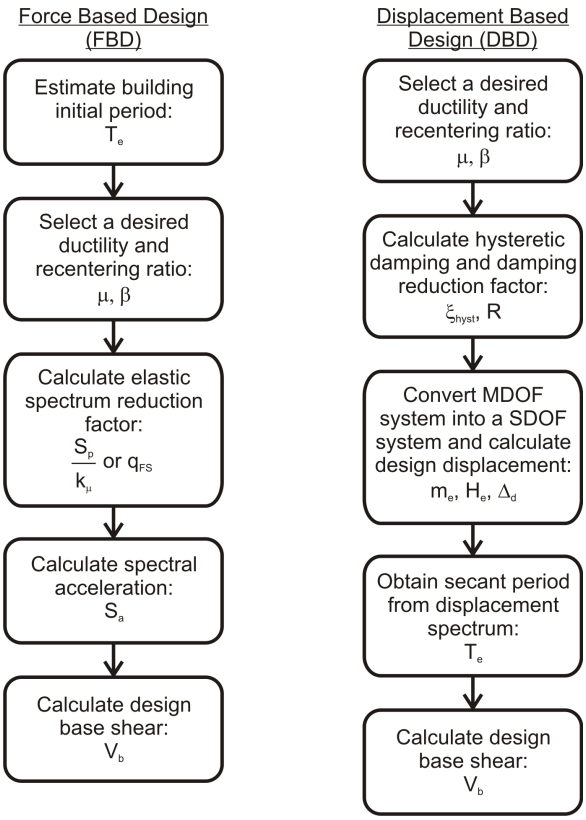

Figure 10.2. Flow chart summary of the application of FBD and DBD

Use of Force Based Design (FBD) for post-tensioned timber frames

The use of FBD in design requires a series of inputs as shown in Table 10.1.

Table 10.1. Inputs required for FBD of a post-tensioned timber frame

Inputs	
Building height	H_n
Building seismic mass	m
Recentering ratio (normally between 0.6-0.8)	β
Ductility	μ
Design hazard acceleration spectrum	S_a

Accurate calculation of the building period requires knowledge of section sizes however at this stage of design (i.e. before moment demand is calculated) it is unlikely that these will be known. Section 7.4 showed that the empirical method suggested by the New Zealand (NZS1170.5 2004) seismic code can be adequate for a first estimation of period:

$$T_1 = 0.11 H_n^{0.75} \tag{10.1}$$

Where:

H_n = Height to the uppermost seismic mass, normally the building height (m)

The procedure proposed by Cardone et al. (2008) for the reduction of the elastic spectrum in order to account for non-linear behaviour is based around the behaviour factor formula for an EPP system, q_{EPP}, as proposed by Newmark and Hall (1973):

$$q_{EPP} = \begin{cases} 1 & T = 0 \\ \sqrt{2\mu - 1} & T = T_g \\ \mu & T > T_C \end{cases} \tag{10.2}$$

Where:

T_g = Characteristic period of the ground motion (i.e. the period associated with the peak spectral acceleration taken as the beginning of the constant acceleration part of the code defined spectrum) (s)

T_C = Corner period associated with the transition between the constant acceleration and constant velocity part of the spectrum (s)

A correction factor is used in order to account for the flag shaped hysteretic behaviour presented by the post-tensioned timber system as follows.

$$q_{FS} = C_\beta q_{EPP} \tag{10.3}$$

$$C_\beta = -2\beta^2 + 1.8\beta + 1 \tag{10.4}$$

Where:

q_{FS} = The structural behaviour factor for the flag shape system

C_β = The q correction factor based on the recentering ratio of the frame (β)

This relationship is then corrected in order to allow for period variation:

$$C_\beta = \begin{cases} 1 & T = 0 \\ C_\beta & T = T_g \\ 1 & T = 0.8 \end{cases} \quad \textbf{(10.5)}$$

Use of Displacement Based Design (DBD) for post-tensioned timber frames

The use of DBD in design requires a series of inputs as shown in Figure 10.2.

Table 10.2. Inputs required for DBD of a post-tensioned timber frame

Inputs	
Building height	H_n
Building seismic mass	m
Recentering ratio (normally between 0.6-0.8)	β
Ductility	μ
Design hazard displacement spectrum	S_d
Outputs	
Base shear	V_b
Column centreline moment	M^*_{cl}

The fundamentals of the Displacement Based Design procedure are shown in Figure 10.3. The steps required for the application of DBD are listed below.

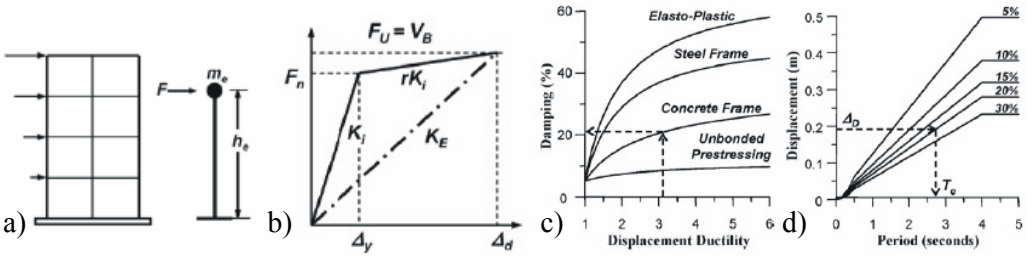

Figure 10.3. Fundamentals of Direct Displacement Based Design Procedure (Priestley et al. 2007)

Conversion of the MDOF system to a SDOF system (Figure 10.3a)

Firstly the normalised inelastic mode shape is calculated:

$$\delta_i = \frac{H_i}{H_n} \text{ For } n \le 4 \quad \textbf{(10.6)}$$

$$\delta_i = \frac{4}{3}\left(\frac{H_i}{H_n}\right)\left(1 - \frac{H_i}{4H_n}\right) \qquad \text{For } n > 4 \tag{10.7}$$

Where:

δ_i = Dimensionless normalised mode shape at floor i

H_i = Height at floor i (m)

H_n = Total height of the structure (m)

n = Total number of storeys in the building

This mode shape is then related to the displacement at the critical storey:

$$\Delta_i = \delta_i\left(\frac{\Delta_c}{\delta_c}\right) \tag{10.8}$$

Where:

Δ_i = Displacement at floor i (m)

Δ_c = Displacement at critical storey (based on the max inter-storey drift) (m)

δ_c = Value of dimensionless mode shape at critical storey

The design displacement of the single degree of freedom structure is then calculated:

$$\Delta_d = \frac{\sum_{i=1}^{n}\left(m_i\Delta_i^2\right)}{\sum_{i=1}^{n}\left(m_i\Delta_i\right)} \tag{10.9}$$

Where:

Δ_d = Design displacement of single degree of freedom structure (m)

m_i = Mass at storey i (tonnes)

Next the effective height and effective mass of the single degree of freedom structure is found:

$$H_e = \frac{\sum_{i=1}^{n}\left(m_i \Delta_i H_i\right)}{\sum_{i-1}^{n}\left(m_i \Delta_i\right)} \quad \textbf{(10.10)}$$

$$m_e = \frac{\sum\left(m_i \Delta_i\right)}{\Delta_d} \quad \textbf{(10.11)}$$

Where:

H_e = The effective height of the single degree of freedom structure (m)

m_e = The effective mass of the single degree of freedom system (tonnes)

Reduction of the elastic displacement spectrum to account for system damping (Figure 10.3b and c)

Displacement based design uses a reduction factor, R, which is a function of the total structural damping (Priestley et al. 2007):

$$R = \left(\frac{7}{2+\xi}\right)^{\alpha} \quad \textbf{(10.12)}$$

Where:

α = is equal to 0.5 and 0.25 for far-field and near field seismic spectra, respectively, (as defined by the local code)

ξ = the system damping ratio of the structure taken as a combination of the elastic damping ξ_{el} and the hysteretic damping ξ_{hyst}:

$$\xi = \xi_{el} + 0.7\xi_{hyst} = 0.03 + 0.7\xi_{hyst} \quad \textbf{(10.13)}$$

$$\xi_{hyst} = \frac{(2-2\beta)(\mu-1)}{\mu\pi(1+r(\mu-1))} \quad \textbf{(10.14)}$$

Calculation of secant system stiffness and base shear (Figure 10.3b and c)

The equivalent stiffness (K_e) of the structure is then found:

$$K_e = \frac{4\pi^2 m_e}{T_e^2} \quad \textbf{(10.15)}$$

From this the base shear is computed:

$$F = V_b = K_e \Delta_d \tag{10.16}$$

Distribution of base shear to determine internal moment demands

The outcome of each of these design methods the base shear (V_b) of the building in the direction of study. An assumption must then be made regarding the ability of the floor diaphragm to transmit load throughout a floor leading to a distribution of the total base shear throughout the frame. Discussion surrounding the rigidity of diaphragm is timber buildings is beyond the scope of this thesis which has made a rigid diaphragm assumption (i.e. total base shear is divided equally between the frames).

Now that a frame base shear has been found it must be distributed throughout the frame:

$$V_b = \sum_{i=1}^{n} V_n^i \tag{10.17}$$

Where:

V_n^i = Shear force at level i

n = Total number of floors

Distribution of the base shear up the frame can be done either following a triangular force distribution or a representation of the buildings first vibration mode and is normally a function of floor weight as a ratio of the total building weight. In most cases post-tensioned timber buildings will be low to medium rise and a triangular force distribution is correct. The current New Zealand seismic code (NZS1170.5 2004) redistributes 8% of the frame base shear to the top storey in order to allow for higher mode effects, this was adopted for the frame designs presented in Chapter 9 and is recommended given the significant impact higher modes have one post-tensioned timber frame response.

Now that base shear has been distributed up the structure it is distributed throughout the frame obtaining design moments. This can be done in two ways. The first method is to develop a simple elastic model, apply the base shear distribution up the frame, and thus obtain the beam and column moments and shears. The second method follows the equilibrium of forces throughout the frame proposed by Priestley et al.

(2007) and elaborated upon by NZCS (2010). The second method was used in the parametric analysis presented in Chapter 9.

Both of these methods require an initial estimate of column base moment capacity to be provided. This assumption has a significant effect on the beam and column demands within the frame. In order to reduce frame deflection it is recommended that the columns be provided with base moment capacity, how this is done is described further in Section 10.3 however for now a simple assumption is made. Given that a key design criterion states that no column hinge shall occur on the underside of the first floor we will set our point of contra-flexure at a height of 60% up the first floor height (i.e. 0.6H). Thus the required moment at each column base becomes:

$$M_b^i = 0.6V_b^i H \tag{10.18}$$

Where:

V_b^i = Base shear of column i

M_b^i = Base moment of column i

H = Interstorey height

As an initial assumption it is possible to say that the column shear will be equally distributed amongst the ground floor columns ($V_b^i = V_b$/number of columns).

Upon conclusion of the above procedure a moment demand at the centreline of the beam on each floor is found (M^*_{cl}). In multi-storey frames it is common practice to average out the demand over two or three storeys in order to minimise variability in system specifications.

10.2.2 Sizing of beams, columns, post-tensioning and reinforcing

From the procedure presented in Section 10.2.1 a moment demand (M^*_{cl}) at the centreline of the column at each level of the structure has been found. The frame must now be dimensioned in order to resist this demand. In reality it is envisaged that most designers who are familiar with the design of post-tensioned timber frames will have adequate understanding and design tools in order miss several of the design steps presented here, however, for completeness all steps are presented.

A flow chart summary of the full design procedure of a post-tensioned timber frame is presented in Figure 10.4. As shown this has been divided into two stages, preliminary

dimensioning and detailed design/final verification. Further discussion of the each step is presented in this section divided under these headings.

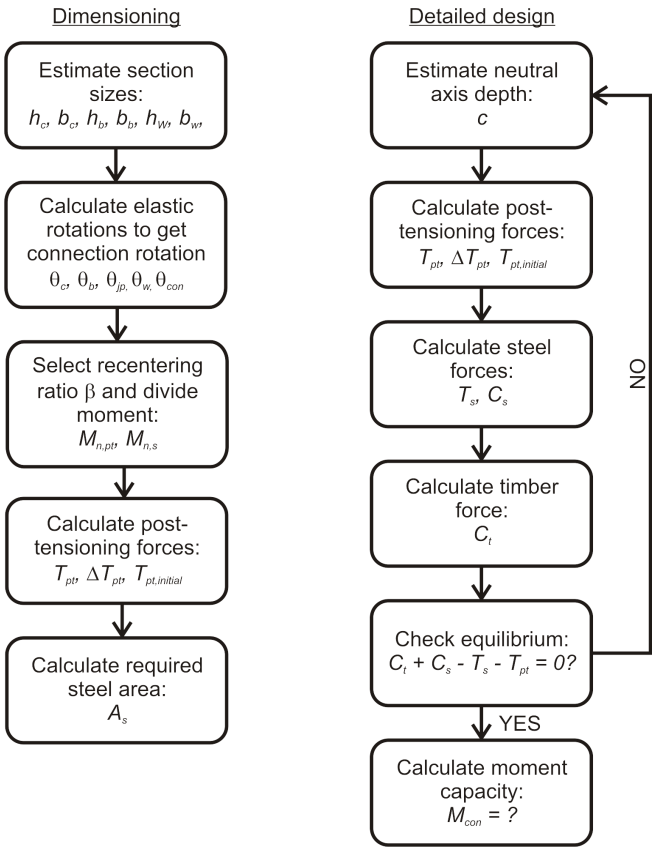

Figure 10.4. Flow chart summary of post-tensioned timber frame design procedure

For frames which have more than one bay it is recommended that design be performed for the internal beam-column joint. This is due to the fact that the elastic rotation of an internal beam-column are larger and therefore finding a suitable (in terms of required dissipation and capacity) solution for an internal beam column joint is normally the critical design case.

Preliminary design – beam and column dimensioning

This part of the preliminary design focusses on the initial selection of the physical beam and column characteristics shown in Table 10.3. Inputs for this design phase are also shown.

Table 10.3. Inputs required and outputs produced by beam and column dimensioning of post-tensioned timber frames

Inputs	
Moment demand	M^*_{cl}
Recentering ratio	β
Design drift	θ_d
Ductility	μ
Outputs	
Column section width	b_b
Column section height	h_b
Beam section width	b_c
Beam section height	h_c

The first step is the definition of the section sizes which adopt an approach based on limiting elastic displacement. As already discussed in Chapters 4, 5 and 7, elastic rotations play a significant role in the lateral response of a post-tensioned timber frame and excessive elastic deformations greatly hinder seismic response. It is likely that member sizes will be governed by elastic deflection and not moment or shear demand and therefore it is logical to design members for elastic limits.

As discussed in Section 5.4 the elastic rotations of post-tensioned timber frames are made up of beam (θ_b), column (θ_c) and joint panel (θ_j) contributions which are calculated about the beam-column centreline using Equations (5.47), (5.48) and (5.49) of Section 5.4.2. Selection of a limit to place on the elastic rotations will rely on the maximum design drift (θ_d) and selected ductility (μ) as discussed in Section 10.2.1. In order to ensure that the ductility used for design is obtained at the design drift the elastic rotations must be limited to less than the design drift divided by this 1.3 times this ductility ($\theta_{el} \leq \theta_d/1.3\mu$). When calculating the elastic rotations the moment demand used should be divided through by any force reduction factor which will be applied to the moment capacity of the beam-column connection (ϕ, in accordance with New Zealand practice and taken as 0.9 for post-tensioned timber systems).

Preliminary design – initial post-tensioning and reinforcing

This part of the preliminary design focusses on the initial selection of the post-tensioning and reinforcing characteristics shown in Table 10.3. Inputs for this design phase are also shown.

Table 10.4. Inputs required and outputs produced by preliminary design of post-tensioned timber frames

Inputs	
Moment demand	M^*_{cl}
Recentering ratio	β
Column section width	b_b
Column section height	h_b
Beam section width	b_c
Beam section height	h_c
Outputs	
Post-tensioning area	A_{pt}
Initial post-tensioning force	$T_{pt,initial}$
Tension force in steel reinforcement	Ts

Once beam and column geometries have been selected post-tensioning area (A_{pt}), initial post-tensioning force ($T_{pt,initial}$) and required tension force in steel reinforcement (T_s) are estimated. The required moment capacity provided by the post-tension (M^*_{pt}) and the reinforcing (M^*_s) are calculated using the re-centering ratio (β) as follows:

$$M^*_{pt} = \frac{\beta M^*_{cl}}{\phi} \quad \textbf{(10.19)}$$

$$M^*_s = \frac{(1-\beta) M^*_{cl}}{\phi} \quad \textbf{(10.20)}$$

Normally before calculating the connection moment demand the centreline moment demand will be translated out to the column face however this will not be performed during the preliminary design phase as the increase in rotation will be cancelled out in part by the interface compression deformation (θ_{int}) discussed in Section 5.3.4. This translation will be performed for the detailed design discussed later.

Terms used in the design of post-tensioned timber beam-column joints have been presented in Figure 5.1 of Section 5.3.2 and are presented again in Figure 10.5 for clarity.

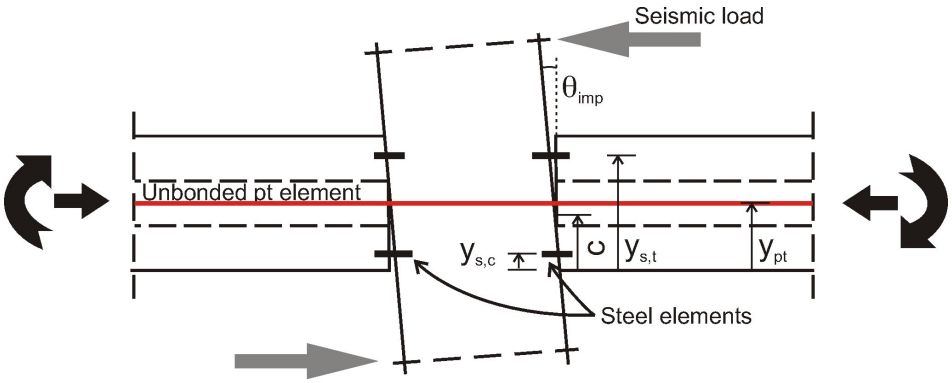

Figure 10.5. MMBA nomenclature for a beam-column joint

The imposed rotation (θ_{imp}, the gap rotation defined during section analysis, θ_{gap}) for the preliminary design is taken as the total rotation minus the beam, column and joint panel rotations calculated during the dimensioning of the beam and column.

In order to estimate the moment capacity a neutral axis depth (c) must be assumed. For a well design seismically dominated frame this will be approximately one third of the beam depth. As discussed in Section 5.3.2 at Ultimate Limit State (ULS) the timber should remain elastic and therefore a triangular stress block should be used meaning the moment capacity provided by the post-tensioning can be calculated as follows:

$$M_{pt}^{*} = T_{pt}\left(y_{pt} - \frac{h_b}{9}\right) \tag{10.21}$$

Rearranging Equation (10.21) the required post-tensioning force at ULS is found:

$$T_{pt} = \frac{M_{pt}^{*}}{\left(y_{pt} - \frac{h_b}{9}\right)} \tag{10.22}$$

The New Zealand concrete code (NZS 3101:1995 2006) places an upper limit on the stress in the post-tensioning at the target drift stating that the total stress in the tendon at the design rotation should not exceed 90% of its yield strength (f_y). The failure hierarchy of a post-tensioned timber frame is discussed further in Section 10.3; it states that the tendon should not yield under Maximum Credible Earthquake (MCE) loading. It is therefore recommended that at ULS the post-tensioning be keep below 70% of its yield strength, thus the required post-tensioning area becomes:

$$A_{pt} = \frac{T_{pt}}{0.7 f_y} \tag{10.23}$$

In order to estimate the initial post-tensioning force estimation must be made of the increase in the post-tensioning due to gap opening (ΔT_{pt}). In order to do this estimation must be made of the gap opening at the level of the post-tensioning (Δ_{pt}):

$$\Delta_{pt} = \theta_{imp}\left(y_{pt} - \frac{h_b}{3}\right) \tag{10.24}$$

Knowing gap opening at the single connection the total gap opening across the frame is found by multiplying by the number of gaps opened (n_{gap}) and the increment in strain in the post-tensioning is found. From this the increase in the post-tensioning force due to gap opening is calculated based on the post-tensioning unbonded length, l_{ub} (normally the total length of the post-tensioned frame).

$$\Delta\varepsilon_{pt} = \frac{n_{gap}\Delta_{pt}}{l_{ub}} \tag{10.25}$$

$$\Delta T_{pt} = \Delta\varepsilon_{pt} E_{pt} A_{pt} \tag{10.26}$$

The total post-tensioning force T_{pt} is made up of the post-tensioning force increase ΔT_{pt} and the initial post-tensioning force $T_{pt,initial}$. Therefore the initial post-tensioning force can be calculated as:

$$T_{pt,initial} = T_{pt} - \Delta T_{pt} \tag{10.27}$$

Estimation of the required force in the reinforcing is done by dividing the required moment (M^*_s) by the reinforcing lever arm (y_s).

$$T_s = \frac{M_s^*}{\left(y_s - \frac{h_b}{9}\right)} \tag{10.28}$$

Reinforcing falling into two main categories was presented in Chapter 3 and design recommendations were provided. Preliminary design using these two forms of reinforcing is as follows:

Angle reinforcing

Example design tables for the dimensioning of dissipative angle reinforcing have been presented in Section 3.6 and full design tables are presented in APPENDIX A. Equation (10.29) provides the estimated tension force required in the dissipative reinforcing by the beam-column joint. Knowing this tension force the design charts presented can be used in order to define required angle physical characteristics.

Fuse type reinforcing

It is suggested that an optimal strain in the tension reinforcing is 3%. This will correspond to a given level of stress (f_s) depending on the characteristics of the steel used. The required area of steel is calculated to be:

$$A_s \geq \frac{M_s^*}{f_s\left(y_{s,t} - y_{s,c}\right)} \qquad \textbf{(10.29)}$$

Where:

$y_{s,t}$ = Tension reinforcing lever arm

$y_{s,c}$ = Compression reinforcing lever arm

10.2.3 Detailed calculation of beam-column connection resistance

The procedure presented in Section 10.2.2 provides sizing of beam and column elements and initial values of post-tensioning and required reinforcement capacity. Beam and column sizes have been based on elastic deformation limits required to ensure adequate system performance. Initial post-tensioning force and required reinforcement has been based on an assumption of neutral axis depth that needs to be verified through the use of the Modified Monolithic Beam Analogy already discussed in Section 5.3.

Following the sizing of the beam and column elements and the initial definition of post-tensioning area, factors accounting for the interface compression deformation (k_{int} from Section 5.3.4) and frame shortening (k_{sho} from Section 5.3.5) are calculated. An initial estimation of the required quantity of column reinforcing is performed using the required post-tensioned tension force (T_{pt}) and the estimated neutral axis depth. Further discussion surrounding column face reinforcement is covered in Section 10.3. The interface deformation factor is calculated as:

$$k_{\text{int}} = \frac{1}{k_{scr} k_{ss}} \tag{10.30}$$

Where:

$$k_{ss} = \frac{h_c}{b_L \ln\left(\frac{h_c}{b_L} + 1\right)} \tag{10.31}$$

$$k_{scr} = 1 + 54 \frac{A_{scr}}{A_t} \left(\frac{l_s}{h_c}\right)^{1.26} \tag{10.32}$$

Where:

b_L = The length of the loaded area (taken as the beam height h_b) (m)

A_t = Total area in compression (m^2)

A_{scr} = Total area of screw reinforcing (m^2)

l_s = Total length of screw (m)

The frame shortening factor is calculated as:

$$k_{sho} = \frac{k_{pt,sho}}{k_{pt}} \tag{10.33}$$

Where:

$$\frac{1}{k_{pt,sho}} = \frac{1}{k_{pt}} + n_b \frac{1}{k_b} + n_{col} \frac{1}{k_c} \tag{10.34}$$

$$k_{pt} = \frac{E_{pt} A_{pt}}{l_{ub}} \tag{10.35}$$

$$k_b = \frac{0.7 E_{t,par} A_b}{L_b} \tag{10.36}$$

$$k_c = \frac{E_{t,perp} A_b}{k_{\text{int}} h_c} \tag{10.37}$$

Where:

n_b = Number of beams

n_{col} = Number of columns

$E_{t,par}$ = Average modulus of elasticity of timber parallel to the grain (kN/m^2)

$E_{t,perp}$ = Modulus of elasticity of timber perpendicular to the grain (kN/m^2)

A_{pt} = Area of post-tensioning (m^2)

A_b = Area of the beam (m^2)

L_b = Beam length (face to face) across the bay which the post-tensioning acts (m)

In Section 10.2.2 the rotation at the centreline of the column in the beam-column joint (θ_{cl}) was calculated by subtracting the elastic beam, column and joint rotations from the total interstorey drift rotation (θ_t). This centreline drift must be transposed in order to find the connection rotation (θ_{con}):

$$\theta_{con} = \frac{\theta_{cl}}{\left(1 - \frac{h_b}{L}\right)} \quad \textbf{(10.38)}$$

Where:

L = Bay length

The MMBA is based on the imposed rotation (θ_{imp}) which is equal to the centreline rotation minus the interface compression rotation (θ_{int}) discussed in Section 5.3.4 and calculated as:

$$\theta_{\text{int}} = k_{\text{int}} \frac{2T_{pt,initial} h_c}{E_{t,perp} h_b^2 b_b} \quad \textbf{(10.39)}$$

Where:

k_{int} = Interface compression factor which accounts for load shearing and interface reinforcement

E_{perp} = Perpendicular to the grain stiffness of the timber

This gives the imposed rotation (θ_{imp}):

$$\theta_{imp} = \theta_{con} - \theta_{\text{int}} \quad \textbf{(10.40)}$$

The use of the MMBA relies on a correct value of the neutral axis depth (c) being used such that the section, shown in Figure 10.6, is in equilibrium.

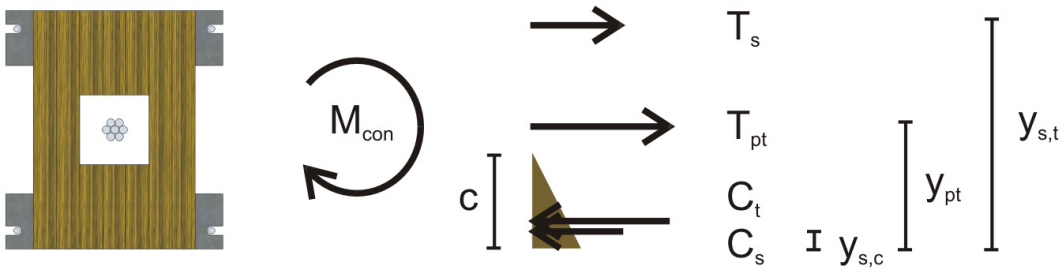

Figure 10.6. Equilibrium for a post-tensioned beam-column joint

The use of the MMBA in the design of post-tensioned timber systems has already been described in Section 5.3 however a brief summary, focused on use during design, is presented. Several iterations may be necessary to find equilibrium.

As during the preliminary design the additional post-tensioning force due to gap opening is calculated with the exception that the actual values of the neutral axis be used and not estimated as before. This correct value of neutral axis is found through iteration until equilibrium is reached.

$$\Delta_{pt} = \theta_{imp}\left(y_{pt} - c\right) \tag{10.41}$$

Now that a precise amount of gap opening has been calculated Equations (10.25) and (10.26) are re-used with the addition of the shortening factor, k_{sho}:

$$\Delta\varepsilon_{pt} = \frac{n_{gap}\Delta_{pt}}{l_{ub}} \tag{10.42}$$

$$\Delta T_{pt} = \Delta\varepsilon_{pt} k_{sho} E_{pt} A_{pt} \tag{10.43}$$

and:

$$T_{pt} = T_{pt,initial} + \Delta T_{pt} \tag{10.44}$$

As in the preliminary design, the calculation of the force in the reinforcing will depend on the type of reinforcing selected. This will be a function of the displacement at the reinforcing level:

$$\Delta_{s,t} = \theta_{imp}\left(c - y_{s,t}\right) \tag{10.45}$$

$$T_s = f\left(\Delta_{s,t}\right) \tag{10.46}$$

$$C_s = f\left(\Delta_{s,c}\right) \tag{10.47}$$

Angle reinforcing

An estimation of the required angle size has been provided during the preliminary design of the beam-column joint. The design tables presented in Section 3.6 and APPENDIX A present yield force (F_y), yield displacement (Δ_y) and post-yield stiffness (r). These values are used in order to find force in the angle under the displacement, Δ_s or Δ_t.

Fuse type reinforcing

The stress in the reinforcing will depend on the steel type used and assumptions made regarding the strain hardening properties of the bar. This is represented by the factor r, the post-yield stiffness ratio. It is recommended that reasonable values of r be used during design (i.e. an elasto-perfectly-plastic assumption is not made). Values of r = 0.02 are recommended based on the testing described in Chapter 3 unless specific values are known.

$$f_s = f_y\left[1 + r\left(\frac{\varepsilon_s}{\varepsilon_y} - 1\right)\right] \tag{10.48}$$

As mentioned above a strain value of 3% is recommended in the tension fuse type dissipative reinforcing in order to obtain optimum performance. This means that the force in the reinforcing becomes:

$$T_s = A_s f_{s,t} \tag{10.49}$$

Where:

$f_{s,t}$ = Stress of selected steel type at a strain of 3%

In order to calculate the stress in the compression reinforcement ($f_{s,c}$) the unbonded length (l'_{ub}) described in Section 3.3 is required. This is done by calculating the required unbonded length to obtain 3% strain in the top reinforcing under its displacement ($\Delta_{s,t}$):

$$l'_{ub} = \frac{\Delta_{s,t}}{0.03} \tag{10.50}$$

Knowing this unbonded length the strain in the compression reinforcing ($\varepsilon_{s,t}$) can be calculated along with the stress using Equation (10.48) and force in the compression reinforcing:

$$\varepsilon_{s,c} = \frac{\Delta_{s,t}}{l_{ub}^{'}} \tag{10.51}$$

$$C_s = A_s f_{s,c} \tag{10.52}$$

As discussed the elastic section of the MMBA is used in order to find the strain in the extreme fibre of the timber (ε_t) under ULS loading. In order to do this the decompression curvature (ϕ_{dec}) of the beam-column joint must be calculated. Checks must be performed to ensure that the timber does remain elastic.

$$\phi_{dec} = \frac{2T_{pt,i}}{k_{gap} E_{t,para} b_b h_b^2} \tag{10.53}$$

$$\varepsilon_t = c\left(3\frac{\theta_{imp}}{L_{cant}} + \phi_{dec}\right) \leq \frac{f_{para}^{'}}{E_{t,para}} \tag{10.54}$$

Where:

L_{cant} = Distance from the interface to the point of contra-flexure, for seismic only loading this is taken as half the beam length

k_{gap} = Modulus of elasticity modification factor (discussed in Section 5.3.6, values found in Table 10.5)

Knowing the strain in the timber and assuming a triangular stress block the stress in the timber is calculated.

$$C_t = 0.5 k_{gap} \varepsilon_t E_{t,par} b_b c \tag{10.55}$$

As discussed in Section 5.3.6 the modulus of elasticity modification factor allows for the material characteristics of timber when loaded in compression. Recommended values for k_{gap} have been presented and are repeated in Table 10.5.

Table 10.5. Recommended values for Modulus of elasticity modification factor (k_{gap})

	Occurrence	kgap
Situations where no perpendicular to the grain action is present	Wall-foundation column-foundation connection, beam-column joints with concrete columns	0.7
Situations where perpendicular to grain action is present but adequate measures have been made to protect the perp to grain properties of timber	Beam-column joints reinforced with screws, epoxied in rods etc.	0.55
Situations where perpendicular to grain action is present and no effort has been made to protect perp to grain properties of timber	Unreinforced beam-column joints (not recommended)	0.1

Summing the tension (post-tensioning and tension reinforcement) and compression (timber compression and compression reinforcement) forces equilibrium is checked. If equilibrium is not satisfied (i.e. the forces do not sum up to or are not close to zero) the neutral axis value must be updated.

$$C_t + C_s - T_s - T_{pt} = 0 \tag{10.56}$$

Once the tension and compression contributions are found the moment capacity of the beam-column joint (M_{con}) can be calculated about any common point. This is then verified against demand using an appropriate reduction factor (ϕ = 0.9 in New Zealand)

$$M^*_{con} \leq \phi M_{con} \tag{10.57}$$

10.3 FURTHER CONSIDERATIONS IN FRAME DESIGN

Section 10.2 provided methodology for the design of an internal beam-column joint as part of a post-tensioned timber frame system. Further considerations must be made when considering this single beam-column joint as part of a full frame. These considerations are described in this section.

10.3.1 Design of external beam-column joint

For frames of more than one bay beam-column joints will be either internal or external. The calculation of capacity for an external joint is performed using the equations described in Section 10.2.3 however some simple considerations must be made.

In several chapters the way in which reductions of the beam, column and joint panel rotations increase gap opening has been described. In an external beam-column joint both the column and joint panel elastic rotations are reduced (Section 5.4.1 and Section 5.4.2, respectively). This increases gap opening and thus strain in both the post-tensioning and reinforcing.

The change in column and joint-panel rotation is simple to allow for in the calculation of strain and force for the dissipative reinforcing with a larger value of gap opening (Δ_s) being used in combination with Equations (10.48), (10.51) and (10.52). It is unlikely that different dissipative reinforcing will be applied to external beam-column joints however this can also be allowed for if desired.

Calculation of the post-tensioning force (T_{pt}) requires more care. In Equation (10.25) the gap opening of the single beam-column interface is multiplied by the number of gaps opening along the frame (n_{gap}). This is based on the assumption that all gap opening values are equal, which for the case of the external columns is not true.

In design it is possible and uncomplicated to iterate in order to find the correct amount of tendon elongation by summing all gaps along the frame:

$$\Delta\varepsilon_{pt} = \frac{n_{gap,external}\Delta_{pt,external} + n_{gap,\text{int}ernal}\Delta_{pt,\text{int}ernal}}{l_{ub}} \quad \textbf{(10.58)}$$

This iteration may become time-consuming however as the tendon elongation, gap opening and moment capacity are all linked.

In most cases for design it is simply possible to take the increase in tendon force (ΔT_{pt}) calculated during the design of the internal joint and apply this to the external joint. This is conservative as the calculation will results in lower tendon forces and thus moment capacity.

10.3.2 Beam and column section checks

The nature of post-tensioned timber connections means that the moment and shear capacity of the individual members is normally significantly stronger than demand. Moment and shear checks, considering capacity design principles and higher mode effects should still however be performed.

Beams

For beams the maximum moment load case must be defined between the seismic loading demand ($M^*_{b,seismic}$) and the gravity loading demand ($M^*_{b,gravity}$). Once complete the relevant timber standard can be used to calculate capacity. In New Zealand (NZS3603:1993 1993) this becomes:

$$\phi M_{n,b} = \phi k_1 k_4 k_5 k_8 f_{tb} Z_b \geq M_b^* \quad \textbf{(10.59)}$$

Where:

k_1 = Load duration factor for strength (1.0 for seismic loading, 0.8 for gravity loading)

k_4 = Parallel support factor (taken as 1)

k_5 = Grid system factor (taken as 1)

k_8 = Stability factor (normally 1 however can be calculated using Section 2.10 of (NZS3603:1993 1993))

f_{tb} = Timber bending strength

Z_b = Beam section modulus

As mentioned the timber section sizes are normally significantly oversized for their required demand therefore a simple assumption of pined-pined support can be used when calculated the gravity load demand. For long spans however this may lead to the beam capacity being exceeded and some fixity at the beam end should be used in order to redistribute loading. Further information on how this can be done is available in van Beershoten et al. (2012).

As with moment demand, maximum shear demand must be identified between the seismic ($V^*_{b,seismic}$) and the gravity cases ($V^*_{b,gravity}$). Again, once complete the relevant timber standard can be used to calculate capacity. In New Zealand (NZS3603:1993 1993) this becomes:

$$\phi V_{n,b} = \phi k_1 k_4 k_5 f_{ts} A_{s,b} \geq V_b^* \quad \textbf{(10.60)}$$

Where:

$A_{s,b}$ = The shear area of the beam

The shear area of the beam can be taken as being 2/3rd of the total beam area in most cases for seismic design. However, in cases where the tendon cavity is large the webs of the beam should be used.

Columns

Column design must include higher mode effects and overstrength considerations as discussed in Section 9.6.2. Firstly the Dynamic amplification factor for higher mode effects (ω_f) must be calculated. This uses the overstrength factor discussed in Section 9.6.2 ($\phi_o = 1.25$) and the ductility assumed in Section 10.2.1:

$$\omega_f = 1.66 + 0.13\left(\frac{\mu}{\phi_o} - 1\right) \tag{10.61}$$

The Dynamic amplification factor at roof level is taken as 1. The moment demand on the column is calculated with relation to the connection moment capacity (M_{con}):

$$M^*_{col} = \phi_o \omega_f \frac{M_{con}}{\left(1 - \frac{h_b}{L}\right)} \tag{10.62}$$

The capacity of the column is calculated using Equation (10.59).

As with the moment demand the shear demand on the column will include dynamic amplification for higher mode effects:

$$V^*_{col} = \phi_o V_E + 0.1\mu V_E \tag{10.63}$$

Additional consideration must be made to the strength capacity of the panel zone in shear. This will be critical for an internal column where, depending on the attachment of the external reinforcing, shear will be highest. The capacity of the column in shear will be calculated using Equation (10.60).

10.3.3 Design of beam corbels for shear transfer

Several tests have been performed historically on corbels designed to transfer shear loading from beams to the column face (Section 2.8.3). During the beam-column testing presented in Chapters 4 and 6 an internally glued tube was used and tested successfully. This tube was designed for a factored maximum gravity load in accordance with recommendations in Appendix B of the New Zealand concrete code (NZS 3101:1995 2006).

This is considered overly conservative however and in reality a risk based assessment should be made based on the contribution of friction at the interface. Minimum values of G + Q (unfactored dead load plus unfactored live load) are recommended.

10.3.4 Considerations for Maximum Credible Earthquake (MCE)

The Maximum Credible Earthquake (MCE) or Maximum Considered Motion limit state must be considered in order to ensure that the structure retains a margin against collapse even under to most severe earthquake shaking to which it is likely to be subjected. In New Zealand (NZS1170.5 2004) this is taken as ground shaking having a 2% probability of exceedance in 50 years (i.e. a 1/2500 return period). Under a performance based design framework this minimum objective is increased however some damage to the post-tensioned frame is acceptable.

Section 10.2.1 discussed the way in which loading for the ULS case is considered. The MCE case loading is found in a similar way. Under MCE loading increased deflections will occur leading to higher ductility demands. Damping values (and thus reduction factors) however will be kept equal to those calculated for the ULS case loading. The amount of EQV damping tends to plateau at higher levels of drift for timber post-tensioned systems as shown in Figure 5.24 of Section 5.5.

Under the revised performance based framework strain limit recommendations are placed for the MCE case in design. These limits are to ensure that a desirable hierarchy of strength is obtained. For post-tensioned timber this hierarchy is: yield of the reinforcement, yield of the timber either in the column or the beam, and finally yielding of the post-tensioning or fracture of the reinforcing. The yielding of the post-tensioning is unlikely however as crushing of the timber will lead to losses in post-tensioning due to plastic deformation. Figure 10.7 shows graphically this hierarchy. Guidance on appropriate strain values in order to ensure this hierarchy of strength are presented in Table 10.6.

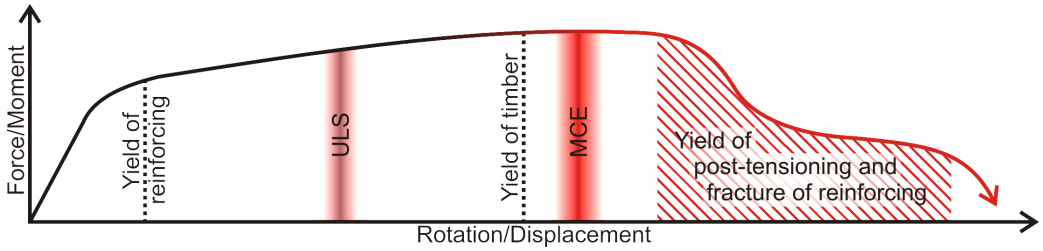

Figure 10.7. Hierarchy of strength for post-tensioned timber structures

Table 10.6. Strain limits for ULS and MCE for post-tensioned timber frames

	ULS	MCE
Reinforcing	3 – 4%	5 – 6%
Engineered timber	0.2%	0.6-0.8%
Post-tensioning	$0.7\varepsilon_y$	$0.9\varepsilon_y$

Further research is required in order to calculate the strain in the timber beyond the elastic limit. Until this research is performed the elastic form of the MMBA can be used to calculate strain provided crushing remains minor (i.e. strains remain close to the elastic limit)

10.3.5 Considerations for long term effects

Long term effects in beams and columns were not within the scope of this research however they do play a significant role in the overall performance considerations and therefore will be briefly discussed with reference to the way in which they impact on frame design.

As mentioned in Section 2.3 moderate post-tensioning losses have been recorded for post-tensioned timber frames where the perpendicular to grain loading of the column was protected and significant losses when no protection was present. The effect of these losses is shown schematically in Figure 10.8. As shown the frame is required to displace further in order to have a capacity equal to the frame demand. In addition residual drifts are increased due to the drop in the recentering contribution. During design it is recommended that a simple push over analysis of the frame be performed in order to establish what increases in drift will occur. The expected amount of losses will depend on the amount of compression perpendicular to the grain present in the frame system. Some discussion regarding the protection of the column can be found in the next paragraph however the long-term performance of these solutions requires further study.

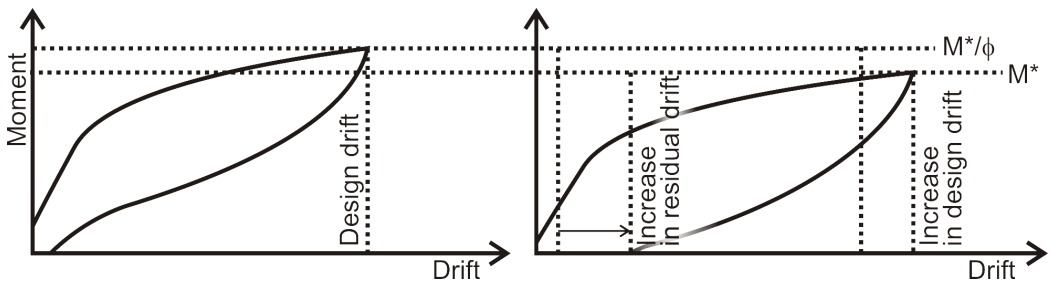

Figure 10.8. Effect of post-tensioning losses on post-tensioned timber frame-performance

10.3.6 Reinforcement of the column face

During both the beam-column testing described in Chapter 4 and the frame testing described in Chapter 5 protection of the column face was provided through the use of screws. The use of screws was necessary as the compression capacity of the column face was not sufficient to resist crushing during rocking.

Numerous methods of column face reinforcement exist as shown in Figure 10.9. Section 5.3.4 and Section 5.3.6 discussed the factors k_{int} and k_{gap} respectively which are related to the reinforcement methods used.

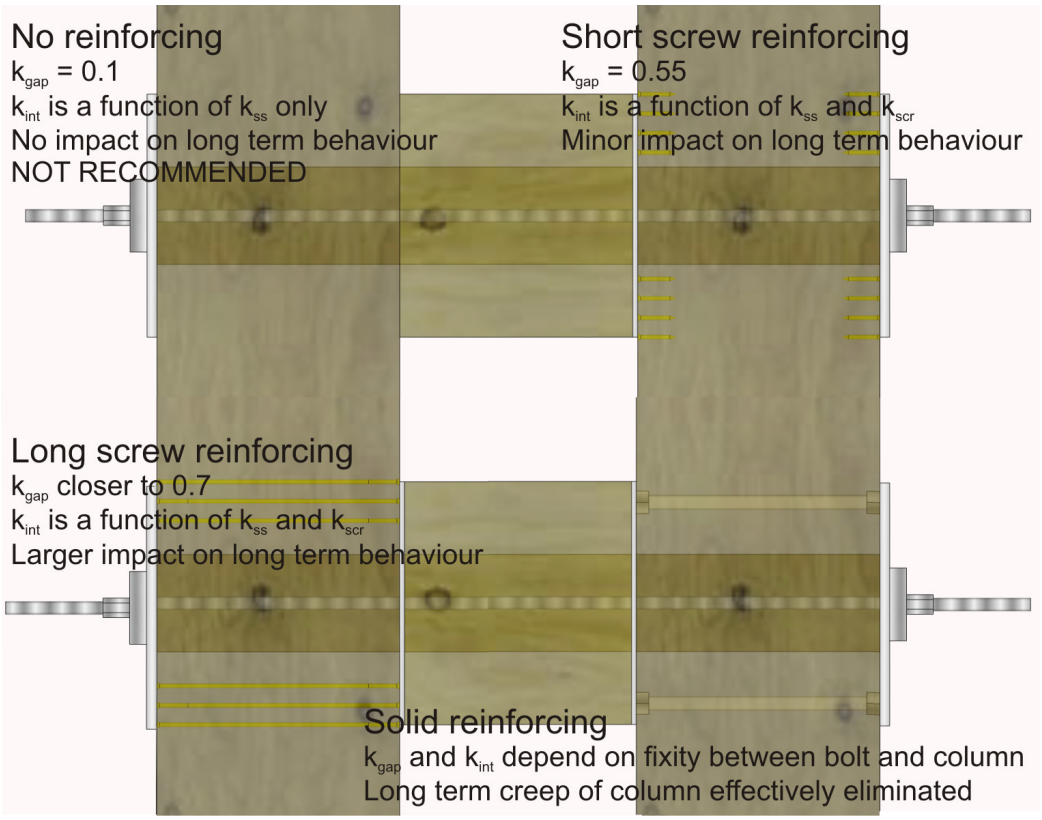

Figure 10.9. Reinforcement methods for beam-column joints

In Figure 10.9 only a summary selection of the many options for the reinforcement of a beam-column joint is shown with various other options being possible. It is important however that the reinforcement option is selected while thinking about what the reinforcement does to the global system response.

Perhaps the most important example of this is the positioning of reinforcement. As shown in Figure 10.10 an unreinforced column can be represented as an almost rigid block on a bed of soft springs, when compressed the bed of soft springs deform

uniformly and create the reduction in stiffness referred to the as interface compression deformation (θ_{int}).

Placing reinforcing in the column effectively introduces stiff springs into the system which when loaded will attract a significant proportion of the initial post-tensioning force ($T_{pt,initial}$). Careful consideration regarding where reinforcement is placed must be made in order to ensure that the placement of reinforcement does not create a hinge in the centre of the beam as shown on the right of Figure 10.10. The creation of this hinge leads to the centroid of the compression zone of the joint being artificially lowered during rocking as shown. This reduces lever arm and thus moment capacity.

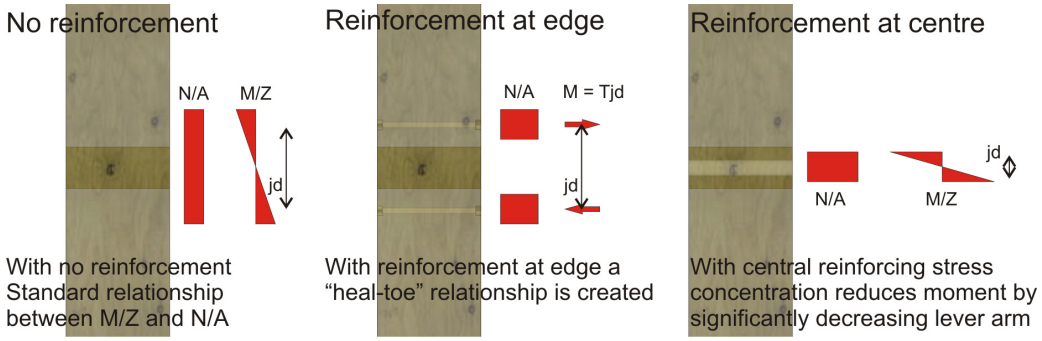

Figure 10.10. Unreinforced, edge reinforced and centrally reinforced and beam-column behaviour

Reinforcement should be concentrated at the edge of the beam as shown. This will create a 'heal-toe' action and will concentrate stress at the edge of the beam. The heal-toe connection will not create the same artificially lowered compression centroid and will not therefore impact on moment response.

10.3.7 Design of columns

As mentioned in Section 10.2.1 during the distribution of forces throughout the frame the base of the columns is assigned a moment capacity based on Equation (10.18), it must therefore be ensured that the column possesses this moment capacity.

The procedure presented in Section 10.2.2 is used in order to calculate the moment capacity. The only elastic contribution to be subtracted is the column rotation (θ_c) as discussed in Section 5.4.3. As the foundation will likely be resting on either a steel base plate or directly on the concrete foundation no interface rotation (θ_{int}) will occur and the modulus of elasticity modification factor (k_{gap}) will be equal to 0.7.

For low to medium rise frames it is likely that the axial load on the column (N) will be adequate to provide recentering and therefore post-tensioning tendons are not required. This axial load should therefore be included in the equilibrium sum in Equation (10.56) and will provide moment capacity. The recentering ratio (β) will also account for the effects of axial load.

The amount of axial load in a column will depend on its tributary area and internal and external columns will have differing axial load values, as will internal and external frames. Furthermore, the axial load in each column will change during seismic loading.

In some cases axial load will not be sufficient in order to satisfy the moment demand required by the selected recentering ratio and lower values (i.e. increased amounts of reinforcing) will be required. This is acceptable provided that the global recentering ratio, which is discussed in the following section, is still adequate. This is likely to occur for external columns which have lower values of axial load. Reinforcing should be increased until the sum of the column moments satisfies the equation below:

$$\sum_{i=1}^{n_{col}} \phi M^{i}_{b,col} \geq 0.6 V_b H \qquad \textbf{(10.64)}$$

Where:

V_b = Total base shear

$M^i_{b,col}$ = Moment capacity at the base of column i

n_{col} = Total number of columns

10.3.8 Global recentering ratio

Section 5.5 discussed the way in which the recentering ratio (β) influences the damping of a post-tensioned timber connection. It must be recognised however that the single connection makes up part of a frame system and it is the combination of the recentering ratios of the whole system which influence frame performance.

In order to calculate the total overturning moment of a frame the individual recentering ratios (β) of the beams and columns are calculated and weighted based on their contribution to the total overturning moment.

Overturning moment (OTM) contribution of the beams at each level (i) is given by:

$$OTM_i = \sum_{i=1}^{n} V_b^i L_{base} \tag{10.65}$$

Where:

V_b = Shear in the beam

L_{base} = Frame length (column centreline to column centreline)

Adding the overturning moment of the columns the total overturning moment of the frame is calculated:

$$OTM = \sum_{i=1}^{n_{col}} M_{b,col}^i + \sum_{i=1}^{n} V_b^i L_{base} \tag{10.66}$$

The total recentering ratio is then weighted based on the proportion provided to this total overturning moment giving:

$$\beta = \frac{\sum_{i=1}^{n_{col}} \beta_i M_{b,col}^i + \sum_{i=1}^{n} \beta_i V_b^i L_{base}}{OTM} \tag{10.67}$$

10.3.9 Distribution of strength amongst frames and the effects of torsion

The impact of torsion on a post-tensioned timber frame has not been previously studied and was beyond the scope of this research however it is unlikely it will create a significant issue if allowed for during design, as with other construction materials. This Chapter has discussed the way in which the strength and stiffness of a post-tensioned timber frame can be controlled though member sizing and the allocation of initial post-tensioning force and dissipative reinforcing. Unbalanced mass distribution can be allowed for through unbalance strength distribution. If eccentricity is an issue in a structure, frames can be designed (through section sizing) to decompress and yield at the same rotation with different strengths thus providing a more uniform performance. It is also expected that the recentering of the post-tensioned timber frame will lead to a reduction in the effects of torsion. This has not been specifically studied but was an observation during the residual displacement analysis discussed in Chapter 2. The distribution of strength will, however, require careful consideration as it is likely that these systems will be paired with timber flooring solutions which, in most cases, cannot be considered rigid.

10.4 CONCLUSIONS FROM CHAPTER 10

Chapter 10 has presented the procedure for the seismic design of post-tensioned timber frames. This has brought together the local and global seismic performance aspects examined during this research.

Historically analytical procedures proposed for post-tensioned timber have mainly focused on the calculation of the capacity of an existing frame and only minor guidance has been given on how to design a new structure.

Firstly in the design process either force based or displacement based design is used in order to calculate the likely base shear demand on the structure for the site where the building is to be constructed. In order to do this a design drift (θ_d), recentering ratio (β), post-yield stiffness (r) and design frame displacement ductility (μ), must be assumed. Although through design these values will vary, the nature of post-tensioned timber frames mean that the following ranges ductility and post-yield stiffness value can be used: $2 \leq \mu \leq 3$ and $r \approx 0.1$. These values require verification post design. The recentering ratio is a design choice however is likely to range between 0.6 and 0.8.

Once the base shear is known any admissible method of frame force distribution can be used. It is suggested that the selection of beam and column sizes be done in order to limit elastic rotations. During the estimation of base shear a design ductility and drift have been selected. In order to ensure that this ductility is obtained at the design drift the elastic rotations must be limited to less than the design drift divided by 1.3 times this ductility ($\theta_{el} \leq \theta_d/1.3\mu$).

Once beam and column sizes have been selected a preliminary design procedure is used in order to set initial values of post-tensioning and dissipative reinforcing. These initial estimations are then checked using the analysis procedure for post-tensioned timber frames presented in Chapter 5. The capacity of the beam-column connection is compared against demand and if satisfied the design procedure is complete.

The design of the initial post-tensioning and dissipative reinforcing quantities makes up one part of the design of a post-tensioned timber frame. The beam and column sections must be verified for shear and moment capacity, including the impact of higher modes on the frame. Details regarding the connection of dissipative reinforcing, and the anchorage of post-tensioning must also be considered carefully.

In a standard post-tensioned timber frame some form of column face reinforcement is likely to be required. The design of this reinforcement requires careful consideration as if poorly designed it can impact negatively on moment capacity. During the complete design of a post-tensioned timber frame hierarchy of strength and long-term performance must also be considered and verified.

Chapter 10 has provided a step by step procedure for the design of post-tensioned timber frames. It has also provided guidance on the selection of beam and column sizes and well and the design of column reinforcing, strength hierarchy and long term effects.

REFERENCES CHAPTER 10

Cardone, D., Di Cesare, A., Ponzo, F. C., and Blonna, B. (2008). "Evaluation of Behaviour Factor for Flag-Shaped Hysteritic Models." International Conference on Engineering Optimization, Rio de Janeiro, Brazil.

Newmark, N. M., and W. J. Hall. (1973). "Procedures and criteria for earthquake resistant design." National Bureau of Standards, U.S. Dept. of Commerce.

NZCS. (2010). *PRESSS Design Handbook*, New Zealand Concrete Society, Wellington New Zealand.

Priestley, M. J. N., Calvi, G. M., and Kowalsky, M. J. (2007). *Displacement-Based Seismic Design of Structures*, IUSS Press.

Sporn, B., and Pampanin, S. (2013). "A “retrofit” solution for Force-Based Design: eliminating the need for iteration and initial period estimation." 2013 New Zealand Society for Earthquake Engineering Conference, Wellington, New Zealand.

van Beerschoten, W. A., Palermo, A., and Carradine, D. (2012). "Gravity Design of Post-Tensioned Timber Frames for Multi-Storey Buildings." ASCE/SEI Structures Congress, Chicago, USA.

NZS 3602:1993. (1993). "Timber Structures." Standards New Zealand.

NZS 1170.5:2004. (2004). "Structural Design Actions Part 5 : Earthquake Actions - New Zealand." Standards New Zealand.

NZS 3101:1995. (2006). "Concrete Structures Part 1. The Design of Concrete Structures." Standards New Zealand.

11 Conclusions and Recommendations for Future Research

11.1 CONCLUSIONS

This thesis has presented a comprehensive look at the seismic performance of post-tensioned timber frames with and without the addition of dissipative reinforcing. Although many observations and conclusions have been made and will be discussed in this chapter and in the concluding remarks of previous chapters, a common theme continued throughout. This was the importance of the deep understanding of displacements within the frame and the impact of these displacements on performance. Created by the inherent increase flexibility of timber as a material, these displacements can impact negatively on planned seismic response by reducing (by up to 50%) the non-linear demand at the beam-column joint. Displacements occur throughout the frame in dissipative reinforcing devices, in the connection of these devices to the frames, in beams, columns and joint panels as well as at the interfaces between members. If understood, these displacements can be designed for and thus ensure that excellent seismic performance, possible using this innovative system, is obtained.

The principal objectives of this research were to review and refine the understanding of the static and dynamic response, the analytical and numerical modelling and the design of post-tensioned timber frames with dissipative reinforcing. In order to achieve these objectives a series of questions were asked as presented in Section 1.3. In order to address these questions a three phase experimental programme was performed in addition to a parametric numerical analysis and extensive analytical and numerical modelling. The responses to these questions are listed below under the headings presented in Section 1.3:

<u>Performance of dissipative reinforcing</u>

1. **What forms of dissipative device can be applied at the beam-column joint?**

Two forms of external dissipative reinforcing device were identified for application at the beam-column joint of post-tensioned timber frame buildings. The first of these was the fused type (‘plug & play’) dissipative reinforcing device consisting of a steel

bar or plate which has been reduced in cross-section over a certain area in order to control strains. The second was a steel angle that yields in bending over an area which has been weakened either through the reduction of the angles width (milled angle) of the drilling of holes (holed angle). Although these two dissipative reinforcing devices have been identified and verified for use in post-tensioned timber structures, research does not exclude the use of other dissipative reinforcing devices at the beam-column joint.

2. **How will the design parameters of initial stiffness, yield strength and post-yield stiffness relate to the physical characteristics of the device?**

Design of the fused type dissipative reinforcing was shown to be relatively straight forward however a slight modification, using a corrective factor k_a, was necessary in order to accurately calculate the yield displacement and thus initial stiffness. A quick design method for both types of dissipative reinforcing angle, which can be used in order to gain a rough estimate of angle size, was provided although being not sufficiently accurate for detailed design. A finite element model, which was confirmed against testing results, was used in order to provide design tables for both the milled and holed angle types.

3. **How will these dissipative devices be connected to the beam-column joint?**

A brief review of common methods of external dissipative reinforcing attachment has been performed concentrating on dowel type connectors (rivets and screws) in shear. Research found that although analytical formulas for the strength of these connections are common and generally in agreement, analytical formulas for the stiffness are rare. It was concluded that the stiffness of these connections, crucial in understanding the response of a displacement-dependent device, requires increased research effort.

<u>Local performance of post-tensioned beam-column joints</u>

4. **How does the ratio of moment capacity provided by the post-tensioning and the moment capacity provided by the dissipative reinforcing relate to the damping capacity?**

During beam-column testing the ratio between the moment capacity provided by the post-tensioning and the total moment capacity (the ratio β) was altered. This provided a range of hysteretic damping results. At the maximum drift level (θ_d = 2.5%) ratios of β ranged between 0.49 and 0.72, displacement ductilities ranged between 2.5 and 3.5 and area based damping values ranged between 9.5% and 19.1%. Equations used

to calculate the area based damping of flag shaped hysteretic systems were reviewed and showed that the current procedure is adequate but slightly overestimates damping for low values of recentering ratio (low β).

5. **Can the prediction of the initial stiffness of post-tensioned beam-column joints as identified by Newcombe (2012) be improved?**

Before decompression an interface compression rotation (θ_{int}) occurs which is a function of the initial post-tensioning value ($T_{pt,initial}$) and was not allowed for in previous design procedures. Formulas were proposed for the calculation of the rotation at which decompression occurs and included the effects which stress spreading and screw reinforcing have on the stiffness of the interface. These formulas were based on compression block testing from literature.

6. **Can improved understanding of the contributions of elastic deformations of the beam, column, joint panel and external dissipative reinforcing attachment be obtained and simple analytical tools be developed?**

The effects of the elastic deformation of dissipation connections were addressed briefly during the testing of the dissipative reinforcing devices however issues with uncertainties surrounding stiffnesses were highlighted and require further research effort. Equations were presented and derived in order to calculate the contributions of the beam (θ_b), column (θ_c) and joint panel (θ_{jp}) elastic rotations to global frame response. These were compared favourably with testing results, however further verification is required due to the limited number of test cases and geometries available. These elastic rotations were then presented together in order to study the way in which the individual rotation components make up the total rotation showing that in some cases these elastic rotations can make up 50% of the total rotations. Of these 50% elastic rotations, approximately one third was due to each of the beam, column and joint panel rotations.

<u>Global performance of post-tensioned frames</u>

7. **Is Laminated Veneer Lumber interchangeable with other engineered timber materials, such as glue laminated timber?**

Testing was performed on a full-scale beam-column joint and a two third scale, three storey frame using glue laminated timber. The results of this testing showed that a post-tensioned timber connection made from glue laminated timber will have the same connection properties as when the system is made from Laminated Veneer

Lumber. One major difference between the two materials however was the reduced strength of glue laminated timber perpendicular to the grain compared with Laminated Veneer Lumber (typical 2/3). This reduced strength will mean that increased reinforcing is likely to be required at the column face when using glue laminated timber. Analytical formulas, originally verified against testing using laminated veneer lumber, were used to successfully predict the system performance.

8. **Do the trends and analytical procedures observed and developed almost entirely during low speed, quasi-static and pseudo-dynamic testing continue during large scale dynamic testing?**

Procedures for the prediction of the beam-column joint performance of a post-tensioned timber frame have been compared against dynamic frame testing results. This comparison showed that the analytical procedure provides accurate predictions of the moment, post-tensioning force and neutral axis depth response. Comparisons of the neutral axis depths versus connection rotation behaviour indicated that the beam-column connection became slightly stiffer under dynamic loading leading to conservative estimations of moment capacity. Finally, the total rotation of the frame (taken from interstorey-drift) was compared against the connection rotation of each floor and the analytical procedures for elastic rotations. This comparison showed the analytical procedures to be accurate with the exception of the first floor. This was likely due to the assumptions made regarding the distribution of moment in the column being inaccurate for the first level (the point of contra-flexure in the column was not close to mid-height as assumed). Overestimation of elastic rotations will lead to conservative designs (increased connection rotations and therefore increased dissipation and moment capacity), however, this possibility must be considered when designing post-tensioning and dissipative reinforcing in order to avoid failure from increased strain demand.

9. **Are the current methods used for the prediction of the dynamic demand and response of post-tensioned timber frames accurate?**

The current methods of calculating dynamic demand (in the form of base shear) have been shown to be accurate provided adequate assumptions are made regarding design displacement ductility and system dynamic characteristics, or iteration to find the correct values, is performed. For a quick estimation the empirical method suggested by NZS1170.5 (2004) for steel frame structures provided, for the testing frame, a sufficiently accurate prediction. Further research effort is required if a quick initial

estimation formula is desired for post-tensioned timber frames. For more detailed information a structural modelling programme was used that only contained information regarding section sizes and boundary conditions. This model did not contain beam-column interface performance information. Two methods of calculation of base shear under a given seismic loading were investigated; Force Based Design (FBD) and Displacement Based Design (DBD). These two design methods were shown to deal with the impact that ductility and damping have on system response in different ways and the failure of FBD, in some cases, to differentiate between the impacts of these two factors led to unconservative results for low damping (low β) systems. In contrast DBD was shown to differentiate between the contributions of these two factors, however it was more susceptible to errors in their values.

10. **How does the dynamic response of a post-tensioned timber frame change when dissipative reinforcing is added to the frame?**

Comparisons between the dynamic shaking table testing of two systems with and without dissipative reinforcing showed a 32% decrease in maximum drift. The reason for this decrease was that the system with dissipative reinforcing had a higher strength capacity and hysteretic capacity when compared to the system without dissipative reinforcing. Comparisons of accelerations between the two test configurations showed that the 32% decrease in drift was not accompanied by an increase in acceleration, but by an 18% increase in base shear.

<u>Numerical modelling and design of post-tensioned timber frames</u>

11. **Do the current methods of numerical computer modelling accurately predict the dynamic performance of post-tensioned timber frames?**

The numerical modelling of the quasi-static beam-column performance provided confirmation that the local, force/moment versus displacement/drift, behaviour of a post-tensioned timber frame can be accurately represented through the use of either a rotational or multi-spring model in either RUAUMOKO or SAP2000. The numerical modelling of the global performance dynamic timber frame testing confirmed that the seismic response of a post-tensioned timber frame can be adequately (errors in the range of maximum 20 – 25%) represented through non-linear time history analysis. Comparison of numerical modelling results versus the dynamic testing response showed the importance of modelling the performance of the column base connection.

It is therefore suggested that the response of column base be at least modelled using a properly calibrated rotational spring in design practice, where it is typically overlooked, in order to provide confidence in numerical modelling outcomes.

12. **Can simplifications to these numerical computer modelling procedures be made in order to render their use more acceptable to practising engineers?**

Dependant on the information required by the designer, it is suggested that the simpler rotational spring model is used for the non-linear modelling of post-tensioned timber frames instead of the more complex and less computationally stable (axial) multi-spring model. It must be noted however that the rotational spring model does not provide correct information regarding the amount of displacement across the gap (which is provided by the multi-spring model). Therefore if information is required regarding gap opening the multi-spring model must be used.

13. **How do the frame characteristics (beam length, number of bays and bay length) as well the quantity of dissipative reinforcing alter section size and required strength and performance?**

Chapter 9 presented the design and analysis of 81 different frames varying beam length (4 m, 6 m, and 8m), number of bays (1, 3 and 5) and number of stories (3, 5 and 7). The recentering ratio was also changed (β = 0.6, 0.8 and 1). Displacement Based Design was used with a design drift value of 1.8%, providing beam areas ranging between A_b = 0.12 m^2 to A_b = 0.425 m^2, an increase of 250% (comparison made between a 5 x 4 m long bay, three storey frame with β = 0.6 and a 1 x 8 m long bay, seven storey frame with no dissipative reinforcing). Beam height did not change with an increase in the number of bays, however as expected an increase of bay length did create an increase in beam height. Decreasing the value of recentering ratio, β, from 1 to 0.8 led to an average 27% reduction in beam area. Decreasing β from 1 to 0.6 led to an average 42% reduction in beam area. Similar trends were observed regarding the initial post-tensioning required to resist moment demand. Minimal change was noted with an increase in the number of bays and moderate increase (approximately 30%) with an increase in number of stories from 3 to 7. A significant increase in initial post-tensioning was observed with an increase in bay length. This was particularly important for the β = 1 post-tensioned only cases which are required to resist any additional moment demand only through increase in post-tensioning

force. The effect of allocating a percentage of moment resistance to the dissipative reinforcing was twofold by decreasing demand and providing moment capacity.

14. **Can the design procedure for post-tensioned timber frames with the addition of dissipative reinforcing devices be refined and simplified in order to make it more linear (with less iteration as is currently required) and easier to use?**

Upon conclusion of this body of research the design procedure for post-tensioned timber frames remains reliant on iteration however the recommendation that elastic rotations be limited as a function of the design displacement ductility will lead to a reduced amount of iteration being required.

11.2 RECOMMENDATIONS FOR FUTURE RESEARCH

As with any body of research all of the questions surrounding the topic of post-tensioned timber frames were not able to be covered in this thesis. The following recommendations are made for the focus of future research efforts regarding this topic:

- During both of the experimental campaigns the connection of the dissipative reinforcing to the frame members displayed performance which was inferior to what it was designed for. This led to reduced frame strength and stiffness as well as reduced dissipative capacity and as a consequence increased demand. This performance was linked to both the manufacture of the connections (inadequate tightening of screws or gluing procedure) and tolerance issues (the widening of holes creating slop in dissipative reinforcing connections delaying yield). As a critical point in the post-tensioned timber frame these connections require further simplification as well as guidance regarding stiffness and manufacture procedures.

- During the presentation of the beam-column joint analysis procedure two factors, k_{int} and k_{gap}, were introduced allowing for the contribution of the column face stiffness to moment-rotation response. These values vary with the addition of armouring and some guidance has been provided regarding these values when screws are applied to the column face. It is recognised however that the addition of screws is only one of many options for column face reinforcement. The impact that different reinforcing methods have on the

factors of k_{int} and k_{gap} remains unknown and as such requires further investigation.

- Investigation into the dynamic behaviour of post-tensioned timber frames was presented based upon the application of a selection of spectrum compatible ground motions to two frame configurations. Although testing has gone a long way in confirming pervious research assumptions and refining design techniques, further testing, on different frame configurations, is required to create a robust base of research to back up current design practice. To this end it is anticipated that testing will continue at the University of Basilicata varying frame capacities and recentering ratios.

- Chapter 9 presented the parametric analysis of a series of post-tensioned timber frame configurations. Several assumptions were made in order to define the cases study which should be reviewed. It is recommended that focus on the influence of tributary width and material stiffness be considered for future studies. The increasing of the number of ground motion records used during the study may also be revised thus decreasing scatter in results.

- Finally, improvement of the estimation of seismic demand, through the removal of the required iteration surrounding the ductility demand is required. In force based design this is not an issue related exclusively to post-tensioned timber and steps to remove inaccuracy and iteration have been proposed by Sporn and Pampanin (2013). Modern displacement based design however, has been able to overcome this hurdle by presenting formulas for the calculation of yield rotations thus becoming 'Direct' Displacement Based Design (DDBD). These relationships are usually a function of beam length and depth and at present are not available for post-tensioned timber frames (or walls).

REFERENCES CHAPTER 11

Newcombe, M. (2012). "Lateral Force Design of Post Tensiond Timber Frame and Wall Buildings ", University of Canterbury, Christchurch.Doctor of Philosophy.

Sporn, B., and Pampanin, S. (2013). "A "retrofit" solution for Force-Based Design: eliminating the need for iteration and initial period estimation." 2013 New Zealand Society for Earthquake Engineering Conference, Wellington, New Zealand.

NZS 1170.5:2004. (2004). "Structural Design Actions Part 5 : Earthquake Actions - New Zealand." Standards New Zealand.

APPENDIX A: Dissipative Reinforcing Angles Design Tools

A.1 MILLED ANGLE DESIGN TABLES

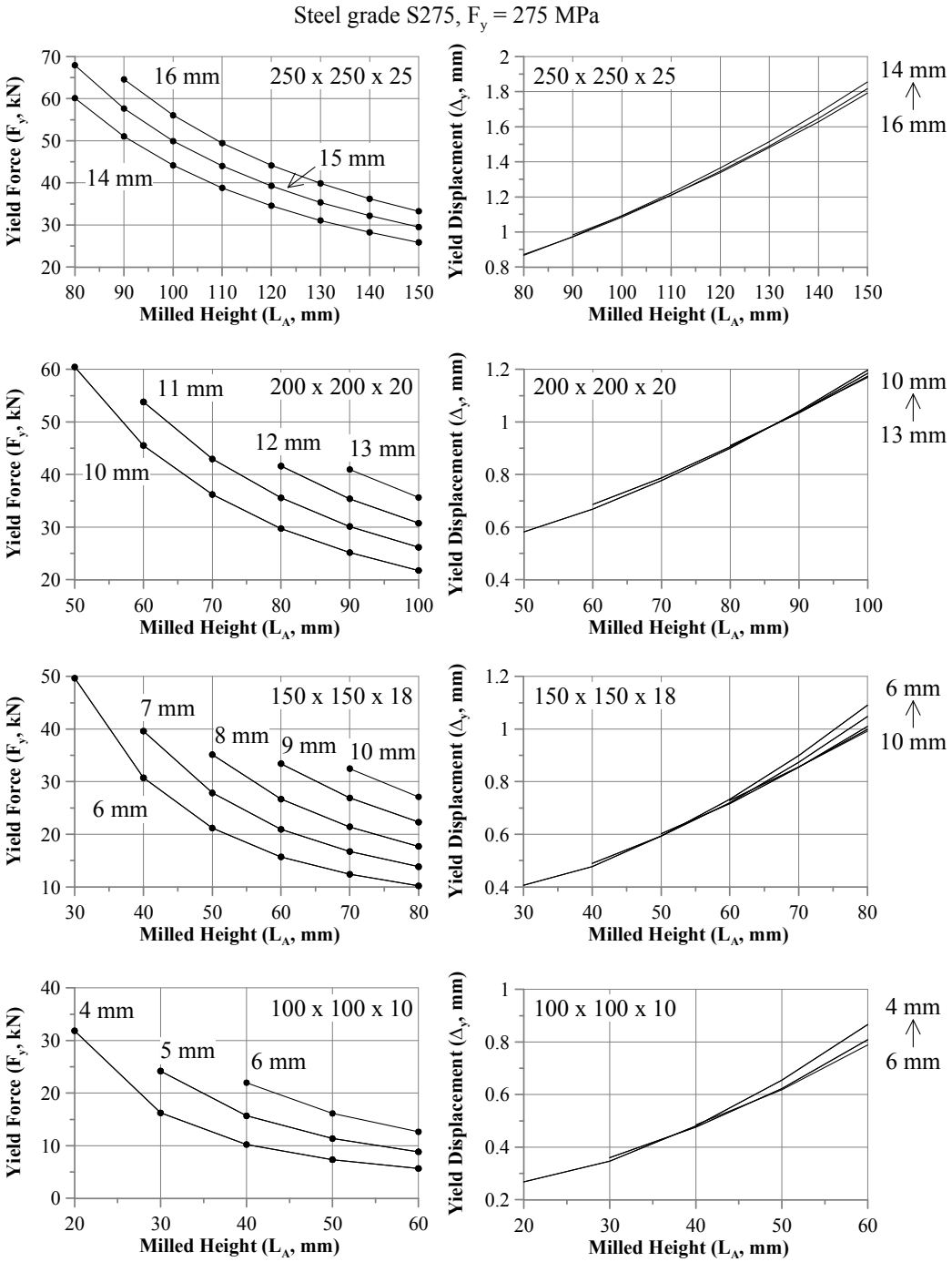

Figure A.1. Milled angle design charts S275 steel

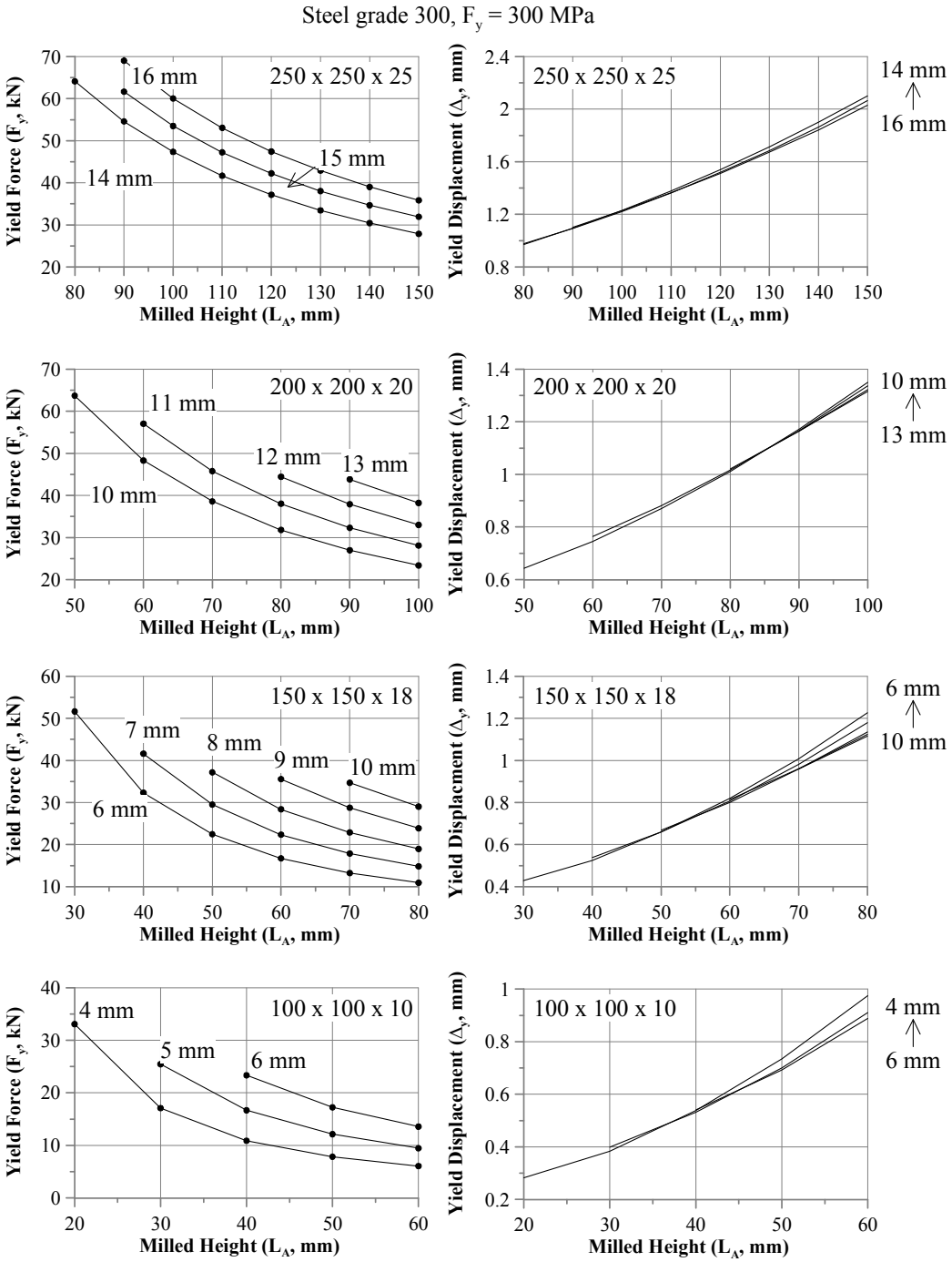

Figure A.2. Milled angle design charts Grade 300 steel

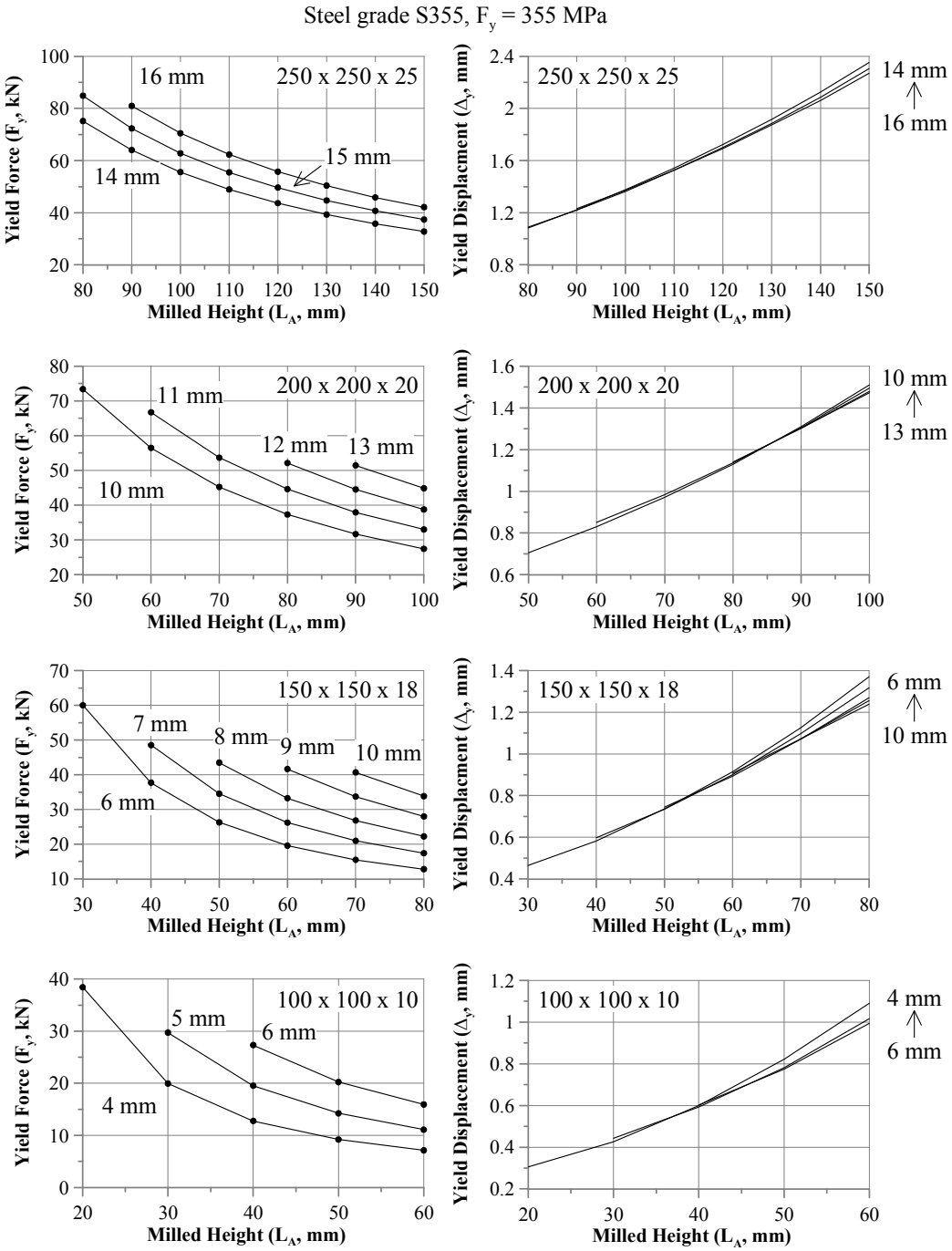

Figure A.3. Milled angle design charts S355 steel

A.2 HOLED ANGLE DESIGN TABLES

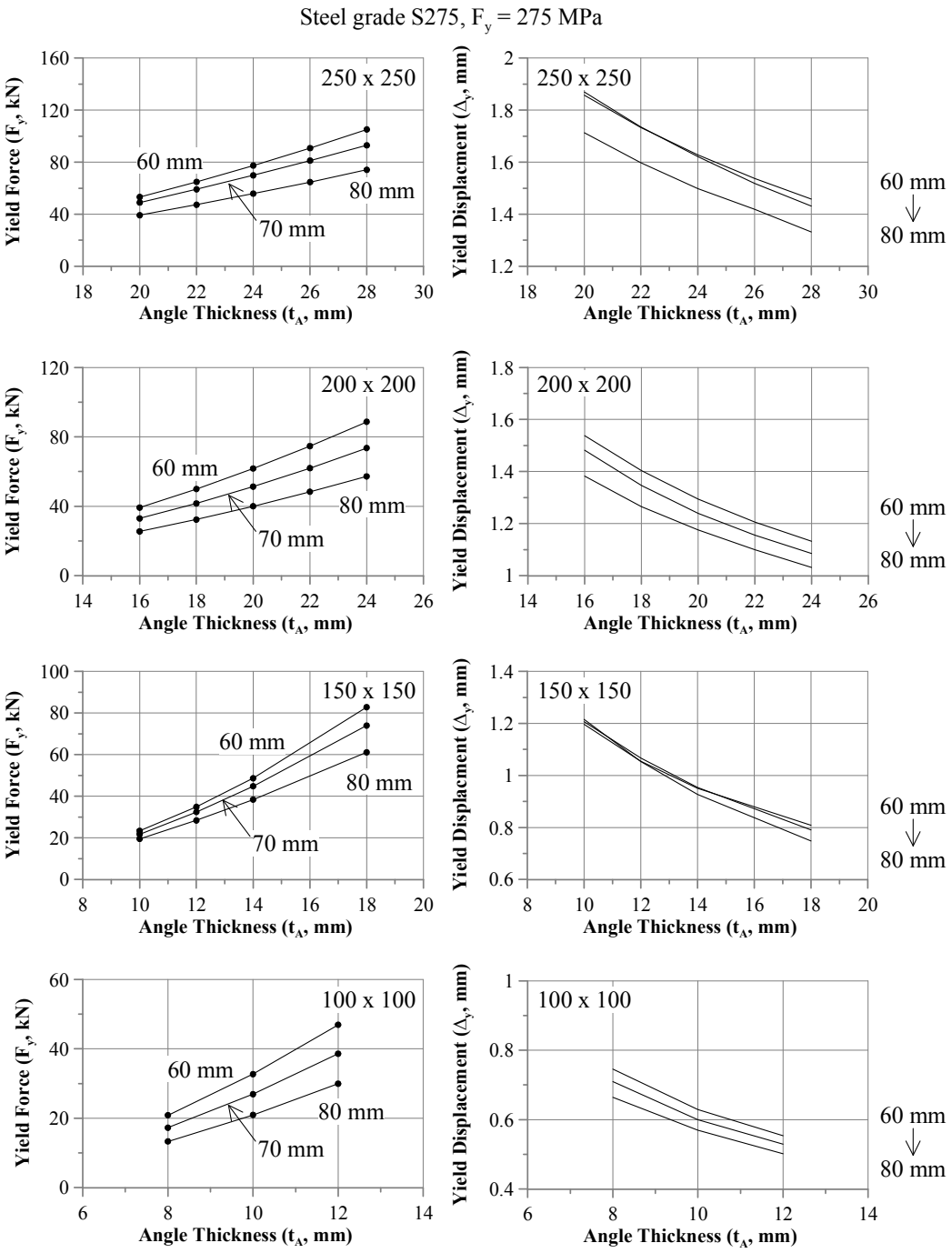

Figure A.4. Holed angle design charts S275 steel

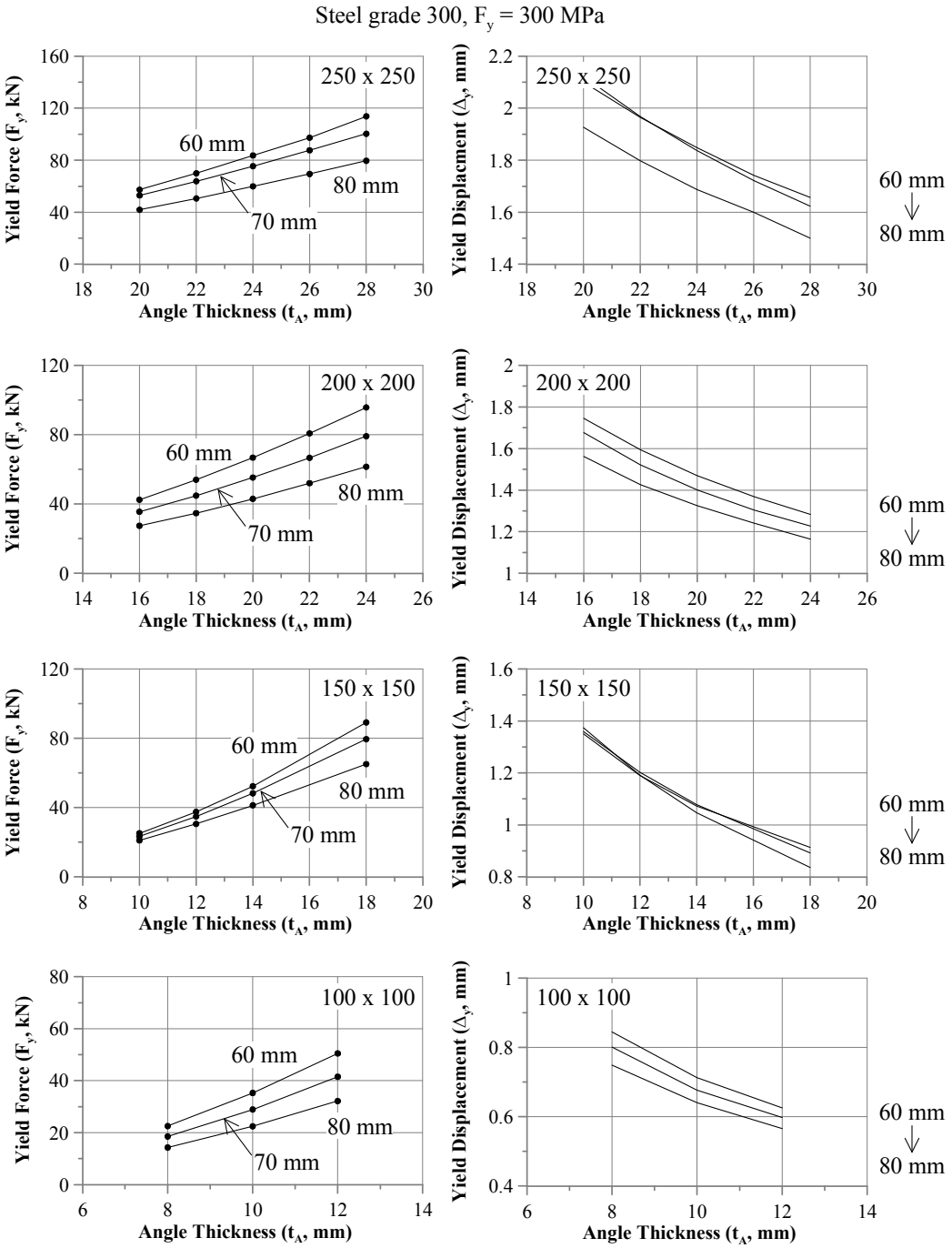

Figure A.5. Holed angle design charts Grade 300 steel

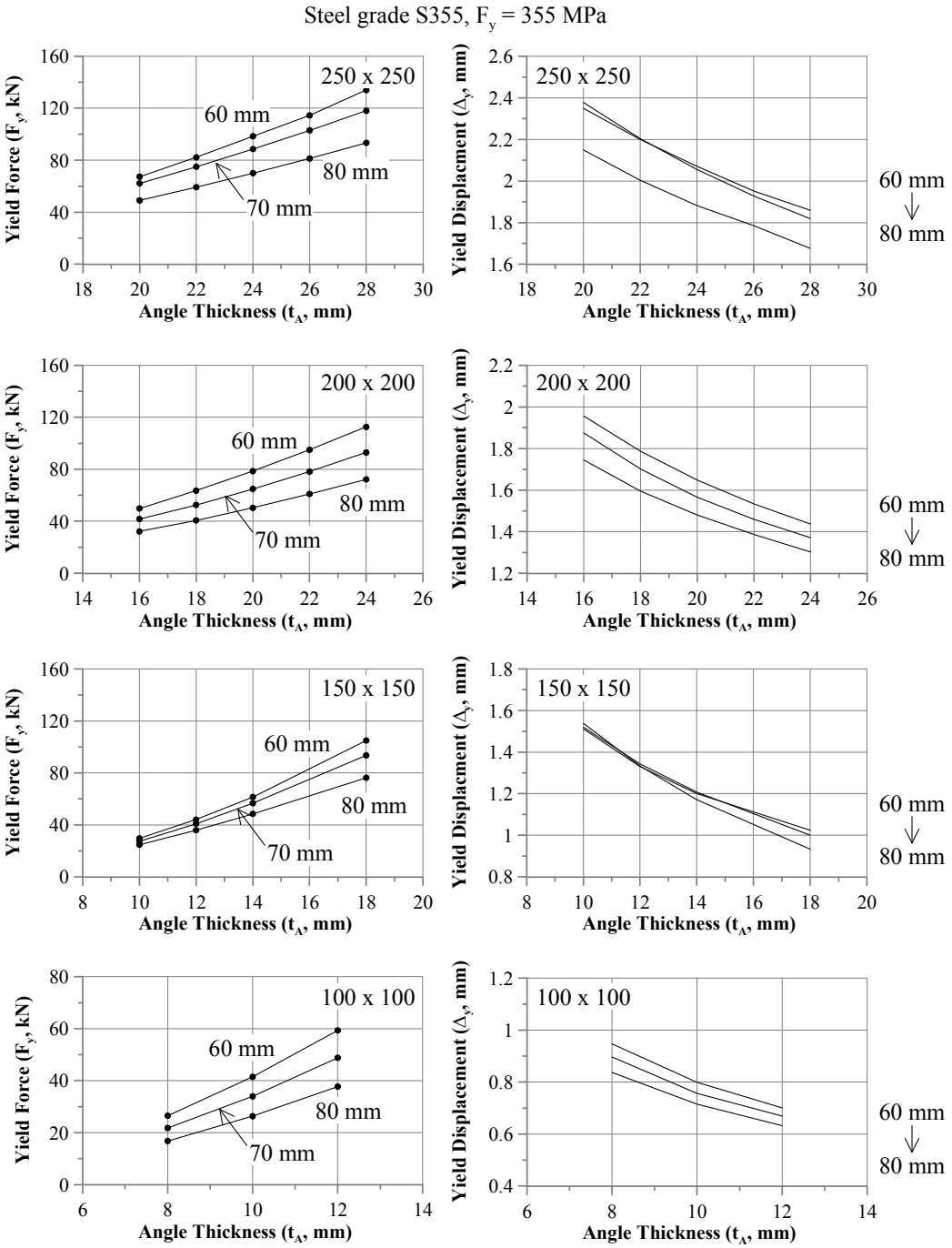

Figure A.6. Holed angle design charts S355 steel

A.3 POST YIELD STIFFNESS

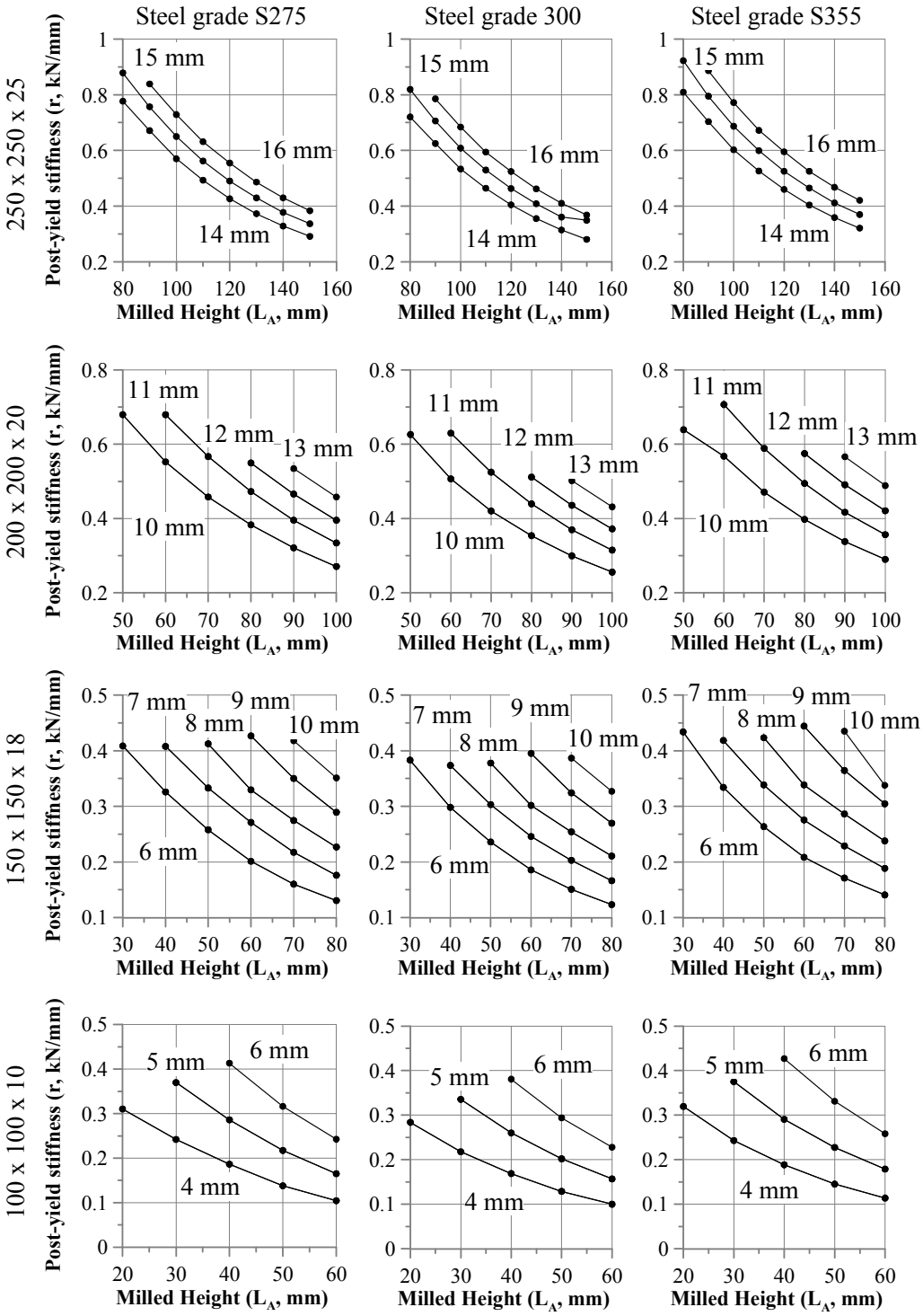

Figure A.7. Post-yield stiffness ratios for milled angles

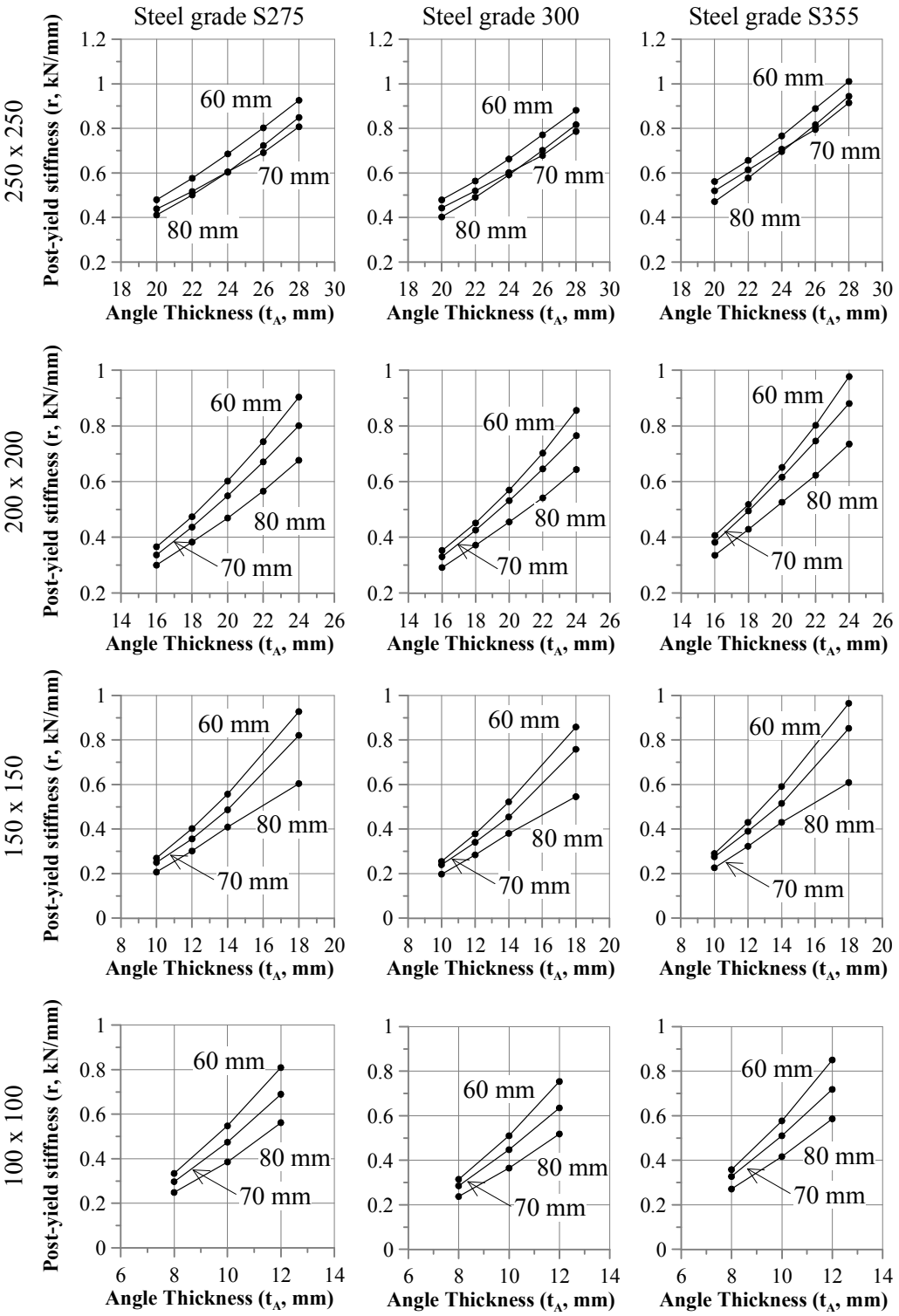

Figure A.8. Post-yield stiffness ratios for holed angles

APPENDIX B: Design of Beam-column Test Prototype Structure

B.1 INTRODUCTION

The following appendix describes the seismic design of the prototype buildings used during the beam-column testing described in Chapter 4. The plan dimensions of the the building were based on an existing test apparatus (Masi et al. 2008).

B.2 DESIGN OF BEAM-COLUMN TESTING PROTOTYPE STRUCTURE

Table B.1 below describes the geometric information regarding the prototype building.

Table B.1. Building Geometric Information

Number of Stories	n_s	5
Interstorey Height	H	3.175 m
Building Bay Length	L_B	4.6 m
Building Tributary Width	W_B	5 m

The building was designed as an office structure with a lightweight flooring solution giving:

Estimated structural dead load G = 2.5 kPa
Building Live Load Q = 3.0 kPa (Table 6.2 EN 1991-1-1:2004)

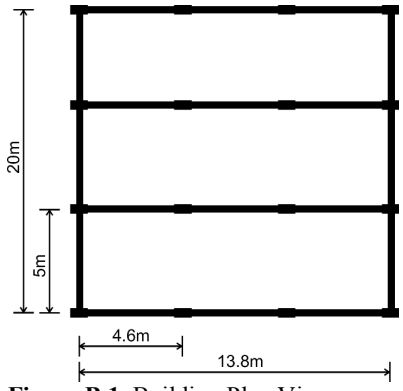

Figure B.1. Building Plan View

The building in plan (Figure B.1) consists of 4 frames and three bays.

Total floor area = 20 x 13.8 = 276 m^2
Seismic weight = G + 0.3Q (Normal)
= 2.5 + 0.3 x 3 = 3.4 kPa
= G + 0.0Q (Roof)
= 2.5 + 0.0 x 3 = 2.5 kPa
Seismic mass = 938 kN, 95.7 t (Floor 1-4)
= 690 kN, 70.3 t (Roof)

The natural period of the building was estimated according to equation 4.6 of EN 1998-1:2003. A value of C_t = 0.085 was used as the building was assumed to be

flexible in a way which is similar to a steel moment frame for which the above value is applied (further discussion regarding this assumption is presented in Chapter 7).

Natural period (H < 40m) $T_1 = C_t H^{3/4}$
$= 0.085 \times 15.9^{3/4}$
$= 0.68s$

The design spectra was defined for the building to be built in Potenza, Italy where the beam-column joint was tested. As an office structure the building was given a nominal life span of 50 years and an importance level of 2. The Peak Ground Acceleration for Potenza is 0.31 g.

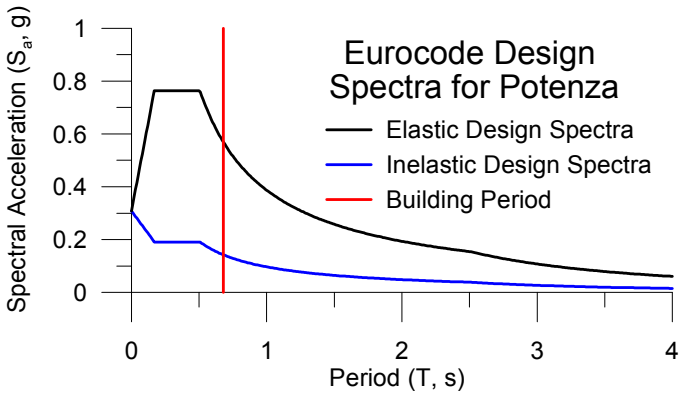

Figure B.2. Design Spectrum for Building

The correct value to be adopted as a structural performance factor has been discussed in Chapter 7 however at the time of design these conclusions had not yet been reached. A structural factor of 4 was therefore selected (Table 8.1 EN 1998-1:2003) due to the ductile and dissipative nature of the system.

Total seismic mass $m = 453$ t (3.2.4(2) EN 1998-1:2003)
From the inelastic design spectra $S_d = 0.142$
Total Base Shear $\Sigma V_b = 0.142 \times 453 \times 9.81$
$= 631.1$ kN
Base Shear per Frame (5 Frames) $V_b = 151.3$ kN

The building forces were distributed up the building according to the estimated first mode shape defined through the use of the mode shape factors shown in Figure B.3 providing the forces applied to each floor shown in Table B.2.

Force applied at each floor $F_i = V_b \frac{s_i m_i}{\sum_{i=1}^{n} s_i m_i}$ (eq. 4.10 EN 1998-1:2003)

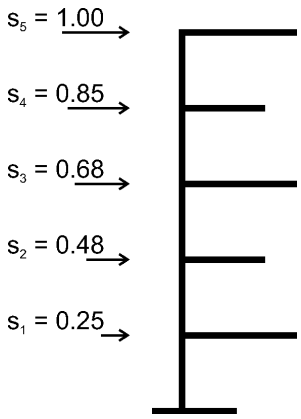

Figure B.3. Mode shape factors

$$\sum_{i=1}^{5} s_i m_i = 0.25\times19.1 + 0.48\times19.1 + 0.68\times19.1 + 0.85\times19.1 + 1\times14.06$$
$$= 57.2$$

Table B.2. Force applied at each level

Floor	Force (kN)
5	31.0
4	35.8
3	28.6
2	20.2
1	10.5

Forces were distributed through the frame using the equilibrium approach (Priestley et al. 2007) employing the following equations:

Column Base Tension Force $$N_E = \frac{\sum_{i=1}^{n} F_i H_i - 0.6 V_b H_i}{L_{base}}$$

Beam Shear $$V_{b,i} = N_E \frac{V_{s,i}}{\sum_{i=1}^{n} V_{s,i}}$$

Beam Moment at Column cl. $$M_{b,i} = \frac{V_{b,i} L_b}{2}$$

Applying the above equations the following Table B.3 was formulated:

Table B.3. Beam moments using equilibrium approach

i	H_i	F_i	F_iH_i	$V_{s,i}$	$V_{b,i}$	$M_{b,i}$	M_n
5	15.875	31.0	492.2	31.0	5.9	13.6	12.1
4	12.7	35.8	454.7	66.8	12.7	29.2	26.1
3	9.525	28.6	272.8	95.5	18.1	41.7	37.3
2	6.35	20.2	128.4	115.7	22.0	50.6	45.2
1	3.175	10.5	33.4	126.2	24.0	55.2	49.4
			Σ = 1381.6	Σ = 435.1			

$$N_E = \frac{1381.6 - 0.6\times126.2\times3.175}{13.8} = 82.7\,\text{kN}$$

REFERENCES APPENDIX B

Masi, A., Santarsiero, G., Dolce, M., Moroni, C., and Nigro, D. (2008). "Il Programma Sperimentale su Nodi Trave-Colonna in C.A. in Corso All'Universita di Basilicata." Con vegno Reluis "Valutazione e Riduzione Della Vulnerabilita Sismica di Edifici Esistenti in c.a", Rome, Italy.

Priestley, M. J. N., Calvi, G. M., and Kowalsky, M. J. (2007). *Displacement-Based Seismic Design of Structures*, IUSS Press.